THE TRANSMISSION OF VIBRATIONS THROUGH STRUCTURES

by

Julian Francis Hardenberg

B.Sc. (Eng), London

Thesis presented for the degree of

Doctor of Philosophy of the University of London

and for the

Diploma of Imperial College

Department of Mechanical Engineering

Imperial College

London S.W.7

August 1971

ABSTRACT

The transmission of vibration through structures depends on impedance matching between elements within each structure. The control of transmission can be achieved by means of inserting suitable paths or 'isolators' to produce an impedance mismatch.

General aspects of isolation are considered and formulations to describe the effectiveness of system modifications are given. Transmissibiiity ratios are used to indicate path characteristics in a standardised source-receiver situation for comparison purposes.

A new type of transmissibility apparatus is described which enables practical isolators to be tested over a large frequency range. Tests have been carried out on rubber tubes and rods, helical springs and a car shock absorber. The apparatus was also used to verify the existence of a damped vibration-cancelling dual path system, shown to be possible theoretically.

Practical vibration isolators tend to be highly complex structures, and an example has been dealt with in detail - namely, a front suspension assembly from a small car. Despite the very considerable complexity necessary to account for all the effects observed, it remains possible to give simple design criteria for the most favourable transmission properties within the limitations imposed by the overall design.

The technique of mathematically modelling complex structures as a set of resonators has been used to produce a simplified method of mobility testing which has been verified by experiments. The generation of mobility functions from modal data enables predictions to be made of bush effectiveness values for suspension models.

Parameter optimisation of suspension models show how target performance can be approached within the restrictions of the model structure and the permissible parameter ranges.

ACKNOWLEDGEMENTS

The Author gratefully acknowledges the support and encouragement of his supervisor, Dr. P. Grootenhuis.

The assistance of Dr. D.J. Ewins is much appreciated, as are the helpful discussions with colleagues.

Mr. R. Gunn gave invaluable help in the laboratory.

This work was partially financed by the Motor Industry Research Association, to whom the Author is indebted.

CONTENTS

		Page
1.	Introduction	10
2.	General Aspects of Vibration Isolation	13
	2.1 Systems and Divisions	13
	2.2 Subsystems	15
	2.2.1 Sources	16
	2.2.2 Paths	26
	2.2.3 Receivers	27
	2.3 Classical Models	27
	2.4 General Formulations	31
	2.5 Qualitative Description	38
	2.6 Role of Damping	43
	2.7 Summary	48
3.	Analytical and Experimental Methods	49
	3.1 Analysis and Solution of Lumped Parameter Models	50
	3.1.1 Notation	53
	3.1.2 Derivation of Equations	55
	3.1.3 Direct Solution of Equations	56
	3.1.4 State Vector Formulation and Solution	57
	3.1.5 Derivation of Mobility Matrices	60
	3.1.6 Alternative Methods	62
	3.2 Immittance and Transmission Matrices	63
	3.2.1 Definitions	63
	3.2.2 Inter-relationship Chart	67
	3.2.3 Experimental Chart	68
	3.2.4 Impedance, Mobility or Transmission?	75

3.3 Modal Equivalent Systems 77

3.3.1 Derivation of Model 78

3.3.2 Physical Interpretation and Consequences 83

3.3.3 Synthesis from Experimental Data 91

3.3.4 Modified Experimental Chart 95

3.3.5 Experimental Verification 99

3.4 Extension to Random Vibration 120

3.4.1 Frequency Response 120

3.4.2 Statistical Energy Methods 121

3.5 Optimisation Techniques 124

3.6 Summary of Computer Programmes 125

4. Special Aspects of Vibration Isolation - Path Control 127

4.1 Theoretical Behaviour of Paths 127

4.1.1 Single Stage Compliance 128

4.1.2 Two-end Multi-Stage Isolators 129

4.1.3 Wave Effects 131

4.1.4 Multi-Path and Cancellation 133

4.2 Test Methods 143

4.2.1 Theoretical Aspects 143

4.2.2 Practical Test Methods 148

4.2.3 Parameter Derivation 151

4.3 Experimental Apparatus 159

4.3.1 Specification 159

4.3.2 Construction 160

4.3.3 Drive and Measurement 165

4.3.4 Proving 171

4.3.5 Modifications and Extensions 176

4.4 Experimental Results 177

4.4.1 Rubber Rods 178

4.4.2 Rubber Tubes 185

4.4.3 Rubber Shear Mount 189

4.4.4 Helical Spring 189

4.4.5 Shock Absorber 200

5. The Transmission of Vibration Through Automobile Suspension Systems 204

5.1 Conceptual Model 205

5.2 Basic Considerations 207

5.2.1 Vehicle Body Mobility 208

5.2.1.1 Excitation away from Centre of Gravity 208

5.2.1.2 Decoupling of Massive Elements 214

5.2.1.3 Plate and Shell Results 214

5.2.1.6 Experimental Data on Car Body Mobility 219

5.2.2 Tyre and Wheel Mobility 224

5.2.3 Suspension - Low Frequency and Static Constraints 228

5.3 Transmission Properties of Individual Suspension Components 232

5.3.1 Principal Vertical Paths 232

5.3.1.1 Main Spring 232

5.3.1.2 Damper Unit 236

5.3.1.3 Wishbones and Links 238

5.3.1.4 Comparison 241

5.3.2 Lateral and Longitudinal Paths 241

5.4 Transmission Properties of Suspension Models 248

5.4.1 Without Links 248

5.4.2 With Links 252

5.4.2.1 Inclined Link with Spring 252

5.4.2.2 Twin Wishbone Model without Damper 254

5.4.2.3 Twin Wishbone Model with Damper 254

5.4.2.4 Twin Wishbone Model with Damper and Spring Surges 256

5.4.3 With Resonant Receiver 259

5.4.3.1 With Engine Resonance 259

5.4.3.2 With Engine and Body Resonances 261

5.5 Discussion and Conclusions 263

6. Experimental Transmission Properties of a Suspension System 268

6.1 Individual Components 269

6.1.1 Damper Unit 269

6.1.1.1 Experimental Apparatus 271

6.1.1.2 Response for Different Force Levels 275

6.1.1.3 Theoretical-Experimental Comparison 281

6.1.1.4 Effect of Parameter Changes 281

6.1.2 Wishbones 283

6.1.2.1 Vertical Transmission 284

6.1.2.2 Lateral Transmission 286

6.1.2.3 Longitudinal Transmission 290

6.2 Suspension Assemblies 292

6.2.1 Apparatus 293

6.2.2 Wishbones Alone 295

6.2.3 Complete Assembly 299

6.3 Discussion of Results 305

7. Conclusions 306

Appendix 1 Dynamic Absorbers 322

Appendix 2 Vibration Isolation Bibliography 342

Appendix 3 Aerostatic Bearing 344

Appendix 4 Transducer Calibration 347

Appendix 5 Mass Cancellation Circuit 352

Appendix 6 Example of Model Derivation 356

Appendix 7 List of Equations 369

Appendix 8 Conversion of Units 395

Appendix 9 Alternative Cancellation Model 396

CHAPTER ONE

INTRODUCTION

Noise and vibration contribute a significant part of the pollution of the environment and are principally the outcome of an industrial, urban society.

The motives for controlling noise and vibration range from purely engineering aspects, such as reduction of failure, fatigue, performance degradation or malfunction, unreliability, wear; to human aspects: physiological - death, pain, noise induced hearing loss, temporary threshold shift, muscle wasting, sickness; and psychological - discomfort, fatigue, reduction of performance, intrusion of privacy. Special motives might include compliance with legislation, secrecy and competition.

Control, at source, of vibration and noise is in many cases impracticable with present technology, and control of propagation is required. For the study of road excited vehicle vibrations, considered in later sections of this work, the transmission paths need to be adapted to lead to satisfactory isolation, since road roughness will always be present.

The motive for this study is to investigate the means by which the transmission of structure-borne vibration, including vibration in the acoustic range of frequencies (hence structure borne sound), may be modified. In essence, the ideal transmission path for vibration isolation is most

frequently a low-pass filter with a very sharp cut-off. The low-pass requirement is necessary for load and stiffness characteristics of the system, and constitutes an external constraint on the system. Multiple-paths and flexibilities of the source and receiver tend to reduce the isolation effectiveness. To express the value of making system changes, some new ratios are employed - receiver, source and receiver-transfer effectiveness which are outlined in Chapter 2 and Chapter 5. Performance of practical isolation mounts is determined experimentally using an original design of apparatus based on transmissibility. Cancellation of vibration through a dual, damped path is shown to be possible theoretically, and has been experimentally observed using rubber tubes, though unfortunately the useful bandwidth tends to be small.

In real isolation systems there may be very considerable complexity in the transmission paths. The use of computers enables quite complex systems to be studied, but excessive complication in modelling tends to lose in accuracy and meaning. For instance, a complete description of a point mobility of a structure requires twenty-one complex parameters for each frequency. Usually, these cannot be derived analytically and experimental determination has shown that large errors can be expected. Statistical energy methods lead to a simplification in approach, but are not at present sufficiently well formulated to lead to direct design criteria for the type of problem considered here.

A vehicle suspension from a small car has been analysed theoretically and tested experimentally, treating the suspension as part of a general isolation system, mainly in the range 10 - 150 Hz, bearing in mind the low-frequency restrictions. Principal vibration paths - vertical, longitudinal, lateral - have been chosen to lead to approximate models. Much information can be obtained from the study of component parts, and design suggestions to improve isolation are given.

Modelling a vehicle body from experimental data shows that it is possible to represent the bare body shell as a multimodal structure. It is shown that as a result of such modelling, mobility testing and data handling can be simplified. Experimental data on body and tyre mobilities is rather incomplete at present and is restricted to single coordinates only. Accordingly, further work is required to lead to a complete description of road noise in vehicles.

CHAPTER TWO

GENERAL ASPECTS OF VIBRATION ISOLATION

A substantial body of theory is available concerning vibration isolation (see Appendix 2 for the bibliography). The purpose in this chapter is to summarise and interpret this theory and to present some generally applicable formulations and conclusions. The topic under consideration is the passive isolation of structure-borne vibration in the field where linear theory holds; examples of where this is not strictly valid being presented also.

2.1 SYSTEMS AND DIVISIONS

The vibration isolation problem is assumed to be present when, within a given system, vibrations are transmitted between parts of the system; and, for reasons indicated in the Introduction, the vibrations at the receiving parts of the system are required to be minimal within a given frequency range. The structural integrity, static and low frequency constraints on the system ensure that structural paths are available for the transmission of vibration. The usual thermodynamic concept of a system is usefully restricted when dealing with vibrations alone. Thus, vibrational energy dissipated into heat is considered lost from the vibration system, and need only be considered when heating effects are significant. Energy will then imply mechanical (vibrational) energy alone.

For the purpose of analysis, the vibration system may be divided into subsystems which are: structures associated with energy inputs, or sources, paths and receivers. The general system will be composed of any number of such subsystems.

The simplest of all the general systems leads to useful concepts and characterises the basic problems involved. This class consists of one source, one path, and one receiver. This is shown schematically in Figure 2.1.1.

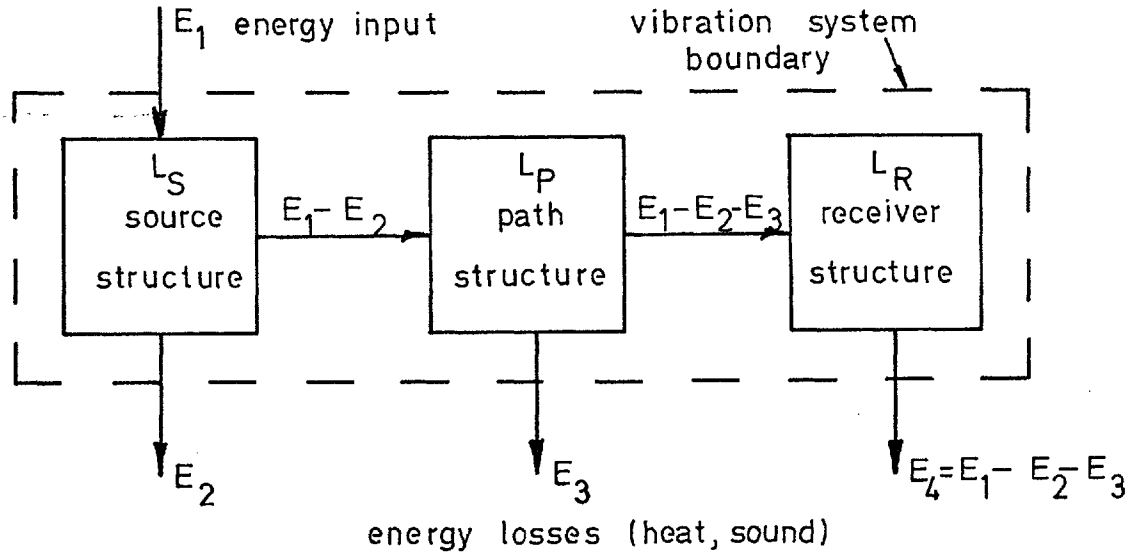


Figure 2.1.1

The system is assumed to exist in the steady state - time average quantities are implied. A primary source of vibrational energy gives a power inflow to the system E_1. Energy is lost from the system at the rates E_2 from the source structure, E_3 from the path and E_4 from the receiver. Kinetic energy levels L_S, L_P, L_R exist in the source, path and receiver. These kinetic energy levels may be normalised by dividing through by the subsystem masses, leading to

'mean specific' energy levels with units of mean square velocity, $\overline{v}^2$ - the mean implying a spatial average. Often, it will be more convenient to relate vibrational energy to the root mean square velocity, $\overline{V}$, or simplify further still to a reference velocity V^*, since for a linear system $\overline{V}$ will be directly related to V^*.

The theory of vibration isolation is concerned with determining the properties of the subsystems, so that given an energy source and certain constraints on the entire system, L_R is reduced to a minimum within a given frequency range. Note that this does not necessarily imply that the power flow into the receiver E_4 is also a minimum.

Before leading on to general formulations of how this is achieved, the system will be discussed in more detail and examples given.

2.2 SUBSYSTEMS

The division of the system into sources, paths and receivers is not unique. The intention of the analysis will readily identify the receiver structure, but the division between the source structure and path structure is often arbitrary and may be determined by analytical convenience alone. General features of these subsystems are shown below.

2.2.1 Sources

It is necessary to distinguish between the primary source of vibration and that part of the system that is associated with it - the source structure. Vibration isolation measures may be concerned with the properties of the source structure, but not with the primary source which is assumed invariable.

For the simplest class of systems, the source structure will have just one (frequency dependent) property - the source mobility M_S (or its reciprocal, impedance). The source structure may be shown as:

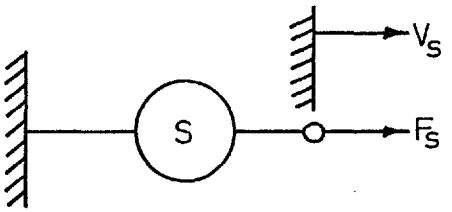


Figure 2.2.1

The source mobility is defined as the free velocity of the source, V_{sf}, divided by the blocked force F_{sb}, i.e:

$$M_s = \frac{V_{sf}}{F_{sb}} \qquad 2.2.1$$

For this one-terminal system is it valid to define the source impedance as the reciprocal of the mobility:

$$Z_s = \frac{F_{sb}}{V_{sf}} = \frac{1}{M_s} \qquad 2.2.2$$

This general linear (ideal) source may be represented as a pure velocity source or a pure force source applied to a subsystem giving the required mobility. This is indicated

below where (F) denotes a pure force source (i.e. force produced regardless of the velocity), and (V) denotes a pure velocity source (i.e. velocity produced regardless of force).

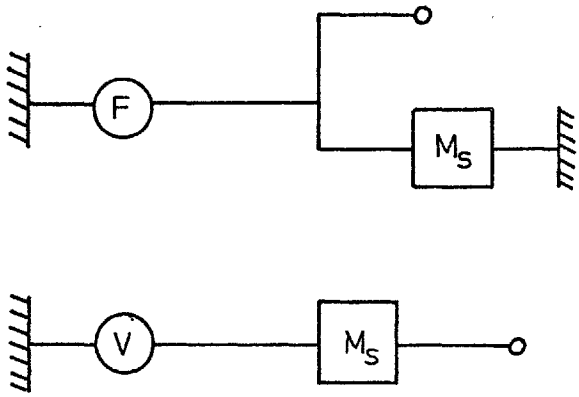


Figure 2.2.2

The source structure may or may not be readily identified as one of the equivalent systems shown.

The road input vibrations to a vehicle may be considered as an almost pure velocity source. The source structure may be taken as the tyre and wheel assembly. The unbalanced force in a machine may be taken as an almost pure force source, with the entire machine treated as the source structure. The acoustic excitation of a panel is an example of where no such primary ideal source is accessible.

Where the primary source is accessible, it is not necessary to measure V_{sf} and F_{sb} to determine the source mobility, but only to 'look into' the output terminal of the source, with the primary source removed - as familiar from electrical circuit theory.

The source structure is then treated as a two-terminal 'black box':

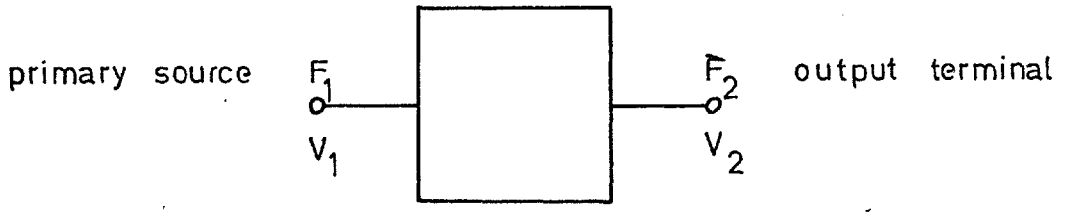


Figure 2.2.3

for which the following relationship holds (see § 3.2.1).

$$\begin{Bmatrix} F_1 \\ V_1 \end{Bmatrix} = \begin{bmatrix} \alpha_{11} & \alpha_{12} \\ \alpha_{21} & \alpha_{22} \end{bmatrix} \begin{Bmatrix} F_2 \\ V_2 \end{Bmatrix} \qquad 2.2.3$$

If the primary source is a velocity source, then

$$V_1 = \alpha_{21} F_2 + \alpha_{22} V_2$$

so that the blocked force is V_1/α_{21} and the free velocity if V_1/α_{22}. The source impedance is then:

$$Z_s = \frac{\alpha_{22}}{\alpha_{21}} \qquad 2.2.4$$

This is identical to measuring the source impedance on the output terminal, $Z_{22} = F_2/V_2$ when the velocity source is removed (i.e. $V_1 = 0$). The interrelationship is given in § 3.2.2.

If the primary source is a velocity source, then

$$F_1 = \alpha_{11} F_2 + \alpha_{12} V_2$$

so that the free velocity is F_1/α_{12} and the blocked force is F_1/α_{11}. The source mobility is then:

$$M_s = \frac{\alpha_{11}}{\alpha_{12}} \qquad 2.2.5$$

This is identical to measuring the source mobility on the output terminal, $M_{22} = V_2/F_2$ when the force source is removed (i.e. $F_1 = 0$).

Using the expression 2.2.2 the relationships are seen to lead to interchangeable results.

Ideal primary force and velocity sources are never encountered exactly in practice. Nevertheless, it seems appropriate to give examples of approximate forms of these which are used later in this work, and to show the inherent limitations.

The rotating unbalanced shaft provides an almost ideal force source, the force increasing with the square of the shaft speed, provided the ensuing accelerations are 'small'. The model is shown below in Figure 2.2.4. By symmetry vibrations are restricted to one dimension only.

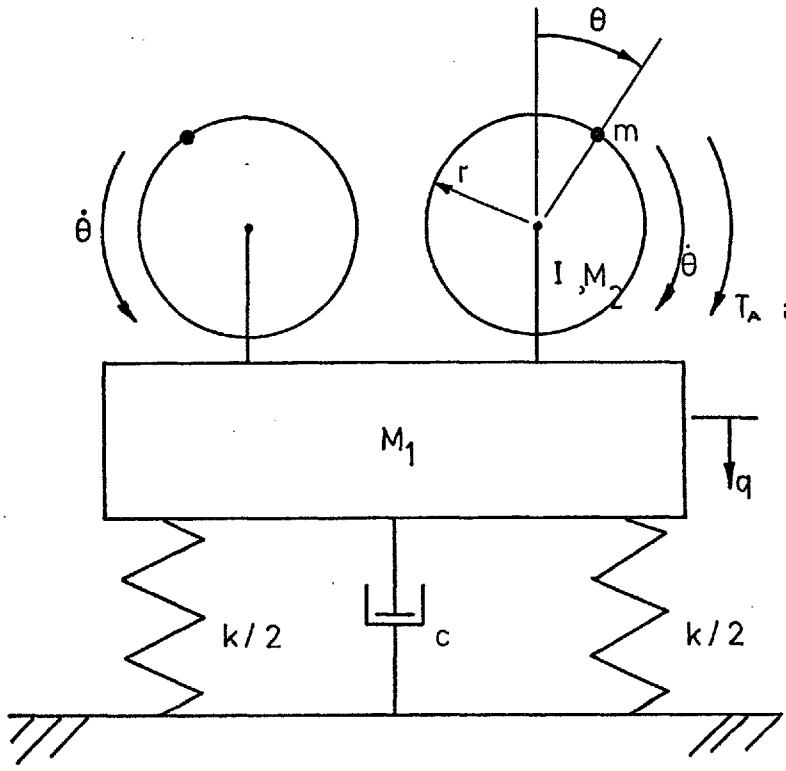


Figure 2.2.4

Two similar contra-rotating shafts of inertia I, mass M_2 with equal amounts of out-of-balance m rotate at speed $\dot{\theta}$. Torque T_n is applied to both shafts equally. The shafts are mounted on mass M_1 by frictionless bearings. The mass is supported on springs and its motion damped by a viscous dashpot. Ignoring gravitational effects, the equations of motion are:

$$M'\ddot{q} - 2mr\sin\theta\ddot{\theta} - 2mr\cos\theta\dot{\theta}^2 + c\dot{q} + kq = 0 \qquad 2.2.6$$

$$I'\ddot{\theta} - 2mr\sin\theta\ddot{q} = T_A \qquad 2.2.7$$

where

$$M' = M_1 + 2M_2 + 2m$$

$$I' = 2(I + mr^2)$$

If T_A = 0 or constant these equations are coupled and non-linear. The only linear case is when $\dot{\theta}$ is constant, say ω, when equation 2.2.6 reduces to the simple form:

$$M'\ddot{q} + c\dot{q} + kq = 2mr\omega^2\cos\omega t \qquad 2.2.8$$

This indicates harmonic forcing increasing with the square of the frequency. The effect on the torque, due to the coupling, is frequently ignored. If no damping is present, i.e. c = 0, equation 2.2.7 leads to:

$$T_A = \left(\frac{4m^2r^2\omega^4}{k - \omega^2 M'}\right)\sin 2\omega t \qquad 2.2.9$$

This shows that a fluctuating torque T_A must be supplied to keep the shaft speed constant, fluctuating at twice the shaft speed. This torque requirement increases as the fourth power of speed at low speeds, and at the square

of speed at high speeds. At the resonant frequency of the system, $\omega_n = \sqrt{k/M'}$, infinite torque fluctuations would be required to maintain the shaft speed constant. This is sketched below in Figure 2.2.5.

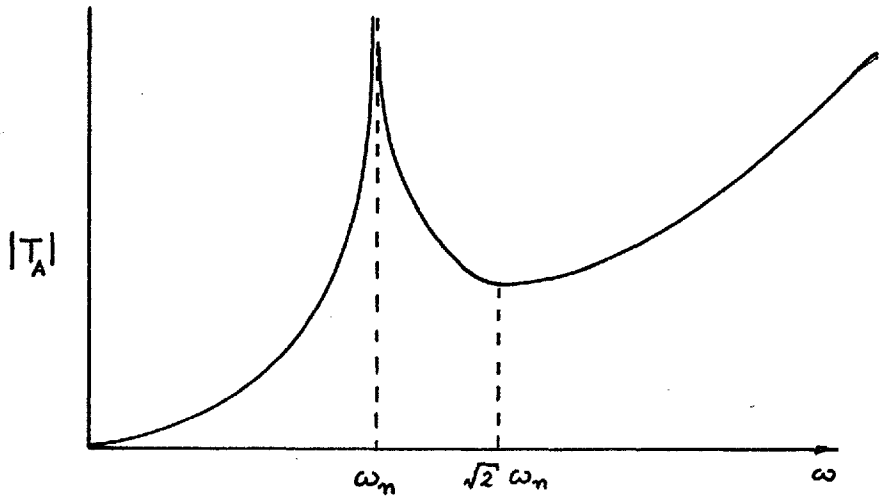


Figure 2.2.5

The minimum in the $|T_A|$ v ω curve is found by differentiating equation 2.2.9 and occurs at $\sqrt{2}\,\omega_n$.

When viscous damping is present, the expression for T_A becomes:

$$T_A = \left(\frac{4m^2r^2\omega^4}{k - \omega^2 M' + i\omega c} \right) \sin 2\omega t \qquad 2.2.10$$

The damping then limits the required torque fluctuations at resonance.

The shaft inertia, I, is usually sufficient to smooth out the torque fluctuations, but, because of the torque requirements near resonance, and at high shaft speeds, the full response curve is not always realised in the practical situation. Where the drive torque is limited, jump phenomena

are experienced (i.e. the Sommerfeld effect). Kononenko (149) describes the non-ideal case in more detail.

A simple model was constructed for confirmation of the effects predicted, of which the behaviour in the unstable region proved of interest. An electric motor with an out of balance rotor was mounted on a cantilever spring, with the rotor axis in the vertical plane.

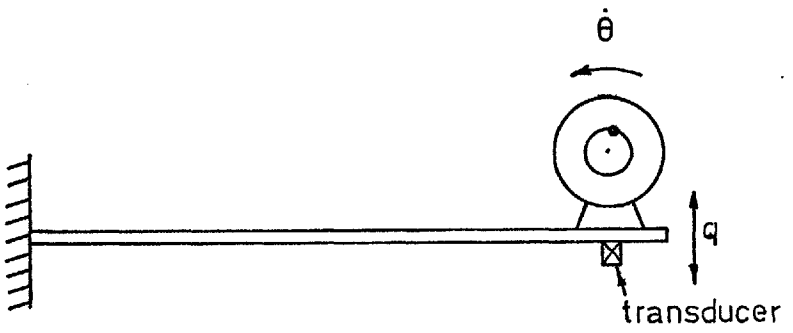


Figure 2.2.6

The response of the motor on the spring in the q-direction is sketched in Figure 2.2.7, showing the accessible regions (i.e. the stable regions).

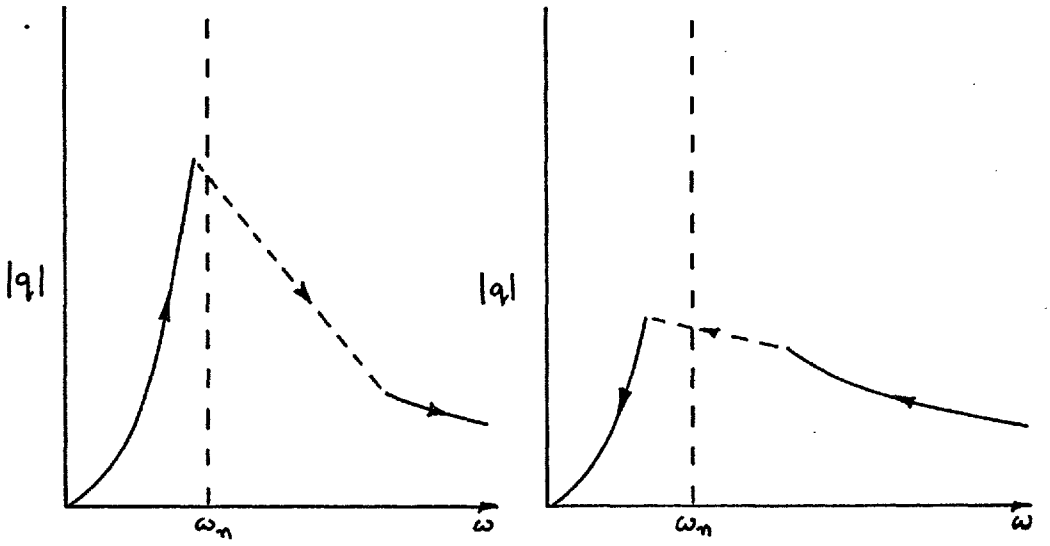


Figure 2.2.7

Starting the motor in the unstable region just above resonance leads to unstable beating between the motor speed, $\dot{\theta}$, and the vibratory displacement, q. This beating persists until one of the modes proves dominant. In one of the cases tested, the motor control was such that 72 beats occured before the vibratory mode finally stabilised the system and regulated the motor speed. The vibratory displacement for this case is shown in Figure 2.2.8.

This special form of non-linearity, due to the source being non-ideal, should be distinguished from the non-linear case where the passive elements are non-linear.

It has been shown that centrifugal forcing may be non-ideal when the ensuing accelerations become large, and this may limit the validity of the linear theory in some cases. It will now be shown that velocity sources are subject to much the same limitations.

The road may be thought of as an almost ideal velocity source to the vehicle travelling over it. This does not extend to tracked vehicles* where there is appreciable elasticity in the track. A highly idealised vehicle is shown in Figure 2.2.9, moving at constant speed along the road, and free to translate vertically. There is no friction between the vehicle and the road, and no loss of contact.

* i.e. steel wheel on steel rail

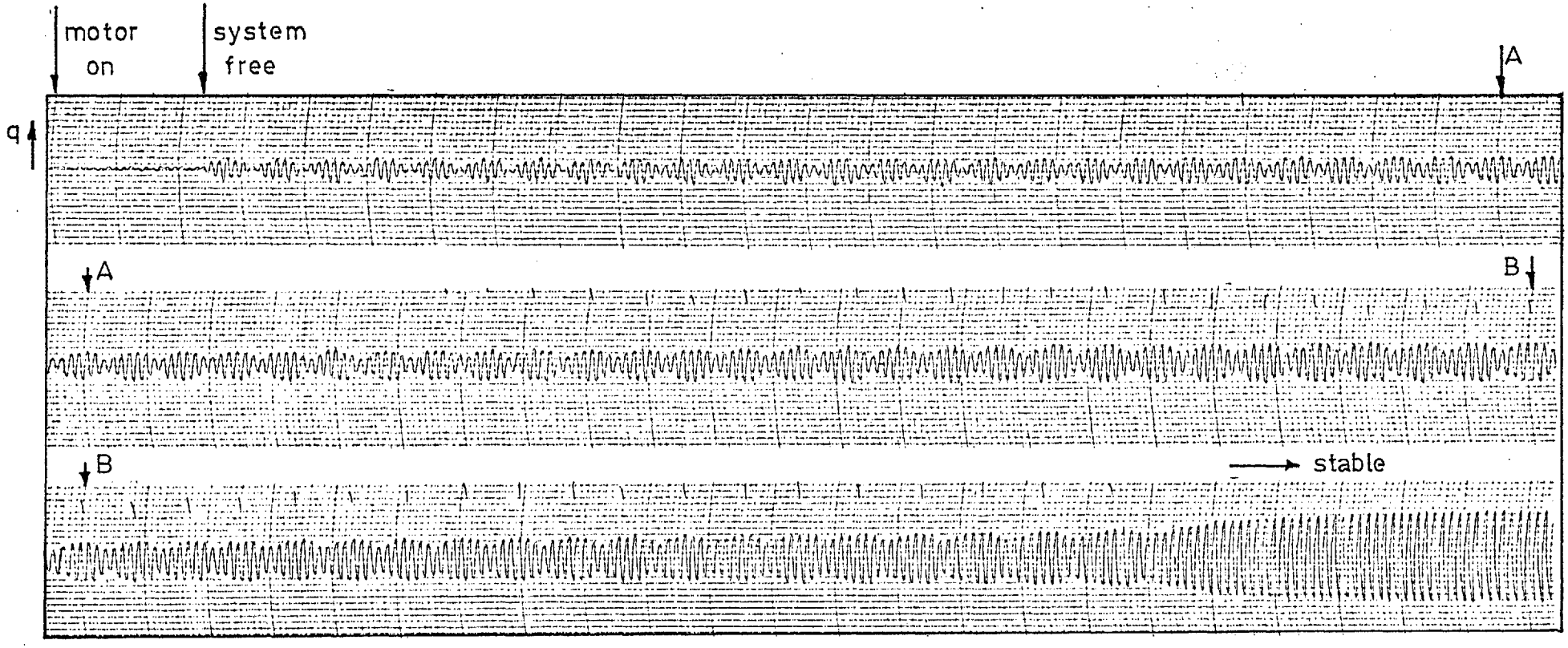


Figure 2.2.8

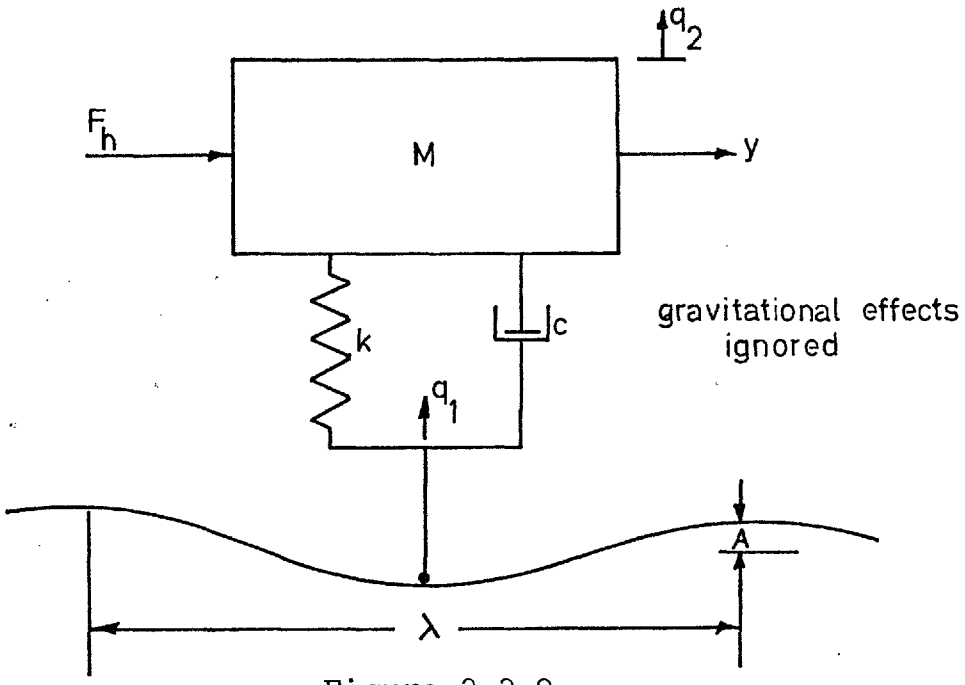


Figure 2.2.9

The road surface is taken as sinusoidal, with wavelength λ, and amplitude A. The vehicle speed is constant, $\dot{y}$, so that the velocity input to the system is $\dot{q}_1$, where

$$\dot{q}_1 = \left(\frac{2\pi\dot{y}}{\lambda}\right) A \sin\left(\frac{2\pi\dot{y}}{\lambda}.t\right) = A\omega \sin\omega t \qquad 2.2.11$$

A horizontal force is required to maintain $\dot{y}$ constant. This turns out to be:

$$F_h = \frac{1}{2}\left\{\frac{\omega^2 M\,(k+i\omega c)\,A}{k+i\omega c - \omega^2 M}\right\} \sin(2\omega t) \qquad 2.2.12$$

Similarly to the previous example, a fluctuating force at twice the vertical forcing frequency must be supplied to keep the vehicle speed constant. The amount of this force is sketched below in Figure 2.2.10. Note that damping leads to increased force requirements at high speeds.

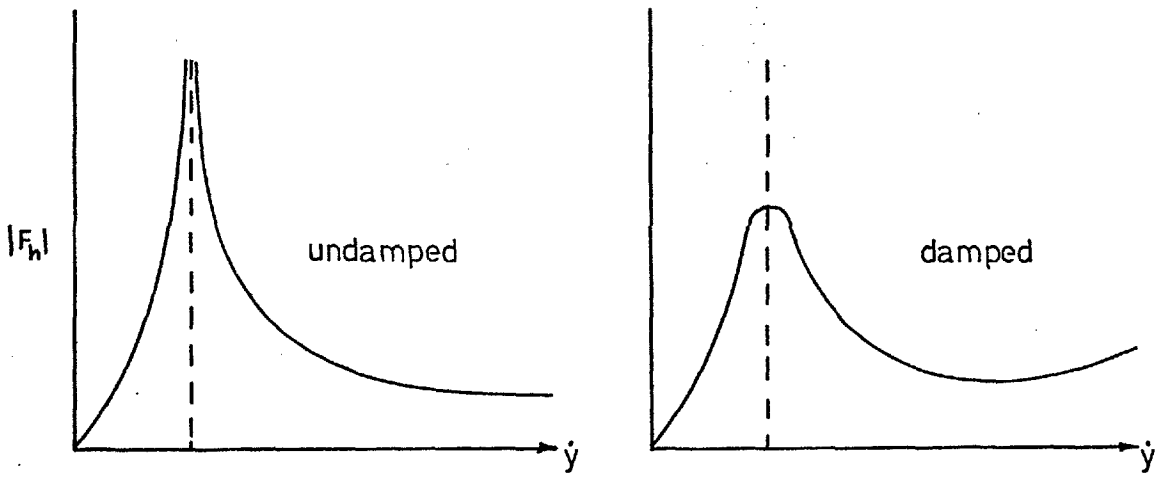


Figure 2.2.10

2.2.2 Paths

Paths provide a dual function in the vibration system. In the first place they provide the low-frequency and static constraints, and load carrying capacity, and in the second place transmit unwanted vibrations at other frequencies. An isolator refers to that part of the system which provides suitable filtering characteristics. The allocation of part of the system as a path is frequently arbitrary for the purpose of analysis.

In the one-path system being described, the properties of the path may be characterised by treating it as a 'black-box' and using immittance or transmission parameters. Generally three parameters will be required to specify its behaviour (for each frequency). The special case of the 'massless' path reduces the number of parameters to one.

The situation where isolation mounts have been preselected as paths for the analysis is discussed more fully

later in the chapter and in Chapter Four.

2.2.3 Receivers

The receivers consist of those parts of the system whose vibration is of interest. In this study they are taken as passive linear systems. In practical cases they may sometimes be taken as secondary sources, if the structure radiates sound, for example.

For a one path system, one parameter is required to characterise its behaviour, its mobility M_R (or the reciprocal, Z_R).

2.3 CLASSICAL MODELS

The 'classical' vibration isolation models lead to some useful conclusions but are limited in scope. Because they are so simple, they are widely used, sometimes inappropriately. The models are envisaged as rigid structures mounted on springs, on a rigid immoveable ground in one case, and to a moving base in the other (see Figure 2.3.1). Straight line motion only is permitted.

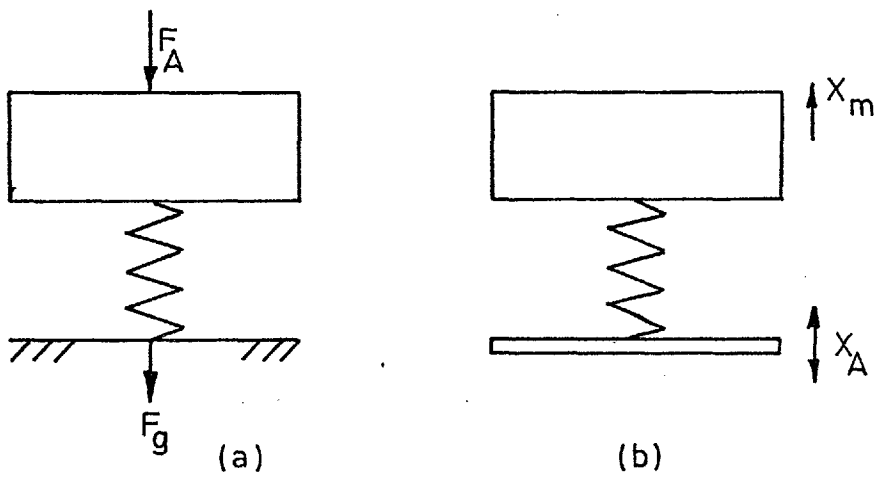


Figure 2.3.1

The transmission of vibrations is defined by force and motion transmissibility ratios. Case (a) is seen to be anomalous, since no energy can be transmitted to the base, and no motion results, so that the force to 'ground' can be of no significance. In practice, however, if the receiver impedance is very high the use of this type of model can lead to useful results.

Case (a) has been called active isolation, and case (b) passive isolation,[10] though this terminology serves to confuse the situation. Both cases are considered here as passive isolation situations, with the term active isolation reserved for the case where an additional energy input is used to effect isolation, as in servo-controlled systems.

The implicit assumptions for these models are:

1. In case (a), F_A is an ideal force source, $M \rightarrow \infty$
2. In case (b), X_A is an ideal velocity source, $M = 0$.

With these assumptions it is possible to define the transmissibilities in a similar fashion to that for effectiveness, defined in the next section. Thus, the force transmissibility T_f is defined by:

$$T_f = \frac{\text{force to ground}}{\text{Applied force}} = \frac{F_g}{F_A}$$

$$= \frac{\text{Force to ground with isolator}}{\text{Force to ground with massless rigid link in place of an isolator}}$$

and the motion transmissibility T_m is defined by

$$T_m = \frac{\text{Motion of receiver}}{\text{Motion of base}} = \frac{X_m}{X_A}$$

$$= \frac{\text{Motion of receiver with isolator}}{\text{Motion of receiver with massless rigid link in place of isolator}}$$

These ratios are in fact identical, leading to the main forms shown in Figure 2.3.2.

For the massless isolator, with complex stiffness $k(1 + i\eta)$, end mounted mass m, the transmissibility is given by

$$T = \frac{1 + i\eta\omega}{1 - a\Omega^2 + i\eta\omega}$$

where a is the stiffness ratio k_o/k_ω

k_o is the stiffness at the resonant frequency

k_ω is the stiffness at frequency ω

η_ω is the loss factor at frequency ω

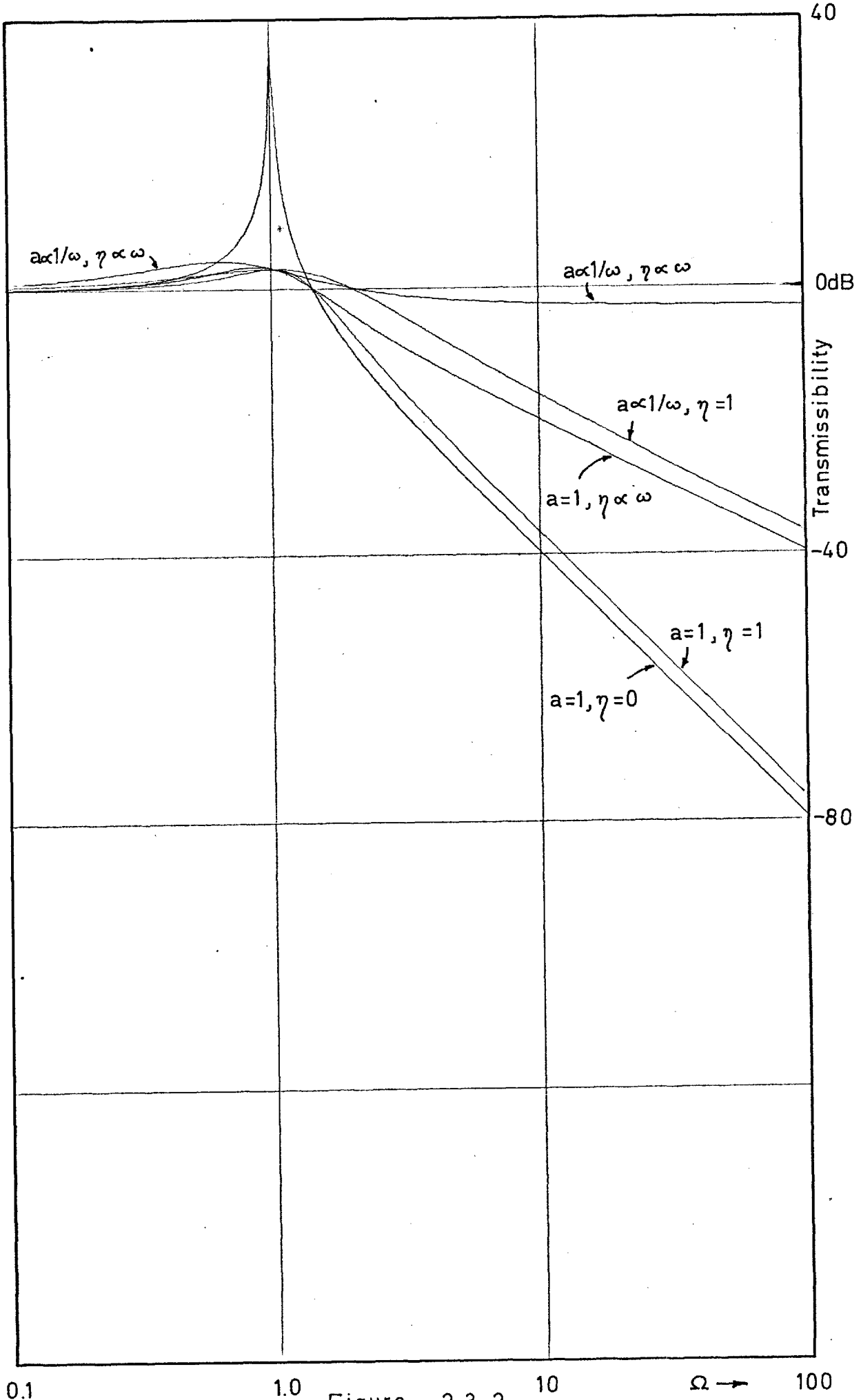
Ω is the frequency ratio ω/ω_n

ω_n is the undamped natural frequency $\sqrt{k_o/m}$

Principal cases include:

1. a = 1, η = 0: undamped spring giving infinite resonant peak and a final high frequency attenuation of 12 dB/octave.

2. a = 1, η = constant: damped spring with constant loss factor (approximated by natural rubber), giving a height



TRANSMISSIBILITY

Figure 2.3.2

of resonant peak $\sqrt{(1/\eta^2 + 1)} \approx 1/\eta$ when η is small. The final high frequency attenuation is again 12dB/octave but at a level $\sqrt{(1 + \eta^2)}$ above the $\eta = 0$ line.

3. a = 1, $\eta \propto \omega$ spring with viscous damping, giving height of peak similar to case 2 (small damping) but a final attenuation slope of 6dB/octave,

4. a $\propto 1/\omega$, η = constant: spring stiffening with frequency, but with constant loss factor (approximated by some high-damping rubbers), again reduces the final attenuation slope to 6dB/octave.

5. a $\propto 1/\omega$, $\eta \propto \omega$: final slope now reduced to 0dB octave.

Numerous other cases exist, referred to in Appendix 2 and in other sections in this work.

2.4 GENERAL FORMULATIONS

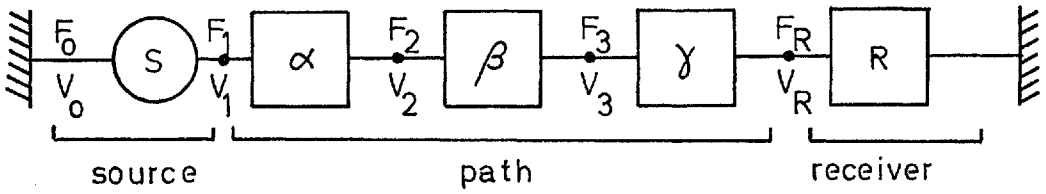
For the more general case where the source and receiver mobilities are arbitrary, some general formulations are available for the one-path system Multi-path systems can be treated to a certain extent by decoupling, or by a more complete analysis of the situation in hand.

This section shows expressions for the effectiveness of system changes in reducing the receiver velocity in the one-path system.

The definition of the path (or isolator) effectiveness E_p, in reducing the receiver velocity is:

$$E_p = \frac{\text{Receiver velocity when source and receiver joined by massless, rigid link}}{\text{Receiver velocity when source and receiver joined by isolator}}$$

Many cases of importance can be derived by treating the path as three systems, and producing certain cases which are nevertheless fairly general in application.



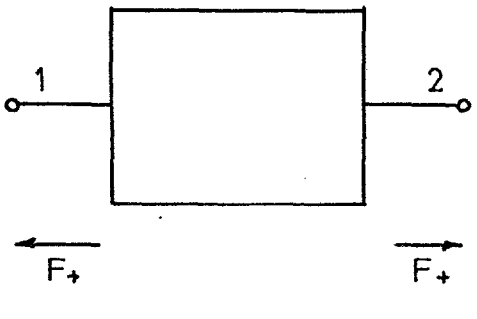
Using transfer matrices, the equation for the system may be formed:

$$\begin{Bmatrix} F_0 \\ V_0 \end{Bmatrix} = \begin{bmatrix} s_{11} & s_{12} \\ s_{21} & s_{22} \end{bmatrix} \begin{bmatrix} \alpha_{11} & \alpha_{12} \\ \alpha_{21} & \alpha_{22} \end{bmatrix} \begin{bmatrix} \beta_{11} & \beta_{12} \\ \beta_{21} & \beta_{22} \end{bmatrix} \begin{bmatrix} \gamma_{11} & \gamma_{12} \\ \gamma_{21} & \gamma_{22} \end{bmatrix} \begin{Bmatrix} F_R \\ V_R \end{Bmatrix}$$

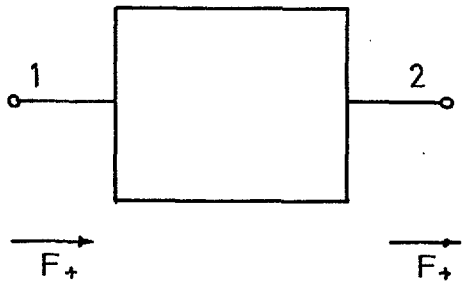
The transfer matrices are discussed more fully in the next chapter. The formulae given are presented in terms of impedance, Z, and mobility, M which must be specified by the boundary conditions and also related to the sign convention used. General relationships are given in the next chapter, but those used here are indicated below.

Sign Conventions

Transfer Matrix



Impedance or Mobility Matrix



For the transfer matrices, there are forward and rearward forms, one the inverse of the other. Note that the determinant of the matrix is unity.

$$\begin{Bmatrix} F_1 \\ V_1 \end{Bmatrix} = \begin{bmatrix} \alpha_{11} & \alpha_{12} \\ \alpha_{21} & \alpha_{22} \end{bmatrix} \begin{Bmatrix} F_2 \\ V_2 \end{Bmatrix}$$

Forward form

$$\begin{Bmatrix} F_2 \\ V_2 \end{Bmatrix} = \begin{bmatrix} \alpha_{22} & -\alpha_{12} \\ -\alpha_{21} & \alpha_{11} \end{bmatrix} \begin{Bmatrix} F_1 \\ V_1 \end{Bmatrix}$$

Rearward form

The definitions of impedance and mobilities are shown below. Note that by comparison with immittance matrices (see next chapter), some of these are 'pseudo' rather than 'true' values.

$$Z_{\alpha 1}^{b} = \frac{1}{M_{\alpha 1}^{b}} = \frac{F_1}{V_1}\bigg|_{V_2=0} = \frac{\alpha_{11}}{\alpha_{21}} \qquad Z_{\alpha 2}^{b} = \frac{1}{M_{\alpha 2}^{b}} = \frac{F_2}{V_2}\bigg|_{V_1=0} = \frac{\alpha_{22}}{\alpha_{21}}$$

$$Z_{\alpha 1}^{f} = \frac{1}{M_{\alpha 1}^{f}} = \frac{F_1}{V_1}\bigg|_{F_2=0} = \frac{\alpha_{12}}{\alpha_{22}} \qquad Z_{\alpha 2}^{f} = \frac{1}{M_{\alpha 2}^{f}} = \frac{F_2}{V_2}\bigg|_{F_1=0} = \frac{\alpha_{12}}{\alpha_{11}}$$

$$Z_{\alpha 12}^{b} = \frac{F_2}{V_1}\bigg|_{V_2=0} = \frac{1}{\alpha_{21}} = \sqrt{\left\{ Z_{\alpha 2}^{b} \left(Z_{\alpha 1}^{b} - Z_{\alpha 1}^{f} \right) \right\}}$$

$$\left(\text{since } \frac{1}{\alpha_{21}^{2}} = \frac{\alpha_{22}}{\alpha_{21}} \cdot \frac{\alpha_{11}\alpha_{22} - \alpha_{12}\alpha_{21}}{\alpha_{22}\alpha_{21}} \quad \& \quad (\alpha_{11}\alpha_{22} - \alpha_{12}\alpha_{21}) = 1 \right)$$

$$\left(\frac{1}{M_{\alpha 12}^{b}} \right)^{2} = \frac{1}{M_{\alpha 2}^{b}} \left(\frac{1}{M_{\alpha 1}^{b}} - \frac{1}{M_{\alpha 1}^{f}} \right)$$

The source mobility has been defined previously, and the receiver mobility is given by $M_R = V_R/F_R$, which does not have a superscript as it is a one coordinate system.

For a rigid mass,

$$Z_m = Z_1^f = Z_2^f = \alpha_{12} \quad , \quad M_1^b = M_2^b = 0$$

and for a massless spring, or isolator,

$$Z_I = Z_1^b = Z_2^b = \frac{1}{\alpha_{21}} \quad , \quad M_1^f = M_2^f = \infty$$

The table 2.4.1 shown effectiveness for a variety of systems, with their mobility diagrams. Massless isolators are denoted ∿∿, rigid masses by shaded boxes, and general systems by unshaded boxes. The first suffix is dropped from the impedance and mobility terms as no ambiguity exists. The formulae are given with both impedance and mobility to simplify appreciation of their significance.

The path or isolator effectiveness depends on the properties of the source and receiver, but only shows the effect of path modifications. The receiver response could be made smaller by alterations to the source and receiver, even though the path might become less effective.

Two other effectiveness ratios might be defined, bringing out the effects of receiver and source control.

Thus, the receiver effectiveness can be defined as

$$\Delta E_R = \frac{\text{receiver velocity with initial receiver mobility}}{\text{receiver velocity with new receiver mobility}}$$

$$= \frac{M_R^{(1)}}{M_R^{(2)}} \left(\frac{M_R^{(2)} + M_{SP}}{M_R^{(1)} + M_{SP}} \right) = \frac{Z_R^{(2)} + Z_{SP}}{Z_R^{(1)} + Z_{SP}}$$

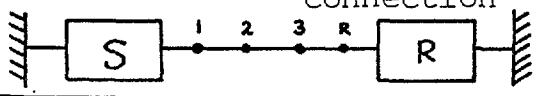
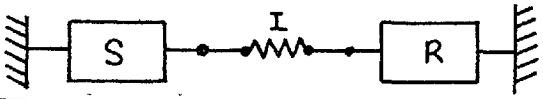
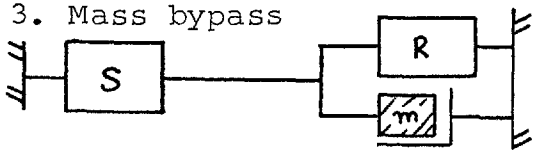
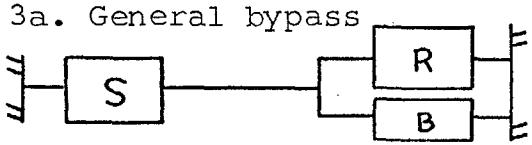
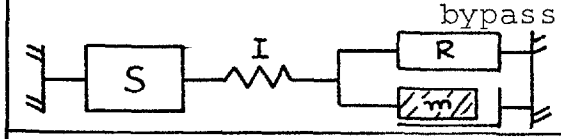
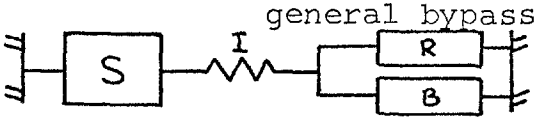
SYSTEM	EFFECTIVENESS (MOBILITY FORM)	EFFECTIVENESS (IMPEDANCE FORM)
1. Reference - direct connection 	$E_p^{(1)} = 1$	$E_p^{(1)} = 1$
2. Massless isolator 	$E_p^{(2)} = 1 + \frac{M_I}{M_S + M_R}$	$E_p^{(2)} = 1 + \frac{Z_S Z_R}{Z_I (Z_S + Z_R)}$
3. Mass bypass 	$E_p^{(3)} = 1 + \frac{M_S M_R}{M_m (M_S + M_R)}$	$E_p^{(3)} = 1 + \frac{Z_m}{Z_S + Z_R}$
3a. General bypass 	$E_p^{(3a)} = 1 + \frac{M_S M_R}{M_B (M_S + M_R)}$	$E_p^{(3a)} = 1 + \frac{Z_B}{Z_S + Z_R}$
4. Massless isolator and mass bypass 	$E_p^{(4)} = E^{(2)} + \frac{M_R}{M_m}\left(\frac{M_S + M_I}{M_S + M_R}\right)$	$E_p^{(4)} = E^{(2)} + \frac{Z_m}{Z_I}\left(\frac{Z_S + Z_I}{Z_S + Z_R}\right)$
4a. Massless isolator and general bypass 	$E_p^{(4a)} = E^{(2)} + \frac{M_R}{M_B}\left(\frac{M_S + M_I}{M_S + M_R}\right)$	$E_p^{(4a)} = E^{(2)} + \frac{Z_B}{Z_I}\left(\frac{Z_S + Z_I}{Z_S + Z_R}\right)$

Table 2.4.1a

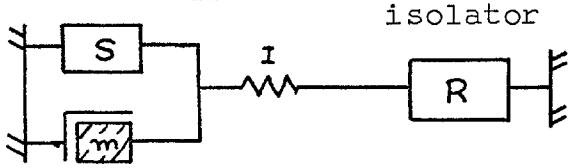
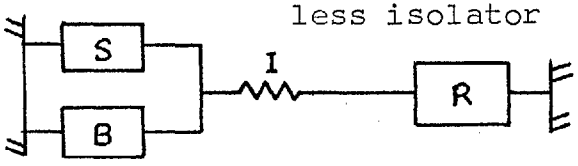
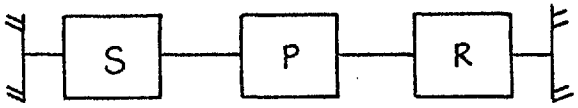
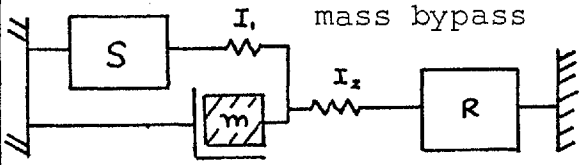
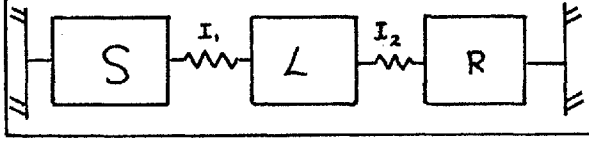
SYSTEM	EFFECTIVENESS (MOBILITY FORM)	EFFECTIVENESS (IMPEDANCE FORM)
5. Mass bypass and massless isolator 	$E_p^{(5)} = E^{(2)} + \frac{M_S}{M_m}\left(\frac{M_I + M_R}{M_S + M_R}\right)$	$E_p^{(5)} = E^{(2)} + \frac{Z_m}{Z_I}\left(\frac{Z_I + Z_R}{Z_S + Z_R}\right)$
5a General bypass and massless isolator 	$E_p^{(5a)} = E^{(2)} + \frac{M_S}{M_B}\left(\frac{M_I + M_R}{M_S + M_R}\right)$	$E_p^{(5a)} = E^{(2)} + \frac{Z_B}{Z_I}\left(\frac{Z_I + Z_R}{Z_S + Z_R}\right)$
6. General isolator 	$E_p^{(6)} = \left(\frac{M_{12}^b}{M_S + M_R}\right)\left[1 + \frac{M_S}{M_1^b} + \frac{M_R}{M_2^b}\left(1 + \frac{M_S}{M_1^f}\right)\right]$	$E_p^{(6)} = \frac{Z_R + Z_2^b + (Z_1^b/Z_S)(Z_R + Z_2^f)}{Z_{12}^b\,(Z_R/Z_S + 1)}$
7. Two stage isolator with mass bypass 	$E^{(2)}$ has $M_I = M_{I1} + M_{I2}$, and $r = \frac{M_{I1}}{M_I}$ $E_p^{(7)} = E^{(2)} + \frac{(M_{I1} + M_S)(M_{I2} + M_R)}{M_m\,(M_S + M_R)}$ opt. $r = \frac{1}{2}\left[1 + (M_R - M_S)/M_I\right]$	$E_p^{(7)} = E^{(2)} + \frac{Z_m\,(Z_S + Z_{I1})(Z_R + Z_{I2})}{Z_{I1}\,Z_{I2}\,(Z_R + Z_S)}$
8. Two stage isolator with general load 	$E^{(8)} = \left(\frac{M_{12}^b}{M_S + M_R}\right) \times \left[1 + \frac{(M_S + M_{I1})}{M_1^b} + \frac{(M_R + M_{I2})}{M_2^b}\left(1 + \frac{(M_{I1} + M_S)}{M_1^f}\right)\right]$	$E_p^{(8)} = \frac{\left\{Z_R Z_{I2}\left[Z_1^b (Z_{I1} + Z_S) + Z_S Z_{I1}\right] + Z_2^b\left[Z_1^f (Z_S + Z_{I1})(Z_R + Z_{I2}) + Z_S Z_{I1}\,(Z_R + Z_{I2})\right]\right\}}{Z_{I1} Z_{I2} Z_{12}^b\,(Z_S + Z_R)}$

Table 2.4.1b

Where Δ is used to indicate the change from an arbitrary receiver mobility, and $Z_{sp} = 1/M_{sp}$ is the source-path impedance, obtained by treating the source and path together as a source.

When $Z_{sp} << Z_R$, when good isolation is already achieved, doubling the receiver impedance will halve the receiver velocity, but if $Z_{sp} \approx Z_R$, little effect can be obtained from modifying the receiver impedance.

Similarly, the source effectiveness can be defined by

$$\Delta E_s = \frac{\text{receiver velocity with initial source mobility}}{\text{receiver velocity with new source mobility}}$$

$$= \frac{M_s^{(1)}}{M_s^{(2)}}\left(\frac{M_s^{(2)} + M_{pR}}{M_s^{(1)} + M_{pR}}\right) = \frac{Z_s^{(2)} + Z_{pR}}{Z_s^{(1)} + Z_{pR}}$$

where $Z_{pr} = 1/M_{pr}$ is the path-receiver impedance, obtained by treating the path and receiver together as the receiver.

The total effectiveness is given by the improvement obtained by altering the source, path, and receiver. Note, however, that this is not the product of the three separate effectiveness ratios, since an improvement in one effectivedess ratio alters the effectiveness of the other ratios.

For example, for a massless isolator employed, with initial source impedance $Z_s^{(1)}$, final $Z_s^{(2)}$ and initial receiver impedance $Z_R^{(1)}$, final $Z_R^{(2)}$, the overall effectiveness is:

$$E_o = \frac{Z_s^{(1)} Z_R^{(2)} (1/Z_s^{(2)} + 1/Z_I) + Z_s^{(1)}}{Z_R^{(1)} + Z_s^{(1)}}$$

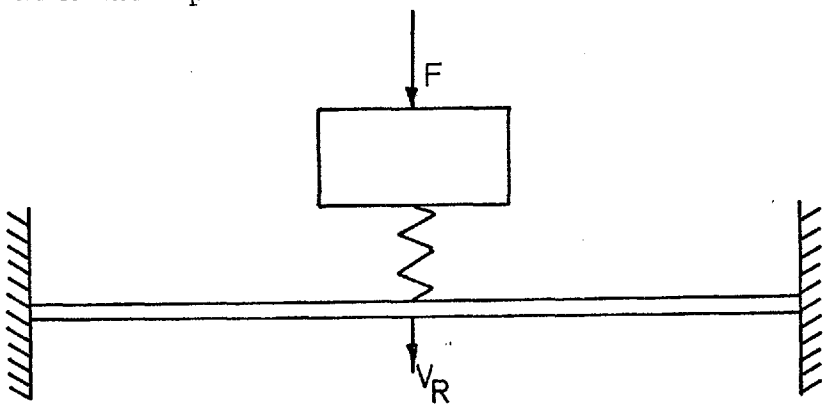
This can be seen to reduce to E_p if $Z_R = Z_R^{(1)} = Z_R^{(2)}$ and $Z_s = Z_s^{(1)} = Z_S^{(2)}$

2.5 QUALITATIVE DESCRIPTION - FREQUENCY RESPONSE

The general formulations given in the previous section do not show the whole picture, since they indicate the effectiveness of system changes only at a given frequency. The overall performance of any measure taken must therefore be obtained by calculating the effectiveness over a complete frequency range.

A description of a simple vibration isolation system is given here, with a graphical approach to the solution which can lead to accurate results for an undamped system.

The system considered is a rigid mass, acted upon by a pure force primary source, mounted with a massless spring on a flexible panel.



The effectiveness of the spring is required, which, from the previous section is known to be:

$$E_p = 1 + \frac{M_I}{M_S + M_R}$$

The source and receiver mobilities are shown in Figure 2.5.1, where the black lines indicate masslike mobilities and the red lines indicate spring-like mobilities. The combined mobility, $M_{RS} = M_R + M_S$ is shown dotted. This

is obtained by addition on the Bode diagram, using the addition Table 2.5.1 below to give guide points.

To derive the effectiveness, it is then necessary to evaluate:

$$E_p = 1 + \frac{M_I}{M_{RS}}$$

This can again be readily derived on the Bode diagram but with an extended addition table used to give the effectiveness. This is given in Table 2.5.2.

The mobility M_{RS} is shown as a full line in the lower half of Figure 2.5.1, and together with the mobility of the isolator. The curve of effectiveness is shown dotted, with the dark shaded areas indicating a reduction of the panel velocity due to the spring, and the red shaded areas showing where the spring amplifies the response. Over the whole frequency range it is seen that the spring, on average, is effective in reducing the panel velocity. From the Table 2.5.2 it is apparent that certain points on the curve can quickly be established to indicate the trend of the curve.

The frequencies A, B, C and D illustrate the type of behaviour the spring introduces, and the corresponding equivalent systems are shown below:

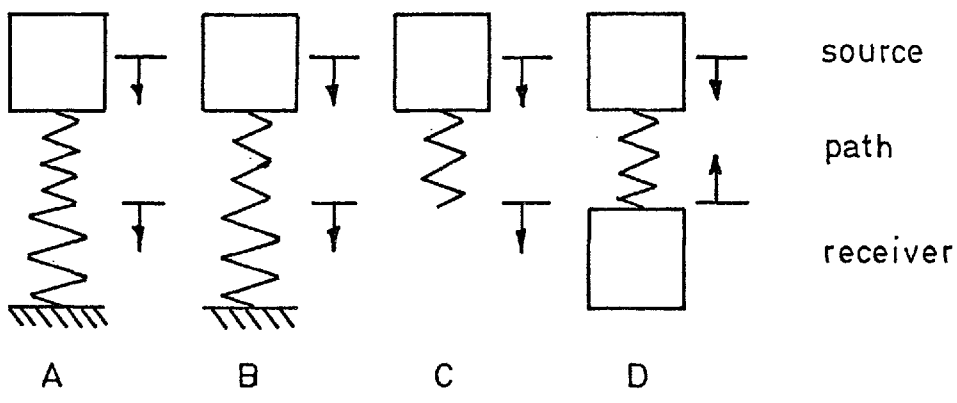
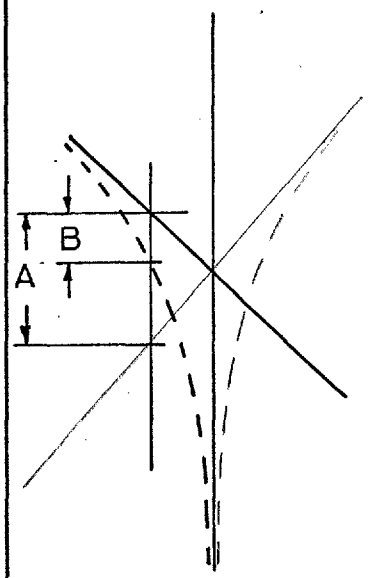
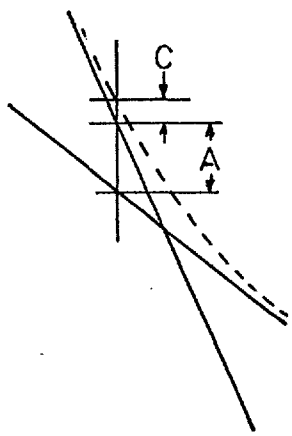
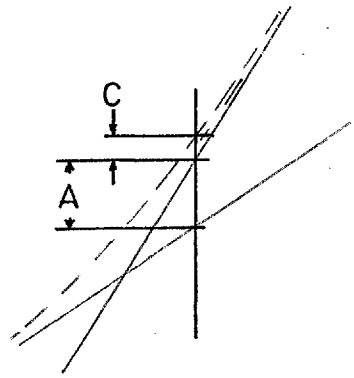


TABLE 2.5.1

ADDITION OF MOBILITIES



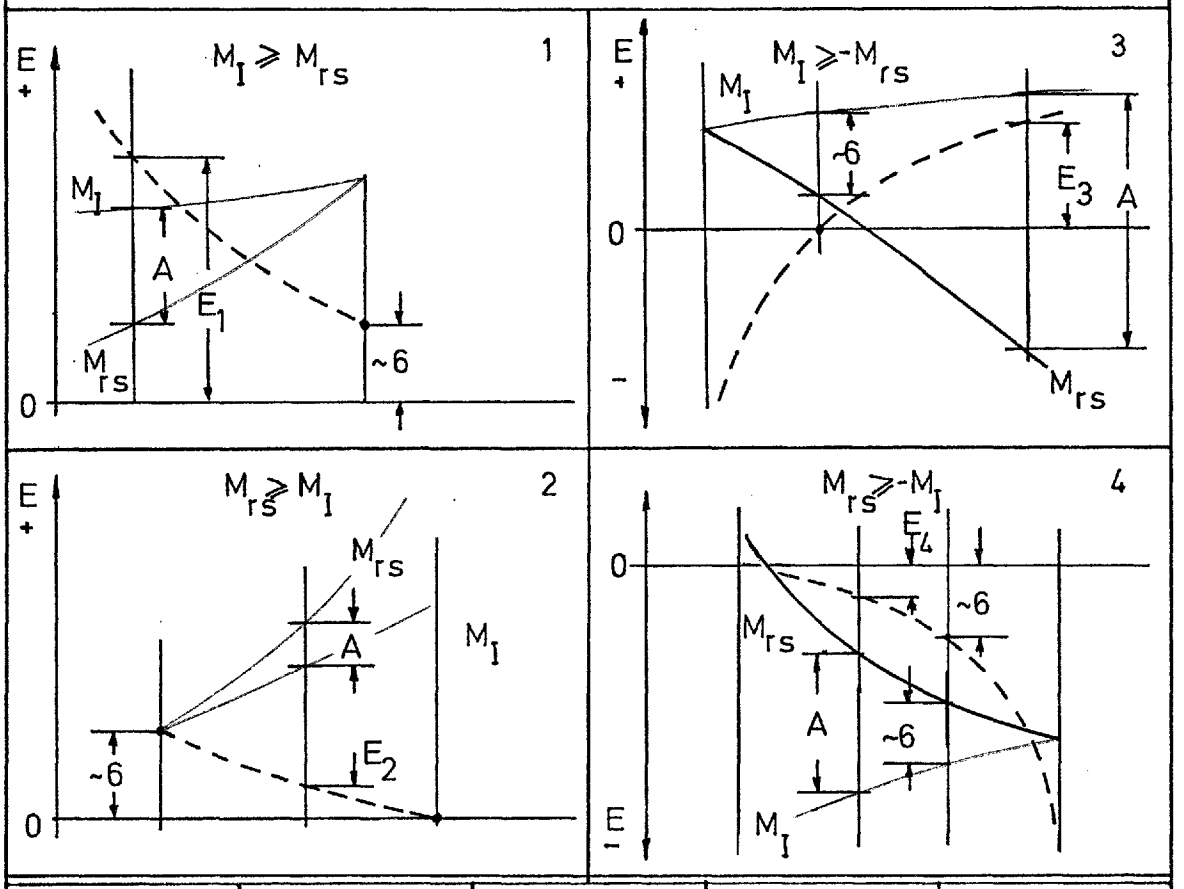




A dB	B dB	C dB
∞	0	0
n >> 30	≈ 0	≈ 0
30	.28	.27
20	.92	.83
10	3.30	2.38
6	6.02	3.52
3	10.72	4.66
2	13.72	5.08
1	19.42	5.54
.5	24.94	5.77
0	∞	6.02

TABLE 2.5.2

EFFECTIVENESS DERIVATION



A db	Effectiveness for each case shown above E_1 dB	E_2 dB	E_3 dB	E_4 dB
∞	∞	0	∞	0
n >> 30	≈ n	≈ 0	≈ n	≈ 0
30	30.27	.27	29.72	-.28
20	20.83	.83	19.08	-.916
10	12.39	3.53	6.70	- 3.30
6	9.53	2.38	-.04	- 6.02
3	7.65	3.52	- 7.68	- 10.72
2	7.08	4.66	- 11.73	- 13.72
1	6.53	5.08	- 19.04	- 19.42
.5	6.27	5.54	- 24.58	- 24.94
0	6.02	6.02	- ∞	- ∞

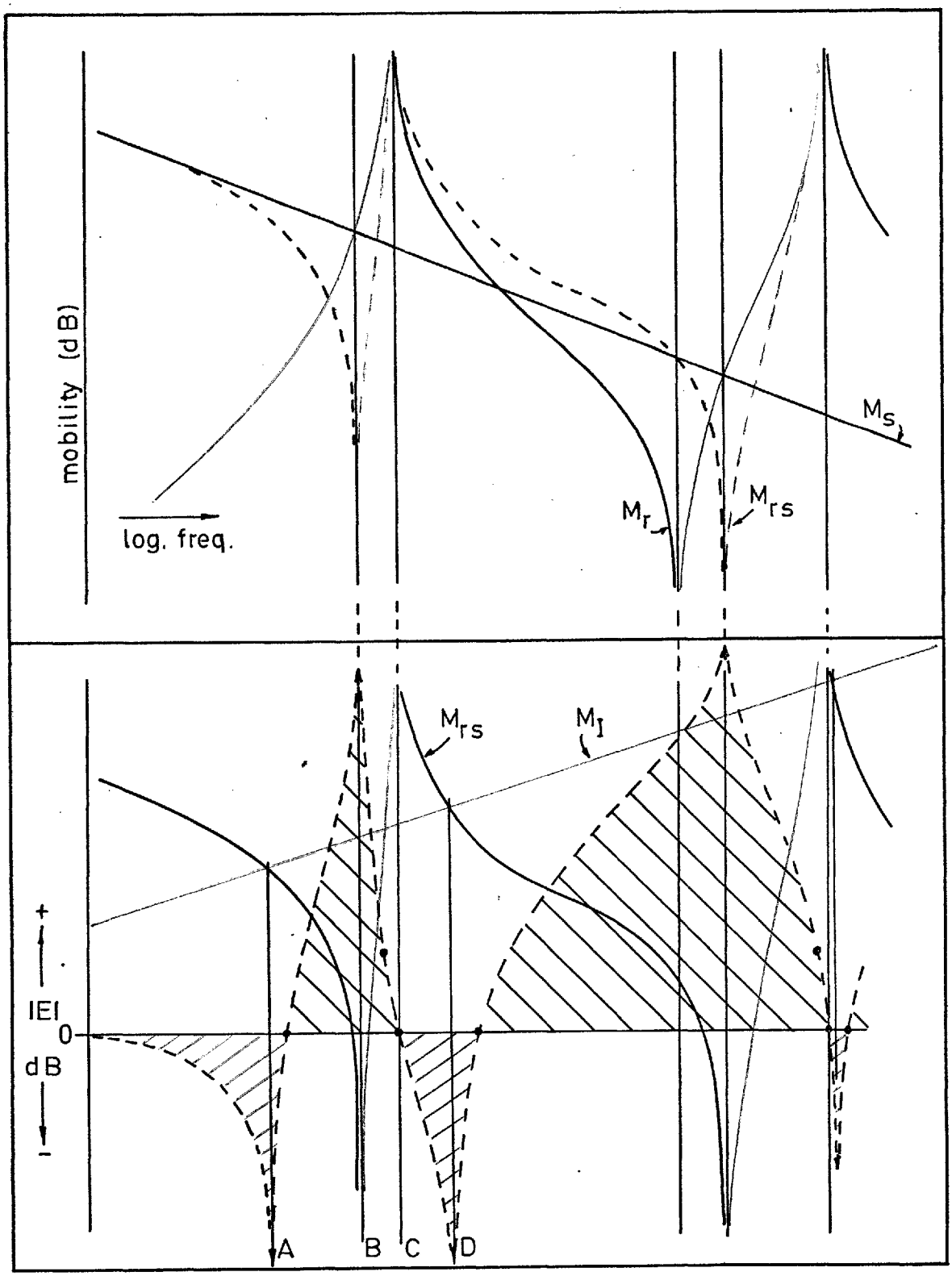


Figure 2.5.1

A. The receiver appears springlike, and the total stiffness is such that resonance occurs. This would not occur without the isolator spring so the effectiveness is zero.

B. The receiver is still springlike, but the system is past the resonant frequency. If the path was replaced by a rigid link, the system would be resonant. Thus the effectiveness is infinite. The effect of the path in A and B is then basically one of shifting the resonant frequencies.

C. At the receiver's resonant frequency, its impedance becomes zero. The isolator cannot be effective - the mounted mass and receiver move together with the same amplitude as the mass would alone in free space.

D. The receiver is masslike, introducing a further resonance into the system.

2.6 ROLE OF DAMPING

The previous section brought out the frequency dependence of isolator effectiveness, but without damping. In this section another graphical description is given to outline the role of damping in simple cases. For more complex systems a more elaborate approach is required.

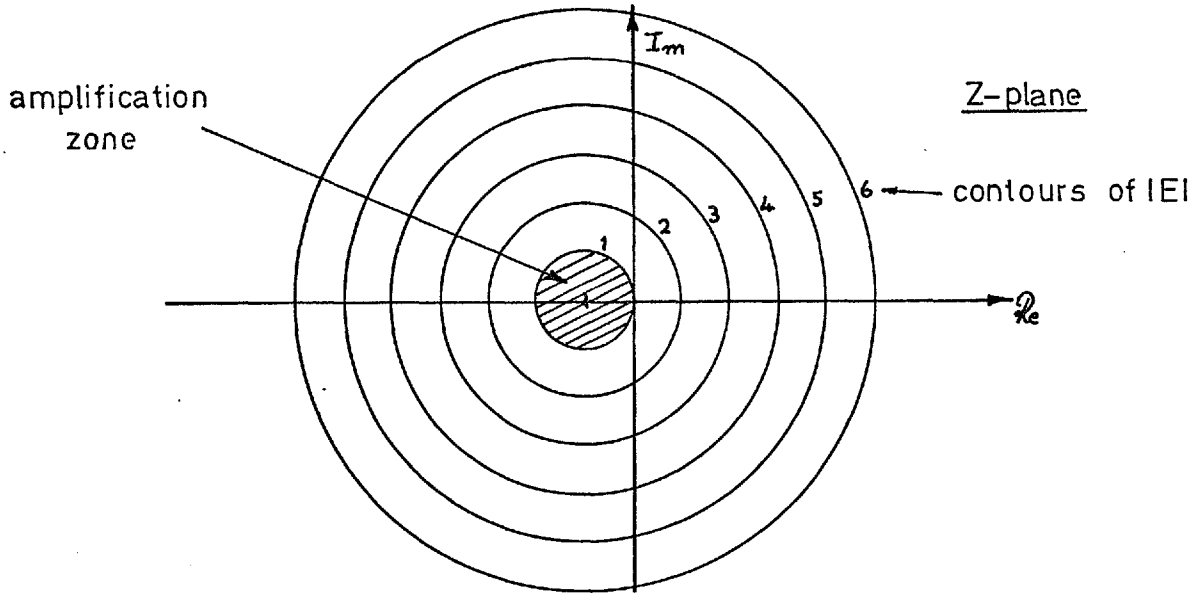
The system described is again that where a massless isolator is used between the source and receiver. Thus we have:

$$E = 1 + \frac{M_I}{M_R + M_S}$$

Using the substitution $Z = M_I/(M_R + M_S)$, and defining the region where the 'isolator' acts as an amplifier, we have a circle on the Z-plane given by:

$$|\geq |E| = |1+Z|$$

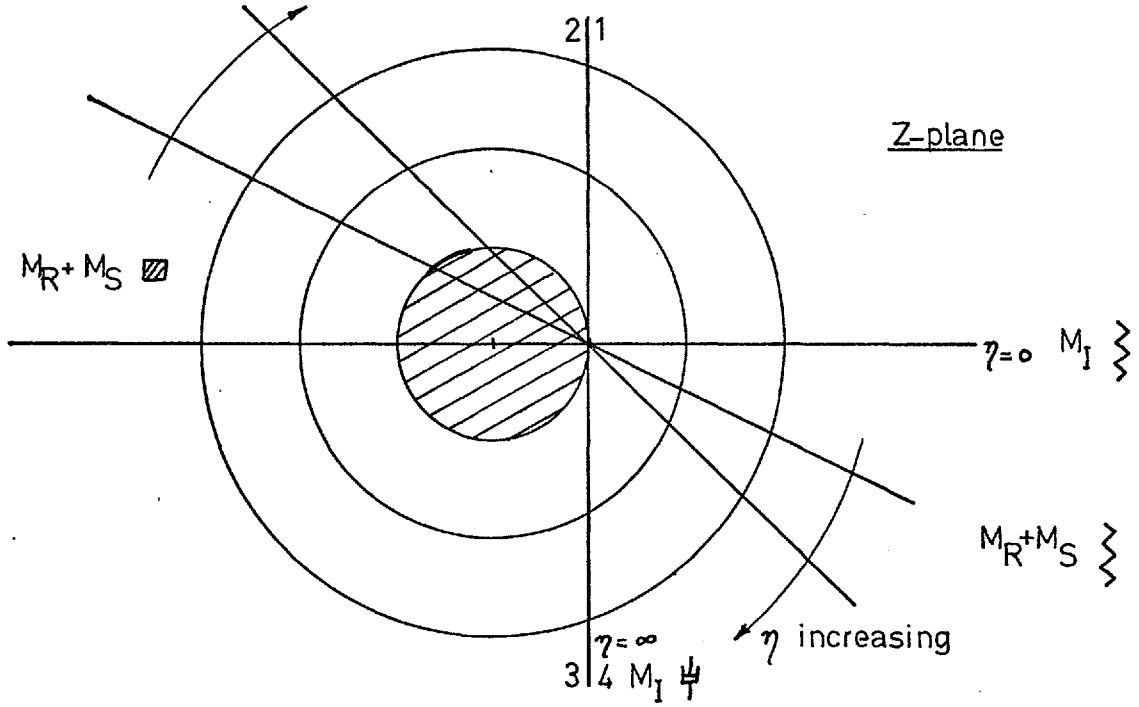
The circle has radius unity, centre (- 1, 0). Defining regions for other values of /E/ shows that the surface of /E/ on the Z-plane is an inverted cone. The isolator is most effective furthest away from the centre of the cone, and gives infinite amplification at (- 1, 0).



Three cases can be distinguished:

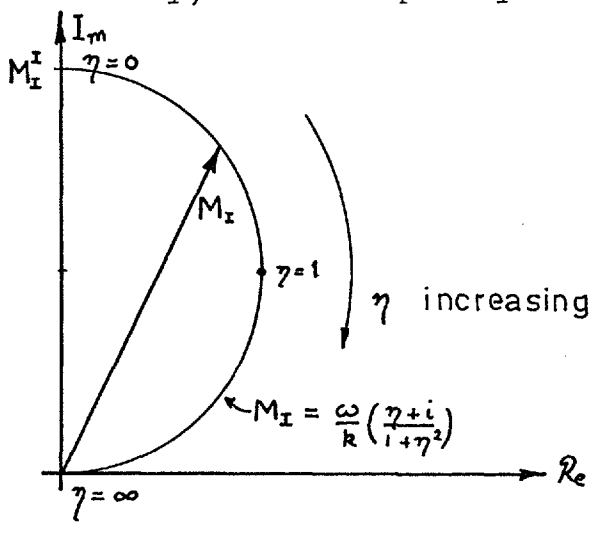
1. Source and receiver undamped, isolator damped or undamped.
2. Source and receiver damped, isolator undamped.
3. Source, receiver, and isolator damped.

In the first case, lines of constant damping for the isolator can be drawn on the Z-plane, and E is constrained to lie along these lines, which are restricted to quadrants 2 and 4.

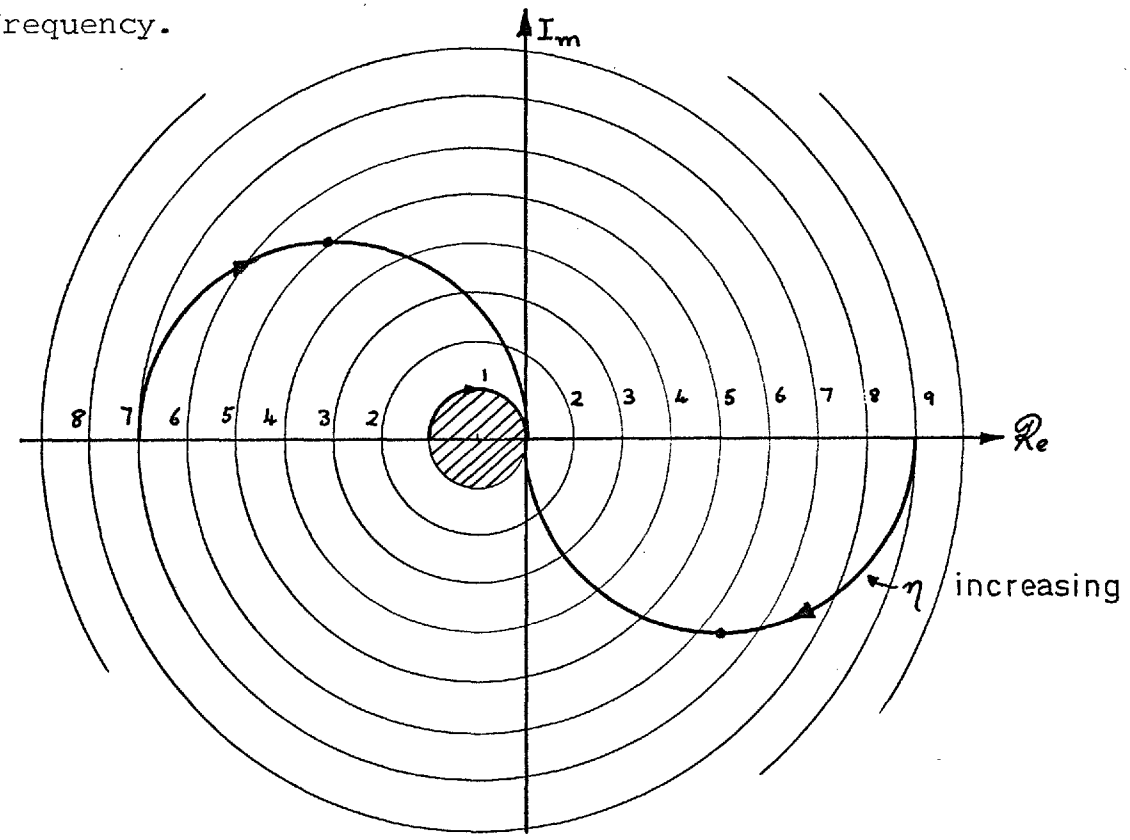


The symbol ∿∿ is used to denote springlike mobilities, and ▨ masslike mobilities. When $\eta = 0$, E lies on the real axis, and thus infinite amplification is possible. The only isolator which cannot give any amplification is a pure dashpot ⏚ , or when $\eta = \infty$. Amplification is only possible when $M_R + M_S$ is masslike, and increasing damping of the isolator reduces the cut of the amplification circle.

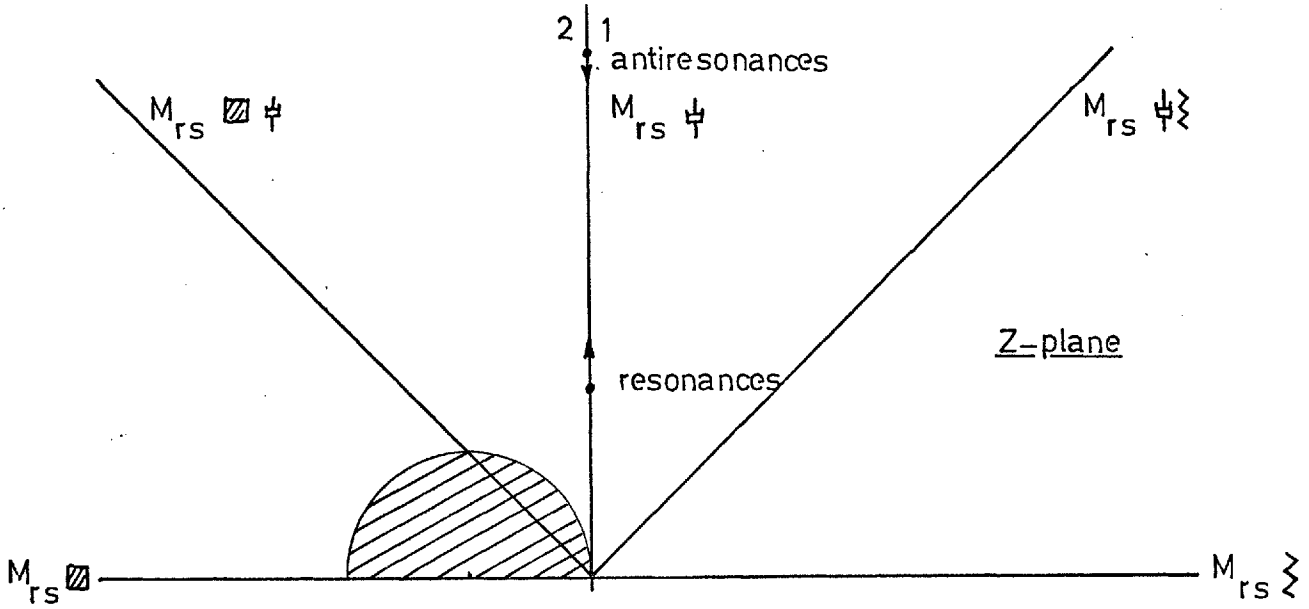
Damping will generally reduce the effectiveness when /E/>1, due to the decrease in the mobility of the isolator. If an isolator of fixed stiffness at a fixed frequency has damping added, then it can be shown that the trajectory of of the isolator's mobility on the complex plane is a semicircle, centre (0, $M_I^I/2$), radius $M_I^I/2$, where M_I^I is the undamped isolator mobility, which is purely imaginary.



The reduction in effectiveness due to damping of the isolator can then be readily obtained by constructing the semicircle on the Z-plane. The figure below shows that for a given isolator mobility, with no damping, /E/ = 7 for $M_R + M_S$ masslike, and 9 for $M_R + M_S$ springlike. Increasing the damping to a loss factor $\eta = 1$ reduces E to 5 and $6\frac{1}{2}$ respectively. Note that when /E/ = 1, there is no change with loss factor. The analogy of this with the transmissibility case is the fixed-point at $\sqrt{2}$ times the resonant frequency.



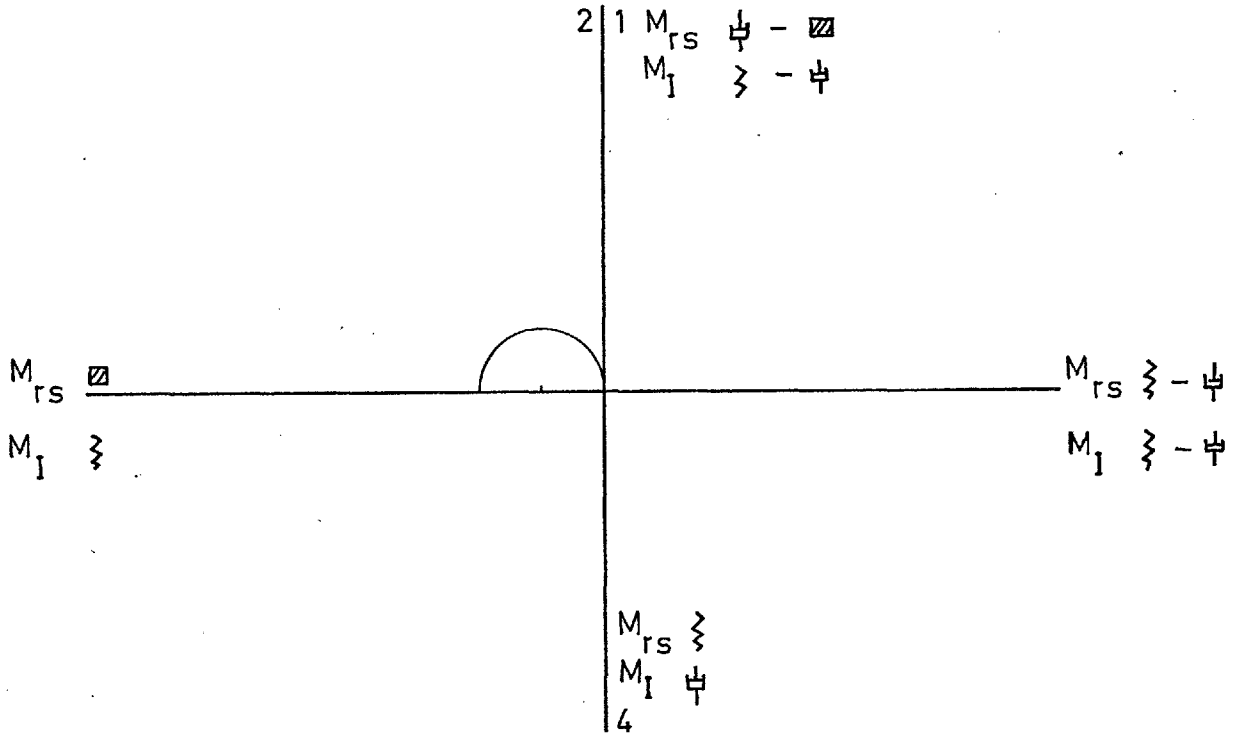
In the second case, when the source and receiver are damped, but the isolator is undamped, then E is restricted to quadrants 1 and 2 as shown below.



Here it can be seen that damping can be beneficial when M_{RS} has a masslike component and amplification can occur. The role of damping in this case is more complex. When M_{RS} is resonant, then, with well spaced modes, M_{RS} is dashpot-like. Increasing the damping increases the effectiveness of the isolator. When M_{RS} is anti-resonant, M_{RS} is again dashpot-like, but increase in the damping of the modes increases the mobility and thus reduces the effectiveness of the isolator.

For the resonant frequencies both the source and receiver must be damped for an increase in effectiveness. The role of damping in this case is one of smoothing out the response of the system.

In the last case, when the isolator is damped as well as the receiver, E is restricted to quadrants 1, 2 and 4. This is shown below with the limiting cases.



2.7 SUMMARY

Elementary aspects of vibration isolation have been discussed by treating a one-path system in detail and giving formulae for the effectiveness of system changes in reducing the receiver velocity. Additional interpretation has been given to the meaning of path effectiveness for the simple case of a massless isolator, but the more complex cases of isolators with appreciable mass have not been discussed.

Multipath systems are amenable to similar analysis but the simple generalisations such as given here are not available, and interpretation is more difficult. Aspects of multipath systems are discussed in later chapters.

CHAPTER THREE

ANALYTICAL AND EXPERIMENTAL METHODS

This chapter deals with the analytical methods used in the study of the dynamic models which are described in the other chapters of this work. The analytical methods are shown in relation to experimental methods that are used to determine or verify the dynamic models. This chapter is divided into six main sections which are summarised below.

The first section outlines the way in which the real system is described by a set of equations, and goes on to enounce the methods for solving the equations. The solution is then extended to the production of the mobility matrix for the system.

Mobility matrices, and related types of system matrices are described in the second section. The relationships between the types of matrices are shown, and the experimental methods required to determine such matrices are outlined, together with some practical details. The question is raised as to which type of matrix is preferable.

A modal equivalent system, based on a series solution for the dynamic model, enables a simplification in the system description to be made, and further enables a simplified experimental procedure to be carried out. This is described in the third section, together with experimental verification provided for some of the predictions arising from such a model.

The fourth section surveys certain aspects of random vibration and the application of statistical energy methods to the topics in hand. Following that, the basic techniques used in optimizing the models are described, and the chapter closes with a list of the more important computer programmes written for the methods dealt with.

3.1 Analysis and Solution of Lumped Parameter Models

In this section the basic mathematical methods used in establishing and solving the equations of motion for lumped parameter models are outlined. The validity of the solutions obtained depend on the following points being true or sufficiently accurate for the purpose of study.

1. The Fundamental Assumptions

Certain fundamental assumptions must be made and generally, the simpler the model, the greater the number of assumptions required. For the models described in later chapters, the following points are assumed:

a) The systems may be described in terms of lumped parameters, that is rigid masses and massless springs, viscous dashpots and hysteretic dampers. This enables the equations of motion to be written in ordinary differential form.

b) The parameters in the system can be specified exactly. In practice each parameter in the system is not, in general, known precisely, and within a set of similar systems each parameter may vary within the set by certain amounts in a random manner. Statistical methods are required to indicate

system performance variations when each parameter may vary at random (126).

c) The lumped parameters in the system are linear. Furthermore, the geometry of the system is such as to lead to linear equations for sufficiently small oscillations. Systems which are inherently non-linear, even for vanishingly small oscillations, are avoided.

Quasi-linear systems may be included with the linear systems as the solution by means of the method described in 3.1.3, page 56 can still follow on the same pattern. Thus springs (such as representing rubber bushes) may be allowed to have a variation of stiffness and loss-factor with frequency, but not with amplitude. For a rubber spring this is admittedly a rather gross assumption; for a complete description, however, other factors such as temperature and strain history must be included.

Linearity is assumed in order to make the mathematics more tractable. In the acoustic range of frequencies of interest, the assumption is probably fair. In the low-frequency, large deflection region, the assumption will not be so good.

2. The Equations

The equations of motion may be derived for a specific case once the assumptions have been made. These equations then form the mathematical model. Certain checks are necessary to ensure that the equations do represent the intended system, especially when the equations are of considerable complexity.

These checks are mainly specific, but some general methods are used.

3. The Numerical Solution

In the arithmetic operations required in solving the equations of motion, rounding errors cause an overall loss of precision in the solution. Prediction of these errors is difficult, owing to the number of operations performed and to variations in errors with different input parameters. Certain sets of equations may be very ill-conditioned.

In the computer programme, the solutions derived may be checked for accuracy by means of back calculation. The solutions so derived are then accurate to at least six significant figures, which is more than sufficient.

It can be seen that when the above points have been satisfied, the solution is correct for the model. To ensure that the model corresponds to the physical reality considered, experimental work is necessary which provides a test of the basic assumptions.

The techniques for the solution of the system equations are now introduced. Some system equations may be capable of reduction to classical normal modes. It can be shown that a necessary and sufficient condition that a damped system possesses classical normal modes is that the damping matrix may be diagonalised by the same transformation which uncouples the undamped system (127). This is an extension of the condition Rayleigh(166) put forward, that the damping matrix

must be a linear combination of the stiffness and inertia matrices. Many systems do not, however, comply with these conditions. With these, if a modal solution is required, it is necessary to convert the n 2nd order differential equations into 2n 1st order differential equations in state vector form (135, 136, 163) as described in § 3.1.4, page 57. This form is common in electrical and control theory (151).

In many instances the modal type of solution is not required, and a more direct solution to the forced response of the system may be obtained by inversion of the system matrices. This approach is described in § 3.1.3, page 56 , and is used in obtaining frequency responses and mobilities.

The way in which the system mobility matrices are obtained is described in § 3.1.5, page 60 . Mobility matrices were chosen for convenience, since they have certain advantages, both from the point of view of the analysis of the models, and of the experimental work, over the inverse (impedance) matrices. This is dealt with in § 3.2.4, page 75 in more detail.

3.1.1 Notation

The notation used in § 3.1.2 and § 3.1.3 is given below:

A, D, E, G	nxn coefficient matrices of inertia, viscous damping, stiffness, and hysteretic damping respectively.
F	nx1 force vector
i, j	indices where subscripted, also $i = \sqrt{-1}$

K	dissipation function
L	Lagrangion (T-V)
n	number of degrees of freedom of system
Q	generalised force
q	generalised coordinate
T	kinetic energy function
t	time
V	potential energy function
ω	angular frequency

Observe that certain changes in the notation are made in the succeeding section, § 3.1.4, which are given below, in order of appearance.

M, C, K	nxn coefficient matrices of inertia, viscous damping, and stiffness, respectively
E	nx1 force vector
q	nx1 displacement vector
ω	exciting frequency (angular)
t	time
A	2n x 2n coefficient matrix for 1st order equivalent system
F	2n x 1 force vector
x	2n x 1 vector which is the state vector of the system and contains the n displacements and the n velocities necessary to describe the state of the system at any time t.
I	unit matrix
p	characteristic root (or eigenvalue)
$\underline{u}$	right hand eigenvectors(columns)

$\underline{v}$ left hand eigenvectors (rows)

$X = X(\omega)$ 2n x 1 steady state response vector in state vector coordinates at frequency ω

$Z = Z(\omega)$ 2n x 1 steady state response vector in the coordinates of the diagonal system at frequency ω.

Some further extensions in the rotation are used when dealing with the mobility matrix derivation, § 3.1.5, which are:

F m x 1 force vector, elements f_i

V m x 1 velocity vector, elements v_i or $\dot{q}_1$

Y m x m mobility matrix, elements y_{ij}

k + ih complex stiffness

3.1.2. Derivation of Equations

The system equations are normally derived using Lagrange's equations:

$$\frac{d}{dt}\left(\frac{\partial L}{\partial \dot{q}_i}\right) - \frac{\partial L}{\partial q_i} + \frac{\partial K}{\partial \dot{q}_i} = Q_i \qquad i = 1, \ldots, n \qquad 3.1.1$$

When the indicated differentials have been performed on the functions L and K, and a steady state response assumed for an excitation at frequency ω, the equations are put in matrix form. To include hysteretic damping (this somewhat contentious form of damping is of great value - Bishop (123) gives an introduction) in the matrix formulation, the compliant elements are assumed to have complex stiffness. The stiffness matrix is then complex, but may be conveniently separated into the inphase stiffness matrix and the out-of-phase hysteretic damping matrix. The resulting matrix

equation is then of the form:

$$[(E - \omega^2 A) + i(G + \omega D)]\{q\} = F e^{i\omega t} \qquad 3.1.2$$

3.1.3 Direct Solution of Equations

The direct solution to equation 3.1.2 at any given frequency ω is obtained by straightforward inversion:

$$\{q\} = [(E - \omega^2 A) + i(G + \omega D)]^{-1} F e^{i\omega t} \qquad 3.1.3$$

The inversion of the complex matrix may be carried out in real arithmetic by means of the following formula:

$$\{q\} = [(G + \omega D)^{-1}(E - \omega^2 A)\{(E - \omega^2 A)(G + \omega D)^{-1}(E - \omega^2 A) + (G + \omega D)\}^{-1} - i\{(E - \omega^2 A)(G + \omega D)^{-1}(E - \omega^2 A) + (G + \omega D)\}^{-1}] F e^{i\omega t} \qquad 3.1.4$$

This formula requires only two matrix inversions to be performed, despite its lengthy appearance. It is necessary, but not sufficient, that $|(G + \omega D)| \neq 0$.

An alternative formulation would require that the matrix $(E - \omega^2 A)$ is non-singular, which would lead to the solution failing whenever ω corresponded to an undamped natural frequency.

Despite the fact that the calculation must be repeated from the beginning for each frequency of interest, it is comparable in speed, for moderate numbers of evaluations, to the method described in the next section.

Hysteretic damping is readily included in this solution, which is a useful model for the damping in rubber and in continuous structures.

The solution is only applicable for forced steady state response, and does not give the natural frequencies or modal damping factors directly. For these additional results, the solution described in the next section is followed.

3.1.4 State Vector Formulation and Solution

The state vector approach is followed when the natural frequencies and modal damping factors are required in the solution. Hysteretic damping is not included. The steady state response is found subsequent to the eigenvalue calculation, and will give a faster computation than the previous method for large numbers of evaluations. The origins of the method have been discussed earlier. The author is indebted to W. N. Caldwell for the format of the solution given below.

The system equations are put in the following form:

$$M\ddot{q} + C\dot{q} + Kq = E e^{i\omega t} \qquad 3.1.5$$

The state vector is defined as the partitioned vector,

$$x = \begin{Bmatrix} x_1 \\ \hline x_2 \end{Bmatrix} = \begin{Bmatrix} q \\ \hline \dot{q} \end{Bmatrix} \qquad 3.1.6$$

which enables equation 3.1.5 to be expressed in partitioned form,

$$\begin{Bmatrix} \dot{x}_1 \\ \hline \dot{x}_2 \end{Bmatrix} = \left[\begin{array}{c|c} 0 & I \\ \hline -M^{-1}K & -M^{-1}C \end{array}\right] \begin{Bmatrix} x_1 \\ \hline x_2 \end{Bmatrix} + \begin{Bmatrix} 0 \\ \hline M^{-1}E \end{Bmatrix} e^{i\omega t} \qquad 3.1.7$$

or, more compactly,

$$\dot{x} = Ax + F e^{i\omega t} \qquad 3.1.8$$

In the first part of the solution is the eigenvalue solution for the matrix A. Wilkinson (184) provides an authoritative account of various eigenvalue methods.

In the absence of an excitation input, equation 3.1.8 becomes: $\dot{x} = Ax$ 3.1.9

and for non-trivial solutions,

$$|A - pI| = 0 \qquad 3.1.10$$

The solution to equation 3.1.9 is then a linear combination of terms of the form

$$\underline{x} = \underline{u}\, e^{pt} \qquad 3.1.11$$

where the column vectors $\underline{u}$ satisfy the homogeneous matrix equation

$$(A - p_i I)\,\underline{u}_i = 0 \qquad i = 1, \ldots, 2n \qquad 3.1.12$$

and are called the right hand eigenvectors of A.

In general, A will not be symmetrical, and if the coefficients of A are restricted to the field of real numbers, then the eigenvalues will occur as either all real numbers or real numbers and complex conjugate pairs. Complex conjugate eigenvalues will lead to complex conjugate eigenvectors.

Left hand row vectors can also be defined for equation 3.1.9, denoted by $\underline{v}_i$; thus:

$$\underline{v}_i\,(A - p_i I) = 0 \qquad i = 1, \ldots, 2n \qquad 3.1.13$$

Since equations 3.1.12 and 3.1.13 are both homogeneous, the magnitudes of $\underline{u}_i$ and $\underline{v}_i$ are undetermined. The $\underline{v}_i$ are scaled so that

$$\underline{v}_i \cdot \underline{u}_i = 1 \qquad 3.1.14$$

$$\underline{v}_i \cdot \underline{u}_j = 0 \qquad (i \neq j) \qquad 3.1.15$$

so that the left hand row vectors are bi-orthogonal to the right hand column vectors.

If U is a matrix where columns consist of the vectors $\underline{u}_i$, and V is a matrix whose rows consist of the vectors $\underline{v}_i$, then a more compact expression for equations 3.1.14 and 3.1.15 is:

$$VU = I \qquad 3.1.16$$

The steady state response is then developed, using the substitution

$$x = Uz \qquad 3.1.17$$

which is inserted into equation 3.1.8, giving:

$$U\dot{z} = AUz + Fe^{i\omega t} \qquad 3.1.18$$

which can be re-arranged, using equation 3.1.16, as

$$\dot{z} = VAUz + VFe^{i\omega t} \qquad 3.1.19$$

Assuming a steady state solution for z as

$$z = Ze^{i\omega t} \qquad 3.1.20$$

and using from the eigenvalue calculation

$$P = VAU \qquad 3.1.21$$

where P is a 2n x 2n diagonal matrix whose diagonal elements are the system eigenvalues, we get:

$$\dot{z} = Pz + VFe^{i\omega t} \qquad 3.1.22$$

from which it follows that

$$Z = (i\omega I - P)^{-1} VF \qquad 3.1.23$$

which yields the final result:

$$X = U(i\omega I - P)^{-1} VF \qquad 3.1.24$$

Certain features are apparent when evaluating the frequency response to a given force vector F. These are:

1. Matrices U, V, P are evaluated once only.

2. Matrix ($i\omega I - P$) is inverted for each frequency, but it is diagonal so that the inversion only requires the elements to be inverted.

3. VF is a column matrix, evaluated once only. Elements represent the components of F exciting each mode of the system

4. The scalar $\{1/(\iota\omega I - p_i)\}\cdot \underline{v}_i F$ represents the response of the ith mode at exciting frequency ω, in modal response coordinates.

5. Pre-multiplication of the modal response vector by U returns the coordinates to the state vector coordinates.

This method provides more information about the system than the direct inversion method, but is unable to take hysteretic damping into account. The eigenvalues provide the damped resonant frequencies and damping factors, and the eigenvectors provide the mode shapes. The forced response is obtained by the summation of the individual modal responses.

3.1.5 Derivation of the Mobility Matrix

Given a system with n degrees of freedom and m external coordinates which may be used for coupling to other systems, there is a mobility matrix defined by:

$$\begin{Bmatrix} v_1 \\ v_2 \\ \vdots \\ v_m \end{Bmatrix} = \begin{bmatrix} y_{11} & y_{12} & \cdots & y_{1m} \\ y_{21} & & & \\ \vdots & & \ddots & \\ & & & y_{mm} \end{bmatrix} \begin{Bmatrix} f_1 \\ \vdots \\ f_m \end{Bmatrix} \qquad 3.1.25$$

This may be expressed more compactly by:

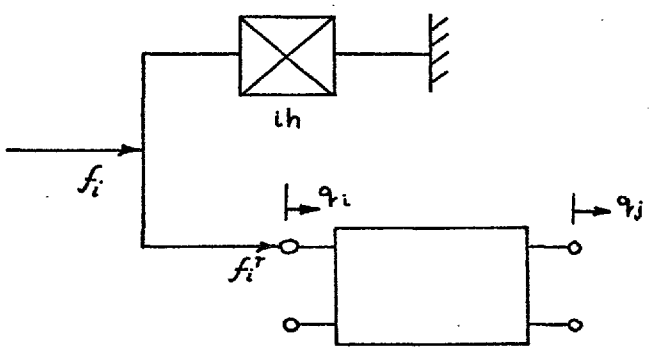
$$V = Y F \qquad 3.1.26$$

where Y is a complex function of frequency in general.

Experimentally, the matrix Y may be determined column by column by applying a force at each of the external coordinates in turn, and measuring the resultant velocities at all the coordinates for each force position. For a linear system, Y is symmetric, and so there is an experimental accuracy check in comparing y_{ij} with y_{ji}.

Analytically, the derivation may proceed on the same pattern, but solution difficulties occur if the system is free in space. Using the method of solution in §§ 3.1.3, for example, the matrix $(G + \omega D)$ will be singular and the method will fail.

To overcome this difficulty, without having to alter the basic technique of solution, the system is grounded by a damper on the coordinate being forced, allowing the matrix $(G + \omega D)$ and derived matrices to be non-singular. Damper-cancellation is later used to allow for this addition.



The value of h is chosen to be compatible with the system as a whole, so that the equations do not remain ill-conditioned. The analysis proceeds to find q_i and the other coordinate displacements for the system and damper under the action of the force f_i. The true force on the system is

calculated by subtracting the force on the damper from the applied force, and is denoted f_i^T.

Then, $$f_i^T = f_i - ihq_i \qquad 3.1.27$$

The true force is then used in calculating the columns of the mobility matrix:

$$y_{ji} = \frac{v_j}{f_i^T} = \frac{\dot{q}_j}{f_i - ihq_i} \qquad 3.1.28$$

Again, checks may be made to see that the derived matrix is symmetrical, and that at very low frequencies a system free in space is masslike.

3.1.6 Alternative Methods

The preceeding sections have indicated the analysis actually used for the dynamic models considered, but alternative methods are, of course, available.

The techniques of control theory may be readily applied, for example. Blackman (125) gives a description of the pole-zero approach, whilst Feinberg (134) and Thompson (177) use the techniques for two-stage isolators in one case, and vehicle suspension in the other. Certain advantages are forthcoming, such as clarification of causality in a complex system, but it does not appear to be as easy, compared with the methods previously discussed, to fit the system analysis into a standard computer routine.

The block-approach for modelling complex systems is used, in any case, in a slightly different form with immittance and transmission matrices, which are described in the next section.

3.2 IMMITTANCE AND TRANSMISSION MATRICES

Immittance (i.e. impedance and admittance) matrices have been well established for calculating the system response from the properties of subsystems. Transmission (or transfer) matrices represent an alternative form of system description.

A plethora of terms has been evolved to describe such matrices, often leading to confusion. This section defines terms, shows interrelationships and goes on to experimental methods which logically follow from the use of such matrices, together with notes on techniques.

3.2.1 Definitions and Terminology

The list below serves to define the matrices and the terms describing them. The preferred terms are shown underlined, with alternatives shown.

The system is assumed to have m coupling coordinates.

Immittance Matrices

Direct Forms (by analogy with equations of motion derived normally)

$$\underset{m \times m}{[A]}\{x\} = \{F\}$$

The external coordinates are given by the vector x and the external forces by the vector $\{F\}$.

$[A]$ is the: dynamic (al) stiffness
apparent stiffness
impedance
dynamic modulus
) matrix

Using velocity, rather than displacement, we have, say

$$[B]\{\dot{x}\} = \{F\}$$

$[B]$ is the: impedance
apparent weight
immobility
) matrix

and extending to using acceleration,

$$[C]\{\ddot{x}\} = \{F\}$$

$[C]$ is the: apparent mass
apparent weight
effective mass
) matrix

Inverse Forms

The matrices here are simply the inverse of those described above

$[A]^{-1}$ is the: receptance
dynamic flexibility
mechanical admittance
compliance
) matrix

$[B]^{-1}$ is the mobility) matrix
mechanical admittance)

$[C]^{-1}$ is the inertance matrix

Transmission (Transfer) Matrices

The direct and inverse forms are more usually considered as forward and rearward, thus:

$$\begin{Bmatrix} \{x_1\} \\ \{F_1\} \end{Bmatrix} = \begin{bmatrix} A \end{bmatrix} \begin{Bmatrix} \{x_2\} \\ \{F_2\} \end{Bmatrix} \qquad \begin{Bmatrix} \{x_2\} \\ \{F_2\} \end{Bmatrix} = \begin{bmatrix} A \end{bmatrix}^{-1} \begin{Bmatrix} \{x_1\} \\ \{F_2\} \end{Bmatrix}$$

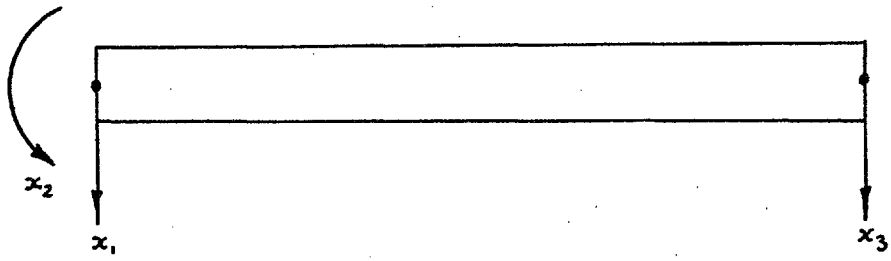
Forward Rearward

The elements of the matrices are sometimes known as four-pole parameters. Velocity or acceleration can be used in place of displacement, and the partitioning of the vectors may often follow certain rules with advantage.

The matrix element names follow from the matrix name, but are usually specified in more detail.

For immittance matrices, the boundary conditions are implicit. Diagonal terms are prefixed by: point, drive-point or direct; whilst the off-diagonal terms are prefixed by: cross or transfer.

A scheme, used here to reduce ambiguity, is outlined here, taking as an example a beam with coordinates shown. Mobility is used, but any other form would serve. It requires that the coordinate numbering is predetermined.



Symbol	Type	Useful form
y_{11}	(translational) point mobility	1-1 point mobility
y_{12}	cross (point) mobility	1-2 cross mobility
y_{13}	transfer mobility	1-3 transfer mobility
y_{22}	(rotational) point mobility	2-2 point mobility

With transmission matrices, there may be ambiguity in terms unless the boundary conditions for the system are specified. This leads to terms such as: blocked mobility (169) or pseudo-mobility (159), free-impedance (169) or pseudo-impedance (159).

Generally, immittance matrices are square, symmetric and dimensionally consistent (apart from rotational and translational units), but they may be singular. Transmission matrices may be neither square nor symmetric, and are not dimensionally consistent. Those that are square have a determinant of $\pm$ 1 (according to sign convention, usually + 1). Whitehead (183) has pointed out that square matrices may be arranged so that symmetry is possible on the cross-diagonal.

3.2.2 Interrelationships

The interrelationships between the different types of system matrix are generally straightforward provided the transmission matrix is square: with tall or wide transmission matrices there will be limitations (168). The chart 3.2.1 shows these relationships for reference (after Rubin (168 ,169)).

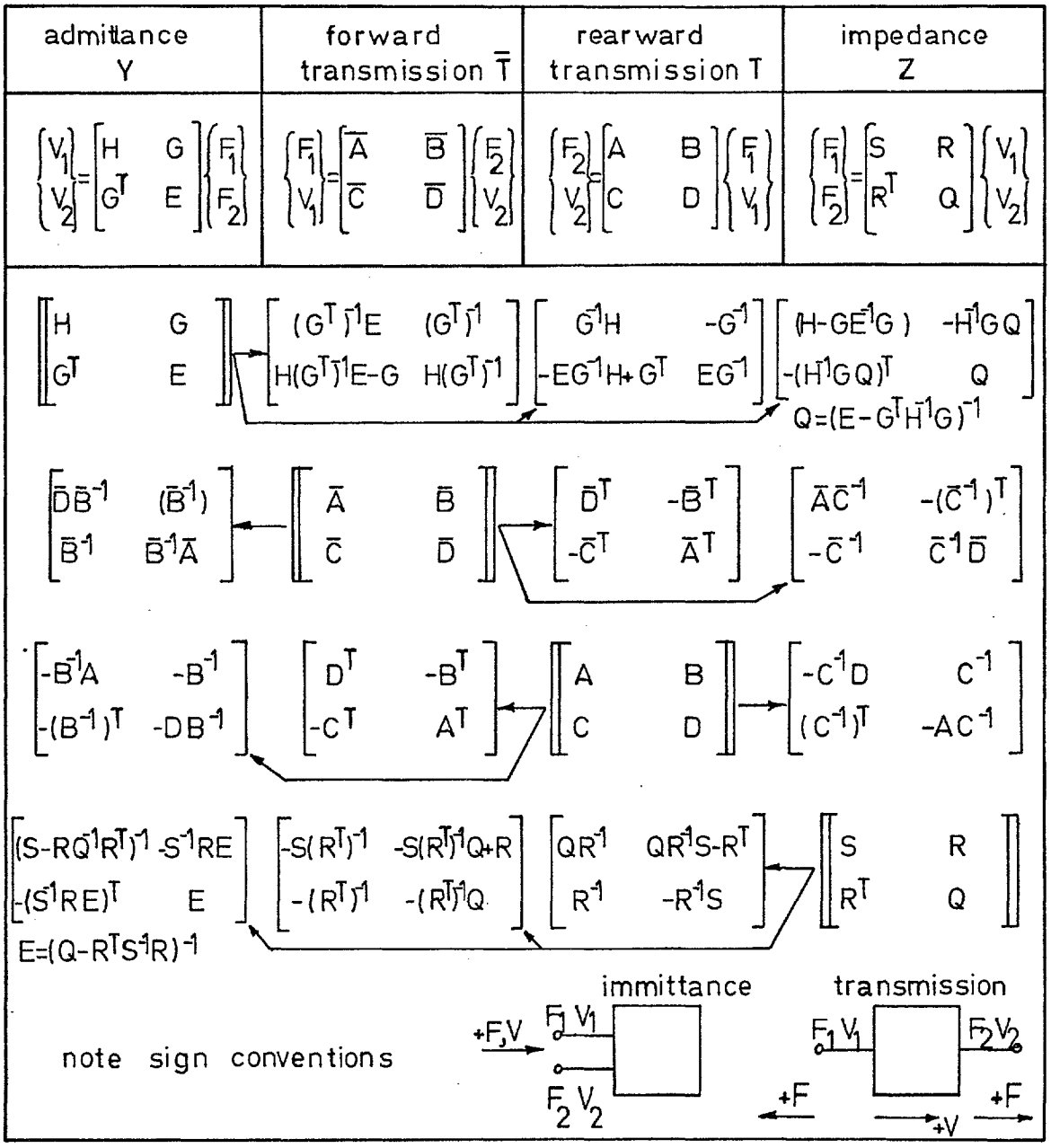


Chart 3.2.1

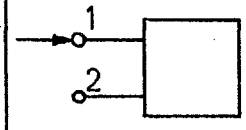
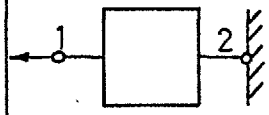
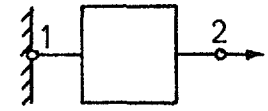
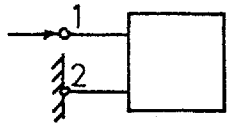
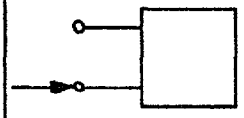
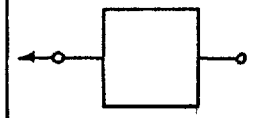
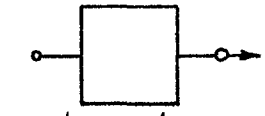
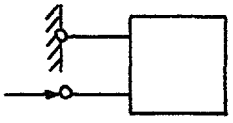
3.2.3 Experimental Chart and Techniques

The chart 3.2.2 shows the tests required to establish immittance and transmission matrices experimentally, for a simple two coordinate system and a branched system. For the branched system it is seen that the elements for the transmission matrices cannot be derived in one step, which makes these matrices less useful. With some appreciation of how the real system will behave under the indicated test, it is possible to choose to measure the most suitable matrix, from the numerical conditioning aspect, at the outset, other factors permitting.

In practical terms, however, it is rarely possible to measure the impedance matrix, especially when there are several significant coordinates at one point. The mobility matrix is subject to experimental difficulties also, but these may be more readily resolved. The following notes use the symbolism in chart 3.2.2 and compare it with the practical situation to exemplify the methods used.

The case considered has been recently reported by Kerlin and Snowdon (hereafter K and S)(147). The system was a cantilever beam, and the object of the work was to determine precisely the beam tip 'impedance'. The tip of the beam has six external coordinates, shown in Figure 3.2.1, with the symbolic representation.

2-Coördinate system

test	Y	$\overline{T}$	T	Z
	$\begin{vmatrix} V_1 \\ V_2 \end{vmatrix} = \begin{bmatrix} y_{11} & y_{12} \\ y_{21} & y_{22} \end{bmatrix} \begin{vmatrix} F_1 \\ F_2 \end{vmatrix}$	$\begin{vmatrix} F_1 \\ V_1 \end{vmatrix} = \begin{bmatrix} a_{11} & a_{12} \\ a_{21} & a_{22} \end{bmatrix} \begin{vmatrix} F_2 \\ V_2 \end{vmatrix}$	$\begin{vmatrix} F_2 \\ V_2 \end{vmatrix} = \begin{bmatrix} b_{11} & b_{12} \\ b_{21} & b_{22} \end{bmatrix} \begin{vmatrix} F_1 \\ V_1 \end{vmatrix}$	$\begin{vmatrix} F_1 \\ F_2 \end{vmatrix} = \begin{bmatrix} z_{11} & z_{12} \\ z_{21} & z_{22} \end{bmatrix} \begin{vmatrix} V_1 \\ V_2 \end{vmatrix}$
1	 → y_{11} , y_{21}	 → a_{11} , a_{21}	 → b_{11} , b_{21}	 → z_{11} , z_{21}
2	 → y_{12} , y_{22}	 → a_{12} , a_{22}	 → b_{12} , b_{22}	 → z_{12} , z_{22}

3-Coördinate system (branched)

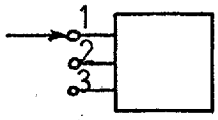
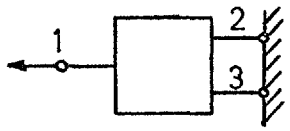
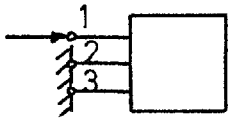
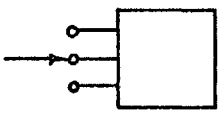
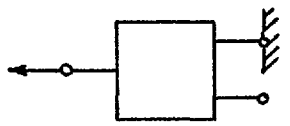
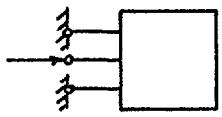
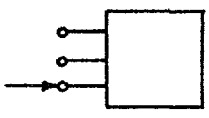
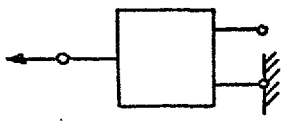
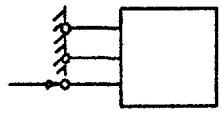
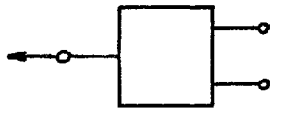
test	Y	T	Z
	$\begin{vmatrix} V_1 \\ V_2 \\ V_3 \end{vmatrix} = \begin{bmatrix} y_{11} & y_{12} & y_{13} \\ y_{21} & y_{22} & y_{23} \\ y_{31} & y_{32} & y_{33} \end{bmatrix} \begin{vmatrix} F_1 \\ F_2 \\ F_3 \end{vmatrix}$	$\begin{vmatrix} F_1 \\ V_1 \end{vmatrix} = \begin{bmatrix} a_{11} & a_{12} & a_{13} & a_{14} \\ a_{21} & a_{22} & a_{23} & a_{24} \end{bmatrix} \begin{vmatrix} F_2 \\ F_3 \\ V_3 \\ V_2 \end{vmatrix}$	$\begin{vmatrix} F_1 \\ F_2 \\ F_3 \end{vmatrix} = \begin{bmatrix} z_{11} & z_{12} & z_{13} \\ z_{21} & z_{22} & z_{23} \\ z_{31} & z_{32} & z_{33} \end{bmatrix} \begin{vmatrix} V_1 \\ V_2 \\ V_3 \end{vmatrix}$
1	 → y_{11} , y_{21} , y_{31}	 → 2 eqns.	 → z_{11} , z_{21} , z_{31}
2	 → y_{12} , y_{22} , y_{32}	 → 2 eqns.	 → z_{12} , z_{22} , z_{32}
3	 → y_{13} , y_{23} , y_{33}	 → 2 eqns.	 → z_{13} , z_{23} , z_{33}
4		 → 2 eqns. total 8 eqns. solvefor'a' forms tri-diag.matrix	

Chart 3.2.2

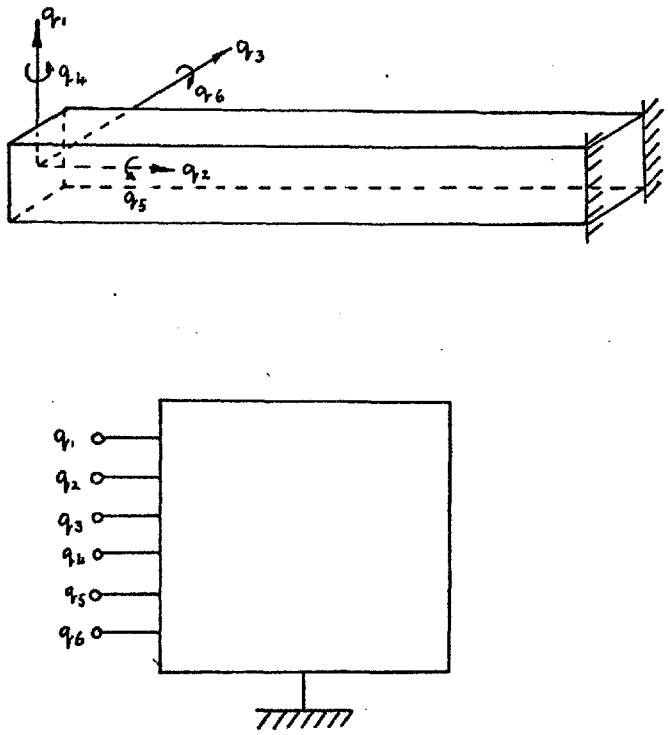


Figure 3.2.1

K and S measured the reciprocal of the 1-1 point mobility - that is the free (pseudo) impedance rather than the true impedance which requires the coordinates two to six to be blocked. (In this case the unqualified use of the term impedance may be justified by arguing that a clamped-free beam is implied, and that any restriction in the q_6 direction cannot be permitted, as such a restriction implies a clamped-sliding beam. The beam is effectively reduced to a one coordinate system and the impedance becomes 'true'). In order to measure the 1-1 point mobility, force must be applied in the q_1 direction without constraining the other coordinates - by no means always easy. In this example, q_3, q_4, q_5 are clearly uncoupled from q_1, q_2 and q_6, and q_2 is only negligibly coupled to q_1 and q_6. This means that any restraint on q_2, q_3, q_4, q_5 will not affect the test. The problem simplifies to reducing the restraint on q_6 as far as possible - i.e.

bending moments on the beam tip should be eliminated.

Decoupling rods are now commonly employed between the driver and the 'impedance' head. The practical arrangement is shown in Figure 3.2.2 for this example, together with the symbolic representation.

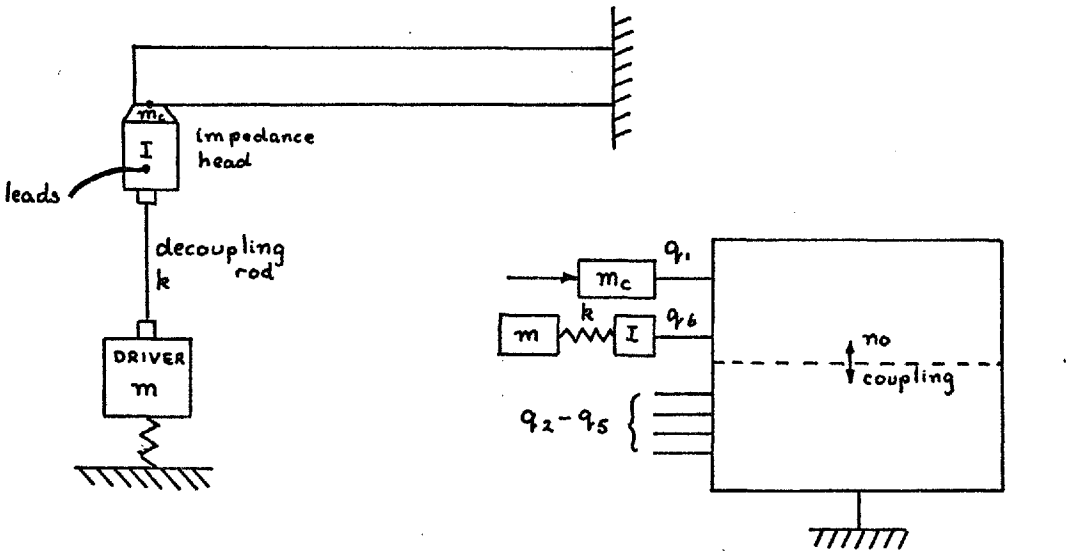


Figure 3.2.2

The effect of the mass in front of the force gauge in the impedance head may be readily cancelled in the test by some simple electronic circuitry. What cannot be simply cancelled, however, is the unwanted system attached to the coordinate q_6 - the inertia of the head, the decoupling rod stiffness, the driver mass and even the connecting leads. The decoupling rod stiffness, k, is usually the only factor amenable to change, and should thus be as small as possible to reduce the load on the q_6 coordinate. The Wilcoxon 'wrap-round' driver features the same basic idea in one unit.

Lateral resonant vibrations of the decoupling rod can also cause additional disturbance on the q_6 coordinate, but this can be avoided by employing different rods for different frequencies. Damping the rods as an alternative is not usually satisfactory, and will render the measured system damping inaccurate, especially if the system damping is small. Smith (174), measuring all six coordinates at a point on the system has cancelled the effects of the drive-block he employed, but only by means of calculation after the test, and with certain loss of precision.

Even the signal leads may present sufficient restraint on the system to be noticeable. K and S used an ususual lead restraint and even resorted to very fine wire coiled connections.

The rotational sensitivity of the accelerometer is a source of inaccuracy. The most noticeable effect of this is when the system is lightly damped and the system is anti-resonant - i.e. the head does not move appreciably in the q_1 direction, but there is appreciable rotation in the q_6 direction. This type of inaccuracy leads to a shift in the observed anti-resonant frequencies, which may be serious if the system is to be modelled as a set of modes, § 3.3, page 77 .

If a stiff coupling rod is employed between the impedance head and the driver, and the mass of the driver is high or attached to the ground, then the coordinate q_6 may be strongly restrained. The measurement now becomes more nearly one of impedance (Figure 3.2.3).

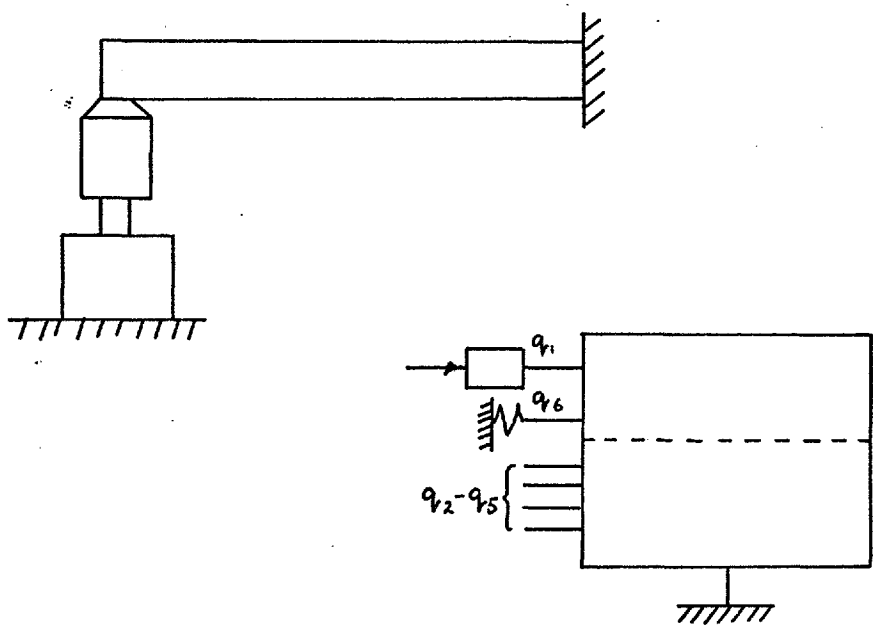


Figure 3.2.3

Frequently, when impedance or mobility tests are reported, little information is given as to the practical arrangement used (and thus the constraints on the other co-ordinates are unspecified), and the test might lie between the two cases shown here. Consequently, such results are at best suspect and at worst useless.

Using a probe on the impedance head eliminates the effect of rotational sensitivity of the accelerometer and the rotational constraint on the system, but other problems occur with this method. This is discussed later in § 3.3.4, page 95.

A probe is also used on a recently marketed portable mobility meter (manufactured by Engineering Design, Ipswich) based on an idea by B. G. Toms of A.W.R.E. and J. Salter of

R.A.R.D.E. In this instrument, the force applied to the system under test is maintained constant by regulating the current in the electrodynamic vibrator, and the resulting motion is measured with a separate accelerometer - either a ring type surrounding the probe or a normal accelerometer placed close to the probe tip. The probe should be light but stiff, and have a rounded end so as not to restrain rotations of the system. Contact is ensured by preloading the probe. Inevitably, there will be certain constraints in the two directions at right-angles to the probe, but these are small.

There are theoretical limitations in this system, however. The first concerns the rotational sensitivity of the accelerometer used, which can lead to shifts in the observed anti-resonances as has been mentioned earlier. The second limitation is the possibility of the probe resonating on the test system, thus amplifying the applied force which is assumed constant. The production instruments have a frequency range limited to 1 kHz, and with the probes supplied the resonance is well outside this frequency range. The design of this instrument is such that many measuring difficulties (due to constraints) are avoided, and ensures that to a large extent the results obtained with it are valid.

If the test system is free in space, difficulties often occur when attempting to support the system with a minimum of constraint. Nodal points for the principal modes are usually employed as support positions, with soft suspension. Mason

and Leventhall (152) have made a comparative study of support methods in the more critical case of measuring the damping of a free-free beam by the logarithmic decrement method, when any energy flow into the supports would have a serious effect on the measured damping of the beam.

It may be concluded that the measurement of mobility is by no means always straightforward - a certain amount of art is still required. At high frequencies and with very stiff structures many other problems, not dealt with here, are found. Ewins (133) has recently summarised some of these; Schloss (171) has reported on many development problems and their solutions.

3.2.4 Impedance, Mobility or Transmission?

The absence of a mobility matrix for a hypothetical massless two-terminal spring clearly suggests that a mobility test on a real spring would lead to a very ill-conditioned matrix, at least at low frequencies: the test would show the massiveness rather than the springyness. An impedance test on a two-terminal mass might be considered also. Transmission matrices are similarly liable to ill-conditioning - an example could be the transfer matrix of a soft spring in series with a large mass at high frequency. Uhrig (179) demonstrates the numerical difficulties of transfer matrix calculations when many sub-systems are joined, as in the analysis of large structures, and surveys reduction methods leading on to the displacement method (180). Pestel and Leckie (162) describe

a modification to the transfer method to avoid the numerical difficulties.

When analysing real systems, a generally flexible approach is necessary in the use of immittance and transmission matrices, and some insight to choose the most suitable for the calculation in hand. It will be shown, however, in the next section that a modal equivalent system will only simply yield a mobility matrix - an impedance matrix would need to be subsequently derived. There is a tendency to think of the mobility matrix as 'natural' and the impedance matrix as 'derived'. O'Hara (159) has previously discussed this from an experimental point of view which is outlined below.

Consider a structure undergoing an immittance test, using four of the coupling coordinates out of those available.

For a mobility test, a force is applied to each coordinate in turn, and the resulting velocities measured. Using the symmetry property of the matrix, ten measurements are required (at each frequency). If a fifth coordinate is then required, the force is applied to this coordinate and five more velocity measurements taken. If coordinates are found to be redundant, the appropriate measurements may be simply discarded.

For an impedance test, a velocity is applied to each coordinate in turn, the coordinates not being excited being blocked, and the resulting forces measured. As for the mobility test, ten measurements are required for a four-coordinate

system. If a fifth coordinate is then required, then the additional coordinate requires blocking during the test. The test must then be repeated from the start - fifteen measurements would be needed now. Similarly, measurements cannot be discarded as in the mobility test if fewer co-ordinates are found to be necessary; the test needs to be repeated from the start.

The mobility matrix is inherently more flexible than the impedance matrix, because of the boundary condition requirements, and may thus be considered the 'natural' form of immittance matrix,

3.3 MODAL EQUIVALENT SYSTEMS

The immittance and transmission matrix elements are frequency responses. For mechanical systems these responses tend to be very complicated in general, requiring the matrix elements to be known for a large number of frequencies to describe the system over even a limited frequency range.

For certain classes of structures, it is well known that they may be represented by an infinite set of uncoupled equations, each implying a single degree of freedom oscillator. Other structures cannot be so represented, due, for example, to damper coupling terms in the equations. Sometimes this coupling may be neglected, but it may be allowed for by reducing the system equations to a finite set and employing the state vector approach.

For the former type of structure it is useful to have a technique to synthesise a modal system from experimentally obtained results in one step. The modal equivalent system must have the same immittance matrix as the structure tested, and will be characterised by the oscillator's (i.e. structures modes) natural frequencies and damping factors, and the coupling to the oscillators from the external coordinates. Fewer data are then required to specify the structure, and simplifications may be made in the measurement procedure. The synthesised system should also be readily compared with the physical structure, so that although complete information about the system is lacking, sufficient is present to suggest any physical effects apparent from the analysis.

In this section, the modal system is described and analysis shown. Experimental verification of the simplified measurement technique possible with this approach is provided.

3.3.1 Derivation of Model

For a linear, homogeneous, isotropic structure with uniform structural (i.e. hysteretic) damping, an infinite set of uncoupled equations may be written for the forced harmonic response (several references, (153) for example):

$$m_i \ddot{\xi}_i + k_i (1 + i\eta_i) \xi_i = \sum_j a_{ij} F_j e^{i\omega t} \qquad i = 1, \ldots, \infty \qquad 3.3.1$$

where ξ_i is the modal response coordinate

m_i is the modal mass

k_i is the modal stiffness, loss factor η_i

a_{ij} is a constant determining the amount of force F_j is applied to mode i

F_j is the externally applied force at point j (distributed forces could also be included)

The constant a_{ij}, where normalised by the modal mass, has been called the excitation constant by Skudrzyk (173, page 220), also identifiable from the mode shape (173, page 303). Bishop and Johnson (124) obtain a partial derivative for a finite system, and characteristic functions for beams and continuous systems. In the present treatment a_{ij} will be thought of as a factor determining the amount of the externally applied force that acts on each mode and is thus denoted coupling factor. The coupling factor is a gemoetrical factor describing the system.

The response, say $\dot{x}_k$, of the structure at point k on the structure due to the applied forces is the summation of the response of all the modes. Strongly coupled modes make large contributions to the response, weakly coupled modes make small contributions. Modes with zero coupling will make no contribution (see for example (124), page 155 et seq.).

The response has been previously expressed in the following terms:

$$M_{ii} = j\omega \sum_{n=0}^{\infty} \frac{1}{\gamma_{ii,n}(\omega_n^2 - \omega^2)} \quad (156)$$

$$\bar{V} = F_0 \sum_{\nu=0}^{\infty} \frac{\omega}{M_\nu^* [j(\omega^2 - \omega_\nu^2) + \omega_\nu^2 \eta]} \quad (173)$$

$$\alpha_{yy} = \frac{(\partial y/\partial p_1)^2}{a_1(\omega_1^2 - \omega^2)} + \frac{(\partial y/\partial p_2)^2}{a_2(\omega_2^2 - \omega^2)} + \cdots$$

$$\alpha_{xh} = \sum_{r=1}^{\infty} \frac{\phi_r(x)\,\phi_r(h)}{a_r(\omega_r^2 - \omega^2)} \quad (124)$$

The derivation will be repeated, possibly by a different path, to bring out a more convenient notation deriving from the outset a mobility matrix. A band-limited model will be used: that is, m_o represents rigid body modes and/or low frequency modes, k_r represents the high frequency modes, and the resonant modes fill the required frequency range (see § 3.3.5, page 99 , for the effects of this approximation). Dotted lines indicate the power flow from the external coordinates (x) to the modes in Figure 3.3.1 below.

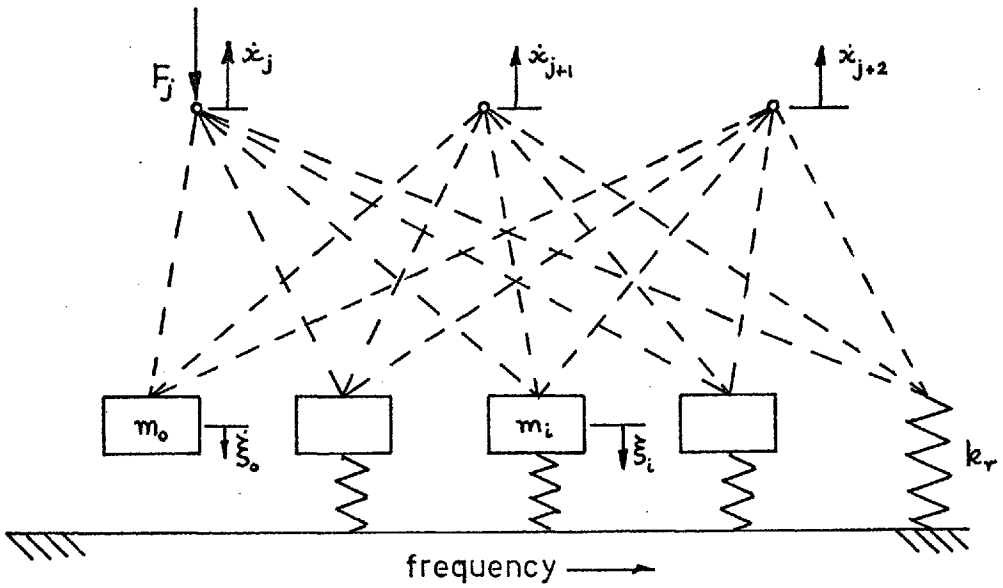


Figure 3.3.1

Assuming that x_j represents the external coupling coordinates and that only one force, $F_j e^{iwt}$, is applied to the system via one of the coupling coordinates, equations 3.3.1 may be written:

$$\left.\begin{aligned} m_o \ddot{\xi}_o &= a_{oj} F_j e^{i\omega t} \\ m_i \ddot{\xi}_i + k_i(1+i\eta_i)\xi_i &= a_{ij} F_j e^{i\omega t} \\ k_r(1+i\eta_r)\xi_r &= a_{rj} F_j e^{i\omega t} \end{aligned}\right\} \qquad 3.3.2$$

The power flow into the system through the coordinate x_j is distributed instantaneously and conservatively to all the modes. As a consequence,

$$\dot{x}_j = a_{oj}\dot{\xi}_o + \sum_{i=1}^{n} a_{ij}\dot{\xi}_i + a_{rj}\dot{\xi}_r \qquad 3.3.3$$

The point mobility of the system is:

$$y_{jj} = \dot{x}_j / F_j \qquad (F_k = o\ ,\ k \neq j)$$

$$= \left[a_{oj}\dot{\xi}_o + \sum_{i=1}^{n} a_{ij}\dot{\xi}_i + a_{rj}\dot{\xi}_r \right] / F_j \qquad 3.3.4$$

Substituting $\omega_i = \sqrt{k_i/m_i}$, the mode natural frequencies in equation 3.3.2 and inserting the result in equation 3.3.4, we get:

$$y_{jj} = i\omega \left[\frac{a_{oj}^2}{-\omega^2 m_o} + \sum_{i=1}^{n} \frac{a_{ij}^2}{m_i(\omega_i^2 - \omega^2 + i\omega_i^2\eta_i)} + \frac{a_{rj}^2}{k_r(1+i\eta_r)} \right] \qquad 3.3.5$$

The free velocity of any other coordinate, x_k, due to the force F_j is, by similar reasoning:

$$\dot{x}_k = a_{ok}\dot{\xi}_o + \sum_{i=1}^{n} a_{ik}\dot{\xi}_i + a_{rk}\dot{\xi}_r \qquad 3.3.6$$

and so the transfer mobility is:

$$y_{kj} = i\omega \left[\frac{a_{oj}\,a_{ok}}{-\omega^2 m_o} + \sum_{i=1}^{n} \frac{a_{ij}\,a_{ik}}{m_i(\omega_i^2 - \omega^2 + i\omega_i^2\eta_i)} + \frac{a_{rj}\,a_{rk}}{k_r(1+i\eta_r)} \right] \qquad 3.3.7$$

It follows that the complete mobility matrix for the system consists of terms of form 3.3.5 on the diagonal, and form 3.3.7 on the off-diagonal. Note that if an impedance matrix were required directly, a whole set of equations of constraint would be necessary, since with F_j applied, all the other coordinates x_k would require to be blocked. This would lead to more elaboration and the need to specify the

number of coordinates, and the number of modes, at the outset.

Inspection of equations 3.3.5 and 3.3.7 shows that, for lightly damped systems, point mobilities show alternating resonances and anti-resonances, whilst the transfer mobilities need not exhibit anti-resonances. This is because a_{ij}^2/m_i must be positive, whilst $a_{ij}\, a_{ik}/m_i$ may be negative.

The kinetic energy level of the system due to an input force F_j may be derived by treating each mode in turn. The energy in each mode is:

$$T_i = \frac{1}{2} m_i \left|\dot{\xi}_i\right|^2 \qquad 3.3.8$$

which, using equation 3.3.2, can be expressed as:

$$T_i = \frac{1}{2} \cdot \frac{\omega^2 a_{ij}^2 F_j^2}{m_i\left[(\omega_i^2 - \omega^2)^2 + (\omega_i^2 \eta_i)^2\right]} \qquad 3.3.9$$

The total system energy is then given by the sum of the modal energies,

$$T = \frac{1}{2} F_j^2 \omega^2 \sum_{i=1}^{n} \frac{a_{ij}^2}{m_i\left[(\omega_i^2 - \omega^2)^2 + (\omega_i^2 \eta_i)^2\right]} \qquad 3.3.10$$

The low frequency/rigid body modes and the high frequency residual stiffness may also be included in equation 3.3.10.

3.3.2 Physical Interpretation and Consequences of the Model

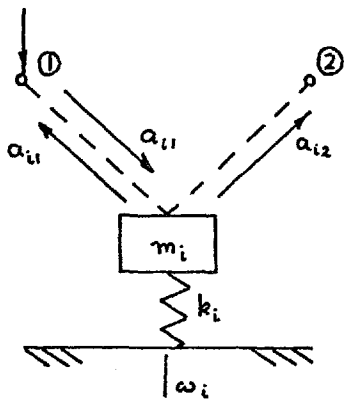
Some space has been devoted to developing the series form solution for the mobility matrix elements. Although the end equations are very similar to forms previously derived, new analogues are apparent and certain consequences arise which have not previously been discussed.

The coupling factors a_{ij} are geometrical descriptions of the system. They relate the position of the coordinate x_j to the nodal pattern for the mode i. The sign of a particular factor, a_{ij}, will change as the forcing position j moves across a node for the mode i, but is arbitrary in sign until compared with other coupling factors. This coupling factor gives a measure of how well the mode is excited. When j is at a node, $a_{ij} = 0$, and so the mode appears infinitely massive. At an antinode, a_{ij} is a maximum, and the mode a appears lighter - approaching the true modal mass.

The modal mass m_i will be seen to be arbitrary in size, as far as the mobility matrix is concerned. The effective modal mass, $m_i/a_{ij}a_{ik}$, alone will be available from external tests on the system. The true modal mass, m_i, is then the measured effective modal mass when the mode i has all the external force applied directly to it, i.e. when $a_{ij} = 1$. This might be estimated from external measurements, knowing that $a_{ij} \neq 1$. Normally the magnitude of m_i may be ignored, and the effective modal mass used.

If a mobility test has determined y_{11} and y_{12} for a

two-coordinate system, say, and m_i/a_{i1}^2 and $m_i/a_{i1}a_{i2}$ have been determined for each mode i (the method is shown later), then the factor a_{i2} may be isolated, hence m_i/a_{i2}^2 for each mode, and so y_{22}. Thus, using this model, only two measurements are required for a 2 x 2 mobility matrix, compared with three with conventional testing. Large savings in measurements are possible with more coordinates (for example six instead of fifteen measurements for a 6 x 6 matrix), provided that none of the coupling factors is zero, or sufficiently close to zero to cause computational difficulties. More important, some otherwise difficult point measurements, such as rotational point mobilities, can be deduced without the need of a rotational driver. Note that for the two-coordinate system discussed, two point measurements would not be sufficient, as an ambiguity in sign would occur. In general, just one column of the mobility matrix needs to be measured, with the above provisions. The points just discussed are summed up in Figure 3.3.2, indicating just one mode.



$y_{11} \rightarrow a_{i1} \cdot a_{i1}$

$y_{21} = y_{12} \rightarrow a_{i1} \cdot a_{i2}$

hence $a_{i2} \rightarrow y_{22}$

if $a_{i1} \cdot a_{i2}$ +ve a_{i1}, a_{i2} like sign

if $a_{i1} \cdot a_{i2}$ −ve a_{i1}, a_{i2} unlike sign

actual signs arbitrary

Figure 3.3.2

Two further points will be made about the model, before the analogues and derivation are shown: mode 'cancellation' and multi-point excitation of the system.

As a consequence of superposition applying to linear systems, a mode excited by a force on one coordinate may be cancelled by a suitable force applied at another coordinate, Figure 3.3.3.

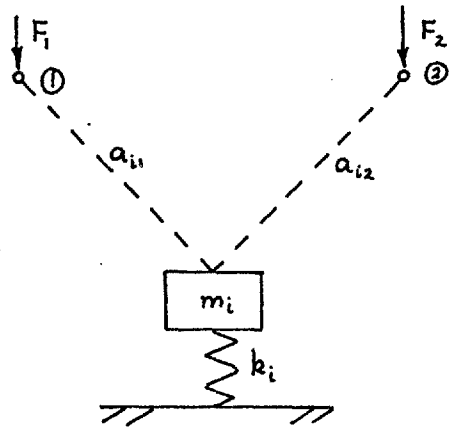


Figure 3.3.3

The requirement is that the net force on the mode is zero, that is,

$$a_{11} F_1 + a_{12} F_2 = 0 \qquad \text{hence} \quad F_2 = -\frac{a_{11}}{a_{12}} F_2 \qquad 3.3.11$$

For two modes to be cancelled, forces will have to be applied to three coordinates, Figure 3.3.4.

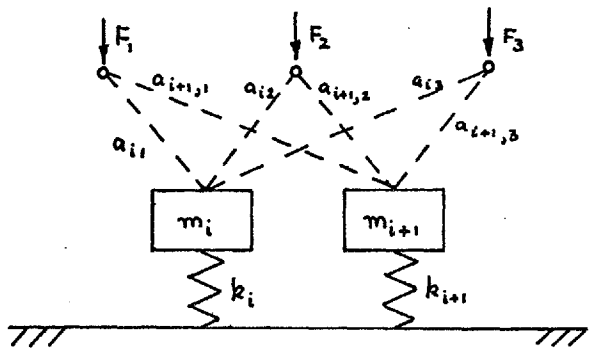


Figure 3.3.4

Now, two simultaneous equations need to be satisfied:

$$\left.\begin{aligned} a_{i1} F_1 + a_{i2} F_2 + a_{i3} F_3 &= 0 \\ a_{i+1,1} F_1 + a_{i+1,2} F_2 + a_{i+1,3} F_3 &= 0 \end{aligned}\right\} \qquad 3.3.12$$

These equations are underdetermined, but the force ratio is required only. Let $F_2 = r_2 F_1$ and $F_3 = r_3 F_1$, then

$$\left.\begin{aligned} a_{i1} + r_2 a_{i2} + r_3 a_{i3} &= 0 \\ a_{i+1,1} + r_2 a_{i+1,2} + r_3 a_{i+1,3} &= 0 \end{aligned}\right\} \qquad 3.3.13$$

which leads to the required force ratios:

$$r_2 = \frac{\begin{vmatrix} -a_{i1} & a_{i3} \\ -a_{i+1,1} & a_{i+1,3} \end{vmatrix}}{\begin{vmatrix} a_{i2} & a_{i3} \\ a_{i+1,2} & a_{i+1,3} \end{vmatrix}} \quad \text{and} \quad r_3 = -\frac{\begin{vmatrix} a_{i2} & a_{i1} \\ a_{i+1,2} & a_{i+1,1} \end{vmatrix}}{\begin{vmatrix} a_{i2} & a_{i3} \\ a_{i+1,2} & a_{i+1,3} \end{vmatrix}} \qquad 3.3.14$$

Extending this process, to cancel n modes, n+1 forcing positions would be required. With this notation used in equation 3.3.13, the equivalent equations become, in matrix form:

$$\begin{bmatrix} a_{i2} & a_{i3} & \cdots & a_{i,n+1} \\ \vdots & & & \vdots \\ a_{i+n,2} & & \cdots & a_{i+n,n+1} \end{bmatrix} \begin{Bmatrix} r_2 \\ \vdots \\ r_{n+1} \end{Bmatrix} = \begin{Bmatrix} a_{i1} \\ \vdots \\ a_{i+n,1} \end{Bmatrix} \qquad 3.3.15$$

or, more briefly

$$[A]\{r\} = \{a_1\} \qquad 3.3.16$$

with the force ratios then given by:

$$\{r\} = [A]^{-1}\{a_1\}$$

Thus n modes of a system may be cancelled by n+1 forces applied at n+1 forcing coordinates (the forces being at the same frequency and in-phase or out of phase as required), provided that the ratio of the force magnitude satisfies the n equations 3.3.17, and singularities do not occur. This applies regardless of frequency and may thus extend to broad-band excitation, provided the forces are correlated.

When particular modes of a structure prove troublesome, and it is not feasible to alter their frequencies, damping, or coupling factors to remove their effects, it would be useful to arrange for this cancellation to occur. The case has been considered where a common source (hence giving correlation to random signals) excites the structure through a set of springs, designed to give the force ratio required, see Figure 3.3.5.

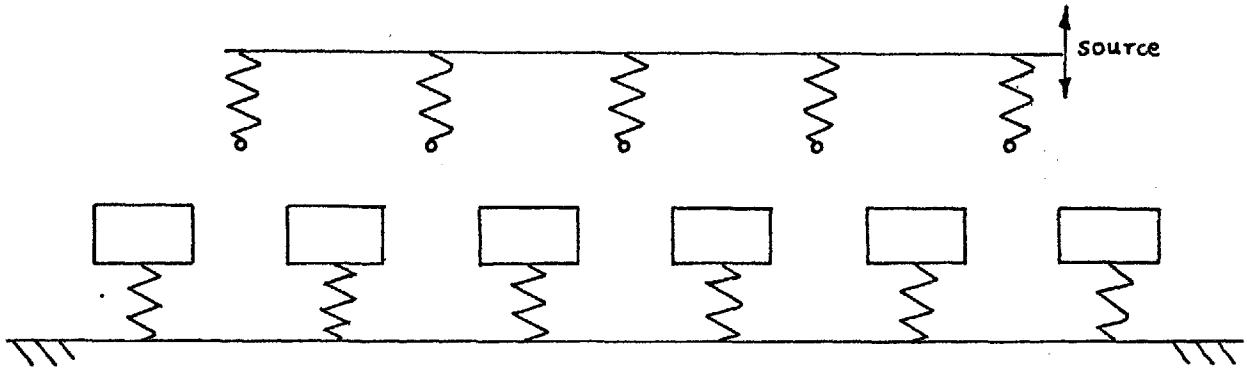


Figure 3.3.5

The analysis (not included here) shows that, because of the effects of the other modes, cancellation cannot be achieved by this means except at one frequency only. Suppression to a certain extent is possible over a limited frequency range, however. The softer the springs, the greater is this range.

The cancellation of modes leads to a simple picture of why multi-point excitation (for example GRAMPA (143), and MAMA (137,167)) can excite relatively pure modes of a structure. If five excitation points are used, with force levels determined by trial, then four modes of the structure may be cancelled. With care, and luck, these may be equally spaced about the mode under investigation. The more distant modes of the structure are then the only, weak, source of modal impurity. This is shown schematically in Figure 3.3.6.

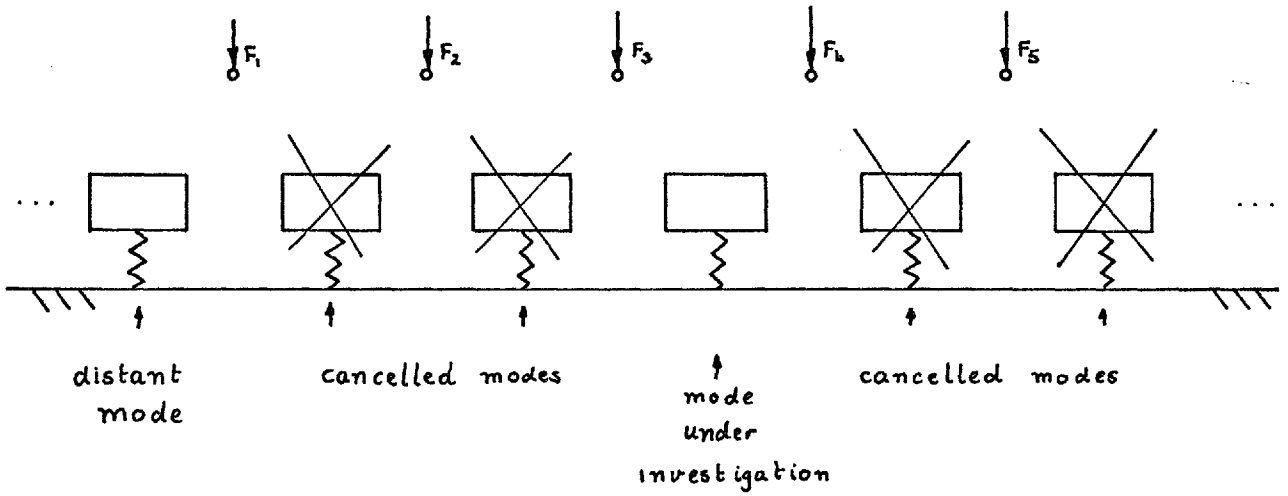


Figure 3.3.6

A physical interpretation has been given to the meaning of coupling factors, and they have been indicated by dashed lines in the previous diagrams. Mechanical, hydraulic and electrical analogues are suggested below to amplify the interpretations. The systems shown satisfy equations 3.2.2, provided that the connecting elements are assumed perfect - frictionless, weightless and so on. They are shown for two coordinates only.

1. Mechanical Analogue

Perfect levers distribute the force, and determine the motion of the drive point as the scaled summation of the modal displacements (equation 3.3.3).

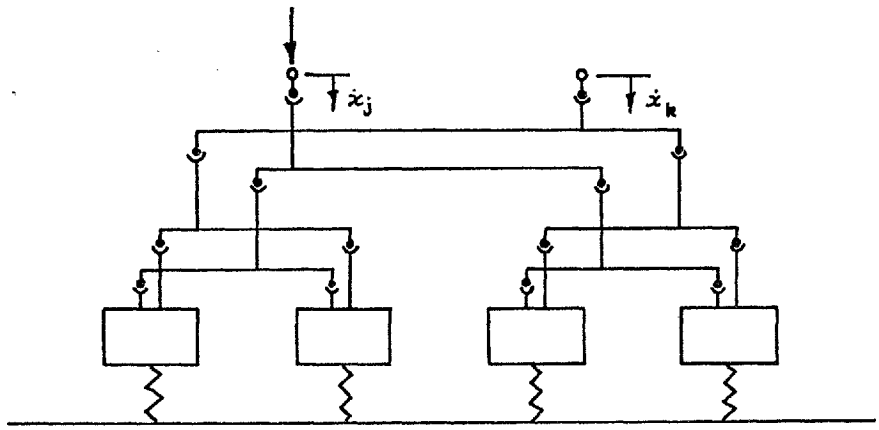


Figure 3.3.7

2. Hydraulic and Mechanical

In this case, the force is distributed hydraulically.

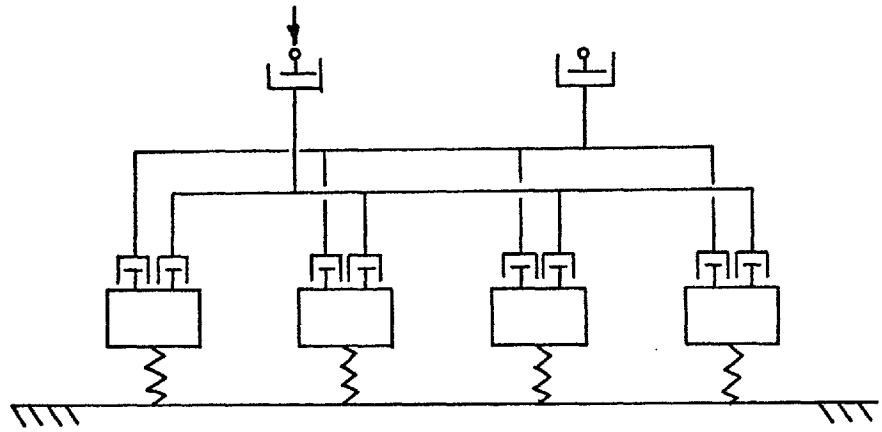


Figure 3.3.8

3. Electrical

This might be compared with the canonical series resonant circuit (for example, see Skudrzyk (173), page 222). The power is distributed by transformers.

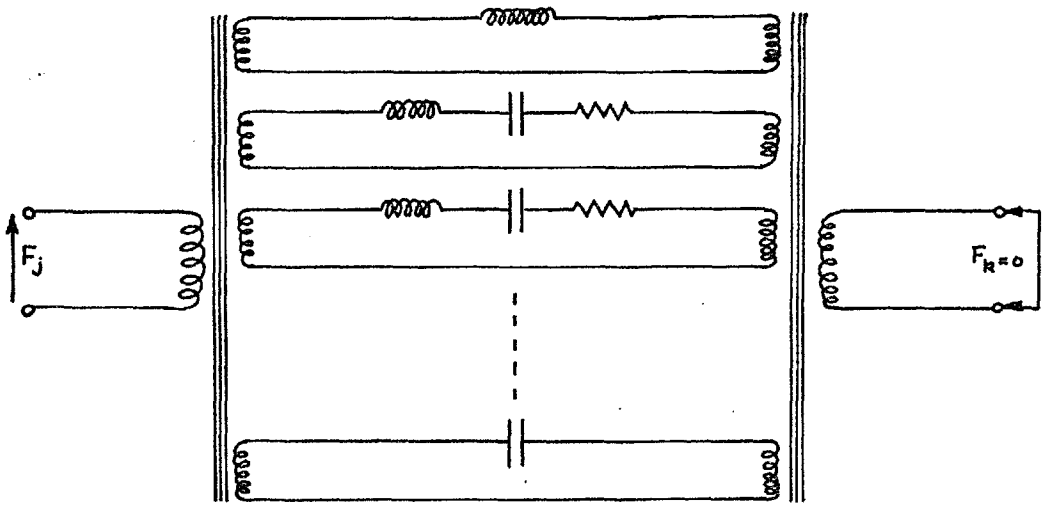


Figure 3.3.9

Subsequent to this derivation it has been noted that Konno and Nakumura (148) have developed a similar model for bars.

For completeness, a conceptual diagram is given, due to Karnopp and Rosenberg (146) in bond-graph form, shown below with one coupling coordinate only

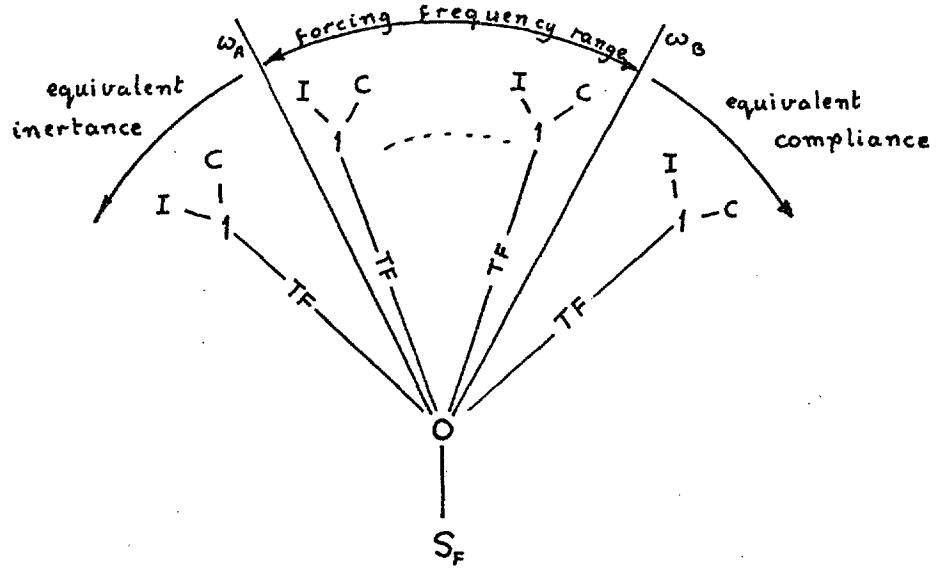


Figure 3.3.10

where I indicates inertance

C compliance

S_F power source

T_F transfer function

0 junction is a flow junction or common effort junction

1 junction is an effort junction or common flow junction

Biot (122), Neubert (156) and Vatz (182) use a model of different conception - a chain of masses and springs in series which is a force-node approach as compared with a velocity-node approach. This appears to make the problem of deriving values for the system harder and makes it more difficult to modify the model. Physical meaning is less obvious as modal velocities are represented by differences between velocities (182).

3.3.3 Synthesis of Model from Experimental Data

It has been known for some time that is is not necessary to measure the complete mobility curve, if the system is known to behave as a set of resonators. Biot in 1940 (122) showed that for a propeller it was only necessary to know its total inertia, and the resonant and antiresonant frequencies on the hub to fully determine the mobility curve. The case might be taken more generally, that for point mobility measurements, provided the structure complies with certain conditions, it is not necessary to use 'impedance'

heads, and less elaborate equipment may suffice.

Biot's equation for the dynamic modulus K (for a one-coordinate system) of the model of shafts and discs was:

$$K = I\omega^2 \cdot \frac{{}^*\omega_1^2\ {}^*\omega_2^2\ {}^*\omega_3^2 \ldots (\omega^2-\omega_1^2)(\omega^2-\omega_2^2)\ldots}{\omega_1^2 \cdot \omega_2^2 \cdot \omega_3^2 \ldots (\omega^2-{}^*\omega_1^2)(\omega^2-{}^*\omega_2^2)\ldots}$$

where I is the total inertia of the system

ω is the exciting frequency

${}^*\omega_i$ anti-resonant frequency i

ω_i resonant frequency i

This enables the point mobility of the system to be deduced, but no more. It applies to free systems only.

Neubert (156) and Vatz (182) developed methods for deriving the constants in the mobility matrix. A simplified method is shown here.

The following methods can be used to evaluate the system parameters from mobility tests using single point excitation.

For an undamped system, the mobility series may be written (shown truncated for brevity - the additional terms are readily included)

$$y_{kj} = i\omega \sum_{i=1}^{n} \frac{a_{ik}\, a_{ij}}{m_i(\omega_i^2-\omega^2)} \qquad 3.3.18$$

The resonant frequencies, ω_i, are first determined in the test. Then n mobility measurements are made at frequencies other than the resonant frequencies, which enable the following matrix equation to be set up:

$$\begin{Bmatrix} y_{kj1} \\ y_{kj2} \\ \vdots \\ y_{kjn} \end{Bmatrix} = i \begin{bmatrix} \frac{\Omega_1}{\omega_1^2 - \Omega_1^2} & \frac{\Omega_2}{\omega_1^2 - \Omega_2^2} & \cdots \\ \vdots & & \\ \frac{\Omega_n}{\omega_1^2 - \Omega_n^2} & & \frac{\Omega_n}{\omega_n^2 - \Omega_n^2} \end{bmatrix} \begin{Bmatrix} a_{1k}a_{1j}/m_1 \\ \vdots \\ a_{nk}a_{nj}/m_n \end{Bmatrix} \qquad 3.3.19$$

or, more briefly

$$\{y\} = [\Omega]\{x\}$$

where Ω_i represents the test frequency. The vector $\{x\}$ is then the column of reciprocals of the effective modal masses. This is simply derived by matrix inversion:

$$\{x\} = [\Omega]^{-1}\{y\} \qquad 3.3.20$$

Thus the effective modal mass, $m_i/a_{ik}a_{ij}$ may be derived. Note that for direct mobilities these must be positive. Also it is possible to have up to (n-1) zeros in the mobility vector - this slightly extends Biot's result in that now just one mobility measurement is required as well as the resonant and anti-resonant frequencies.

From all the mobility tests on a system it is then possible to obtain a complete coupling matrix for each mode:

$$m_i \begin{bmatrix} 1/a_{i1}^2 & 1/a_{i1}a_{i2} & \cdots \\ \vdots & & \\ & & 1/a_{in}^2 \end{bmatrix} \qquad 3.3.21$$

In order to improve on the accuracy of the model, if random errors occur in the mobility levels (but not the frequencies), equation 3.3.19 may be written:

$$\{y\} = [\Omega]\{x\} + \{\epsilon\} \qquad 3.3.22$$

where $\{\epsilon\}$ represents the random errors in $\{y\}$.

Then, by linear regression, the least squares estimate of $\{x\}$ is given by:

$$\{x\} = (\Omega^T \Omega)^{-1} \Omega^T \{y\} \qquad 3.3.22$$

and the more mobility values measured, the more accurate the ensuing model is likely to be. The method might be improved by an investigation into the types of error likely to occur, as the estimate obtained in this way tends to be biased. Even with overdetermining the solution in this way, considerably fewer input data are required to define the system than if modelling were not employed.

When the system is appreciably damped, the Kennedy-Pancu diagram is usually employed to determine the resonant frequencies, mode damping and effective mass. See Figure 3.3.11 below.

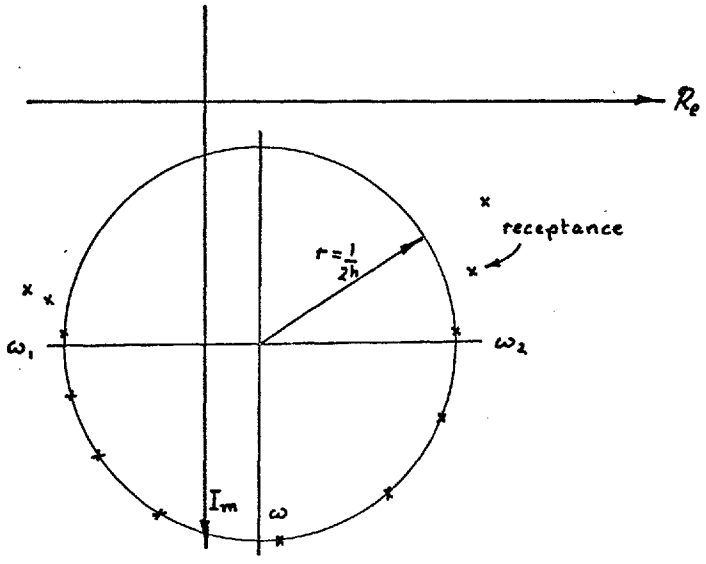


Figure 3.3.11

From the half-power points, the mode loss factor is determined:

$$\eta \simeq \frac{\omega_1 - \omega_2}{\omega}$$

and from the radius of the 'best fit' circle, the damping value is obtained leading to the effective mode stiffness:

$$r = \frac{1}{2h} \qquad \therefore\ h = \frac{1}{2r} \qquad k = h/\eta$$

this, together with the resonant frequency then gives the effective modal mass - $m = k/\omega^2$.

The derived values of η and m are subject to certain errors. The loss factor η depends on the small difference between two large quantities, especially when the damping is light. The derived mass depends both on η and on the radius of the 'best fit' circle and is thus subject to increased error. The method, with care, can give good accuracy for η, but is not very reliable for the effective modal mass.

For a lightly damped system, combining the techniques for the undamped case and the damped case can lead to satisfactory results. The Kennedy-Pancu method, with care, ensures that the mode damping can be well established, whilst the solution for the undamped case determines the effective modal masses.

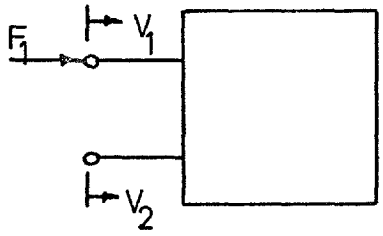
3.3.4 Modified Experimental Chart and Techniques

The modal equivalent system has been seen to yield only a mobility matrix directly. The modified experimental procedure, shown in Chart 3.3.1, shows the derivation of a mobility matrix only.

For an undamped (or lightly damped) system with two coupled coordinates (for example, a beam) the following scheme

2-Coördinate system

undamped or high Q



Apply F_1 , measure y_{11} , res. freqs. ω_r & anti-res. freqs. ω_a

y_{21} at ω_a

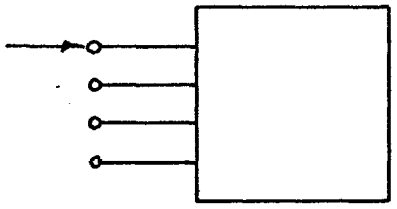
damped

include 1/2 power points for each res. freq.

or Kennedy - Pancu plot

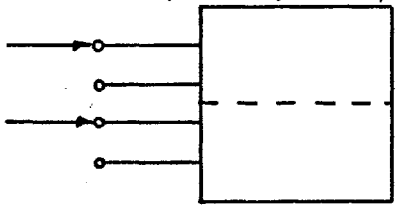
Multi - Coördinate system

all coupled



as above + y_{31} , y_{41} ..... at ω_a

partially coupled



treat as separate systems

Chart 3.3.1

has been found to provide satisfactory measurements - Figure 3.3.12.

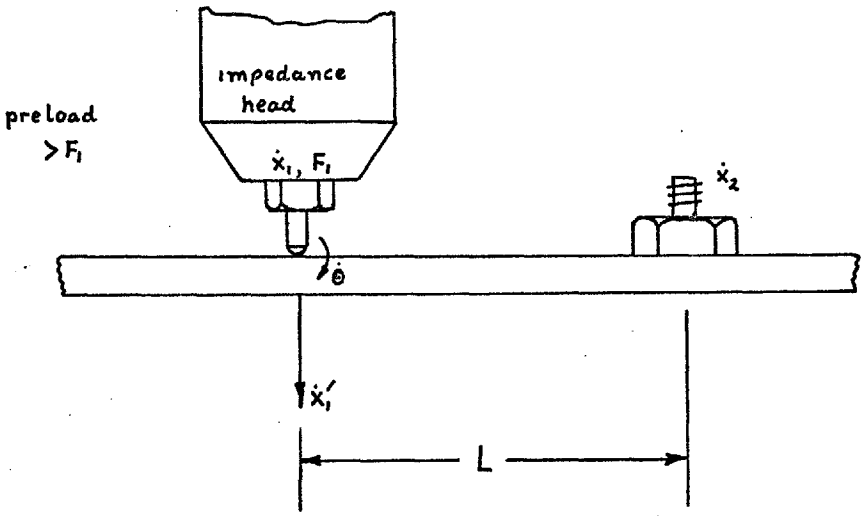


Figure 3.3.12

A probe with a small hemispherical end transmits the applied force without introducing restraining bending moments, and is preloaded to maintain contact. At anti-resonant frequencies, the rotational sensitivity of the accelerometer in the impedance head is no longer significant, but the accuracy of the observed anti-resonant frequencies depends on the probe stiffness, which should be sufficiently great that $\dot{x}_1' \approx \dot{x}_1$. For the cross mobility, an accelerometer, giving $\dot{x}_2$ and hence $\dot{\theta}$ is mounted distance L away from the probe, L being large enough to provide sufficient signal but small enough for the bending effects in the beam in that region to be negligible. Only $\dot{x}_2$ is required to give the rotation in this case, since the rotation need only be measured at the anti-resonant frequencies (i.e. with $\dot{x}_1 = 0$). When there is appreciable damping, so that at the anti-resonant frequencies $\dot{x}_1$ is not neglibible compared with $\dot{x}_2$, the rotation must be derived from the scaled difference of the two

signals. The circuit, shown in Figure 3.3.13, might be used in this case.

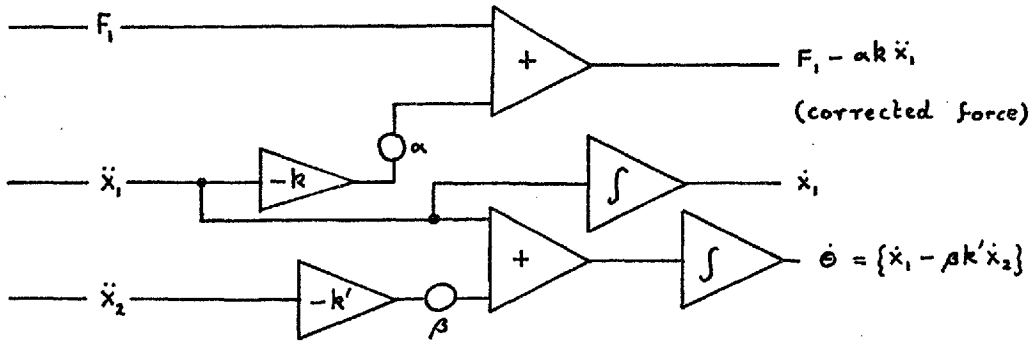


Figure 3.3.13

With the portable mobility meter (manufactured by Engineering Design, Ipswich), the use of a summing amplifier and two accelerometers can lead to the same measurements - Figure 3.3.14.

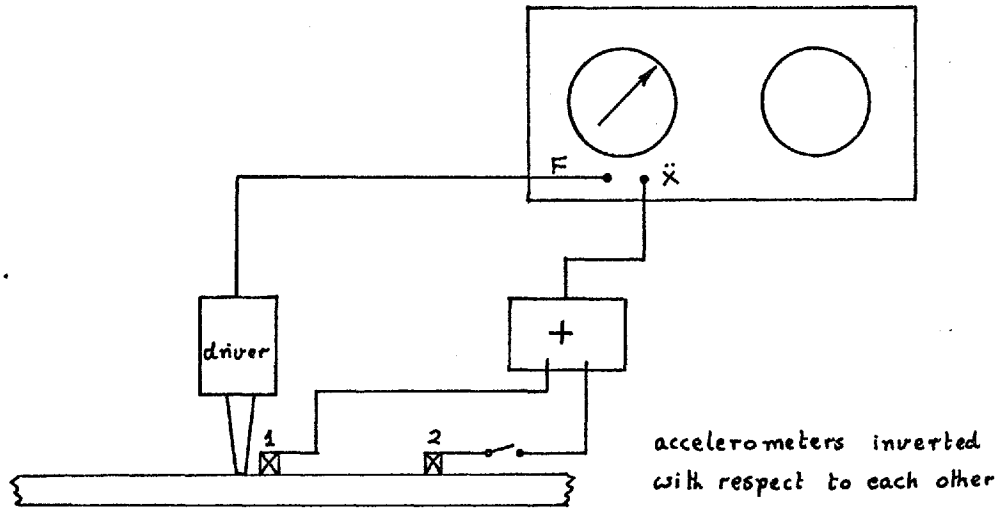


Figure 3.3.14

In this case, accelerometer number 2 needs to be cut-out when determining the point anti-resonant frequencies and the resonant frequencies, and is switched in subsequently to give the rotation.

The method can be extended to measure two rotations, as shown in Figure 3.3.15, as for measuring the two-rotational point mobilities of a plate.

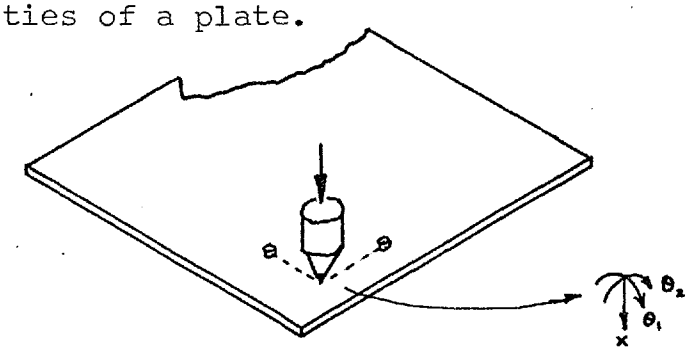


Figure 3.3.15

3.3.5 Experimental Verification

It was shown earlier that it is possible to predict point mobilities and other mobilities from just one column of the mobility matrix when the system has been modelled. This does not appear to have been attempted in practice, however. Smith (174), when measuring the total structural (point) matrix used a procedure basically in accordance with the methods shown in §§ 3.2.3, page 68 ; this required extensive instrumentation.

A simple experiment was devised to predict the rotational point mobility at the end of a free-free beam, using linear excitation only. A closed form solution for the beam is available, enabling an exact-theoretical comparison. The tip mobilities of the beam are denoted by y_{11}, y_{12}, y_{22} defined in Figure 3.3.16.

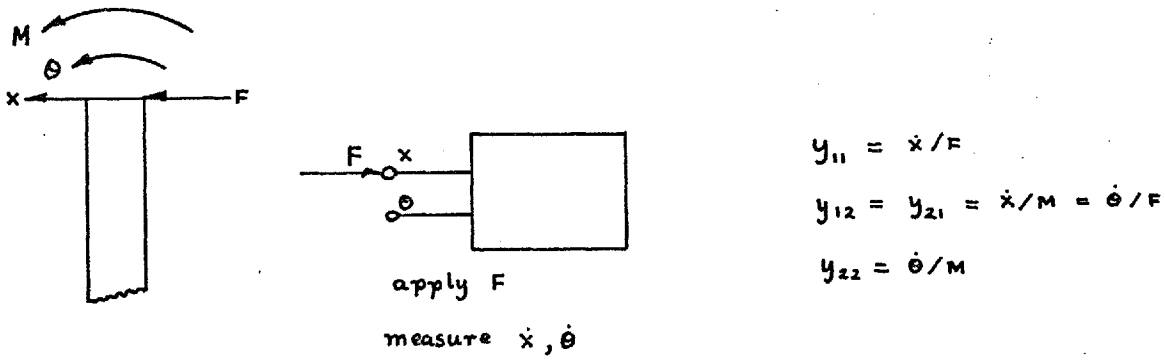


Figure 3.3.16

Figure 3.3.17 shows the experimental arrangement.

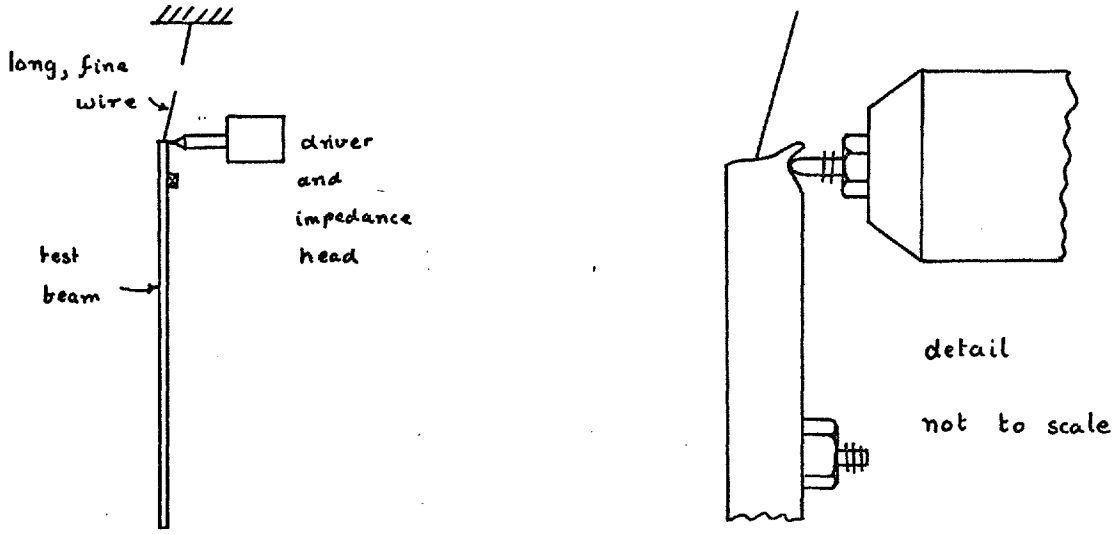


Figure 3.3.17

The beam used was made of mild steel, 57.06 in. long, 1.5 in. wide and 0.25 in. thick, weighing 5.99 lb wt. It was suspended vertically from the measurement end with very fine wire supports (as several modes were to be investigated, the nodal point approach would have been tedious; in any case this method was found to provide a very satisfactory solution and little stiffening occured) these wires being slightly inclined from the vertical so as to preload the impedance head probe. An accelerometer was placed 2 in. from the drive end to measure the rotation of the beam; the beam being assumed to be virtually straight in this region for the modes tested.

The resonant and 1-1 anti-resonant frequencies were measured, and the 1-2 point mobility at the 1-1 anti-resonant frequencies. The low frequency behaviour was derived by calculating the rigid body behaviour from the beam constants, although this could have been measured experimentally.

The measured frequencies are shown in Table 3.3.1 compared with the theoretical frequencies assuming a Bernoulli-Euler beam, with Young's modulus 30 x 10^6 lbf/in^2.

Resonant frequencies (Hz)			1-1 anti-resonant frequencies (= resonant frequencies of free-pinned beam) (Hz)		
Experi-mental	Theore-tical	% diff-erence	Experi-mental	Theore-tical	% diff-erence
16.25	16.05	+1.21	11.01	11.06	- .431
43.096	44.26	-2.63	35.41	35.83	-1.17
85.464	86.76	-1.51	73.83	74.77	-1.258
141.50	143.8	-1.6	126.40	127.88	-1.16
			192.68	195.2	-1.29

Table 3.3.1

Four resonant and five anti-resonant frequencies were measured which is sufficient for a five mode plus residual stiffness model to be calculated - that is, one rigid body mode representing both translational and rotational modes, four resonant modes and a residual stiffness term.

It is seen that generally good agreement with the theoretical values was found. Good mass cancellation of the impedance head could be made, as individual adjustment for each test frequency could be made.

The measured and theoretical 1-2 point mobilities are shown in Table 3.3.2, at the 1-1 anti-resonant frequencies.

Experimental		Theoretical		
1-1 anti resonant frequencies (Hz)	1-2 point mobilities rad/s/lbf	1-1 anti resonant frequencies (Hz)	1-2 point mobilities rad/s/lbf	% difference
11.01	+ .2575	11.06	+ .236	+ 9.1
35.41	+ .2275	35.83	+ .250	- 9.0
73.83	+ .252	74.77	+ .250	+ 0.8
126.4	+ .249	127.88	+ .250	- 0.4
192.68	+ .209	195.2	+ .251	-16.8

Table 3.3.2

The calculated low frequency (rigid body) behaviour of the beam is: at 1 rad/s, 1-1 point mobility equals 258 in/s/lbf and the 1-2 point mobility equals - 6.78 rad/s/lbf. Together with the experimental measurements these provide the necessary information to define the complete point mobility matrix for the beam tip.

Figures 3.3.18 - 29 show the results of this beam test, and provide material for a discussion of the errors involved (and errors in other similar tests). The first set of figures, i.e. Figures 3.3.18 - 23, shows the model

with a residual stiffness term.

In Figure 3.3.18, the closed-term solution is shown compared with the experimentally derived 1-1 point mobility curve. The model is valid up to the fifth anti-resonance. Note that damping has been ignored - the height of the peaks and depth of the notches is determined by the step length used in plotting. The two curves show generally good correspondence. In Figure 3.3.19, the 1-2 point mobility curves are shown - the correspondence detween the curves is not quite so good. The 2-2 point mobility curves are shown in Figure 3.3.20, demonstrating quite clearly that it is possible to predict this mobility from other results, though the errors tend to be cumulative.

Figures 3.3.21 - 23 show similar curves, but instead of experimental measurements, the closed form values for the beam are substituted into the modal model (subject to truncation errors). These show that systematic errors tend to predominate over the random errors. The random (experimental) errors are shown in Table 3.3.3, the errors being related to the coupling factors with the modal masses arbitrarily set to unity.

THEORY + EXP YOO

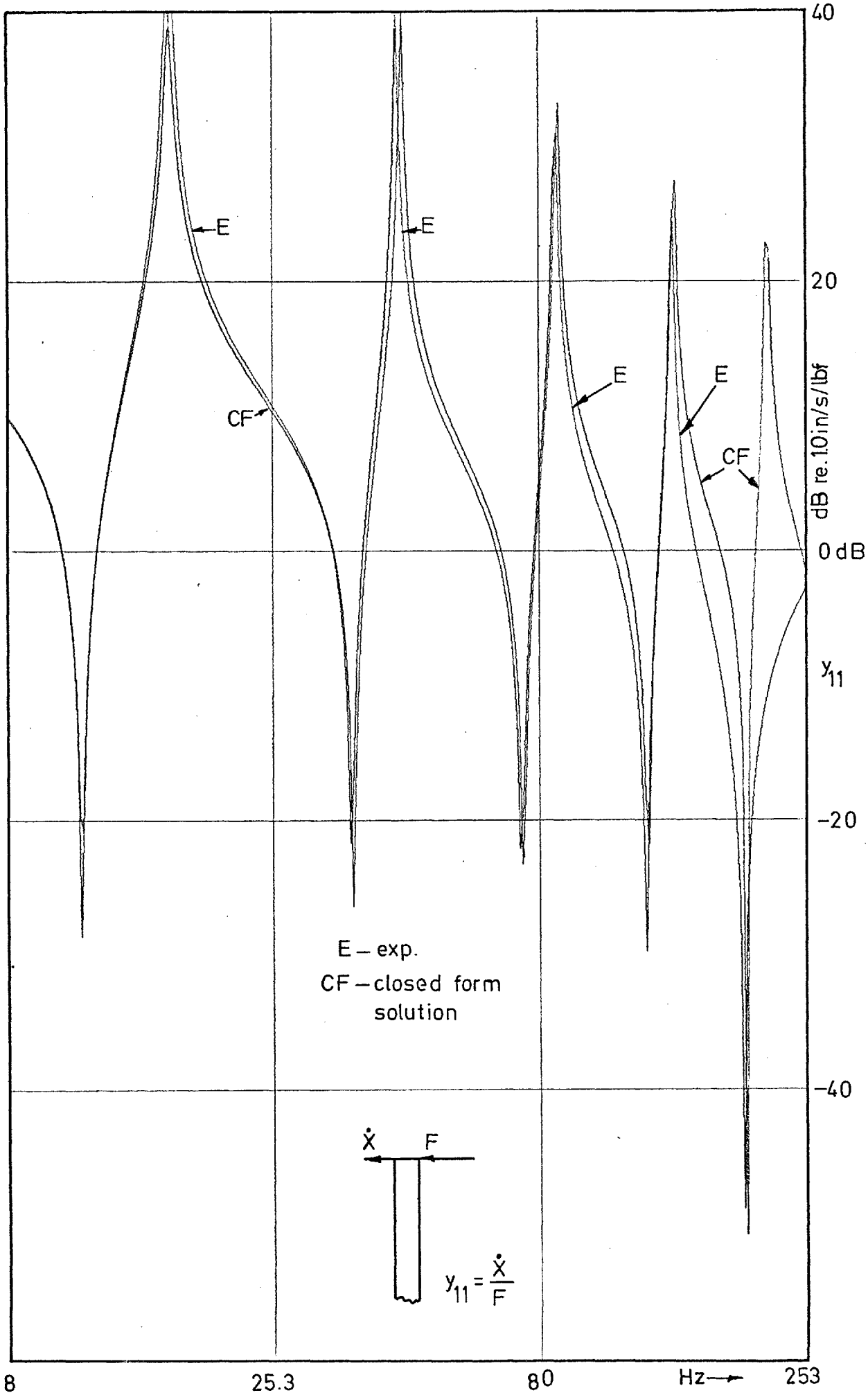


Figure 3.3.18

THEORY + EXP YOO/

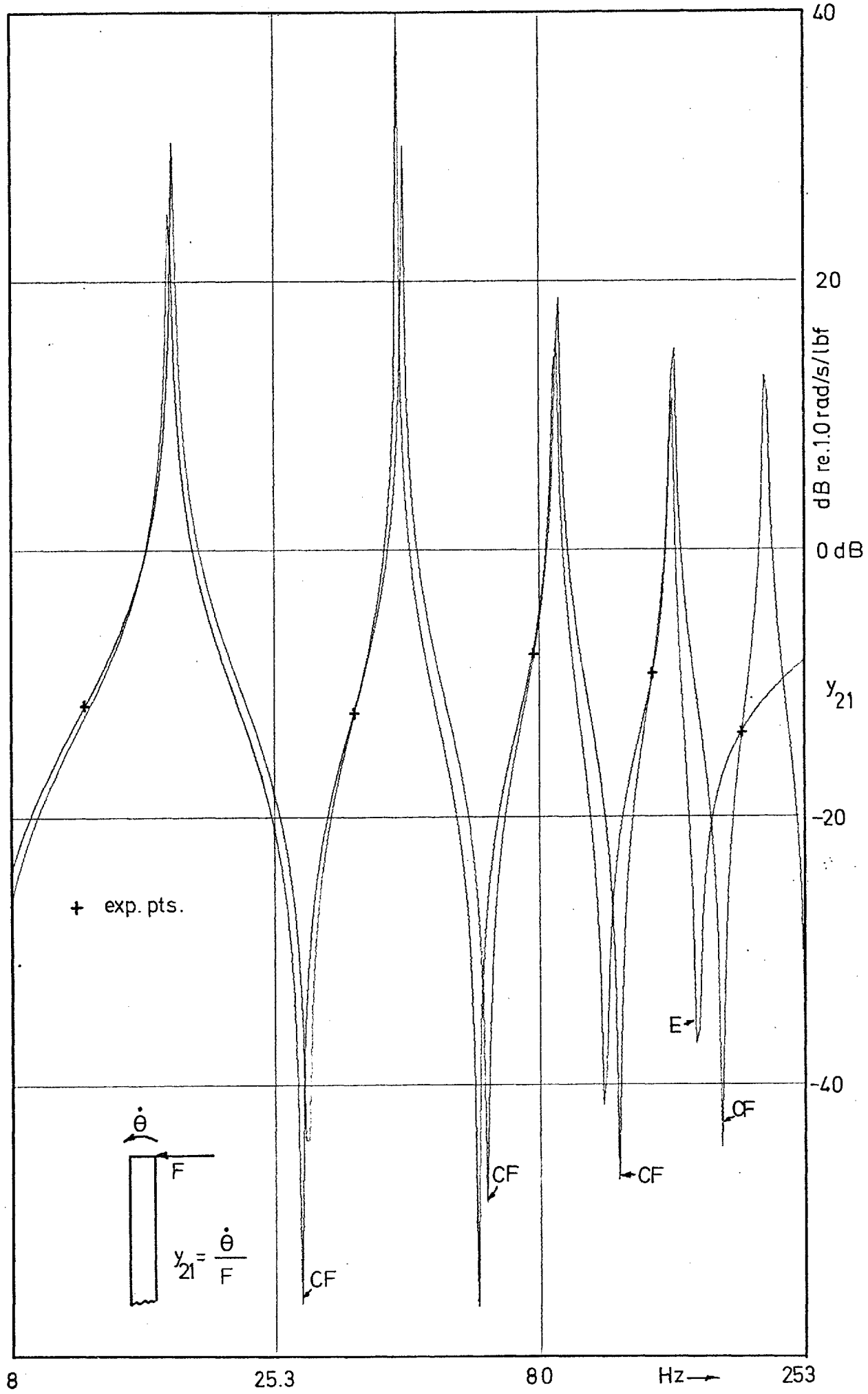
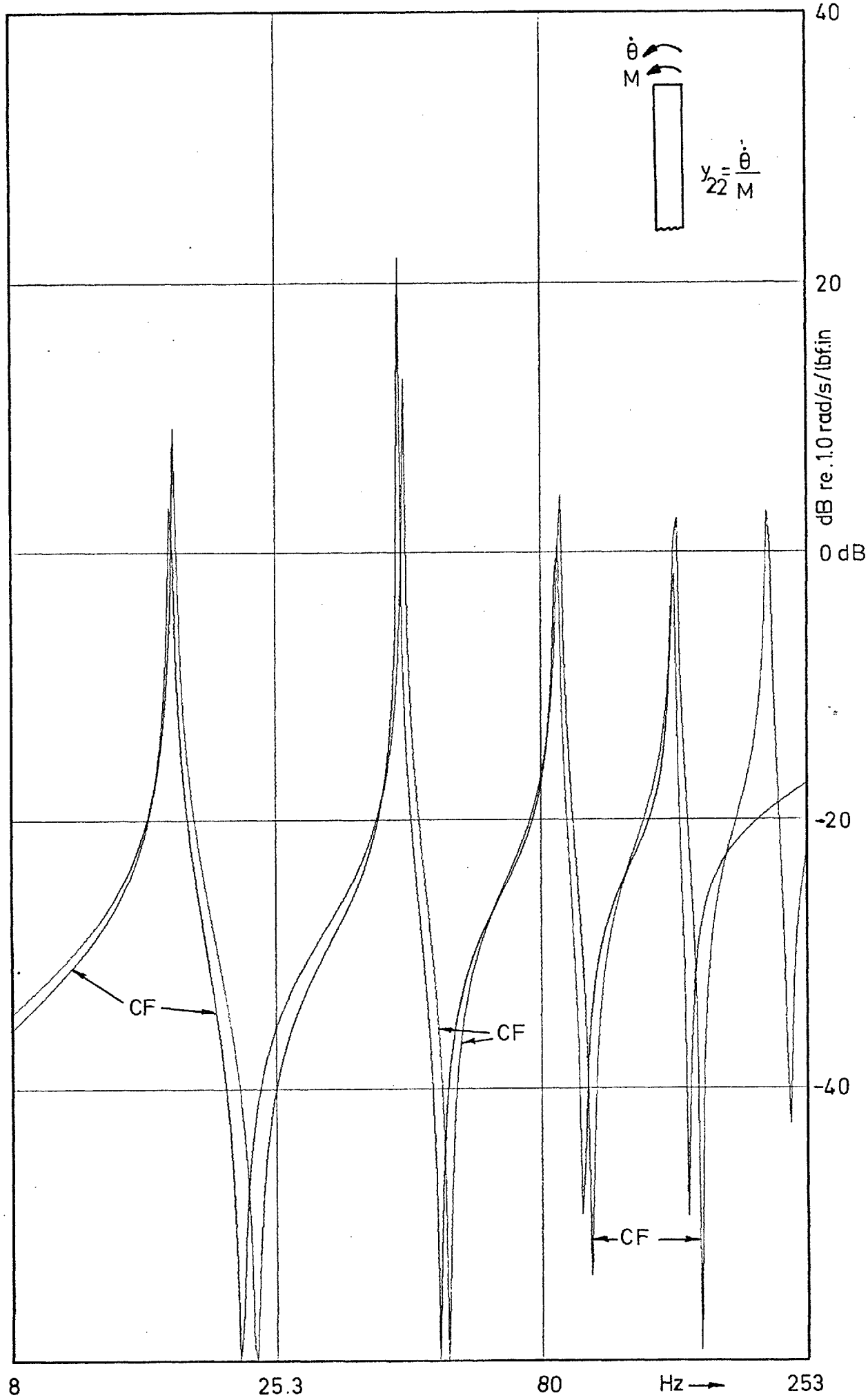


Figure 3.3.19



THEORY + EXP YO/O/

Figure 3.3.20

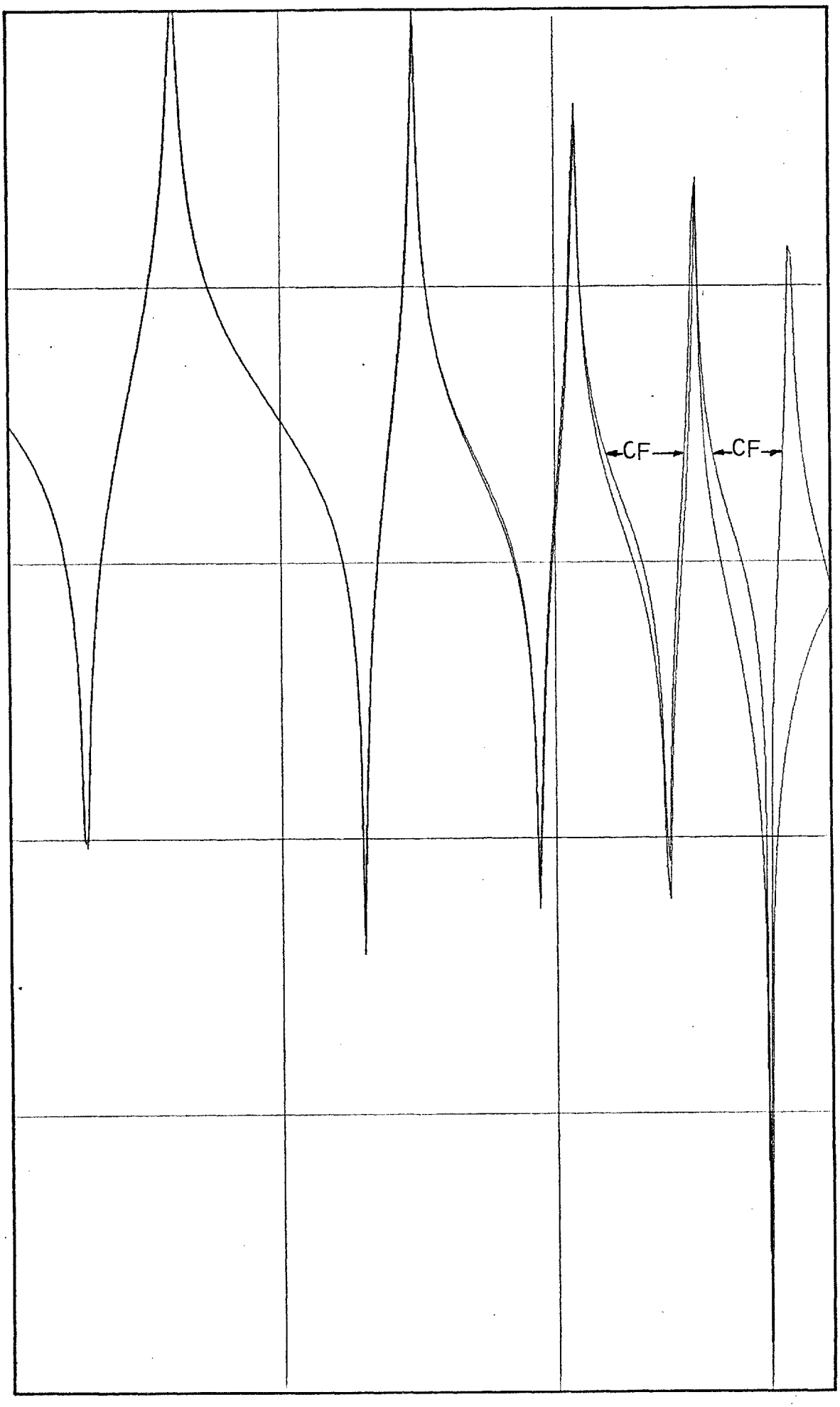


Figure 3.3.21

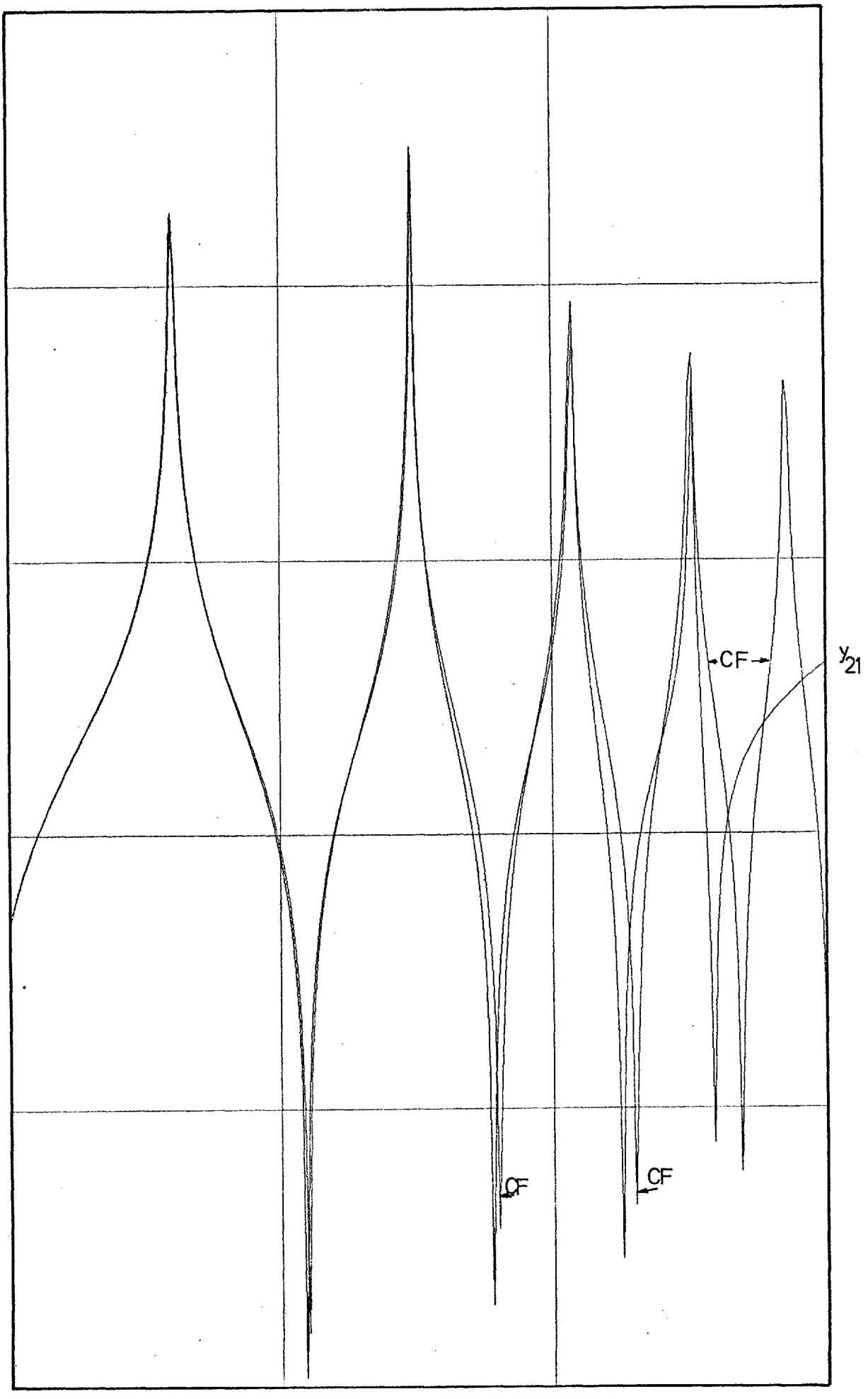


Figure 3.3.22

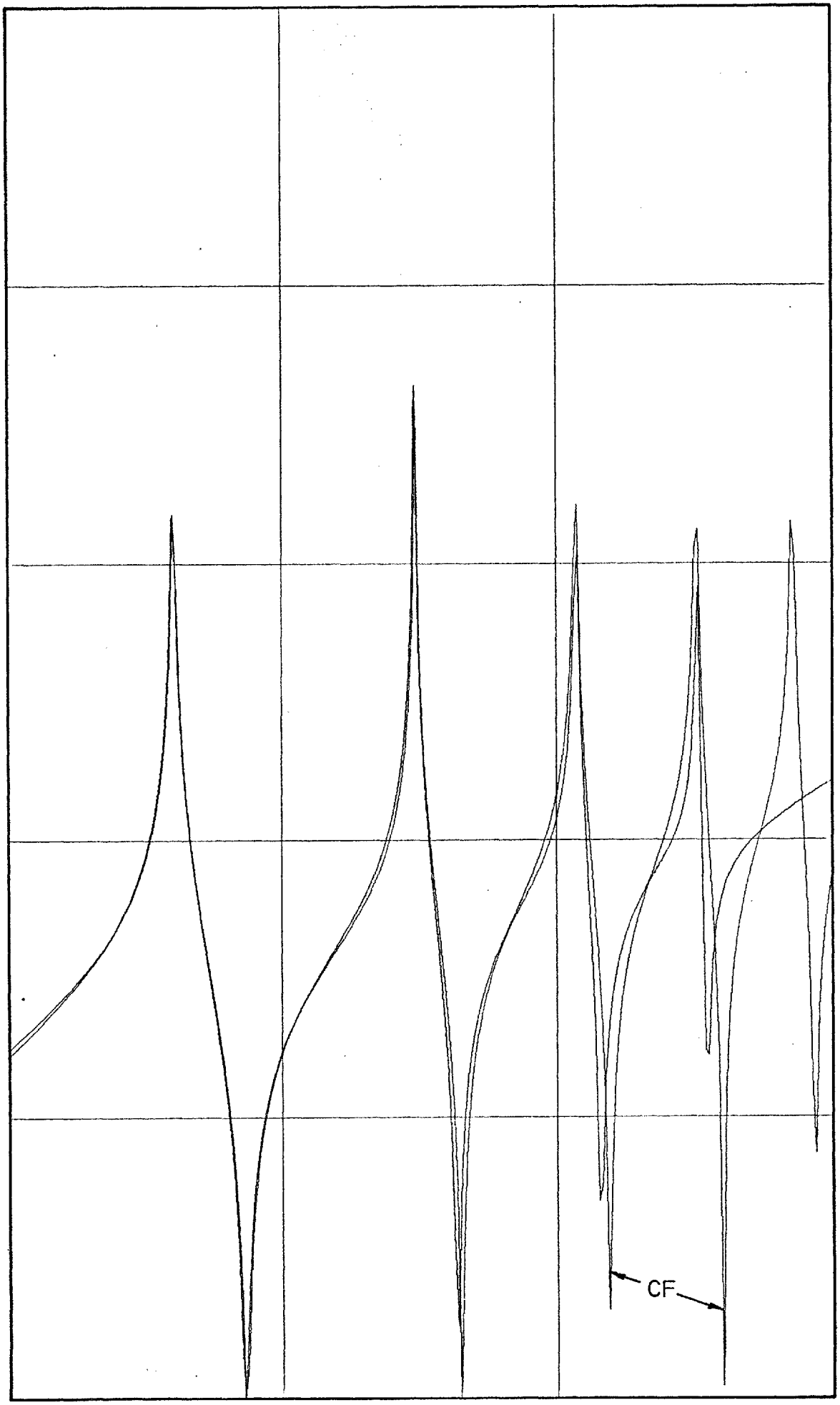


Figure 3.3.23

Mode	Coupling factors ($m_i = 1$)						Errors in effective modal mass		
	1 - direction			2 - direction			1 - 1	1 - 2	2 - 2
	Theory	Exp.	% Change	Theory	Exp.	% Change	% heavy (+) or light (-)		
0	16.0725	16.0656	- .043	.426581	.422336	- 1.0	+ .086	+ 1.043	+ 2.0
1	16.0341	16.5355	+3.13	1.29123	1.43842	+11.4	-6.26	-14.43	-22.8
2	15.8160	15.5306	-1.8	2.06982	1.92144	-7.2	+3.6	+ 9.0	+14.4
3	14.9554	14.8419	- .76	2.59311	2.64007	+1.81	+1.52	- 1.05	- 3.62
4	12.7180	12.4582	-2.04	2.46545	2.92636	+18.6	+4.04	-16.56	-37.2
res. stiffness	0.030652	0.03089	+ .775	0.0105716	0.0097869	-7.35	+1.55	+ 6.58	+14.7

Table 3.3.3

The systematic error is due to the mobility of the residual stiffness term. The fifth mode is close to the fourth mode (about 50% higher frequency) which means that the mobility of the residual terms about the third and fourth modes is greater than that given by the spring term alone. For this systematic error to be neglibible, the frequency of the highest mode measured should be about 5 x the highest frequency of interest. Alternatively, the residual stiffness term may be eliminated, and the modal series terminated by a mode. The highest mode considered is then not a true mode, but represents the true mode plus the effects of the higher modes. Again, the series will not give an exact representation, but the systematic error should be reduced.

To allow for this, and to represent the first five modes of the beam, the fifth resonant frequency is required. This was not measured experimentally, and so, for the results shown here, the value used together with the experimental values - 210.95Hz - represents the same order of error (1.6%) from the exact value (214.4 Hz) as the frequencies measured experimentally.

Figures 3.3.24 - 26 show the closed form solution compared with the experimentally derived curves recalculated as indicated above, and Figures 3.3.27 - 29 show the closed form solution compared with the curve calculated from the theoretical input data (subject to truncation errors).

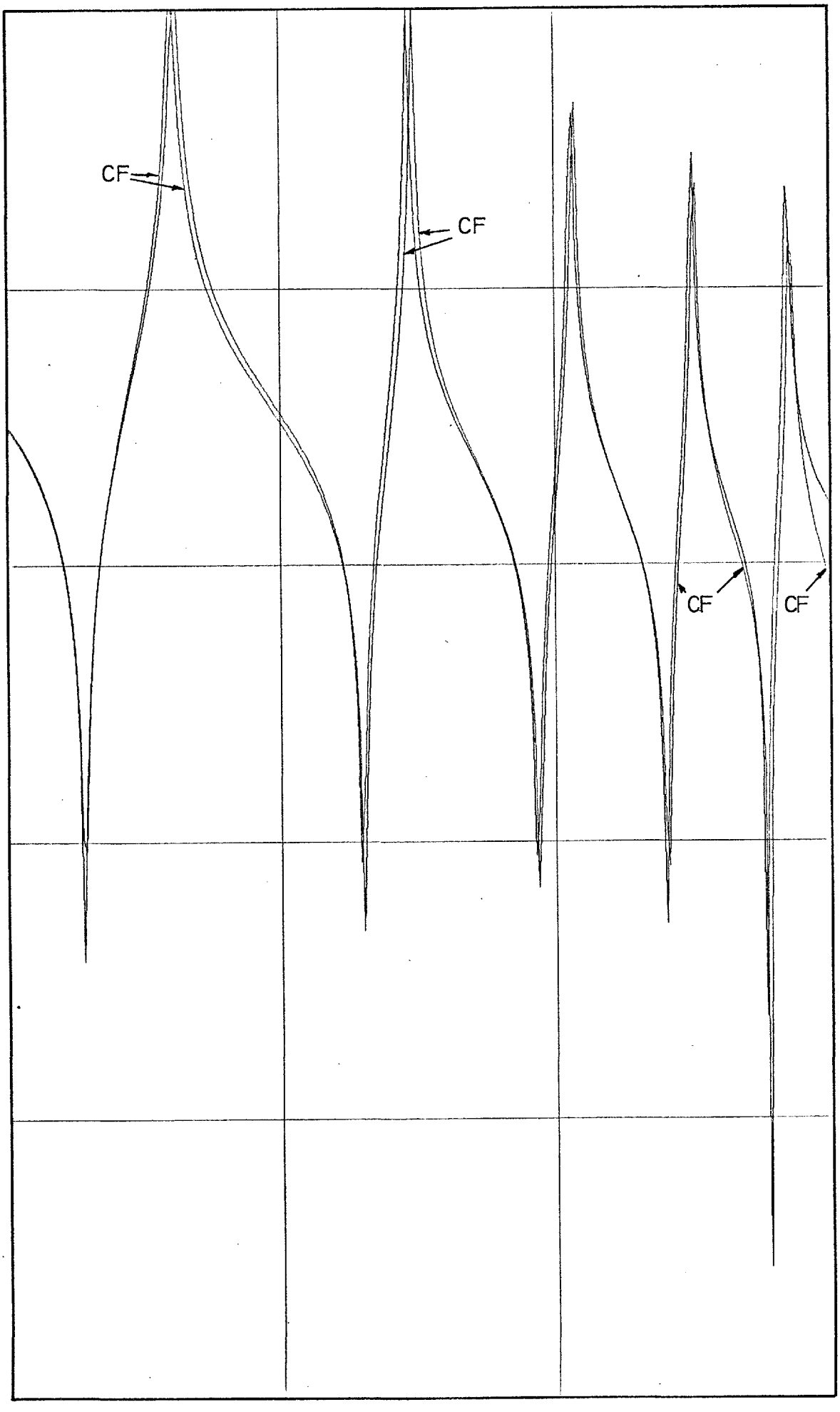


Figure 3.3.24

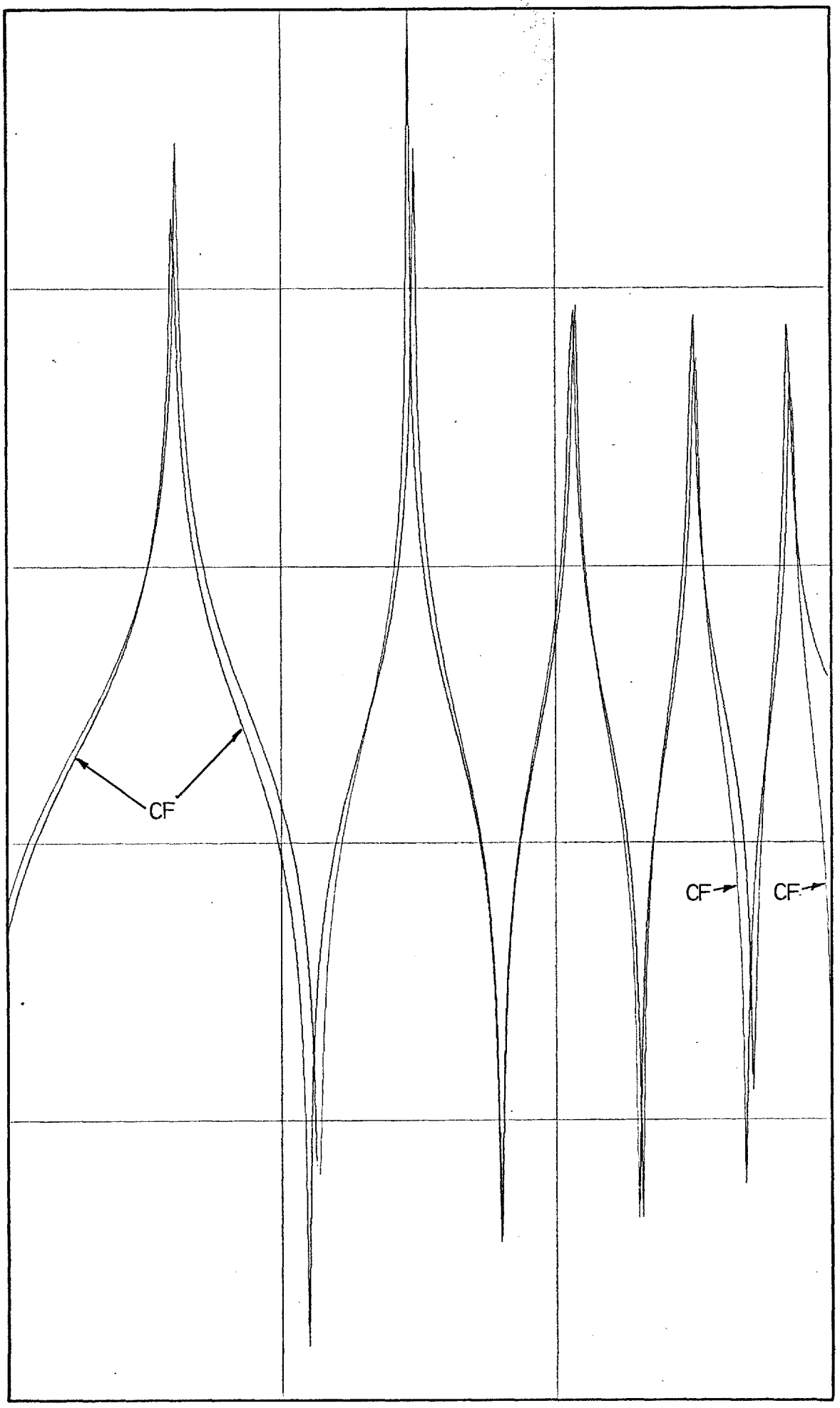


Figure 3.3.25

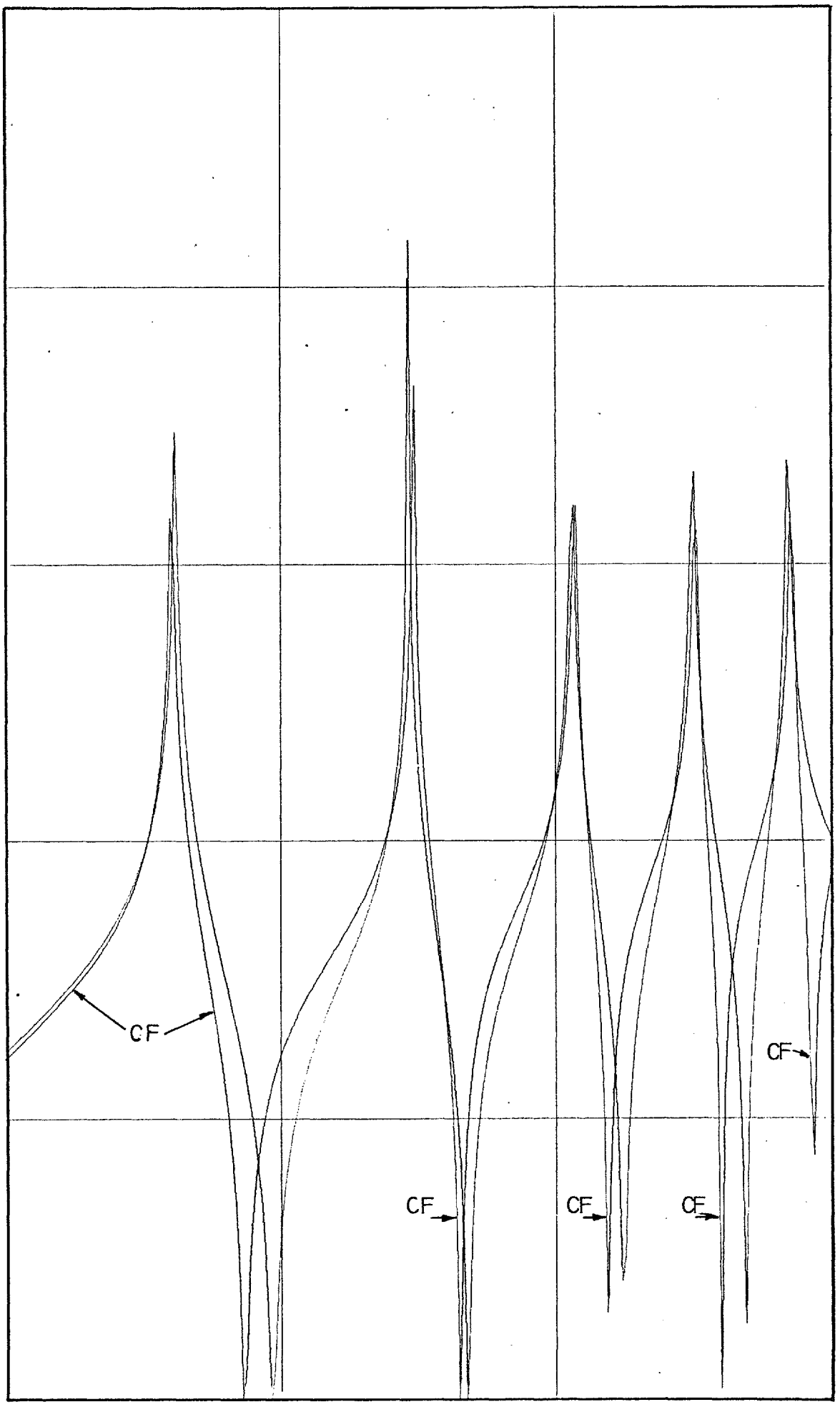


Figure 3.3.26

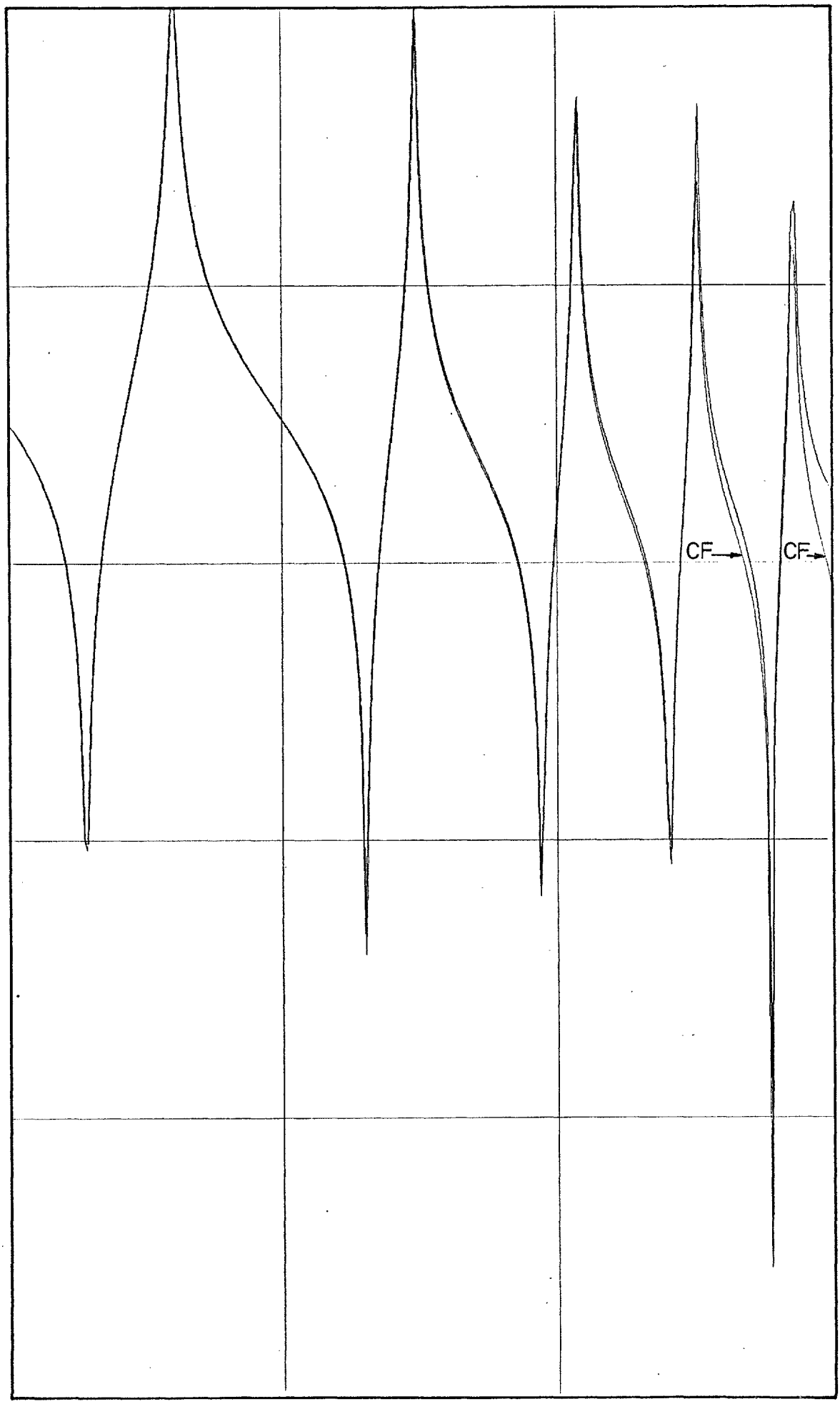


Figure 3.3.27

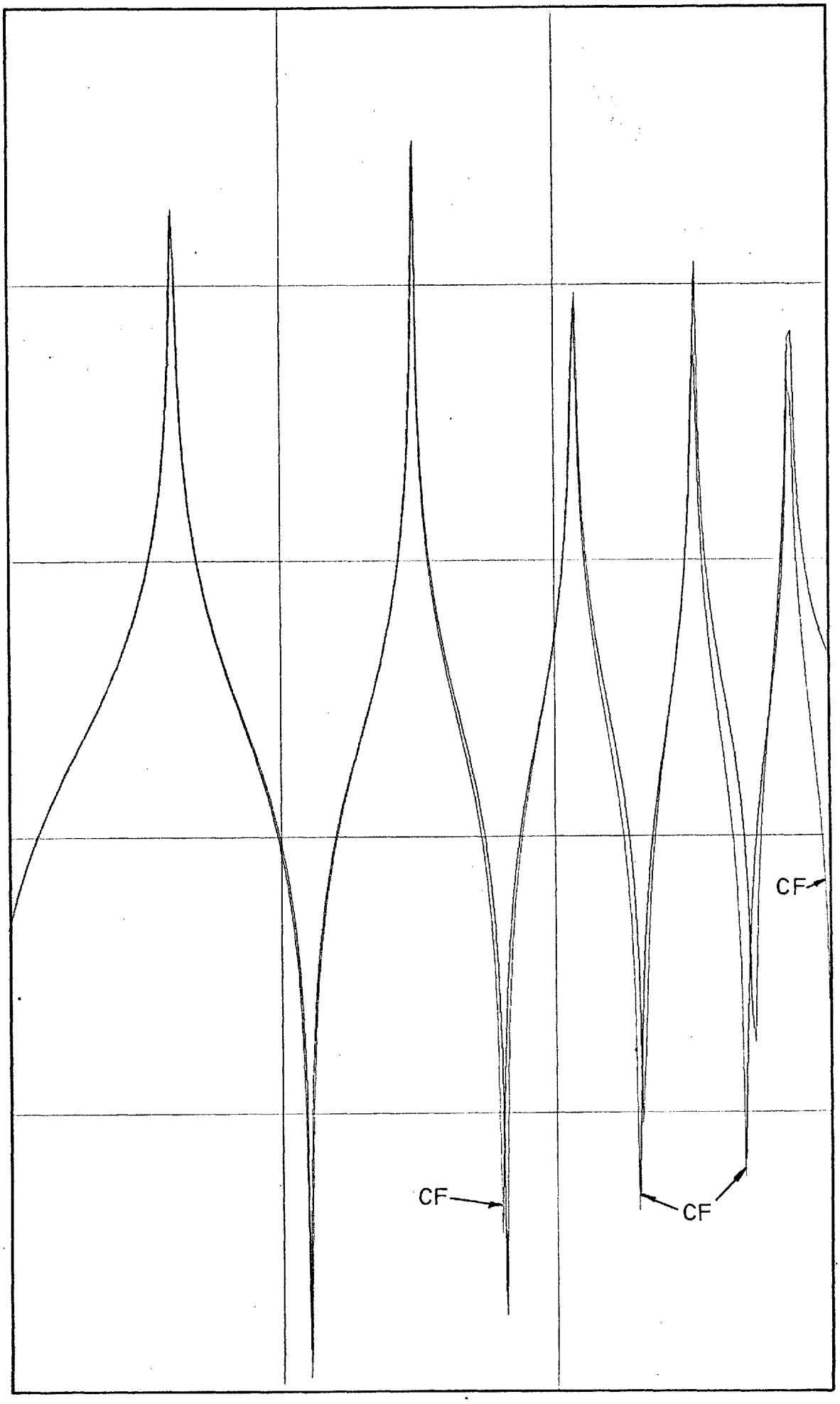


Figure 3.3.28

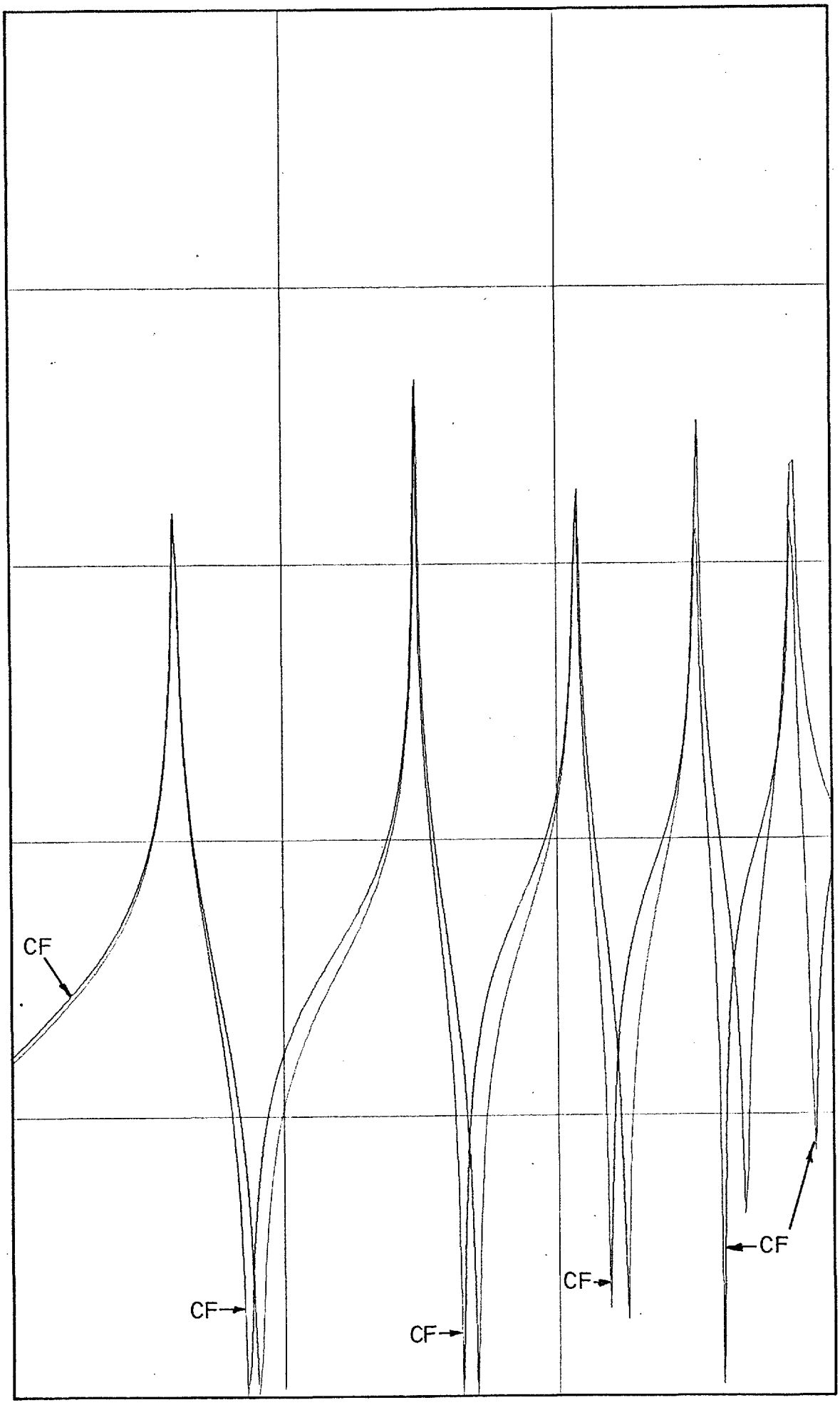


Figure 3.3.29

The representation of the 1-1 point and 1-2 point mobilities is seen to be markedly improved, but the 2-2 point mobility appears to have slightly increased error. Table 3.3.4 compares the errors in coupling factors and the ensuing errors in the effective modal masses.

These errors might be considered with those in Tables 3.3.1 and 2. The size of the errors for the 1-1 point mobility is about 3 x the error in the frequency measurements. For the 1-2 point mobility, the errors are about the same size as the experimental errors, whilst the 2-2 point mobility predictions are subject to up to twice the errors of the 1-2 point mobility measurements. The frequency measurements are subject to less error than the mobility measurements - this is probably true in most cases. It should be noted that the accuracy of the model depends on all the measurements - one wrong measurement will affect the calculated coupling factors for all the modes.

The model shows generally very good agreement with the closed term solution (which is itself liable to error if the physical constants are not exact), and the prediction of the rotational point mobility has been established. The series solution is short (six terms) but compares well with a twenty term model used by Neubert (156).

Mode	Coupling factors ($m_i = 1$)						Errors in effective modal mass		
	1 - direction			2 - direction			1 - 1	1 - 2	2 - 2
	Theory	Exp.	% Change	Theory	Exp.	% Change	% heavy (+) or light (-)		
0	16.0613	16.0656	- .0268	.419198	.422333	+ .675	+ .0536	- 0.648	- 1.35
1	16.0680	16.5847	+ 3.21	1.31002	1.46536	+ 11.9	- 6.42	- 15.11	- 23.8
2	16.1529	15.8652	- 1.78	2.26284	2.09071	- 7.62	+ 3.56	+ 9.4	+ 15.24
3	16.3428	16.2338	- .668	3.28881	3.25792	- 0.94	+ 1.34	+ 1.61	+ 1.88
4	17.1347	16.7977	- 1.98	4.66765	4.56496	- 2.2	+ 3.96	+ 4.18	+ 4.4
5	19.1017	18.5943	- 2.65	6.66324	5.89126	- 11.58	+ 5.30	+ 14.23	+ 23.16

Table 3.3.4

3.4 RANDOM VIBRATION

The following brief notes refer to the role of random vibration theory in the present context of vibration transmission and isolation. It is not intended to form a complete review of the subject.

3.4.1 Frequency Response

When the system is deterministically described, but the excitation is random in nature, then certain basic results are readily obtained, given for example by Crandall (128). Given a linear system, with a complex frequency response $H(\omega)$, and an excitation $f(t)$ leading to a response $x(t)$, an important result is:

$$S_x(\omega) = |H(\omega)|^2 S_f(\omega)$$

where $S_x(\omega)$ is the spectral density of the response
and $S_f(\omega)$ is the spectral density of the excitation

From the point of view of isolation theory, an input is presupposed, and the form of $S_f(\omega)$ is, ideally, known. The theory becomes concerned with the nature of $H(\omega)$ to give a satisfactory response. As such, the study of the frequency response $H(\omega)$ may be continued, without the application of further statistical theory to lead to a satisfactory vibration isolation solution.

3.4.2 Statistical Energy Methods

For highly complex structures, a deterministic description is likely to fail, or become impractical to use. This state occurs when the modal density of the structure is so great that the average spacing between the structure's modes is less than the modes' bandwidths, for example. Statistical energy methods refer to those methods applied when the system, as well as the vibration, is statistically described. Wilson, in 1909, showed that analogies exist between statistical properties of a system and the elementary thermodynamics of a gas, though no engineering results were obtained. In the last decade, a substantial body of theory has been evolved, mainly by workers at Bolt, Beranek and Newman, Inc., (96—118). The advantage of the method is that complex vibration problems (mainly cases like jet noise excitation) can be treated by much simpler energy balances.

Some of the basic points are outlined here, presented recently in a summarising paper by Ungar (118), and refer to the cases of the two coupled modes, and two sets of coupled modes.

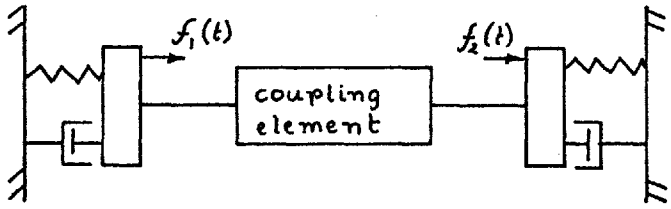


Figure 3.4.1

Figure 3.4.1 shows the model for two coupled modes, The theory leads to the conclusion that: "the steady-state time average power flow from one mode to another is proportional to their time average kinetic energies of the two modes provided that:

1. The coupling is linear, conservative and light, and purely springlike and/or gyroscopic; and

2. the forces acting on the two modes are uncorrelated and have relatively flat spectra (as compared with the system admittance spectra) within the frequency band encompassed by the resonances of the coupled systems".

Between two sets of coupled modes, the theory leads to the conclusion that: "the steady-state time average power flow from one set of modes to another is proportional (or approximately proportional) to the difference between the set and time-average modal kinetic energies of the two sets provided that:

1. The mode-to-mode coupling satisfies the conditions above, and

2. either a) the mode-to-mode coupling is (at least approximately) the same for all mode pairs

   or b) all the modes in a set have (at least approximately), equal time average kinetic energies".

This applies to statistically independent forcing on the two sets of oscillators - Fahy (100) deals with the case

where the modal forces are not independent. The energy approach leads to mean square results - this has been extended by Lyon (108) and Stearn (116) to estimate the likely variations about the mean, and the prediction of response concentrations in the structures.

Generally, the present usefullness of the theory is limited by the amount of information on coupling coefficients and damping (118) - non-linear coupling and more than two sets of modes can be included in the theory. Sound-structure coupling has been estimated in some cases, but structure-structure coupling has proved much more difficult.

In the range of problems considered in this work, the structures considered are sometimes complex. Nevertheless, the application of statistical energy methods would lead to only very approximate solutions. Very few of the conditions outlined above are satisfied even approximately. The number of modes in a car body, for instance, is quite large in the frequency range of interest - but satisfactory modelling has been achieved from experimental data.

The body of theory called 'statistical energy methods' has been surveyed, but it has not been found suitable for the problems of concern here, although the qualitative descriptions can be of value.

3.5 OPTIMISATION TECHNIQUE

The method used in optimising a given dynamic model was to establish an objective function for the model in mathematical form, and minimising the error of the model's response from the objective by variation of the model's parameters. An example of the use of such a technique is given in the section on vibration cancelling paths, §§ 4.1.4, page 133.

If the response of a trial model is given by $\emptyset = \emptyset(\underline{x})$, and the objective response is $\emptyset^*(\underline{x})$, where $\underline{x}$ is a vector of independent parameters, then the objective is reached when $f(\underline{x}) = \sum(\emptyset^* - \emptyset)^2$ is a minimum or zero. If the number of parameters is sufficient, and they are allowed a free range of values, the objective can be reached. Normally, however, there will be constraints on the range of values of the parameters, and equations describing these constraints must be included. In this case, only a minimum of $f(\underline{x})$ will be found. A minimisation routine, due to Powell (164) was used for searching for the minimum. This does not require derivatives of the function, and is claimed to be efficient. An inbuilt function checks, once a minimum has been found, whether other minima exist by introducing large parameter variations and starting a new search. The minimum found depends ultimately on the equations of constraint - these are given for the particular cases discussed.

3.6 SUMMARY OF COMPUTER PROGRAMMES

A variety of computer programmes was developed to deal with the computational work associated with the methods described in this chapter. Only the principal routines are outlined here - these have undergone a development period and are made as general as possible. Many other minor routines were written for a variety of other calculations.

Programme 014C

This programme solves the matrix equations for a system by the matrix inversion method outlined in §§ 3.1.3, page 56 . It features adjustable and self-adjusting input - output routines and eight basic options for normal usage, including an accuracy checking option. Associated subroutines provide for setting up the system matrices from the system parameters, and for producing mobility matrices. Standard routine used was a matrix inversion routine.

Programme 016

This is similar in performance to the above routine, but uses the state-vector approach, §§ 3.1.4, page 57 , producing eigenvalues and eigenvectors. Standard routine used - eigenvalues and eigenvectors of a real matrix, produced by W. N. Caldwell from SHARE programmes.

Both of the above programmes have been used in conjunction with subroutine VA04A (minimisation of a function of several variables), to form optimising versions.

Programme MODAL

This programme produces the parameters for a modal equivalent system, as described in §§ 3.3.3, page 91 , from experimental input data, and subsequently produces mobility values (or complete matrix) over the required frequency range to complete the data and provide an output check.

CHAPTER FOUR

SPECIAL ASPECTS OF VIBRATION TRANSMISSION

The emphasis throughout the present work is on path control. The effectiveness of any vibration path in amplifying or reducing vibration depends on the characteristics of the source and receiver as well as the properties of the path itself. If these characteristics are known or assumed, then the path performances can be calculated as was shown in Chapter 2. This chapter deals with the properties of the paths from theoretical and practical viewpoints. It discusses how path properties may be measured and describes experimental apparatus built for this purpose, and includes experimental results.

4.1 THEORETICAL BEHAVIOUR OF PATHS

The general formulations for path effectiveness have been given earlier. This section briefly summarises some typical paths and extends path behaviour to the more complex case of two-paths. Transmissibility is used as a simple guide to the path properties for comparison.

4.1.1 Single Stage Compliance

When a massless compliant element is effective as an isolator, the effectiveness depends on its mobility. The essential requirement is then the maximum mobility of element, which is decreased by damping. If the source and receiver are undamped, then damping of the compliant element is necessary to limit the amplification in the frequency range where the compliant element is ineffective, as was shown in Chapter 2.

The general requirement for a suitable stage compliance, taking into account the practical behaviour of real systems, is that the stiffness does not increase with frequency and the loss-factor does not increase indefinitely with frequency.

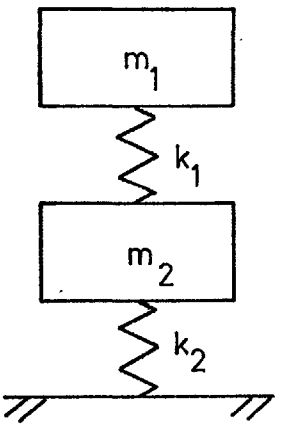
Considering rubber-like materials for the compliant elements Snowdon (26) has shown that natural and butyl rubbers most closely satisfy the requirements. Most high damping rubbers usually exhibit a substantial increase in stiffness with frequency. Snowdon (92) has also analysed a parallel mounting, where natural rubber and a high damping rubber are employed, to give good creep resistance, moderate loss factor and a compromise in the frequency dependent properties.

A useful reference slope on the transmissibility curves is given by the undamped spring with constant stiffness - 12 dB/octave at high frequency. A loss factor of unity

independent of frequency increases the transmissibility by 3 dB, but the slope of the line remains at 12 dB/octave.

4.1.2 Two- and Multi-Stage Mounts

In the transmissibility form, the two-stage (or compound) mount appears as shown below:



This has been dealt with fairly extensively in the literature, and optimum design parameters are known. The final slope on the transmissibility curve is 24 dB/octave for the undamped case - double that of the simple mounting - but two resonances occur. The optimum condition for a given amount of secondary mass, m_2, is for the ratio of the two resonant frequencies, ω_2/ω_1, to be as small as possible.

Snowdon (26), for example, shows that the optimum stiffness ratio is

$$\frac{k_2}{k_1} = \theta = 1 + \beta$$

where β is the mass ratio m_2/m_1. The ratio of the resonant frequencies is then given by:

$$\frac{\omega_2}{\omega_1} = \left\{ \frac{(1+\beta) + \sqrt{(1+\beta)}}{(1+\beta) - \sqrt{(1+\beta)}} \right\}^{1/2}$$

When β is small, then a ratio $\Theta = 1$ gives nearly optimum conditions, but β should be made as large as possible to make the ratio ω_2/ω_1 small.

From Chapter 2 it can be seen that an alternative derivation of the optimum mobility (or stiffness) ratio is given by:

$$r_{opt} = \frac{1}{2}\left(1 + \frac{M_R - M_S}{M_I}\right)$$

where $r = \frac{M_{I1}}{M_I}$, $1 - r = \frac{M_{I2}}{M_I}$

$$M_I = M_{I1} + M_{I2}$$

$$\text{i.e. } \Theta = \frac{r}{1-r}$$

Which shows that if $|M_I| >> |M_R - M_S|$, when good isolation is achieved, $r_{opt} \approx \frac{1}{2}$, hence $\Theta \approx 1$. Thus this approach leads to almost the same condition as in the former case, but is more general in application.

The multi-stage mount can then be envisaged as a further compounding of the simple mount, leading to n resonances for an n-stage mount, with a final attenuation of 12 n dB/octave. The increase in spread of the additional resonances would tend to make such a mount unlikely to be useful, however.

4.1.3 Wave Effects

The continuum model of a real compliant element forms in effect a multi-stage mount where $n \rightarrow \infty$. The effect of distributed mass in the element leads to resonances (or wave effects) which can only be controlled by damping directly on (or in) the compliant element. Wave effects have been considered by several workers (30, 36, 141, 142, 181), and are discussed more fully later in the chapter. The effect of the resonances is to increase the transmissibility, until high order resonances occur which are damped out along the element. Three main regions may be distinguished:

1. Wavelength of the vibration transmitted through the compliant element is much greater than the length of the element: the compliant element functions as a massless spring.

2. Wavelength the same order as the element length – region of low-order resonances and increased transmissibility.

3. Wavelength much less than the length of the compliant element - high order resonances - the vibration now attenuated as it passes through the compliant element, depending on the damping of the material. Leads to a very steep final transmissibility slope.

Practical mounts should avoid region 2, and region 3 generally implies very long compliant elements or very high frequencies. Design in general should be for region 1. In the case of rubber springs this implies that the transmission path should be very short.

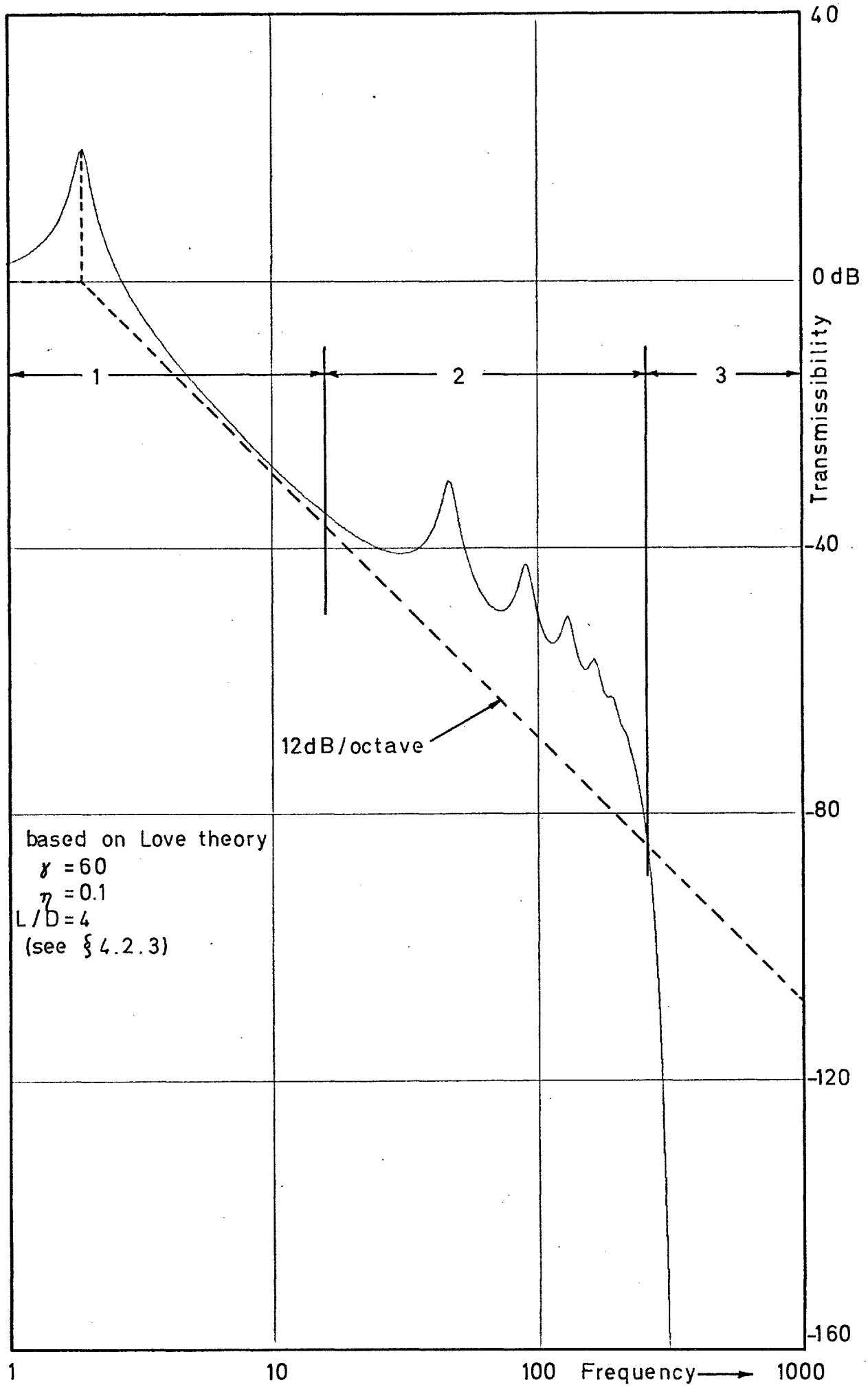
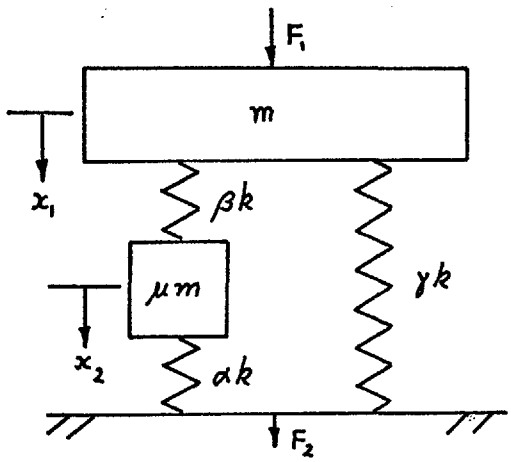

40
0 dB
-40
-80
-120
-160
Transmissibility
1
2
3
12dB/octave
based on Love theory
γ = 60
η = 0.1
L/D = 4
(see § 4.2.3)
1
10
100
Frequency
1000

Figure 4.1.1

Figure 4.1.1. shows diagramatically the significance of wave effects on transmissibility.

4.1.4 Multi-Path Mounts and Cancellation

Where more than one path exists between the source and receiver, possibilities exist for cancellation of vibrational forces at the receiver end. The process might also be considered as the destructive interference of waves travelling along the paths. Sykes (175) has referred to a two-path system exhibiting this effect, implying the model shown below:



The cancellation condition occurs at one frequency only, when the forces due to αk and γk are equal and opposite:

$$\text{i.e.} \quad F_2 = \alpha k x_2 + \gamma k x_1 = 0 \qquad 4.1.1$$

The cancellation frequency ω is given by

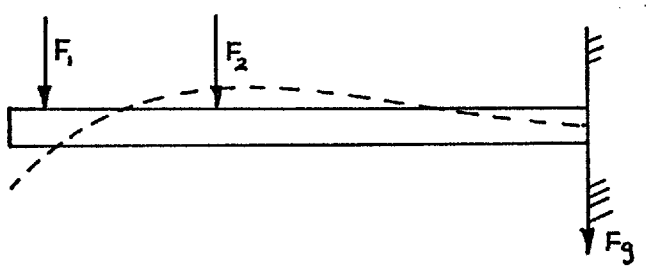
$$\omega^2 = \frac{(\alpha\beta + \beta\gamma + \gamma\alpha)}{\gamma\mu} \omega^{*2} \qquad 4.1.2$$

$$\text{where} \quad \omega^{*2} = \sqrt{k/m} \qquad 4.1.3$$

The system can be seen to degenerate to a tuned dynamic absorber attached to the source ($\alpha = 0$) or to the

base (β = 0) and consequently does not reveal the benefits of cancellation when the system is damped.

Snowdon (92) has considered an alternative aspect - splitting the source into two parts and applying to different parts of one path, such as a cantilever beam. The diagram below shows two forces F_1 and F_2 acting on the beam in the correct proportion and position such that the second mode of the beam (shown dotted) in cancelled.

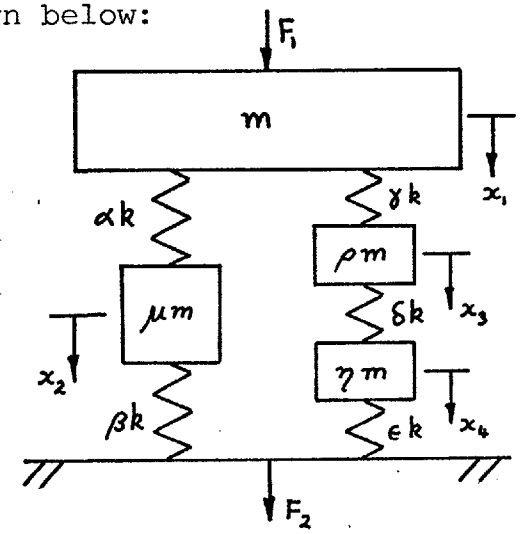


By this means, cancellation of one mode of the beam is achieved, but not a complete zero of transmissibility unless the beam is undamped, though a minimum occurs between the third and fourth modes. The beam modes are analogous to the wave effects discuseed previously, and this technique takes advantage of their properties. The practical application of these forces remains a problem, however, as was seen in Chapter 3.

Cancellation, complete or partial, has been observed in the models of the suspension system (Chapter 5), with rubber tubes (§ 4.4.2), and apparently in tyres (160). In general, it might be stated that any multiple path system might have a zero (or zeros) of transmissibility, regardless of the amount of damping in the paths, provided certain conditions are fulfilled.

The section following describes a lumped parameter model which produces a zero of transmissibility, and discusses the capabilities and limitations involved.

Three masses and two paths are required to produce cancellation conditions when the springs are damped. Initially the system will be considered in the undamped state, shown below:



$$\omega^{*2} = k/m$$

The requirement is that

$$F_2 = \beta k x_2 + \epsilon k x_4 = 0 \qquad 4.1.4$$

and the cancellation frequencies, $\omega_{1,2}$ are obtained from the roots of the frequency equation:

$$\alpha\beta\rho\eta\,\omega^4 - \{\alpha\beta[\eta(\gamma+\delta) + \rho(\delta+\epsilon)] + \gamma\delta\epsilon\mu\}\,\omega^{*2}\omega^2 + \{\alpha\beta[(\gamma+\delta)(\delta+\epsilon) - \delta^2] + \gamma\delta\epsilon(\alpha+\beta)\}\,\omega^{*4} = 0 \qquad 4.1.5$$

This is of the form $ax^2 + bx + c = 0$ which has two real roots provided $b^2 - 4ac > 0$.

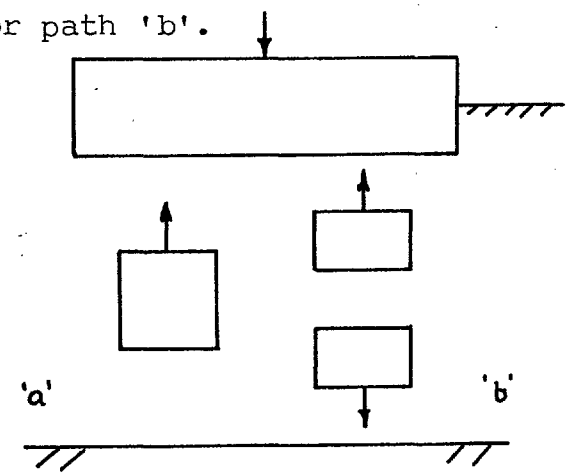
This system may degenerate to one having two dynamic absorbers, attached to the source and receiver ($\delta = 0$), giving:

$$\omega^2 = \frac{\gamma}{\rho}\,\omega^{*2} \quad \text{and} \quad \frac{\epsilon}{\eta}\,\omega^{*2}$$

or in any of several other ways.

For the complete model both cancellation frequencies will not be realised, however, as the higher frequency turns out to be anti-resonant (so that the transmissibility becomes indeterminate). This higher frequency might be designated a blocking frequency.

Parameters may be derived by the following simplification. The mounted mass is assumed stationary, and the resonant frequencies of the two paths are made equal - the second mode for path 'b'.



The requirement is then that

$$\left.\begin{aligned} \alpha k x_2 + \gamma k x_3 &= F_1 \\ \beta k x_2 + \epsilon k x_4 &= F_2 = 0 \end{aligned}\right\}$$

Then, if ω_2 is the resonant frequency, and the following simplifications are made in the parameters:

$$\alpha = \beta \qquad \gamma = \delta = \epsilon \qquad \eta = \rho$$

the blocking frequency ω_2 is given by

$$\omega_2^2 = \frac{2\alpha}{\mu}\omega^{*2} = \frac{3\delta}{\rho}\omega^{*2} \qquad 4.1.6$$

$$\therefore \alpha = \frac{3}{2}\frac{\mu}{\rho}\delta \qquad 4.1.7$$

Before extending the model to the damped case, a numerical example is given to show the type of transmissibility curve of such an undamped transmission path. This is shown from a range of such models analysed.

The system parameters are:

$$\alpha = \beta = 3/8$$

$$\gamma = \delta = \epsilon = 1$$

$$\mu = 1/8$$

$$\eta = \rho = 1/2$$

so that equation 4.1.5 becomes

$$9\omega^4 - 104\,\omega^{*2}\omega^2 + 300\,\omega^{*4} = 0$$

$$\therefore \omega_{1,2}^2 = \left[\frac{104 \pm 4}{18}\right]\omega^{*2}$$

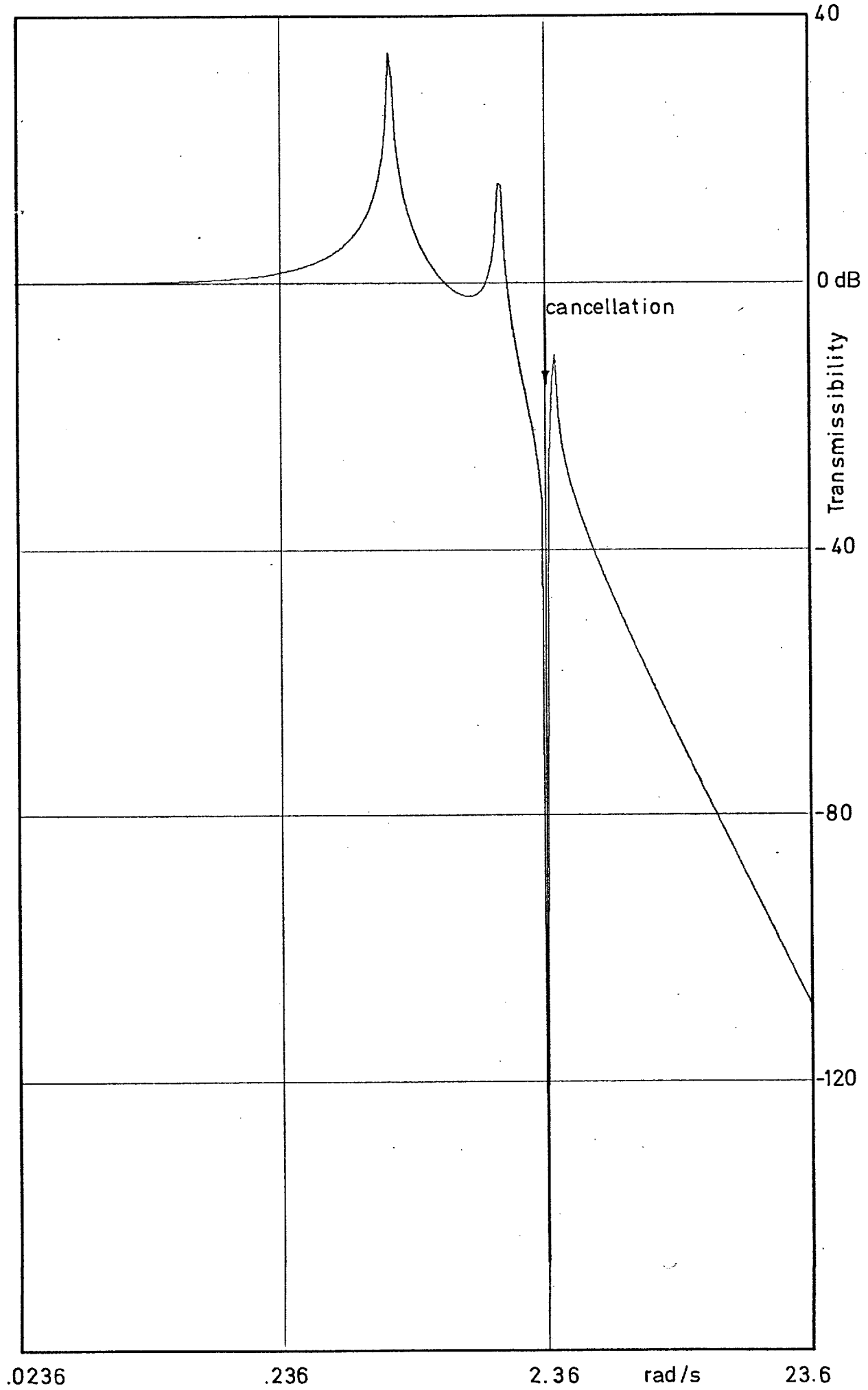
$$i.e. \quad \omega_{1,2} = 2.358 \text{ and } 2.449 \text{ rad/s} \quad \text{with } \omega^{*2} = 1 \text{ rad/s}$$

The parameters were chosen to satisfy equation 4.1.7, so the blocking frequency, from equation 4.1.6 is

$$\omega_2 = \sqrt{\frac{36}{\rho}}\,\omega^{*2} = \sqrt{6} = 2.449 \text{ rad/s}$$

Thus the vibration cancellation frequency occurs at a frequency of 2.358 rad/s. The complete transmissibility curve is shown in Figure 4.1.2.

This cancellation condition should be distinguished from the troughs usually experienced in transfer mobility curves for systems, mounts using nodal lines at the forcing point and dynamic absorbers. In these cases, the trough depth is determined by the lack of damping. The model shown above can be heavily damped whilst still exhibiting the



TRANSMISSIBILITY S7

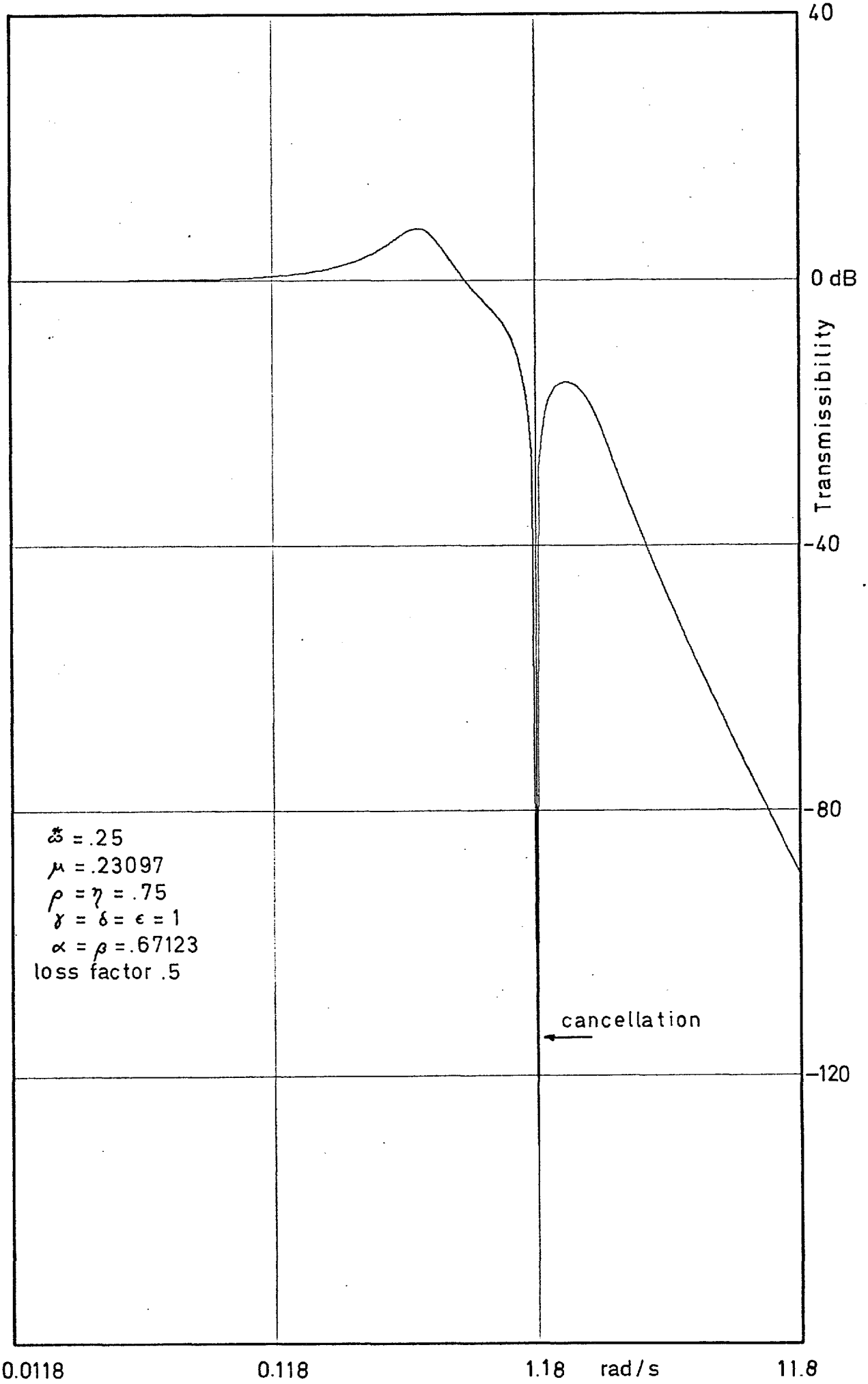
Figure 4.1.2

cancellation condition.

If hysteretic damping is included for each of the springs (i.e. $k \rightarrow k\ (1 + i\eta)$) the equations of motion become more complex and it is difficult to derive suitable parameters by inspection. Furthermore, the parameters do not form real variables as they are restricted to a certain range of positive values. Consequently, in order to derive the parameters, the cancellation condition was set up as a minimisation problem. With certain simplifications (and so leading to a restricted class of models) the number of parameters required to be free to vary is two. An example of this approach is now shown.

The mounted mass and the two-mass path are taken as fixed, and all the springs are made to have a loss-factor of 0.5. The mass and spring stiffnesses in the one-mass path are free to vary, but the spring stiffnesses are equal. That is, μ and $\alpha = \beta$ are the free parameters. The function to be minimised is the transmissibility at the required cancellation frequency, i.e. $|T|\ \omega_1$. The fixed path provides a constraint on the lowest resonant frequency of the system.

Figure 4.1.3 shows an example of a transmissibility curve produced from the minimisation programme. The cancellation frequency is achieved at about three times the fundamental frequency and a generally efficient overall transmissibility curve is obtained. The high frequency attentuation is somewhat better than 24 dB/octave of the two-stage mount, showing that partial cancellation is achieved



TRANS MODEL 20V

Figure 4.1.3

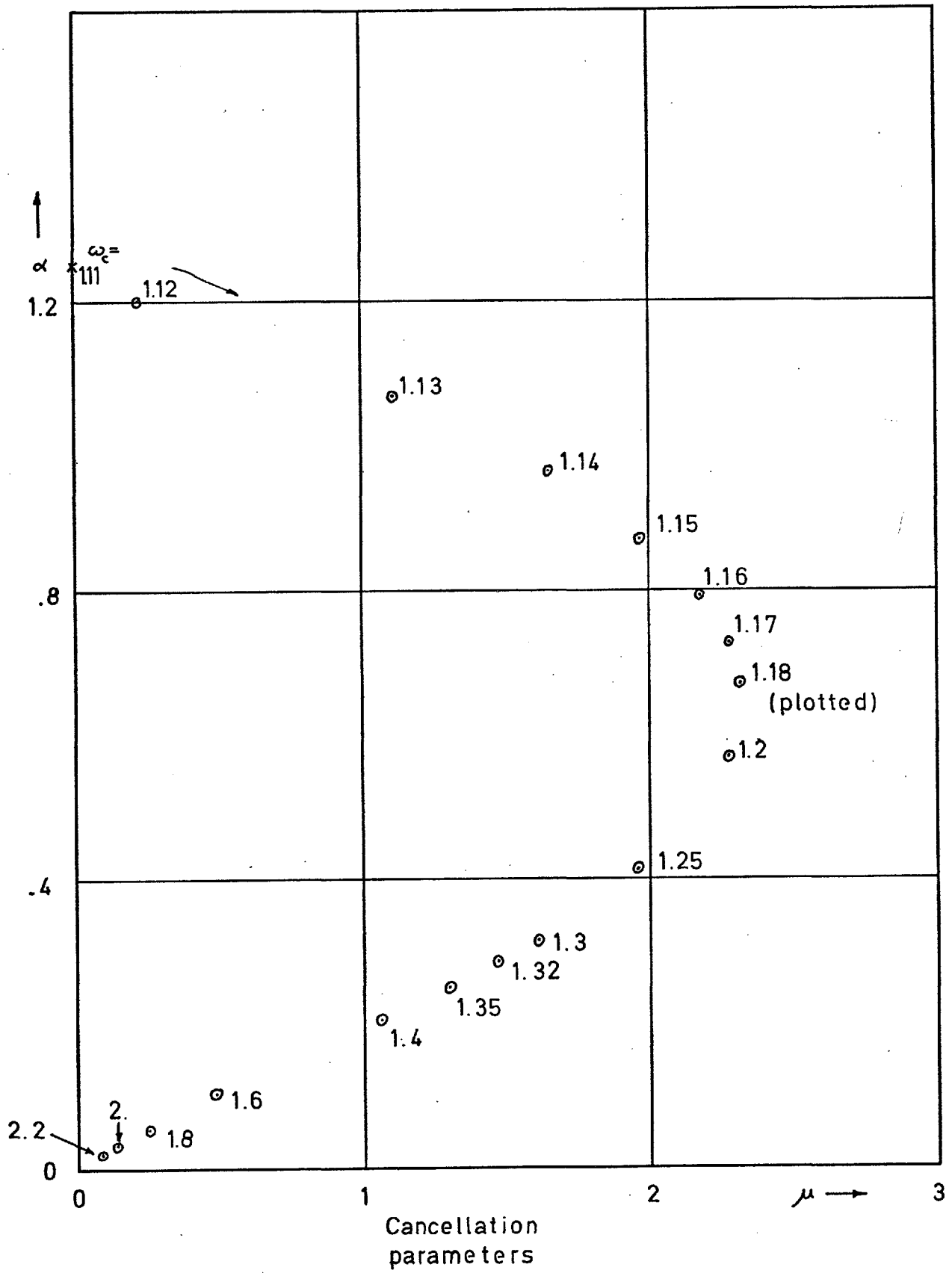

α
ω_c=
1.11
1.12
1.2
1.13
1.14
1.15
1.16
.8
1.17
1.18
(plotted)
1.2
1.25
.4
1.3
1.32
1.35
1.4
1.6
2.
1.8
2.2
0
0
1
2
μ
3
Cancellation
parameters

Figure 4.1.4

in this range also. The low-frequency response also compares well with the single-stage mounting. The cancellation region is, however, very narrow.

Figure 4.1.4 shows the range of permissible values for α and μ, and the range of possible cancellation frequencies, for this model. Cancellation depends quite critically on the precision of the parameter values, though the figure makes it clear that if maximum mass is used, the sensitivity to stiffness variations is a minimum.

Such a model can then be thought of as a notch-filter, and in theory a series of such units can lead to a succession of cancellation frequencies - though such a series would lower the fundamental resonance and thus make all the cancellation frequencies relatively higher.

The limitation of the model is that the final attenuation obtained depends mainly on the strongest path - in this case the one-mass path. A better final attenuation slope could be obtained at high frequencies if this path were to be removed, giving a slope of 36 dB/octave.

4.2 TEST METHODS

In this section some experimental methods are outlined for the determination of the dynamic properties of rubberlike materials and isolation mounts. A large number of methods have been established to measure the dynamic properties from less than 0.1 Hz to more than 120 kHz, and over a large frequency range. Prior to a description of the apparatus used, the theoretical basis behind the methods is outlined.

Results from a number of experiments have been pre sented by Snowdon (92) using the method of reduced variables.

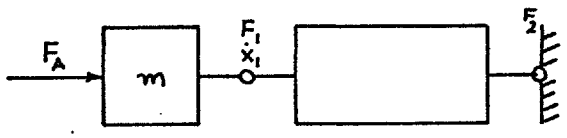
4.2.1 Theoretical Aspects

The dynamic modulus and loss factor are the desired properties for the rubberlike materials, whilst for practical isolation mounts the stiffness rather than the dynamic modulus is required. It is evident that an impedance or transfer type test is needed, rather than a mobility test, to show up these properties. Wave propagation is another form.

1. In most test methods, the specimen or isolation mount is treated as a two-terminal 'black box' although certain prior assumptions are made about its properties. Four main sections summarise the type of test performed on this system.

a. Mass fixed to terminal 1, terminal 2 blocked

The system is shown symbolically below



The test methods are:

(i) Free decay. Initial displacement x_1 given and then x_1 observed as a function of time. The system is assumed purely springlike (or has 1/3 of its mass added to m). The loss-factor of the system needs to be fairly small (< 0.2) to enable an accurate determination. Measures the properties at discrete frequency intervals only.

(ii) Resonant vibration. The dynamic stiffness F_A/x_1 is measured over the resonant frequency range. This permits the properties to be measured at constant x_1 to show strain effects.

(iii) Transmissibility. Measuring F_2/F_A enables properties to be obtained at the resonant frequency and at high frequencies continuously below the wave-effect frequencies of the specimen. This method is equivalent to that shown below in c.

General limitations: The rigid end condition is difficult to achieve satisfactorily when the specimen is very stiff and/or very high frequencies are involved. When large static loads are required, or m is very large, the added mass may no longer be sufficiently rigid.

b. Impedance test

The system is shown symbolically below:



If the mass of the specimen is negligible (below wave effects), then $F_1 \approx F_2$. The choice of measuring direct or transfer impedance is then available.

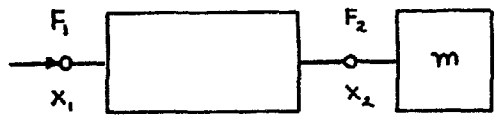
(i) Direct Impedance, $F_1/\dot{x}_1$. This will give the properties continuously as a function of frequency. However, in practice, a certain amount of mass inevitably lies between the force gauge and specimen. Whilst mass cancellation may be employed, at high frequency the impedance of the mass can become greater than that of the specimen, and the correction becomes ill-conditioned.

(ii) Transfer Impedance, $F_2/\dot{x}_1$. This can provide a more reliable force guide as no mass cancellation is required, provided the test frequency is small enough.

(iii) Tests (i) and (ii) together give complete information for a symmetrical specimen (for a non-symmetrical specimen tests (i) and (ii) should be repeated with the specimen reversed) - the previous assumptions can serve to simplify the procedure.

(iv) From the resonances of the specimen, the loss factor and stiffness of the specimen can be obtained at discrete frequencies.

c. Mass placed on terminal 2



This gives the usual form of transmissibility test.

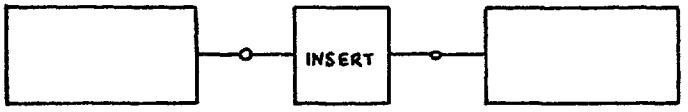
(i) Low frequency resonance: ratio x_2/x_1 gives stiffness and loss factor at resonant frequency.

(ii) High frequency, but no wave effects: the mass moves much less than x_1, and approximates to fixed end. Acceleration $\ddot{x}_2$ leads to the force F_2. Use of $\dot{x}_1$ and $\dot{x}_2$ leads to the transfer impedance.

(iii) With wave effects: when x_2 is small test becomes one as in b.(iv); when x_2 is appreciable, modelling the response can also lead to material properties at discrete frequencies.

The use of mass as an approximation to a fixed end has certain advantages over a frame designed to provide such a fixed end, because resonances can be avoided more easily.

d. Insert to a system



Change in the system due to the insertion of the specimen leads to specimen properties.

2. More completely, when coupling can exist within a path, the specimen should be treated as a multi-terminal box. The previously described tests can be extended to deal

with the more complex system, though in practice this is likely to be difficult.

With knowledge of the material properties and the form of the specimen, it is probably better to calculate the complete system matrix, with simplifications to reduce the coupling considered.

Thus, for a straight elastic bar, the complete transfer matrix can be produced from four low-order sub-matrices as shown below (162).

$$\begin{pmatrix} S_1 \\ S_2 \\ S_3 \\ S_4 \end{pmatrix}_i = \begin{bmatrix} A & 0 & 0 & 0 \\ 0 & B & 0 & 0 \\ 0 & 0 & C & 0 \\ 0 & 0 & 0 & D \end{bmatrix} \begin{pmatrix} S_1 \\ S_2 \\ S_3 \\ S_4 \end{pmatrix}_{i+1}$$

where

A, B are 2 x 2 matrices

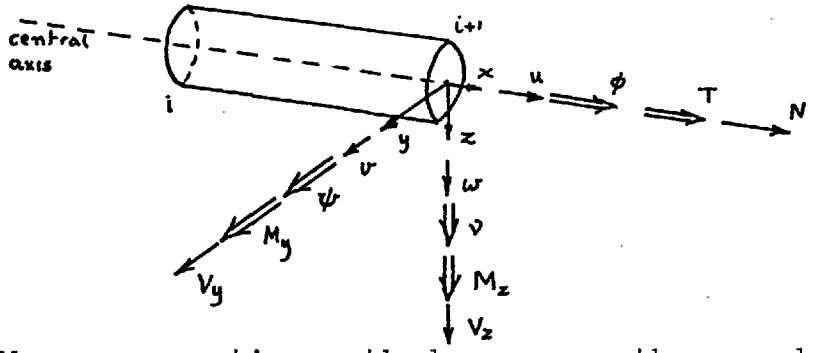
C, D are 4 x 4 matrices

0 is a null matrix

and S_1 is the vector (u, N), S_2 is (ϕ, T)

S_3 is $(v, \nu, M_z, -V_y)$ and S_4 is $(-w, \psi, M_y, V_z)$

with the coordinates, forces, moments and deflections defined in the diagram below:



3. Wave propagation methods measure the speed and decay of waves through the specimen, which is made sufficiently long so that standing waves are not encountered. From these measurements the dynamic modulus and loss factor can be derived directly. In practice however, the detector for the waves can act as a reflector, and standing waves occur.

The test then becomes one like in b.(iv).

4.2.2 Practical Test Methods

Most practical test methods for the determination of the dynamic properties of rubber-like materials fall into one or other of the categories outlined in the previous section. Surveys of such methods have been given by Nolle (158), Gehman (138), Payne and Scott (161), Kainradl and Handler (145), Praefcke (165), and, for the particular case of high static loads, Newland (157).

A summarising table is given below to give the characteristics of examples of the principal methods, following the order of the previous section.

Apparatus was required to measure the material properties of rubber up to a frequency of 1 kHz. Furthermore, the effects of resonances were to be observed, and the apparatus was to be adaptable to a variety of specimen sizes and also accommodate complete isolation mounts. Motion in only one direction was required. This eliminates from the test methods available all except the impedance tests and the transmissibility tests. Lack of suitable impedance equipment (at the time of design) lead to a decision to use a transmissibility test as the most practical solution. Apparatus already available in the laboratory was limited to that developed by Praefcke (165) which was unsuitable from the frequency range available. Transmissibility

Type and Name	Frequency Range (Hz)	Static Constraints	Advantages	Limitations	Reference
1.a(i) Rocking beam oscillator	0.1 - - 25	elongation 5% to limit set by specimen	precise indication of temperature behaviour at nearly constant frequency	loss factor less than 0.2	Nolle (158)
1.a.(ii) Vibrating reed	10 - 500	none	study of low frequency stiffening	loss factor < 0.2 for accurate results	Nolle (158)
Compression	20 - 40	deadweight of applied mass	easy control of strain	Static load and frequency interdependent	Grootenhuis (140)
1.b.(i) Shear strain	10 - 300	arbitrary compression load	easy control of strain	material stiffness; mass cancellation at high frequencies	Grootenhuis (140)
1.b.(iii) Impedance	20 - 5k	up to 10,000 lbf static compression	Testing of complete isolation mounts	Frame stiffness Phase accuracy	Schloss (172)
1.b.(iv) Strip resonance	set by specimen, lower frequency by half-wavelength, higher frequency by attenuation	1 - 2% elongation	precise indication of temperature effect on modulus	loss factor < 0.2	Nolle (158)
Bar transmission	" "	2% compression	convenient	" "	Morris, James and Guyton (155)

Summary of Experimental Methods

Type and Name	Frequency Range (Hz)	Static Constraints	Advantages	Limitations	Reference
1.c.(i) Transmissibility	5 - 50	Deadweight of mounted mass	testing of practical isolation mounts	High frequency response limited	Praefcke (165)
	50 - 10k	"	wave effects shown and high frequency response	small specimens	Harrison, Sykes and Martin (142), Snowdon(26)
1.d Magnetostriction	12k - 120k	10% or more possible	no loss factor restriction, small sample, wide temperature range	Sample controlled so that resulting Q-factor of system >10. Frequency deviation small.	Nolle (158)
2. No complete test known					
3. strip transmission	1k - 40k	2% elongation	automatic operation continuous frequency coverage	Not suitable for very stiff materials. Possible flexural wave interference. Material attenuation must be less than 40dB/cm and more than 0.25dB/cm.	Nolle (158)

Summary of Experimental Methods (Contd.)

apparatus was designed, similar in scope to that used by Harrison, Sykes and Martin (142) and Snowdon (25) but adapted to the particular requirements outlined above. This apparatus is described later after the parameter derivation for this type of test is shown in the next section.

4.2.3 Parameter Derivation

The formulae and techniques for deriving the important parameters from transmissibility tests are shown here. For an existing mount, these parameters are stiffness and loss factor as a function of frequency, and the effects of distributed mass. For material properties, such as Young's modulus and shear modulus, the geometry of the specimen must be taken into account. The expressions given imply linearity - non-linear effects may be deduced to a certain extend by repeating tests at different amplitudes, static loads and so forth.

The section is divided into three main parts, with subdivisions:

1. Massless spring
   a. frequency independent properties
   b. frequency dependent properties
2. Appreciable mass in spring
   a. low frequency effects
   b. wave effects by Love and long-rod theories.
3. Geometrical factors for material properties.

1.a The system is shown in Figure 4.2.1 below. The spring is presumed to have a frequency independent loss factor η.

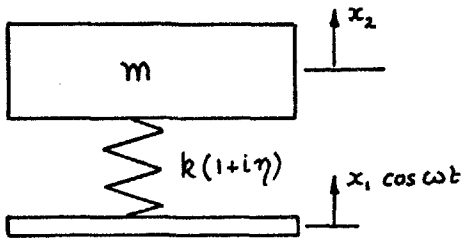


Figure 4.2.1

The transmissibility, T, for this case is given by the complex expression:

$$T = \frac{x_2}{x_1} = \frac{1 + i\eta}{1 - \Omega^2 + i\eta} \qquad \text{where} \quad \Omega = \omega/\omega_n, \quad \omega_n = \sqrt{k/m}$$

in modulus form this is:

$$|T| = \left\{ \frac{1 + \eta^2}{(1-\Omega^2)^2 + \eta^2} \right\}^{1/2}$$

If T_R denotes the real part of T, and T_I the imaginary part, then the equation for a circle can be derived, on the complex plane:

$$\left(T_I - \frac{1}{2\eta}\right)^2 + \left(T_R - \frac{1}{2}\right)^2 = \frac{1}{4}\left(1 + \frac{1}{\eta^2}\right)$$

This circle has a radius r given by:

$$r = \frac{1}{2}\sqrt{\left(1 + \frac{1}{\eta^2}\right)}$$

and the position of the centre is given by $\left(\frac{1}{2}, -\frac{1}{2\eta}\right)$

This circle is similar to the Kennedy-Pancu diagram,

but there are certain noticeable differences. The diagram is shown below in Figure 4.2.2 with the important quantities marked on. Note that there are four exact means by which η may be determined, and two approximate formulae - though only one determination of $\Omega = 1$ and thus stiffness.

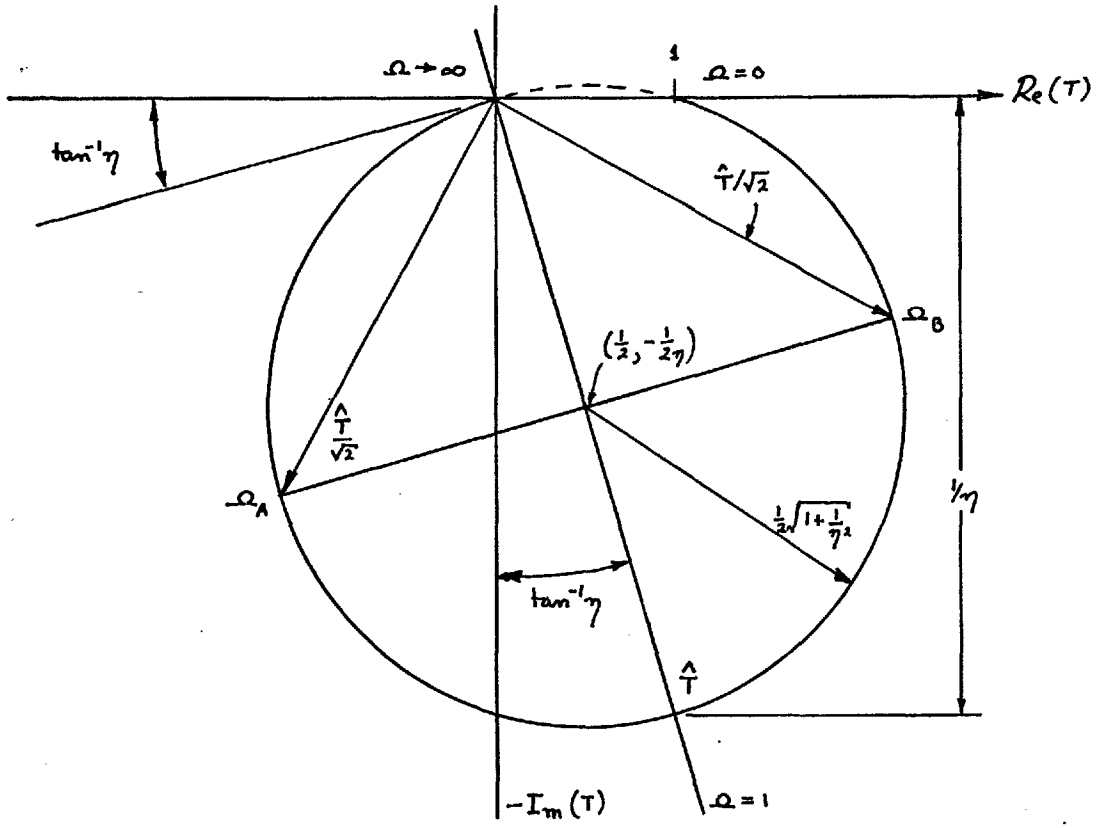


Figure 4.2.2

Exact formulae for η

$\eta = 1/T_I$ at $\Omega = 1$

$\eta = \tan(90 - \angle T)$ at $\Omega = 1$

$\eta = \tan(180 - \angle T)$ as $\Omega \to \infty$

$\eta = \frac{1}{2}(\Omega_A^2 - \Omega_B^2)$

Approximate formulae

$\eta \simeq 1/\hat{T}$ $\quad o(\epsilon) \sim \eta^2$

$\eta \simeq \Omega_A - \Omega_B$ $\quad o(\epsilon) \sim \eta^3$

The frequencies Ω_A and Ω_B correspond to the levels of transmissibility 3dB down from the peak transmissibility, and a Bode diagram can be used to give these.

1.b When the parameters in the system show appreciable frequency dependence, the transmissibility is given by

$$T = \frac{1 + i\eta_\omega}{1 - a\Omega^2 + i\eta_\omega}$$

where η_ω is the loss-factor as a function of frequency and a is the stiffness ratio, k_o/k_ω where k_o is the stiffness at $\Omega = 1$ and k_ω is the stiffness at frequency ω. To determine these functions, the high frequency attenuation slope and phase angle curves are used. The asymptotic condition is observed from the Bode diagrams of transmissibility.

Then, as $\Omega \to \infty$

$$T \approx \frac{-1}{a\Omega^2}(1 + i\eta_\omega)$$

The loss factor is determined by the phase angle, i.e.

$$\eta \simeq \tan(180 - \angle T)$$

whilst the combined stiffness ratio, k_ω/k_o is given by

$$\frac{1}{a}(1 + i\eta_\omega) = \frac{k_\omega}{k_o}(1 + i\eta_\omega) = -\Omega^2 T$$

In this way, the top mass behaves as a load cell and the bottom acceleration is used to give the spring displacement. In effect, the test becomes one of a dynamic modulus test - the motion imposed on terminal 1 of the spring, the force measured on terminal 2 (blocked). The direct stiffness is the same as the transfer stiffness as the mass of the spring is neglected.

2.a Where there is appreciable mass in the spring, this must be allowed for in the low-frequency calculations. Assuming that the spring deflects uniformly at the fundamental resonance, one third of the spring mass must be added

to the mounted mass for the calculation of stiffness from the frequence of the resonance. The high frequency behaviour shows an increase in the level of the transmissibility curve, and also wave effects.

2.b Resonances in the spring exhibit the phenomena usually referred to as wave effects, or surges in the case of coil springs. For homogeneous, uniform cross-section rods the Love theory and the long-rod theory (92) can be used to predict the effects.

The expression for the modulus of the transmissibility from the Love theory is:

$$T = 1/\{[cp.chq - \gamma(p.sp.chq - q.cp.shq)]^2 + [sp.shq + \gamma(p.cp.shq - q.sp.chq)]^2\}^{1/2}$$

where cp, sp, chp, shp imply the cos, sin, cosh, sinh of p, etc. The terms are given by:

$$p = [(\phi + \mu)/2]^{1/2}$$

$$q = [(\phi - \mu)/2]^{1/2}$$

$$\phi = [\mu^2 + \chi^2]^{1/2}$$

$$\mu = [P^2 - Q^2 - R^2(P^2+Q^2)]/\xi$$

$$\chi = 2PQ/\xi$$

$$\xi = [1 - 2R^2(P^2-Q^2) + R^4(P^2+Q^2)]$$

$$P = \eta L[(D_E+1)/2]^{1/2}/D_E$$

$$Q = \eta L[(D_E-1)/2]^{1/2}/D_E$$

$$D_E = (1+\eta^2)^{1/2}$$

$$R = D/(2\sqrt{2}) \quad \text{(round rod)}$$

$$\eta = fc$$

$$c = 2\pi\sqrt{\frac{\rho}{E}}$$

The input data required to specify the transmissibility are :

γ = mass ratio = mounted mass / spring mass

ρ = density of spring

L = length of spring

E = Young's Modulus of spring

η = loss factor of spring

D = Diameter of spring

f = frequency in Hz

The Love theory allows for the lateral expansion of the rod, but is not exact. The long-rod theory is a simplification, excluding the lateral expansion. Putting D = 0, the terms simplify to:

$$\left.\begin{aligned} p &= P \\ q &= Q \end{aligned}\right\}$$

the form of the transmissibility equation being exactly the same as for the Love theory.

To derive the system parameters, referring now to cylindrical rubber specimens in compression, the following procedure can be followed.

1. Obtain the transmissibility curve, including wave effects.

2. From the low-frequency resonance, obtain E_o using the shape factor (see below) and the loss factor η_o. The loss factor η_ω can be obtained at the higher resonant frequencies by the bandwidth method.

3. Use Love theory to predict transmissibility curve from obtained values. From position of resonant peaks, find the change in stiffness (if any) of the material and fit approximate laws to η_ω and E_ω.

4. Recalculate transmissibility curve with frequency dependent parameters and compare with the experimental curve.

Note that in this case, the properties can only be determined at certain frequencies, as compared with the massless specimen where the stiffness and loss-factor can be determined continuously as a function of frequency.

3. In order to determine the material properties of a specimen from the measured stiffness values, the geometry must be considered.

For rubber-like materials (for which the bulk modulus is much greater than the shear modulus), $E = 3G$ where G is the shear modulus, and it implies a Poisson's ratio of 0.5.

The stiffness of the spring is then related to the apparent Young's Modulus E_a or shear modulus G_a by the relation

$$k = \frac{E_a A}{L} = \frac{3 G_a A}{L} \qquad A \text{ is c/s area}$$

The apparent moduli are related to the actual moduli by an expression using the shape factor S:

$$E_a = E(1 + 2\alpha S^2) = 3G(1 + 2\alpha S^2)$$

The shape factor S is defined as one loaded area divided by the free area of the rod. For a cylindrical specimen, $S = D/(4L)$ using the previous notation. The constant α depends on the material, and the hardness. The

values shown here, obtained from Lindley (150) show some values for natural rubber, compared with hardness and Young's Modulus.

Table 4.2

Hardness IRHD ± 2	Young's Modulus lbf/in^2	α
30	130	0.93
35	168	0.89
40	213	0.85
45	256	0.80
50	310	0.73
55	460	0.64
60	630	0.57
65	830	0.54

For the harder grades of natural rubber (with lamp-black as filler), Lindley (150) points out that the relationship $E = 3G$ no longer holds, but becomes more nearly $E = 4G$.

For a specimen in shear, the shear modulus is more readily obtained from $G = Lk/A$.

4.3 EXPERIMENTAL APPARATUS

Apparatus was constructed to measure the transmission properties of rubber specimens and isolation mounts, the principle of operation being the same as that used in apparatus developed by Harrison, Sykes and Martin (142) and Snowdon (26). Differing in many practical details from those previously developed, this apparatus enabled fairly large specimens and parts to be tested (for example a car shock absorber). This section gives details of the design, instrumentation and proving of the aparatus.

4.3.1 Specifications

The test below shows the working specifications of the apparatus as constructed. The frequency and transmissibility ranges depend upon both mechanical and electronic limitations, and are thus capable of extension. Larger top weights are also possible, and the use of preload.

1. Measure transmissibility in the frequency range 5Hz - 1kHz.
2. Minimum measureable transmissibility: - 80dB
3. Maximum applied vibratory force: 25 lbf.
4. Maximum motion of top weight: $\frac{1}{4}$in. amplitude.
5. Minimum/maximum top weight: 6.8/13.7 lb. wt.
6. Maximum specimen height: 20 in.
7. Maximum specimen support diameter: 4 in.

8. Top weight constrained to linear motion without friction.

4.3.2 Construction

The overall view and principal dimensions of the apparatus are shown in Figure 4.3.1. The vibration generator 1 drives the bottom mounting part 2 . The top mass 3 is supported in an air-bearing on a sliding mounting plate 4. This mounting plate can be moved on three supporting pillars 5 to accommodate the specimen, the pillars being located at the top by a circular plate. The whole apparatus stands on a very firm base 6 . The deadweight on the vibrator is relieved by elastic cords (not shown) attached to the bottom mounting.

The top weight and air-bearing are shown in more detail in Figure 4.3.2. The top weight 1 consists of a conical part and a cylindrical shaft. Holes are drilled in the conical part to allow the fixing of an adaptor plate (and ring) 2 , and to give space to mount an accelerometer internally 3 , with a lead hole 4 . The top of the shaft has tapped holes 5 to allow additional weights to be attached. The shaft slides freely in the air-bearing which consists of an inner sleeve 6 mounted in an outer case 7 which is fixed to the mounting plate. Two rows of jets at quarter stations provide the required air-flow in the bearing - design details are given in Appendix 3. The radial clearance of the bearing is very small (< .001 in.) which constrains

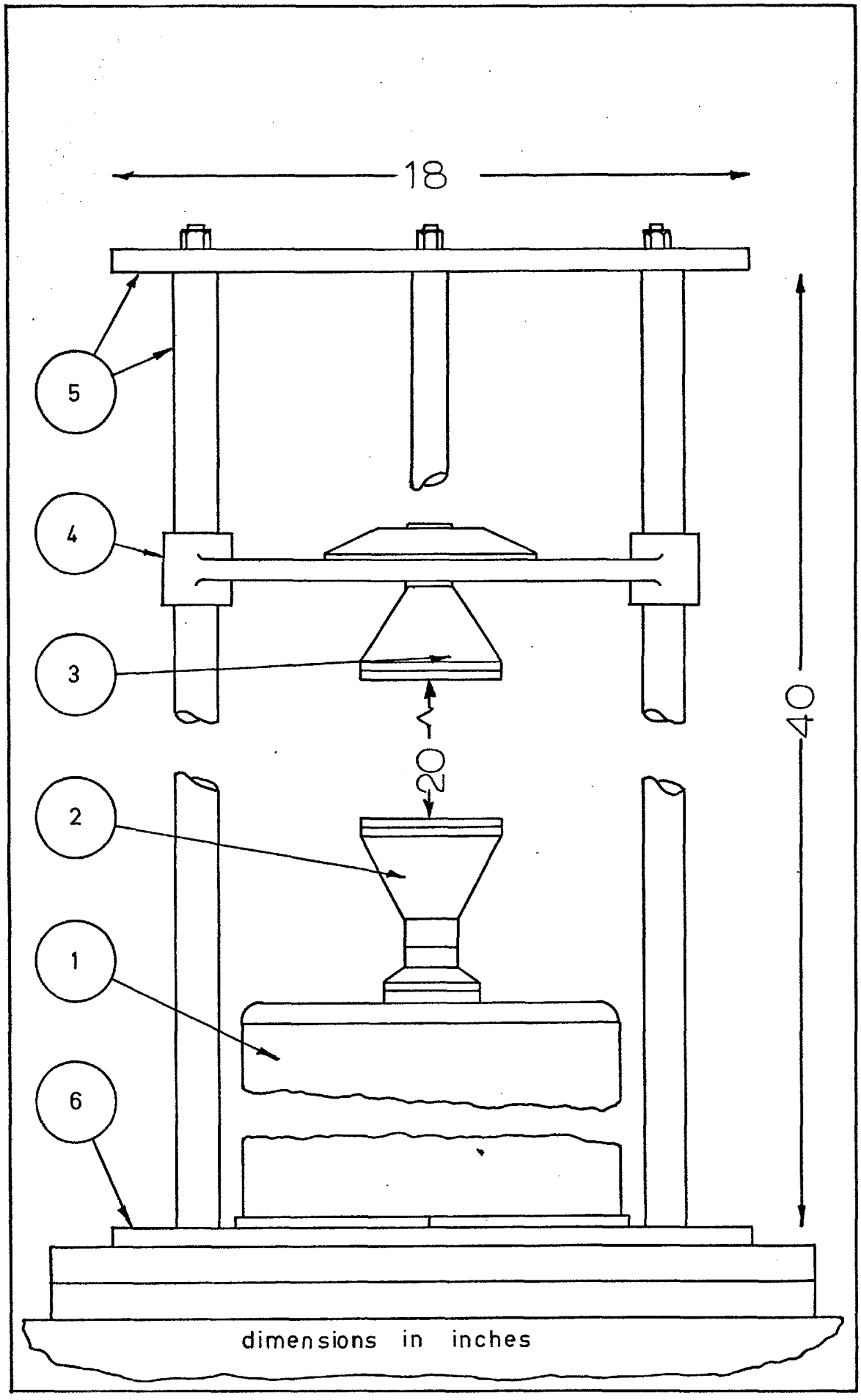


Figure 4.3.1

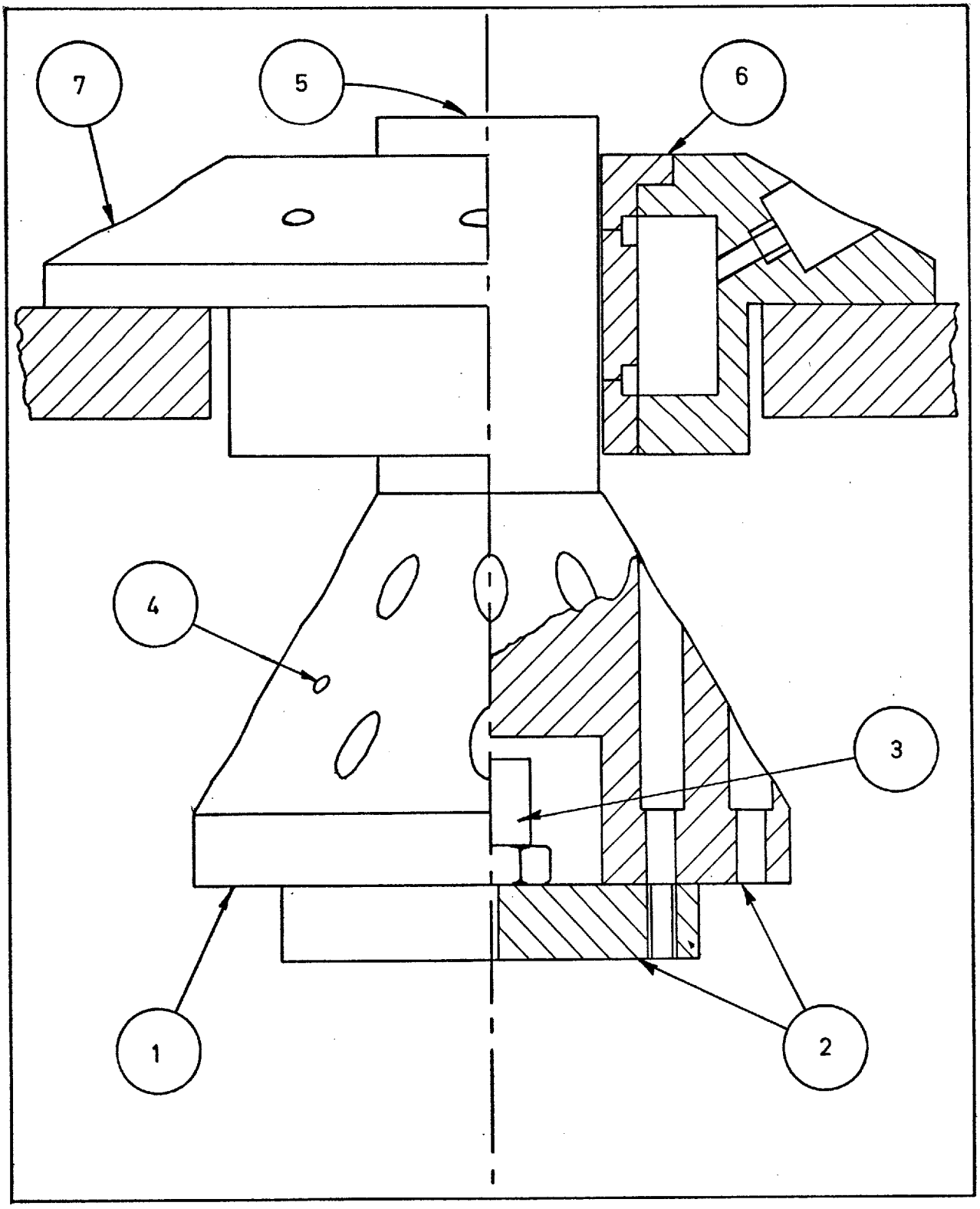


Figure 4.3.2

the top weight horizontally without introducing any appreciable frictional constraints vertically.

The bottom mounting, shown in Figure 4.3.3 is similar in design to the top weight, but is made from duralumin to keep the weight down, whereas the top weight was made of mild steel. An adaptor plate and ring 1 can be attached. The accelerometer 2 and lead hole 3 are as in the top weight. A large stud 4 connects the mounting to the adaptor piece 5 for attachment to the vibrator. The split construction is to enable all nine mounting holes on the vibrator table to be used. Three studs 6 enable elastic cords to be attached to relieve the vibrator of the static load imposed.

Clean, dry air is required for the air bearing at a pressure of 80 psig and low pressure cooling air is necessary for the vibrator if prolonged running at high output is envisaged. Figure 4.3.4 shows the essential features of the air supply, including a safety cut-out switch, which cuts off the vibrater supply should the air-bearing pressure fall below a preset value. This last feature was later modified to an electrical cut-out switch.

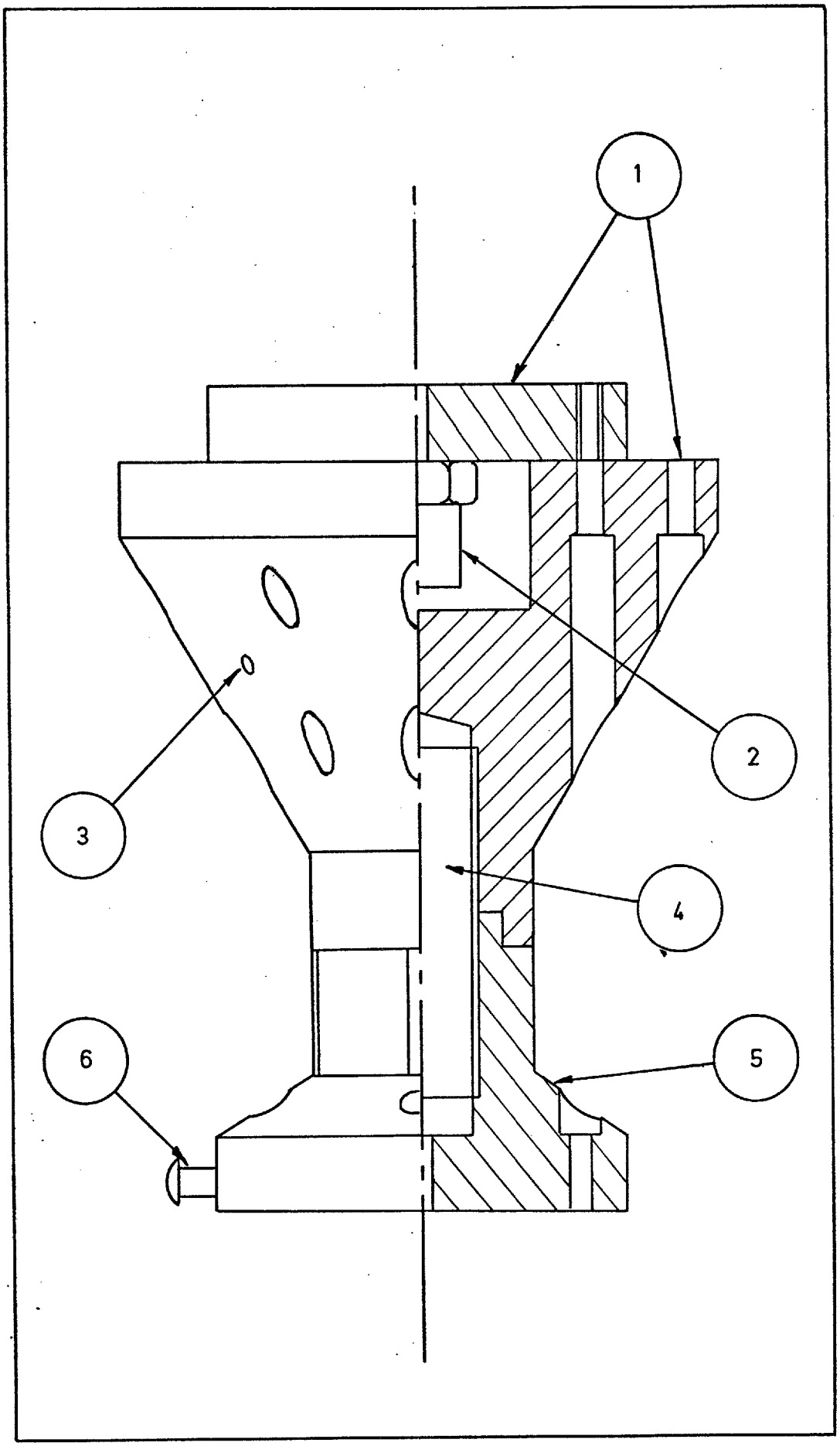


Figure 4.3.3

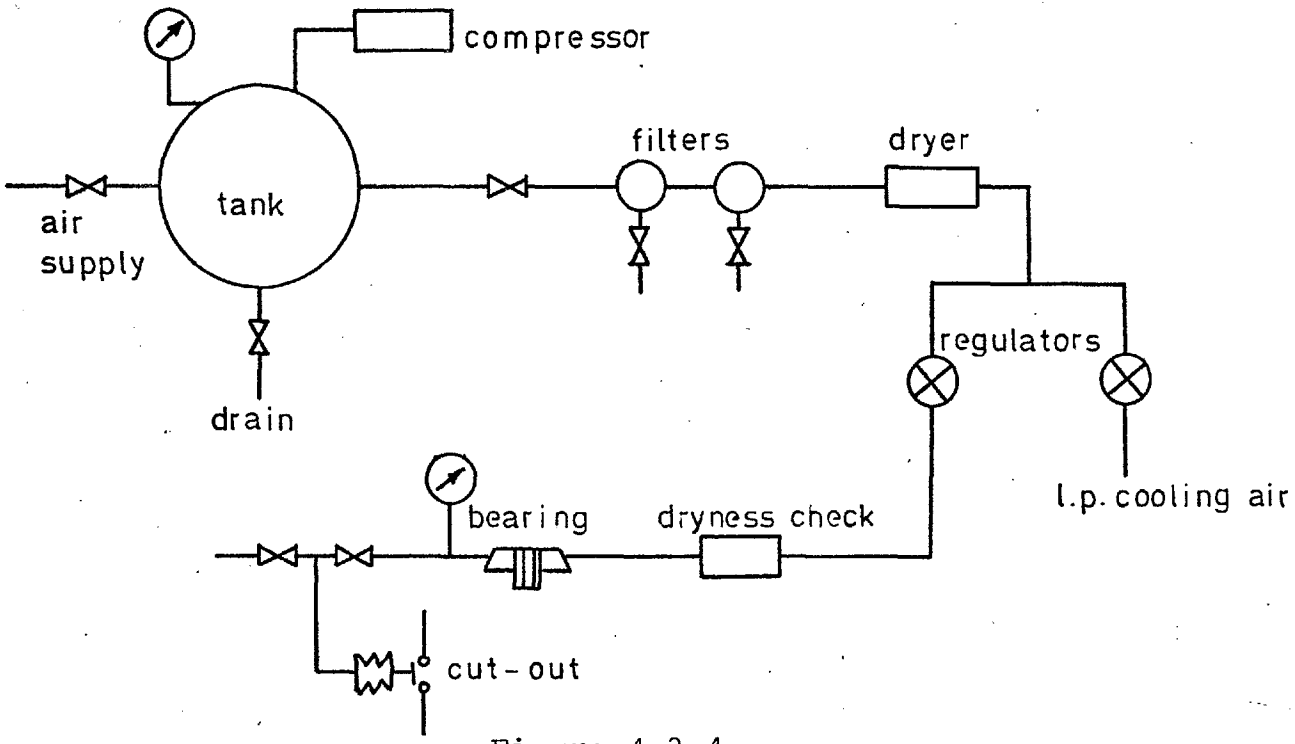


Figure 4.3.4

4.3.3 Drive and Measurement Circuits

The choice of vibration generator was determined in the design of the apparatus - an electrodynamic generator (Derritron VP4) was chosen to satisfy the bandwidth and force requirements. The drive and measuring circuits, however, were developed as a result of operating experience and due to an influx of new transducers and electronic devices. The development of these circuits is outlined below, with notes on operating experience and limitations.

Circuit 1

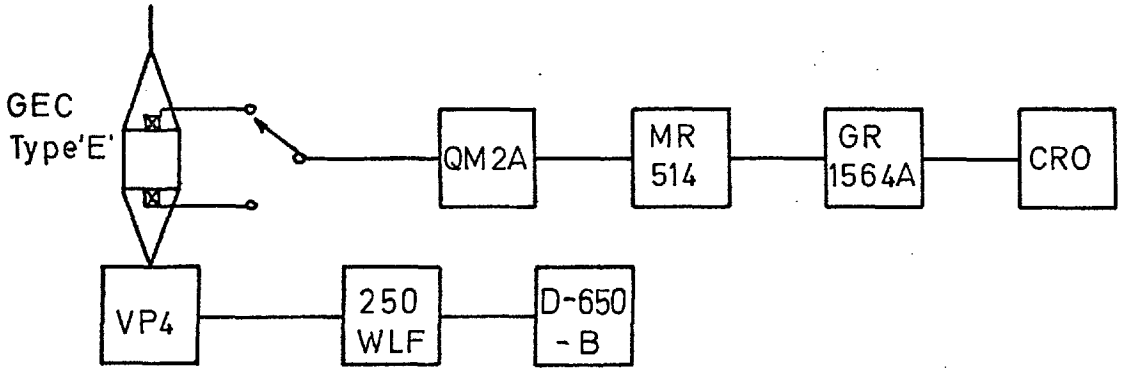


Figure 4.3.5

The first circuit was essentially an interim circuit used whilst new equipment was being ordered. The equipment is listed below:

Oscillator	-	Muirhead type D-650-B
Power Amplifier	-	Derritron type 250 WLF
Accelerometers	-	GEC type E
Charge Amplifier	-	Environmental Equipment type QM2A
Preamplifier	-	Southern Instruments 'Minirack' DC type MR514
Tuneable Voltmeter	-	General Radio analyser type 1564-A
Oscilloscope	-	Telequipment type D41 with type A amplifiers

This circuit required duplication to give phase readings. Severe noise was apparent at low power output, and mains 'hum' was intrusive. It was found desirable to bond the specimens firmly to the adaptor plates.

Circuit 2

A Goodmans control amplifier E501 was tried, to control the input acceleration on the specimen, but severe hum was introduced, and it was not used further.

The accelerometers and cables used were considered notoriously misleading. Large amounts of cable induced noise (i.e. triboelectricity) and cable attachment sensitivity (on the seismic mass of the accelerometers) made a change in accelerometers essential, though for this circuit there were no others available.

An extra charge amplifier, phase-meter and valve-voltmeter enabled the required circuit duplication to be carried out, but with no filtering. The signal required to be clean for the phase-meter, which limited the range of transmissibility that could be measured.

Figure 4.3.6 shows this circuit, and the additional equipment is listed below.

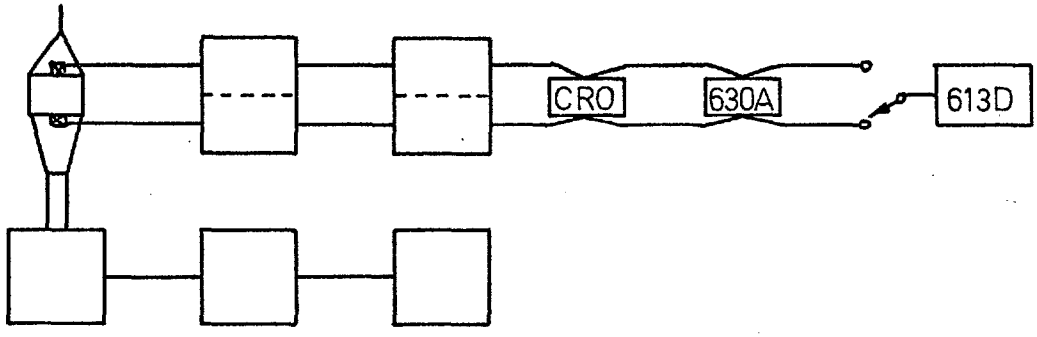


Figure 4.3.6

Phase-meter - Dawes type 630A

Valve-voltmeter - Dawes type 613D

Circuit 3

New accelerometers, cables and charge amplifiers became available. With the circuit otherwise as shown in Figure 4.3.6 the new equipment was:

Accelerometers - Environmental Equipment type AQ40 with subminiature coaxial leads

Charge Amplifiers - Environmental Equipment type CVA2

The new leads did not have the same motion sensitivity as those previously used, although some high frequency noise could be produced. The lead attachment was found satisfactory. These transducers and leads were finalised

as acceptable primary measurement devices.

Mains hum now appeared as a problem at high frequency, due to the relative transmission of the 50Hz hum and the signal. This produced gross distortion of the output signal even though the input signal appeared clean. In order to observe real signal distortion, due to the specimen, it was decided to build a hum correcter which would inject, with suitable magnitude and phase, a mains frequency signal into the power amplifier to cancel that being generated.

The circuit, shown in Figure 4.3.7, cured the problem of hum in a satisfactory manner. The power amplifier was sufficiently well corrected for harmonics of the mains frequency to be insignificant.

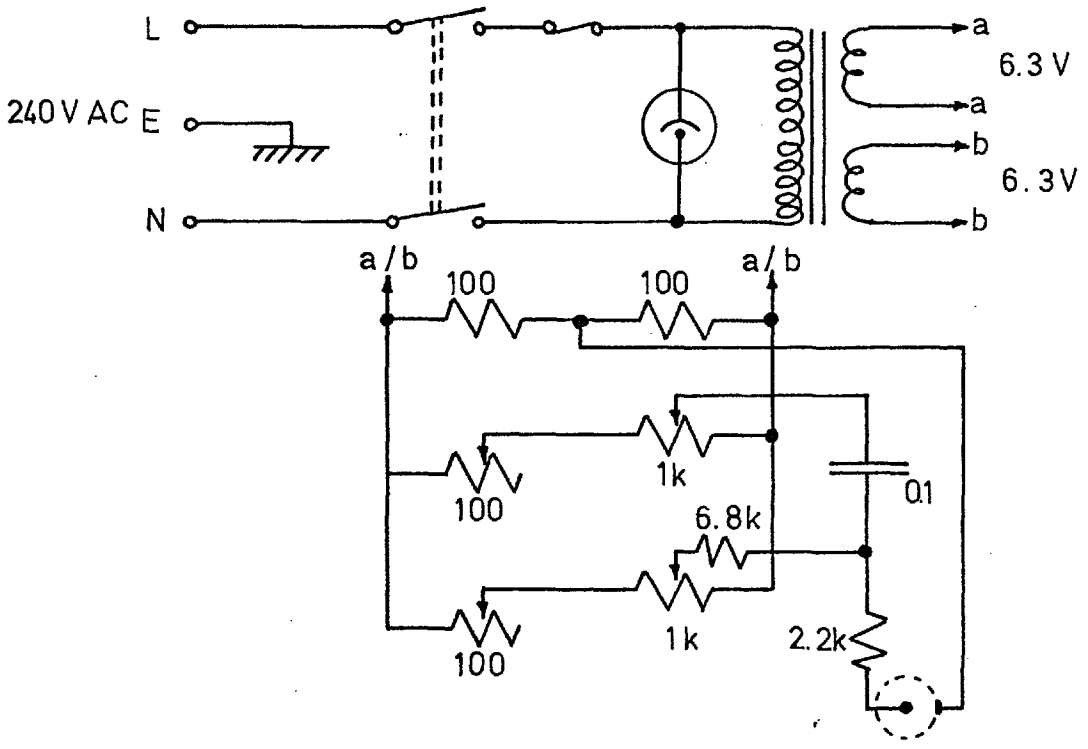


Figure 4.3.7

Circuit 4

The previous circuits did not permit filtering or the signal for phase measurements. The circuit shown below in Figure 4.3.8 permitted both phase measurements and filtering (and thus extending the range of measurements) but was slow and tedious in operation.

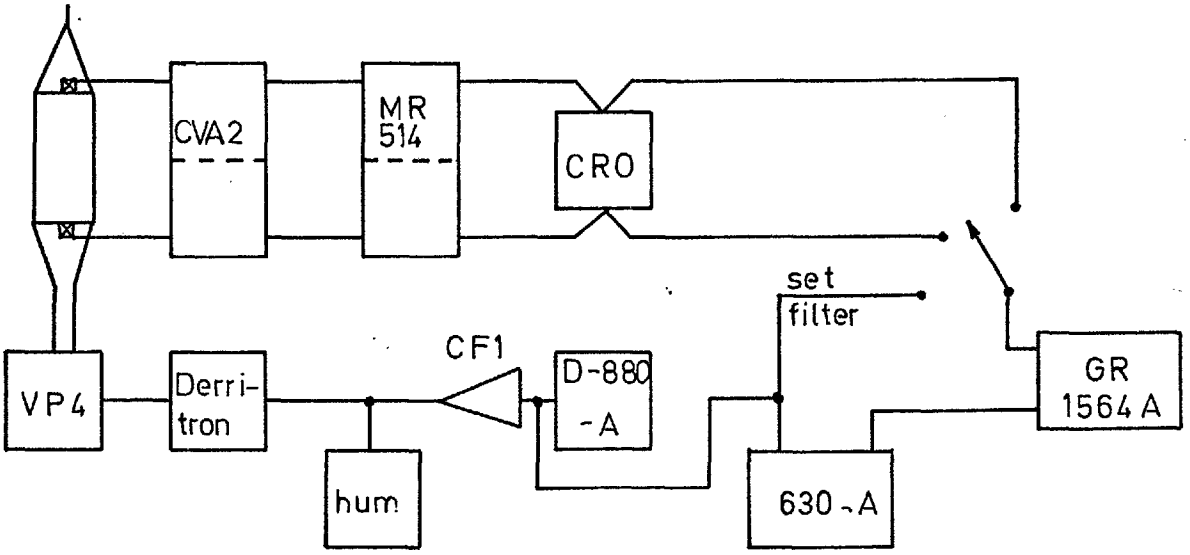


Figure 4.3.8

Power Amplifier - Derritron Solid State 100 Watt

Oscillator - Muirhead D-880-A or or Levell TG-66A

Cathode Follower - Langham Thompson type CF1

An alternative safety cut-out circuit was employed to detect air-bearing failure (i.e. contact of shaft in bearing), using magnetic flip-flop relays and indicator lamps. This is shown below in Figure 4.3.9.

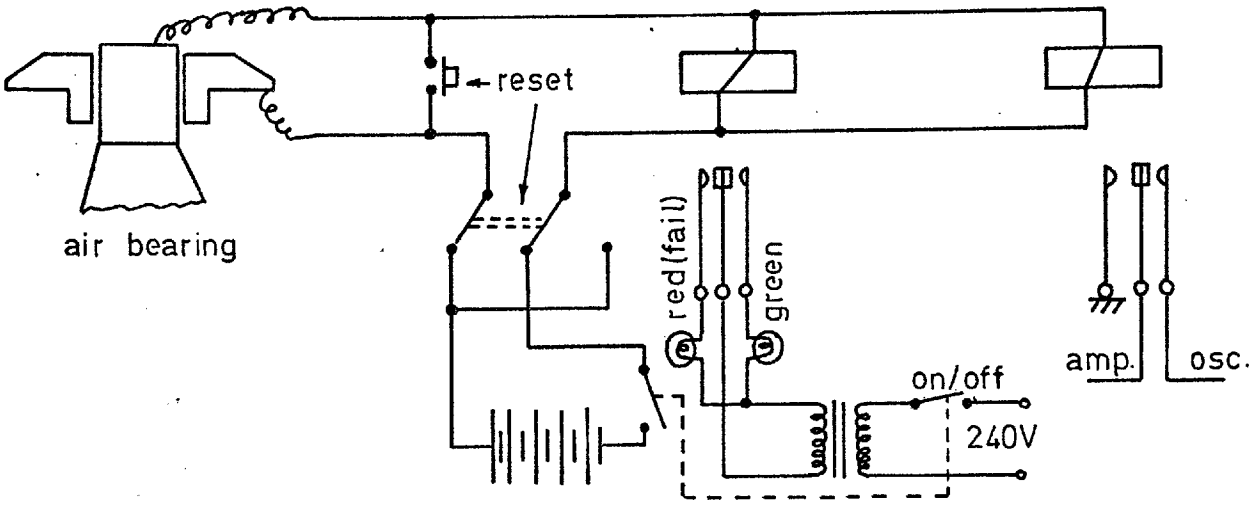


Figure 4.3.9

Circuit 5

An alternative circuit was available, using a resolved component indicator. This circuit, and a similar circuit using a digital transfer function analyser provided a more convenient circuit for phase measurements with filtering. The digital transfer function analyser was only available at a late stage, and did not cover the full frequency range. After this work was finished, a high frequency extension unit became available which would permit the whole frequency range to be used. The circuit is shown in Figure 4.3.10, including the hum corrector. This is not essential for the measurement, but enables the real signal distortion to be observed prior to filtering. For greatest accuracy of phase measurement in the high frequency region, where the material loss factor is derived directly from the phase angle between the top and bottom accelerometer signals, it is desirable for the digital equipment to see a signal at some multiple of 45° relative to the source signal. A passive R-C network was constructed to act on the output of the

transfer function analyser to produce this phase shift as required. For low damping materials, when both top and bottom signals have very similar phase, a considerable increase in accuracy can be obtained than if the phase-shift network were not employed.

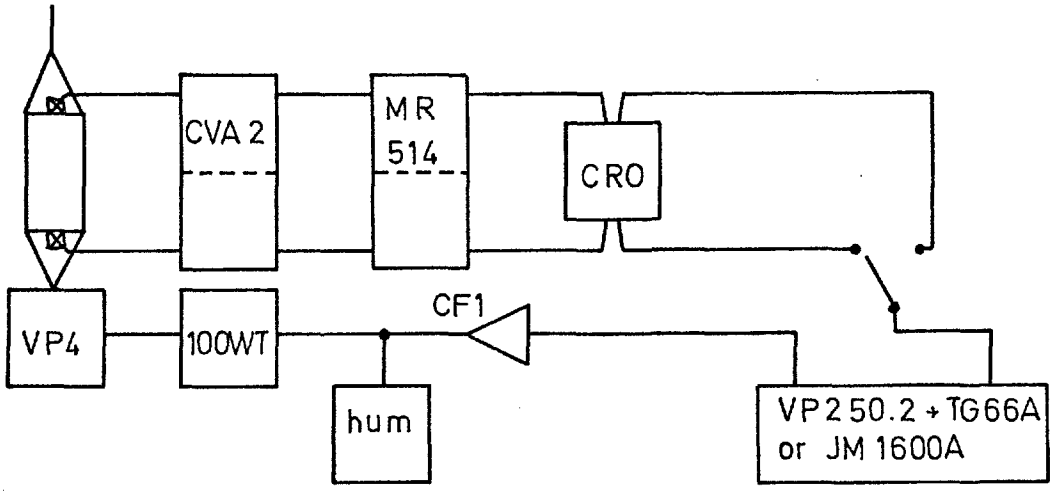


Figure 4.3.10

Resolved component indicator - Solatron VP2502

Digital transfer function analyser - Solatron JM1600A

(Extension unit, not used, - Solatron JM1639)

4.3.4 Proving

Certain points inherent in the design of the apparatus require that testing of the apparatus itself is an essential step. These points are:

1. That the top-weight and bottom mounting remain rigid in the specified frequency range.

2. The air-bearing introduces no appreciable damping of the top mass, nor induces lateral resonances.

3. No appreciable flanking paths exist for the vibration to the top weight.

Taking these points in order, it was found that a frequency of at least 6 kHz was required before any noticeable deviation from the rigid body behaviour was observed for the top weight and bottom mounting.

For the second point, it was found that for a helical steel spring, a Q-factor of nearly 500 could be measured, near the limit of the instrumentation. This indicates that for most practical mounts and rubber specimens, the damping of the top mass was entirely negligible. A rocking mode (or rather two modes at nearly equal frequencies) existed for the top mass alone in the bearing at about 16 Hz (dependent upon air pressure), with a Q-factor of 42. The normal accelerometer mounting position is insensitive to this mode, and with symmetrical specimens there will be no coupling. The existence of this mode did not cause any difficulty. Due to the lack of rotational constraint of the top mass, a helical spring could cause coupling to the rotational mode of the top mass. Should this occur, the cure could simply be the addition of extra weight on the top weight to change the moment of inertia.

The point requiring greatest attention was that of flanking paths to the top weight. That is, vibration transmitted via the columns, bearing mounting plate, and air-

bearing to the top weight which could lead to incorrect transmissibility readings. Whilst by virtue of the design the flanking paths are weak, when measuring transmissibilities as small as -80 dB only the smallest possible amount of flanking vibration is permissible. Really firm mounting of the apparatus on a solid concrete base ensured that the frame motion was negligible in the specified frequency range. It was not sufficient to rest the apparatus on the concrete (as high spots caused a low contact stiffness leading to a resonance at about 100 Hz), nor even to use a thin rubber sheet to ensure a larger contact area. The final solution employed, and found to be satisfactory, was to bond a 1 in. thick, 24" diameter ground steel plate to the concrete floor, and to attach the apparatus to the plate with a very thin layer of grease. This spreads the contact area to the full diameter of the base plate whilst not stressing the apparatus, and also allows the use of the base plate for other experiments. The comparison of the top weight acceleration in the vertical and horizontal directions to a given amount of force input to the base, with the top weight suspended from above, between the apparatus mounted with the rubber sheet and bonded to the steel plate is shown in Figures 4.3.11 and 4.3.12. The scale is that of dBre 10^{-3} g/A, the current in the vibrator being used as a measure of the force. Considerable improvement is shown in the final mounting (shown ●) over the mounting on the rubber sheet (shown X), and as such shows that, unless exceptional attenuation is observed in the specimen, flanking paths are not significant.

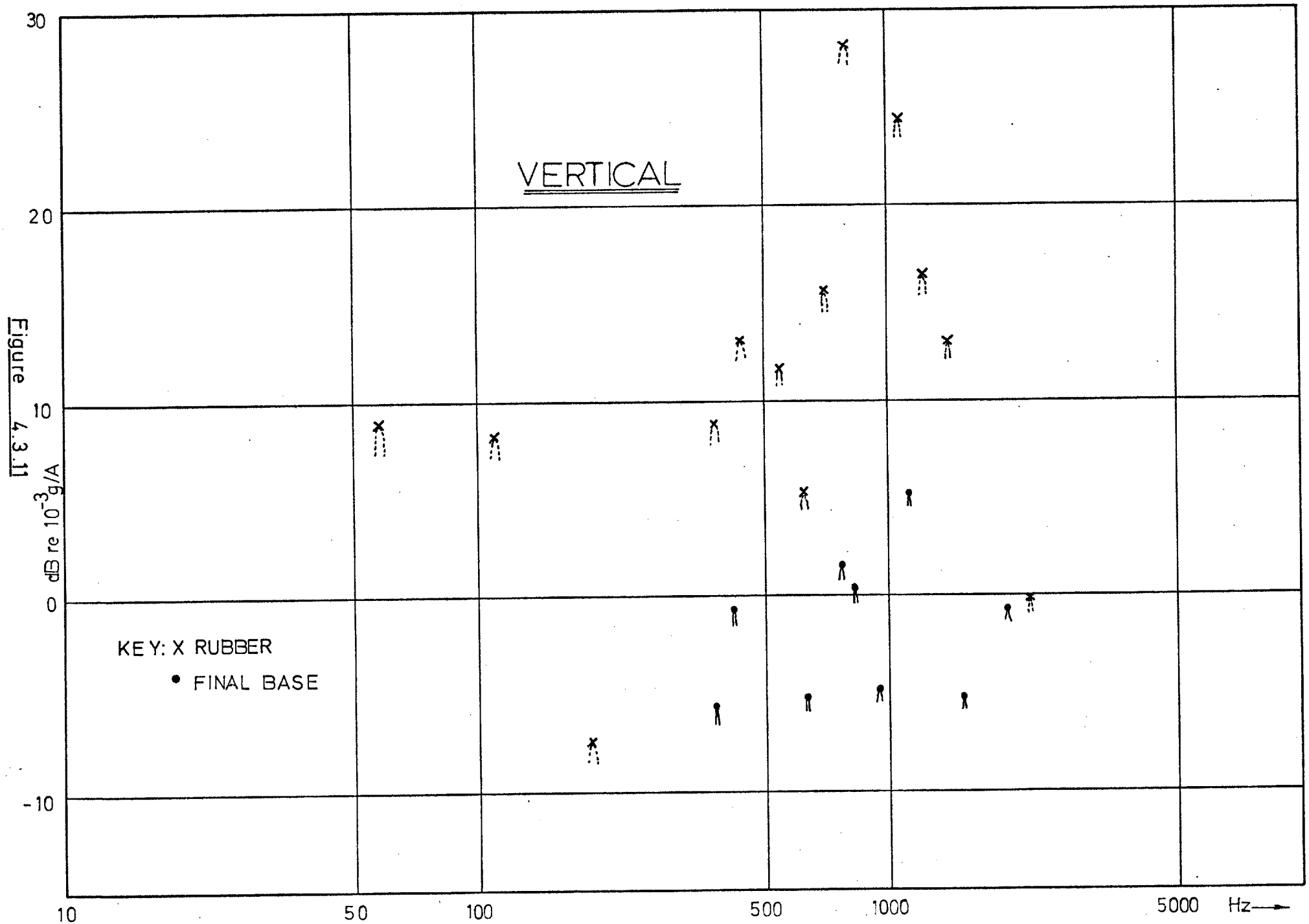

VERTICAL
30
20
10
0
-10
dB re 10^{-3}g/A
KEY: X RUBBER
• FINAL BASE
10
50
100
500
1000
5000
Hz

Figure 4.3.11

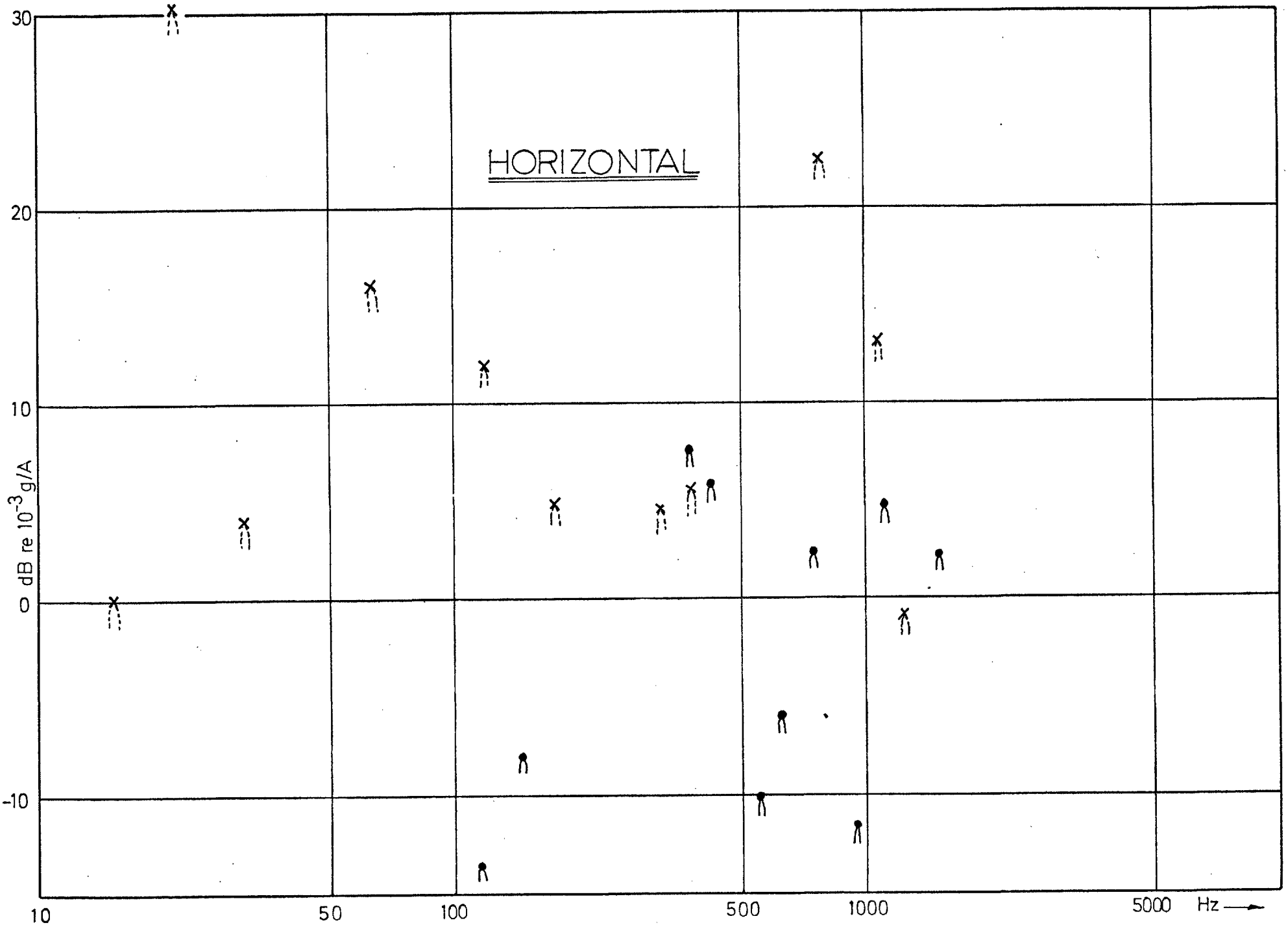


Figure 4.3.12

4.3.5 Modifications and Extensions

To increase the usefulness of the apparatus, the method shown in Figure 4.3.13 may be used to preload the specimens to the desired compression or stress. A pair of specimens would be required in ring form in the particular arrangement shown

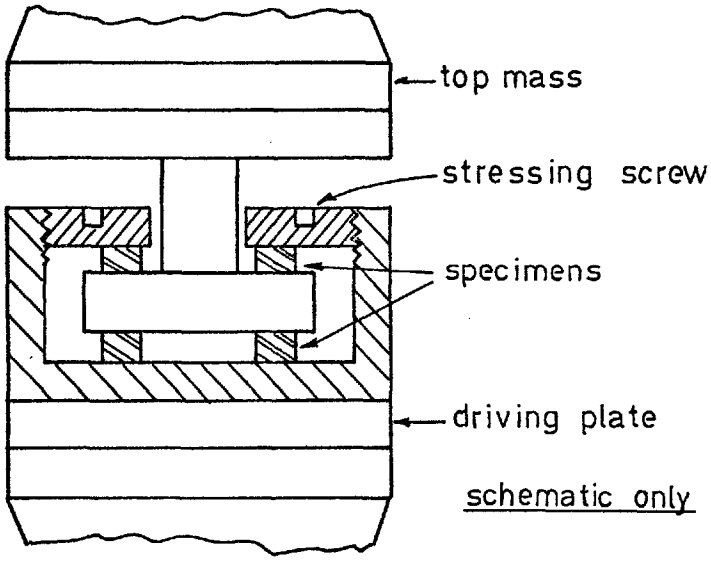


Figure 4.3.13

When testing a car shock-absorber, preloading was applied, similar to that employed in the vehicle installation. The arrangement is shown in Figure 4.3.14.

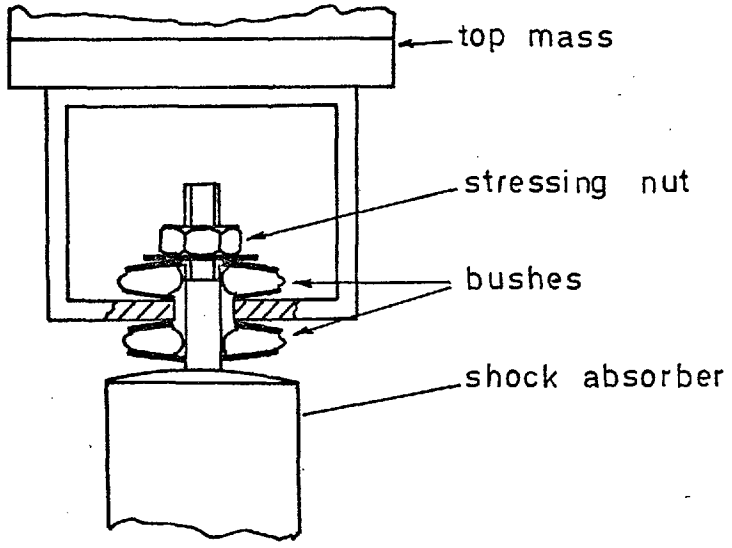


Figure 4.3.14

In the low-frequency range it is desirable to obtain the specimen displacement directly to observe strain dependent effects. The required quantity is $\underline{x}_2 - \underline{x}_1$ where $\underline{x}_2$ and $\underline{x}_1$ are the phasors for the top and bottom displacements or the displacement. In the high-frequency region, $\underline{x}_2 \approx 0$, and the top weight functions as a load cell, so that the specimen is the input displacement, and no modification is required. For the low-frequency end, it would be possible to use a displacement gauge to measure $\underline{x}_2 - \underline{x}_1$, but the existing circuits could be modified as shown below in Figure 4.3.15 to provide the modification more simply.

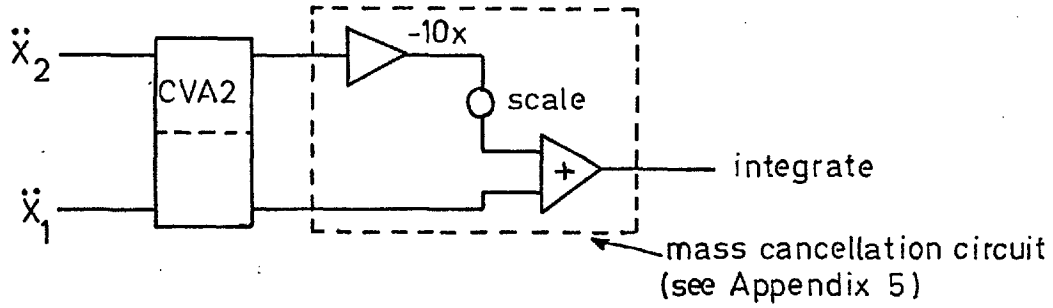


Figure 4.3.15

4.4 EXPERIMENTAL RESULTS

Results from some* of the experiments performed using the apparatus described in the previous section are shown

* Some of the earlier results, obtained with inferior measurement circuitry are omitted. The final circuit, using the digital transfer function analyser, was available too late to repeat all of the results obtained.

here. They serve to indicate that the apparatus is a reliable piece of equipment with fairly versatile performance. Besides tests on special rubber components, the apparatus was used for measuring the transmissibility through a car shock absorber, and the properties of rubber bushes used in a vehicle suspension system.

4.4.1 Rubber Rods

The performance of rubber rods was studied with the transmissibility apparatus to compare the wave effects found with the theoretical predictions, and to deduce the dynamic properties of the rubber.

PB50

The first result shown here is on a high damping rubber called PB50. The specification is shown below. Two different types of transmissibility curve are shown here for the low frequency region. The first, Figure 4.4.1 shows the modulus of transmissibility against frequency, whilst the second, Figure 4.4.2, shows the polar form of plot. The marked inclination of the circle shows the extent of the damping, the phase angle at the undamped natural frequency being 76°. On the enlarged scale the high frequency response is shown, indicating that a heavily damped resonance occurs in the region of 280-340 Hz. The scatter on the results is generally small, though the results were obtained with early circuits.

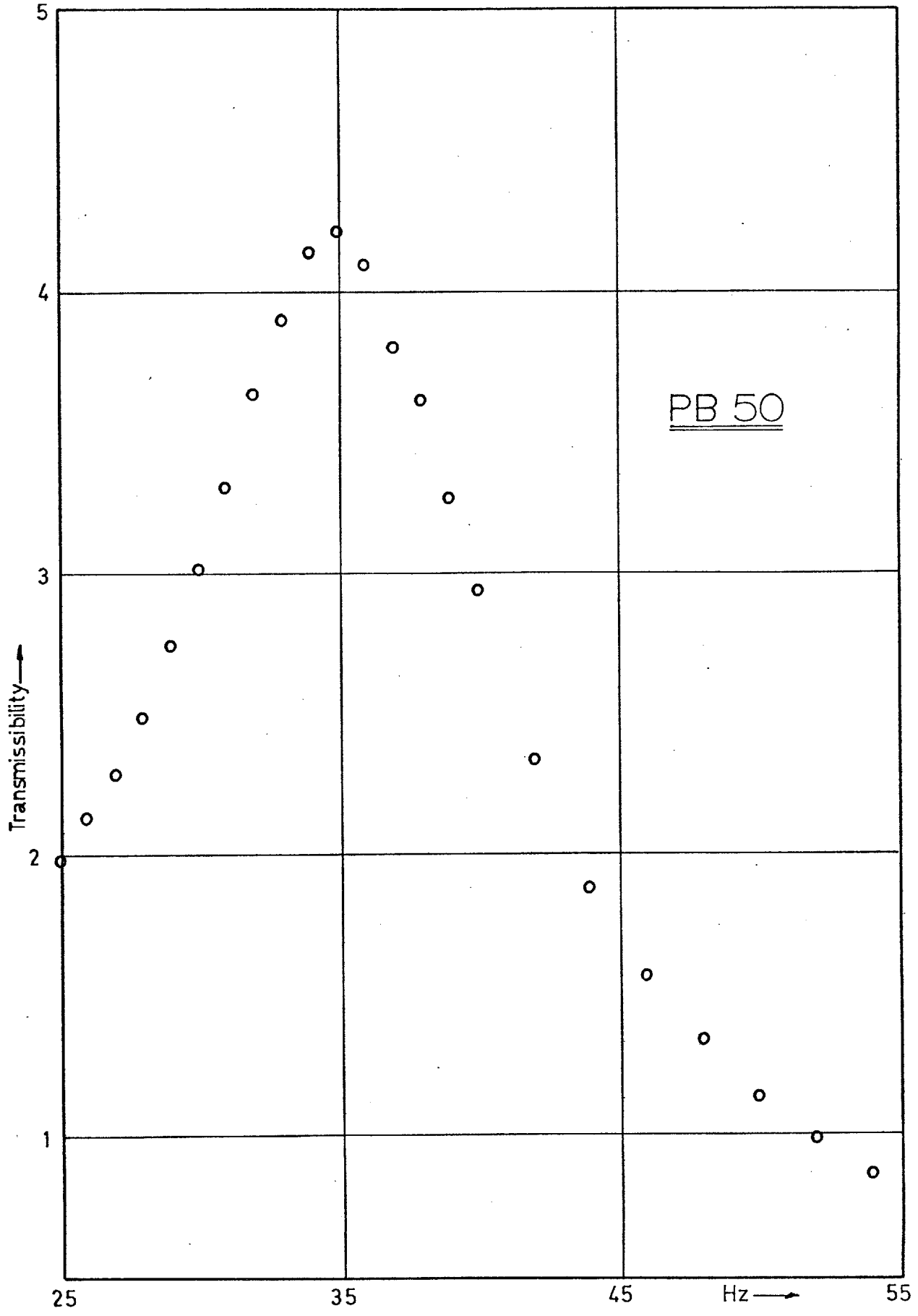


Figure 4.4.1

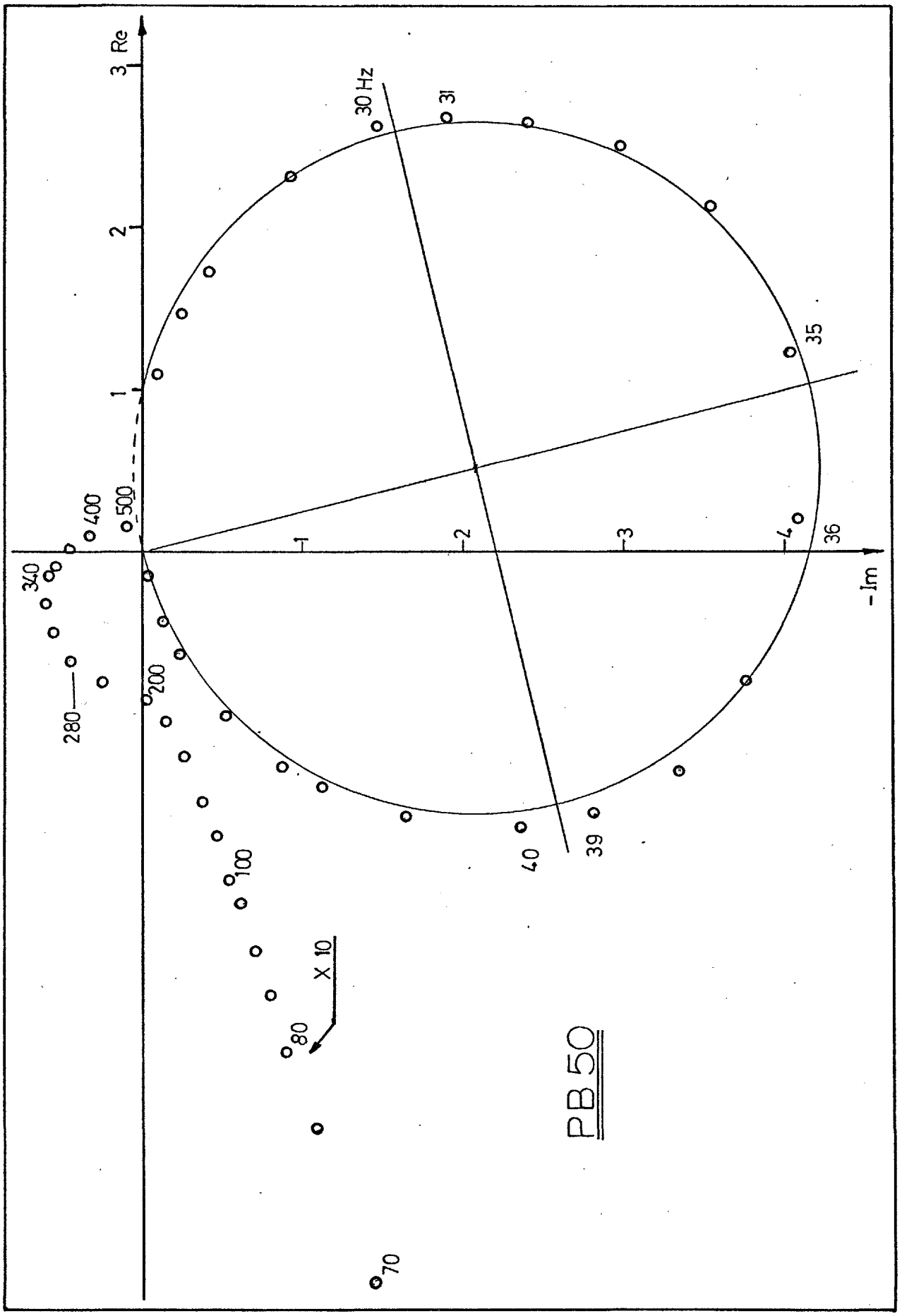

3 Re
2
1
30 Hz
31
35
36
-Im
1
2
3
4
400
500
340
280
200
100
80
70
40
39
X 10
PB 50

Figure 4.4.2

PB50 Manufactured by James Walker and Co. Ltd.

Specification: Medium nitrile rubber (butadiene acrylo nitrile) of 60% rubber content (comprising 30% nitrile and 70% butadiene), balance: carbon black, plasticisers and accelerators, etc., hardness $50^{\circ} \pm 5$ BS.

Test Conditions:

Ambient temperature	$22.4^{\circ}C$
Specimen size	5.975 in. x 2.790 in. diam.
Specimen weight	1.5 lb. wt.

Young's Modulus at 35.2 Hz - 904 lbf/in^2

Loss factor at 35.2 Hz:

by phase lag η = 0.249 (at resonance)

by bandwidth η = 0.252 (exact formula)

The two measures of damping give fair agreement.

AFG

The second results shown use the Bode diagram to indicate the transmissibility curve. The rubber in this case is a natural rubber with some carbon black. Figure 4.4.3 shows the experimental points obtained with a theoretical curve using the derived material properties. The theoretical curve used the Love theory which is subject to certain errors in the end boundary conditions. Nevertheless, excellent agreement is seen between the experimental and theoretical values up to the fourth wave effect. Using the experimental values obtained for the rubber properties, the transmissibility curve was calculated for a different mounted mass. The experimental results again show good agreement

with theory, except for a very slight shift in the low frequency resonance. The wave effects occur at a low frequency due to the length of the specimen used. The details of the rubber and the test results are shown. below.

AFG Manufactured by James Walker and Co. Ltd.

Specification: High quality natural rubber 90 - 95%, balance carbon blocks, etc. Hardness $45^{\circ} \pm 5^{\circ}$ BS.

Test Conditions

Ambient Temperature	$22.8^{\circ}C$
Specimen size	6.075 in. x 2.806 in. diameter
Specimen weight	1.395 lb. wt.
Young's Modulus	392 lbf/in^2 at 22.38 Hz
Loss factor	η = 0.0279 at 22.38 Hz

Using Love theory to show stiffness variation leads to the predictions

$$E = 400 \text{ lbf/in}^2 \text{ at } 22.38 \text{ Hz}$$
$$= 436 \text{ lbf/in}^2 \text{ at } 167 \text{ Hz}$$
$$= 442 \text{ lbf/in}^2 \text{ at } 305 \text{ Hz}$$

Plotting these on a log-log plot gives an almost straight line. An empirical stiffness versus frequency law was fitted

$$E = 10^{(2.5435 + .04183 \log f)} \text{ lbf/in}^2$$

where f is the frequency in Hz, in the range 20 - 300 Hz.

From the measured loss-factor at the wave effects

$$\eta = .0765 \text{ at } 172.5 \text{ Hz}$$
$$= .1086 \text{ at } 315 \text{ Hz}$$

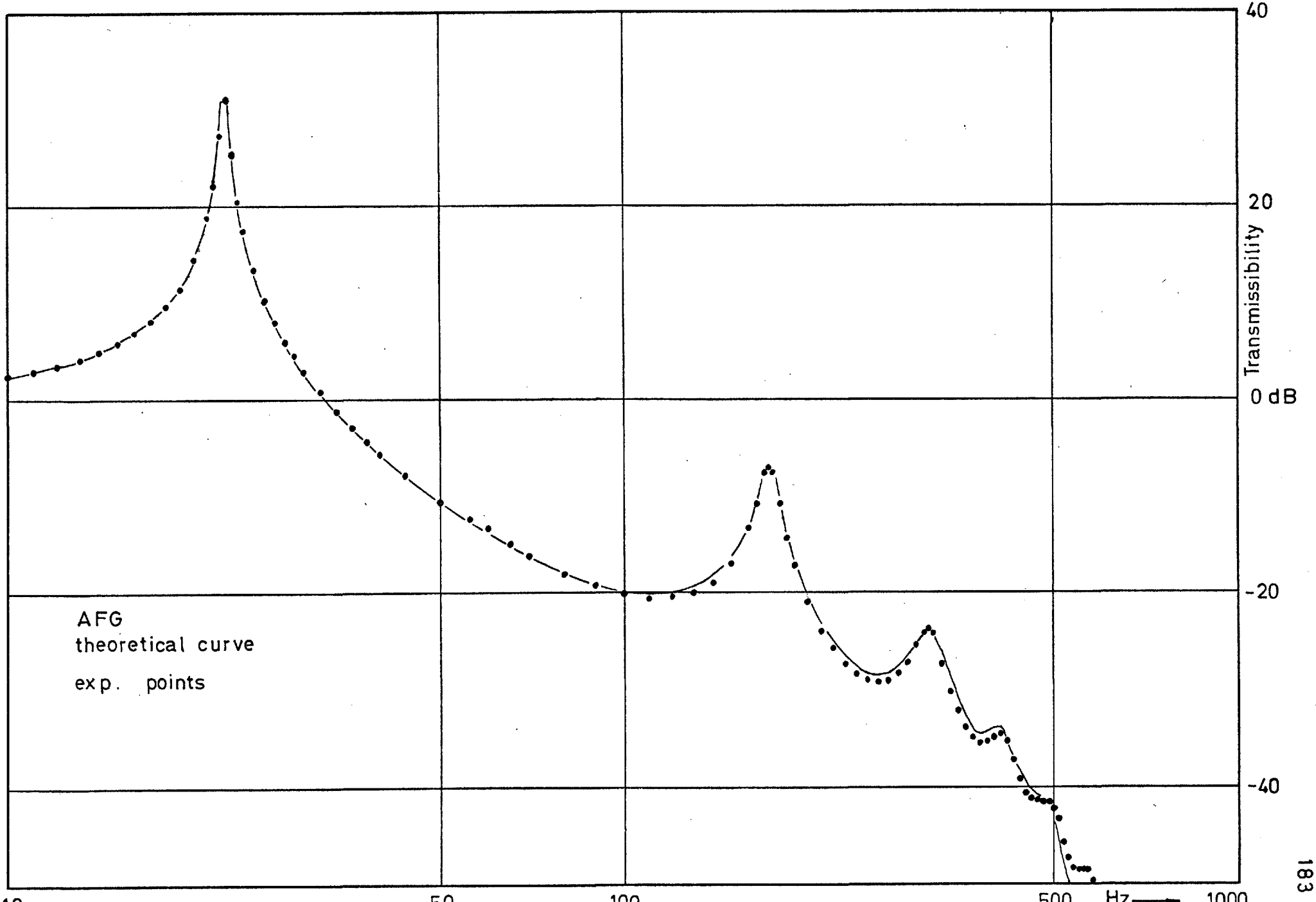

40
20
0 dB
-20
-40
Transmissibility
AFG
theoretical curve
exp. points
10
50
100
500
Hz
1000

Figure 4.4.3

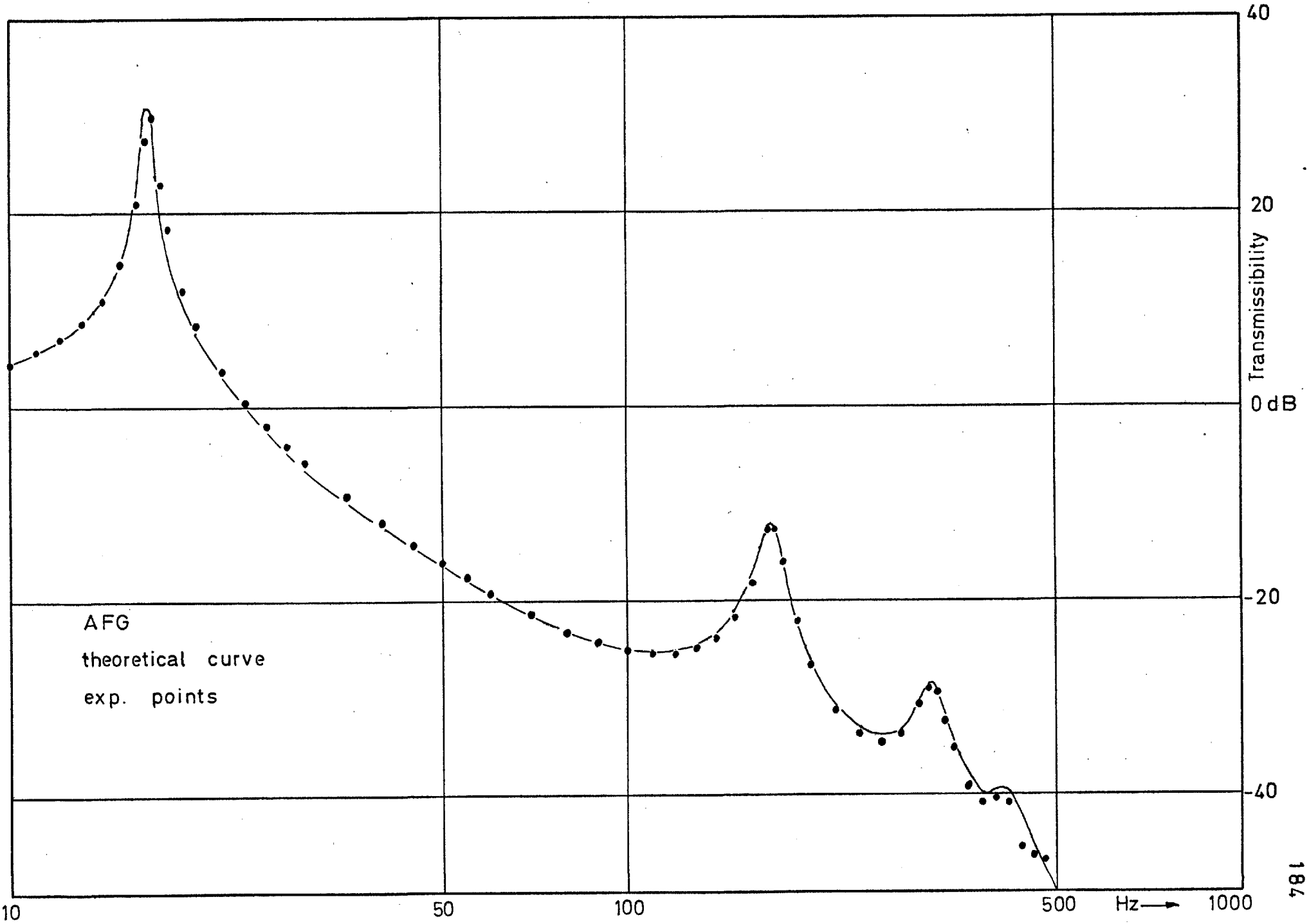

40
20
0 dB
-20
-40
Transmissibility
AFG
theoretical curve
exp. points
10
50
100
500
Hz
1000

Figure 4.4.4

an almost straight line could be obtained on a log-log plot giving the following empirical loss factor versus frequency law.

$$\eta = 10^{(-2.2235 + .4935 \log f)}$$

The theoretical curve shown in Figures 4.4.3 and 4 use these laws for the material properties of the rubber.

Test Conditions (2)

For the second curve, Figure 4.4.4, a larger mounted mass was used and the ambient temperature was 21.7°C.

4.4.2 Rubber Tubes

Employing rubber tubes instead of rods enables additional resonances to be excited, in the form of bending standing waves as well as the longitudinal standing waves. In figures 4.4.5 and 6 the transmissibility is shown using a tube of AFG of approximately the same area as the rods previously tested. An interesting condition reached is that cancellation through the paths is achieved - a very deep trough (-59.4 dB) being obtained at 197 Hz, independent of the mounted mass and very deep compared with the heights of the resonant peaks. Good repeatability is shown between the two curves of transmissibility using different mounted mass. The existence of the dual path through the tube leads to a markedly inferior high frequency transmissibility curve, and the bending resonances are seen to be primarily responsible for this effect.

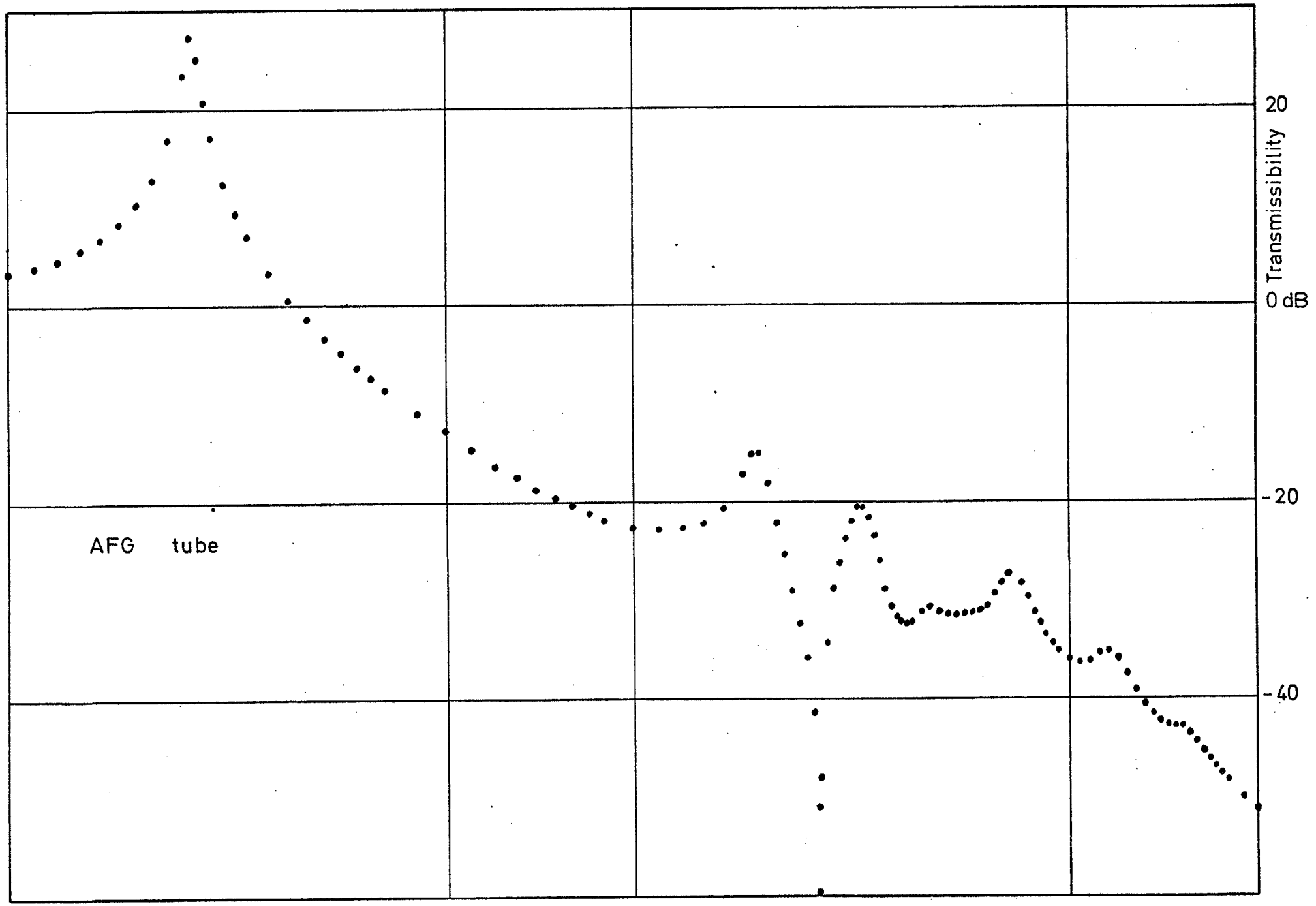


Figure 4.4.5

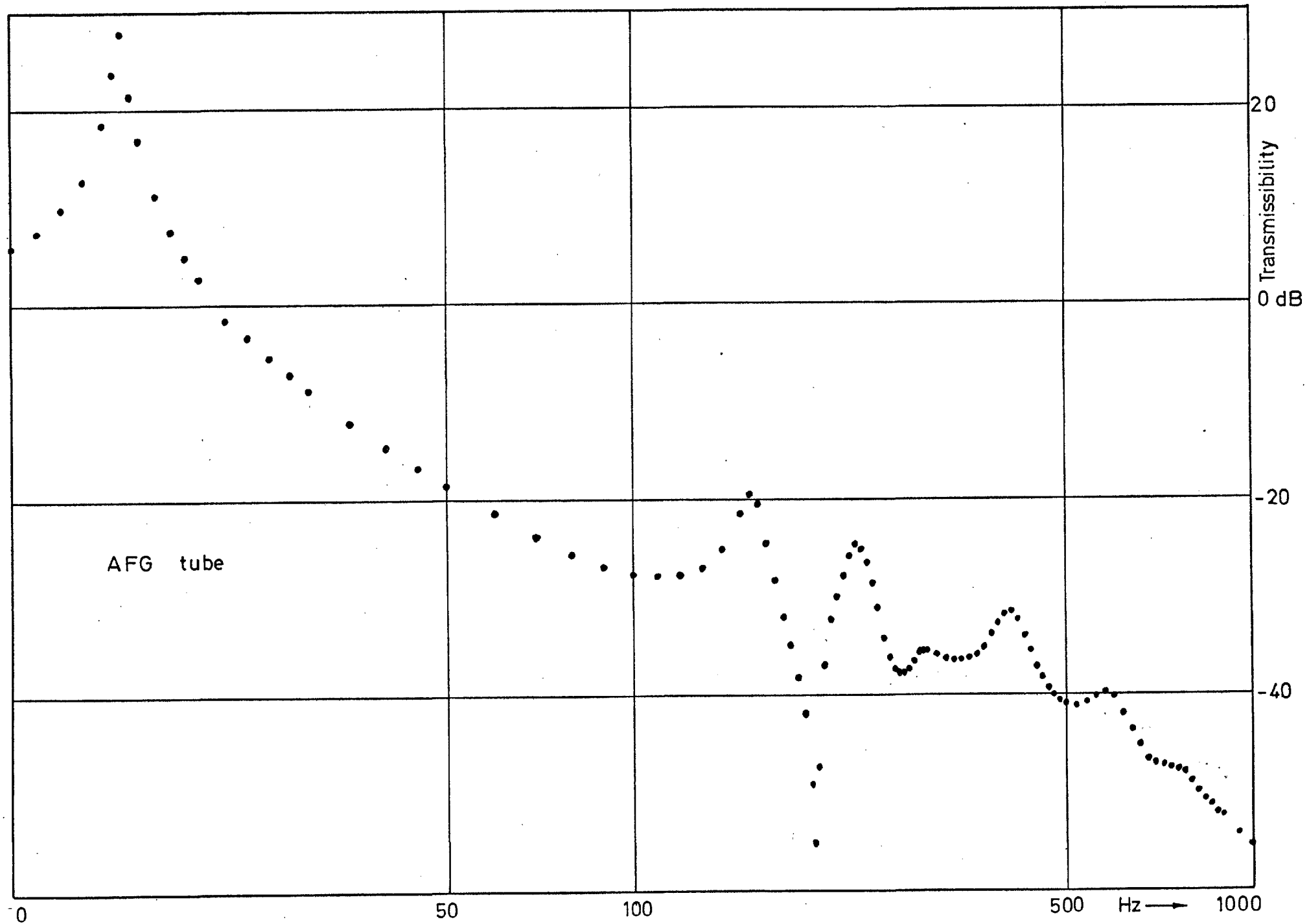


Figure 4.4.6

AFG Manufactured by James Walker and Co. Ltd.

Specification: High quality natural rubber 90 - 95%, balance carbon blacks, etc. Hardness $45^{\circ} \pm 5^{\circ}$ BS.

Specimen size: 5.942 x 3.995 in. O.D., 2.975 in. I.D.

Specimen weight 1.17 lb. wt.

Test 1 - Ambient temperature $22^{\circ}C$ (Figure 4.4.5)

Young's Modulus at 19.6 Hz = 363 lbf/in^2

Loss factor at 19.6 Hz = .045 from peak amplitude

= .048 from bandwidth

Test 2 - Ambient temperature $23.5^{\circ}C$ (Figure 4.4.6)

Young's Modulus at 15 Hz = 364 lbf/in^2

Loss factor at 15 Hz = .041 from peak amplitude

= .046 from bandwidth

The results for the Young's Modulus of AFG give fair agreement with those obtained for the rod. From the law obtained in the previous section, the Young's Modulus is 397 lbf/in^2 at 19.6 Hz and 392 lbf/in at 15 Hz. The loss factor, however, is about twice that obtained for the rod. The most likely explanation for this is that considerable air-damping was produced as restricted air flow is possible at the tube ends. The contained air is also likely to be of considerable effect on the production of the resonances at higher frequencies.

4.4.3 Rubber Shear Mount

Shear mounts are commonly used for vibration isolation. Figures 4.4.7 and 8 show the transmissibility of a typical small mount. Low damping rubber is employed, and the transmissibility curve follows the ideal case until 300 Hz, when the transmissibility increases from the ideal line leading to a resonance at 760 Hz.

Shear mount. Metalastik double-U type 31/149C
Ambient temperature at test 21.8°C
Stiffness of mount at 21.4 Hz = 354 lbf/in
Approximate shear modulus = 133 lbf/in^2
Young's modulus = 398 lbf/in^2
Loss factor at 21.4 Hz = .056 from peak
= .058 from bandwidth

The static stiffness of the mount appears from the literature to be 250 lbf/in, but the rubber composition is not known precisely.

4.4.4 Helical Spring

Helical metal springs are commonly used as isolation mounts, but their high frequency performance is known to be poor because of spring surges. These surges can also contribute to secondary noise generation when the coils clash - noticeable in compression springs with flattened ends. High damping rubber in the form of a pad at the end of the coils is commonly advocated to reduce the surges, but can have little effect on the lower spring modes.

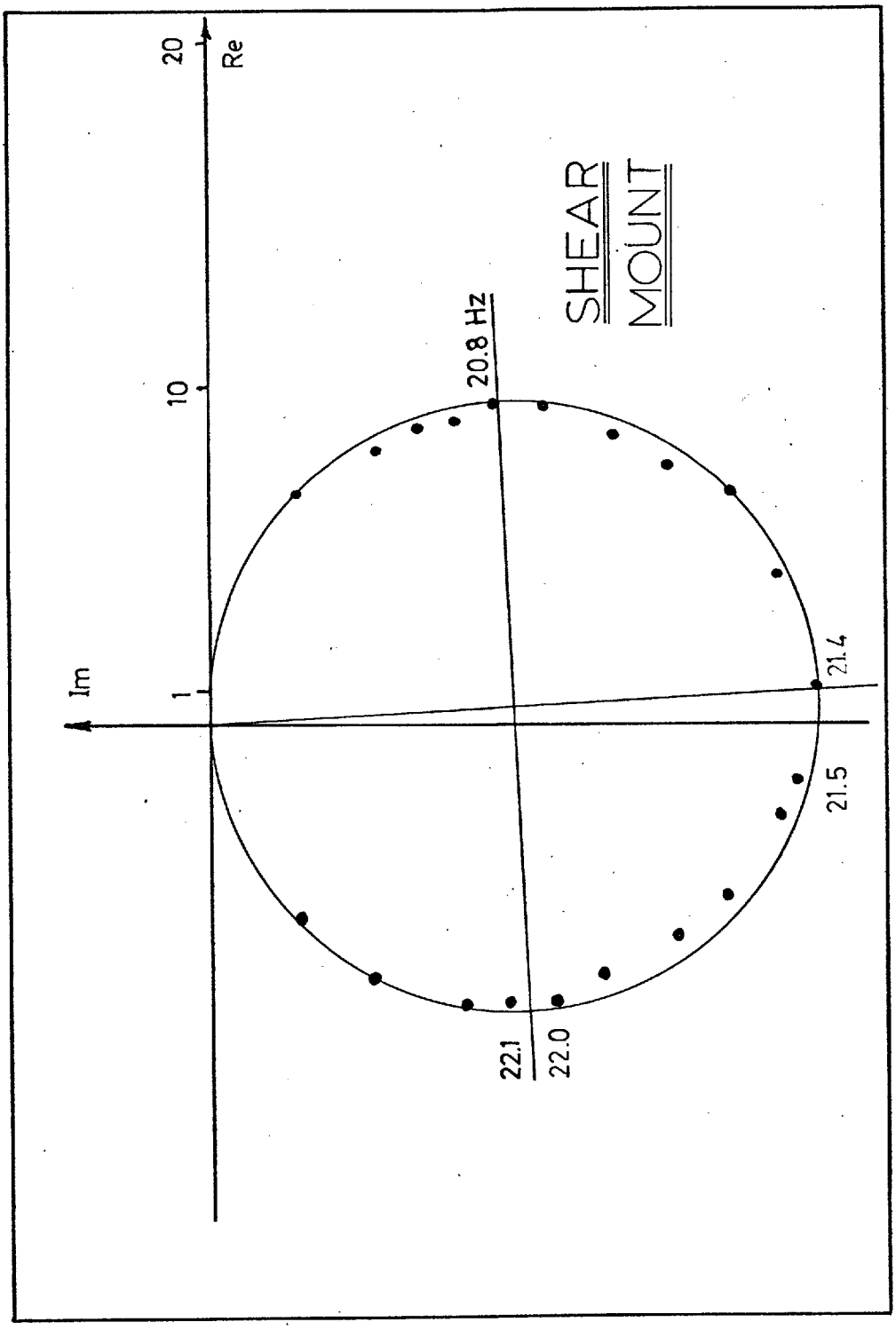


Figure 4.4.7

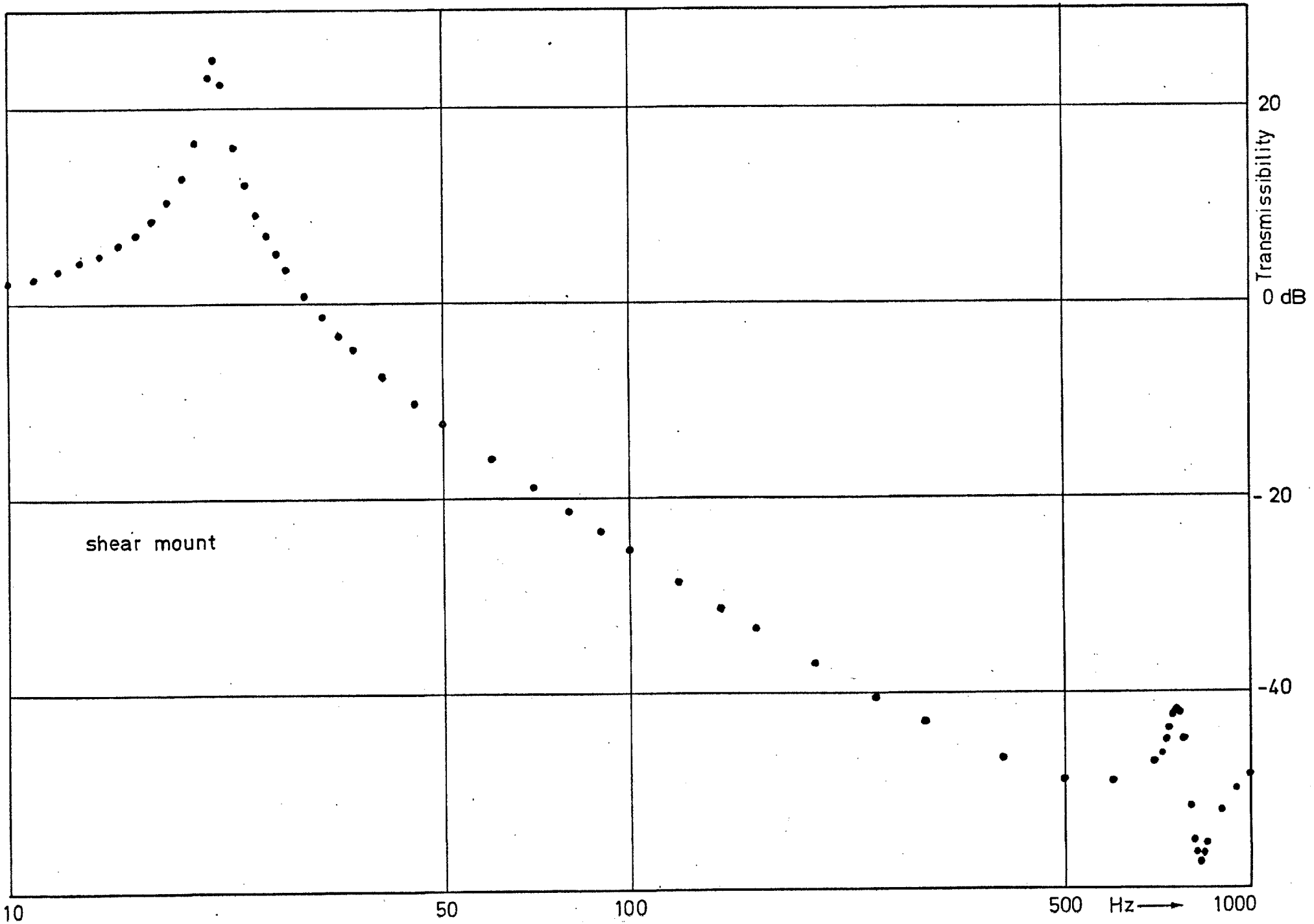

20
0 dB
- 20
-40
Transmissibility
shear mount
10
50
100
500
Hz
1000

Figure 4.4.8

A helical spring was tested in the transmissibility apparatus for two reasons - in the first place to determine the damping in the air bearing as part of the proving, and secondly to show the effects of various practical means of suppressing the spring surges.

Figure 4.4.9 shows the transmissibility through an undamped compression helical spring. The Q-factor for the first resonance is 490, showing that for the other mounts tested the damping from the air bearing is negligible. After the first spring surge, the real spring behaviour is seen to diverge from the simple resonant behaviour predicted theoretically due to real excitation of torsional and bending modes, but generally follows the expected envelope of behaviour up to the fourth mode. The behaviour after this became extremely complicated.

Spring details are shown below:

Helical compression spring - material spring steel

shear modulus 11.5×10^6 lbf/in^2

density .285 lb wt/in^3

number of active coils $8\frac{1}{2}$

wire diameter .28 in.

mean coil diameter 2.7 in.

calculated spring stiffness 52.1 lbf/in.

experimental spring stiffness 51.6 lbf/in.

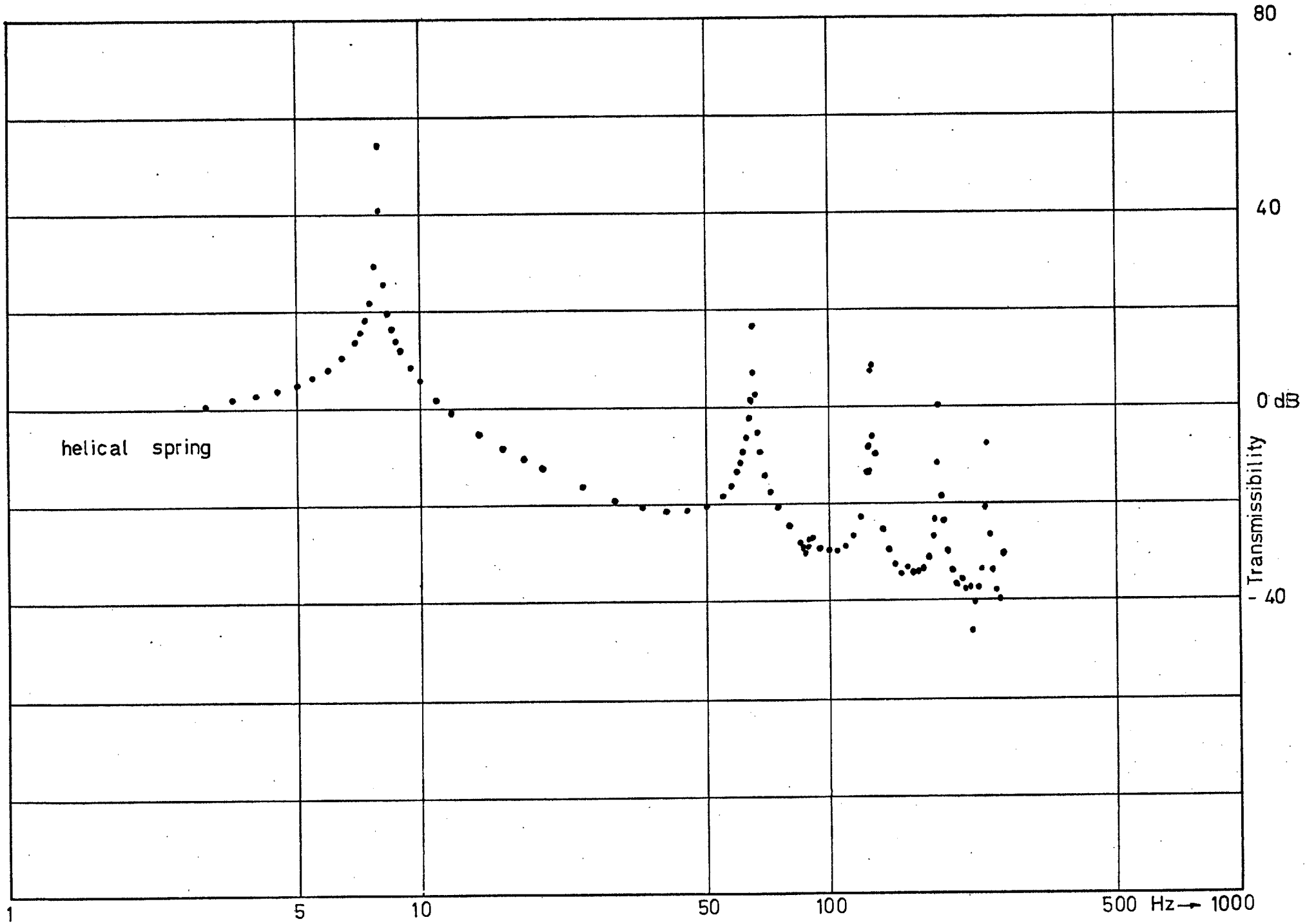

helical spring
80
40
0 dB
- 40
- Transmissibility
1
5
10
50
100
500 Hz→ 1000

Figure 4.4.9

Blocked natural frequencies (theoretical)	Peak transmissibility frequencies (experimental)
63.6	65.4
127.2	127.1
190.8	185.5
254.4	244.0

Figure 4.4.10 shows the effect of the first damping treatment - two strips of velbex p.v.c. ($\frac{1}{2}$ in. wide, 1/16 in. thick) were bonded to the spring on opposite sides. Velbex has a high loss factor, in the region of 0.5 in the frequency range here. Considerable damping is introduced (the loss factor at the fundamental resonance is 0.115), but the surges still increase the level of the transmissibility curve, although heavily damped. The strips increase the stiffness of the spring by 42% to 73.4 lbf/in, which, if a loss factor of 0.5 is assumed, lead to a predicted overall loss factor of 0.147, reasonably close to that measured.

Figure 4.4.11 shows the effect of four damping strips similar to those used previously. If the resonant frequencies are matched it is seen that the high frequency performance is considerably improved. The experimentally determined loss factor at the fundamental resonance is 0.206, and the overall spring stiffness is raised to 100 lbf/in. The estimated loss factor from the properties of velbex is 0.216.

Frictional damping is often advocated. Figure 4.4.12 shows the effect of 1/16 in. sheet of velbex wrapped all round the spring, but not bonded, being wired in position. The low

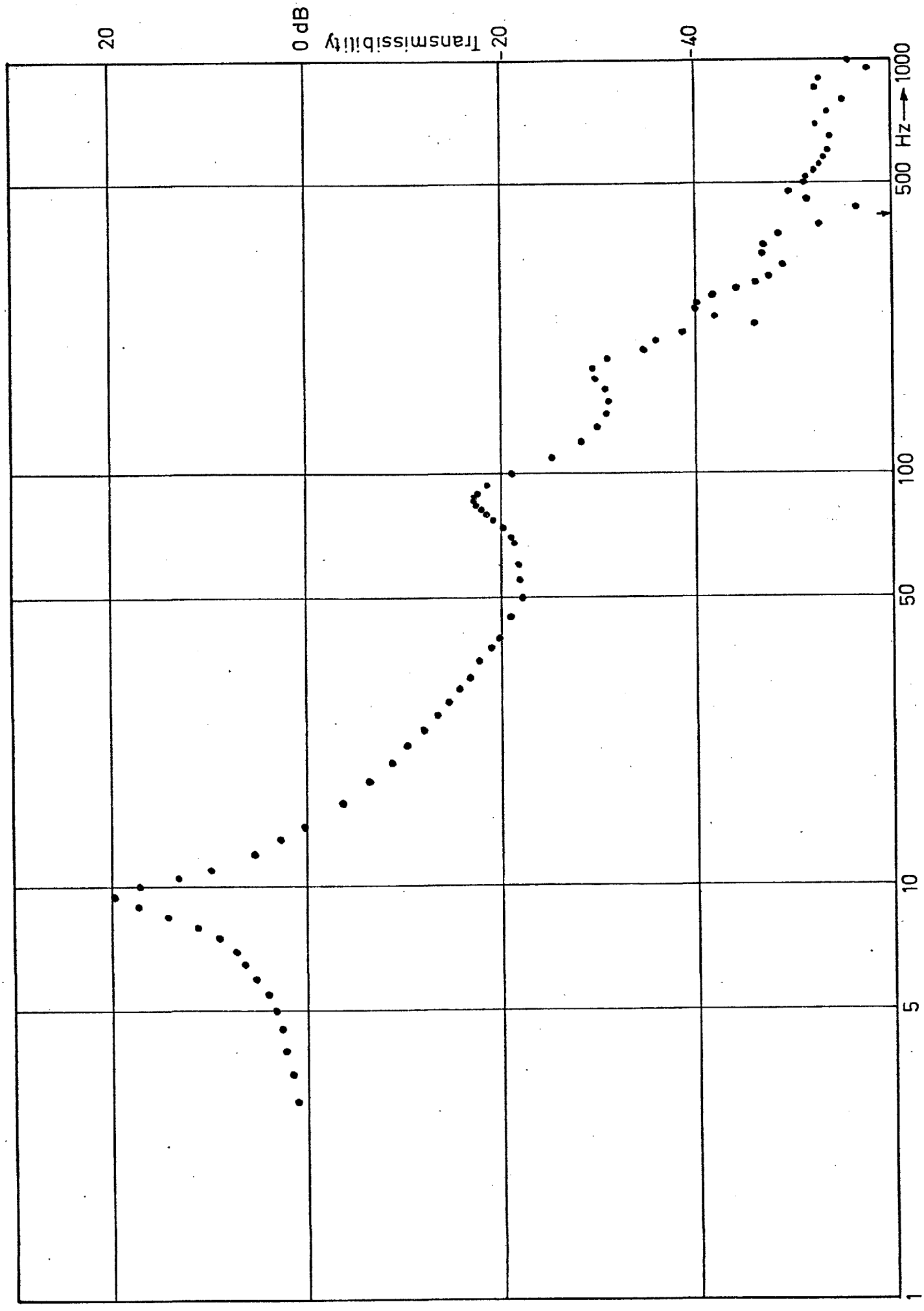


Figure 4.4.10

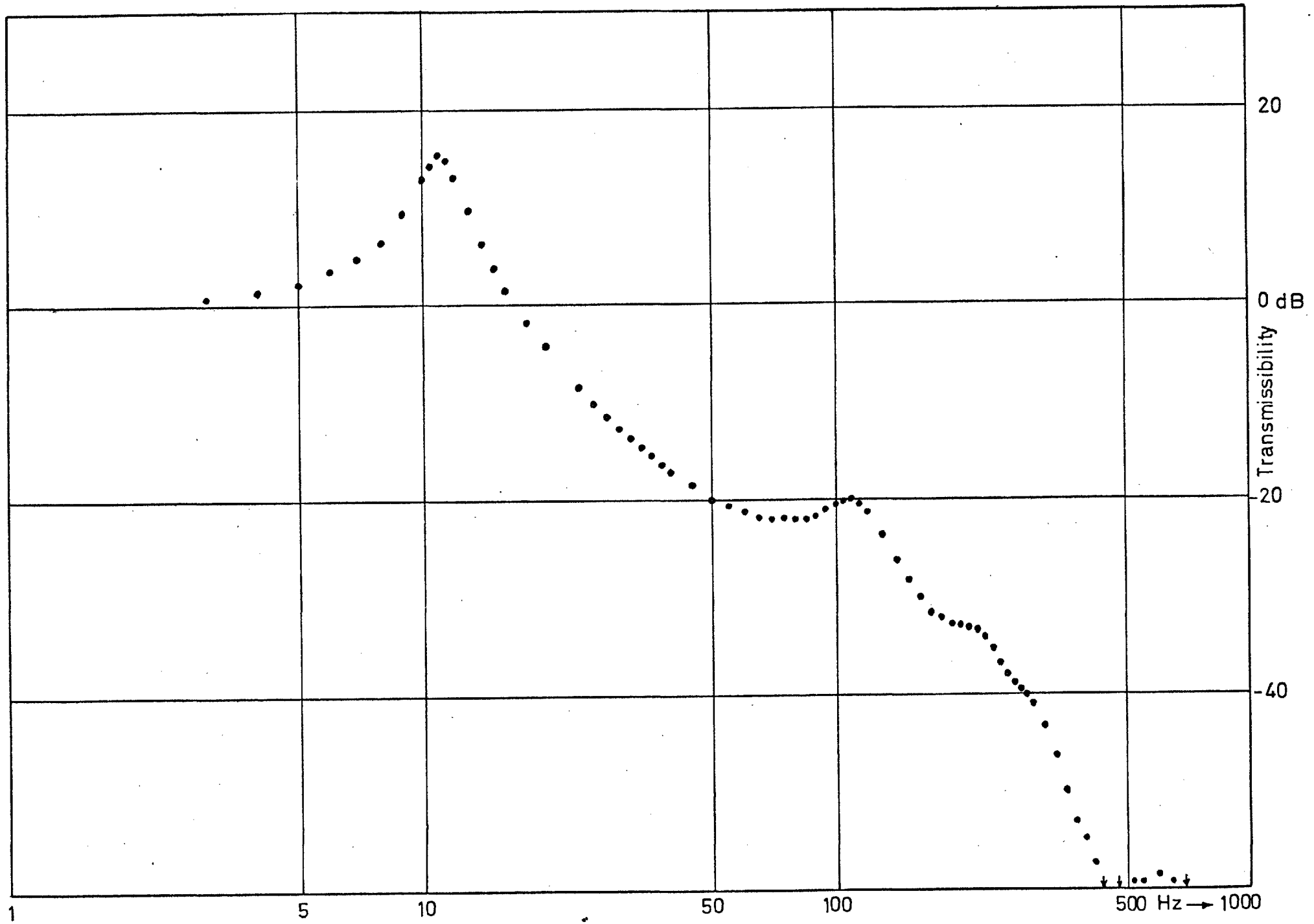


Figure 4.4.11

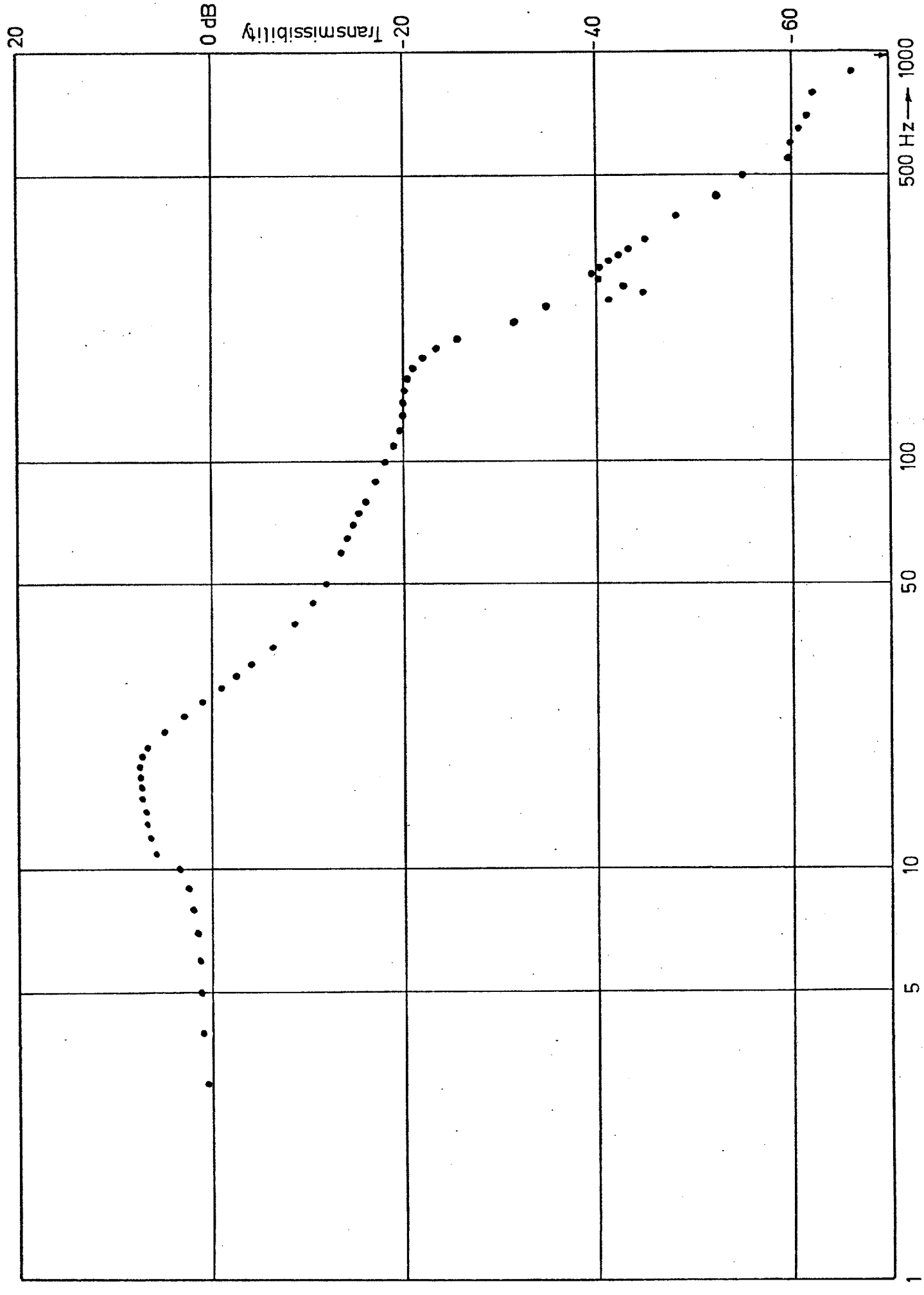


Figure 4.4.12

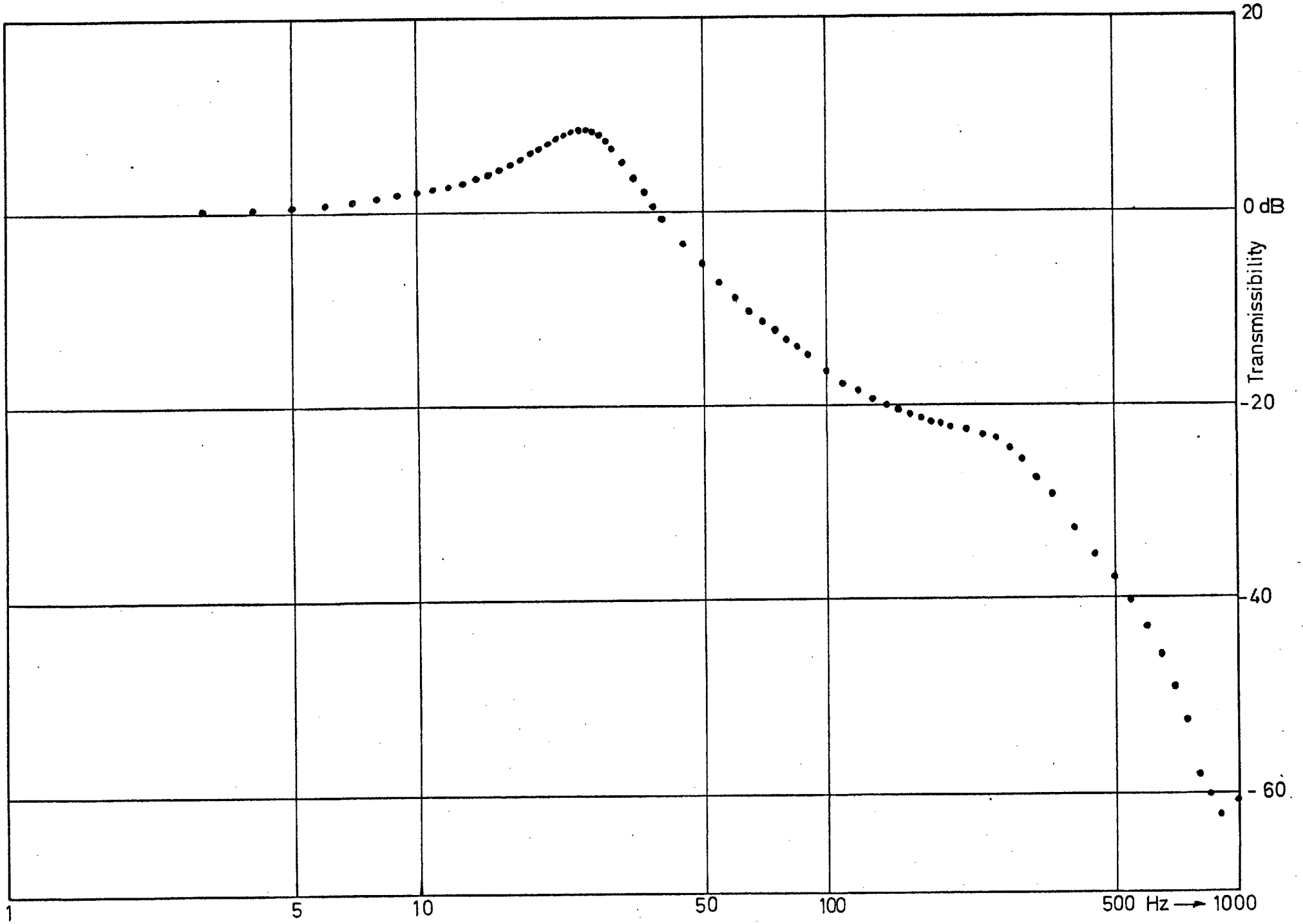


Figure 4.4.13

frequency resonant behaviour is strongly non-linear and the peak is ill-defined (a maximum magnification of 7.4 dB is reached). After the first spring surge, the isolation is seen to be superior to that achieved with the bonded strips, if the resonant behaviour is matched.

Bonding the sheet to the spring gives the transmissibility curve shown in Figure 4.4.13. The transmissibility at resonance is actually increased to 8.6 dB, giving an overall loss factor of 0.475. The overall stiffness of the spring is raised to 550 lbf/in, an increase of 970% over the original spring, which leads to an expected loss factor of about 0.46. Again, fair agreement is achieved. The overall performance is strongly determined by the velbex, and the high frequency behaviour is not quite so good as in the unbonded state.

The following conclusions may be drawn:

1. The damping introduced by the air-bearing in the apparatus is negligible when testing rubber mounts.

2. Helical spring behaviour generally follows the expected form but additional bending resonances are likely to occur.

3. Practical damping treatments can be very effective in reducing the height of resonant peaks, and thus also suppress secondary noise generation, but to be effective the damping must be fairly heavy. As a consequence, when using high damping elastomers the significant change in stiffness must be allowed for.

4. The general level of the transmissibility curve, even for the wall-damped spring, is considerably higher than the ideal 12dB/octave line. The spring surge frequency should be made as high as practicable to keep the surge effects to a minimum.

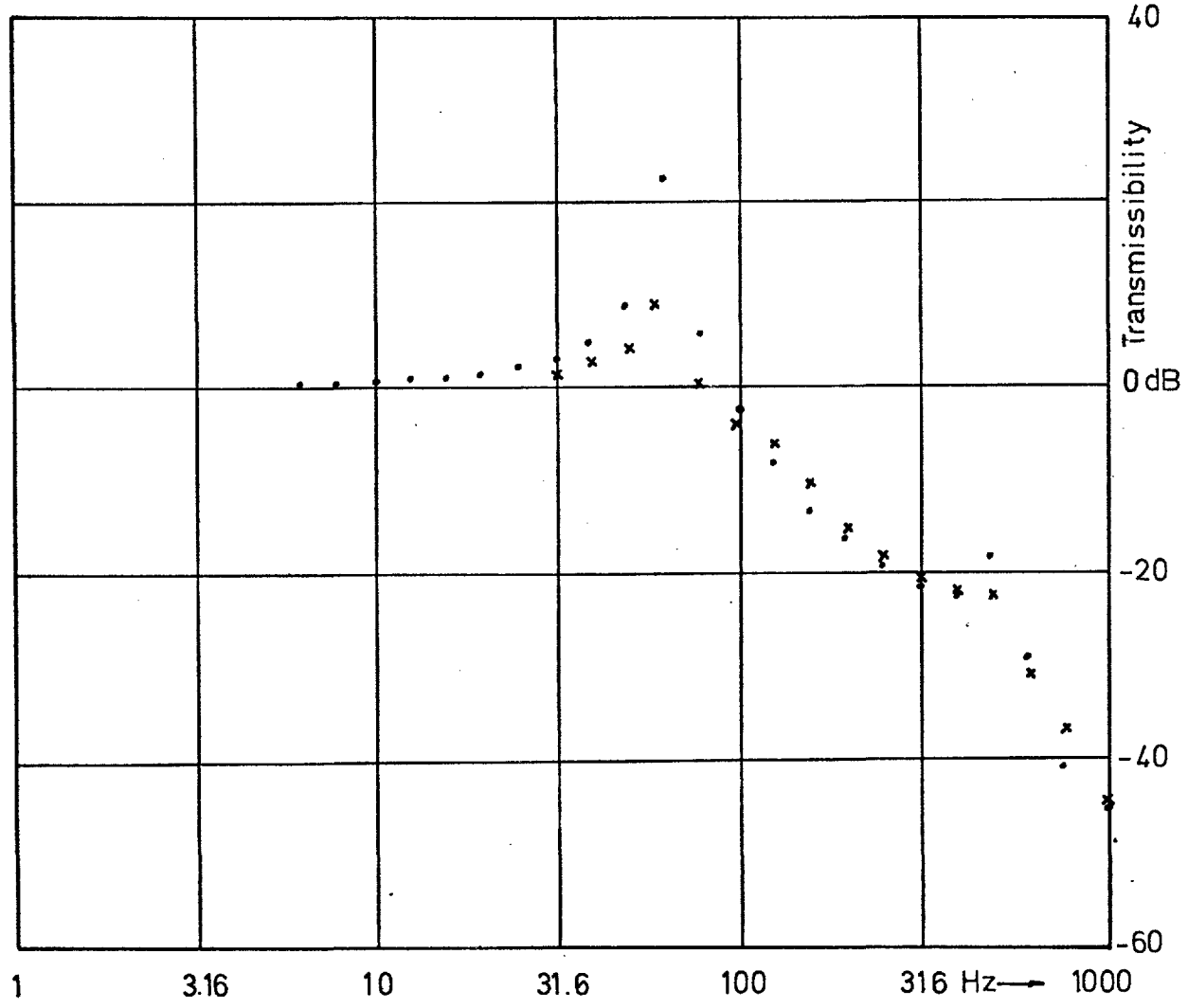
4.4.5 Shock Absorber

The transmissibility apparatus enabled a car shock absorber to be tested, though in the locked state due to stiction, as the forces involved were small. The case where larger forces were used is discussed in Chapter 6. This test enabled the stiffness of the end bushes to be determined as the absorber performed as a two-stage mount.

Figure 4.4.14 shows the transmissibility through the shock absorber. Two resonant peaks are in evidence. After the second peak the attenuation approaches the ideal 24dB/octave line, but levels off near 1 kHz. The high frequency peak is clearly disadvantageous, and increases the transmissibility by up to 7db than if the bottom (very stiff) bush were removed, which would lead to the 12dB/octave line being followed. From the resonant frequencies and knowledge of the weight of the absorber, the bush stiffnesses were calculated. The top bush stiffness was 3,250 lbf/in, with $\eta \approx .07$ at 63 Hz, and the bottom bush stiffness 28,500 lbf/in, with $\eta \approx .15$ at 500 Hz. The top bush was preloaded, as shown earlier and as in the vehicle installation.

• harmonic force

× white noise - 1/10 oct. filter



shock absorber

Figure 4.4.14

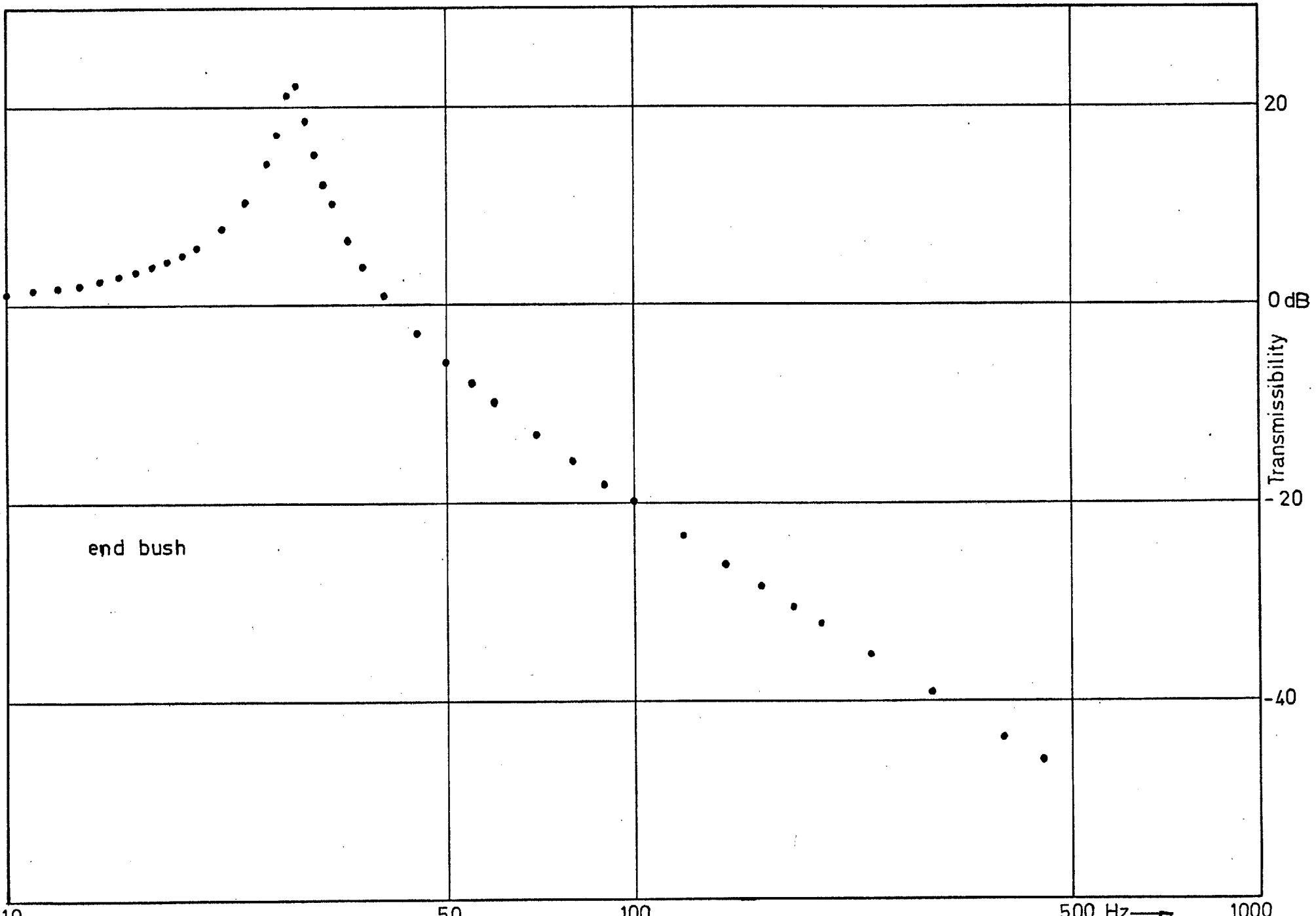


Figure 4.4.15

One half of the bush was tested separately without preload, the transmissibility curve obtained being shown in Figure 4.4.15. The bush stiffness is 618 lbf/in at 29 Hz with a loss factor of 0.059, the properties showing very little change with frequency. The preloading of the bushes previously employed considerably increased their loaded area of the rubber and shortened their length, and led to an increase in the bush stiffness over the unstressed condition by a factor of about 2.6. In the vehicle installation it is evidently possible to make large changes in the bush stiffness.

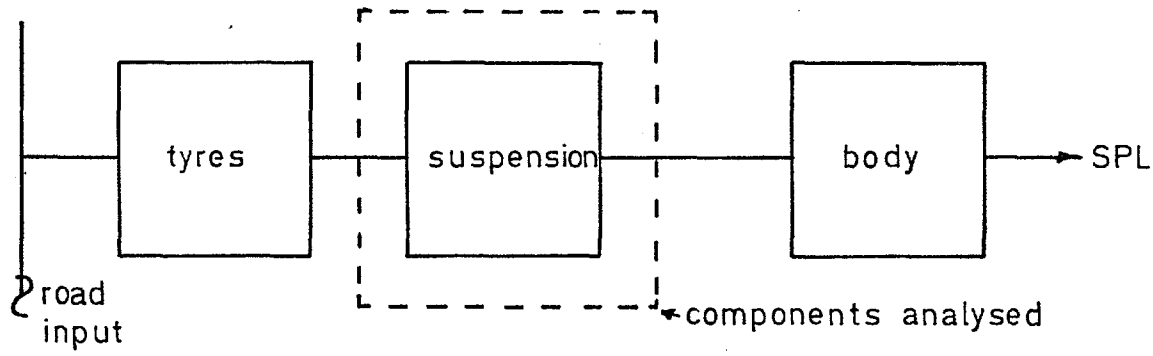
CHAPTER 5

THE TRANSMISSION OF VIBRATION THROUGH AUTOMOBILE SUSPENSION SYSTEMS

The ultimate concern of this work is the relationship between road fluctuations and the interior sound pressure level of an automobile. The engine and associated components are most frequently the prime sources of noise, and have received much attention, but road-induced interior noise can still be of significant proportions. Modern lightweight construction has tended to accentuate the noise levels produced, and no altogether satisfactory means has been found to reduce the noise in the type of vehicle considered - the cheap, mass produced small car where economy is paramount. The aspects of the problem considered here are concerned with the role of the suspension as an isolator of structure-borne vibration, and acoustic paths are not considered. The objective is to model the suspension from drawing board data to a reasonable degree of accuracy, and to compare the predicted response with experimental trials on a typical small car suspension. Considerable complexity is found to be required to model the suspension for a frequency range up to several hundred cycles per second.

5.1 CONCEPTUAL MODEL

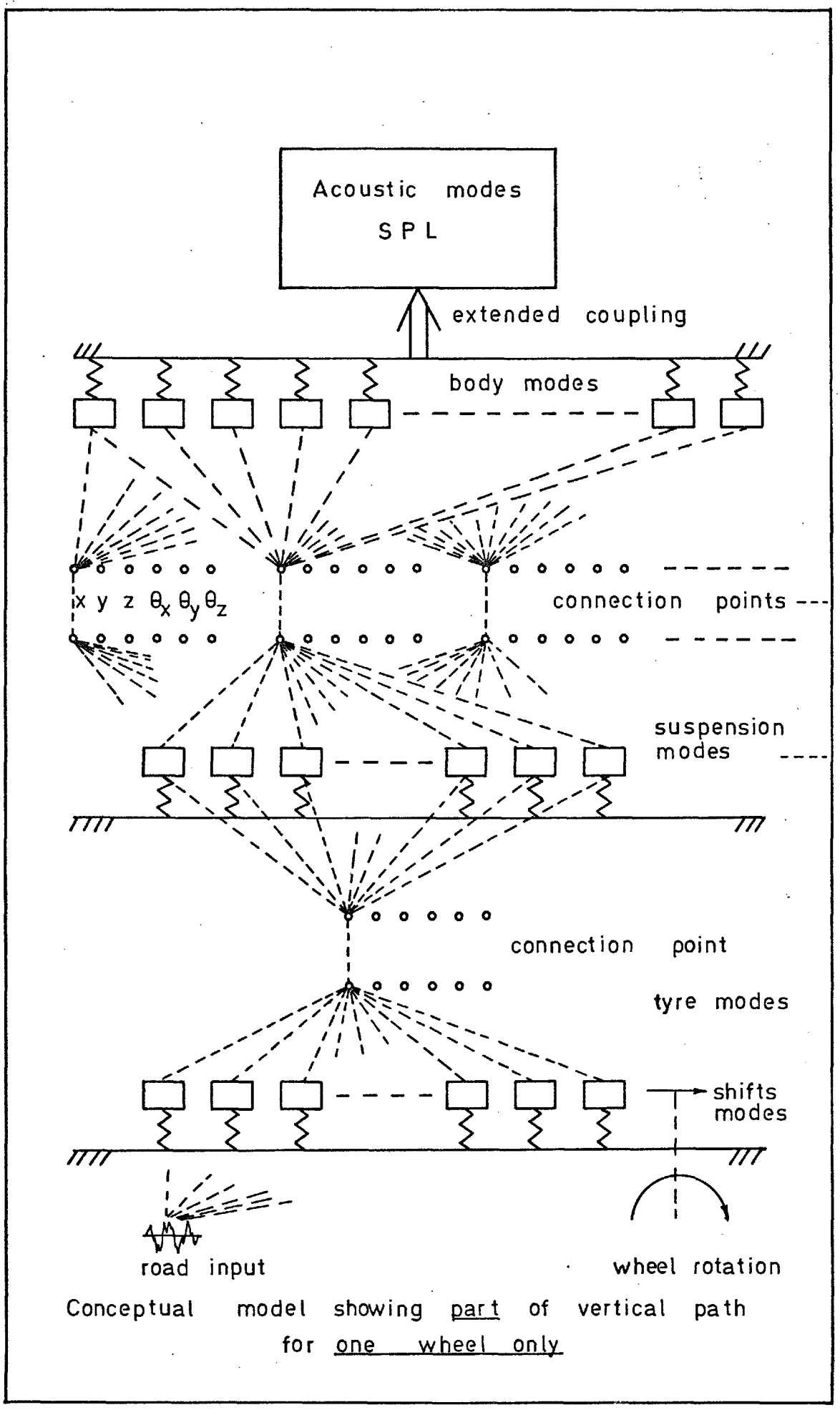
The diagram below shows a conceptual model of the problem considered



For a given vehicle, the sound pressure level depends on the state of the body (windows open or closed, number of passengers), the road speed and the road surface. These may be regarded as external parameters over which there is little control.

The components over which direct control can be influenced are the tyres, suspension and body. The performance of the suspension as an isolator depends on the behaviour of the tyres and body and for these experimental data is used. The complexity of the problem can be envisaged from a more complete representation of the system (Figure 5.1.1).

Multiple coupling occurs between the road input (assumed a velocity-like source) to the tyre modes, thence to the various suspension components, the body modes and thus to the interior sound pressure level which can be influenced by cavity resonances. Between each mechanical connection there are six coupling coordinates, which might mean 120 coupling coordinates to the body alone from the



Conceptual model showing part of vertical path for one wheel only

Figure 5.1.1

suspension. Drastic simplifications are required to reduce the amount of coupling considered, whilst still retaining sufficient information to describe the system adequately.

5.2 BASIC CONSIDERATIONS

The performance of the suspension as an isolator of structure-borne vibration is demonstrated by treating the tyre and wheel as the source and the body as the receiver. The effectiveness of the suspension (defined in Chapter 2) is limited for the following reasons:

1. The suspension provides a multiplicity of paths for vibration, and some are very stiff for handling and tyre wear reasons.

2. The tyre and wheel provide a fairly high mobility source, exacerbated by tyre resonances.

3. The body mobility is much greater than its mass alone would suggest due to its flexibility and position of excitation.

The car body is usually treated first in attempts to reduce the noise, by means of stiffness and damping alterations. There is a definite limit to the amount of noise reduction possible by these means (121).

This section continues to outline in more detail the points raised above before the suspension is considered in depth.

5.2.1 Vehicle Body Mobility

Three basic reasons exist for the high mobility of the vehicle body:

1. The excitation from the suspension is removed from the centre of mass.

2. Significant massive elements - engine, gearbox, - and other elements (driver, passengers) require low frequency support but do not contribute significantly to the vehicle impedance at high frequency as they become decoupled.

3. The body is flexible and displays numerous resonances.

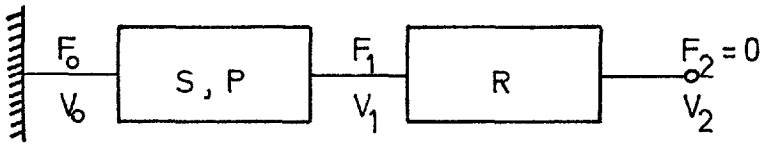
These points are discussed in the following sub-sections.

5.2.1.1 Excitation away from Centre-of-Gravity

The free-impedance of a rigid body will be less than that given by the total mass of the body if the line of excitation does not pass through the centre of gravity. Thus, in a car, the excitation from the suspension is near the corners, a position of low impedance even if the body remains rigid. The suspension (path) and receiver effectiveness ratios will thus be less than if the suspension were to be centrally situated. However, the position of the significant part of the receiver (i.e. the central portion) means that the transfer impedance might be large.

The idea of receiver effectiveness has been disuussed in Chapter 2. This may be extended to cover the transfer case for the receiver giving the interesting result that increasing the receiver impedance may have no effect on the transferred vibration, or even increase it, whilst at the same time the path and receiver effectivensss ratios are improved.

The one-path system is shown thus:



The source and path are lumped together, giving a source-path impedance Z_{sp}. The point impedance of the receiver is Z_R which, when changed to Z'_R gives the receiver effectiveness (with alternative mobility form):

$$E_R = \frac{Z_R' + Z_{SP}}{Z_R + Z_{SP}} = \left(\frac{M_R}{M_R'}\right)\left(\frac{M_R' + M_{SP}}{M_R + M_{SP}}\right)$$

Thus, as shown earlier, increasing Z_R is effective in reducing the receiver velocity V_1 at the drive-point. The receiver-transfer effectiveness is defined by the ratio V_2 with initial receiver properties to V_2 with modified receiver properties, where V_2 is the free velocity of any part of the receiver. Denoting the transfer impedance of the receiver by $Z_T = F_1/V_2$, the receiver-transfer effectiveness is:

$$E_{RT} = \frac{Z_T' Z_R}{Z_T Z_R'}\left(\frac{Z_R' + Z_{SP}}{Z_R + Z_{SP}}\right) = \frac{M_T}{M_T'}\left(\frac{M_R' + M_{SP}}{M_R + M_{SP}}\right)$$

If the transfer impedance is assumed unchanged, then the effect of increasing the point impedance only is given by:

$$E_{RT} = \frac{Z_R}{Z_R'}\left(\frac{Z_R' + Z_{sp}}{Z_R + Z_{sp}}\right) = \frac{M_R' + M_{sp}}{M_R + M_{sp}} = \frac{Z_R}{Z_R'} E_{RT}$$

To show up the significance of this equation, the curve plotted in Figure 5.2.1 shows the regions (shaded) where $|E_{RT}| > 1$ - i.e. the velocity is reduced - with the significant boundaries indicated. It is assumed that the system is undamped and that

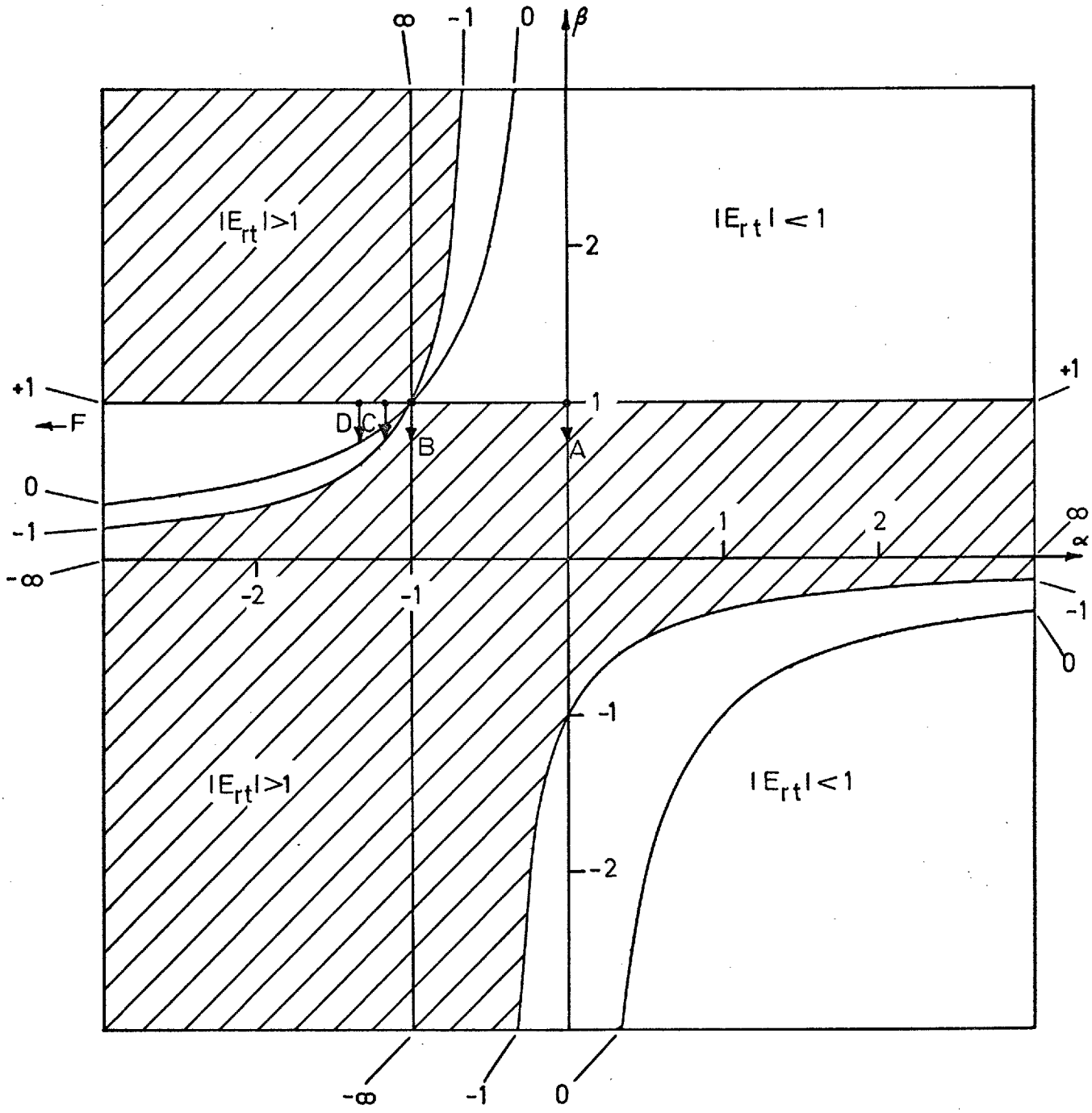
$$Z_R = \alpha Z_{sp}$$

$$Z_R' = \beta Z_R = \alpha\beta Z_{sp}$$

$$\text{i.e. } E_{RT} = \frac{1}{\beta}\left(\frac{\alpha\beta + 1}{\alpha + 1}\right)$$

For example, if α is assumed large positive, an increase in the receiver impedance, $\beta > 1$, reduces the effectiveness. The qualitative reason can be given that increasing β, i.e. the receiver impedance, whilst decreasing V_1 results in the source applying more force to the receiver. Hence, with Z_T fixed, the transferred velocity V_2 must be increased.

Increasing Z_T is seen to effect a direct improvement. In practice however, Z_R and Z_T will be interelated. A simple example is given below to show how a reduction in Z_R, due to excitation away from the centre of gravity, can lead to either no change or an improvement.



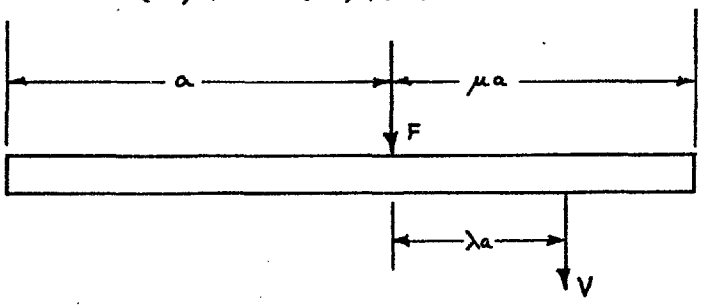
singularities at $\alpha = -1, \beta = 0$ & $\alpha = -1, \beta = 1$

boundaries at $E = 0, \pm 1, \pm \infty$

Figure 5.2.1

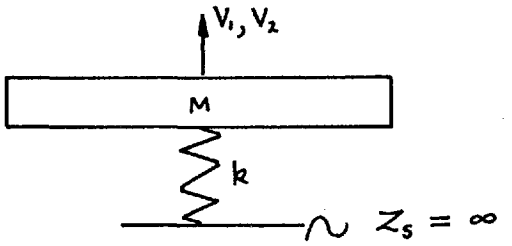
The free-impedance of a uniform, rigid beam, of total mass M, with geometry as shown below, is given by:

$$\frac{Z}{i\omega M} = \frac{(1+\mu)^2}{(1+\mu)^2 + 3(1-\mu)(1-\mu+2\lambda)} \quad , Z = \frac{F}{V}$$



The direct point impedances are obtained putting $\lambda = 0$, and the transfer impedance with $\lambda \neq 0$.

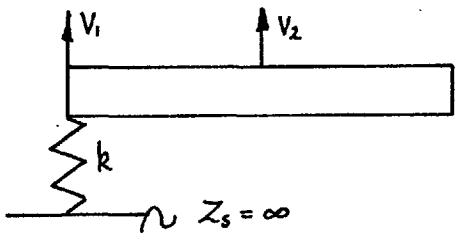
In the initial configuration of the system, the beam is driven from a velocity source through a spring at the midpoint. The midpoint velocity is of interest ($= V_2$).



$$Z_R = Z_T = i\omega M \qquad (\mu = 1\ ,\ \lambda = 0)$$

$$Z_{sp} = k / i\omega$$

The system is then changed to driving at the end of the beam:

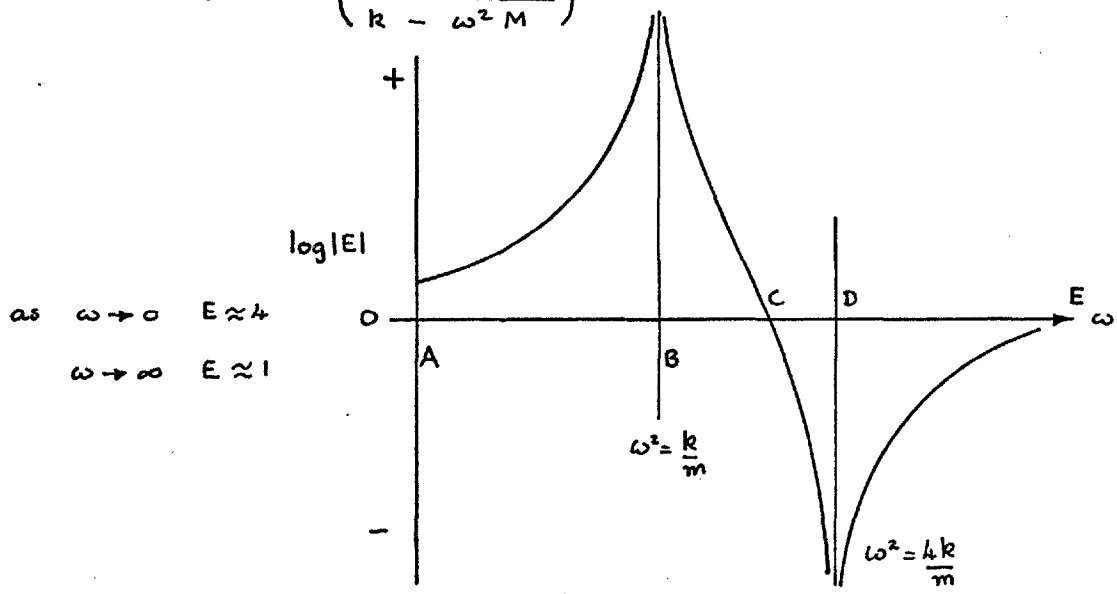


so that

$$Z_R' = \frac{i\omega M}{4} = \frac{Z_R}{4} \qquad (\mu = 0, \lambda = 0)$$

$$Z_T' = i\omega M \qquad (\mu = 0, \lambda = -\tfrac{1}{2})$$

$$\therefore \; E_{RT} = 4\left(\frac{k - 0.25\omega^2 M}{k - \omega^2 M}\right)$$



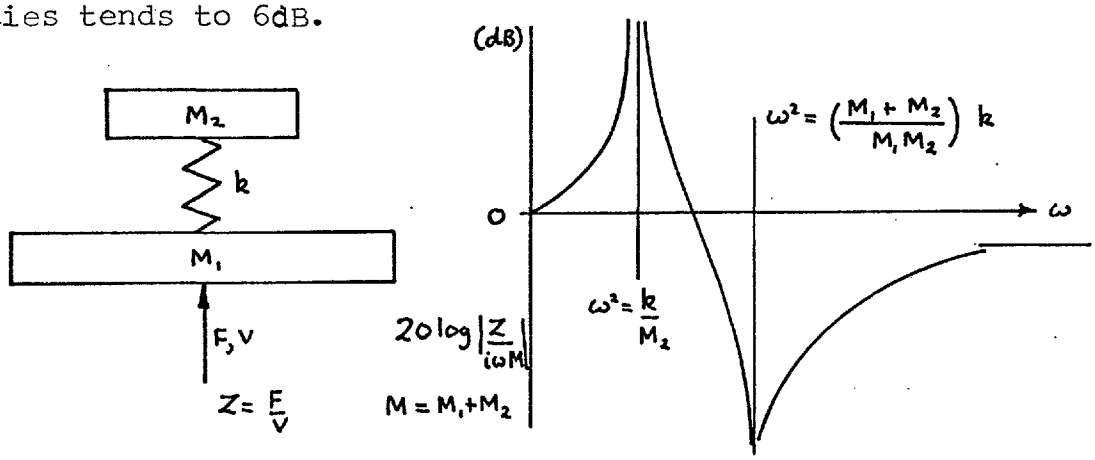
The shifts on the $\alpha - \beta$ plane at frequencies A, B, C, D, and F are shown on Figure 5.2.1. In this simple beam example, the transfer impedance for end excitation can be made infinite - i.e. $V_2 = 0$ regardless of force if $\lambda = -2/3$ - the point at which V_2 is measured then rotates only with zero translation.

Snowdon (92) has shown for the flexible free-free beam that $|Z_T/i\omega M|$ can be made larger than unity for most of a frequency range covering five resonances, for $\mu = 3.348$, $\lambda = 2.5$ with an internal loss factor of unity. Damping, on average, increases Z_T and is thus beneficial.

The approach shown above is somewhat simplified as more than one coordinate is necessary to specify the receiver response, In the case of the beam, if the rotation had been considered, then the system change is disadvantageous as rotation now occurs together with the vertical response.

5.2.1.2 Decoupling of Massive Elements

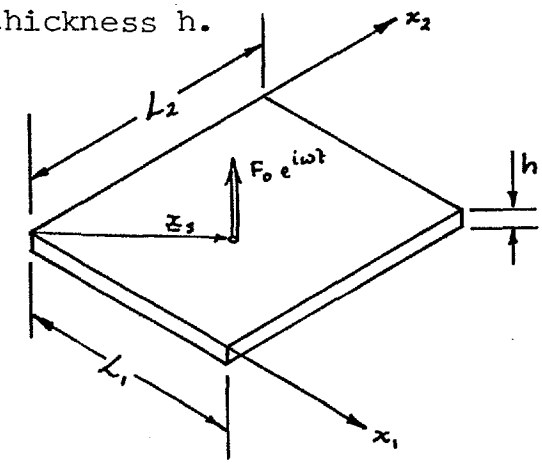
Massive elements within the car structure, such as the engine, are often spring mounted. Thus whilst for low-frequency and static conditions their mass must be considered, and the suspension made stiff enough, at high frequencies they no longer contribute significantly to the body impedance. The simple model below demonstrates the point. If $M_2 = M_1$ then the loss of impedance at high frequencies tends to 6dB.



5.2.1.3 Plate and Shell Results

Plate and shell results can give useful clues for the reasons for the high mobility of the flexible body structure and lead to indications of the important parameters for controlling mobility.

Consider first the simply-supported isotropic rectangular plate, with the bending wavelength λ_b much greater than the plate thickness h.



The plate has a Young's Modulus E, density p, Poisson's ratio ν. Constants for the plate are given by:

$$c_l = \sqrt{\frac{E}{\rho(1-\nu^2)}} \quad , \quad \kappa = \sqrt{\frac{h^2}{12}}$$

(a) Modal density $n(\omega)$ = number of modes/unit frequency

$$= \frac{L_1 L_2}{4\pi c_l \kappa}$$

for sufficient modes considered. Note that $n(\omega) \propto$ area, independent of frequency. It is reasonable to assume for high order modes that the boundary conditions become irrelevant and thus the formula can be applied more generally.

(b) Point mobility of plate - with structural loss factor η

$$M(i\omega) = \frac{4}{\rho h L_1 L_2} \sum_n \sum_m \left[\frac{i\omega \sin^2 k_n x_{1s} \sin^2 k_m x_{2s}}{\omega_{nm}^2 - \omega^2(1-i\eta)} \right]$$

where k represents the wave number and x_{1s} and x_{2s} specify the position of the drive point.

The expectation of $M(i\omega)$, that is the average of

$M(i\omega)$ over frequency and position, is, for small η:

$$E[M(i\omega)] = \frac{1}{8\rho h c_t \kappa}$$

(c) For an infinite plate, letting L_1, $L_2 \to \infty$, the point mobility is:

$$M_\infty(i\omega) = \frac{1}{8\rho h c_t \kappa \sqrt{1-i\eta}}$$

which is the same, for small damping as $E[M(i\omega)]$.

For a steel plate, for example

$$Z_\infty = \frac{1}{M_\infty} \cong 99.2 \times h^2 \quad kg/s$$

where h is measured in mm . Thus for a plate 0.04 in.(1.016mm) thick,

$$Z_\infty = 101 \quad kg/s$$

$$\text{or} \quad M_\infty = 9.9 \times 10^{-3} \quad s/kg$$

(d) For a finite plate, $M(i\omega)$ fluctuates rapidly with frequency at low frequency, but at high frequency tends to $M(i\omega)$. This condition is sensibly reached when:

$$\omega\eta > \Delta\omega_n = 1/n(\omega)$$

that is, when the mode bandwidth exceeds the average mode spacing.

(e) The infinite plate (M_∞) mobility becomes much larger than the mobility of the plate if it remained rigid - say M_o

$$\left|\frac{M_\infty}{M_o}\right| = \left|\frac{i\omega A}{8 c_t \kappa}\right| = \left|\frac{i\omega\rho A h}{8\sqrt{\rho h D}}\right| = \frac{\pi^2}{2}\frac{A}{\lambda_b^2}$$

where $A = L_1 L_2$

D = plate flexural rigidity = $Eh^3/[12(1-\nu^2)]$

Thus, for high order modes, $A >> \lambda_b^2$

(f) The mean power flow into an undamped infinite plate is given by:

$$\Pi = F_o^2/(16\rho h c_t \kappa)$$

(g) In the case of rotational mobilities for a plate - i.e. the rotational velocity to an applied moment - the result obtained depends on the form of application of the moment. Thus, for a moment applied as a dipole of forces with mutual distance d: (144)

$$M_{rot}^{\infty} = \frac{\omega}{4D}\left[\frac{1}{4} + \frac{i}{\pi}(1 - \ln kd)\right] \qquad kd \ll 1$$

whilst for the moment applied over a disc of radius a

$$M_{rot}^{\infty} = \frac{\omega}{4D}\left[\frac{1}{4} - \frac{i}{\pi}\ln ka\right] \qquad ka \ll 1$$

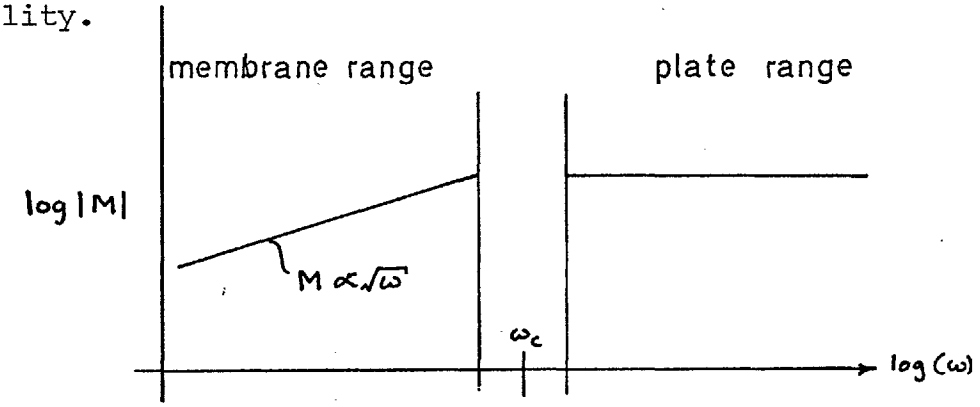
where $k = \omega/c$ = wave number for bending waves

c = propagation velocity for bending waves.

Thus for a or $d \to 0$ the mobility becomes infinite. These difficulties exist even if more accurate bending wave equations are used.

(h) Certain distinct changes from the above results are apparent in the mobility of a cylindrical shell. With certain basic assumptions, i.e. the shell is neither very thick or very short, the following results can be obtained (173):

1. In the membrane range, i.e. $\omega < \omega_c$ where ω_c is the radial resonant frequency, the characteristic point mobility increases proportionally to the square root of the frequency, attaining the plate mobility at ω_c. It then increases by a factor about 0.15 ln (8OR/h) where R is the shell radius over a small frequency range and then stays constant at twice the plate mobility.



2. The modal density increases in the membrane range, reaches a peak at $\omega = \omega_c$ and then settles down to a steady value twice as great as that of a plate of the same area and thickness.

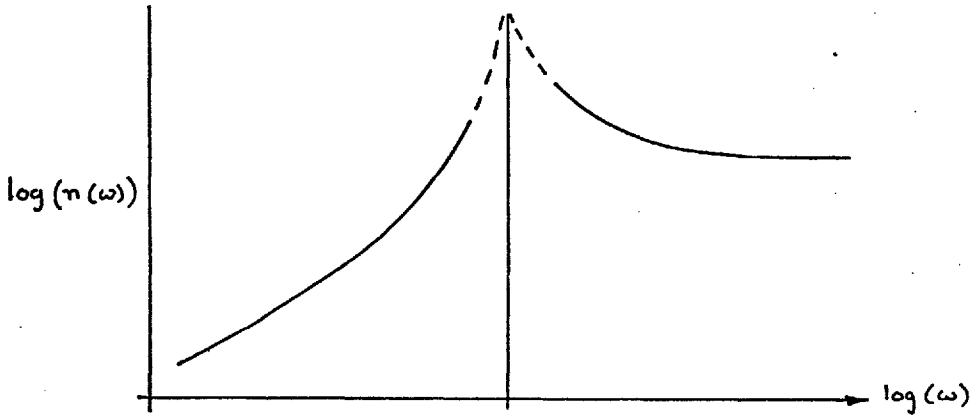


Plate and shell results must be applied with a certain amount of caution to a real car structure, but they partially explain the reasons for the high body mobility. Damping has only a small effect on M_∞, but will increase the transfer impedance. Its primary importance is the suppression of resonant peaks in the low frequency range. Increase of the plate flexural rigidity of the car body components decreases M_∞ and $n(\omega)$, but the increased modal separation leads to larger excursions of mobility from the mean at low frequencies and thus renders individual resonances more significant. The central portion of a car body can be crudely represented as a cylindrical shell, and this form of construction has the effect of generally increasing the modal density and mobility from that of a flat plate-like structure.

5.2.1.4 Experimental Data on Car Body Mobility

There is a certain amount of published data on car body mobilities. Data presented by Dunn (130), Dunn and Aspinall (131), and Rodgers (167) will be discussed here.

Table 5.2.1 shows the number of modes excited in 10Hz frequency bands for a vehicle 'C' with different excitation positions (131).

Excitation position	Total	Frequency (Hz)											
		10 - 20	- 30	- 40	- 50	- 60	- 70	- 80	- 90	- 100	- 110	- 120	- 130
2	45	0	1	3	3	5	3	5	5	5	4	6	5
3	42	0	1	3	3	5	5	4	3	4	6	3	5
4	43	0	0	3	5	4	3	4	4	5	6	5	4
5	47	0	1	3	5	4	4	5	5	4	4	6	6
6	40	0	1	3	2	5	4	5	4	4	3	4	5
7	39	0	1	3	2	5	4	6	2	3	6	3	4
12	37	0	1	3	2	5	4	4	3	3	6	2	4
13	50	0	1	4	2	5	4	5	5	4	6	7	7
15	47	0	1	4	2	6	3	5	4	5	7	5	5
Average		0	.89	3.21	2.89	4.89	3.78	4.78	3.89	4.12	5.34	4.55	5.0

Table 5.2.1

Ideally, for such a structure there is no ambiguity about the modes and each column should contain the same numbers. Certain modes are weakly excited and there is some doubt as to whether small peaks are spurious or do represent true modes. Also, the exact boundary conditions are not known for the test. Two mobility plots were eliminated from the table as atypical and misleading.

Using the average number of modes in each frequency band as an estimate of the modal density, a plot of modal density can be formed (Figure 5.2.2).

Reference (131) contains one mobility plot with a frequency scale up to 1.5 kHz. Figure 5.2.3 shows the estimate of modal density in 100 Hz bands, together with the modal density for vehicle bodies tested by Dunn (130) and Rodgers (167) in the 0-100 Hz frequency range.

The accuracy of the higher frequency modal density must be taken as slightly suspect, as limited information is available. The modal density of the body is thus seen to rise to a broad peak in the 50 - 100 Hz band and then decreases to an almost steady value after 400 Hz. In this respect the behaviour crudely approximates to the variations of modal density of a cylindrical shell. The larger vehicle 'C' is seen to have a greater modal density than the other vehicles tested.

To give some idea of the amplitude variation of the mobility curves, the number of resonant peaks greater than

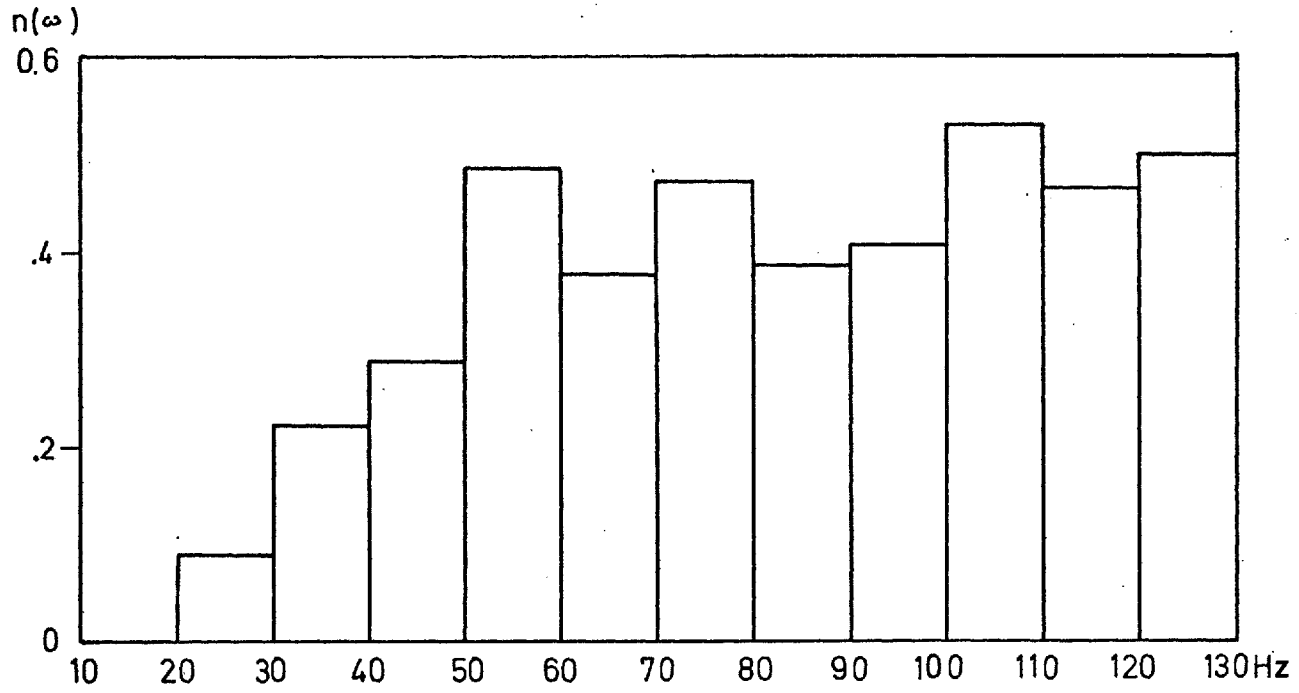


Figure 5.2.2

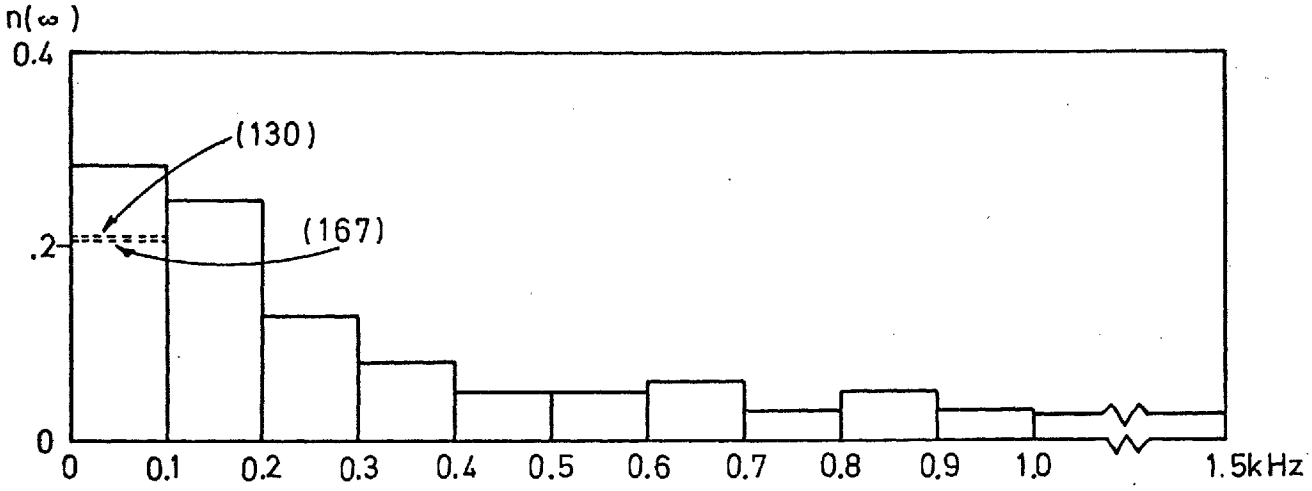


Figure 5.2.3

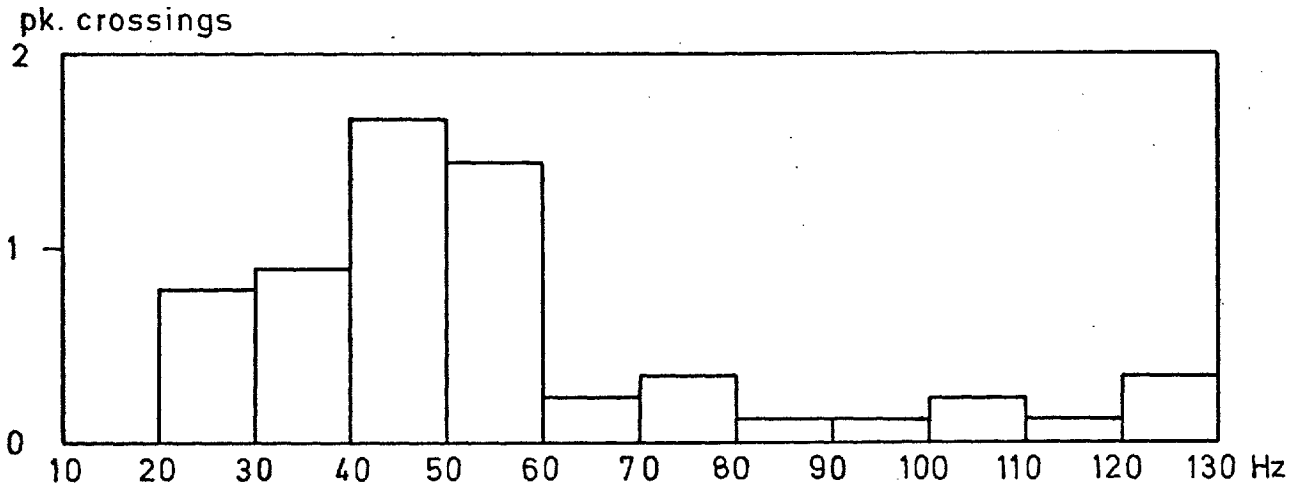


Figure 5.2.4

- 10 dB re 10^{-3} s/kg in each frequency band, averaged out as in the results above, for vehicle 'C', are plotted in Figure 5.3.4.

The regions of highest modal density do not coincide with the regions of highest peak mobility. This may be due to the fact that the low frequency modes are very strongly excited compared with the higher frequency modes.

These results apply to the bare body shell. Adding the doors, windows, bonnet and bootlid significantly increases the damping of the structure (130), reducing the fluctuations in mobility to generally 20 dB. Average mobility levels tend to be in the region of - 20 dB re 10^{-3} s/kg. Structural modifications (167), such as fitting windows, have marked effects on the position of the low frequency modes, but do not appear to change the average mobility very much. Differences between similar production models, and prototypes are evident in detail, but not in average level. Considerable differences in mobility can be found at different excitation positions on a body, and often the stiff-looking drive point does in fact display low mobility. The bare structure appears quite linear, testing at different force levels showing only small changes with generally higher damping for higher force levels (167).

Dunn (130) showed that the enclosing of the vehicle by the addition of doors and windows generally increased the interior sound pressure level for a given input force on the body, most noticeable at frequencies below 60 Hz where the air is springlike. The floor was found to be the primary

noise generator in this region, with the roof as the higher frequencies. Becher (121) used a pipe model to explain the acoustic resonances within the car body. Saunders (170) when measuring internal sound pressure levels of a car in service found that low-frequency air fluctuations tended to overload the measuring equipment. Such infra-sound may have an effect on the passengers and cause discomfort.

Using the experimental data for point mobilities of a car body, and the modelling technique shown in Chapter 3, a modal equivalent system can be derived. Figure 5.2.5 shows the result of such modelling, together with the input experimental points. Q-factors for the modes were presented with the experimental data. The agreement is considered very good, bearing in mind the complexity of the mobility function. It would seem doubtful, however, that the modelling could adequately represent the built-up structure. For comparison purposes, the mobility of a rigid 200 kg mass is shown. The car body is seen to have significantly higher mobility from frequencies of 26 Hz upwards.

5.2.2 Tyre and Wheel Mobility

The source mobility of the tyre and wheel is obtained by fixing the tyre tread at the contact point and measuring the mobility at the wheel. A first simple model for a tyre and wheel is shown below, together with a sketch of the source mobility, for vertical vibrations.

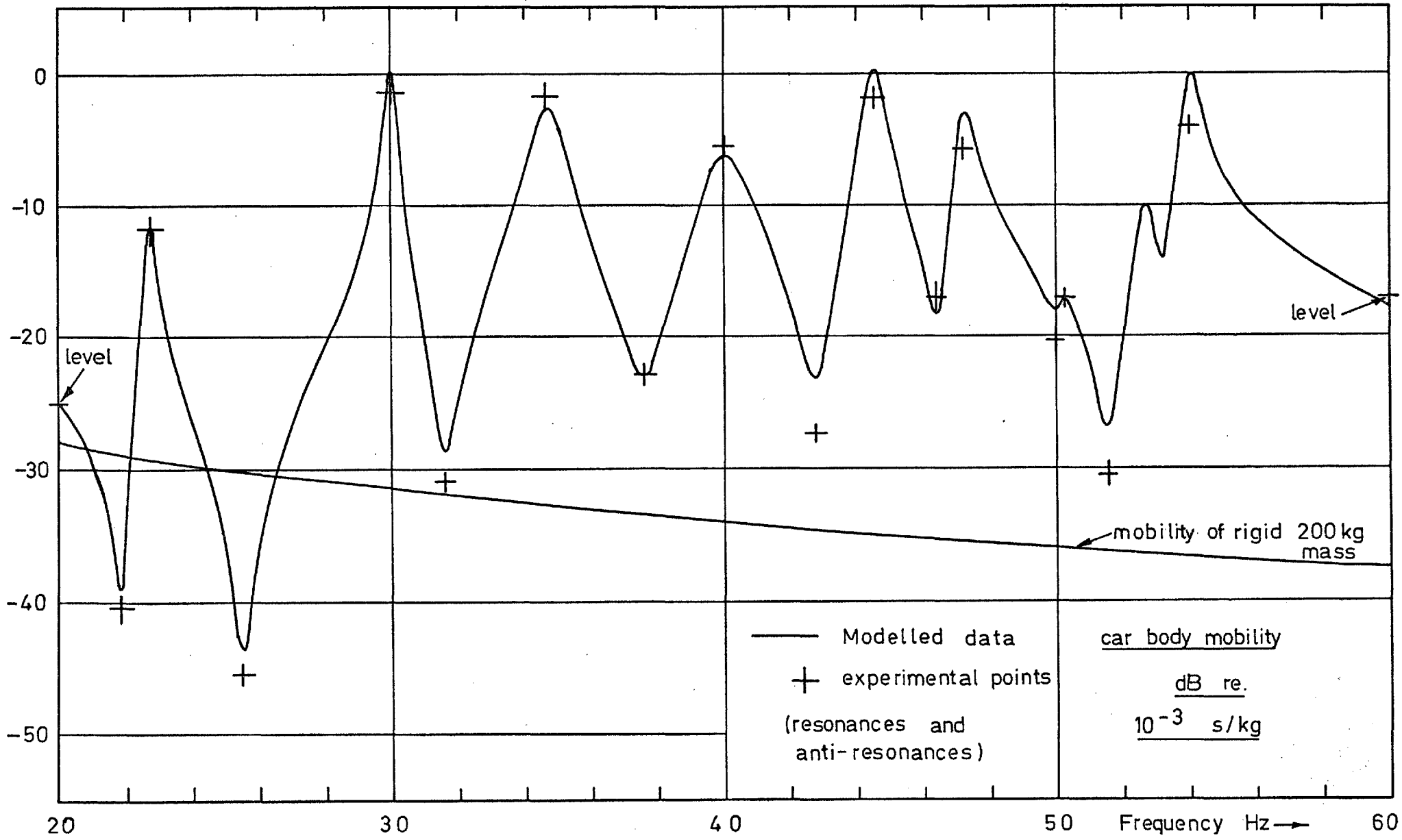
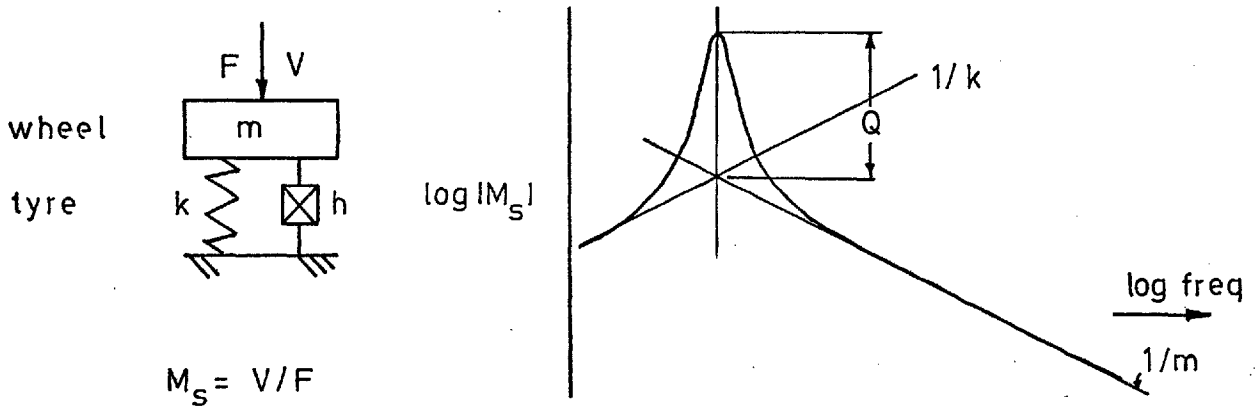
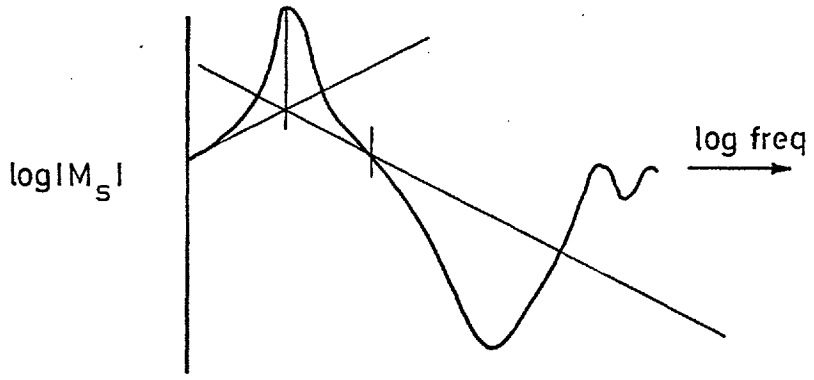

0
-10
-20
-30
-40
-50
level
level
mobility of rigid 200 kg mass
Modelled data
experimental points
(resonances and anti-resonances)
car body mobility
dB re.
10⁻³ s/kg
20
30
40
50
60
Frequency Hz

Figure 5.2.5



The behaviour of this model is very straightforward. In particular, it is seen that at high frequencies (in the range of interest) the mobility is controlled principally by the wheel mass. Thus variations of the tyre stiffness (k + ih) with frequency have only a small effect on M_s. A similar type of model could be used for the lateral behaviour of the tyre as well as the vertical.

Dunn and Mills (132) have experimentally measured M_s for a stationary tyre. The appreciable distributed mass in the tyre means that tyre resonances occur at fairly low frequencies. The figure below shows a sketch of the tyre mobility found for a radial ply tyre, and probably characterises the type of behaviour for this type of tyre in general.



A Q factor in the region of eight is found for the lowest resonant peaks. The effect of the tyre behaviour is to reduce the mobility of the source from the mass line in

the region 30 - 92 Hz, by as much as 26 dB. Above this frequency the mobility is much greater than the mass line, reaching peaks of 16 dB and 12 dB above the mass line at frequencies of 106 Hz and 123 Hz. Over the whole frequency range from 30 - 130 Hz the source mobility is thus similar to the mass line on average, but the effect of the resonances is to introduce significant fluctuations in Ms and thus make the tyre resonances obtrusive in the overall vehicle response at high frequencies. The effect of the tyre rolling has not been given.

The fluctuations in tyre mobility are controlled by the tyre modal mass and damping. Damping is generally undesirable in the tyre because of heat generation, and so the main parameters for controlling the high frequency response are the tyre modal masses and the coupling factors.

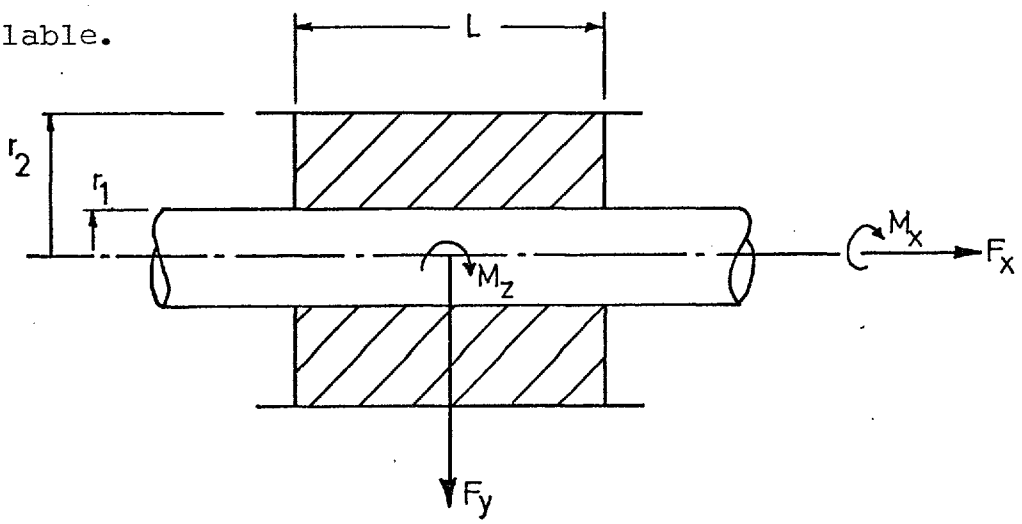
It would appear likely that the lateral and longitudinal responses of the tyres would show a generally similar trend, as the same tyre modes would be excited.

The real tyre and wheel behaviour is thus seen to be inferior to the case of the simple model, and in the higher frequency range tends to reduce the effectiveness of the suspension.

5.2.3 Suspension - Low Frequency and Static Constraints

In this section some of the effects of compliance introduced by the use of rubber bushes on the inboard pivots of a twin-wishbone front suspension are discussed for low-frequency and static conditions. Only the stiff suspension paths are considered, with the object of finding the softest bushes for a given amount of overall stiffness required for handing and ride requirements. Rubber bushes are commonly employed on the inboard pivots to stop noise generation, but do provide compliance that can lead to some vibration isolation at high frequencies, though this is by no means automatic.

The annular rubber bush is able to provide stiffness in all directions which can be tailored to meet the requirements by means of changing its shape. The formulae for the simple bush are shown below, after Davey and Payne (129). There are four separate bush stiffnesses, and two pairs of similar bush stiffnesses. However, since there are only three parameters independently variable, it will not be possible to satisfy each stiffness requirement exactly. Practical bushes differ somewhat from this simple case, and for these sufficient independent parameters will be available.



$$\frac{F_x}{x} = \frac{2\pi LG}{\ln(r_2/r_1)} \qquad \frac{F_y}{y} = \frac{7.5\pi LGf}{\ln(r_2/r_1)}$$

where G is shear modulus

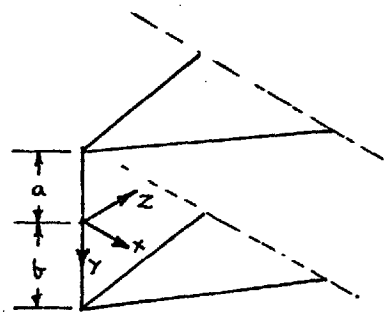
$$f = 1 + \frac{0.0097L^3}{(r_2 - r_1)^3}$$

$$\frac{M_x}{\theta_x} = \frac{4\pi LG}{\left(\frac{1}{r_2^2} - \frac{1}{r_1^2}\right)} \qquad \frac{M_z}{\theta_z} = \frac{\pi L^3 G (X^2+1) N}{(X^2+1)\ln X - (X^2-1)} \quad \text{(not accurate)}$$

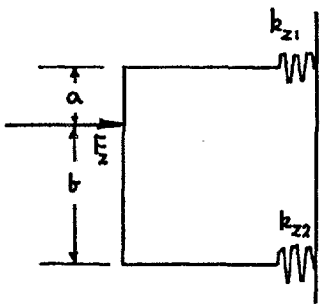
where $N = 1/3$ for long bushes, $4/3$ for short bushes

$X = r_2/r_1$

The suspension considered is highly simplified, and comprises two wishbones and a stub axle only. Ball joints are considered on the outboard pivots, and rubber bushes for the inboard pivots. The forces acting on the stub axle are considered, with the vertical force neglected as this will be primarily carried by the main spring. The torsional (θx) stiffness of the bushes then contributing a certain (unnecessary) stiffness.



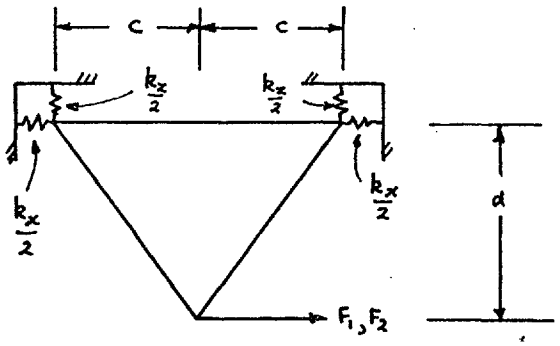
Considering the force in the z-direction first, the suspension can be represented as shown below, where k_{z1} represents the combined radial stiffness of the upper wishbone bushes, and k_{z2} the lower bushes.



A simple form of optimum for this case is that only a pure translation results from F_z, thus

$$\frac{k_{z1}}{k_{z2}} = \frac{a}{b}$$

The displacement of each wishbone due to a force in the x-direction is given by:



$$x_1 = F_1 \left(\frac{1}{k_{x_1}} + \frac{1}{r^2 k_{z1}} \right)$$

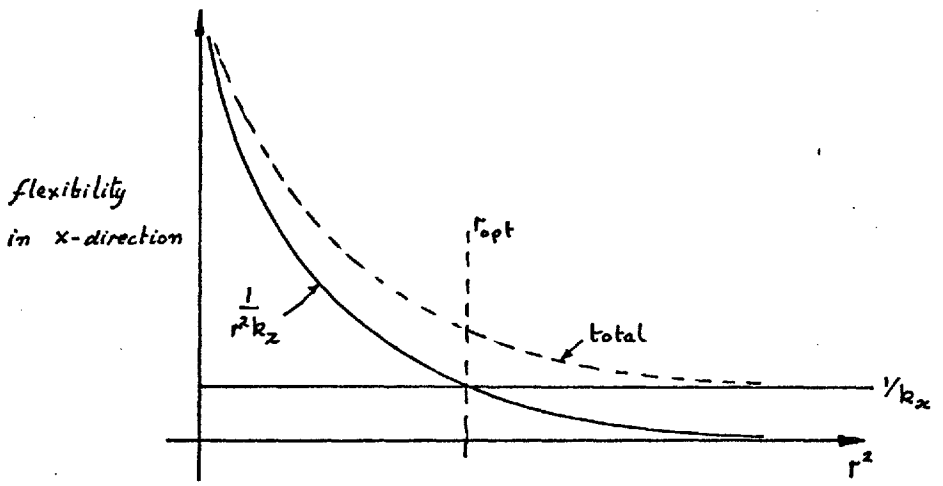
$$x_2 = F_2 \left(\frac{1}{k_{x_2}} + \frac{1}{s^2 k_{z2}} \right)$$

where r = c/d for the upper wishbone

s = c/d for the lower wishbone

The torsional (θ_z) stiffness of the bushes is neglected in the above equations, and small displacements are assumed.

There is no minimum flexibility in the x-direction, but a reasonable optimum is when the bush stiffnesses in both the x- and z- directions make equal contributions, as shown below.



This 'optimum' is then given by

$$r^2\theta_1 = 1 \quad , \quad s^2\theta_2 = 1$$

$$\text{where} \quad \theta_1 = \frac{k_{z1}}{k_{x1}} \quad , \quad \theta_2 = \frac{k_{z2}}{k_{x2}}$$

Thus, for any given geometrical factor r for the wishbone, the required stiffness ratio can be found.

For the force F_x applied at the stub axle, the requirement, for a pure translation to result is that:

$$\frac{a}{b} = \frac{\left(\frac{1}{k_{x1}} + \frac{1}{r^2 k_{z1}}\right)}{\left(\frac{1}{k_{x2}} + \frac{1}{s^2 k_{z2}}\right)} = \frac{k_{x2}}{k_{x1}}$$

Thus, as a result, the factors determining the shape of the wishbone suspension, for equal stiffness contributions by all bushes, and translational responses only to the applied forces, are given by:

$$\frac{a}{b} = \frac{s}{r}$$

and this represents some form of optimum. It is of some interest to note that for the suspension investigated, from a small saloon car, the ratio a/b = 1.5 and s/r = 1.43 which is close to the optimum as defined above.

5.3 TRANSMISSION PROPERTIES OF INDIVIDUAL SUSPENSION COMPONENTS

This section describes the transmission properties of individual suspension components from a small car twin-wishbone front suspension unit, and uses transmissibility plots to provide a quick comparison and enable initial design criteria to be formed. It must be emphasised, however, that the combined response of the assembled suspension will be considerably more complex than the combination of transmissibility plots would suggest, due to the interaction of components with each other. Also, transmissibility plots only demonstrate the effectiveness of the suspension for a special case - that is for a masslike receiver (here), for a source of zero mobility - and they give an optimistic picture to the effectiveness in the real system.

The many possible vibration paths are reduced to just three uncoupled paths for this description - vertical, lateral and longitudinal.

5.3.1 Principal Vertical Paths

The main vertical forces are transmitted via the main spring and damper unit, and less importantly, the wishbones.

5.3.1.1 Helical Coil Spring

The ideal massless spring gives a transmissibility curve as shown in Figure 5.3.1, where small material damping

is considered. The slope of the curve at high frequencies tends to 40 dB/decade, providing a useful reference slope.

The real spring exhibits highly resonant behaviour, a continuum model being shown on the same figure. Besides the effect of the resonant peaks, the slope of the trough line is reduced to 20 dB/decade which means that the high-frequency effectiveness is markedly reduced.

Also shown on the same plot is a lumped-mass approximation to the continuum model which successfully predicts the first two resonant frequencies, but afterwards deviates noticeably.

To minimise the effects of spring resonances it is necessary to damp the coils and also shift the resonances to as high a frequency as possible. The effect of coil damping has been demonstrated experimentally, and the use of high damping strips found to be successful. This was described in Chapter 4. In the combined spring-damper unit, such coil damping can be effective without obstructing the airflow over the damper. Damping at the end of the coils can have little effect.

To increase the resonant frequencies of the coils for a given overall stiffness, a large D/d ratio is required, where D is the coil diameter and d is the wire diameter.

The helical coil stiffness is given by:

$$k = \frac{G d^4}{8 D^3 n}$$

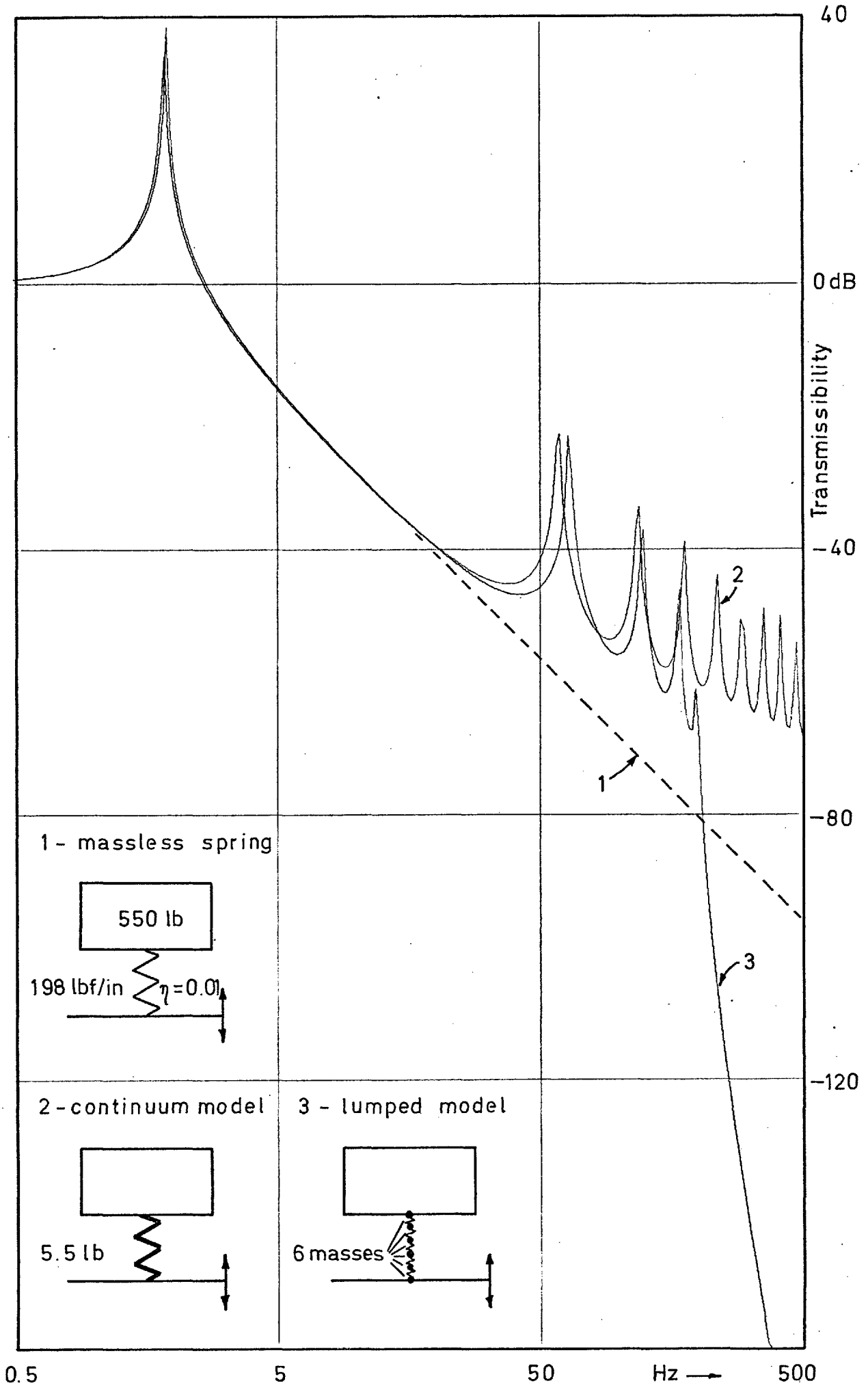

40
0dB
-40
-80
-120
Transmissibility
1
2
3
1 - massless spring
550 lb
198 lbf/in
η=0.01
2 - continuum model
5.5 lb
3 - lumped model
6 masses
0.5
5
50
Hz
500

Figure 5.3.1

where G is the shear modulus of the material, and n is the number of active coils. The lowest natural frequency for spring resonances, for the case where both ends of the coil are clamped (approximately the case in the vehicle suspension) is given by:

$$f_n = \frac{2d}{\pi D^2 n}\sqrt{\frac{Gg}{32\gamma}} \quad (Hz)$$

where γ is the material density, g the acceleration of gravity, and inch units are employed.

The requirement is then that

$$\frac{f_n}{k} = \frac{2d}{\pi D^2 n}\sqrt{\frac{Gg}{32\gamma}} \cdot \frac{8D^3 n}{Gd^4} \propto \frac{D}{d^3}$$

is a maximum. Thus, for a given material, D/d^3 should be large, but this implies high stressing, as the peak stress τ for a given force is (uncorrected case):

$$\frac{\tau}{F} = \frac{8D}{\pi d^3}$$

Conservative spring design is thus disadvantageous from the point of view of vibration isolation, which requires the highest possible stressing.

Modifying the coilspacing at the end of the spring in order to make the surges become non-linear, will limit the height of the resonant peaks, but the resulting closing up of the coils will itself provide a source of noise.

In summary, from the point of view of vibration isolation, high stressing is required coupled with coil

damping.

5.3.1.2 Damper Unit

The damper unit is basically disadvantageous as damping here decreases the mobility of the suspension, and this particular unit provides the most significant vertical path in the intermediate frequency range. It would be preferable to damp the source and receiver, for example by dynamic absorbers as shown in Appendix 1, though this is not popular in practice.

For the pure viscous damper (of constant mobility) the slope of the transmissibility curve tends to 20 dB/decade. The mobility can be increased by a spring in series (relaxation tyre damping or the Maxwell body) which improves the transmissibility slope to 40 dB/decade when the spring becomes more mobile than the damper (Figure 5.3.2).

The real damper may use two springs (in the form of rubber bushes at the ends of the unit) and also possesses mass. These introduce a resonant peak into the transmissibility curve which is predominantly controlled by the spring damping. After the resonant peak there is good attenuation. If one spring only is employed, this resonant peak is removed which leads to a gain in effectiveness in one region offset by an increase in transmission at higher frequencies. The high frequency behaviour becomes independent of the damping coefficient and is controlled by the spring stiffness.

MAX, VISC, EM010

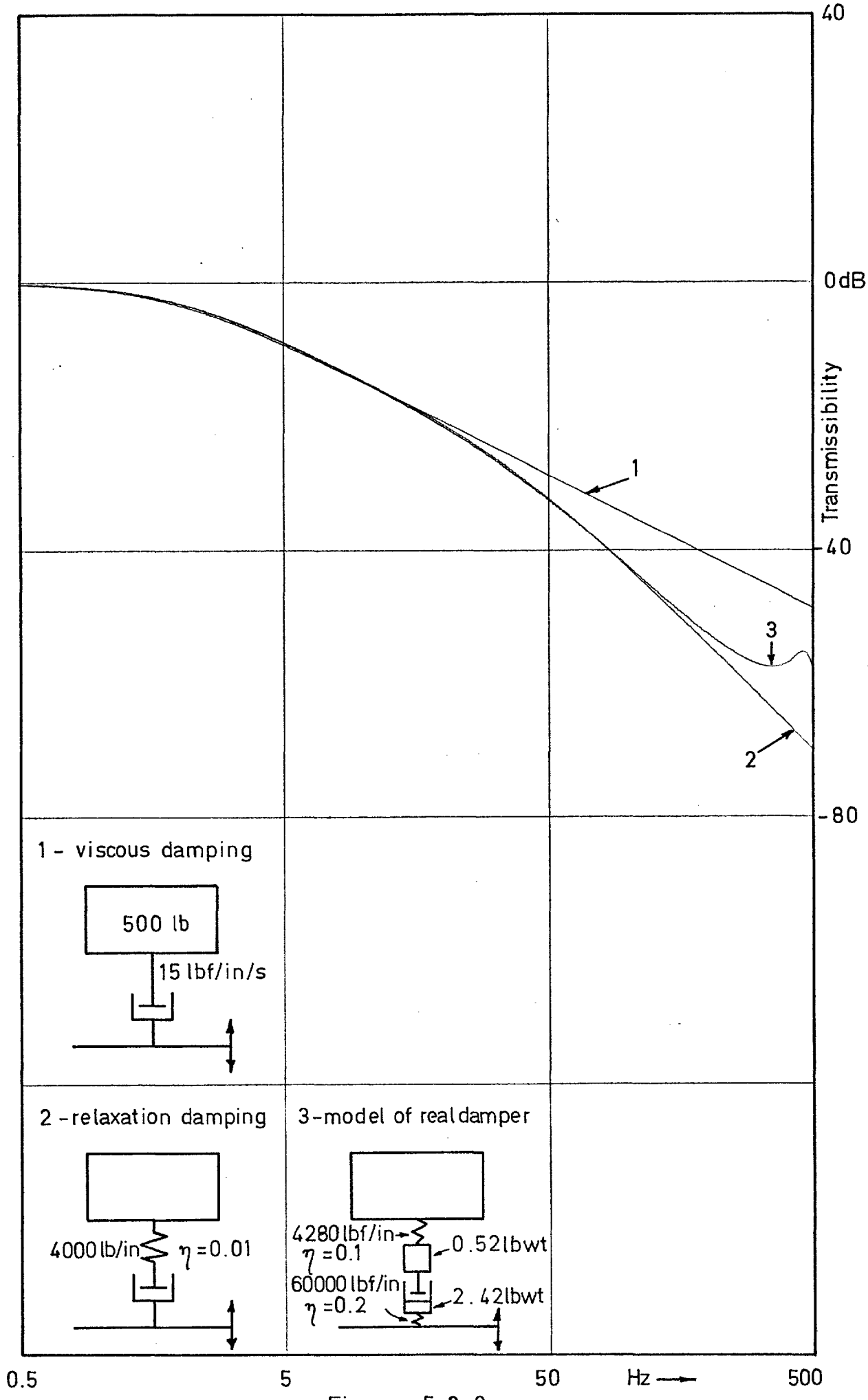


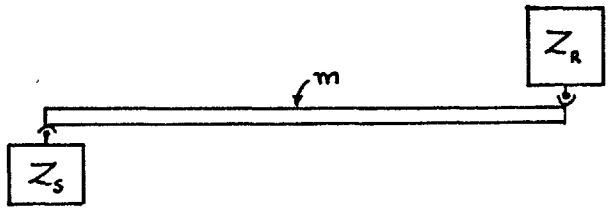
Figure 5.3.2

This will be much greater than the main coil stiffness, and so this path will tend to be a much better transmitter.

The best compromise in the design of the damper unit is then to employ just one end bush (as the lower frequency behaviour will be more important than the high frequency) which should be as compliant as possible whilst still enabling sufficient damping to be provided for the damper to fulfill its main duty. A low-frequency model to derive such an optimum is given in Appendix 1 for comparison with the use of dynamic absorbers.

5.3.1.3 Wishbones and Links

The effectiveness of a uniform rigid beam with freely pivoted end joints can be readily derived.



Using the formula for the impedance of the rigid beam, and for the general isolator effectiveness, we have:

$$E_p = 2 + \frac{6\alpha\beta}{\alpha+\beta} + \frac{1}{2(\alpha+\beta)} \quad \left(\approx \frac{6\alpha\beta}{\alpha+\beta} \text{ for large } \alpha,\beta\right)$$

where $\alpha = Z_S/i\omega m$, $\beta = Z_R/i\omega m$ and m is the mass of the beam. The transmissibility, where m' is the mass of the receiver, is given by:

$$T = \left[\frac{6m'}{m} + 2\right]^{-1}$$

The transmissibility is then small provided $m \ll m'$ which will normally be the case. Viscous damping at the pivots will increase the low frequency transmissibility (Figure 5.3.3) and is thus disadvantageous. An inboard bush with radial and torsional stiffness will also generally increase transmissibility. The torsional stiffness increases the low frequency transmissibility, whilst at high frequency the link will resonate due to the radial stiffness. The curve shown also includes a lateral weakly excited resonance, which occurs when the link is inclined from the horizontal. After these high frequency resonances, the radial stiffness of the bush increases the isolation of the link, but the advantage of this is offset by the resonances. The transmission in the freely pivoted case can be made zero, as was shown before, if the inboard pivot is two-thirds along the length of the beam, provided it remains rigid. This is simple dynamic balancing. For the non-uniform case of the practical wishbone the proportion will, of course, be different. The flexible beam will increase the transmissibility above that of the rigid case, as is also shown on the figure, and high damping should be employed to damp the resonances.

General design criteria are: links should be light, very stiff and well damped, with a free inboard pivot ideally. If a flexible bush is used (to eliminate noise generation from clearance), the radial stiffness in the vertical direction should be extremely high or very low (the latter introducing a resonance in the working range), whilst the torsional

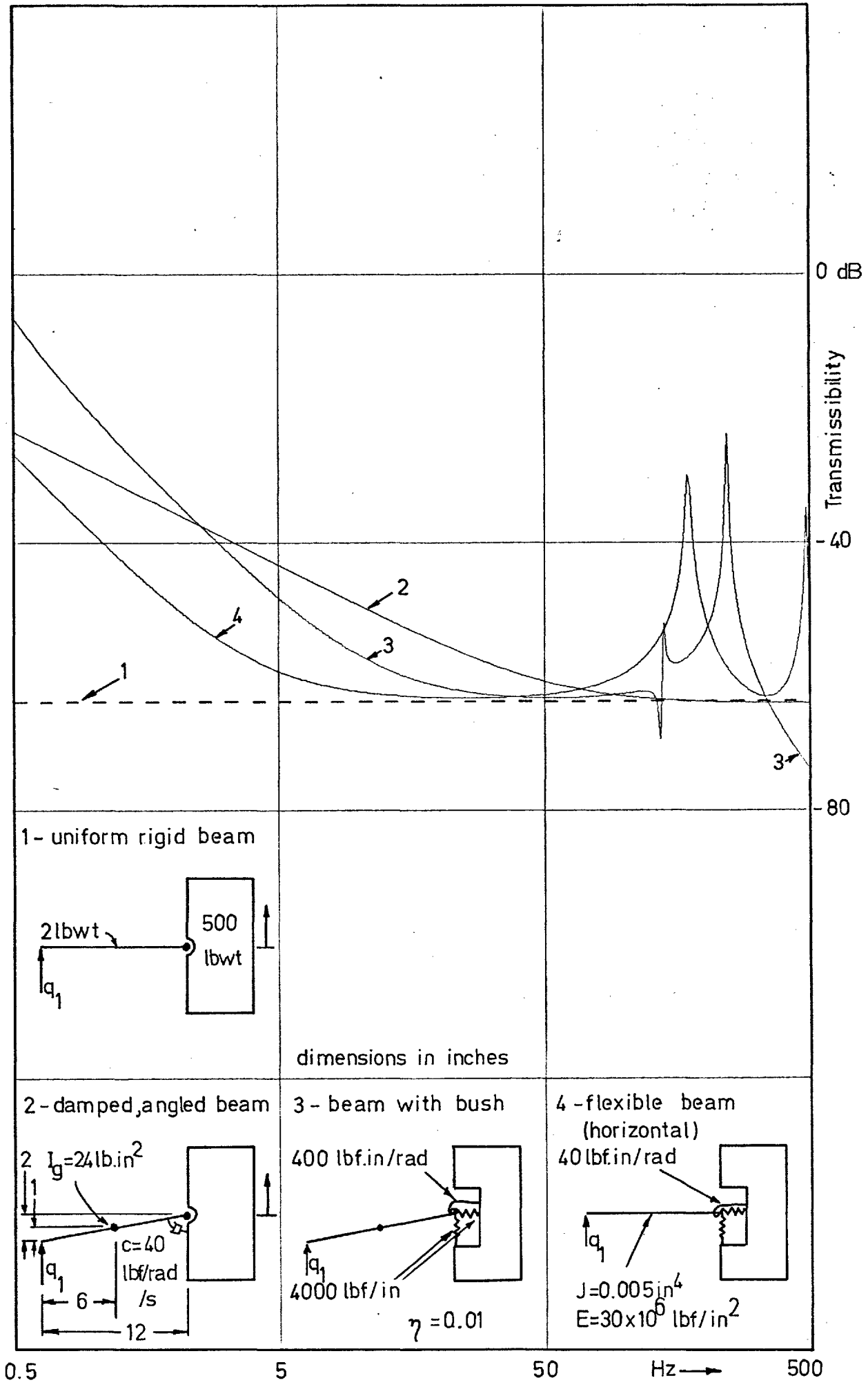

0 dB
- 40
- 80
Transmissibility
1
2
3
4
3
1 - uniform rigid beam
2 lbwt
500 lbwt
q_1
dimensions in inches
2 - damped, angled beam
2
1
I_g=24 lb.in^2
q_1
c=40 lbf/rad /s
6
12
3 - beam with bush
400 lbf.in/rad
q_1
4000 lbf/in
η =0.01
4 - flexible beam (horizontal)
40 lbf.in/rad
q_1
J=0.005 in^4
E=30x10^6 lbf/in^2
0.5
5
50
Hz
500

Figure 5.3.3

stiffness should be low unless designed to share the load of the main spring. The outboard pivot should also be as free as possible. Correct balancing of the wishbones and links will reduce their transmission, with zero transmission theoretically possible.

5.3.1.4 Comparison

The relative significance of the different paths depends on the parameters chosen for the separate components. The Figure 5.3.4 shows a comparative set of curves for fairly representative components, and gives the regions of significance. For the static to the lowest resonant frequency, the spring provides the principal path. In the intermediate frequency range, the damper unit is predominant. At the high frequency end of the curve all three paths become of comparable importance.

5.3.2 Lateral and Longitudinal Paths

The source of excitation is the lateral and longitunidal directions is not so straightforward as in the vertical direction. In Chapter 2, a simple model showed that coupling exists between the vertical and longitudinal directions, and this is basically non-linear - the linear form being a special case, giving longitudinal excitation at twice the vertical frequency. At higher frequencies,

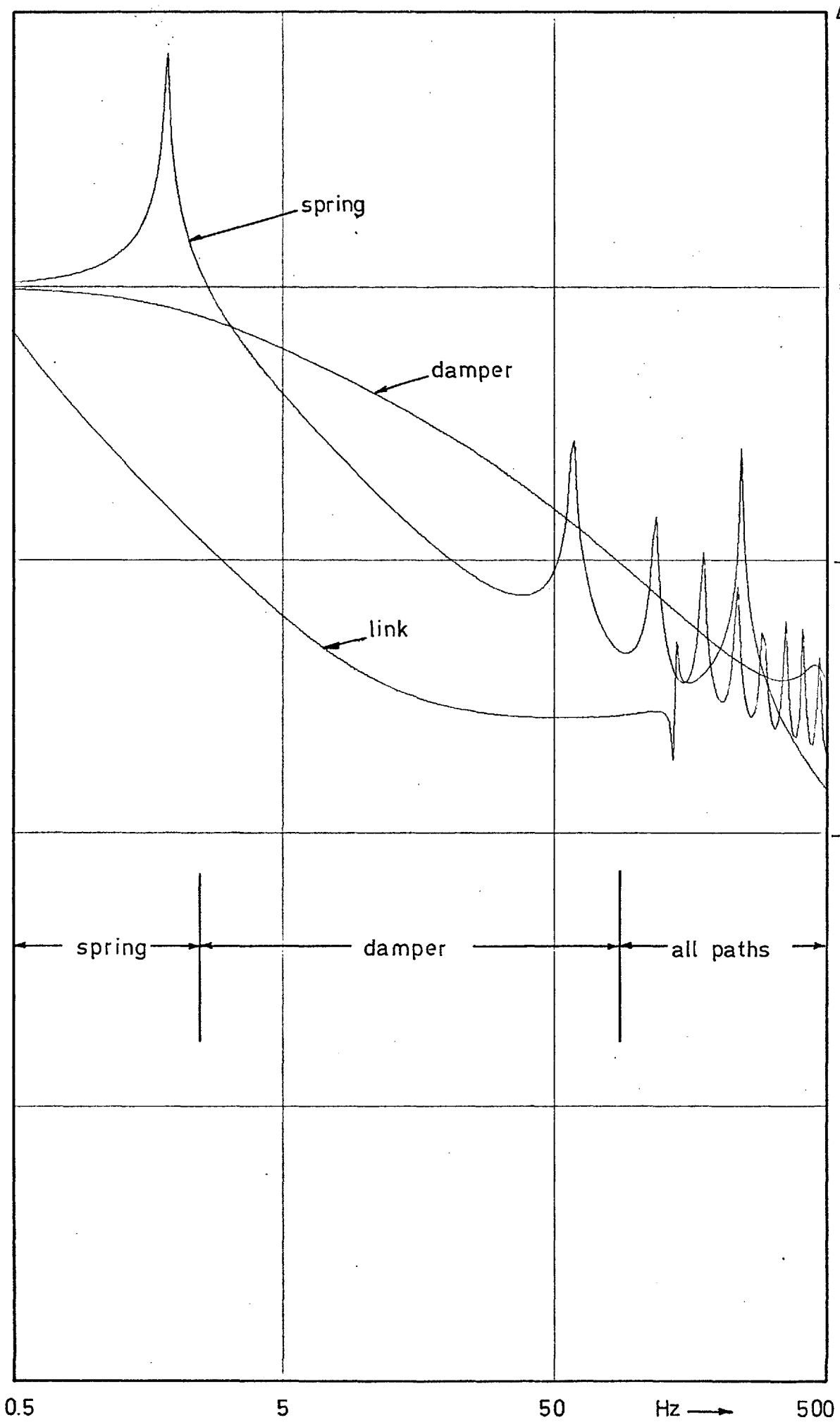

40
0 dB
-40
-80
Transmissibility
spring
damper
link
spring
damper
all paths
0.5
5
50
Hz
500

Figure 5.3.4

the coupling exists as a result of tyre properties and rotation, as has been shown by Tiekling (178). Experimentally, tyre properties appear to have a more significant effect in the longitudinal direction than in the vertical (119). Greater flexibility than usual has been shown to be effective in reducing the transmission of vibration, but may lead to handling difficulties (120). For both the longitudinal and lateral paths there is little scope for achieving really effective isolation in the suspension. ~~since the bush stiffnesses needed for handling are very great.~~

For the lateral direction, the path can be represented by a massless spring for the inboard rubber bushes, with the wishbones, wheel and tyre lumped for the source and the body as the receiver. Treating the system as having single coordinate coupling, as shown in Figure 5.3.5, and assuming that in the frequency range considered (20 - 60 Hz) the source mobility can be represented by a massline, the bush effectiveness can be found. This gives an order-of-magnitude approximation to the effectiveness of the bushes for the real case, subject to the errors incurred in neglecting the tyre modes and cross-coupling of the body coordinates, for which there is no information. For the body mobility, the connecting coordinates are treated as one, using the point mobility previously shown modelled in Figure 5.2.5, representative of a small saloon car. The modelling simplifies the input data, and fills in the deficiencies of the experimental data - in this case, no phase angle information was presented experimentally, only Q-factors for the principal

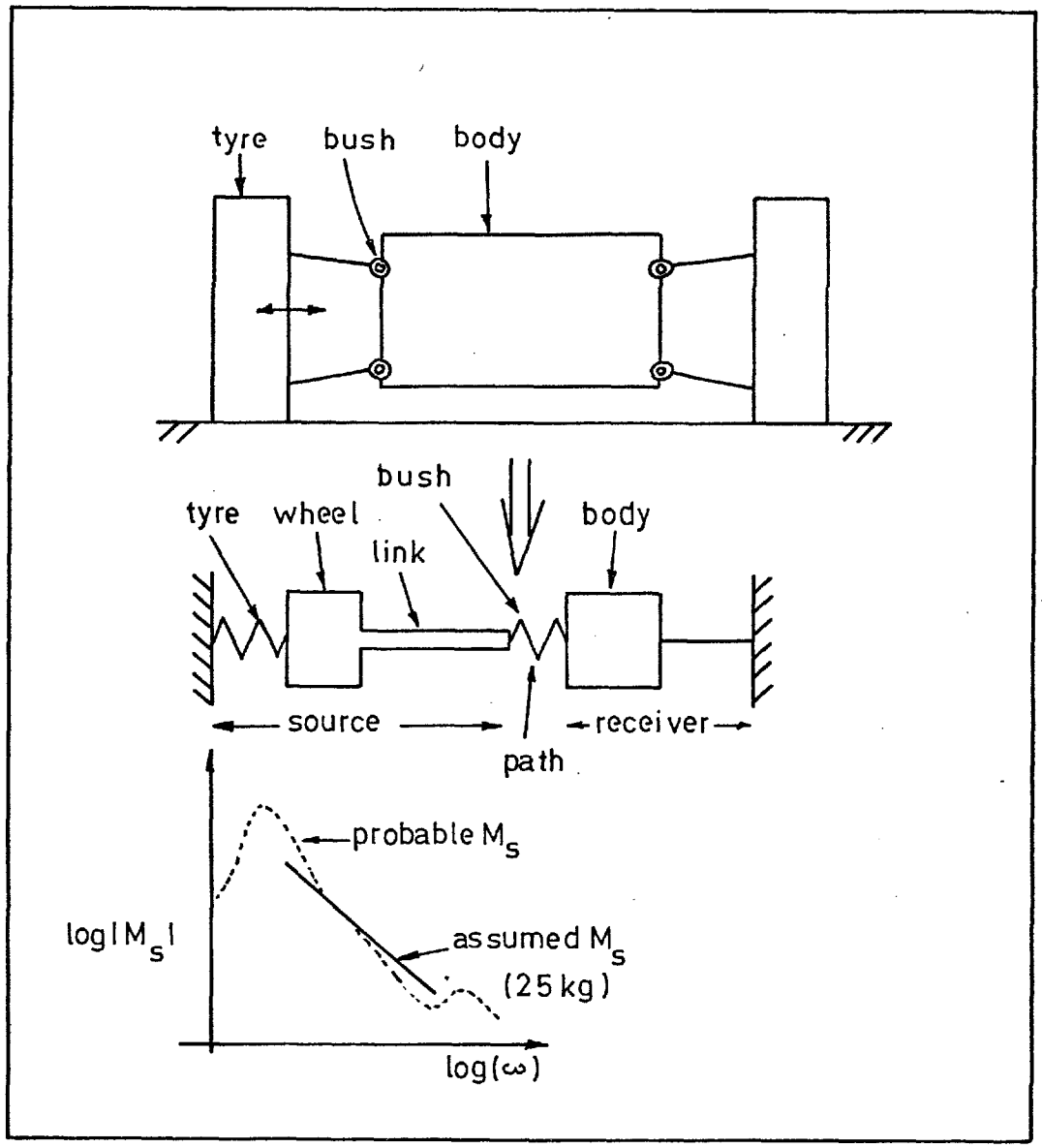

tyre
bush
body
bush
tyre
wheel
link
body
source
receiver
path
probable M_s
log|M_s|
assumed M_s
(25 kg)
log(ω)

Figure 5.3.5

modes. The model can generate the complete mobility function at any required frequency in the range of validity.

Figure 5.3.6 shows the effectiveness for two values of bush stiffness - the higher (3.4 MN/m or 19,400 lbf/in.) being fairly representative of the level of stiffness used in practice showing for the most part in this frequency range amplification of the vibration (the bush stiffness in fact exceeding the dynamic stiffness of the body for many regions along the frequency scale), with the second curve showing the effectiveness for a stiffness value ten times lower. The latter is seen to be generally effective, but this advantage is offset by the significant amplification region at low frequencies.

The lateral bush stiffness also partially determines the longitudinal stiffness of the suspension as shown earlier, where a relationship between the longitudinal to lateral stiffness was obtained. A longitudinal force on the outboard end of the suspension leads to a couple as well as a force being applied to the body. No information is available for the cross-coupling between the suspension attachment points, so that the effect of the couple cannot be predicted with any accuracy. The transmissibility (to a rigid mass) in the longitudinal direction is shown in Figure 5.3.7, showing how this transmission path forms basically a two-stage mounting, introducing an undesirable resonance at high frequencies.

The lateral and longitudinal paths for the conventional suspension do not appear to be effective isolators, nor can

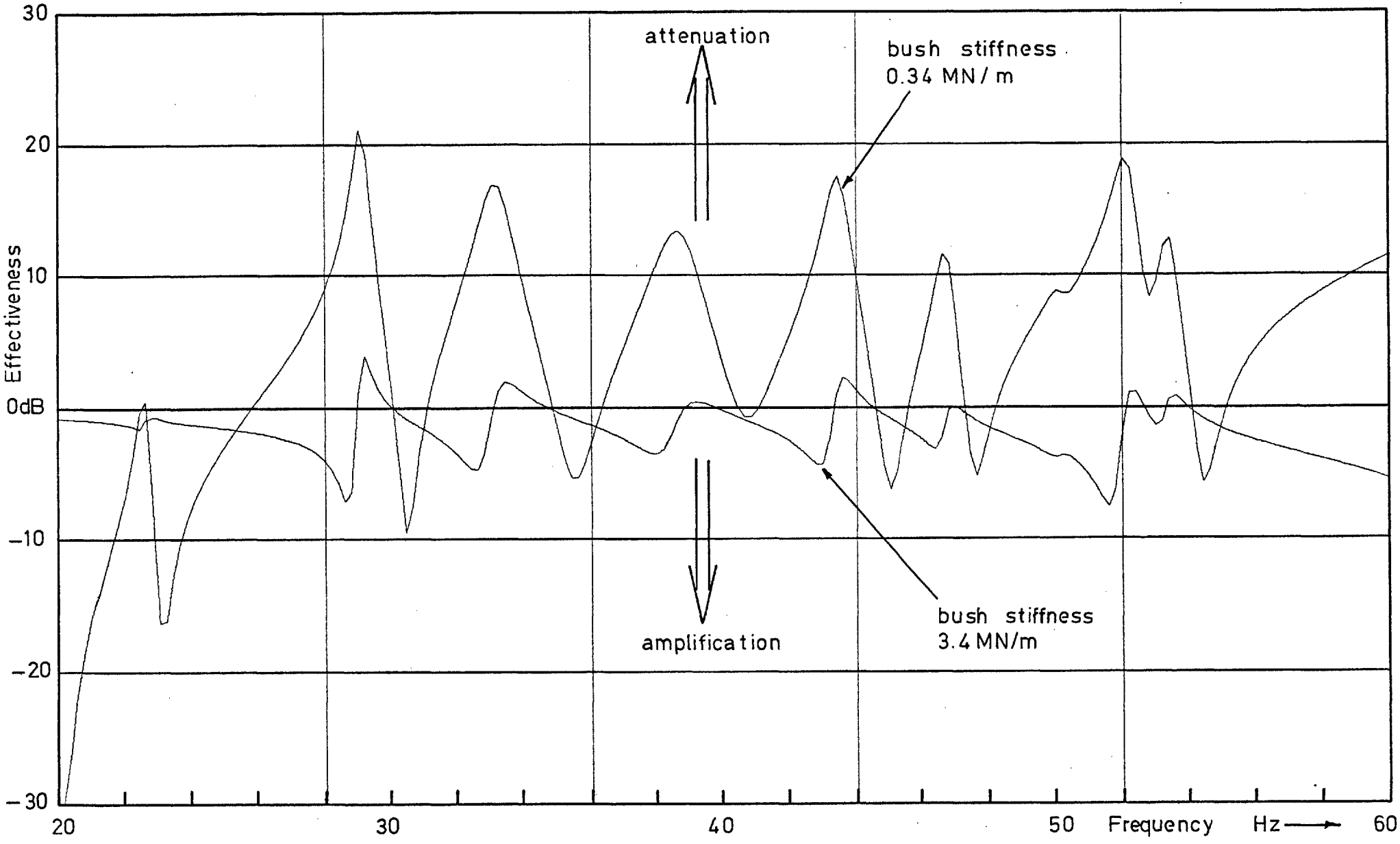

30
20
10
0dB
−10
−20
−30
Effectiveness
attenuation
bush stiffness
0.34 MN/m
amplification
bush stiffness
3.4 MN/m
20
30
40
50
Frequency Hz ⟶
60

Figure 5.3.6

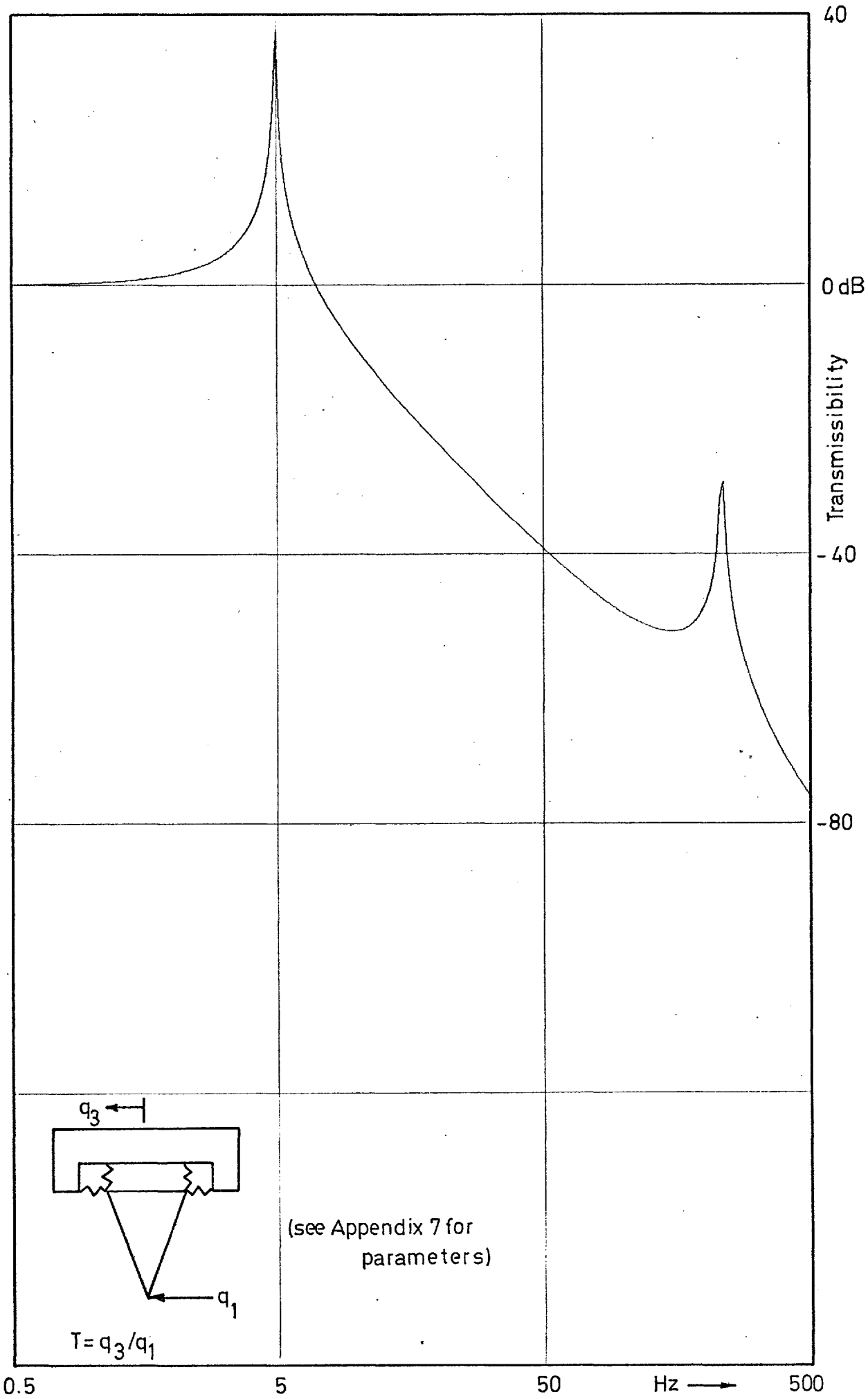


Figure 5.3.7

SSH1P01 TRANS

great gains be expected from changes in the parameters. The low-frequency stiffness characteristics are in direct conflict with the isolation effectiveness at higher frequencies. The most flexible bushes possible for satisfactory handling should be employed, but it should be appreciated that many amplification regions can be encountered. High damping is desireable in the bushes for the control of the low frequency amplification regions, but generally high damping rubbers show an increase in dynamic stiffness with frequency and so are less effective than natural rubber at high frequencies. The combined materials isolator, using a combination of natural and high damping rubber, as suggested by Snowdon (92) would appear to offer a reasonable compromise.

5.4 TRANSMISSION PROPERTIES OF SUSPENSION MODELS

The models described below build up to the complete suspension model in stages, and show the effects of components interacting.

5.4.1 Without Links

The first model consists of a massless main spring with the damper unit, and the transmissibility for this case is shown in Figure 5.4.1. If this is compared with the damper model shown in Figure 5.3.2 it is seen that the

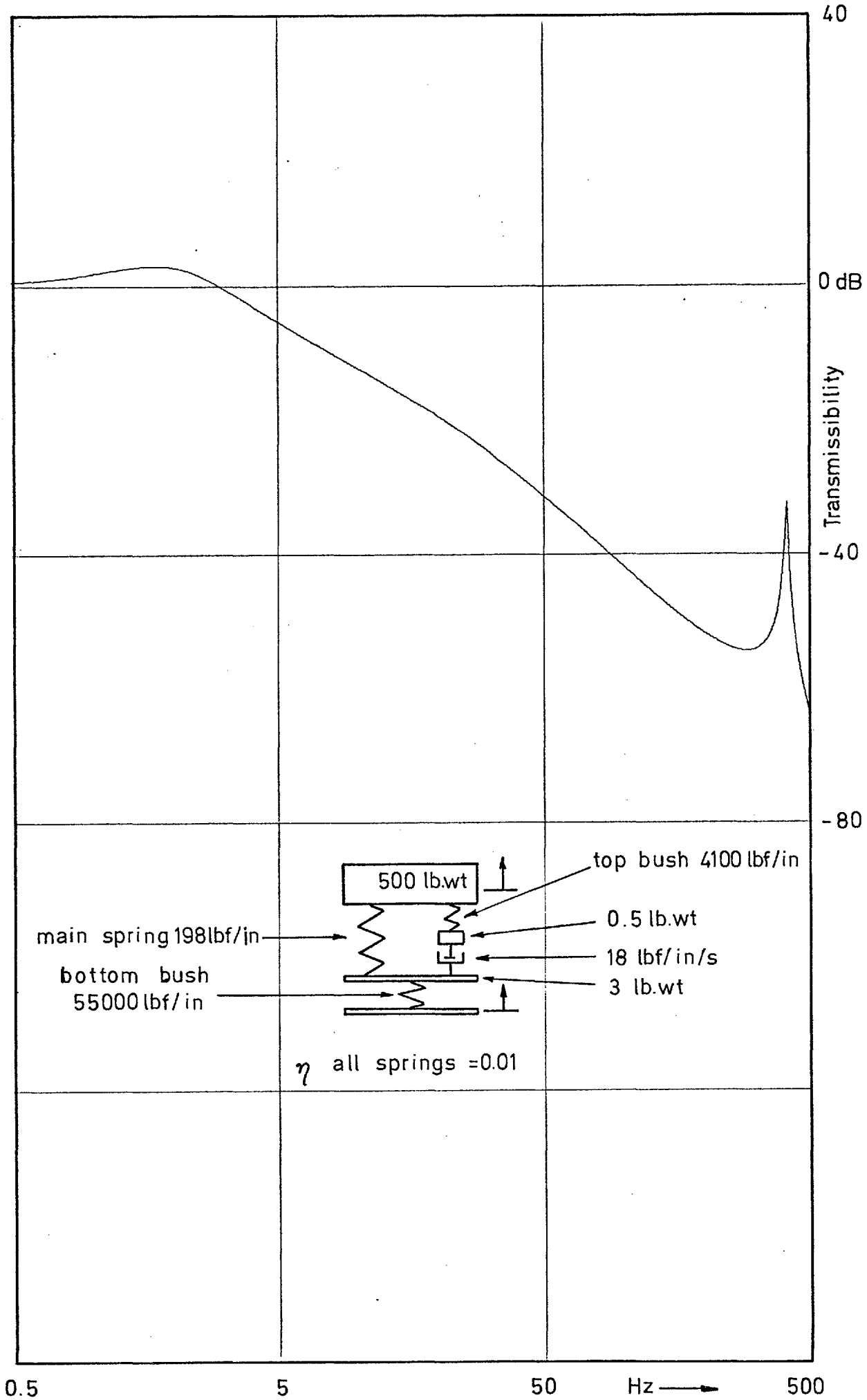

40
0 dB
- 40
- 80
Transmissibility
500 lb.wt
top bush 4100 lbf/in
0.5 lb.wt
18 lbf/in/s
3 lb.wt
main spring 198 lbf/in
bottom bush
55000 lbf/in
η all springs =0.01
0.5
5
50
Hz
500

Figure 5.4.1

main spring controls the low-frequency behaviour only, with the damper heavily suppressing the resonant peak. At high frequencies the transmissibility is primarily controlled by the damper unit, with the bush providing the main attenuation. Introducing the lumped parameter model for the main spring shows the effect of spring surges (valid for the lower modes). The almost undamped spring leads to sharp peaks in the transmissibility curve (Figure 5.4.2). Control of the spring damping will reduce these peaks, as shown earlier, though the overall effect on energy transmission will be small, compared with the damper unit. It is of interest to note that partial cancellation occurs between the first and second spring surge, and again between the third and fourth modes. This is due to the phase differences of the force transmitted by the damper unit compared with the force transmitted by the spring. This (first) cancellation region is fairly broad-band (66 - 115 Hz) with at least 4 dB reduction compared with the damper unit alone. Thus for this section of the curve, the increased transmissibility of the spring due to surges is favourable. It should be possible to utilise the cancellation region to compensate for regions of high source or receiver mobility, e.g. tyre resonances, to give a slight improvement, by means of changing the weight of the spring. Between the second and third spring surge, the phase relation changes, and reinforcement occurs.

This model, shown in detail in Appendix 7, does in fact provide a fairly accurate model for the vertical transmission of vibration over a limited frequency range, since the transmission through the links is small at medium frequencies. It

MODEL WITH SURGES

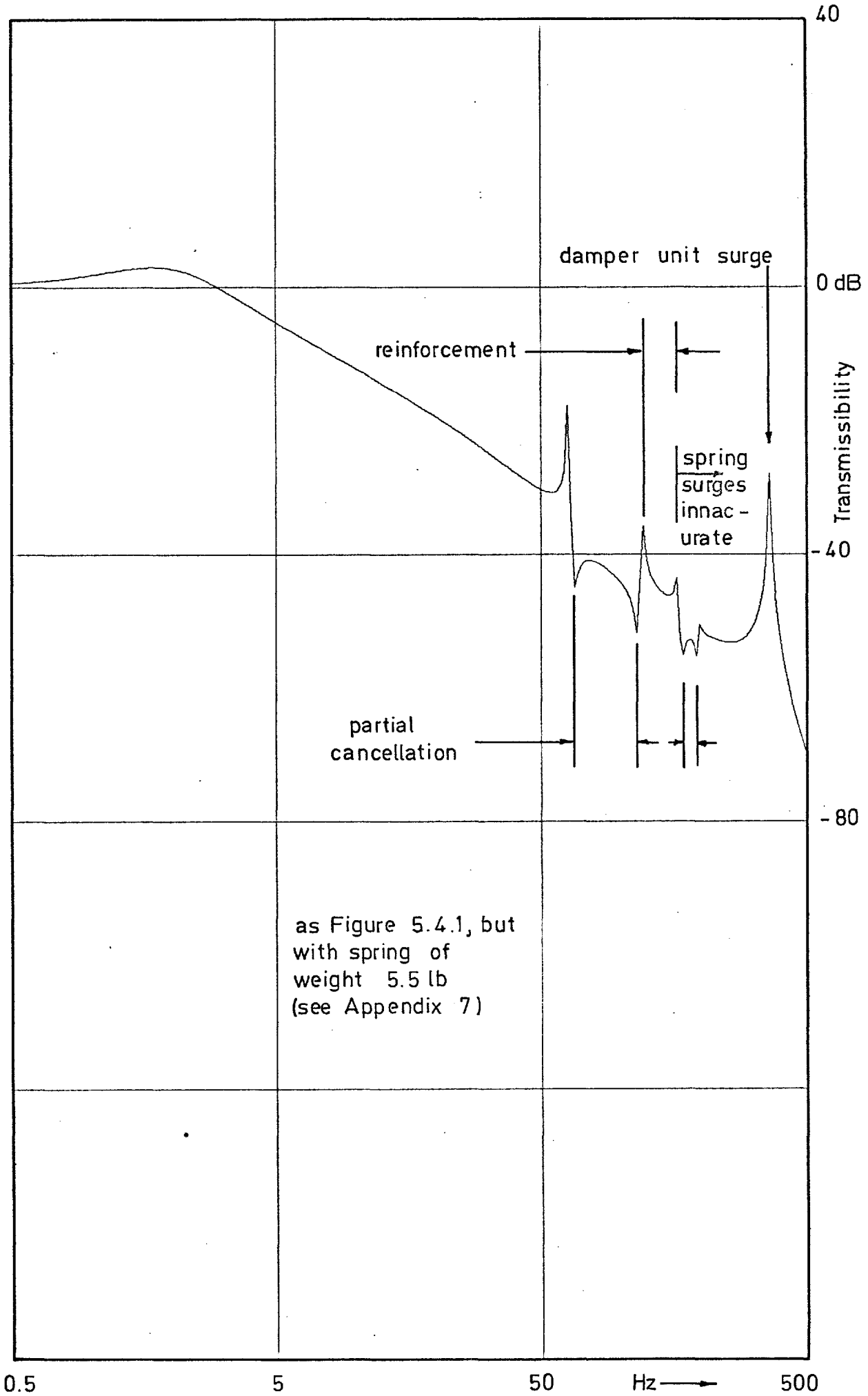


Figure 5.4.2

further has the advantage over the later models in extreme simplicity.

5.4.2 With Links

As shown earlier, the links or wishbones on the suspension unit can have comparable transmission properties to the damper unit and spring at high frequencies. The models shown now build up to a complete suspension model to include the effects of the wishbones and stub-axle. In-plane vibrations are assumed only - that is, vertical vibration can cause lateral and in-plane rotations, but coupling to the longitudinal and out-of-plane rotations is not considered. Further, it should be noted that the bush stiffnesses used are made deliberately lower than would be usual in practice, to demonstrate the effects of resonances. Also the links are assumed rigid. The model equations are given in Appendix 7.

5.4.2.1 Inclined Link with Spring

Figure 5.4.3. shows the transmissibility of one inclined link with a massless main spring. The main spring almost entirely regulates the low-frequency behaviour, but at high frequencies the transmissibility curve levels off towards the link transmissibility curve (c.f. Figure 5.3.3). The low bush stiffness leads to a weak lateral resonance followed by a stronger vertical resonance. For a very stiff bush, in the vertical radial direction, the curve would remain

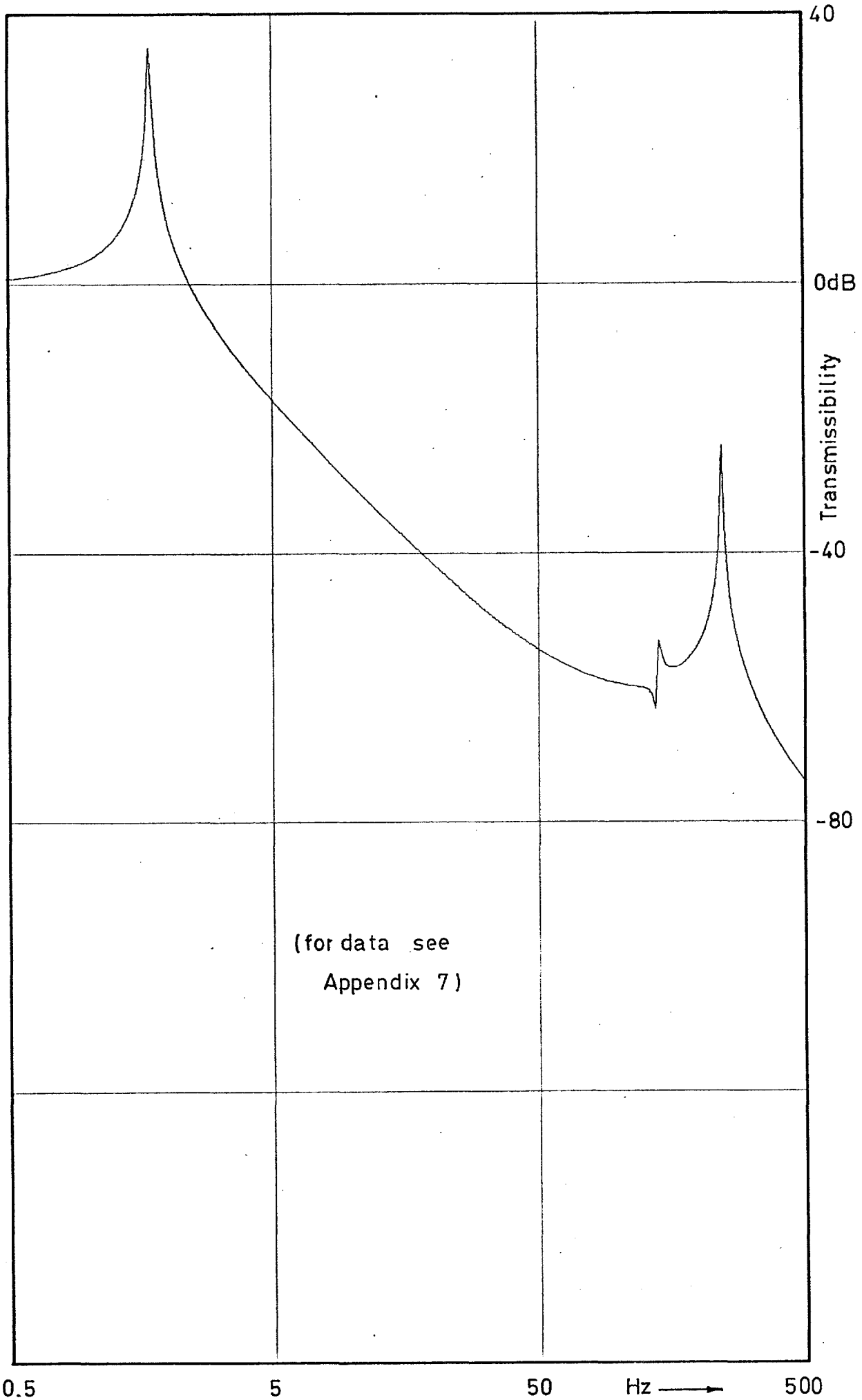


Figure 5.4.3

AWM2V01 TRANS

level in this region, thus giving a more favourable response.

5.4.2.2 Twin Wishbone Model without Damper

To allow for the in-plane motions of the stub axle and both wishbones, a considerable increase in complexity is required. The suspension is characterised by coordinates relating the position of the drive and connecting points, and the position of the centre of gravity of each element. Viscous damping is assumed for the outboard pivots, and no clearance is allowed. The stages in developing the equations for this model are shown in Appendix 6. The damper unit is not included, and the main spring is assumed massless. Figure 5.4.4 shows the transmissibility for this model. More resonances can occur than previously, but due to the triple path partial cancellations of the transmitted force are in evidence. Again, as in the previous model, if very stiff bushes (in the radial direction) were used, the transmissibility curve would become level at high frequencies and the resonances would be at a much higher frequency. Due to the fact that two links are now used, this level will be higher than for the one link case.

5.4.2.3 Twin Wishbone Model with Damper

This model extends the previous model by the insertion of the damper unit. In this and the following model certain compromises had to be made in the completeness of the model to limit the number of degrees of freedom required. These

SS2DU05 TRANS 0S6L

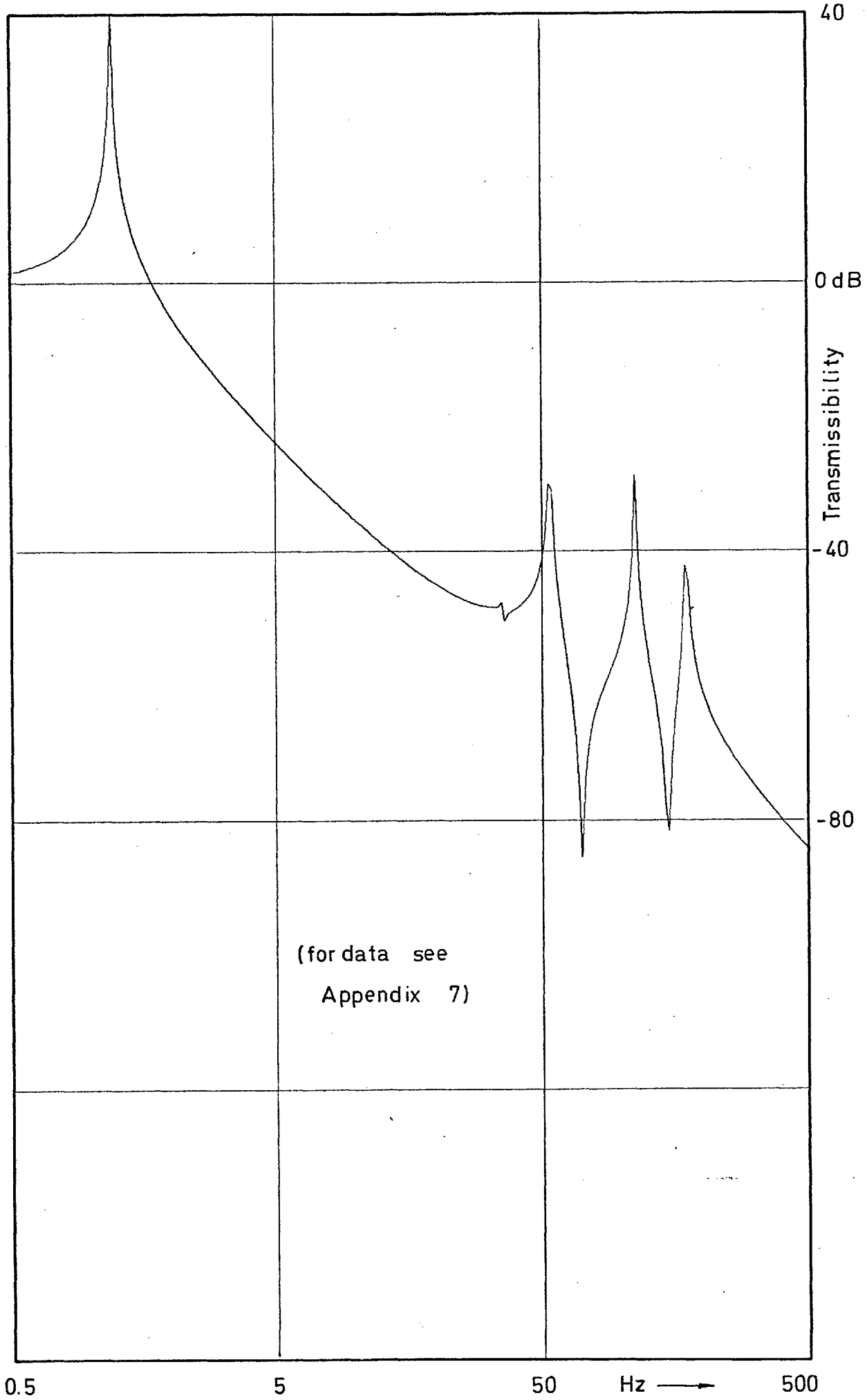


Figure 5.4.4

are noted in Appendix 7. The result is that for the low-frequency response constraints are apparent which do not occur in practice. It is useful to consider this as a band-limited model, so that the model such as shown in Figure 5.4.1 is valid (with the appropriate assumptions) for low frequencies and the present model (Figure 5.4.5) for the higher frequencies. The damper unit is seen to introduce an additional resonance into the system. The increase in transmissibility due to the damper is mainly apparent in the intermediate frequency range.

5.4.2.4 Twin Wishbone with Damper and Spring Surges

This model represents the final development of the suspension models, and is of considerable complexity. It requires 12 degrees of freedom and 58 independent parameters to describe the system. Figure 5.4.6 shows the transmissibility curve for this model showing the many resonances which can be excited which are not controlled significantly by the damper unit. Again, as in the previous examples, bush stiffnesses are made deliberately low to show possible effects. The transmissibility curve with parameters found in the suspension unit tested is shown in Chapter 6.

Although partially obscured, the cancellation condition from the spring and damper unit combination is still in evidence. The existence of the various troughs in the

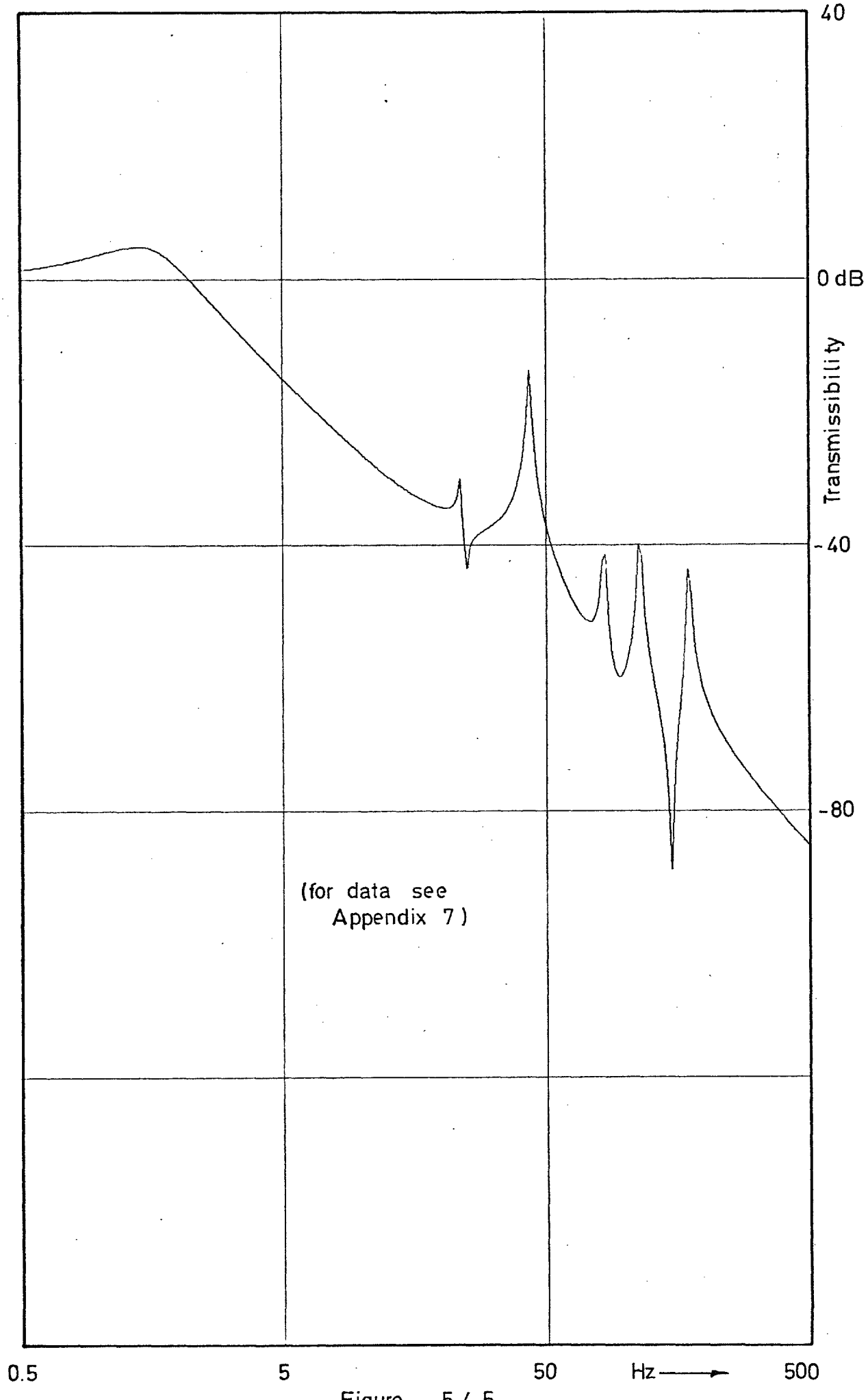
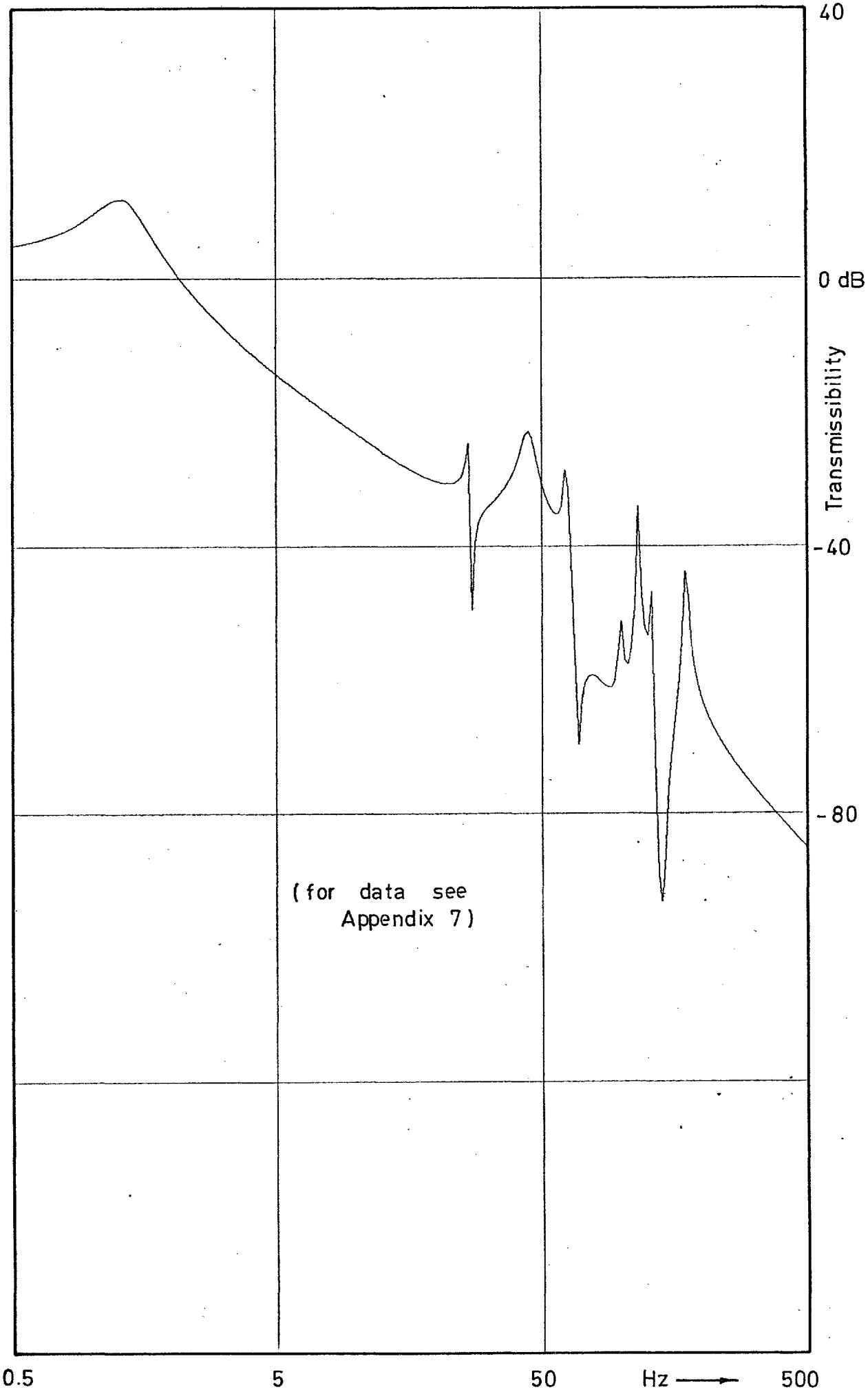


Figure 5.4.5

SS2DD01 TRANS 0S6L



SS2DSS03 TRANS

Figure 5.4.6

response can be used to advantage in designing the suspension to match up with regions of high mobility of the tyres and body, though it should be emphasised that very substantial improvements are unlikely.

5.4.3 With Resonant Reciever

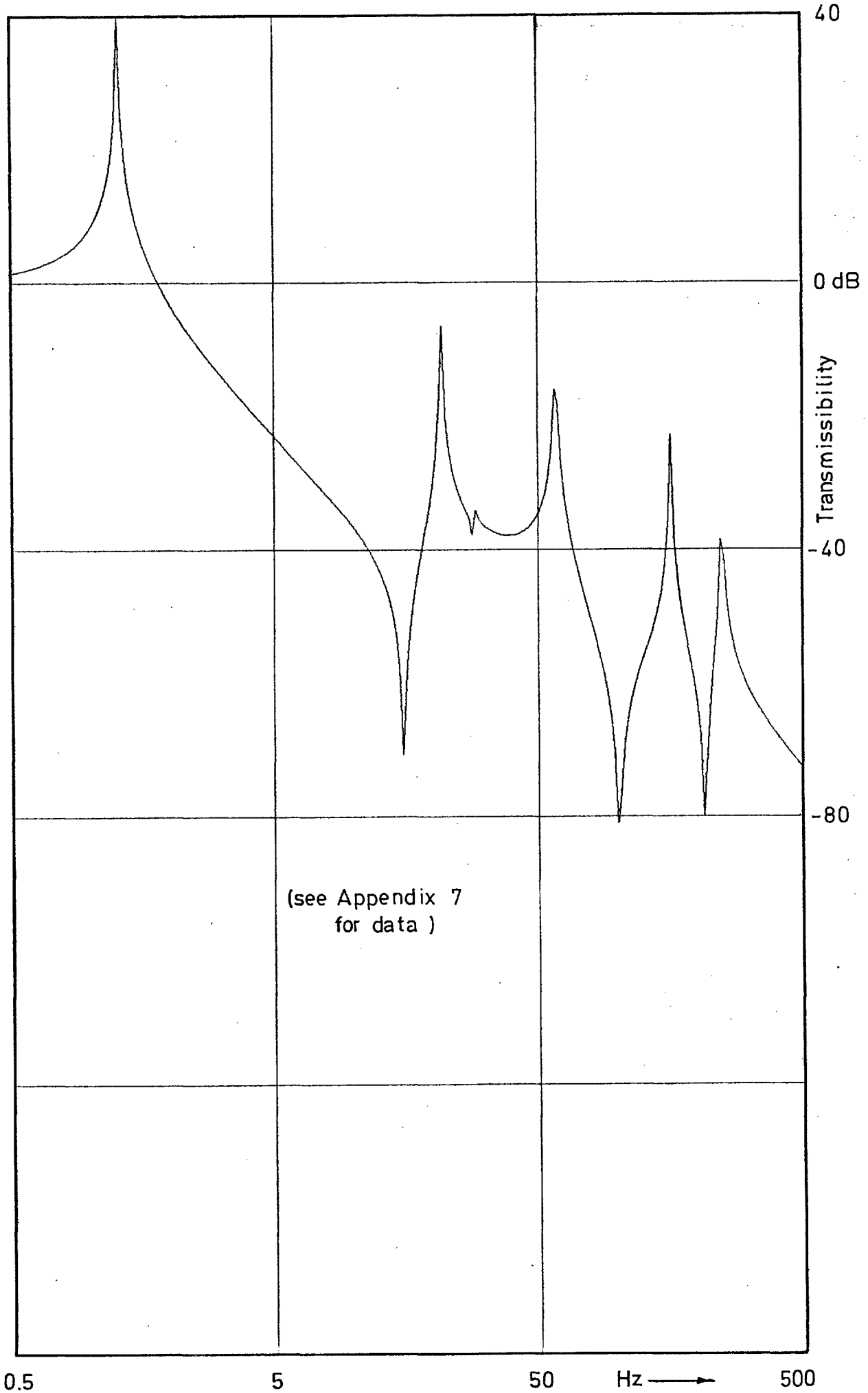
The transmissibility curves shown in the previous sections, whilst giving indications of the important transmission paths and the means of improvement, give an over-optimistic picture to the effectiveness of the suspension when the effects of high source and receiver mobility are considered.

An exact representation of all the effects of this is as yet unsolved, due to a very substantial degree of complexity required.

The models shown in the following sections show, on a very simple level, the sort of effect when the receiver (car body) mobility is greater than the ideal mass line.

5.4.3.1 With Engine Resonance

Using the twin-wishbone model without the damper unit, and allowing for one (vertical) resonance of the engine, leads to the model shown in Figure 5.4.7. At low frequencies, the engine resonance leads to the dynamic absorber effect, giving a deep trough in the transmissibility



SS2DUE01 TRANS

Figure 5.4.7

curve. At higher frequencies, the engine mass becomes decoupled from the body leading to a loss of impedance (as shown earlier), and consequently the transmissiblity curve shows an overall upward shift.

5.4.3.2 With Engine and Body Resonances

With the same suspension model, and allowing for two body modes of the receiver, the transmissibility curve shown in Figure 5.4.8 is obtained. The body resonances cause a further loss of receiver impedance, and so the transmissibility curve shows a further upward trend.

The suspension is seen to be far less effective for this case, and the response extremely irregular.

From this simple example it is clear that the body mobility, compared with that for a mass, strongly reduces the suspension effectiveness. Despite the complexity of the response, the body mobility is made ideally simple - in the frequency range considered perhaps 100 body resonances might occur in practice, leading to further increases in transmissibility.

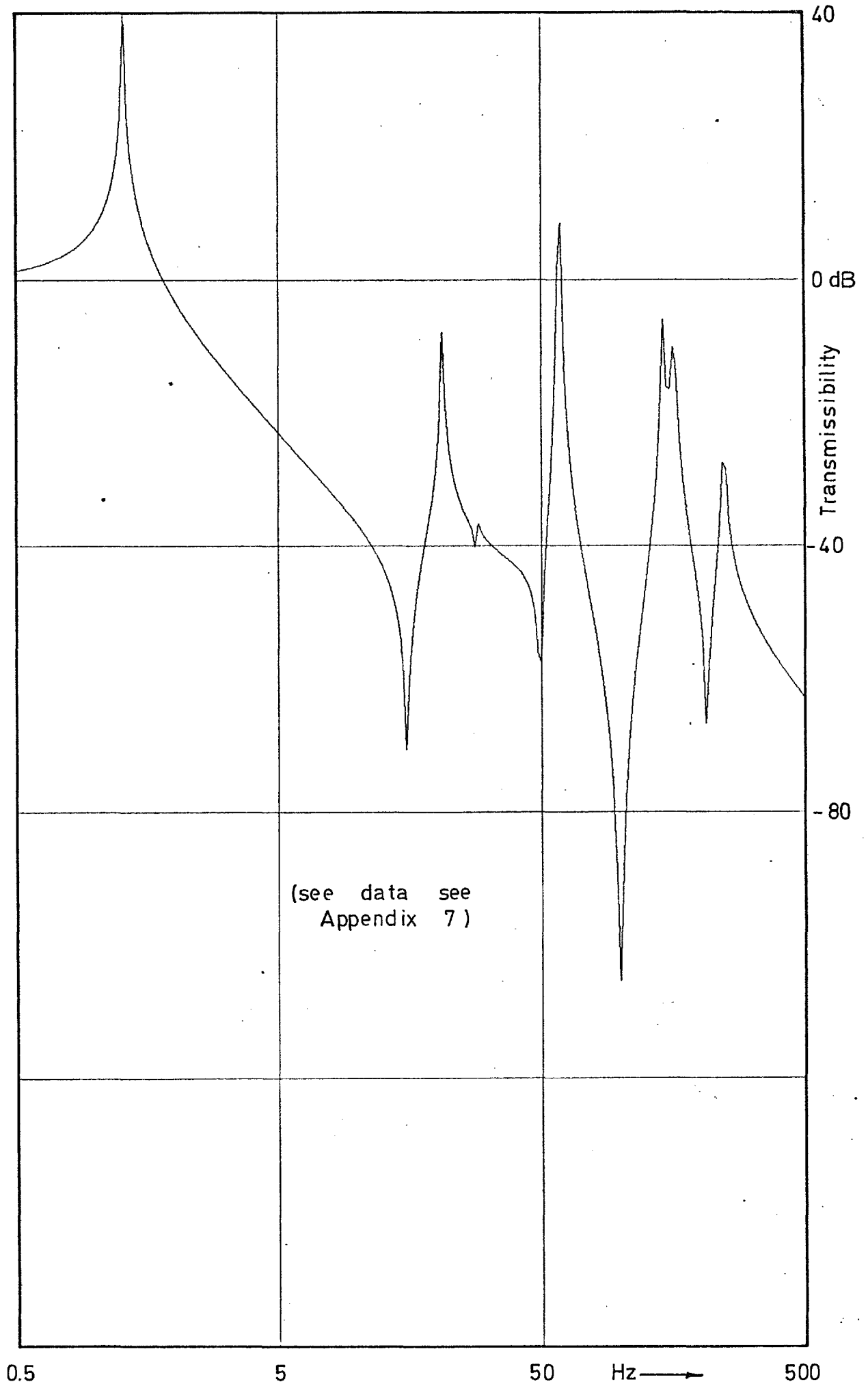


Figure 5.4.8

SS2DUER01 TRANS

5.5 DISCUSSION AND CONCLUSIONS

The transmissibility plots shown earlier, whilst leading to useful results, do not describe every detail of the suspension model. Complete response curves (185) have been presented earlier and aid the interpretation of the responses, but tend to result in a surfeit of information. When joining systems together, mobility matrices can be used, formed as shown in Chapter 3. Figures 5.5.1 and 2 show the matrix elements in modulus versus frequency form, for a 2 x 2 mobility matrix for the vertical behaviour of the twin wishbone model both without and with the damper unit. It is difficult to produce transfer or impedance matrices directly because of the boundary condition requirements. The restraints implicit in the model have been avoided here by treating the damper unit as upright, so that the low-frequency asymptote to the mass-line is formed. The curves show the considerable complexity of the suspension in isolation (i.e. without the body response) but as only two coupling coordinates are used, the description is not complete.

To a first approximation the vertical transmission path depends on the damper unit up to about the second spring surge. In turn, the damper unit transmission in the higher frequency range (> 30 Hz) depends mainly on the damper bush stiffness - one bush only is seen to be preferable, (§5.3.1.2) shown for the unit tested in Chapter 6. Thus, the simple design criterion for minimising vertical transmission is that the damper unit bush is as flexible as

SS2DU09 Y11, Y21, Y22

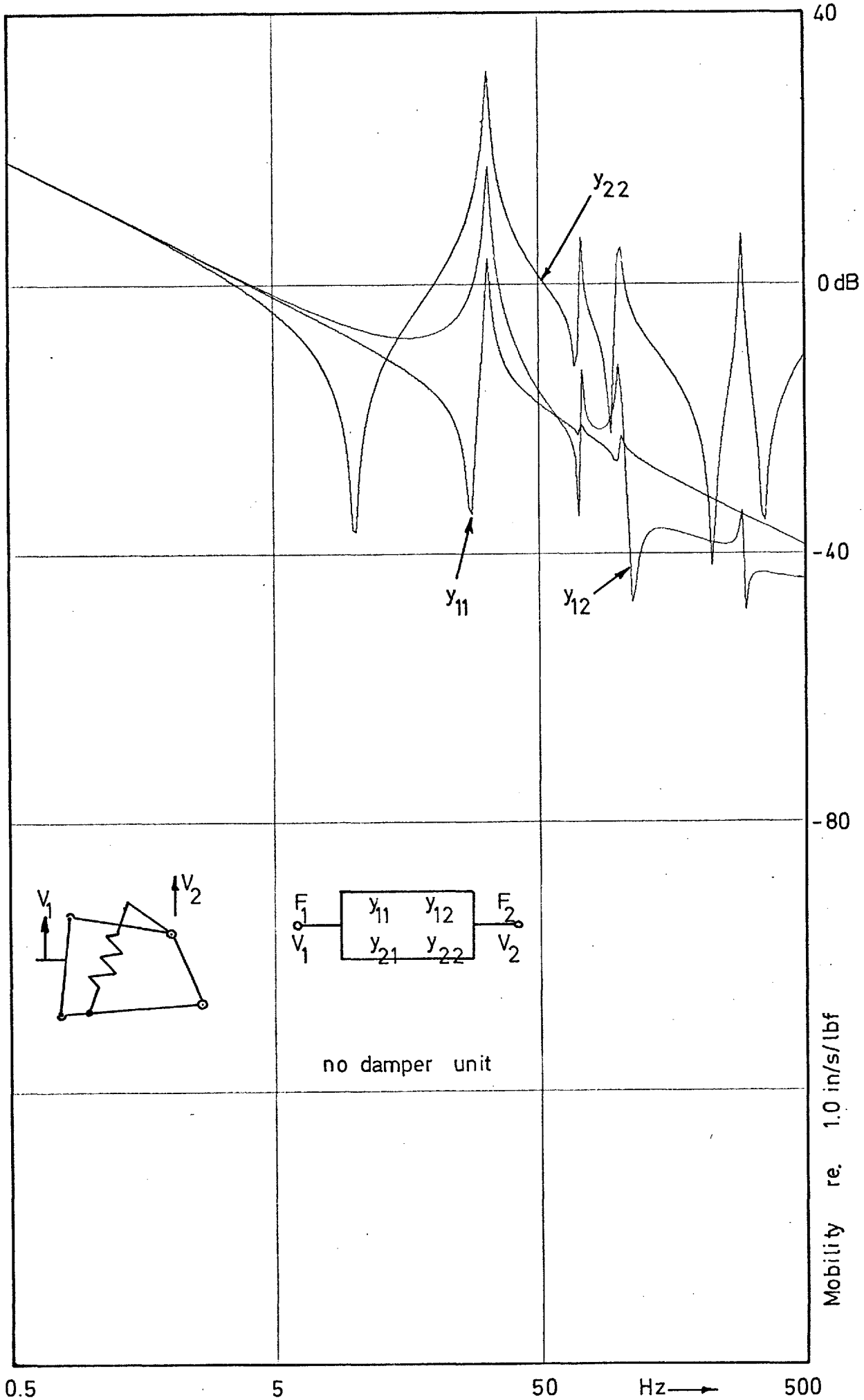


Figure 5.5.1

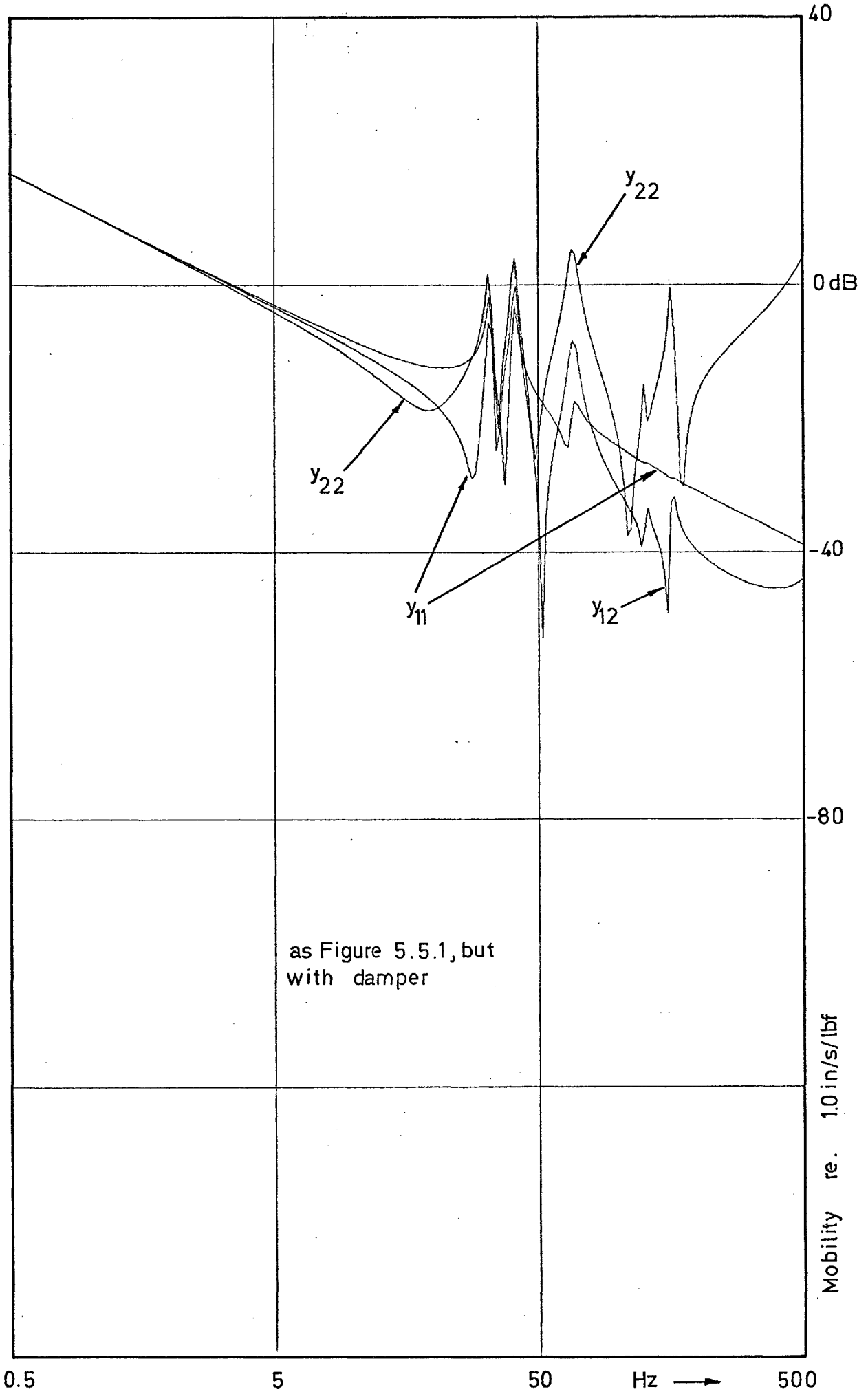


Figure 5.5.2

SS2DD04 Y11, Y21, Y22

possible whilst maintaining the effectiveness of the damper in its prime function. In Appendix 1, a suspension model is shown optimised for damping of the wheel-hop and body bounce modes, and for this model it is found that the damper bush stiffness required is about thirty times greater than the stiffness of the main spring. This requirement severely limits the effectiveness of the suspension as an isolator. An alternative to the damper unit, using dynamic absorbers, reduces the vertical transmission by up to 26 dB and is thus a significant improvement - but at the expense of less efficient damping of the low frequency modes and increased complexity(Appendix 1).

The lateral and longitudinal paths can similarly be seen to depend almost entirely on the inboard bush stiffness. To be effective as isolators they must be as flexible as possible in the horizontal plane (in the vertical direction they are required to be stiff). Very stiff bushes are seen to be almost totally ineffective as isolators, and can in fact act as amplifiers for much of the frequency range, though the amplification will be small. Very flexible bushes, on the other hand, will be generally effective as isolators at high frequencies but can cause considerable amplification at low frequencies with consequent handling difficulties. Design should thus be for the most flexible bushes compatible with handling - this will depend on tyre properties, and at present it would seem that practical testing is still necessary.

Suspension models have been discussed analytically and design inertia given - it is seen that bush stiffnesses provide the principal means of affecting the transmission properties of the suspension. Radical changes in the suspension properties cannot be expected, only fairly small improvements, unless radical changes are made in the suspension design - such as the use of dynamic absorbers.

CHAPTER SIX

EXPERIMENTAL TRANSMISSION PROPERTIES OF A SUSPENSION SYSTEM

Experimental work was conducted at various stages to confirm that the idealised models used for the suspension conform reasonably well to the real components and the complete suspension system. The experimental results as such apply, of course, only to the particular suspension tested, but show that the theoretical models predict the real system behaviour with fair accuracy, and so the models can be used to predict the performance of other suspension systems with the requisite parameter changes.

The precise methods of testing to deduce the immittance or transmission matrices, as shown in Chapter 3, are not always feasible to use when testing real components. Compromise in the test procedures have to be made according to the apparatus available. For the experimental work described here, a model for the system is previously assumed, and parameter derivation and confirmation of the predicted behaviour is required. The tests study the behaviour of the system within a known system, and it is not always possible to deduce the system matrix directly, but only from the model.

6.1 INDIVIDUAL COMPONENTS

The practical behaviour of the component parts of the suspension was studied first - notably the damper unit and the wishbones. The behaviour of the vehicle coil spring was not studied, but a smaller coil spring was tested, shown in Chapter 4, and the effect of damping demonstrated. The behaviour was seen to conform to that of a simple continuum model for the first four spring surges; at higher frequencies the behaviour became extremely complex. The behaviour of the damper unit in the locked state was also shown in Chapter 4.

6.1.1 Damper Unit

The damper unit or shock absorber tested was of the telescopic type with rubber end bushes, shown in Figure 6.1.1.

The model used for this unit is shown on the same figure. Hysteretically damped springs represent the end bushes, an equivalent viscous damping coefficient represents the damping action, and the masses represent the mechanical parts and the working fluid.

A compression test on the unit performed by applying a steady load and measuring the resulting velocity shows that the damper unit is highly non-linear - see Figure 6.1.2. The mass distribution, due to the working fluid is also not constant, and so severe approximations are made in the model.

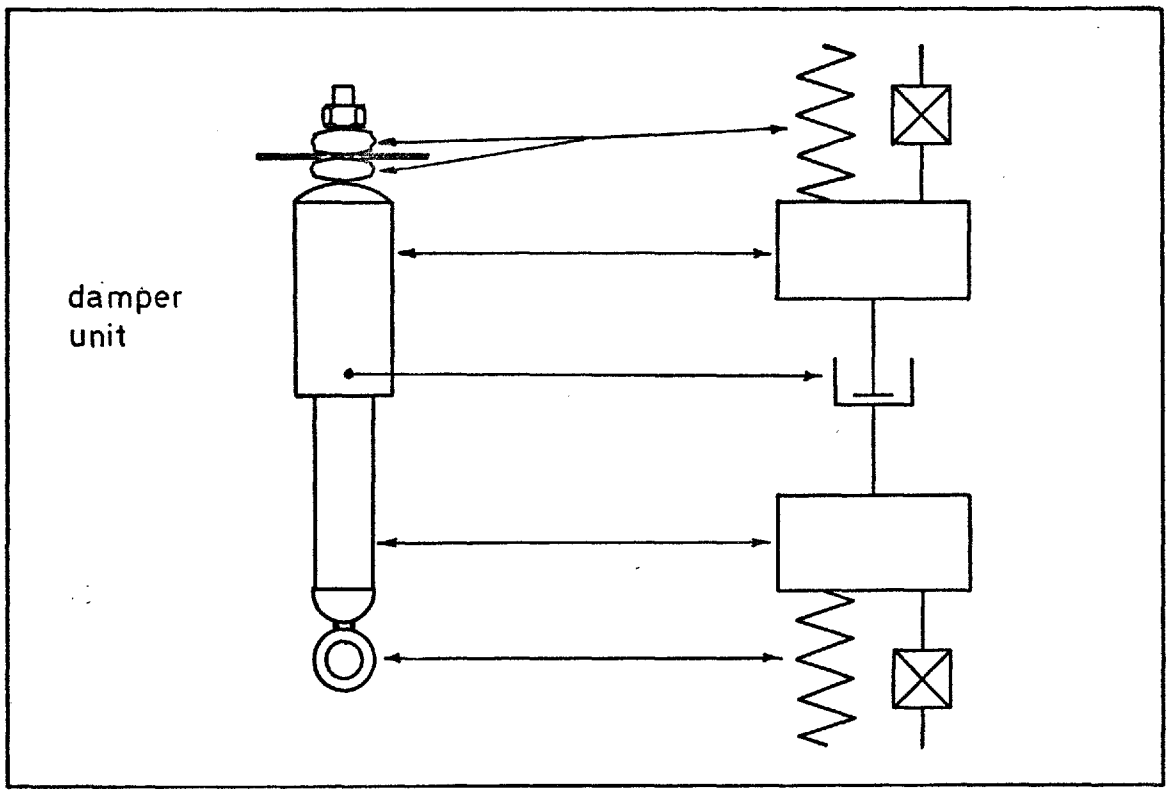


Figure 6.1.1

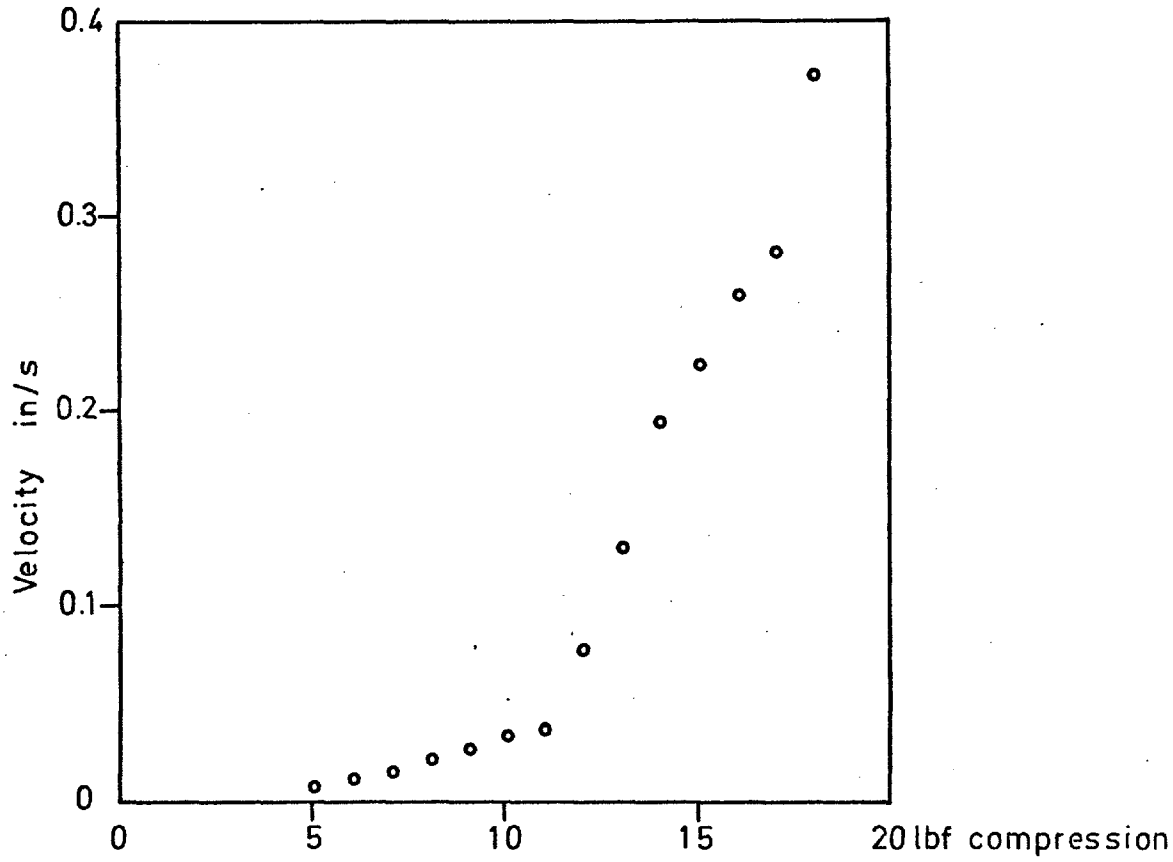


Figure 6.1.2

These do not, in fact, tend to be serious in the high frequency range as the end bushes become much more mobile than the damper itself, and thus principally determine the transmission properties. Temperature effects mean that in any case the damping available will vary with service conditions.

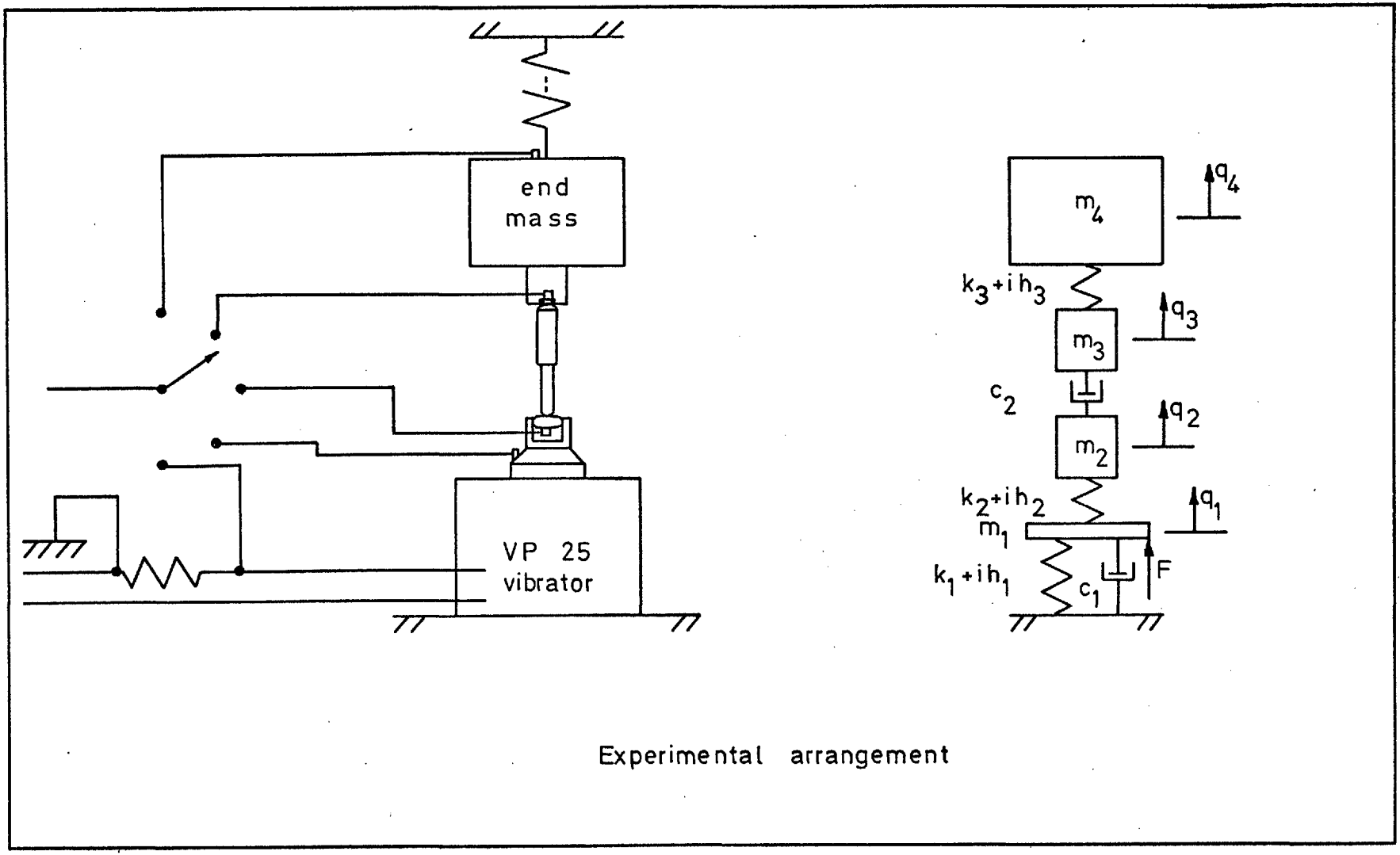
The unit had a total weight of 2.83 lb, and the weight distribution was estimated by measuring the position of the centre of gravity with the unit fully extended and fully compressed - giving the weight of the top part as 0.517 lb, and the bottom part 2.313 lb. The bush stiffnesses had been previously estimated as shown in Chapter 4.

6.1.1.1 Experimental Apparatus

To enable the damper unit to function correctly, sufficient vibratory force must be applied across it to break the stiction present. A rigid termination is not feasible for the frequencies tested (up to 1 kHz), and so a large end mass was employed. Vibrator current was used as a measure of applied force, since suitable force gauges were not available.

The overall arrangement is shown in Figure 6.1.3. It should be borne in mind that the damper unit must be in an upright position to prevent aeration.

The end mass was a solid steel block of weight 298 lb, suspended by a soft spring with coil damping, giving a free



Experimental arrangement

Figure 6.1.3

natural frequency of 0.71 Hz. The effect of the spring on the motion of the end mass was considered negligible at the test frequencies, and so was not included in the model.

The vibrator table and suspension, and the weight of the bottom adaptor had to be included in the model, and for these a separate test was required.

To determine the table mass, m_T, suspension stiffness k_1, and damping, h_1, c_1 for the vibrator, the displaced frequency method was used. This involved measuring the vibrator characteristics with the table first unloaded, and then with a known additional mass m_A. The vibrator current was measured by observing the voltage drop across a low-value, high-wattage resistor in series with the vibrator coil.

For small damping, we have $\omega_1^2 = k_1/m_T$ and $\omega_2^2 = k_1/(m_T + m_A)$ where ω_1 and ω_2 are the resonant frequencies for the table unloaded and loaded respectively. Thus, $m_T = m_A\ \omega_2^2/(\omega_1^2 - \omega_2^2)$ and $k_1 = m_T\ \omega_1^2$.

The damping was found to be small, but increased slightly with frequency, and was modelled as hysteretic plus a viscous component. The force calibration was obtained from the asymptotic low-frequency deflection. The receptance of the vibrator table, and with the additional mass (in fact the bottom adaptor for the damper unit) is shown in Figure 6.1.4, and indicates that this method

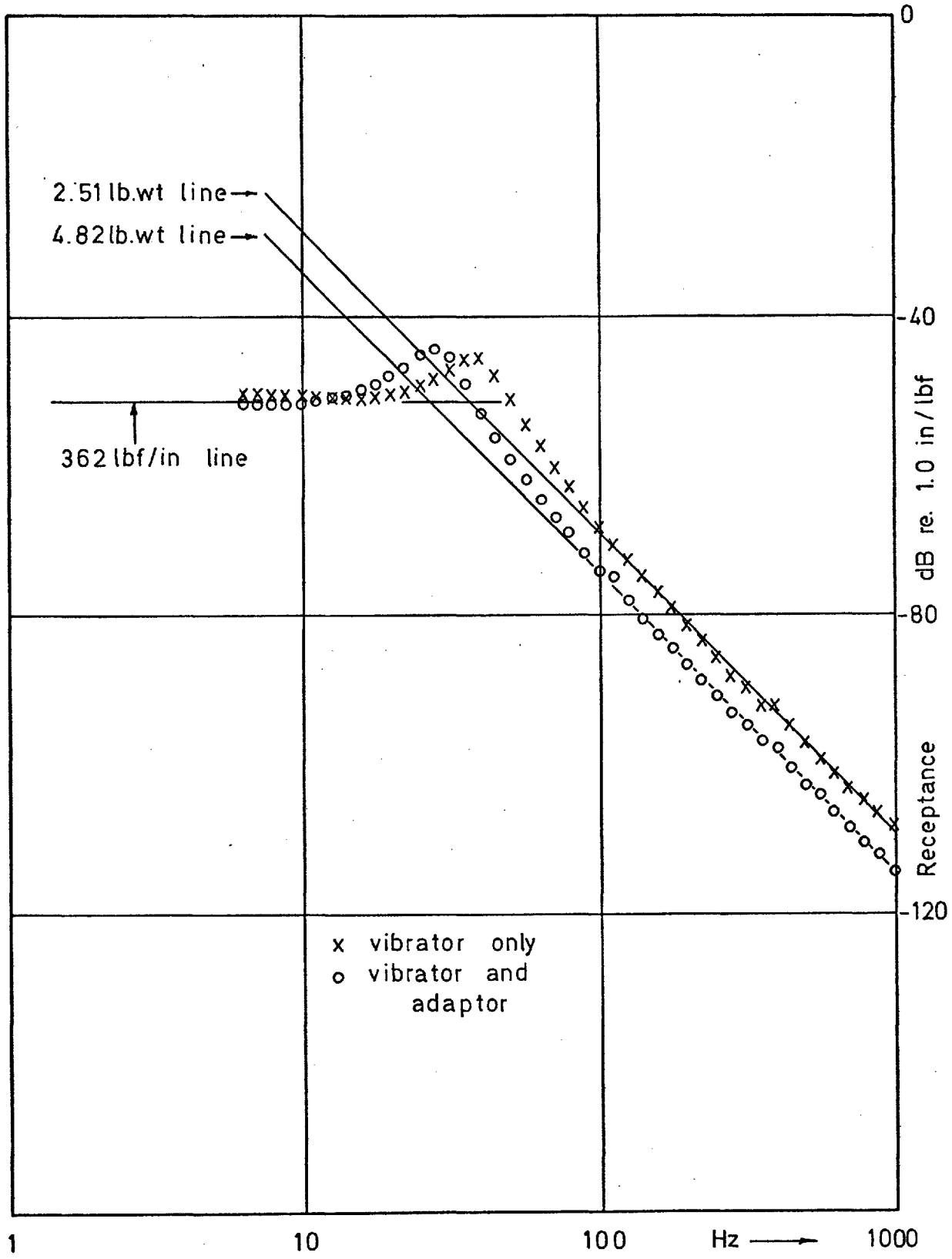

2.51 lb.wt line
4.82 lb.wt line
362 lbf/in line
x vibrator only
o vibrator and adaptor
0
-40
-80
-120
dB re. 1.0 in/lbf
Receptance
1
10
100
Hz
1000

Figure 6.1.4

of force measurement is adequate, though small deviations of up to 1 dB could be expected due to spurious resonances in the vibrator.

The vibrator characteristics were found to be:

m_T = 2.51 lb wt	h_1 = 90 lbf/in
m_A = 2.307 lb wt	c_1 = 0.437 lbf/in/S
k_1 = 362 lbf/in	F = 4.35 lbf/mV

Accelerometers were mounted on the large end mass, on the damper unit ends, and the vibrator table, corresponding to coordinates q_1 - q_4 on Figure 6.1.3. This enabled the complete response to be monitored, and also enables the transmissibility ratio (q_4/q_1) for the particular case to be derived.

6.1.1.2 Response for Different Force Levels

The damper unit was tested at different force levels, to show up the effects of damping changes. The results for these tests are shown in Figures 6.1.5 - 7, with the theoretical response of the model with parameters derived from the tests.

The top-bush stiffness k_3 is found by using the frequency 'A' at which the top mass m_4 is anti-resonant on the damper unit. This bush is slightly non-linear as this frequency depends upon amplitude (and preload), giving frequencies between 11.3 Hz and 11.9 Hz. Taking the mean

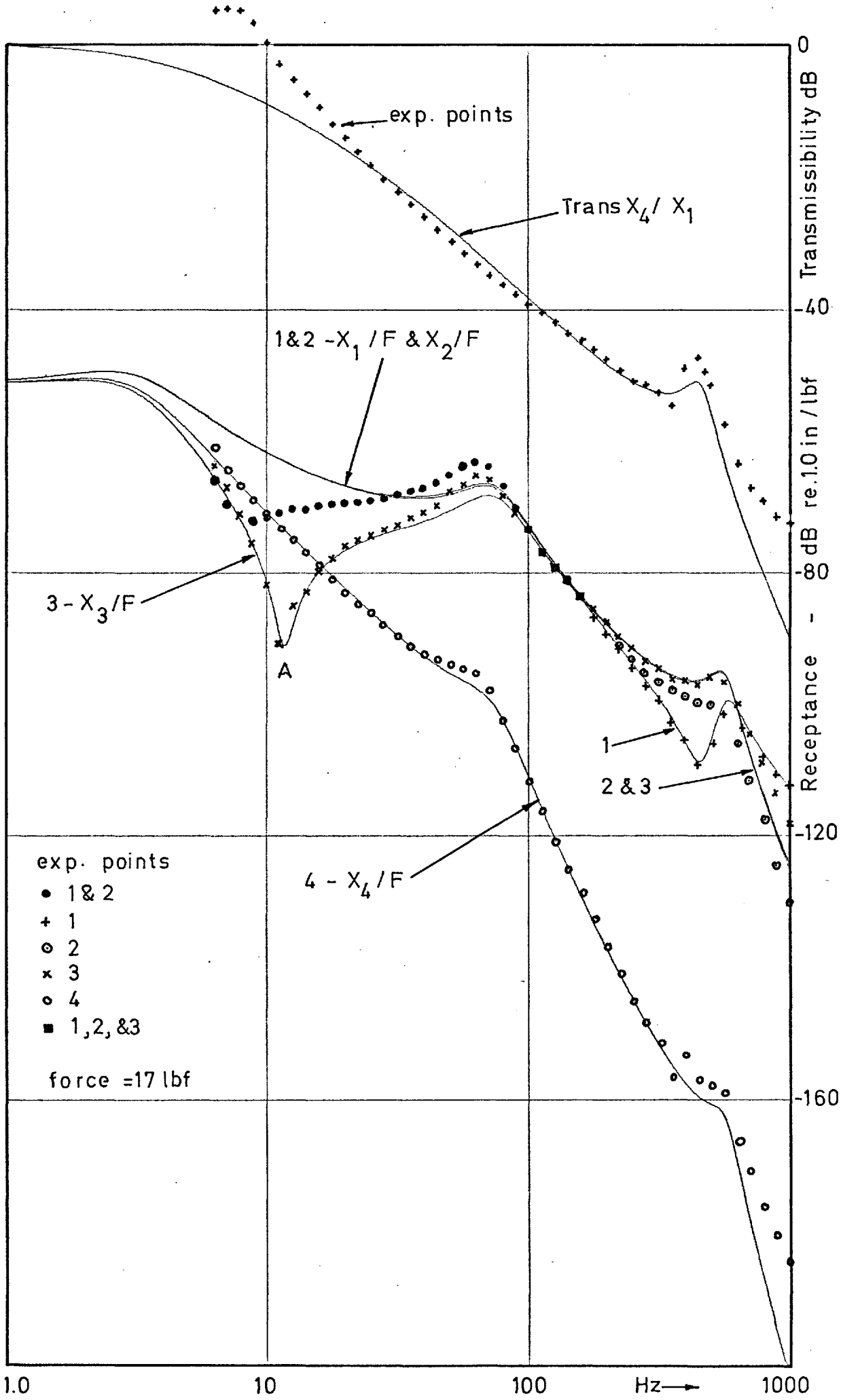


Figure 6.1.5.

EMOOSI ALL

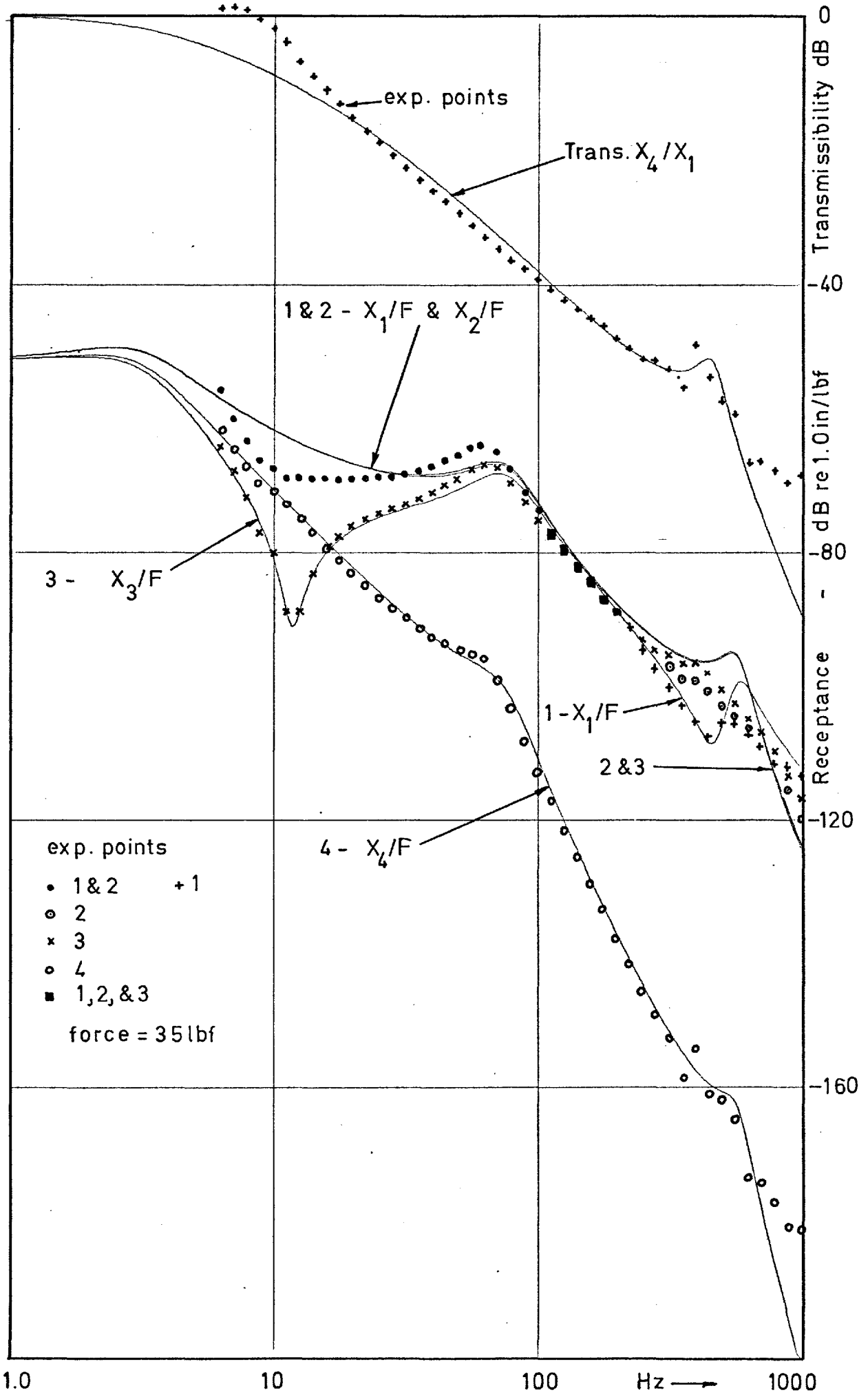


Figure 6.1.6

EM005R ALL

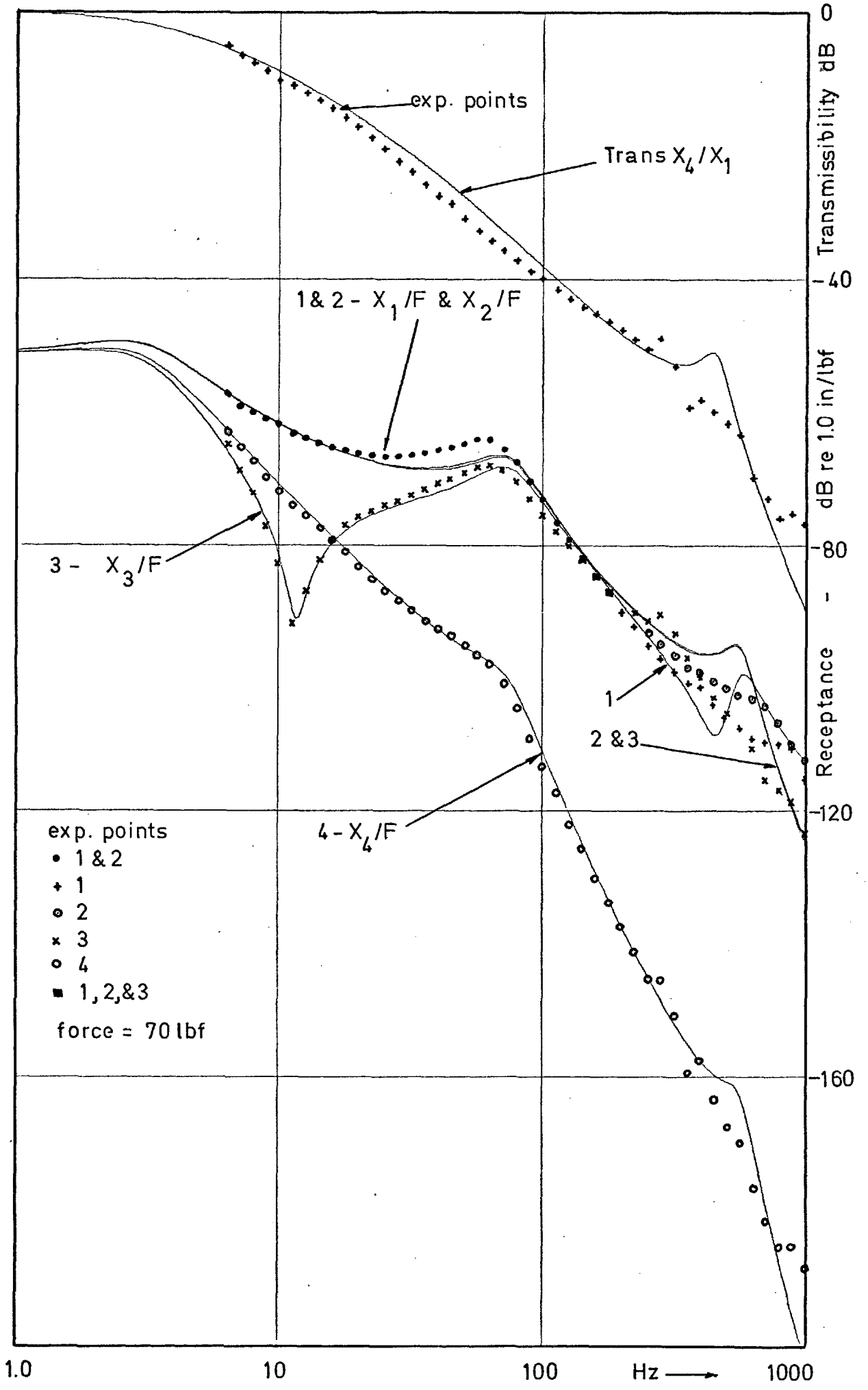


Figure 6.1.7

EMOOSR ALL

value of 11.6 Hz then leads to a bush stiffness of 4,100 lbf/in.

The bottom bush stiffness is deduced from the second resonance, when the damper is effectively locked and resonant between two clamped ends. This resonance occurs at about 450 Hz - though this is masked at higher force levels. This leads to a combined stiffness $k_2 + k_3 =$ 59,100 lbf/in, and thus $k_2 =$ 55,000 lbf/in. Loss factors for the bushes (by the bandwidth method) are $\eta_3 = 0.13$ and $\eta_2 = 0.22$. The bush stiffnesses and loss factors are assumed constant with frequency.

At low frequencies, the variations in damping are apparent, low force levels leading to increased transmissibility as frictional effects become more significant. The equivalent viscous damping coefficient used was 18 lbf/in/S which fits the 70 lbf excitation level quite well. At high frequencies, the damper unit tends to 'lock-up', so that after about 30 Hz the transmission of the unit depends very little on the damper characteristics, but is principally determined by the bush stiffnesses and the mass of the unit. This locking of the damper unit occurs in the theoretical model also - due to the relative mobilities of the bushes and damper and not due to stiction.

Figure 6.1.8 shows the transmissibility using pink and white noise excitation. The signal was analysed using a 1/10 th octave filter and thus some detail is lost. The

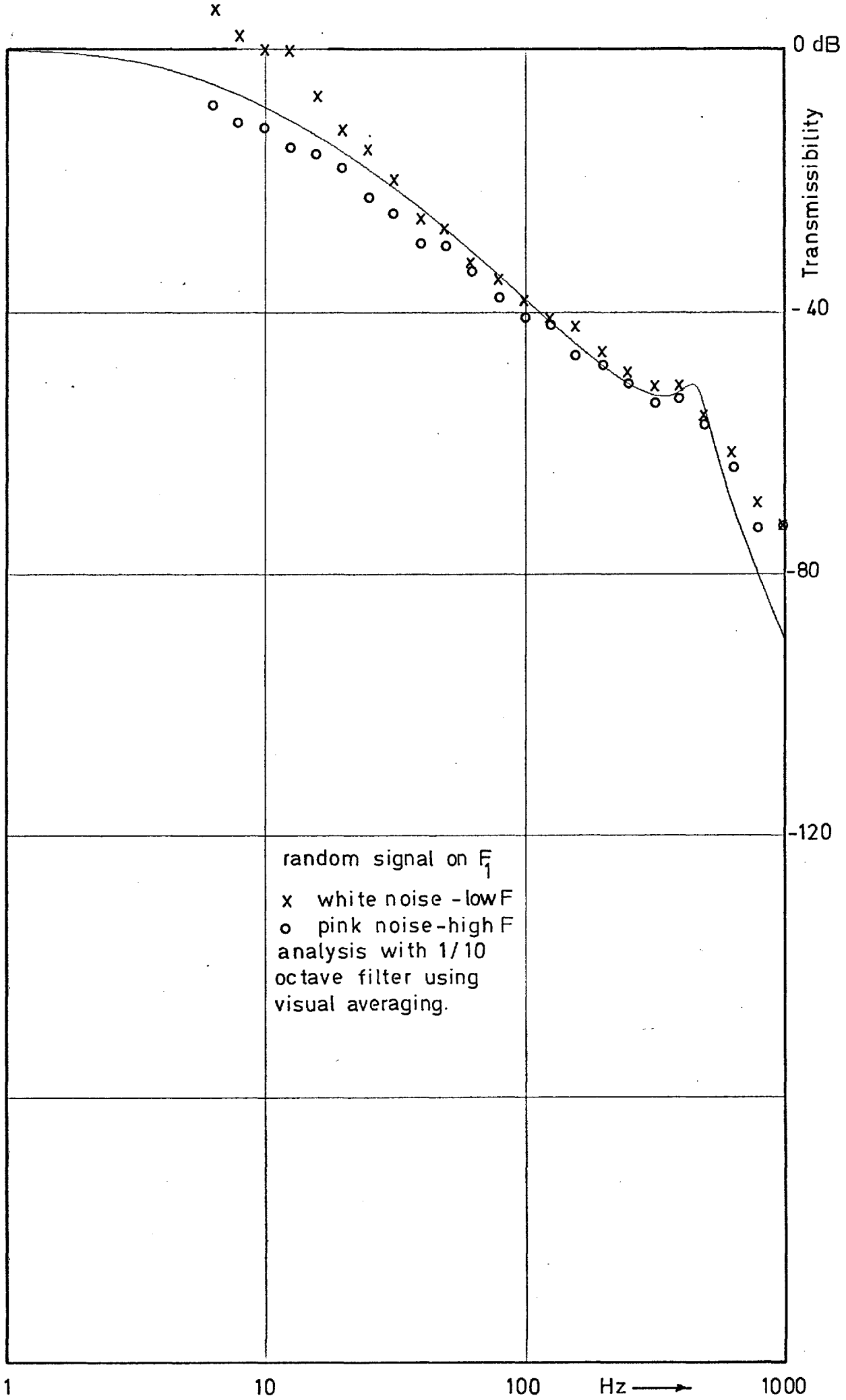


Figure 6.1.8

EM0051

results show that the frequency response curves give a good representation of the system in the more realistic environment of random vibration.

6.1.1.3 Theoretical - Experimental Comparison

Figures 6.1.5 - 8 showed the theoretical response of the model with experimentally obtained parameters, for comparison with the experimental results. The top bush is seen to provide the main compliant element in the middle frequency range, until at high frequencies (> 450 Hz) the bottom bush increases the mobility, after first causing a resonance.

Clearly the model gives an adequate description of the damper unit, especially in the higher frequency range.

6.1.1.4 Effect of Parameter Changes

The effect of modifications to the damper unit can then be predicted. Figure 6.1.9 shows, for comparison with the present unit, the effect of equalising the bush stiffnesses (with the same overall stiffness) which gives, to a first approximation, the 'optimum' for a two stage mount as was shown in Chapter Four. Also shown is the effect of removing the bottom bush, with all the compliance in the top bush. Equalising the bush stiffnesses is seen to lead to increased transmissibility in the region of 60 - 280 Hz,

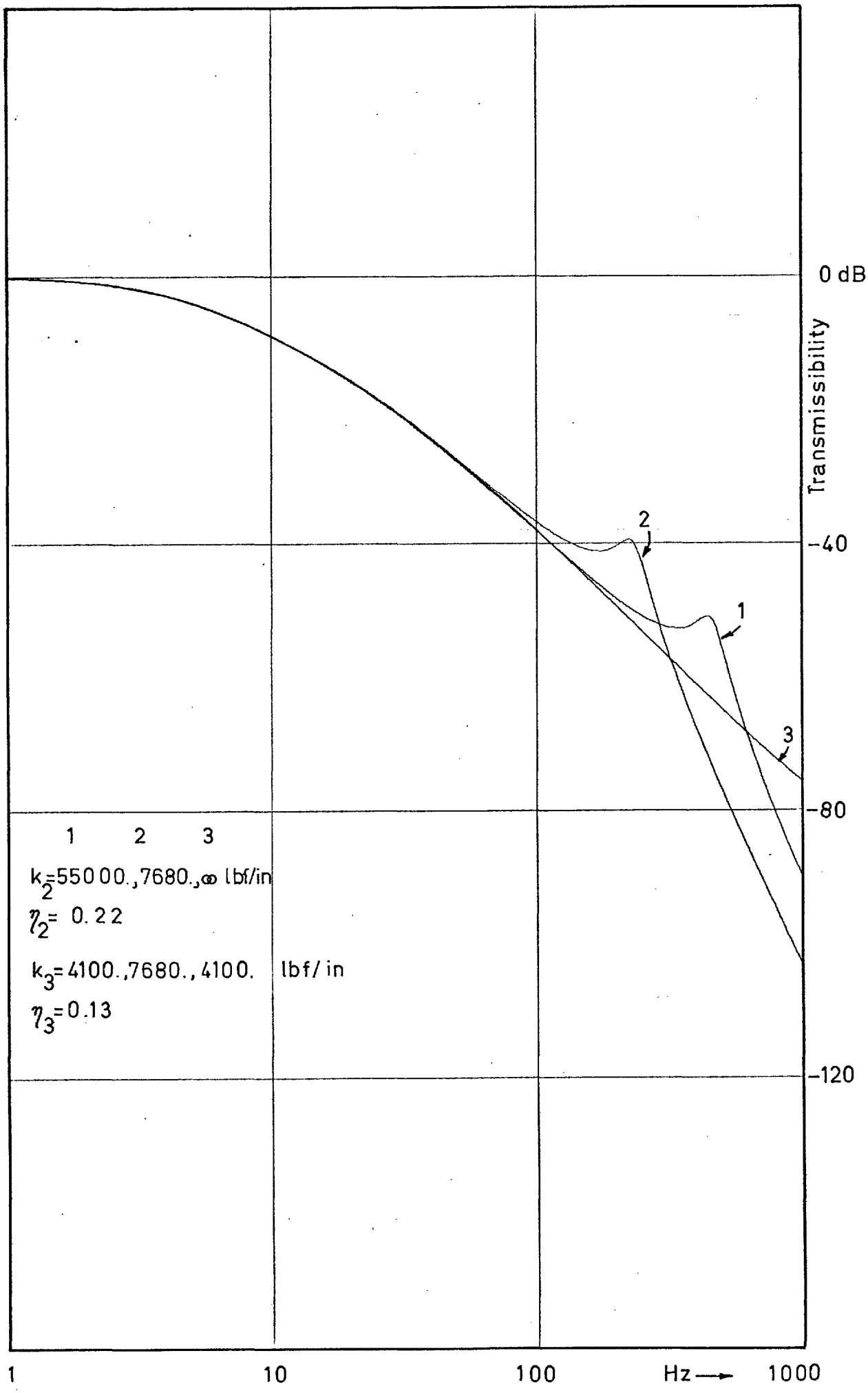

0 dB
-40
-80
-120
Transmissibility
1
10
100
Hz
1000
1
2
3
1 2 3
k2=55000.,7680.,∞ lbf/in
η2= 0.22
k3=4100.,7680.,4100. lbf/in
η3=0.13

Figure 6.1.9

of up to 10 dB due to resonance, and a decrease in transmissibility of around 10 dB at higher frequencies. This modification is thus disadvantageous as far as low frequency isolation is concerned. The removal of the bottom bush removes the resonant peak and so increases the isolation in the range 220 - 560 Hz, thereafter giving more transmission than the unit tested.

It is clear that for the best low-frequency response only one compliant element should be used to avoid the resonance, and for isolation purposes this should be as compliant as possible. In Appendix 1 it is shown how the required bush stiffness can be obtained to retain the damper's effectiveness. This compliant element will always tend to be much stiffer than the main suspension spring and will therefore be a much better transmitter.

6.1.2 Wishbones

The lower wishbone was tested by making impedance and transmissibility measurements with a steel block as the end constraint. This block, designed to test the complete suspension, is described in detail in §§ 6.2.

6.1.2.1 Vertical Transmission

The physical and schematic test arrangements are shown in Figure 6.1.10.

The terminal mass was softly suspended from the ceiling, with a pivot point, consisting of stiff rubber pads, distant from the excitation point. The block was then effectively free to move vertically. The inboard pivots of the wishbone were rubber bushes, with the outboard pivot a plain bearing. Two basic difficulties needed to be overcome - that of not introducing bending moments with the vertical excitation, and not constraining the wishbone laterally. For the frequency range tested (10 - 150 Hz), the bearing already part of the suspension was employed and found to be satisfactory. Keeping the amplitude small on the input ensured that lateral motion of the wishbone end was kept to a negligible amount.

The transmissibility ($\ddot{X}_2/\ddot{X}_1$) and apparent mass ($F_1/\ddot{X}_1$) of the wishbone were measured, shown in Figure 6.1.11. Apart from a slight resonance at 55 Hz, due to the end beams on the terminal block, the behaviour conformed well with that predicted. The wishbone construction was such that it could be adequately described as a uniform beam, of weight 2.915 lb. The weight of the terminal block was 160 lb effectively at the excitation point. For the freely pivoted case, the transmissibility is given by:

$$T = \lfloor 6m'/m + 2 \rfloor^{-1} = -50.4 \text{ dB}$$

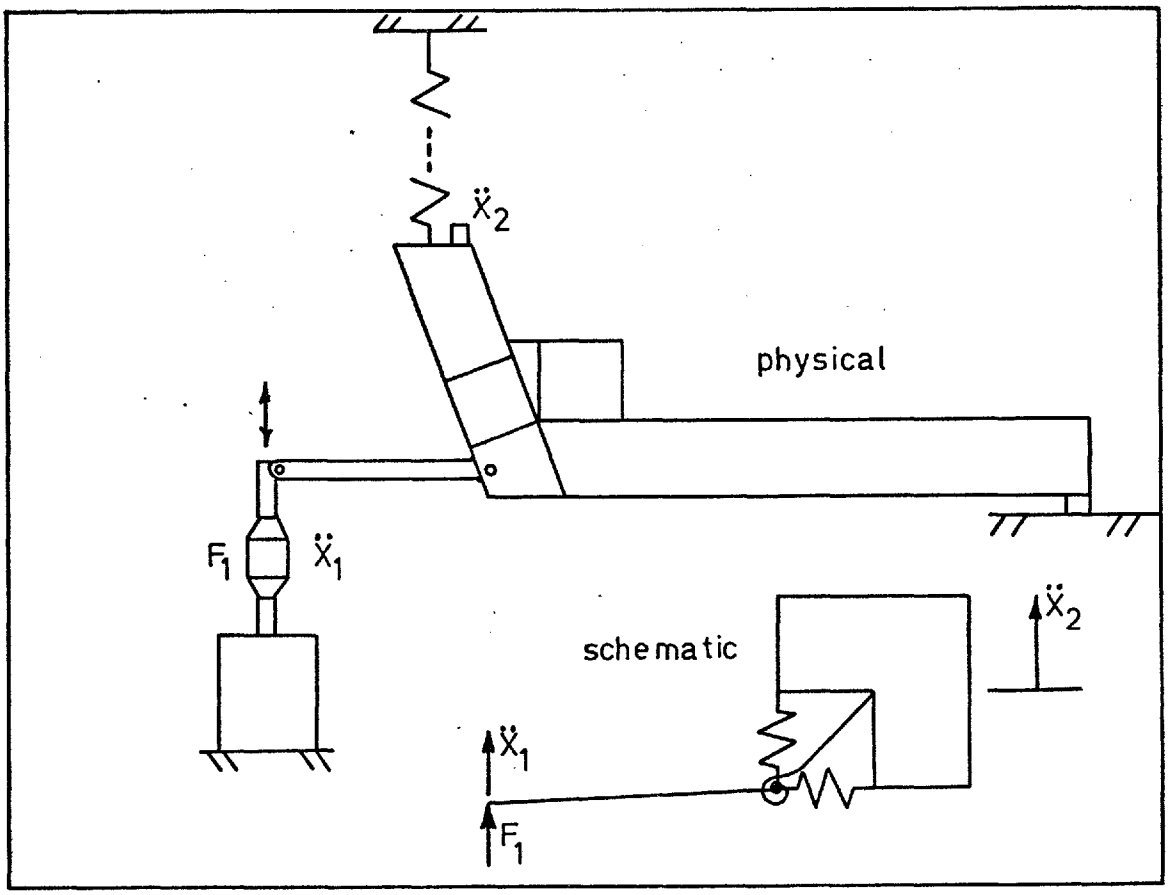


Figure 6.1.10

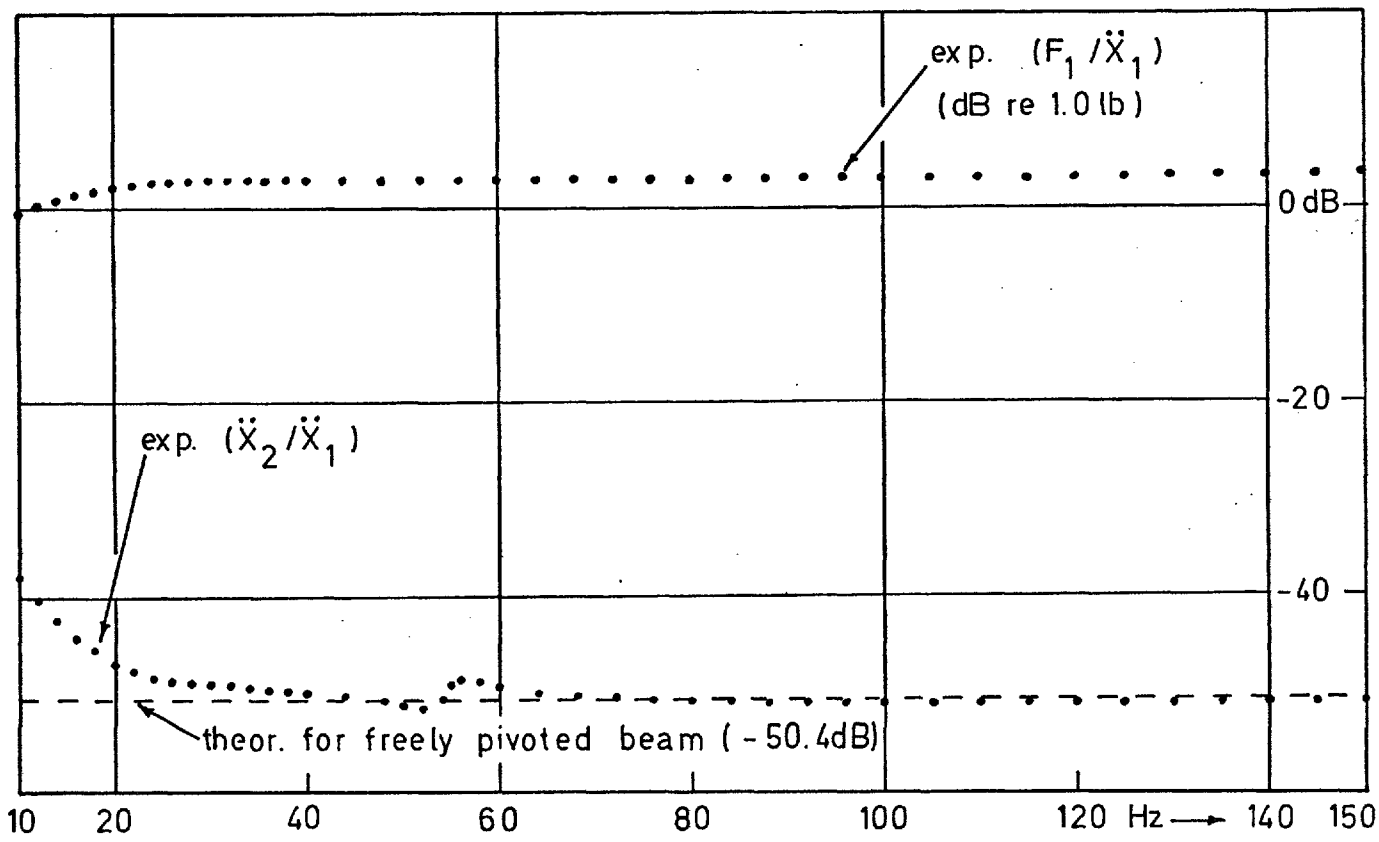


Figure 6.1.11

as has been shown previously. After the torsional stiffness controlled region, the experimental curve remains level at -51 dB giving good agreement with theory. The radial stiffness of the inboard bushes is so high that no resonance is caused, and it plays no part in the vertical transmission of vibration. The torsional stiffness of the bushes was more readily determined by free-decay methods, since the torsionally controlled resonance occurs below the available test frequencies (and so, in fact, the torsional stiffness is somewhat irrelevant).

This test gave the torsional stiffness as 60.5 lbf in/rad with a loss factor of 0.08. Some slippage can occur between the bush and the mounting, so that this value will be variable in practice - it represents a value about four times smaller than might be expected from the bush dimensions.

6.1.2.2 Lateral Transmission

As shown in Chapter 5, the lateral transmission path is seen to depend primarily on the inboard bush stiffnesses of the wishbones, and knowing the bush stiffnesses it is possible to make an estimate of the effectiveness of the bushes as isolators. The arrangement of the lateral transmission test to give the bush stiffnesses is shown in Figure 6.1.12.

The terminal block was suspended from the ceiling and is free to rotate as well as translate, so that the effective mass of the end block in this case is less than

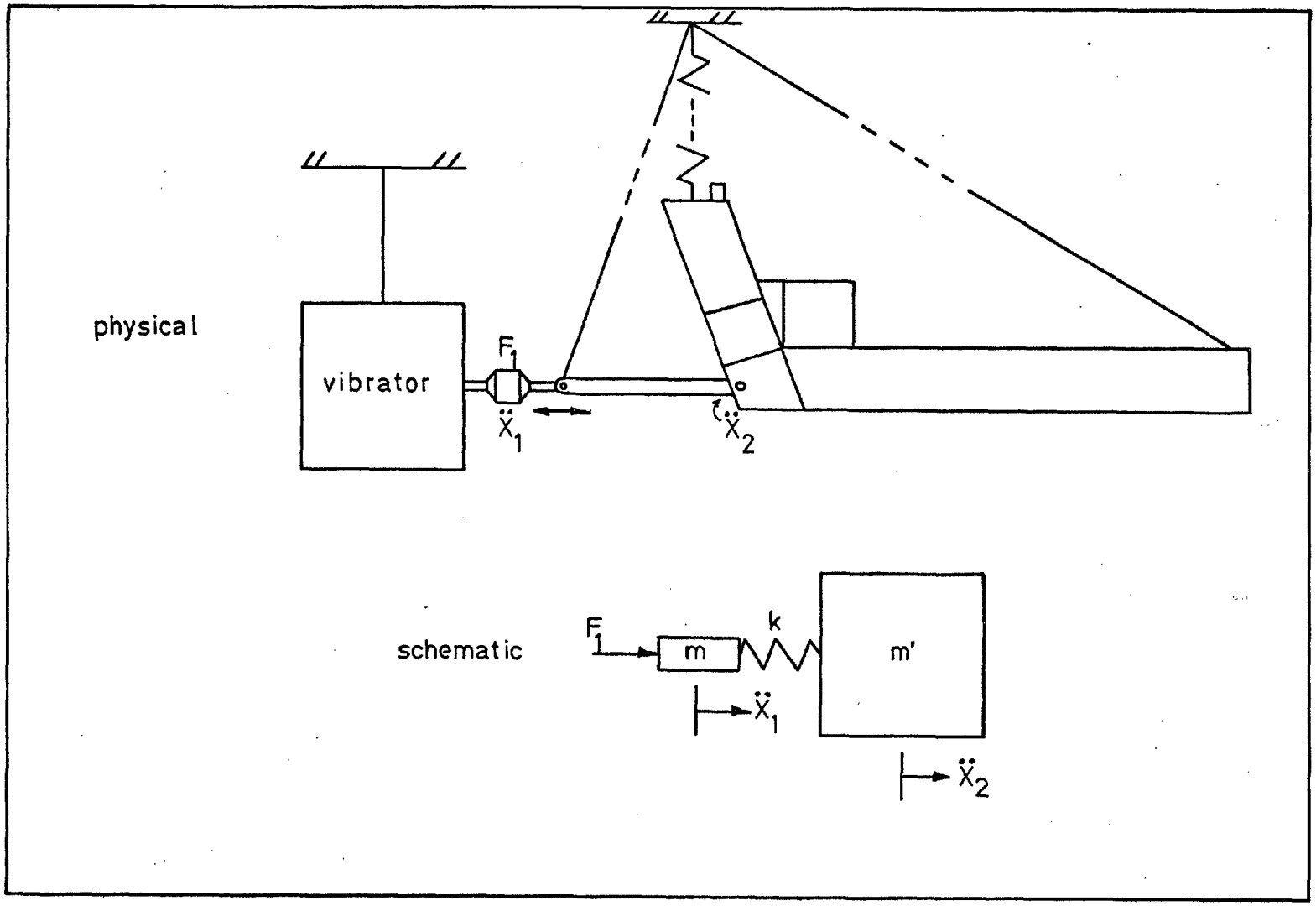

physical
vibrator
F_1
$\ddot{X}_1$
$\ddot{X}_2$
schematic
F_1
m
k
m'
$\ddot{X}_1$
$\ddot{X}_2$

Figure 6.1.12

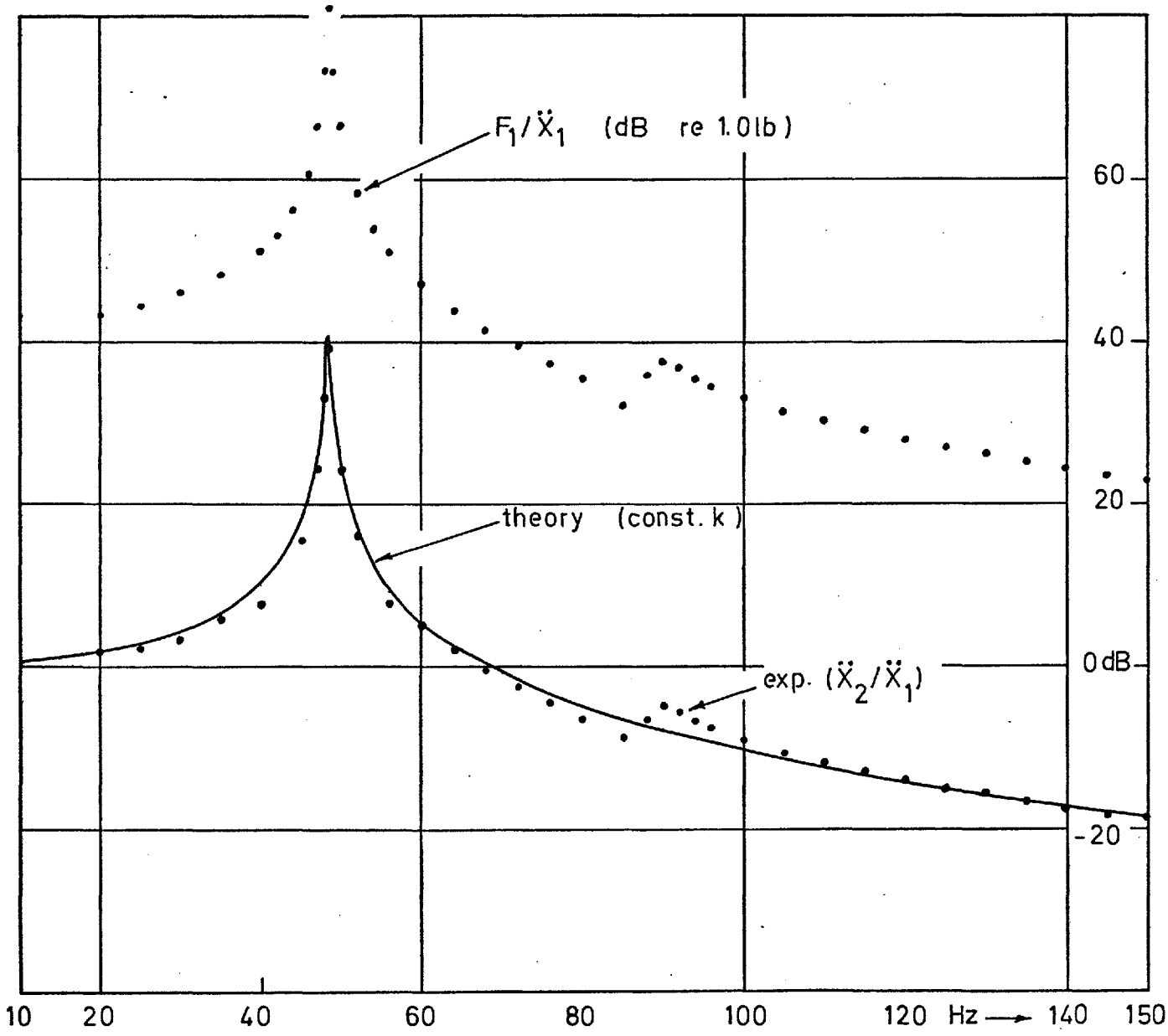

$F_1/\ddot{X}_1$ (dB re 1.0lb)
theory (const. k)
exp. $(\ddot{X}_2/\ddot{X}_1)$
60
40
20
0dB
-20
10
20
40
60
80
100
120
Hz
140
150

Figure 6.1.13

the total mass of the block.

In the practical arrangement the wishbone is inherently unstable to an applied lateral point force, and a rigid connection was found to be necessary between the impedance head and the wishbone to suppress coupling to the vertical response of the wishbone due to any small misalignment. The rigid connection in this case does not affect the validity of the test - see Chapter 3 on experimental techniques.

The apparent mass ($F/\ddot{X}_1$) and transmissibility ($\ddot{X}_2/\ddot{X}_1$) curves for this test are shown in Figure 6.1.13. From the low-frequency asymptote of the apparent mass curve the total effective mass of the system ($m + m^1 \simeq$ 103 lb wt) can be estimated. The wishbone mass m is already known by weighing, but could be obtained from the high frequency asymptote. From the anti-resonant frequency ω_A = 48.3 Hz, the combined bush stiffness can be obtained i.e. $k = m^1 \omega_A^2 \simeq$ 24,000 lbf/in. The amplification at resonance is seen to be 40 dB (subject to errors of $\pm$ 2 dB due to limitations in the digital measuring equipment - a poor signal-to-noise ratio was encountered about this frequency), which leads to the bush loss factor of 0.01.

A slight spurious resonance is seen at 90 Hz, due to the beams of the terminal mass. This frequency is seen to be different from the previous case, due to the difference in boundary conditions. Apart from this effect, the real behaviour of the wishbone is seen to comply well with the simple model proposed for it. From the transmissibility curve, the bush stiffness is seen to remain effectively

constant over this frequency range.

6.1.2.3 Longitudinal Transmission

The apparatus was not well adapted to measure the longitudinal transmission through the wishbones, and consequently the test was performed to study the general form of tranmmission only - it is difficult to draw definitive conclusions. The arrangement used is shown in Figure 6.1.14, and the transmissibility for this case shown in Figure 6.1.15 compared with the theoretical response using the longitudinal wishbone model shown in Chapter 5. The general form of agreement is seen to be good, indicating that the proposed model is valid.

The receiving mass tends to rotate about a vertical axis 'A' and a horizontal axis 'B' - and as a consequence the terminal impedance is low. Furthermore, due to this rotation, at very low frequencies the transmissibility is less than unity - in fact tends to -8 dB. The terminal effective mass was deduced from the low frequency apparent mass asymptote ($F_1/\ddot{X}_1$), referred to the receiver end, and was estimated at 61.5 lb. With the measured bush stiffness from the lateral test, and this terminal effective mass, it was not possible to predict the resonant frequency precisely with reasonable estimates of longitudinal and torsional stiffness values of the wishbone bushes. The lateral radial stiffness of the bushes has been increased some 54% for the theoretical model to predict the resonant peak successfully, and

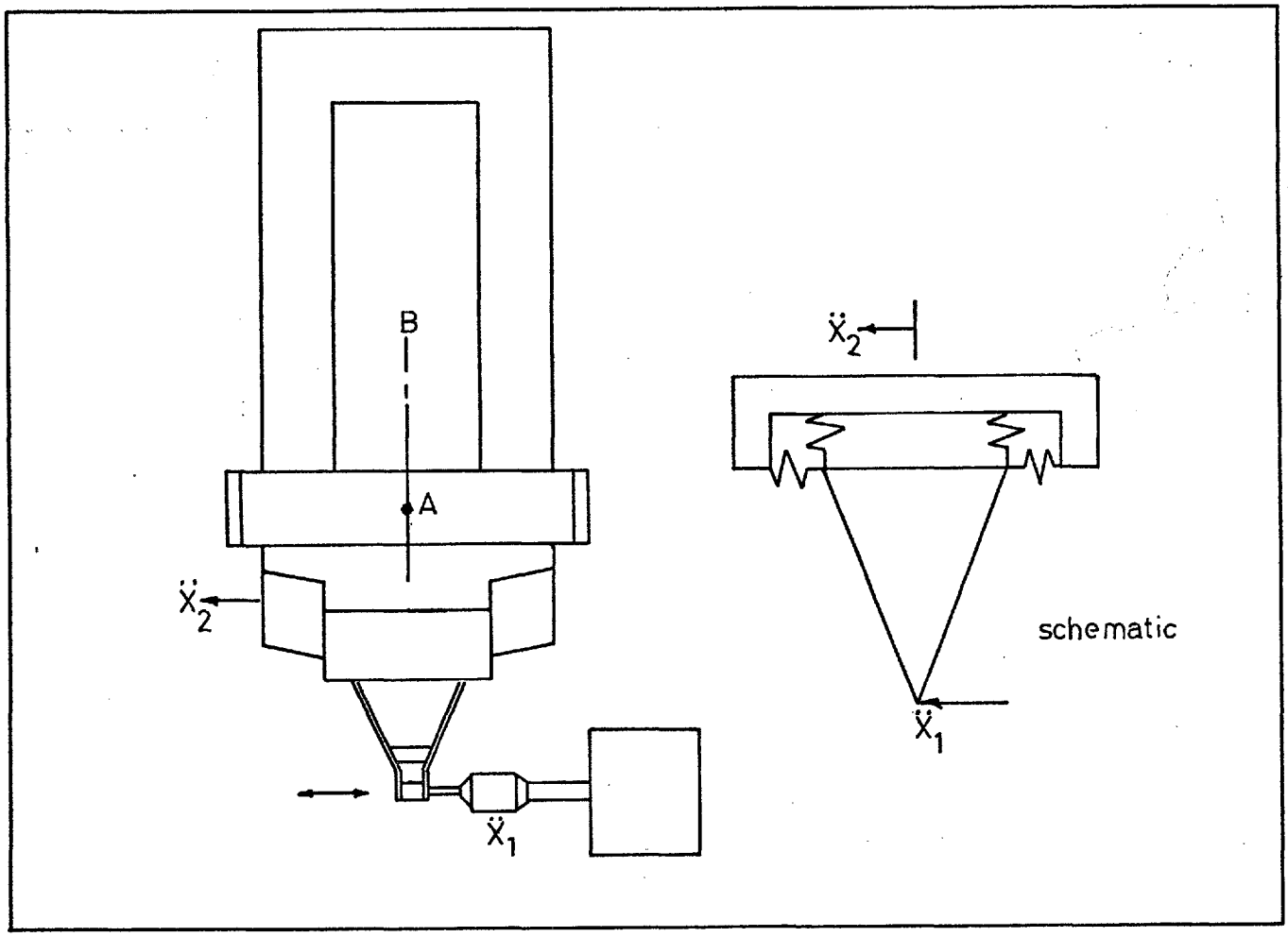


Figure 6.1.14

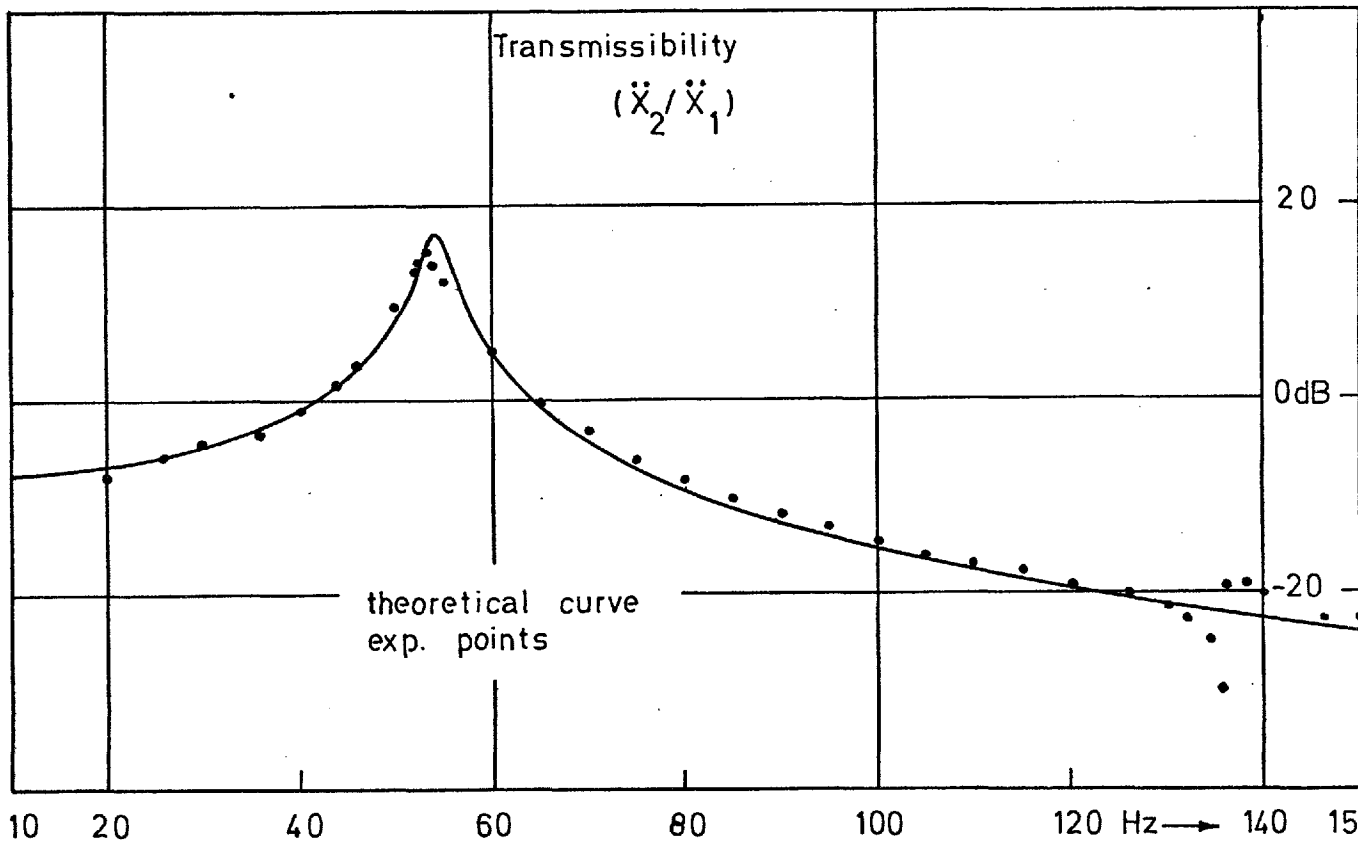


Figure 6.1.15

8 dB subtracted from the transmissibility to account for the rotation effects. A spurious resonance is noted around 138 Hz.

6.2 SUSPENSION ASSEMBLIES

Suspension assemblies leading up to the complete suspension system formed the final stages in testing.

For the complete suspension, there are certain practical difficulties for standard impedance tests:

1. there are five output-points (the wishbone ends and the spring-damper unit) as well as one input point, and the correct orientation must be preserved between the components,
   and
2. appreciable static load must be applied through the damper-spring unit to give this orientation.

The electromagnetic exciter used to supply the vibratory signal was unable to accept the static load.

A transmissibility type test was arranged, with a rigid end mass as the receiver to lead to results to give a reasonable comparison with the plots shown in Chapter Five.

6.2.1 Apparatus

The mean static load required across the suspension to simulate average laden conditions is about 550 lbf. It was decided to use a smaller amount of mass than would produce this load, and to adjust the static load by means of springs. The form of the apparatus is shown in Figure 6.2.1. The suspension unit is mounted onto a 4 in. thick steel plate, with mounting points to give the correct suspension orientation. Box-section beams 4 in. square lead out rearwards from the mounting plate to a pivot point (in fact very stiff rubber pads), so that for small motions the mounting plate is free to translate approximately vertically. The static load from the suspension is borne by a pneumatic spring (in place of the tyre - the wheel and tyre would obstruct the driving), using an adaptor from the spring to the stub-axle. By adjusting the air pressure in the pneumatic spring, and the tension of the loading springs, the whole apparatus can be correctly aligned with the requisite static load on the suspension.

Ideally, the form of the model for this arrangement is as in the models described in Appendix 7, except with a smaller end mass attached to ground with a spring. In practice, despite the massive construction of the end mass, it does not remain entirely rigid in the frequency range tested, (10 - 150 Hz), due principally to resonances of the box-beams - and these resonances are to some extent variable according to the boundary conditions at the beam ends. Thus, the receiver

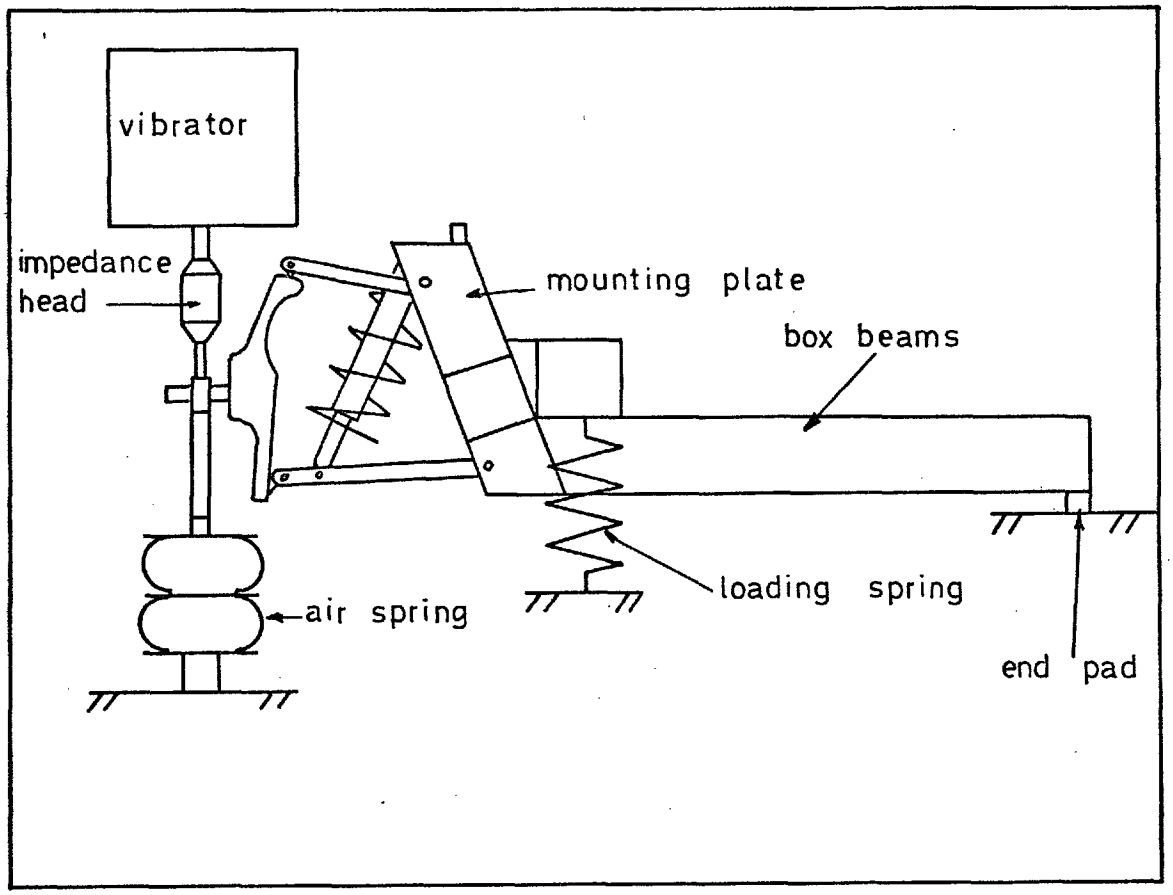

vibrator
impedance
head
mounting plate
box beams
air spring
loading spring
end pad

Figure 6.2.1

does not give the simple spring mass system as is ideally the case. Furthermore, it was not possible to measure the impedance of the receiver in the 'in-service' condition, because of the static load requirements. The impedance of the receiver will, in any case, vary across the mounting points. As a consequence, it was necessary in the first instance to assume that the simple receiver behaviour was followed, and then to investigate unexpected resonances by measuring the receiver amplitude at various positions on the mounting plate and beams. It was found by this means that resonances in the box-beams did occur. In the case of the wishbones-only test, one of these resonances was included in the modelling. For the complete suspension unit, more resonances were encountered, but could not be included in the model as the model complexity was near the limiting case for accurate computer solutions. In this case, it was necessary to explain the occurence of spurious peaks in the response, after searching over the receiver with an accelerometer.

6.2.2 Wishbones Alone

The step from the single wishbone model to two wishbones and stub-axle assembly was seen to result in a considerable increase in complexity, principally in the inertia matrix allowing for the rotations of the elements.

The lower wishbone tested previously was seen to have only small outboard pivot friction. The pivot for the upper wishbone, a ball joint, was found to have very considerable

friction and was thus expected to give very non-linear behaviour.

The experimental arrangement for testing the wish-bones alone is shown in Figure 6.2.2. A soft spring is used to relieve the static load on the suspension. The experimental transmissibility ($\ddot{X}_2/\ddot{X}_1$) for this case is shown in Figure 6.2.3, for both high and low applied force (F_1). In the low-frequency range very appreciable differences in transmissibility are seen, more than 20 dB at 10 Hz between the two force limits, and this effect is attributed directly to the friction on the upper pivot. In the theoretical model, the energy loss at the pivots had previously been obtained by assuming equivalent viscous damping, but the slope of the curve in the low-frequency region cannot be explained by this mechanism.

The energy loss per cycle for pure Coulomb damping is given by:

$$\Delta E_c = 4 R x_o$$

where R is the frictional force and x_o is the amplitude of vibration.

The hysteretic damper provides a model for frequency-independent energy-loss per cycle, i.e.

$$\Delta E_h = \pi x_o^2 h$$

where h is the hysteretic damping value.

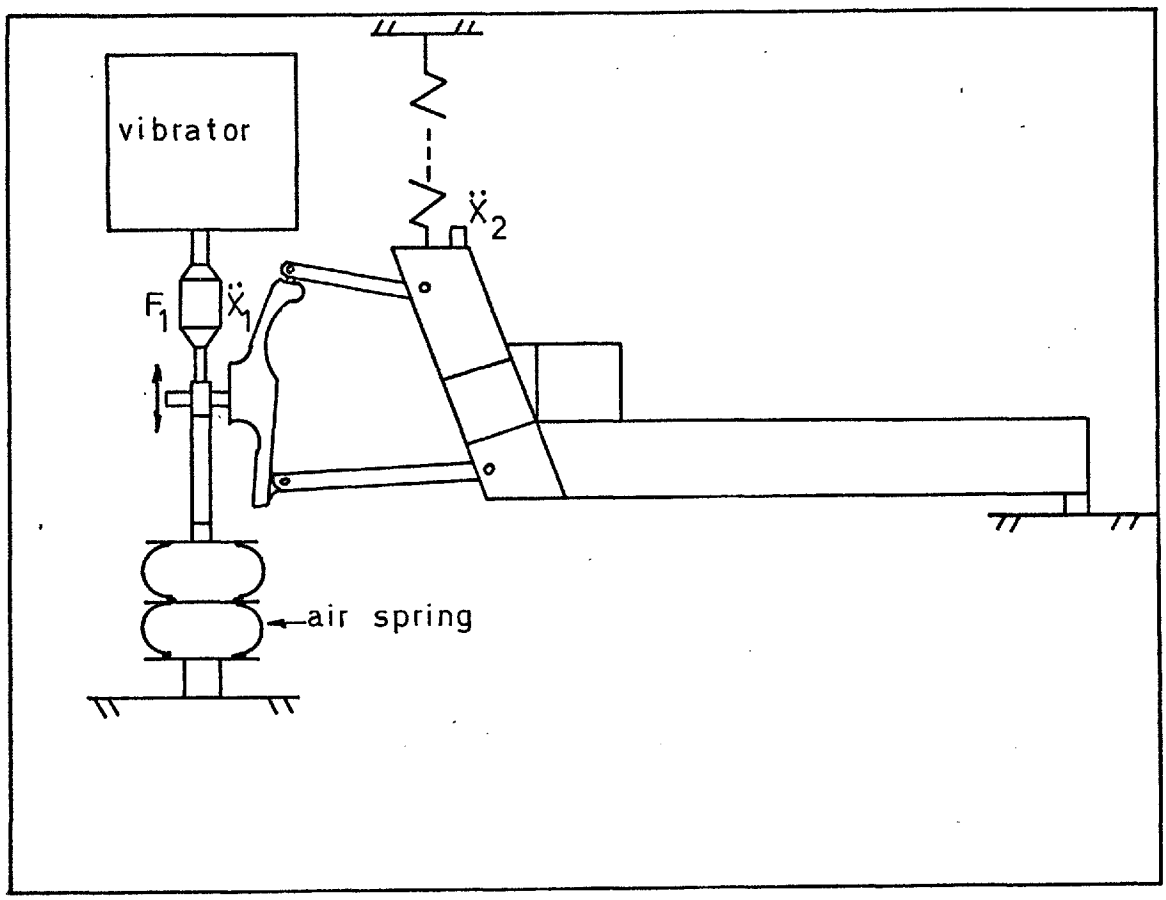


Figure 6.2.2

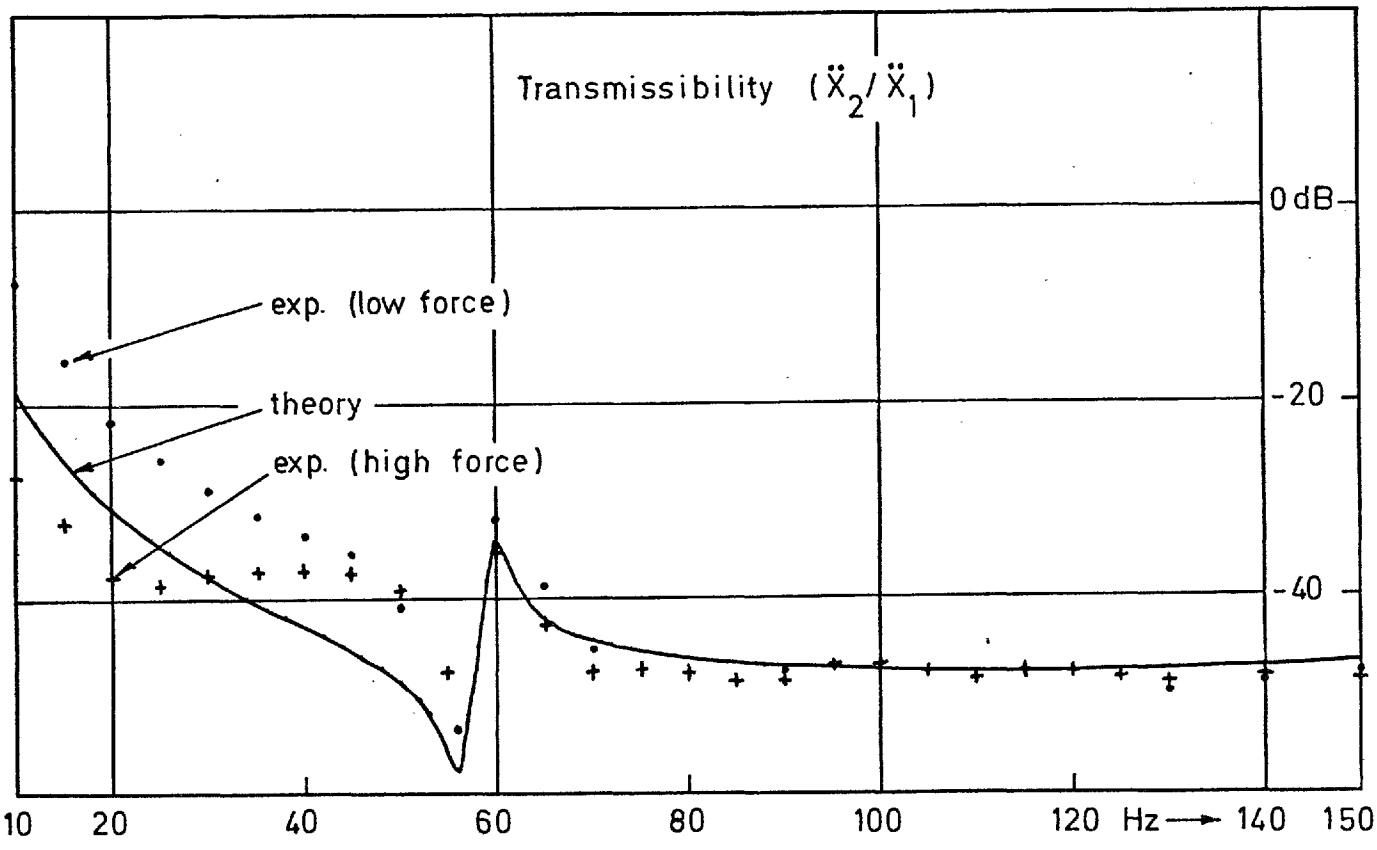


Figure 6.2.3

Thus, for constant amplitude it is possible to replace, for equal energy loss, Coulomb damping by hysteretic. This procedure is followed here, although it is not strictly valid, to provide a mean line between the high and low force levels. Note that no statement is made about the actual mechanism of energy loss at the pivots, merely a model of approximately the right form has been employed to simulate the loss. Receiver resonances at 60 Hz (strong) and 100 Hz (weak) were found, the former being modelled in the response. With these adjustments the theoretical response is calculated (see Appendix 7 for data), giving reasonable correlation with the experimental results. In the higher frequency range, the non-linear effects are less in evidence than at low-frequencies (where the model can only cope most approximately), with high and low forces giving closely similar results.

The low-frequency behaviour, depending so much on pivot friction, will be very variable in service. The effect on the complete suspension properties will, however, be small as the wishbones form a weak path. The large variations in frictional behaviour with force are thus unlikely to have more than a small effect on the transmissibility when the spring-damper unit provides the main path.

6.2.3 Complete Assembly

The complete suspension assembly was tested, arranged as shown in Figure 6.2.1, and shown without the vibrator in Plate 1. In this case there is appreciable load on the pivots, and the friction here is likely to be changed - though it is not possible to separate out the effects of this. The transmissibility for this test is shown in Figure 6.2.4. The damper unit is seen to remain in the locked state, as only small vibratory forces could be applied, and the primary transmission path is through the damper top bush. The loading and constraints on the damper unit give a higher bush stiffness than previously encountered. Spring surges at 70 Hz and 138 Hz demarcate the partial cancellation region referred to in Chapter 5, but spurious resonances, due to the box-beam resonances tend to obscure this zone. By slight adjustments to the boundary conditions (i.e. by moving the end rubber pads) it was seen that the spurious resonances could be changed when the test was repeated, whilst the suspension resonances remained closely repeatable. The theoretical curve fitted to the results is thought to give a reasonable representation of the real behaviour, but one point remains not completely explained - that is, the apparent increase in the damper top-bush stiffness which, in the model, although increased from that value previously measured, still underestimates the low-frequency resonant peak, and would thus appear to need to be stiffer still. This would lead to too high a frequency 'A' on the input inertance plot (Figure 6.2.5) and so a compromise

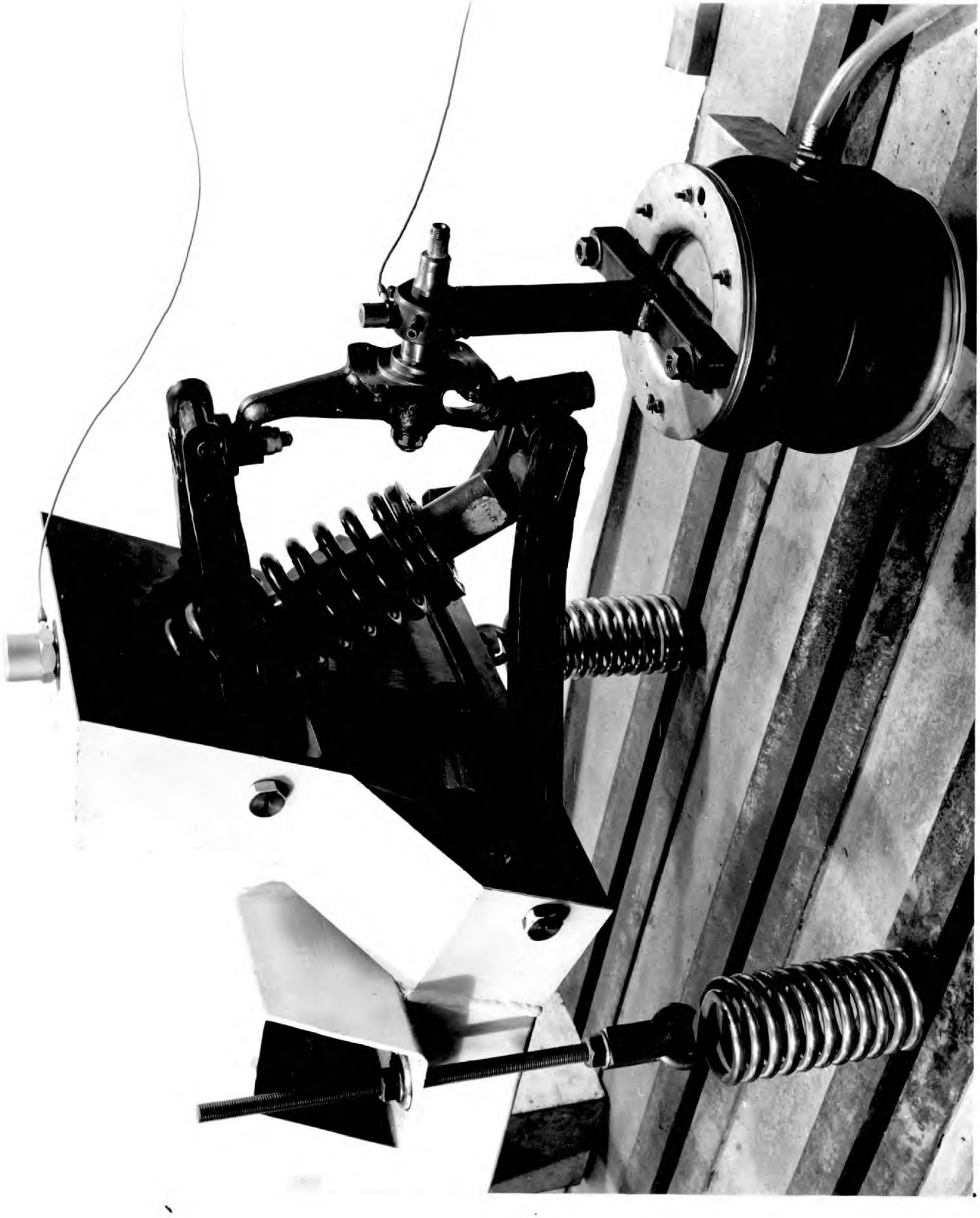


Plate 1

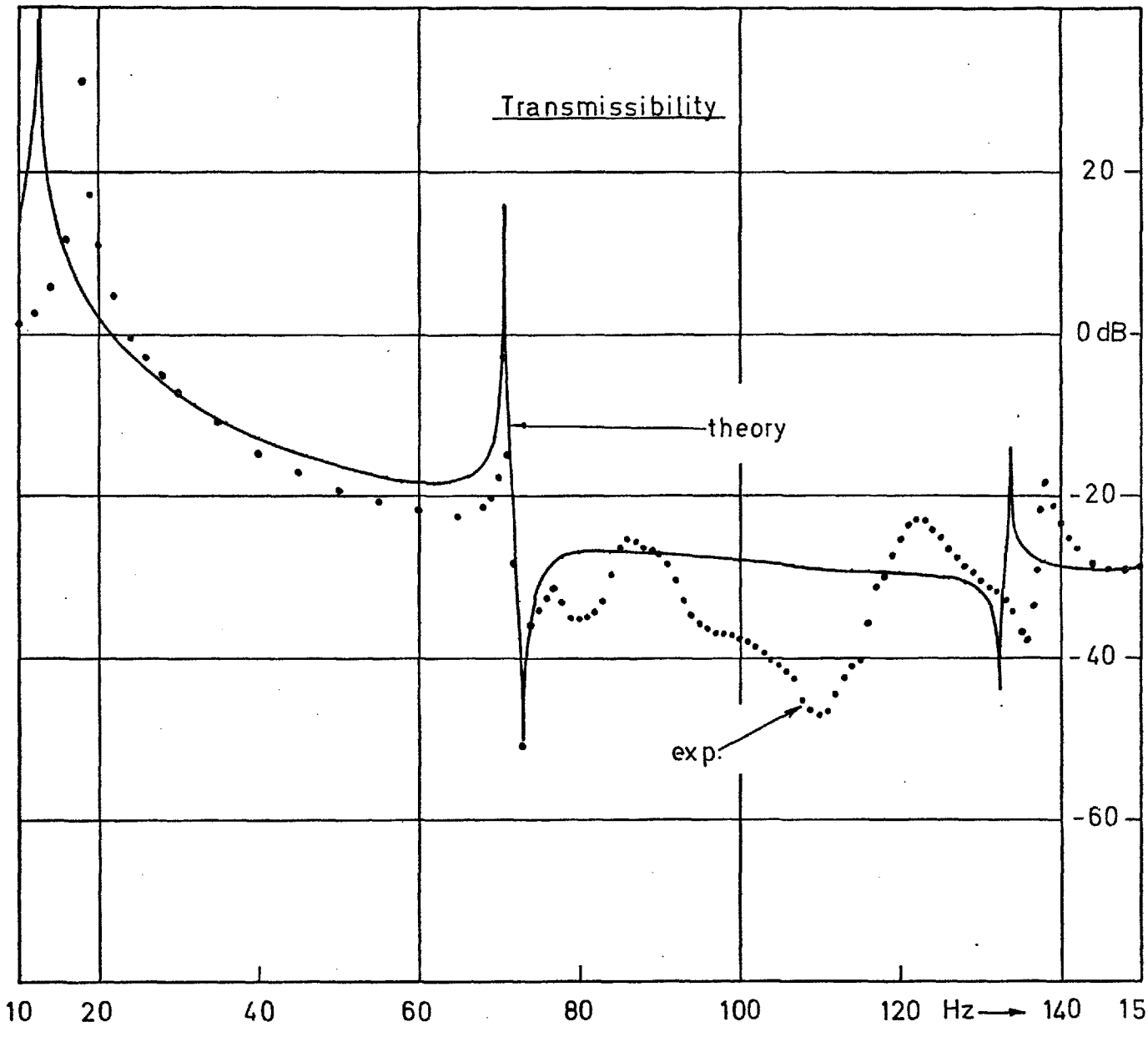

Transmissibility
20
0 dB
-20
-40
-60
theory
exp.
10
20
40
60
80
100
120
Hz
140
15

Figure 6.2.4

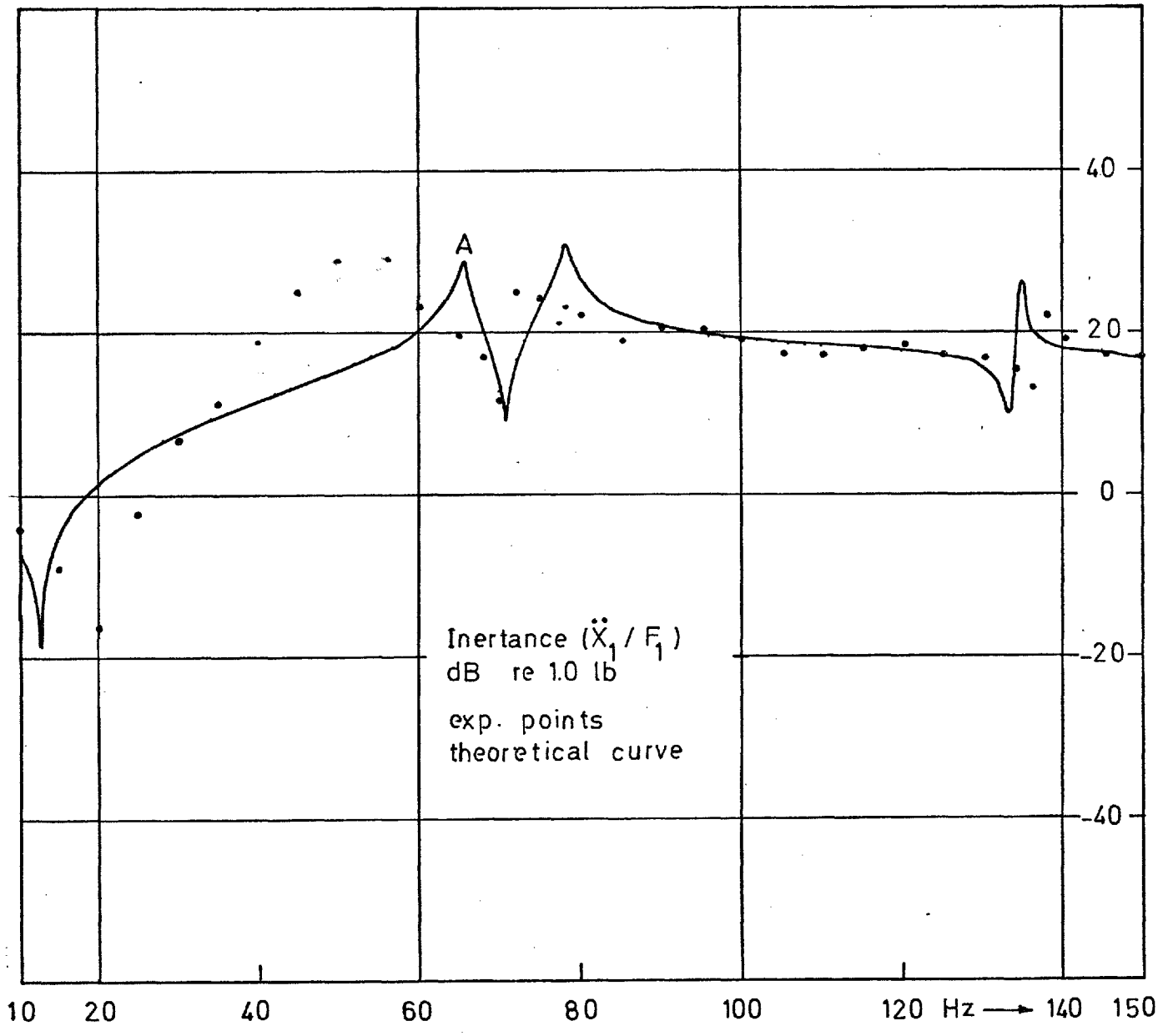

A
40
20
0
-20
-40
Inertance ($\ddot{X}_1$ / F_1)
dB re 1.0 lb
exp. points
theoretical curve
10
20
40
60
80
100
120
Hz
140
150

Figure 6.2.5

value was found necessary.

The lumped parameter model for the main spring was found to underestimate the spring surge frequencies (this is a fundamental limitation of such modelling) and so for the results shown here, the spring mass in the model has been artificially reduced from the true value to match up the first spring surge with that observed. The model still underestimates the second surge frequency, accounting for the small shift seen in Figure 6.2.4.

Bearing these points in mind, it is concluded that the theoretical model gives a reasonable representation of the true behaviour. Figure 6.2.6 shows the predicted transmissibility of this model with a receiver of mass 550 lb over a more extended frequency range. The low frequency behaviour is seen to be strongly constrained due to limitations in the model previously discussed (and which can be avoided), but the higher frequency behaviour is valid, showing the partial cancellation region between the first two spring surges, and rather complex resonant behaviour at higher frequencies.

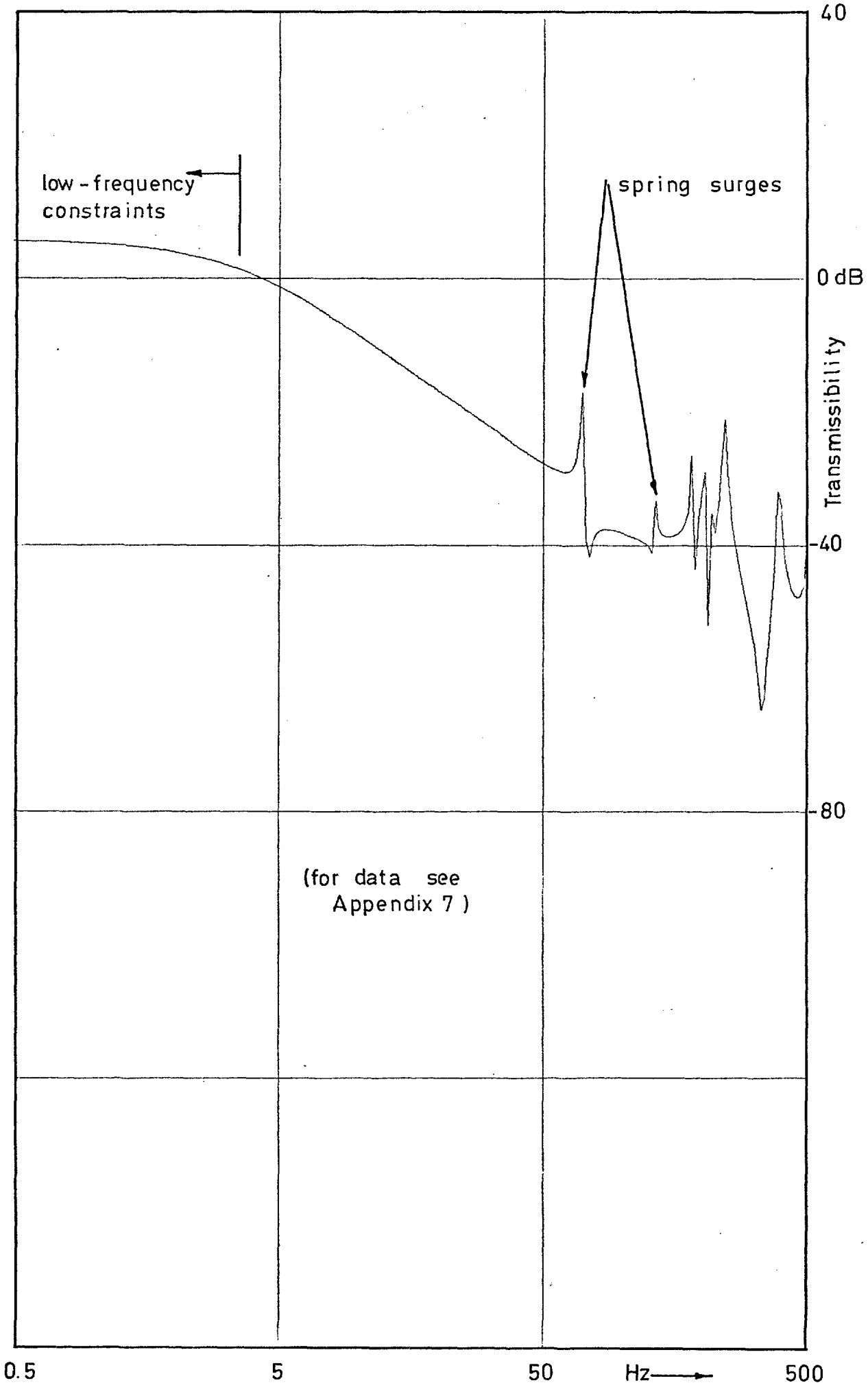


Figure 6.2.6

SS2DSSOX TRANS

6.3 DISCUSSION OF RESULTS

Generally good correlation between the theoretical models' and the real systems' behaviour has been observed, showing that the modelling of what constitutes a highly complex transmission path is a feasible proposition, and that reasonable reliance may be placed on the mathematical models of the suspension. The strongly non-linear properties of the suspension, due to friction, mean that the low-frequency behaviour can be rather indeterminate, but in the acoustic range of frequencies these effects diminish in importance. The frequency range of the modelling is limited by the degree of complexity permitted - thus here the links have been assumed rigid - for higher frequencies link flexure must be allowed for and this requires a very substantial increase in complexity that is probably unwarranted.

CHAPTER 7

CONCLUSIONS

The effectiveness of system changes in reducing the receiver velocity for a given source of excitation has been expressed in equation form in Chapter 2 with an extension noted in Chapter 5. Given the necessary impedance or mobility values for the subsystems it is then comparatively easy to compute the effectiveness of system changes. Transmission paths with appreciable mass lead to quite complex equations, and since it is not always possible to change one mobility parameter independently of the others in real systems it may be difficult to predict the effects of real system changes.

Plurality of transmission paths tends in general to increase transmission, but cancellation conditions can also be achieved. Excessive complication can ensue if every path is considered, and so the approach of considering paths individually is considered, with the objective of optimising each path separately - though by this simplification certain interactions are neglected.

Transmissibility gives a useful indication to transmission path performance, especially for comparison purposes. The principal value of this factor lies in the rapid interpretation of path changes in a standardised source-receiver situation. The relationship between transmissibility and

effectiveness depends on the source and receiver, and generally transmissibility plots tend to give over-optimistic indications as to the effectiveness of an isolator. With this in mind, a new form of transmissibility apparatus was designed and proved.

Real vibration isolators, such as the vehicle suspension system considered, tend to be of such great complexity that the simplified approach noted above needs to be followed. Design criteria for improving performance may be realised using quite simple models. Theoretical predictions in this case have been found to be valid, though experimental work is useful in re-establishing assumptions about the model considered - such as was the case for pivot friction in the suspension.

The linear theory of isolation pre-supposed an ideal-source of vibration, which is, of course, a convenient fiction. Path modifications can lead to the source behaviour being noticeably non-ideal (as shown in Chapter 2) which can result in the path and receiver strongly modifying the source characteristics. As with transmissibility plots, caution must be exercised in interpreting values of effectiveness.

Theoretical and experimental studies on a car suspension system have lead to the following conclusions:

1. Because of the relative mobility of the damper unit and its end bushes, at frequencies of excitation above about 30 Hz the damper unit is effectively locked and vibration

transmission is determined principally by the bush mobility. Friction can lock the damper unit at lower frequencies when the applied force is low.

2. The damper forms the most significant vertical transmission path for most of the frequency range 10 - 200 Hz apart from peaks due to spring surges. One compliant element (or bush) in series with the damper is seen to be preferable to two so that a high frequency resonance is avoided.

3. The desirable bush stiffness for the damper unit to give satisfactory control of body-bounce and wheel-hop modes is obtained from a five parameter optimisation study of a simplified model.

4. Eliminating the damper unit and using dynamic absorbers has been shown theoretically to lead to significant improvements in the vertical transmission properties of the suspension, at the expense of greater complexity and some reduction of damping effectiveness.

5. Spring surges lead to high peaks of transmissibility, and also give rise to partial cancellation of vibration in the spring and damper unit combination. The spring surges can be readily damped by attachment of longitudinal damping strips on the coils.

6. Vertical transmission through the wish-bones is generally small, and depends primarily on the wishbone mass. Radially compliant end bushes can lead to high frequency

resonances. At high frequencies, wishbone resonances can increase transmission, and damping (such as with damping layers) is required.

7. Lateral and longitudinal transmission through the suspension is seen to depend primarily on the wishbone geometry and inboard bush stiffness. Effectiveness calculations show how a very stiff bush is of little benefit, and can act as a weak amplifier, whilst a more compliant bush is generally more effective but can give rise to large low-frequency amplifications.

8. The theoretical models have been verified by experiments on a small car suspension and the adequacy of the models demonstrated.

Further work on the suspension system can be envisaged when more data are available on tyre behaviour and the body mobility. In particular, work is desirable on mobility testing of vehicle bodies especially on the effect of widely spaced correlated excitation such as occurs in longitudinal vibration of the wishbones, and the coupling between different body coordinates.

REFERENCES

(Each section is in alphabatical order)

Vibration Isolation Section

1. Anon (1970); Development of Hydroelastic Suspension; Automobile Engr., 60(2), 65-5 (Feb).

2. Barson, C.W. et al (1964-5); Tyre and Vehicle Vibration; Proc. Auto. Div. Instn. Mech. Engrs., 179 (2A), No.7, 213-229.

3. Bender, E.K. (1968); Optimum Linear Preview Control with Application to Vehicle Suspension; J. Basic Engng, 90 (2), 213-21.

4. Efstathiades, G.J. et al (1967); Vibration Isolation using Non-Linear Springs; Int. J. Mech. Sci. 9 (1) 27-44.

5. Exner, M. (1952); Schalldämmung durch Gummi - und Stahlfedern; Acustica 2, 213-21.

6. Fiala, E. et al (1970); Zur Optimierung von Fahrzeug-federungen; Auto. -tech. Z., 72(1), 1-3.

7. Grootenhuis, P. et al (1965); Vibration of a Spring Supported Body; J. Mech. Engng. Sci. 7 (2), 185-92.

8. Gupta, K.M. (1967); Force Transmissibility provided by inclined Isolators...; J. Insts. Engrs. India 47 (11), 507-22.

9. Gurtin, M.E. (1961); On the Use of Clearance in Viscous Dampers to Limit High Frequency Force Transmsssion; J. Engng. Ind. 83, 50-2.

10. Haringx, J.A. (1949); On Highly Compressible Helical Springs . . . (IV) Philips Res. Repts. 4 261-290.

11. Harris, C.M. and Crede, C.E. (Eds.); Shock and Vibration Handbook, McGraw Hill, 1961.

12. Henry, R.F. et al (1959); Instability and Steady State Coupled Motions in Vibration Isolation Systems; J. Mech. Engng. Sci. 1 (1), 19-29.

13. Horovitz, M. (1957-8); Suspension of Internal Combustion Engines in Vehicles; Proc. Auto. Div. Instn. Mech. Engrs., No. 1, 17-35.

14. McDowell, E.L. (1953); A Mathematical Model of a Rubber Resilient Mounting; Proc. 1st. Midwest Conf. Solid Mech, 175-9.

15. McDuff, J.N. and Curreri, J.R; Vibration Control; McGraw Hill, 1958.

16. Moulton, A.E. and Turner, P.W. (1956-7); Rubber Springs for Vehicle Suspension; Proc. Auto. Div. Instn. Mach. Engrs, 17-26.

17. Porter, B (1967); Synthesis of Optimal Suspension Systems; Engineer 223, 619-22.

18. Rossini, L.R. (1969); Application of Statistical Criteria to the Investigation of Vertical Vibration of the Suspension System; ATA 22 (10), 513-521; MIRA Trans 7/70.

19. Ruzicka, J.E. et al (1958); Vibration Isolation; Mach. Des., Oct. 16, 114-121.

20. ———— (1961); Analysis and Design of Tangent Elasticity Vibration Isolators; J. Engng. Ind 83, 53-60.

21. ———— (1967); Resonance Characteristics of Uni-Directional Viscous and Coulomb Damped Vibration Isolation Systems; J. Engng. Ind 89 (4) 729-40.

22. Sekiguchi, H et al (1970); The Isolation of Random Vibration; Bull JSME 13 (56), 248-57.

23. Skudrzyk, E.J. (1959); Theory of Noise and Vibration Insulation of a System with Many Resonances; J. acoust. Soc. Am, 31 (1), 68-74.

24. Smollen, L.E. (1966); Generalised Matrix Methods for Design and Analysis of Vibration - Isolation Systems; J. Acoust. Soc Am, 40 (1), 195-204.

25. Snowdon, J.C. (1956); The Reduction of Structure Borne Noise; Acustica 6 118-125.

26. ———— (1958); The Choice of Resilient Materials for Anti-Vibration mountings; Br. J. appl. Phys. 9 (12), 461.

27. ———— (1960); Dynamic Mechanical Properties of Mechanical Vibration; Noise Control, 6 (2), 18.

28. ———— (1961); Reduction of the Response to Vibration of Structures possessing Finite Mechanical Impedance, J. acoust. Soc Am, 33, 1466.

29. ———— (1962); Isolation from Vibration with a Mounting Utilizing low - and high - Damping Rubber-like Materials; J. acoust. Soc. Am, 34, 54.

30. ——— (1965); Occurrence of Wave Effects in Rubber Antivibration Mountings; J. acoust. Soc Am, 37 (6), 1027-32.

31. ——— (1965); Rubberlike Materials, their Internal Damping and Role in Vibration Isolation; J. Sound Vib, 2 (2), 175-93.

32. —— et al (1959); Isolation from Mechanical Shock with one - and two - Stage Mounting Systems; J. acoust. Soc. Am, 31 (7), 967-76.

33. Soliman, J.I. et al (1968); Vibration Isolation between Non-rigid Machines and Non-rigid Foundations; J. Sound Vib., 8 (2), 329-51.

34. ——— et al (1966); Self-damped Pneumatic Isolator for Variable Frequency Excitation; J. mech. Engng. Sci., 8 (3), 284-293.

35. Sykes, A.O. (1960); A Study of Compression Noise Isolation Mounts Constructed from a Number of Rubber and Rubber like Materials; DTMB Rept. 845 (revised).

36. ——— (1960); Isolation of Vibration when Machine and Foundation are Resilient and when Wave Effects Occur in the Mount; Noise Control 6, 115-130.

37. Tajer-Ardabili, D. (1966); Servo-Controlled Isolation Systems; Ph.D. Thesis, Univ. of London.

38. Thompson, A.G. (1970); Optimum Damping in Randomly Excited Non-Linear Suspension; Instn. mech. Engrs, AD P8/70.

39. Timoshenko, S (1937); Vibration Problems in Engineering; Van Nostrand, 3rd ed.

40. Ungar, E.E. et al (1966); High-Frequency Vibration Isolation; J. Sound Vib., 4, 224-41.

Dynamic Absorbers and Variants

41. Anon (1971); A Vibration Damper for Ships; Chart. mech. Engr. 18 (6), Ad 428.

42. Abu-Akeel A.K. (1967); The Electro-dynamic Vibration Absorber as a Passive or Active Device; J. Engng Ind. 89 (4), 741-53.

43. Arnold, R.N. (1947 The Tuned and Damped Gyrostatic Vibration Absorber; Proc. Inst. mech. Engrs, 157, 1-19.

44. Bogy, D.B. (1963); An Evaluation of the Fixed Point Method of Vibration Analysis for a Particular System with Initial Damping; J. Engng Ind., 85 (3), 233-6.

45. Bosch, Ir J.J. (1966); On Roll Damping by Free Surface Tanks; Trans. R. Instn. nav. Archit, 108, 345-61.

46. Boyle, A. et al (1968); A Theoretical Investigation into the Characteristics of a Feedback Controlled Damping Unit; 9th Int. MTDR Conf. Sept. Preprint No. 50.

47. Brock, J.E. (1946); A Note on the Damped Vibration Absorber; Trans ASME, 68, A-284

48. Crede, C.E. (1947); Damping of Textile Mill Movement by the Frahm System; Trans. ASME, 69, 937.

49. Crossby, F.R.E. (1953); The Forced Oscillation of the Centrifugal Pendulum with Wide Angles; Trans. ASME, 75, 41-7.

50. Den Hartog, J.P. (1956); Mechanical Vibrations; McGraw Hill, 4th ed.

51. Egle, D.M. (1967); An Investigation of an Impact Vibration Absorber; J. Engng. Ind., 89, 653-61.

52. Falcon, K.C. et al (1967); Optimisation of Vibration Absorbers.... J. mech. Engng Sci., 9 (5), 374-81.

53. Flannelly, W.G. (1963); Gyroscopic Vibration Absorber Research Proposal; Kaman Aircraft Corp. Rept. R-499, 26 Mar.

54. ———— (1963); Gyroscopic Vibration Absorber Test Report; Kaman Aircraft Corp. Rept AIR 63-4, 30 Aug.

55. ———— (1965); Analytical Research on a Synchronous Vibration Absorber; NASA CR 338.

56. Frahm, H. (1911); Neuartige Schlingertanks zur Abdamfung von Schiffsrollsbewegungen und ihre infolgreiche Anwendung in der Praxis, Jarbuch der Schiffbanteschnischen Gesellschaft.

57. Grover, G.K. et al (1968), A Study of the Overhung Damped Dynamic Vibration Absorber with Tuning Optimisation, 9th Int. MTDR conf, Preprint 68.

58. Henderson, J.P. (1966); Energy Dissipation in Vibration Damper Utilising Viscoelastic Suspension; S and V Bull, 35 pt 7, 213-29.

59. Hooper, W.E. (1967); Self-Adaptive Vibration Balancing Device for Helicopters; S and V Bull, 36, 113-27.

60. Horn, F. (1911), Theorie des Frahmschen Schlingerdamfungstanks; Jarbruch der Schiffbantechnischen Gesellschaft, p 453.

61. Jones, D.I.G. (1967); Response and Damping of Simple Beam with Tuned Dampers; J. acoust. Soc. Am., 42 (1),50-3.

62. Jones, R (1967), The Gyroscopic Vibration Absorber; J. Engnd Ind; 89 (4), 706-12.

63. Knyazev, A.S et al (1966); Application of Electromechanical Feedback for the Damping of Plate Vibrations and Radiation; Soviet Physics - Acoustics, 12, 330.

64. Laufer, T (1960); A Vibration Absorber for Two-Bladed Helicopters; NASA TT F-43..

65. Lawther, J.M. et al (1965); Compensating Technique for Active Damping Improvement; J. acoust. Soc. Am., 38, 481-4 (L).

66. Lewis, F.M. (1955); The Extended Theory of the Viscous Vibration Damper; J. appl. Mech., 22, 377-82.

67. Lieber, P. et al (1945); An Acceleration Damper; Development, Design and Some Applications; Trans ASME, 67, 523-30.

68. Masri, S.F. (1967); Effectiveness of Two-Particle Impact Dampers; J. acoust. Soc Am., 41(6), 1553-4.

69. _____ et al (1966); On the Stability of the Impact Damper; J. Appl. Mech., 33, 576-92.

70. _____ (1967); Electric-Analog Studies of Impact Dampers; Exp. Mech., 7(2), 49-55.

71. _____ (1970); General Motion of Impact Dampers; J. acoust. Soc. Am., 47 (1 pt 2), 229-37.

72. Murotsu, Y. et al (1967); The Optimisation of Vibration Absorber; Bull. Univ. Osaka Pref. Series A., 16(2), 235-45.

73. Newland, D.E. (1964); Non-Linear Aspects of the Performance of Centrifugal Pendulum Vibration Absorbers; J. Engng Ind., 86, 257-63.

74. Ormondroyd, J. et al (1928); The Theory of the Dynamic Absorber; Trans ASME, APM-50-7.

75. Pipes, L.A. (1953); Analysis of Non-linear Dynamic Vibration Absorber; J. appl. Mech., 75, 515-8.

76. Pringle, O.A. (1953); Use of Centrifugal Governor Mechanism as a Torsional Vibration Absorber; Trans ASME, 75, 59.

77. Radziszewski, B et al (1966); On the Possibility of Improvement of the Characteristics of a Dynamic Vibration Absorber for the Centrifugal Force Excitation; Zagadnienia Drgan Nieliniowych, 6, 71-81.

78. Reed, F.E. (1949); The Use of the Centrifugal Pendulum Absorber for the Reduction of Linear Vibrations; J. appl. Mech., 16(2), 190-4.

79. Ro, M de (1968); The Magnetic Exciter as Applied to Active Damping of Machine Tools; 9th Int. MTDR conf., Preprint 69.

80. Robertson, R.E. (1952); Synthesis of Nonlinear Vibration Absorber; J. Franklin Inst., 254(3), 205-20.

81. Rockwell, T.H. et al (1964); Theoretical and Experimental Results on Active Vibration Dampers; J. acoust. Soc Am., 36(8), 1507.

82. ———— (1965); Investigation of Structure Borne Active Vibration Dampers; J. acoust. Soc. Am., 38(4), 623-8.

83. Sadek, M.M. (1965-6); Behaviour of Impact Damper; Proc. Instn. Mech. Engrs., 180(38), 895-906.

84. Sallet, D.W. (1967), A Vibration Absorber for the Determination of the Transient Vibration Process (in German); Ing-Arch, 35(5), 292-304.

85. Sauer, F.M. et al (1949); Performance of the Viscously Damped Vibration Absorber Applied to Systems having Frequency Squared Excitation; J. appl. Mech., 16(2), 109-17.

86. Sciarra, J.J. (1967); Application of Direct Stiffness and Mobility Method to Vibration Absorber Studies; ASME - Paper 66 Vibr 65 for meeting Mar. 29-31.

87. Snowdon, J.C. (1954); Transient Behaviour of the Dynamic Absorber; J. acoust Soc. Am, 31(12), 1668-75.

88. ———— (1959); Steady-State Behaviour of the Dynamic Absorber; J. acoust. Soc. Am., 31(8), 1096-1103.

89. ———— (1964); Steady-State Behaviour of the Dynamic Absorber - Addendum; J. acoust. Soc. Am., 36(6), 1121-23.

90. ———— (1965); Reduction of Response of Lumped and Distributed Parameter Systems by the Application of Dual Dynamic Absorbers (Abstract); J. acoust. Soc Am., 38(5), 924A.

91. ———— (1966); Vibration of Cantilever Beams to which Dynamic Absorbers are Attached; J. acoust. Soc. Am. 39(6), 78-86..

92. ———— (1968), Vibration and Shock in Damped Mechanical Systems; J. Wiley and Sons.

93. Warburton, G.B. (1957); On the Theory of the Acceleration Dampers: Discussion; J. appl. Mech., 24, 322-4.

94. Watts, P. (1883); On a Method of Reducing the Rolling of Ships at Sea; Trans, Instn. Nav. Archit., 24, 165-90.

95. Young, D. (1948); Vibration of the Beam with Concentrated Mass, Spring and Dashpot, Trans ASME, 70, 65.

Statistical Energy Methods

96. Anon (1964); Sound and Structural Vibration; Bolt, Beranck & Newman Inc, Rept. No. 1156.

97. Bogdanoff , J.L. (1965); Mean - Square Approximate Systems and their Applications in Estimating Response in Complex Disordered Linear Systems; J. acoust. Soc. Am., 38(2), 244-52.

98. Eichler, E. (1965); Thermal Circuit Approach to Vibration in Coupled Systems and the Noise Reduction of a Rectangular Box; J. acoust. Soc. Am. 37(6), 995-1007.

99. Fahy, F.J. (1969); Vibration of Containing Structures by Sound in the Contained Fluid; J. Engng Ind., 91(4), 939-50.

100. ———— (1970); Energy Flow between Oscillators: Special Case of Point Excitation (Letter); J. Sound Vib., 11(4), 481-3.

101. Gray, A.H. (1967); Some Energy Bounds for Randomly Excited Beams; J. acoust. Soc. Am., 41(3), 615-7.

102. Heckl, M. (1962); Measurement of Absorption Coefficients on Plates; J. acoust. Soc. Am., 34(6), 803-8.

103. Karnop, D.K. et al (1966); Plastic Deformation in Random Vibration; J. acoust. Soc Am., 39, 1154.

104. Lyon, R.H. et al (1962), Power Flow between Linearly Coupled Oscillators; J. acoust. Soc. Am., 34, 623-39.

105. ———— et al (1964); Random Vibration of Connected Structures; J. acoust. Soc. Am., 36(7), 1377-54.

106. ———— et al (1965); Vibrational - Energy Transmission in a Three-Element Structure; J. acoust. Soc Am., 38(2) 253-61.

107. ———— et al (1966); (Reply to ref 111); J. acoust. Soc. Am, 39(4), 755L.

108. ———— (1967); Spatial Response Concontrations in Extended Structures; J. Engng. Ind., 89(4), 754-8.

109. Maidanik, G. (1966); The Influence of Fluid Loading on the Radiation from Orthotropic Plates; J. Sound Vib., 3(3), 288-99.

110. Newland D.E. (1966); Calculation of Power Flow between Coupled Oscillators; J. Sound Vib. 3(3), 262-76.

111. ———— (1966); (Comment on ref. 106); J. acoust. Soc. Am., 39(4), 755L.

112. ———— (1966); Power Flow between a Class of Coupled Oscillators; Sub. to J. acoust. Soc. Am.

113. Ribner, J.S. (1966); Response of a Flexible Panel to Turbulent Flow - Running Wave versus Modal Density Analysis; J. acoust. Soc. Am., 40, 721.

114. Rosselli, A. (1965); The Transmission of Random Vibrations between Connected Plates; DIC Dissertation, London.

115. Scharton, TD. et al (1968); Power Flow and Energy Theory in Random Vibration; J. acoust. Soc. Am., 43(6), 133.

116. Steam, S.M. (1970); Spatial Variations of Stress, Strain and Acceleration in Structures Subject to Broad Frequency Band Excitation; J. Sound Vib., 12(1), 85-97.

117. Ungar, E.E. (1966); Fundamentals of Statistical Energy Analysis of Vibrating Systems; Bolt, Beranck and Newman Inc. Rept AFFDL-TR-66-52.

118. ———— (1967); Statistical Energy Analysis of Vibrating Systems; J. Engng. Ind. 89(4), 626-36.

General.

119. Anon (1965); Rilievi Vibrazionali su Vetture Falcon E Galaxie; Pirelli Rept No. 9.

120. Barone, G. (1967); Report on the Tests Carried Out on the Opel Rekord 1900 Car; SAGA Rept. No. 170.

121. Becher, G.W. et al (1958); Limits of Noise Reduction to be Achieved by Damping of Structure Borne Noise in Motor Vehicles; Acustica, 8(1), 11-18. MIRA Trans 47/65.

122. Biot, M.A. (1940); Coupled Oscillations of Aircraft Engine and Propeller Systems; J. aeronaut. Sci., 7, 376-82.

123. Bishop, R.E.D. (1956); The General Theory of 'Hysteretic Damping'; Aeronaut Q., 60-70. (Feb).

124. ———— et al (1960); The Mechanics of Vibration; C.U.P.

125. Blackman, P.F. (196); The Pole-Zero Approach to Systems Analysis; Control Monograph No. 2 (Rowse Muir Pub).

126. Bogdanoff, J.L. et al (1961); Dynamics of some Disorganised Linear Systems; Int. J. mech. Sci., 3 157-169.

127. Caughey, T.K. (1960); Classical Normal Modes in Damped Linear Dynamic Systems; J. appl. Mech., 27(2), 269-71.

128. Crandall, S.H. (Ed) (1964); Random Vibration, I; M.I.T. Press.

129. Davey, A.B. et al (1964); Rubber in Engineering Practice; Maclaren & Sons.

130. Dunn, J.W. (1967); An Analysis of the Dynamic Characteristics of a Saloon Car Structure Applied to the Generation of Low-Frequency Noise; MIRA Dept. No. 1967/8.

131. ———— et al (1970); A Study of the Vibration and Acoustic Characteristics of Saloon Car Bodies; MIRA Dept.

132. ———— et al (1971); An Instrumentation System for the Analysis of the Forced Vibration Characteristics of Stationary and Rolling Tyres; SEE Dynamic Testing Symp., London.

133. Ewins, D.J. (1971); Some Whys and Wherefores of Impedance Testing; SEE Dynamic Testing Symp, London.

134. Feinberg, M. (1965); New Methods Simplify Analysis of Vibration-Isolation Systems; Mach. Des. July 22, 138-44 & Aug 5, 142-9.

135. Foss, K.A. (1958); Coordinates which Uncouple the Equations of Motion of Damped Linear Systems; J. appl. Mech., 25(3), 361-4.

136. Frazer, R.A. et al (1938); Elementary Matrices; C.U.P.

137. Gaukroger, D.R. (1967); Resonance Tests on a Model Dam; RAE Tech, Rept. 67083.

138. Gehman, S.D. (1957); Dynamic Properties of Elastomers; Rubber Chem. Technlgy., 30, 1203.

139. Grassam, N.S. et al (Eds) (1964); Gas Lubricated Bearings; Butterworths.

140. Grootenhuis, P. (1967); Measurement of the Dynamic Properties of Damping Materials; Proc. Int. Symp on Damping, Belgium.

141. Harrison, M. et al (1951); Wave Effects in Isolation Mounts; D.T.M.B. Rept 776.

142. ———— et al (1952); Wave Effects in Isolation Mounts; J. acoust. Soc. Am., 24(1), 62-71.

143. Hawkins, F.J. (1965); GRAMPA - An Automatic Technique for Exciting the Principal Modes of Vibration of Complex Structures; RAE Tech, Rept. No. 65142.

144. Heckl, M.A. (1961); Compendium of Impedance Formulae; Bolt; Beranck and Newman, Inc. Rept. No. 774.

145. Kainradl (1958); Messung der Dynamischen Eigenschaften von Vulkanisaten; Kautschuk & Gummi 11, 193.

146. Karnopp, D. et al (1968); Analysis and Simulation of Multiport Systems; MIT Press.

147. Kerlin, R.L. et al (1970); Driving-point Impedance of Centilever Beams - Comparison of Measurement and Theory; J. acoust. Soc. Am., 47 (1 pt 2), 220-8.

148. Konno, M et al (1965); Equivalent Electrical Network for the Transversely Vibrating Uniform Bar; J. acoust. Soc. Am., 38(4), 614-22

149. Kononenko, V.O. (1969); Vibrating Systems with a Limited Power Supply; Iliffe, London.

150. Lindley, P.B. (1964); Engineering Design with Natural Rubber; NRPRA Tech. Bull. No. 8.

151. MacFarlane, A.G.L. (1963); Notes on the Use of Matrix Theory in the Analysis of Linear Feedback Circuits; Proc. Inst. elect. Engrs., 110(1), 139-48.

152. Mason, J.M. et al (1970); Efficiency of Various "Free-Free" Support Systems for a Flexing Beam; Acustica 23(6), 348-50.

153. Meirovitch, L. (1967); Analytical Methods in Vibrations; MacMillan, N.Y.

154. Mitton, C.A. (1965); Application of a Hydrostatic Air Bearing to a Vibration Generator; Proc. Instn. mech. Engrs. 180(3A) 13-17.

155. Morris, R.E. et al (1956), A New Method for Determining the Dynamic Mechanical Properties of Rubber; Rubb. Age, 78(5) 725-31

156. Neubert, V.H. (1965); Series Solution for Structural Mobility; J. acoust. Soc. Am., 38, 867-76.

157. Newland, D.E. (1971); Methods of Dynamically Testing Rubber Building Materials under High Static Pressure; SEE Dynamic Testing Symp., London.

158. Nolle, A.W. (1948); Methods for Measuring Dynamic Mechanical Properties of Rubber-Like Materials; J. app. Phys., 19, 753-74.

159. O'Hara, G.H. (1967); Mechanical Impedance and Mobility Concepts; J. acoust. Soc. Am., 41(5), 1180-4.

160. Overton, J.A. et al. (1969 - 70); The Vertical Response Characteristics of the Non-Rolling Tyre; Proc. Auto. Div. Instn. Mech. Engrs., 184 (2). 25-40.

161. Payne, A.R. et al. (1960); Engineering Design with Rubber; MacLaren and Sons.

162. Pestel, E.C. et al. (1963); Matrix Methods in Elasto-mechanics; McGraw Hill

163. Pipes, L.A. (1963); Applied Mathematics for Engineers and Physicists; Prentice Hall.

164. Powell, M.J.D. (1964); An Efficient Method for Finding the Minimum of a Function of Several Variables Without Calculating Derivatives; Comput. J. 7, 303.

165. Praefcke, R. (1964); Determination of the Dynamic Properties of Rubber-like Materials; D.I.C. Thesis, London.

166. Rayleigh, Lord (1945 ed); Theory of Sound; Dover, N.Y.

167. Rodger, M. (1970); The Experimental Investigation of Body Structural Vibration; Joint Symp. on Body Engng., Cranfield.

168. Rubin, S. (1964); Transmission Matrices for Vibration and their Relationship to Admittance and Impedance; J. Engng. Ind., 86 (1), 9 - 21.

169. _____ (1967); Mechanical Immittance - and Transmission - Matrix Concepts; J. Acoust. Soc. Am., 41 (5), 1171-9.

170. Saunders, D.J. (1970 , May); Human Reaction to Noise and Vibration in Motor Cars; Environ. Engng. No. 44, 12-16.

171. Schloss, F. (1963); Recent Advances in Measurement of Structural Impedances; DTMB Dept. 1584.

172. _____ (1965); Recent Advances in Mechanical Impedance Instrumentation and Applications; DTMB Dept. 1960.

173. Skudrzyk, E. (1968); Simple and Complex Vibratory Systems; Pennsylvania State U.P.

174. Smith, J.E. (1970); Measurement of the Total Structural Mobility Matrix; S and V Bull No. 40, pt. 7, 51 -84.

175. Sykes, A.O. (1963); Passive Vibration-cancelling Isolation Mounts; J. Acoust. Soc. Am., 35 (5), 797A.

176. Taylor, G.A. et al. (1969); MAMA - a Semi-Automatic Technique for Exciting the Principal Modes of Vibration of Complex Structures; Min. Tech. ARCR and M No. 3590.

177. Thompson, A.G. (1965); Synthesis of Active and Passive Automobile Suspension Systems by Pole-Zero Methods; Ph.D. Thesis, Univ. of Adelaide.

178. Tiekling, J.T. (1965); Plane Vibration Characteristics of a Pneumatic Tyre Model; S.A.E. No. 650492.

179. Uhrig, R. (1966); The Transfer Matrix Method Seen as One Method of Structural Analysis among Others; J. Sound Vib., 4 (2), 136 - 48.

180. _____ (1966); Reduction in the Number of Unknowns in the Displacement Method Applied to Kinetic Problems; J. Sound Vib., 4 (2), 149-55.

181. Ungar, E.E. (1963); Wave Effects in Viscoelastic Leaf and Compression Spring Mounts; J. Engng. Ind., 85 (3), 243-6.

182. Vatz, I.P. (1968); Determination of Modal Mass from Test Data; S and V Bull, No. 38, pt. 2, 271-98.

183. Whitehead, D.S. (1969); A Symmetry Property of Transfer Matrices; Aeronaut. J., 73 (704), 686 - 8.

184. Wilkinson, J.H. (1965); The Algebraic Eigenvalue Problem; Clarendon Press, Oxford.

185. Refers to Reports Nos. 1 - 4 by the Author to MIRA on the progress of the work described herein.

APPENDIX I

DYNAMIC ABSORBERS

There are two distinct ideas behind the term 'dynamic absorber'. The function of the device depends on the type of system excitation. Thus we have:

1. For broad band excitation the models discussed by Den Hartog and Haringx for example, more precisely termed 'auxiliary mass dampers' or 'damped absorbers'

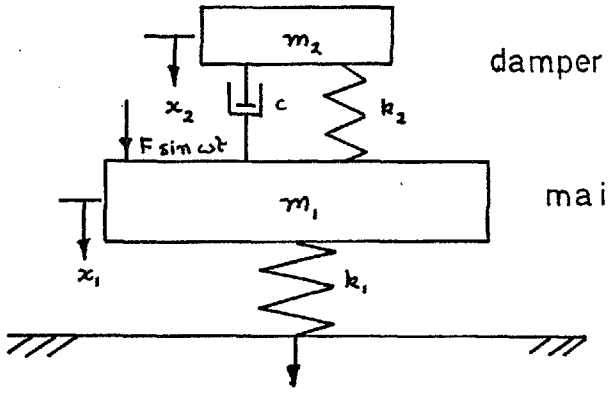
and

2. For narrow band excitation the models discussed, for example, by Robertson, more precisely termed 'auxiliary mass neutralizers' or the 'undamped dynamic absorber'.

In the first case, broad band excitation can also be taken to mean harmonic or narrow band excitation that can vary over a wide frequency range with time. The function of the absorber is to introduce damping into the system. In vibration isolation work it enables rigid body modes of the source and receiver to be damped enabling undamped (and thus more effective) massless compliant paths to be used, as was shown to be desirable in Chapter 2. When compliant paths are used with appreciable distributed mass, damping in the path is required in general to suppress resonant peaks.

Thus, in the classical case, we have a mass on a spring system - the spring being undamped for good transmissibility performance at high frequencies. As excitation occurs,

or can occur, at all frequencies, the resonant peak must be suppressed by introducing damping.



$\omega_1 = \sqrt{k_1/m_1}$

$\omega_2 = \alpha\,\omega_1 = \sqrt{k_2/m_2}$

$m_2/m_1 = \rho$

$\mu = 1/(1+\rho)$

$\Omega = \omega/\omega_1$

Using the auxiliary mass damper, two resonant peaks are formed, with the optimum response dependent on the type of excitation. Examples are sketched in Figure A.1.1.

Optimisation makes use of fixed 'cross-over' frequencies and bilinear equations. For case (A) the procedure is to find the frequency ratio 'a' to provide the cross-over frequencies at the same height on the receptance axis, and then select 'c' so that the slope of the receptance curve is approximately zero at the cross-over frequencies. The heights of the resonant peaks are then (approximately) equal with their minimum values. For a given amount of auxiliary mass, this is more effective than the Lanchester damper (that is, $k_2 = 0$). The performance near optimum is shown sketched in Figure A.1.2 with shaded regions showing where the response must lie for values of damping between zero and infinity, for the auxiliary mass damper (a.m.d.) and the Lanchester damper (L.d.).

For case 'a', the optimum values for a given mass ratio μ are:

$$\frac{k_2}{k_1} = \mu(1-\mu) \quad \text{and} \quad \frac{c}{\sqrt{m_1 k_1}} \approx (1-\mu)\sqrt{1.5(1-\mu)}$$

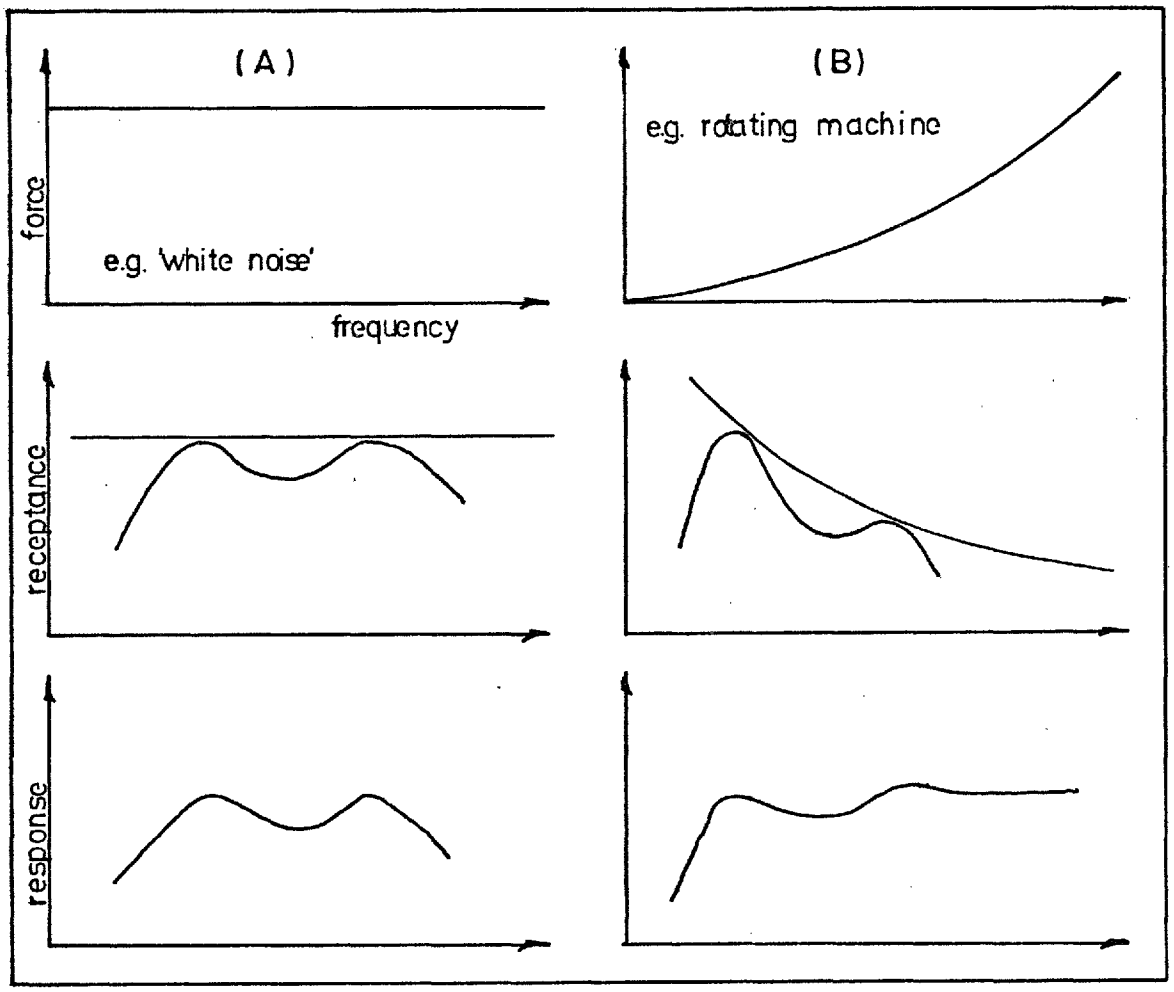


Figure A.1.1

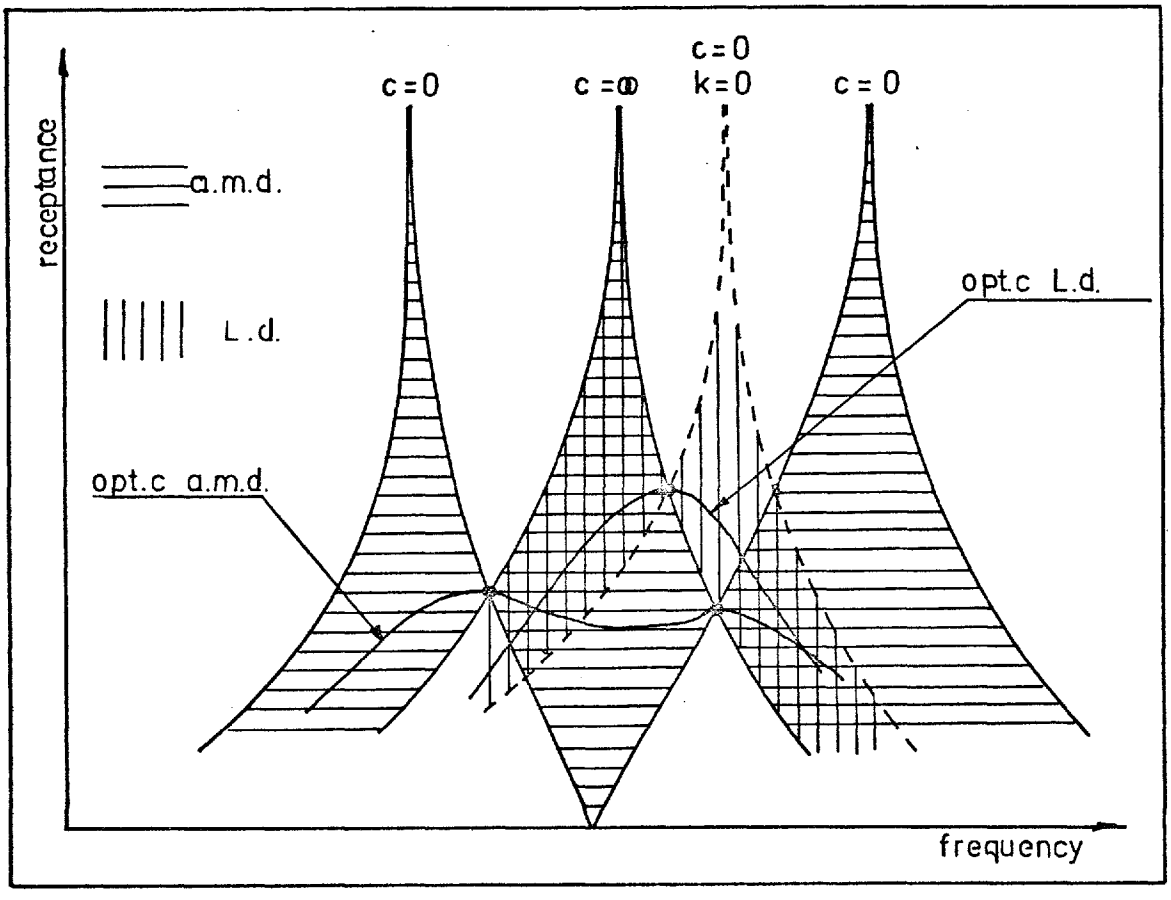


Figure A.1.2

For case 'B', the optimum will, of course, depend on the form of excitation. Also, other criteria such as velocity rather than displacement may be used, and different forms of damping.

In the second type of absorber, where narrow band excitation is predominant, the requirement is to react the vibratory forces as completely as possible, and the height of the resonant peaks is of little concern, as shown in Figure A.1.3.

The concept of suppression bands is used, denoted by $S(1,\Omega^2)$ which is the set of Ω^2 for which $|A_1| \leq 1$, where A_1 is the non-dimensionalamptitude of the main mass. For the system shown, without damping,

$$A_1 = \frac{k_1 x_1}{F} = \frac{a^2 - \Omega^2}{\Omega^4 - (1 + a^2 + a^2\rho)\Omega^2 + a^2}$$

and the bounds for this region can be found for the plane (a^2, Ω^2) from

$$A_1 = \begin{cases} 0 \\ +1 \\ -1 \\ \infty \end{cases}$$

obtaining respectively:

$$a_0^2 = \Omega^2$$

$$a_{+1}^2 = \Omega^2/(1+\rho)$$

$$a_{-1}^2 = \Omega^2(\Omega^2-2) / (\Omega^2 + \rho\Omega^2 - 2)$$

$$a_{\infty}^2 = \Omega^2(\Omega^2-1) / (\Omega^2 + \rho\Omega^2 - 1)$$

Sample curves for the above functions are plotted in Figure A.1.4 on the (a^2, Ω^2) plane for $\rho = 0.1$ and $\rho = 1.0$.

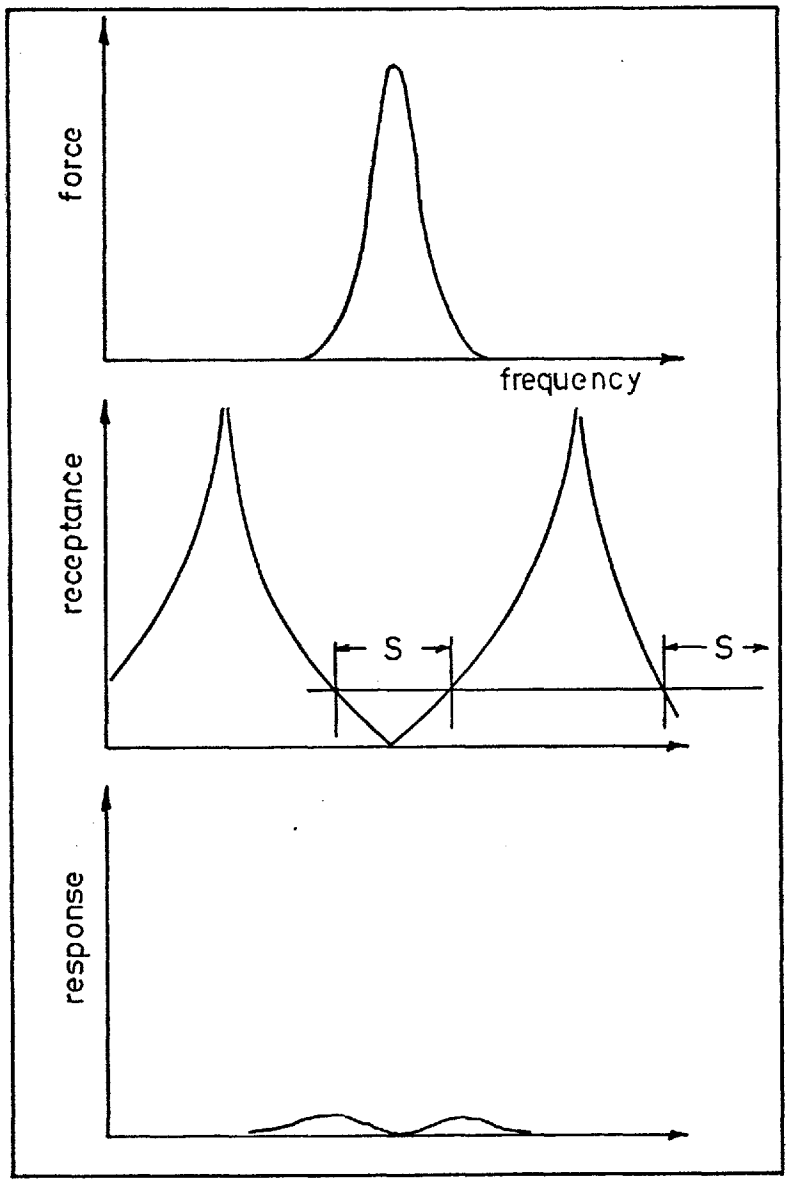


Figure A.1.3

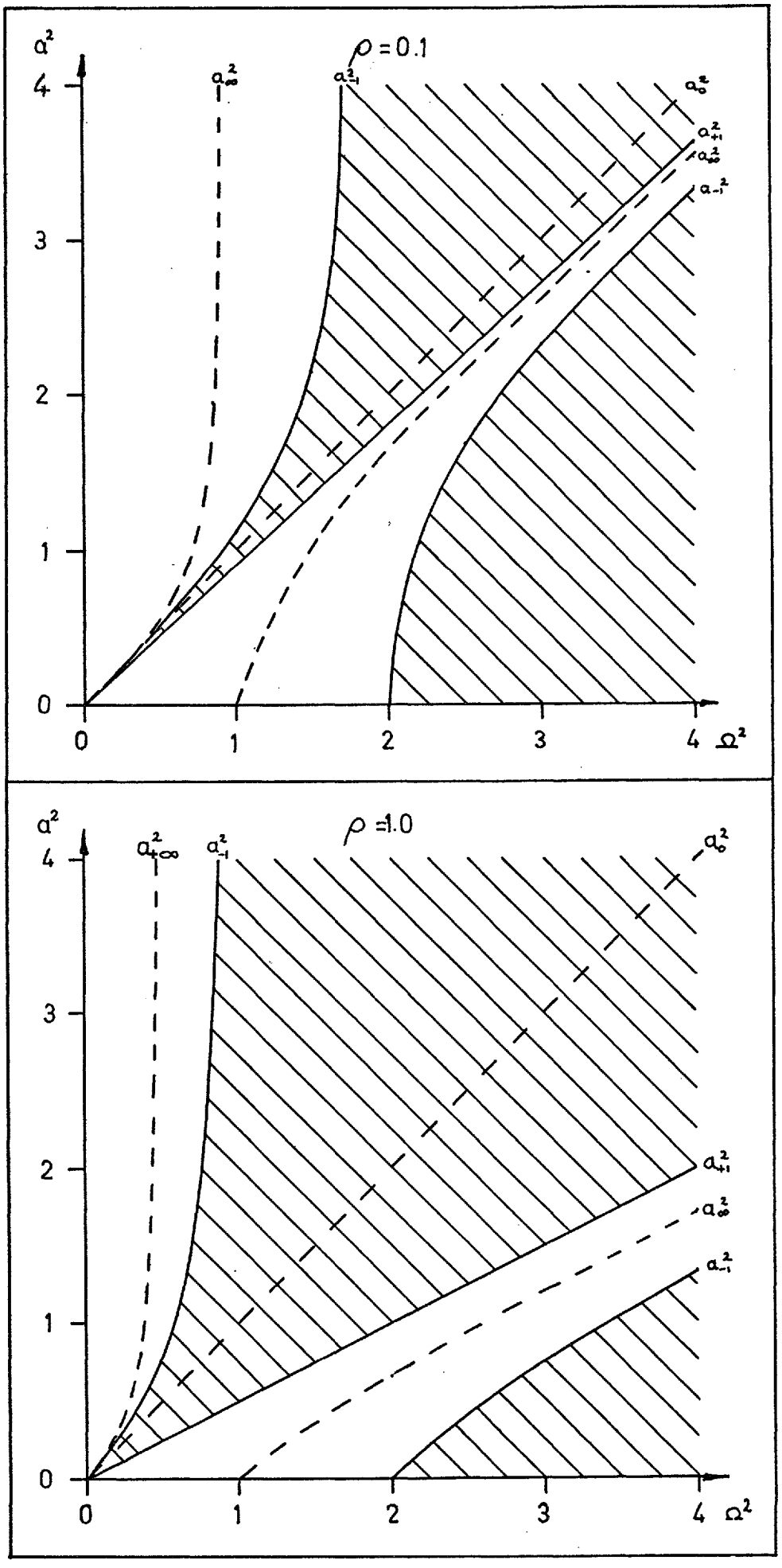
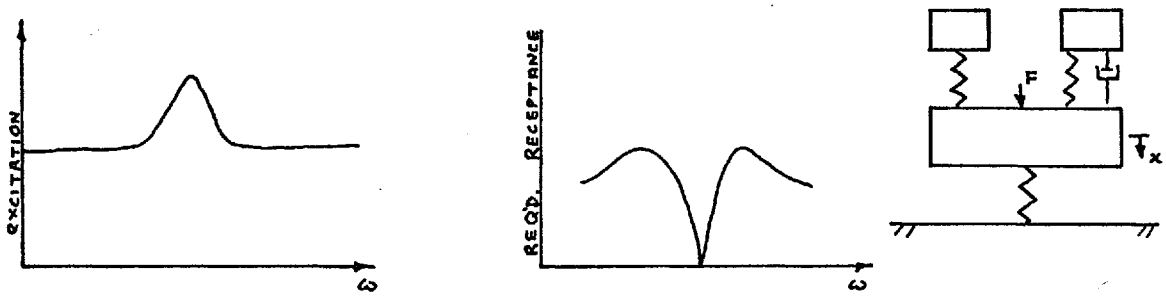

a^2
$\rho = 0.1$
$a^2_{+\infty}$
a^2_{-1}
a^2_0
a^2_{+1}
a^2_∞
a^2_{-1}
0
1
2
3
4
Ω^2
a^2
$\rho = 1.0$
$a^2_{+\infty}$
a^2_{-1}
a^2_0
a^2_{+1}
a^2_∞
a^2_{-1}
0
1
2
3
4
Ω^2

Figure A.1.4

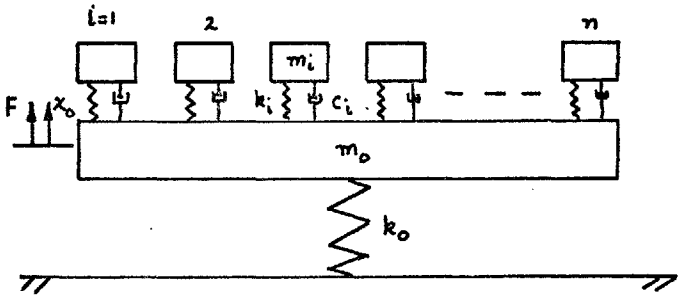
The amplitude-frequency plots can be readily visualised from the set of (a^2, Ω^2) curves. The conclusion readily drawn from the above plots is that both a^2 and ρ should be made as large as possible to give the largest suppression band. However, the suppression point i.e. $A_1 = 0$ is determined solely by a^2 and will be decided by the centre frequency of the excitation.

Light damping might be employed to cope with any weak broad-band excitation present, but will tend to reduce the suppression band. Non-linear springs can serve to improve the suppression bandwidth.

A mixed type of absorber, combining the features of both absorbers can be useful (in theory at least) when substantial broad band excitation coexists with narrow band peaks. The damped and undamped absorber thus give an overall damped response, with the narrow band excitation suppressed by the undamped absorber. This is sketched below.



A logical extension to the simple model is the case where n absorbers are attached.



$$\rho_i = m_i / m_o$$
$$\omega_i = a_i \omega_o$$
$$\omega_o = \sqrt{k_o / m_o}$$
$$\Omega = \omega / \omega_o$$

The non-dimensional amplitude of the response, A_o, is then given by

$$A_o \left(= \frac{k_o x_o}{F} \right) = \left\{ (1-\Omega^2) - \sum_{i=1}^{n} \frac{\rho_i a_i \Omega^2}{\rho_i (a_i^2 - \Omega^2) + i 2 c_i \Omega} - i \sum_{i=1}^{n} \frac{2 c_i \rho_i \Omega^3}{\rho_i (a_i^2 - \Omega^2) + i 2 c_i \Omega} \right\}^{-1}$$

where the undamped absorbers are obtained by putting $c_i = 0$. The effect of many dampers on the system is thus similar to attaching a flexible structure with many resonances. If damping is ignored, then:

$$A_o = \frac{\prod_{i=1}^{n} (a_i^2 - \Omega^2)}{(1-\Omega^2) \prod_{i=1}^{n} (a_i^2 - \Omega^2) + \sum_{i=1}^{n} \left(-\rho_i a_i^2 \Omega^2 \prod_{\substack{j=1 \\ j \neq i}}^{n} (a_j^2 - \Omega^2) \right)}$$

which forms a model for general multimodal structure, principally specified by the anti-resonances ($a_i^2 = \Omega^2$) but otherwise leading to similar results to the model used in Chapter 3. The application of more than a very few absorbers is likely to be limited.

The application of the damped dynamic absorbers to a vehicle suspension is attractive in theory as considerable gains in low-frequency isolation can be achieved. It has not, however, been popular in practice. An example of the application of absorbers to a highly simplified suspension system is shown below and the results compared with an

optimised conventional system.

The vehicle is represented by a rigid mass, with a massless main spring and tyre, and rigid wheel, as shown in Figure A.1.5. Tyre damping is neglected. The model is essentially a representation of low frequency behaviour only.

An approximate optimum for uniform broad-band excitation can be derived very simply by using approximate single-degree-of-freedom systems for the body-bounce and wheel-hop modes. Absorber weights of 100 lb. for the body-bounce mode and 15 lb. for the wheel-hop mode are used. Using the optimum parameters as described earlier, we have:

a) for the body-bounce mode

μ = 0.8

absorber k = 20.5 lbf/in

absorber c = 1.37 lbf/in/s

b) for the wheel-hop mode

μ = 0.727

absorber k = 188.2 lbf/in

absorber c = 1.732 lbf/in/s.

For comparison purposes, an optimised version of a conventional suspension system is shown, subject to similar simplifications also in Figure A.1.5. The damping used is of the relaxation type, and again tyre damping is ignored. The parameters shown are obtained by minimizing the error

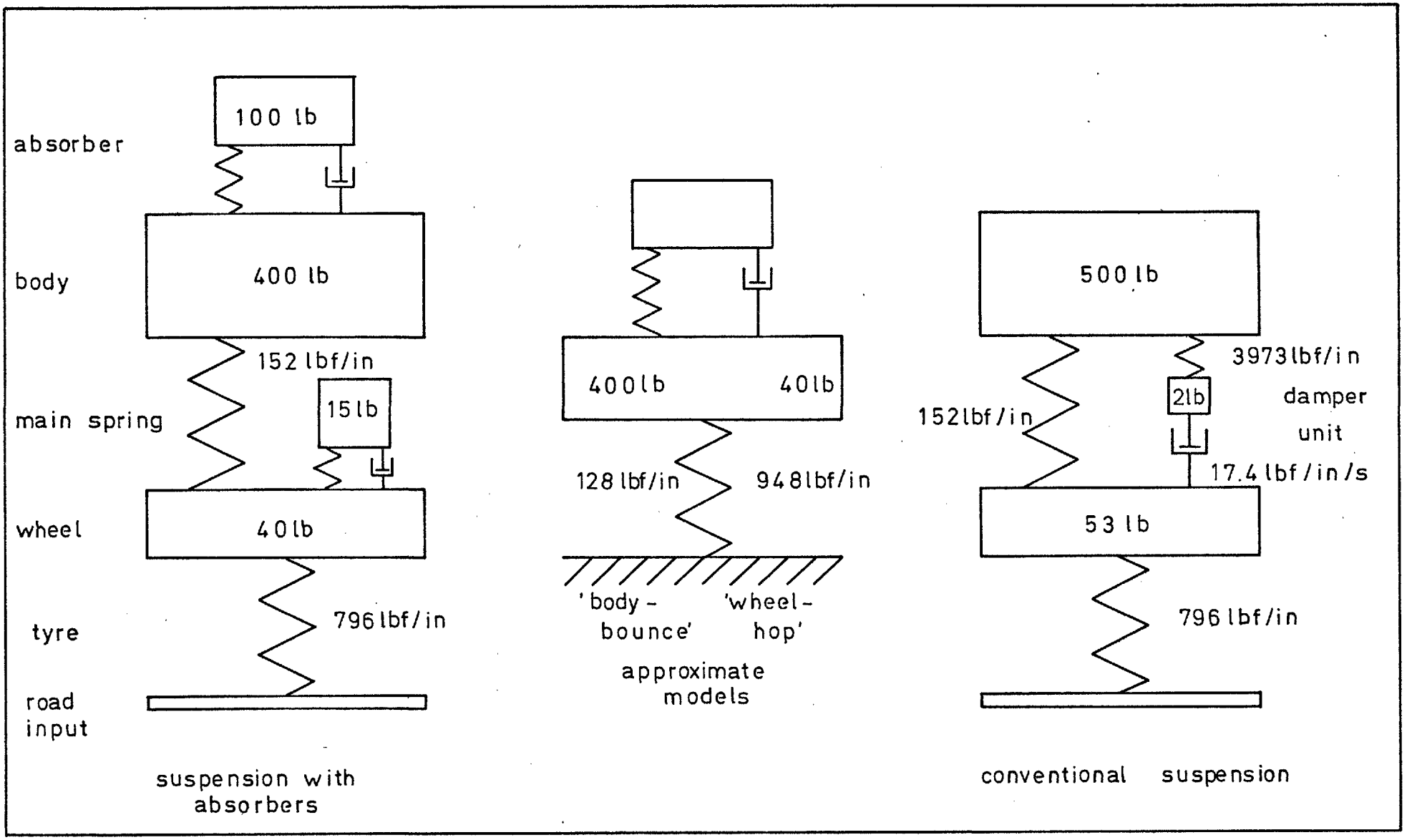

absorber
100 lb
body
400 lb
152 lbf/in
main spring
15 lb
wheel
40 lb
tyre
796 lbf/in
road input
suspension with absorbers
400 lb
40 lb
128 lbf/in
948 lbf/in
'body - bounce'
'wheel - hop'
approximate models
500 lb
3973 lbf/in
2 lb
damper unit
152 lbf/in
17.4 lbf/in/s
53 lb
796 lbf/in
conventional suspension

Figure A.1.5

between the model's performance and the target performance. The target performance is that both the wheel-hop and body-bounce modes have the same damping ratio of 0.585 such that the model returns to equilibrium very rapidly after an input disturbance. Also, the body-bounce frequency is to be 10 rad/s (1.59 Hz) and other modes are to be over-damped and thus non-oscillatory. The one damper unit is then required to perform equally efficiently for both modes of vibration.

The target lines for the model on the complex plane (α, ω) for the complex frequencies ($\varphi = \alpha \pm j\omega$) of the model are shown in Figure A.1.6, together with the complex frequencies for the initial parameters. The parameters available for change (but subject to constraints) are the tyre, main spring, and damper bush stiffnesses, the wheel mass and the damper viscous damping coefficient. The target is reached exactly with such a free-range, though with fewer parameters only a minimum would be found. Figure A.1.7 gives an interpretation of the response of modes characterised by points on the complex plane.

In Figure A.1.8 the response of the body and wheel to the suspension with absorbers is shown to a road input. The heights of the peaks indicate that the approximate approach was quite adequate and reasonable damping was achieved on the modes of vibration - the wheel being better controlled due to a more favourable mass ratio. Figure A.1.9 shows the response of the optimal conventional system, showing

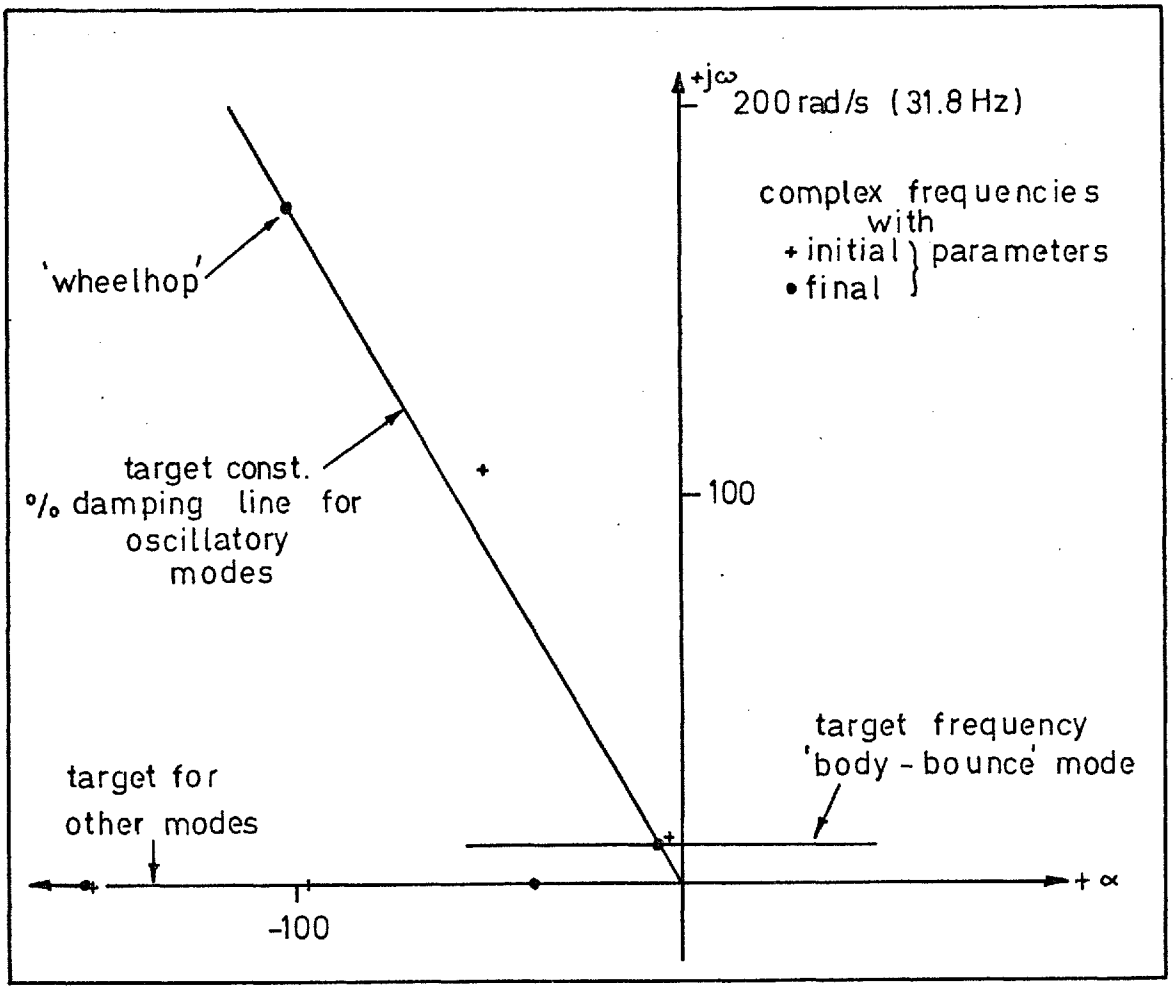


Figure A.1.6

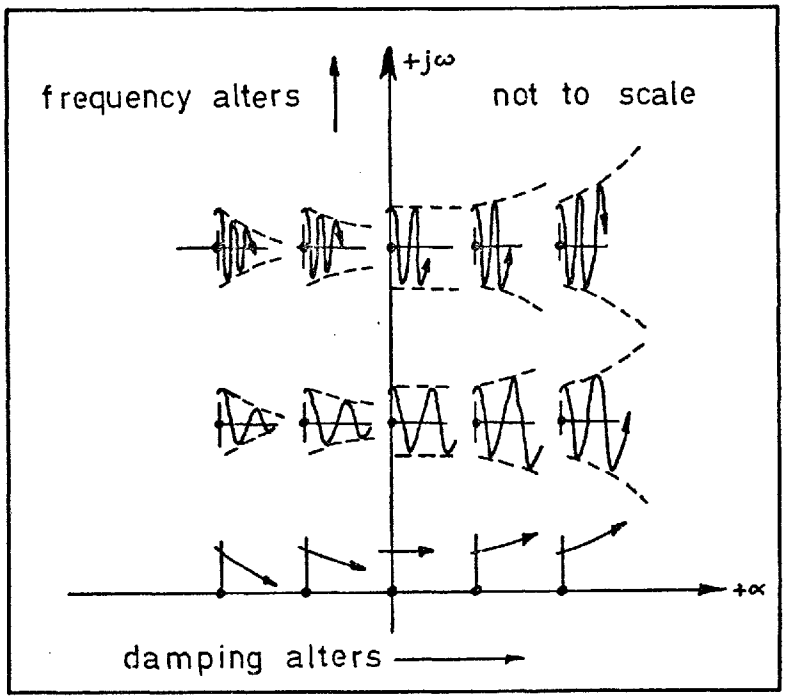


Figure A.1.7

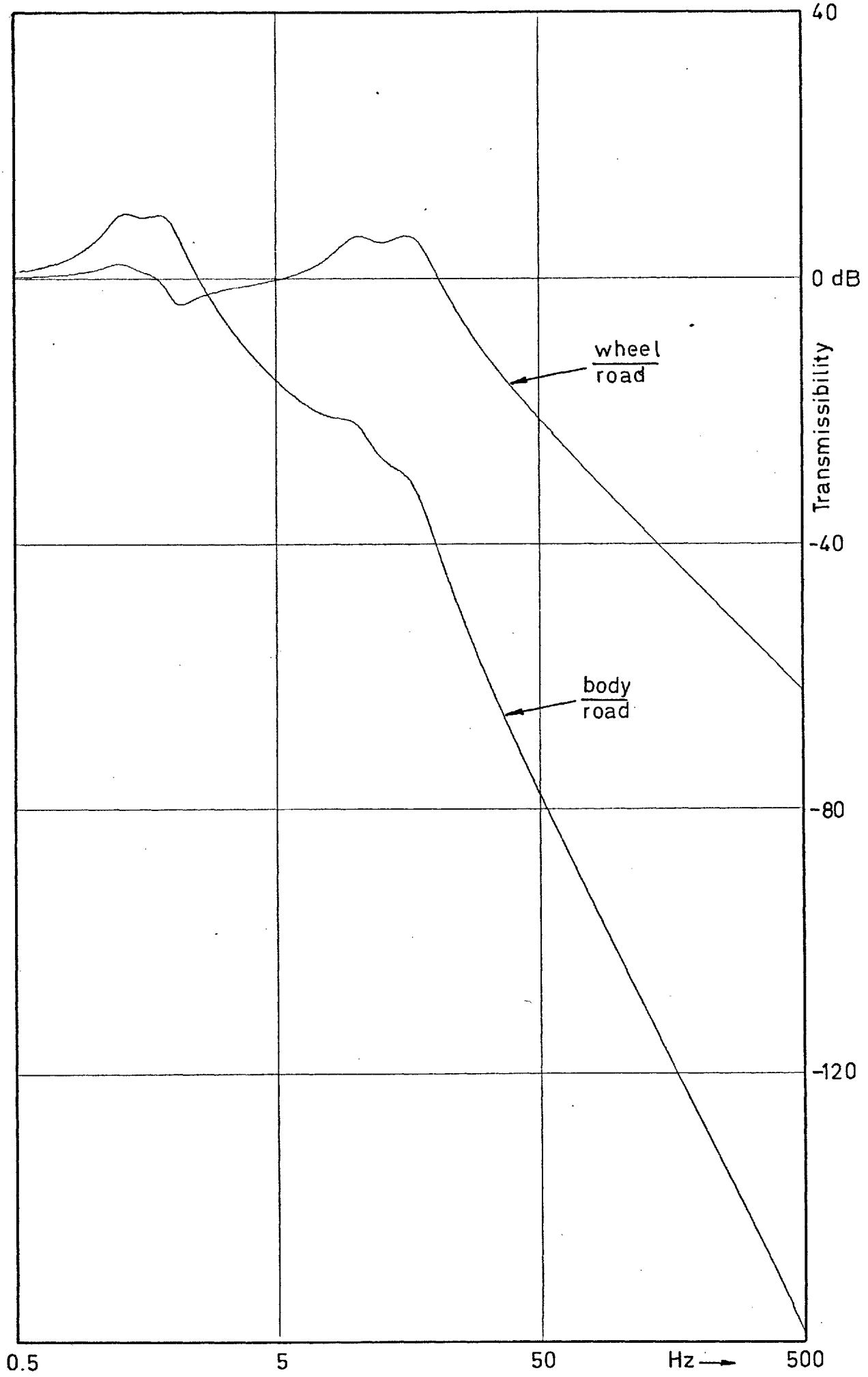


Figure A.1.8

CSWA04 4-1,2-1

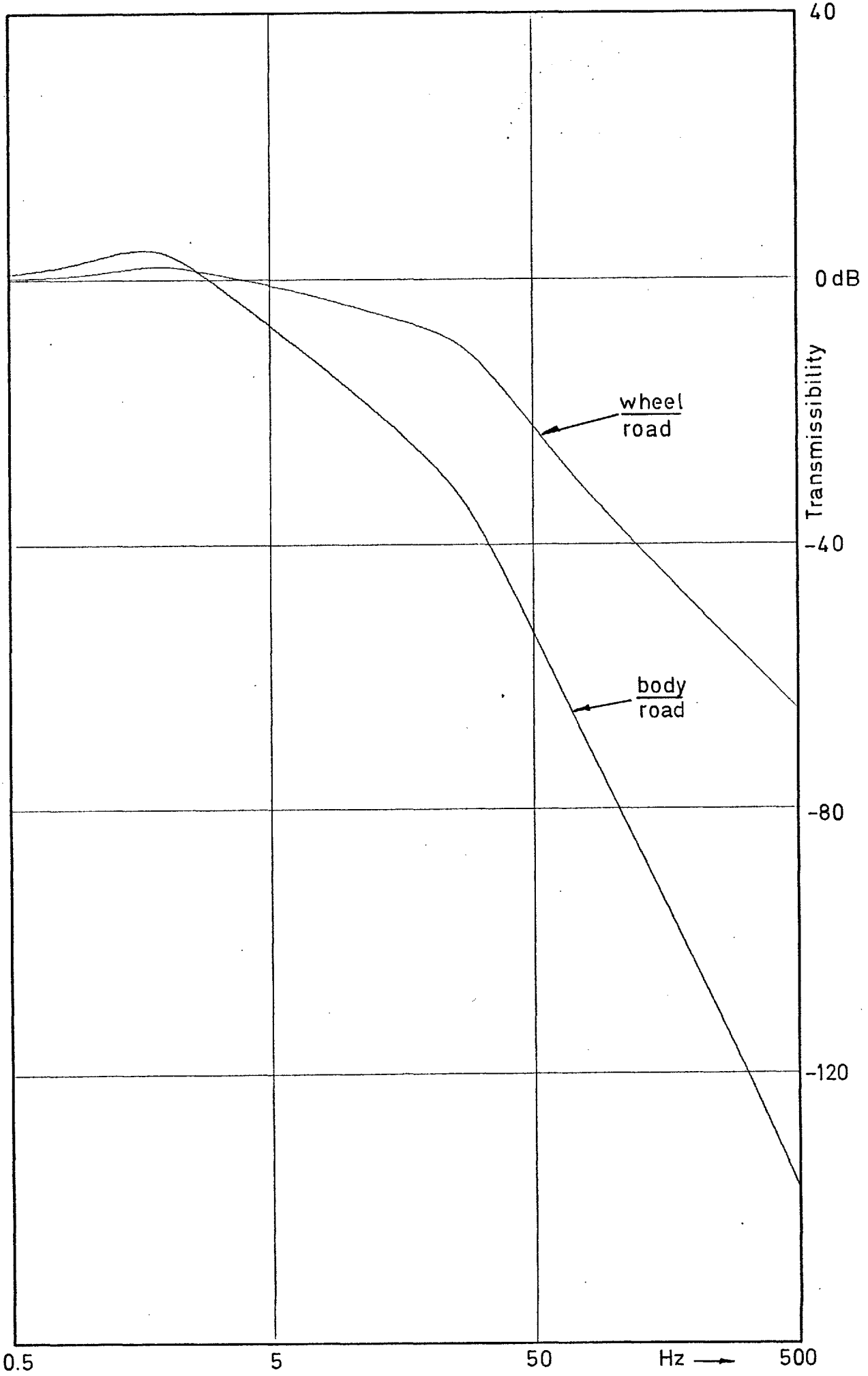


Figure A.1.9

LFSMD02 4-1,2-1

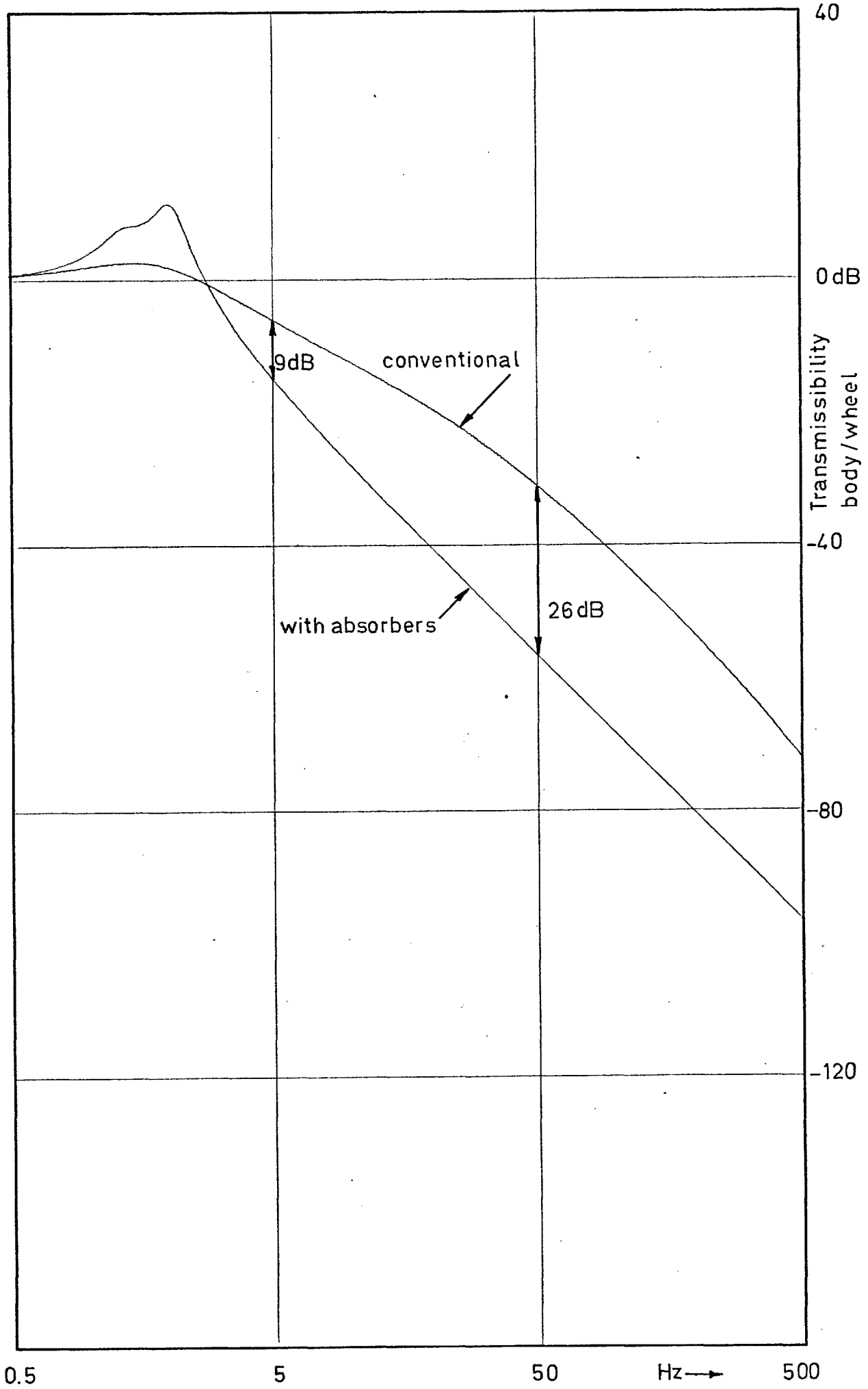


Figure A.1.10

CSWA04,LFSMD01 4-2

the extremely heavy damping available giving excellent control of the body and wheel.

Figure A.1.10 shows the transmissibility from the wheel to the body for both models, as an indication of suspension effectiveness. The system with absorbers shows an appreciable gain in effectiveness over the conventional system due to the more mobile path, even at low frequencies, at the expense of slightly less efficient damping. The gain, of course, extends to higher frequencies.

The conventional model might have as an alternative target the softest possible damper bush to improve the transmissibility characteristics, but a reduction in available damping must be considered. For reasonable damping, the top bush cannot be made sufficiently soft for the suspension to compete with the absorber system in effectiveness.

Optimum damping, in practice, is usually obtained by changing the damper setting only, and due to the non-linear characteristics will vary according to the excitation. However, it is clear from the above model, that several different parameters need to be changed to lead to a true optimum and a long iterative procedure is necessary to achieve this.

The use of dynamic absorbers is unlikely to be widespread in practice despite their theoretical advantages, but it should be noted that the same absorber mass can be used in different directions to increase the efficiency for a given overall weight.

Brief Review of Literature

For the purpose of this brief review, the term 'dynamic absorber' will be applied in a wide sense to include most devices which can be attached to a system or structure to limit its vibration, either conservatively or non-conservatively. 'Built in' methods, such as damping introduced by sandwich construction with viscoelastic materials are not considered.

The origin of the dynamic absorber is usually attributed to Frahm, though Watts (84) in 1883 fitted anti-roll tanks to a Frigate and thereby reduced its rolling by 20 - 30%, and the method used approximated to that of the dynamic absorber. It is of interest to note that whilst such tanks are now obsolete (they were used on the German luxury ships Bremen and Europa (11)), modern references appear on the use of water as a means of effecting roll damping - for instance Bosch (45, 1966) and more recently in ref. 41, 1971. Early theory and practice of anti-roll tanks were given by Frahm (56, 1911) and Horn (50, 1911). Frahm in 1911 took out U.S. Patent Number 989,958 entitled "device for damping vibrations of bodies" and thus became the usually acknowledged inventer of the dynamic absorber.

In 1928 a very complete describtion of the dynamic absorber was given by Ormondroyd and Den Hartog (74), covering the cases of 'absolute' and 'relative' viscous damping, the use of dual absorbers to relieve stresses and for two working frequencies, torsional applications and the equations

for solid (i.e. hysteretic) damping. Den Hartog later consolidated the optimisation procedure (50, 1st ed. 1934), and Brock (47, 1946) supplemented the formulae for optimum tuning, and included the Lanchester damper. A practical application of the 'Frahm absorber' was given the following year by Crede (48). Later work on the absorber includes analyses with hysteretic damping by Snowdon (88, 1959; 92, 1968).

Robertson (80, 1952) pointed out that numerous patents to increase the usefullness of the 'Frahm absorber' by means of non-linear elements had been taken out since 1914 but had not been properly exploited, and showed that the non-linear absorber is less sensitive to frequency drift and tuning than the linear case. Using the concept of suppression bands as a criterion for synthesis he established the advantages of non-linearities. Pipes (75, 1953) extended the analysis to another form of non-linearity, but by a 'significantly different procedure'.

Centrifugal force excitation, requiring modified performance criteria, has been considered by Sauer (85, 1949) and Radziszewski (77, 1966). Other optimisation procedures have been given, of which two of the more recent are Murotsu (72, 1967) and Falcon (52, 1967). The transient response of the absorber has been considered by Snowdon (87, 1959).

Cases where the absorber has been attached to a beam (thus representing a fairly complex structure) have been given by Young (95, 1948), Snowdon (91, 1966), and Jones (61, 1967). The case of dual or multiple absorbers has been considered by Snowdon (89, 90; 1964-5) and Grover (57, 1968).

The acceleration or impact damper was first invented in 1944 by Lieber (67, 1945). It presents interesting analytical problems which have been extensively discussed, for instance by Warburton (93, 1957), Sadek (83, 1965-6), Masri (68 - 71; 1966-70), and Egle (51, 1967).

The application of servo-controlled or active dampers is a logical step from the use of passive devices. Rockwell and Lawther (65, 81, 82; 1964-5), Knyazev (63, 1966), Abu-Akeel (42, 1967), Ro (79, 1968), and Boyle (46, 1968) each deal with aspects of active damping. Earlier results (82) showed extensive operational bandwidth, and the introduction of damping equivalent to a loss factor of 0.2 was achieved. Whilst attractive in theory, one may wonder at the philosophy of providing power and fairly elaborate equipment to counteract the vibration in a system unless exceptional results can be obtained.

The use of rotary devices greatly enlarges the scope of absorbers. The simplest of these are the rotary forms of the Frahm or Lanchester dampers. A slight modification for torsional oscillations is the pendulum absorber, discussed by Crossley (49, 1953) and Newland (73, 1964) allowing for large angles of swing. Other torsional vibration absorbers include the gyrostatic (Arnold (43, 1947)) and the governor type (Pringle (76, 1953)). There is also a self-adaptive balancing device for shafts (Hooper (59, 1967)).

Pendulum type absorbers on rotating shafts may also be employed to deal with axial vibrations, as shown by Reed (78, 1949) and Laufer (64, 1960).

Gyroscopic absorbers may be employed to deal with linear vibrations and may be synchronised to the main excitation frequency as their anti-resonant frequency is a function of the rotor speed. Flannelly (53 - 55; 1963 - 65) and Jones (62, 1967) have analysed these.

APPENDIX 2

VIBRATION ISOLATION BIBLIOGRAPHY

Papers referring specifically to vibration isolation are given in the first section of the list of references (1 - 40). General background may be found in Macduff and Curreri (15), Timoshenko (39) and Ruzicka (19). The 'classical' models in differing forms are shown by Gurtin (9), McDowell (14), Ruzicka (20, 21), Sekiguchi (22), and with wave effects Snowdon (30). The performance of practical forms of isolators is given by Exner (5) and Haringx (10) considering steel and rubber springs, and rubberlike materials by Snowdon (26, 27, 29, 31) and Sykes (35). The two-stage mount for shock has also been considered by Snowdon.(32).

Equations for the effectiveness of isolators given in Chapter 2 have been given by Harris and Crede (11) - equation $E^{(6)}$ in impedance form, and equations $E^{(2)}$ - $E^{(7)}$ in mobility form by Ungar (40). The other equations were derived from first principles. The general single path system has also been dealt with by Skudrzyk (23), Snowdon (25, 28) and Sykes (36), and with extensions to multiple paths, Soliman (33).

Pneumatic isolators have been considered by Soliman (34), and with servo-control, by Tajer-Ardabili (37).

Multi-degree of freedom systems for general rigid body motions have been considered by Efstathiades (4), Grootenhuis (7), Gupta (8), Henry (12) and Smollen (24).

Vibration isolation in vehicles has been considered by Barson (2), dealing with tyres, with suspension by (1), Fiala (6), Moulton (16), Porter (17), Rossini (18) and Thompson (38). Active isolation has been considered by Bender (3), and engine suspension by Horovitz (13).

The above list is not, of course, inclusive, but briefly covers the field. Other references to vibration isolation are given in the complete list.

APPENDIX 3

AEROSTATIC BEARING

The use of aerostatic bearings in vibration systems is somewhat unusual, and problems have been encountered (154). As such, the use of an aerostatic bearing in the transmissibility apparatus described in Chapter 4 could not be guaranteed a succes at the design stage.

The requirement for the bearing was a high lateral stiffness, with reasonable load bearing capacity, with virtually no restraint in the vertical direction.

Design criteria from Grassam and Powell (139) were used to meet these requirements. Due to manufacturing difficulties, the minimum jet size available was 1/64 in, and so fewer jets than desirable had to be used, with a certain loss in performance.

The design details are:

bearing length 2.0 in.

bearing diameter 1.5 in.

radial clearance 0.001 in. (design), 0.0007 in. (actual)

jets, 2 rows of 4 at quarter stations, each 1/64 in. diameter

air pressure 70 - 80 psig

As shown in Chapter 4, the behaviour of the airbearing was in almost every respect satisfactory, and air

consumption was minimal. Complete absence of dirt and oil in the bearing, and the supply of clean, dry air were essential for the correct performance of this bearing.

The lateral stiffness of the bearing compares well with the theoretical predictions at the design pressure - see Figure A.3.1.

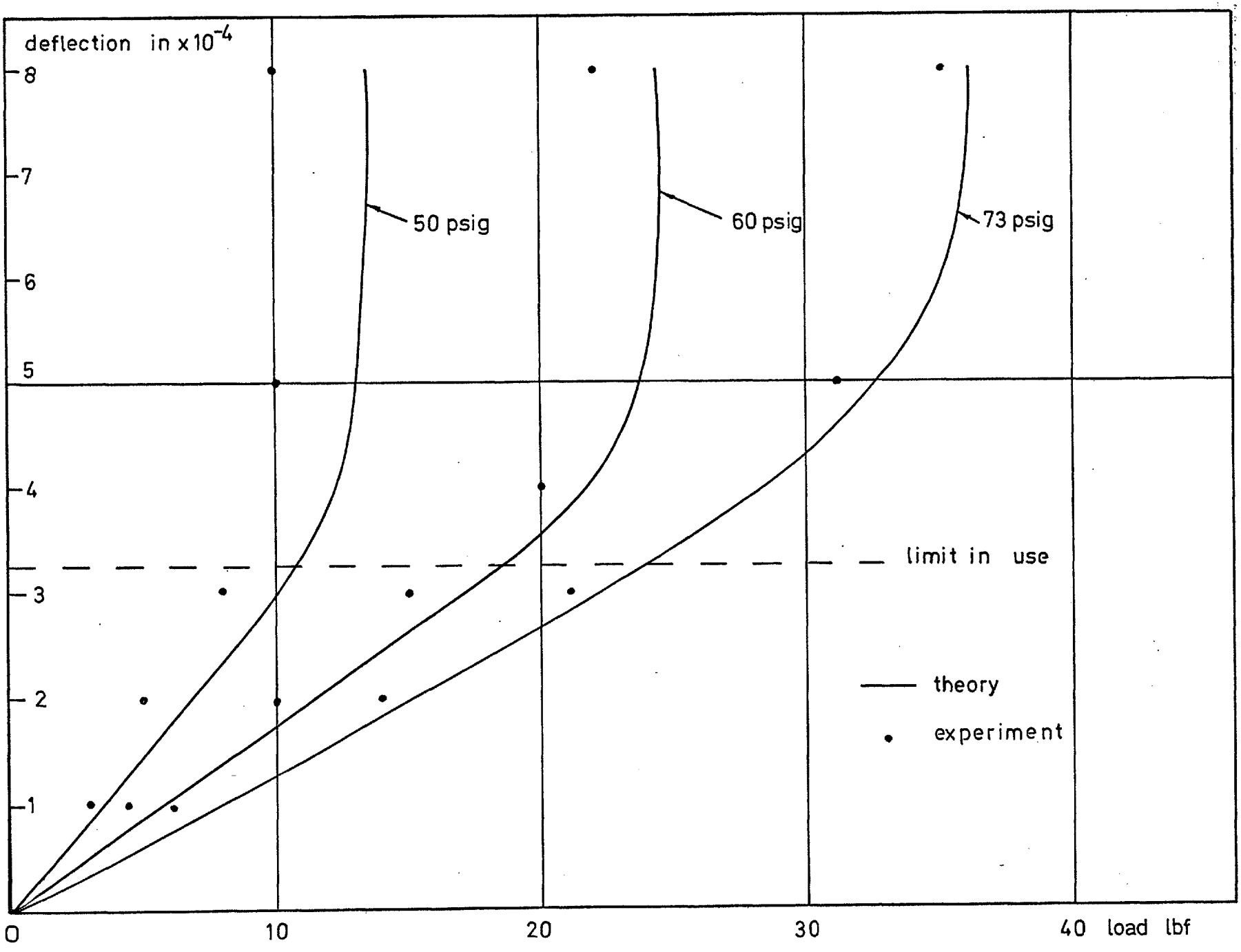

deflection in x10^-4
8
7
6
5
4
3
2
1
50 psig
60 psig
73 psig
limit in use
theory
experiment
0
10
20
30
40 load lbf

Figure A.3.1

APPENDIX 4

TRANSDUCER CALIBRATION

To ensure reasonable confidence in the accuracy of measurements using accelerometers a form of absolute calibration is desirable - using quoted accelerometer sensitivity values and amplifier gain values can lead to an accumulation of errors.

A small calibration block was designed to supply a readily measurable motion input to the accelerometer, enabling an overall calibration to be performed using the same measuring circuit for the calibration as the experimental work. The overall calibration obtained is then scale reading (volts)/g.

The calibration block consists of a 1 in x 1 in square, 1.5 in. long piece of stainless steel with highly polished sides. On two of these sides, very fine lines were scribed at spacings of 2, 4, 10 and 20 x 10^{-3} in and 1., .2, .5 and 1 mm, to an accuracy of 10^{-5} in.

Set amplitudes of the block are obtained by vibrating the block vertically and observing with a microscope when the lines merged.

Twelve adaptor bolts could be screwed into the block, tapped with the various screw threads necessary to test any accelerometer in the laboratory. Another adpator was made to enable the block to be attached to the vibrator.

The complete assembly with accelerometer and vibrator is shown in Figure A.4.1.

The range of operation is limited by the lowest frequency observable by the eye without image loss, the line spacing, and the thrust of the vibrator, and is shown in Figure A.4.2.

Several readings are taken for the calibration, the frequency and amplitude giving acceleration, the independent variable, y, with scale reading, x (volts), as the dependent variable. A line $x = ay$ is fitted by a least squares fit, i.e.

$$a = \frac{\Sigma x_i y_i}{\Sigma (y_i)^2}$$

This is chosen as the errors tend to be small and random. Whilst it is not really meaningful to discuss standard deviations without gross assumptions, an estimate of the errors can be made - these were usually found to be within 3% with occasional errors up to 10%.

The calibration errors provide some idea as to the expected errors in measurement using the accelerometers. Some systematic errors are eliminated by the observer using the same meter for calibration and measurement (except, of course, with digital equipment), but systematic errors may occur in reading the calibrating block. These errors are likely to be the same for all accelerometers being tested, and thus there may be a (small) systematic error for the

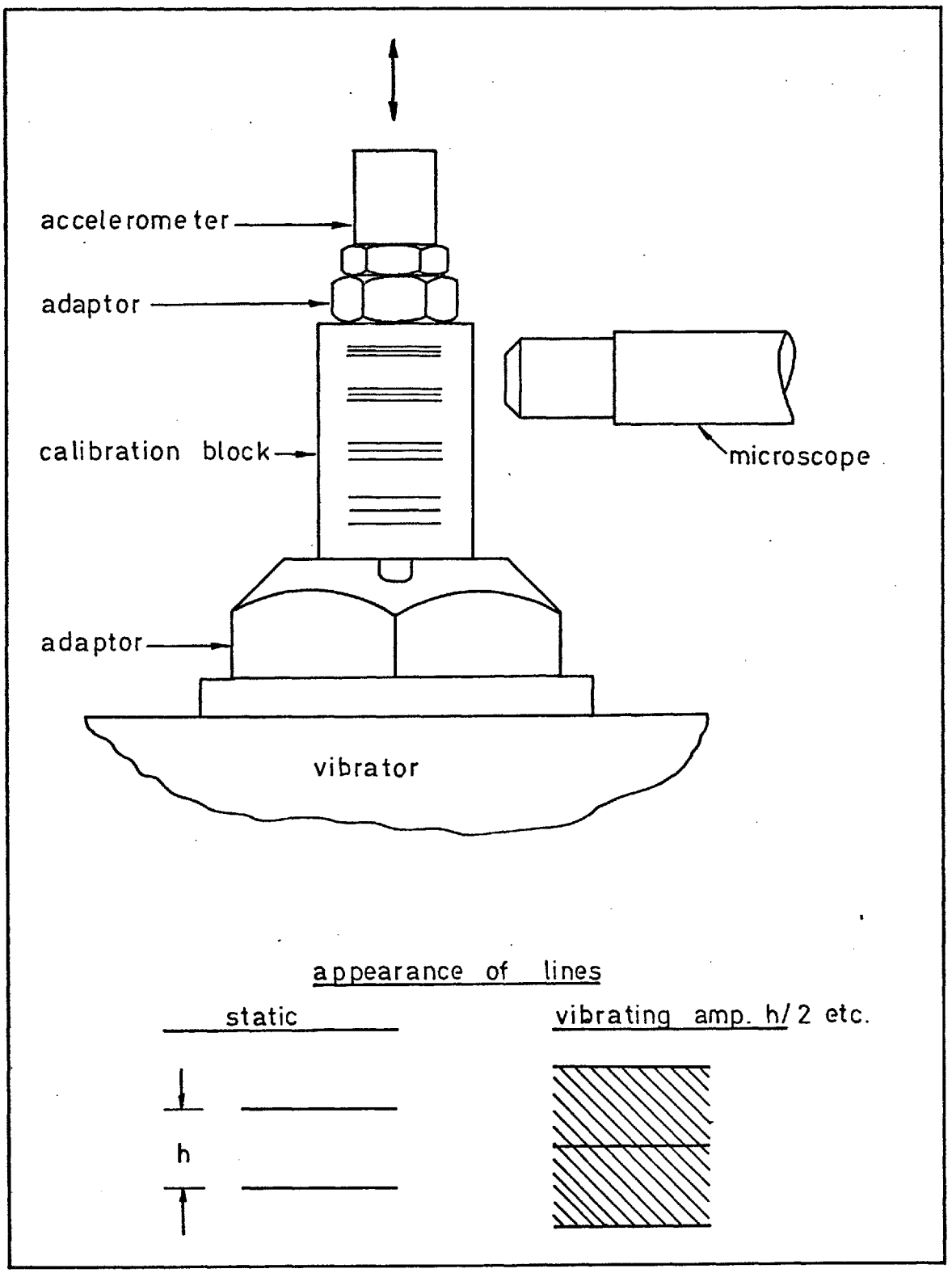

accelerometer
adaptor
calibration block
microscope
adaptor
vibrator
appearance of lines
static
vibrating amp. h/2 etc.
h

Figure A.4.1

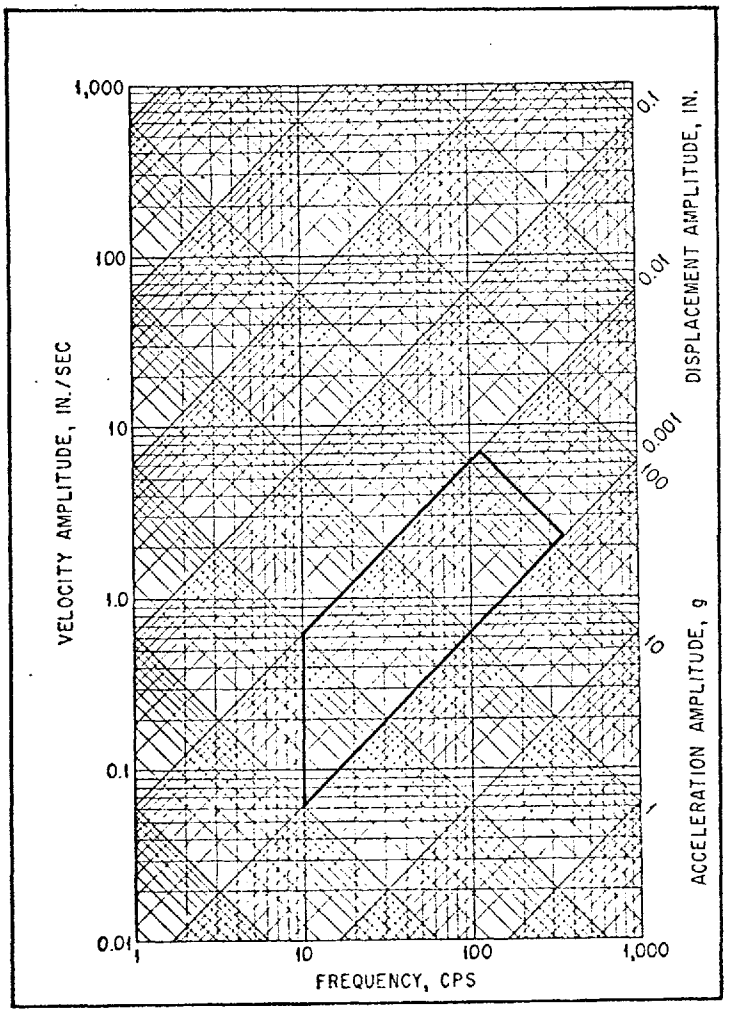

1,000
100
10
1.0
0.1
0.01
VELOCITY AMPLITUDE, IN./SEC
1
10
100
1,000
FREQUENCY, CPS
0.1
0.01
0.001
100
10
1
DISPLACEMENT AMPLITUDE, IN.
ACCELERATION AMPLITUDE, g

Figure A.4.2

experimental results. These can be kept small by using the larger displacements.

The accelerometers and amplifiers are assumed to be linear throughout their working range. With those used this was found to be the case within the limits of error of the calibration.

The calibration block could also be used to calibrate force gauges, by using the block as a loading device as well as indicating the displacement. Additional mass can readily be attached.

Impedance heads can also be calibrated in this way. For these, however, a relative calibration between force and acceleration is usually sufficient. For this relative calibration is only necessary to drive a known mass if the mass cancellation circuit is used, or two different masses to obtain the calibration and the effective mass at the end of the impedance head.

APPENDIX 5

MASS CANCELLATION CIRCUIT

Cancellation of the mass between the force gauge of an impedance head and the structure being tested is necessary for accurate measurements, especially when the structure's impedance is low. As is shown in Figure A.5.1, only F can be measured by the force gauge, whilst the true force F_T acting on the structure must be deduced, using the relation:

$$F_T = F - m\ddot{x}$$

where m is the mass in front of the force gauge (assumed rigid), and the common acceleration $\ddot{x}$ is measured by the accelerometer. A rigid connection to the structure in the forcing direction is assumed.

Circuits to perform the required function were not available (at the time of testing), and so the circuit shown in Figure A.5.2 was constructed, using integrated circuit operational amplifiers.

The circuit specification is:

Power supply 240 V AC

Input impedance (both inputs) 10 kΩ

Output impedance 220 Ω

Maximum input voltage $\pm$ IV on $\ddot{X}$, $\pm$ 10V on F

Maximum output voltage $\pm$ 10V

Output short-circuit protection - complete

Bandwidth DC - 1kHz

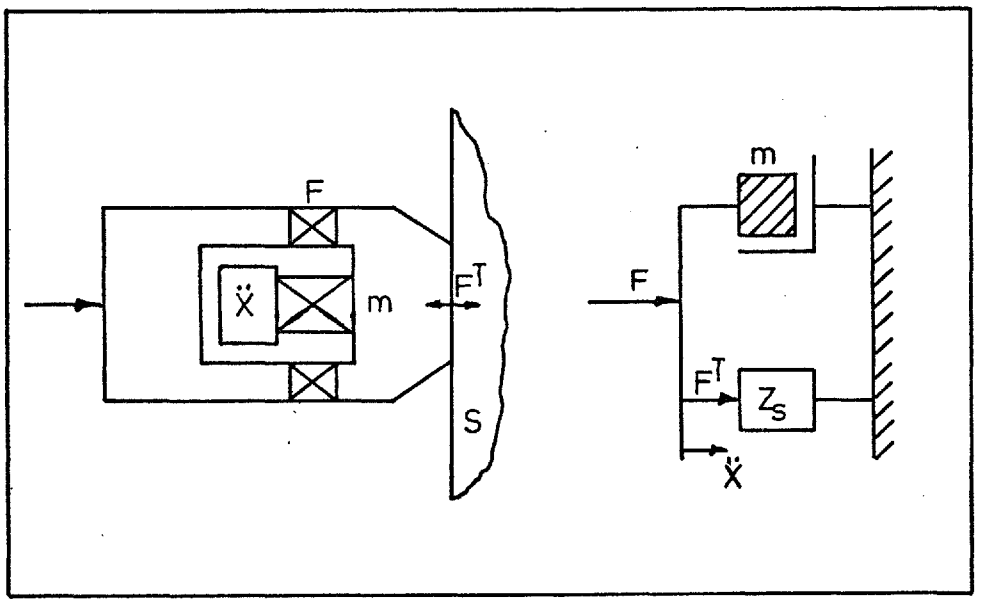


Figure A.5.1

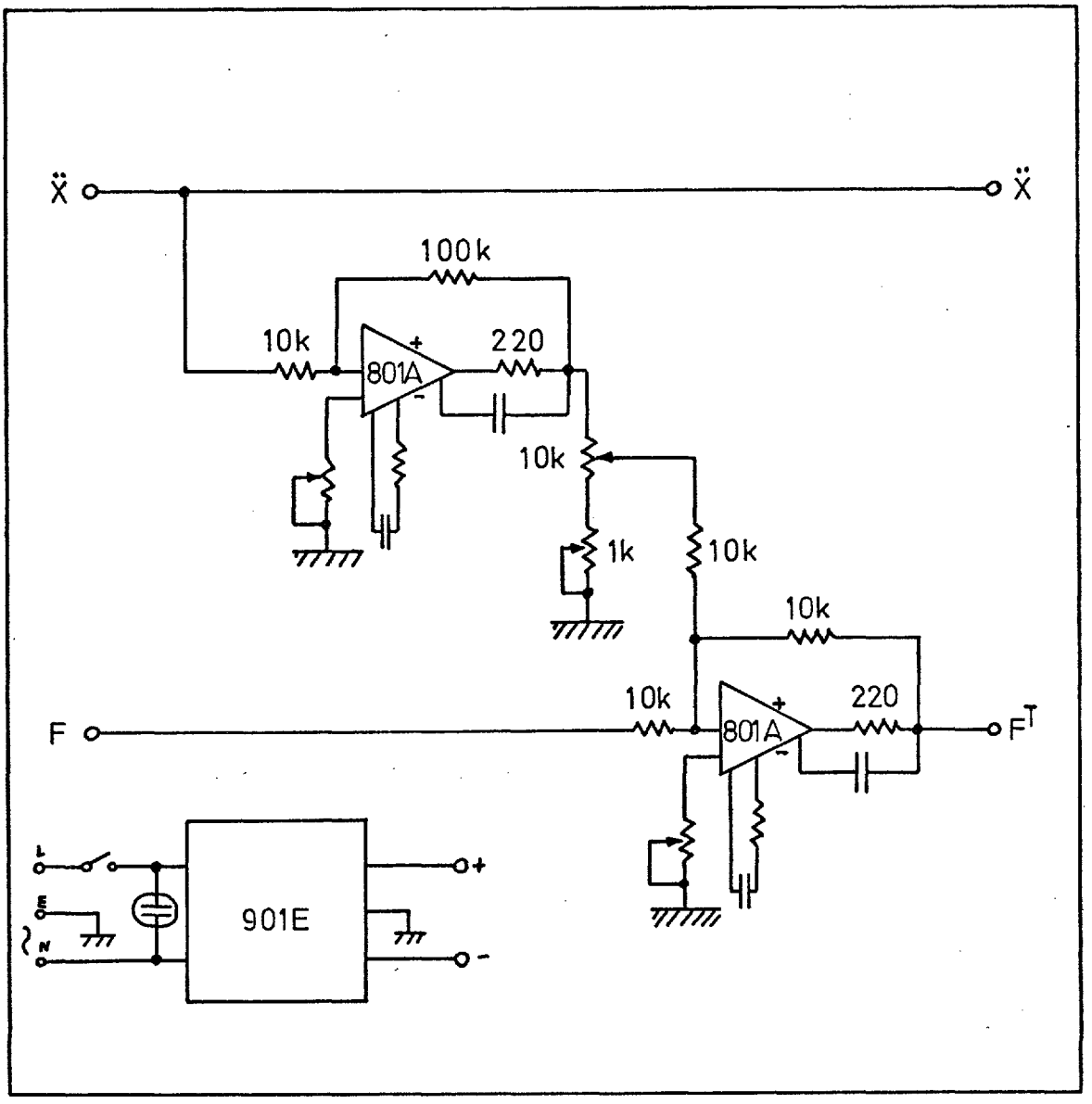


Figure A.5.2

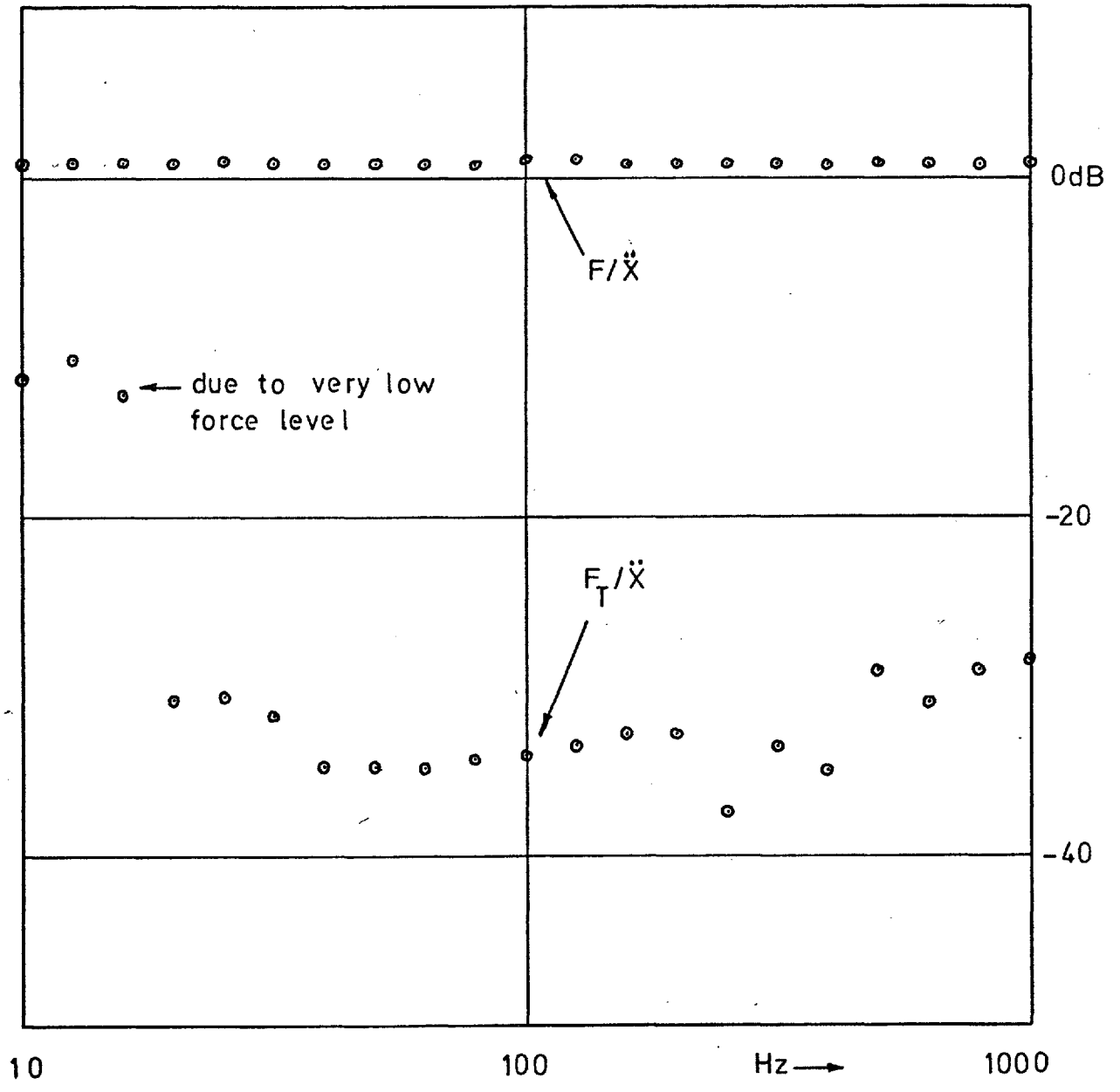


Figure A.5.3

The circuit was tested by feeding both inputs with a common signal from an oscillator, and setting the potentiometers to give a minimum output on the force channel. The minimum was found to be at least -80dB relative to the input over the operating range and thus the circuit was seen to perform with high accuracy.

Using an impedance head as the signal supply, the effects of the mass in front of the force gauge were reduced over most of the frequency range by more than 30 dB. A typical trial using a Wilcoxon impedance head is shown in Figure A.5.3. Small phase and gain shifts introduced by the transducers and amplifiers account for the fact that the amount of mass cancellation achieved in practice is less than would be expected from the behaviour of the mass cancellation circuit alone. Because of the frequency dependence of such shifts it is possible when taking measurements at spot frequencies to achieve better than 30dB cancellation by adjustment of the gain potentiometers.

The circuit can also provide the relative displacement between the top and bottom blocks in the transmissibility apparatus.

APPENDIX 6

EXAMPLE OF MODEL DERIVATION

The derivation of the equations of motion for the twin wishbone model without the damper unit are shown here to characterise the approach taken and the type of assumptions made in the modelling.

The skeleton form of the suspension model is shown in Figure A.6.1. The following initial assumptions are made:

1. Component parts are rigid, springs massless.
2. In-plane, small vibrations considered only.
3. No clearances.
4. Outboard pivots viscously damped, inboard pivots rubber bushes.
5. End mass constrained to move in x-direction only.

Right-hand Cartesian coordinates are used, x corresponding to the vertical direction.

The generalised coordinates are chosen as being suitable for measurement and forcing, and are:

q_1 - x-direction motion of stub-axle (point a)

q_2 - y-direction motion of stub-axle (point a)

q_3 - θ_z-direction rotation of stub axle (point a)

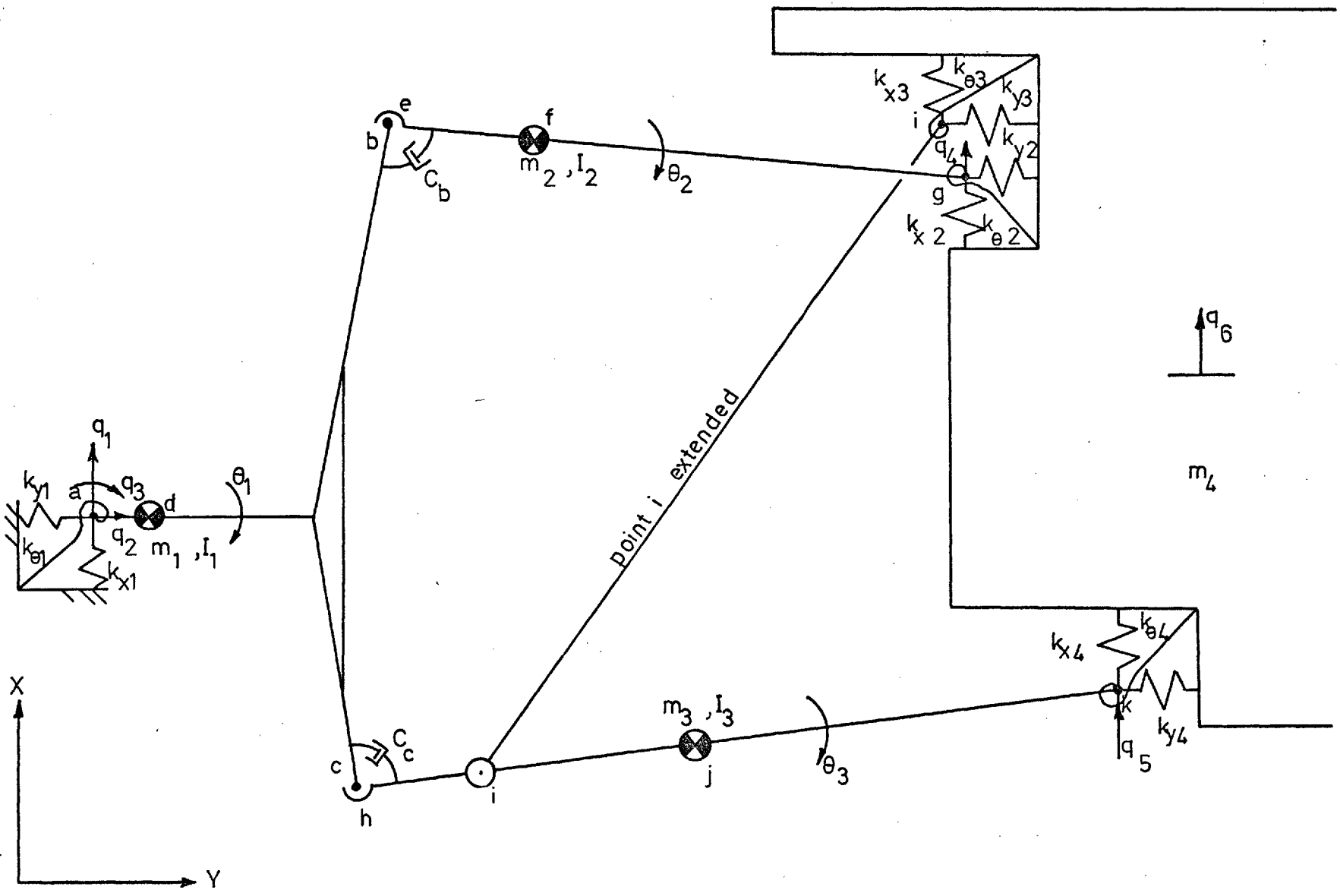

k_{x3}
$k_{\theta 3}$
k_{y3}
k_{y2}
k_{x2}
$k_{\theta 2}$
i
g
q_4
e
f
b
C_b
m_2, I_2
θ_2
q_6
m_4
q_1
k_{y1}
a
q_3
d
θ_1
$k_{\theta 1}$
q_2
m_1, I_1
k_{x1}
point i extended
k_{x4}
$k_{\theta 4}$
k
k_{y4}
q_5
m_3, I_3
j
θ_3
C_c
c
h
i
X
Y

Figure A.6.1

q_4 - x-direction motion of inner end of upper wishbone (point g)

q_5 - x-direction motion of inner end of lower wishbone (point k)

q_6 - x-direction motion of end mass.

Auxiliary coordinates are used to give the motions of other points on the model, and are denoted by the vector form of the point name:

e.g. $\underline{\dot{a}} = \dot{a}_x \underline{i} + \dot{a}_y \underline{j} = \dot{q}_1 \underline{i} + \dot{q}_2 \underline{j}$

is the velocity of point a, where $\dot{a}_x$ and $\dot{a}_y$ are the components of velocity, and $\underline{i}$ and $\underline{j}$ are unit vectors in the x and y directions respectively.

Position vectors ($\underline{r}$) specify the geometry of the model. They refer the position of any point on a rigid link to the position of the input point (characterised by the lowest letter) of that link.

e.g. $\underline{r}_k = r_{xk} \underline{i} + r_{yk} \underline{j}$

means the position of point k referred to point h (see Figure A.6.1).

The points d, f, j specify the positions of the centre of mass of the stub-axle and wishbones.

Other system parameters are:

k_{x1} - spring stiffness, spring number 1, direction x (this may be complex, to include hysteretic damping)

c_b - viscous damping coefficient, number b

m_2 - mass, number 2

I_3 - moment of inertia of rigid body number 3 about centre of mass in XY plane (i.e. about z axis)

Each spring is represented by three uncoupled stiffnesses - vertical (k_x), horizontal (k_y) and torsional (k_θ). The spring k_1 is seen in place of the tyre, and is included for numerical reasons - it need not affect transmissibility calculations (q_6/q_1), or the mobility matrices where spring-damper cancellation is used.

The equations are set up using Lagrange's formulation, requiring expressions for the energy and dissipation of the system. Thus, we have:

kinetic energy, T

$$= \tfrac{1}{2} \left\{ m_1 |\dot{\underline{d}}|^2 + I_1 |\dot{\underline{\theta}}_1|^2 + m_2 |\dot{\underline{f}}|^2 + I_2 |\dot{\underline{\theta}}_2|^2 + m_3 |\dot{\underline{j}}|^2 + I_3 |\underline{\theta}_3|^2 + m_4 |\dot{\underline{i}}|^2 \right\}$$

potential energy, V

$$= \tfrac{1}{2} \left\{ k_{x1} a_x^2 + k_{y1} a_y^2 + k_{\theta 1} \theta_1^2 + k_{x2} (g_x - l_x)^2 + k_{y2} g_y^2 + k_{\theta 2} \theta_2^2 + k_{x3} (i_x - l_x)^2 + k_{y3} i_y^2 + k_{\theta 3} \theta_3^2 + k_{x4} (k_x - l_x)^2 + k_{y4} k_y^2 + k_{\theta 4} \theta_3^2 \right\}$$

dissipation function, - D

$$= \tfrac{1}{2} \left\{ c_b (\dot{\theta}_1 - \dot{\theta}_2)^2 + c_c(\dot{\theta}_1 - \dot{\theta}_2)^2 \right\}$$

Forces applied externally to the generalised coordinates correspond to the generalised forces, Q.

The expressions above require to be modified into expressions containing the generalised coordinates (q) only. Considering the kinematic relations first, we have:

1. for the stub axle:

$$\underline{\dot{d}} = \underline{\dot{a}} + \underline{\dot{\theta}}_1 \wedge \underline{r}_d$$

2. for the upper wishbone:

$$\underline{\dot{e}} = \underline{\dot{b}} = \underline{\dot{a}} + \underline{\dot{\theta}}_1 \wedge \underline{r}_b$$

$$\underline{\dot{g}} = \underline{\dot{e}} + \underline{\dot{\theta}}_2 \wedge \underline{r}_g = \underline{\dot{a}} + \underline{\dot{\theta}}_1 \wedge \underline{r}_b + \dot{\theta}_2 \wedge \underline{r}_g$$

$$\underline{\dot{f}} = \underline{\dot{a}} + \underline{\dot{\theta}}_1 \wedge \underline{r}_b + \underline{\dot{\theta}}_2 \wedge \underline{r}_f$$

3. for the lower wishbone:

$$\underline{\dot{h}} = \underline{\dot{c}} = \underline{\dot{a}} + \dot{\theta}_1 \wedge \underline{r}_c$$

$$\underline{\dot{k}} = \underline{\dot{a}} + \underline{\dot{\theta}}_1 \wedge \underline{r}_c + \underline{\dot{\theta}}_3 \wedge \underline{r}_k$$

$$\underline{\dot{j}} = \underline{\dot{a}} + \underline{\dot{\theta}}_1 \wedge \underline{r}_c + \underline{\dot{\theta}}_3 \wedge \underline{r}_j$$

$$\underline{\dot{l}} = \underline{\dot{a}} + \underline{\dot{\theta}}_1 \wedge \underline{r}_c + \underline{\dot{\theta}}_3 \wedge \underline{r}_i$$

Consider the terms needed for T:

$$\underline{\dot{d}} = \underline{\dot{a}} + \underline{\dot{\theta}}_1 \wedge \underline{r}_d$$

$$= (\dot{q}_1 - r_{yd}\,\dot{q}_3)\,\underline{i} + (\dot{q}_2 + r_{xd}\,\dot{q}_3)\,\underline{j}$$

hence $$\underline{\dot{d}}^{\,2} = \dot{q}_1^{\,2} + \dot{q}_2^{\,2} + r_d^{\,2}\dot{q}_3^{\,2} - 2\dot{q}_1\dot{q}_3 r_{yd} + 2\dot{q}_2\dot{q}_3 r_{xd} \qquad (1)$$

where $$r_d^{\,2} = r_{xd}^{\,2} + r_{yd}^{\,2}$$

and $$\underline{\dot{\theta}}_1^{\,2} = \dot{q}_3^{\,2}$$

For the rotation of θ_2, we have

$$\underline{\dot{\theta}}_2 \wedge \underline{r}_y = \underline{\dot{g}} - \underline{\dot{a}} - \underline{\dot{\theta}}_1 \wedge \underline{r}_b$$

hence $$\dot{\theta}_2 = \frac{1}{r_{yg}}(\dot{q}_1 - \dot{q}_4 - r_{yb}\,\dot{q}_3)$$

so that $$\underline{\dot{f}} = \underline{\dot{a}} + \dot{\theta}_1 r_b \underline{u}_b + \frac{1}{r_{yg}}(\dot{q}_1 - \dot{q}_4 - r_{yb}\dot{q}_3)\, r_f \underline{u}_f$$

(where $r\,\underline{u} = -r_y\,\underline{i} + r_x\,\underline{j}$)

then $$\dot{f}_x = \dot{a}_x - \dot{\theta}_1 r_{yb} - \frac{1}{r_{yg}}(\dot{q}_1 - \dot{q}_4 - r_{yb}\,\dot{q}_3)\, r_{yf}$$

$$= \dot{q}_1 - r_{yb}\,\dot{q}_3 - \frac{r_{yf}}{r_{yg}}(\dot{q}_1 - \dot{q}_4 - r_{yb}\,\dot{q}_3)$$

using the substitutions

$$A_1 = \frac{r_{yf}}{r_{yg}}, \qquad A_2 = 1 - A_1$$

leads to:

$$\dot{f}_x^{\,2} = A_2\dot{q}_1^{\,2} + r_{yb}^{\,2}A_2^{\,2}\dot{q}_3^{\,2} + A_1^{\,2}\dot{q}_4^{\,2} - 2r_{yb}A_2^{\,2}\dot{q}_1\dot{q}_3$$

$$+ 2A_1A_2\dot{q}_1\dot{q}_4 - 2r_{yb}A_1A_2\dot{q}_3\dot{q}_4$$

whilst for $\dot{f}_y$, we have

$$\dot{f}_y = \dot{a}_y + \dot{\theta}_1 r_{xb} + \frac{r_{xf}}{r_{yg}}(\dot{q}_1 - \dot{q}_4 - r_{yb}\,\dot{q}_3)$$

using the substitutions

$$A_3 = \frac{r_{xf}}{r_{yg}} \quad , \qquad A_4 = (r_{xb} - \frac{r_{yb}\, r_{xf}}{r_{yg}})$$

leads to

$$\begin{aligned} \dot{f}_y^{\,2} &= A_3^{\,2}\, \dot{q}_1^{\,2} + \dot{q}_2^{\,2} + A_4^{\,2}\, \dot{q}_3^{\,2} + A_3^{\,3}\, \dot{q}_4^{\,2} + 2A_3\dot{q}_1\dot{q}_2 \\ &+ 2A_3A_4\, \dot{q}_1\dot{q}_3 - 2A_3^{\,2}\, \dot{q}_1\dot{q}_4 + 2A_4\, \dot{q}_2\dot{q}_3 \\ &- 2A_3\, \dot{q}_2\dot{q}_4 - 2A_3A_4\, \dot{q}_3\dot{q}_4 \end{aligned}$$

Thus, for the third term in T, we have

$$\begin{aligned} |\underline{\dot{f}}|^2 &= \dot{f}_x^{\,2} + \dot{f}_y^{\,2} \\ &= \left\{A_2^{\,2} + A_3^{\,2}\right\}\, \dot{q}_1^{\,2} + \dot{q}_2^{\,2} + \left\{ r_{yb}^{\,2}\, A_2^{\,2} + A_4^{\,2} \right\}\, \dot{q}_3^{\,2} \\ &\qquad + \left\{A_1^{\,2} + A_3^{\,2}\right\}\, q_4^{\,2} \\ &+ 2A_3\, \dot{q}_1\dot{q}_2 + 2(A_3A_4 - r_{yb}A_2^{\,2})\dot{q}_1\dot{q}_3 + 2(A_1A_2 - A_3^{\,2})\dot{q}_1\dot{q}_4 \\ &+ 2A_4\, \dot{q}_2\dot{q}_3 - 2A_3\, \dot{q}_2\dot{q}_4 \\ &- 2(r_{yb}\, A_1A_2 + A_3A_4)\, \dot{q}_3\dot{q}_4 \end{aligned} \tag{3}$$

Using the substitution

$$A_5 = \frac{1}{r_{yg}^{\,2}}$$

we get, for the fourth term in T,

$$\begin{aligned} |\underline{\dot{\theta}}_2|^2 &= A_5\, \dot{q}_1^{\,2} + r_{yb}^{\,2}\, A_5\, \dot{q}_3^{\,2} + A_5\, \dot{q}_4^{\,2} - 2A_5\, \dot{q}_1\dot{q}_4 \\ &- 2r_{yb}\, A_5\, \dot{q}_1\dot{q}_3 + 2r_{yb}\, A_5\, \dot{q}_3\dot{q}_4 \end{aligned} \tag{4}$$

By similar analysis, using the substitutions:

$$A_6 = \frac{r_{yj}}{r_{yk}}, \quad A_7 = \left(1 - \frac{r_{yj}}{r_{yk}}\right), \quad A_8 = \frac{r_{xj}}{r_{yk}},$$

$$A_9 = \left(r_{xc} - \frac{r_{yc}\, r_{xj}}{r_{yk}}\right)$$

we get:

$$|\dot{\underline{i}}|^2 = (A_7^2 + A_8^2)\dot{q}_1^2 + \dot{q}_2^2 + (r_{yc}^2 A_7^2 + A_9^2)\dot{q}_3^2 + (A_6^2 + A_8^2)\dot{q}_5^2$$

$$+ 2A_8 \dot{q}_1\dot{q}_2 + 2(A_8A_9 - r_{yc} A_7^2)\dot{q}_1\dot{q}_3 + 2(A_6A_7 - A_8^2)\dot{q}_1\dot{q}_5$$

$$+ 2A_9 \dot{q}_2\dot{q}_3 - 2A_8 \dot{q}_2\dot{q}_5$$

$$- 2(r_{yc} A_6A_7 + A_8A_9)\dot{q}_3\dot{q}_5 \qquad (5)$$

and $|\dot{\underline{\theta}}_3|^2 = A_{10} \dot{q}_1^2 + r_{yc} A_{10} \dot{q}_3^2 + A_{10} \dot{q}_5^2 - 2A_{10} \dot{q}_1\dot{q}_5$

$$- 2r_{yc} A_{10} \dot{q}_1\dot{q}_3 + 2r_{yc} A_{10} \dot{q}_3\dot{q}_5 \qquad (6)$$

where $A_{10} = \frac{1}{r_{yk}^2}$

and for the last term $|\dot{\underline{i}}|^2 = \dot{q}_6^2$ (7)

Summing the terms 1 - 7, the expression for kinetic energy in terms of the generalised coordinates is :

$$
\begin{aligned}
2T = {} & \left\{ m_1 + (A_2^2 + A_3^2)m_2 + A_5 I_2 + (A_7^2 + A_8^2)m_3 + A_{10} I_3 \right\} \dot{q}_1^2 \\
& + (m_1 + m_2 + m_3)\dot{q}_2^2 \\
& + \left\{ (m_1 r_d^2 + I_1) + (r_{yb}^2 A_2^2 + A_4^2)m_2 + r_{yb}^2 A_5 I_2 + \right. \\
& \qquad (r_{yc}^2 A_7^2 + A_9^2)m_3 \\
& \qquad \left. + r_{yc}^2 A_{10} I_3 \right\} \dot{q}_3^2 \\
& + \left\{ (A_1^2 + A_3^2)m_2 + A_5 I_2 \right\} \dot{q}_4^2 \\
& + \left\{ A_6^2 + A_8^2)m_3 + A_{10} I_3 \right\} \dot{q}_5^2 \quad + \quad m_4 \dot{q}_6^2 \\
& + 2(A_3 m_2 + A_8 m_3)\dot{q}_1\dot{q}_2 + 2\left\{ -r_{yd} m_1 + (A_3 A_4 - r_{yb} A_2^2)m_2 \right. \\
& \quad \left. - r_{yb} A_5 I_2 + (A_8 A_9 - r_{yc} A_7^2)m_3 - r_{yc} A_{10} I_3 \right\} \dot{q}_1\dot{q}_3 \\
& + 2\left\{ (A_1 A_2 - A_3^2)m_2 - A_5 I_2 \right\} \dot{q}_1\dot{q}_4 \\
& + 2\left\{ (A_6 A_7 - A_8^2)m_3 - A_{10} I_2 \right\} \dot{q}_1\dot{q}_5 \\
& - 2\left\{ r_{xd} m_1 + A_4 m_2 + A_9 m_3 \right\} \dot{q}_2\dot{q}_3 - 2A_3 m_2 \dot{q}_2\dot{q}_4 - 2A_8 m_3 \dot{q}_2\dot{q}_5 \\
& - 2\left\{ (r_{yb} A_1 A_2 + A_3 A_4)m_2 - r_{yb} A_5 I_2 \right\} \dot{q}_3\dot{q}_4 \\
& - 2\left\{ (r_{yc} A_6 A_7 + A_8 A_9)m_3 + r_{yc} A_{10} I_3 \right\} \dot{q}_3\dot{q}_5
\end{aligned}
$$

From this expression for T, it is then possible to write down the inertia matrix elements by inspection - these are shown in Appendix 7.

Considering now the potential energy, we require additional expressions for:

$$g_y \,, \quad i_x \,, \quad i_y \quad \text{and} \quad k_y$$

now $\underline{g} = \underline{a} + \underline{\theta}_1 \wedge \underline{r}_b + \underline{\theta}_2 \wedge \underline{r}_g$

so $g_y = q_2 + q_3 r_{xb} + \frac{r_{xg}}{r_{yg}} (q_1 - q_4 - q_3 r_{yb})$

$$= B_1 q_1 + q_2 + B_2 q_3 - B_1 q_4$$

where $B_1 = \frac{r_{xg}}{r_{yg}}$, $\quad B_2 = r_{xb} - \frac{r_{yb} r_{xg}}{r_{yg}}$

then $g_y^2 = B_1^2 q_1^2 + q_2^2 + B_2^2 q_3^2 + B_1^2 q_4^2$

$$+ 2 B_1 B_2 q_1 q_2$$

$$+ 2 B_1 B_2 q_1 q_3 - 2 B_1^2 q_1 q_4 + 2 B_2 q_2 q_3$$

$$- 2 B_1 q_2 q_4$$

$$- 2 B_1 B_2 q_3 q_4 \qquad (8)$$

and $\underline{i} = \underline{a} + \underline{\theta}_1 \wedge \underline{r}_c + \underline{\theta}_3 \wedge \underline{r}_i$

so $i_x - q_6 = B_4 q_1 - r_{yc} B_4 q_3 + B_3 q_5 - q_6$

where $B_3 = \frac{r_{yi}}{r_{yk}}$, $\quad B_4 = 1 - B_3$

so that $(i_x - q_6)^2 = B_4^2 q_1^2 + r_{yc}^2 B_4^2 q_3^2 + B_3^2 q_5^2 + q_6^2$

$$- 2 r_{yc} B_4^2 q_1 q_3 + 2 B_3 B_4 q_1 q_5 - 2 B_4 q_1 q_6$$

$$- 2 r_{yc} B_3 B_4 q_3 q_5 + 2 r_{yc} B_4 q_3 q_6$$

$$- 2 B_3 q_5 q_6 \qquad (9)$$

and $i_y = B_5 q_1 + q_2 + B_6 q_3 - B_5 q_5$

where $B_5 = \frac{r_{xi}}{r_{yk}}$, $B_6 = r_{xc} - \frac{r_{yc}\, r_{xi}}{r_{yk}}$

so that $i_y^2 = B_5^2 q_1^2 + q_2^2 + +B_6^2 q_3^2 + B_5^2 q_5^2$

$+ 2B_5 q_1q_2 + 2B_5B_6 q_1q_3 - 2B_5^2 q_1q_5$

$+ 2B_6 q_2q_3 - 2B_5 q_2q_5$

$- 2B_5B_6 q_3q_5$ (10)

whilst for k_y, we have

$k_y = B_7 q_1 + q_2 + B_8 q_3 - B_7 q_5$

where $B_7 = \frac{r_{xk}}{r_{yk}}$, $B_8 = r_{xc} - \frac{r_{yc}\, r_{xk}}{r_{yk}}$

so that $k_y^2 = B_7^2 q_1^2 + q_2^2 + B_8^2 q_3^2 + B_7 q_5^2$

$+ 2B_7 q_1q_2 + 2B_7B_8 q_1q_3 - 2B_7^2 q_1q_5$

$+ 2B_8 q_2q_3 - 2B_7 q_2q_5$

$- 2B_7B_8 q_3q_5$ (11)

The expression for the potential energy can now be formed, and is:

$$
\begin{aligned}
2V = {} & \{k_{x1} + B_1^2 k_{y2} + A_5 k_{\theta 2} + B_4^2 k_{x3} + B_5^2 k_{y3} + A_{10} k_{\theta 3} + B_7^2 k_{y4} \\
& \qquad + A_{10} k_{\theta 4}\} q_1^2 \\
& + \{k_{y1} + k_{y2} + k_{y3} + k_{y4}\} q_2^2 \\
& + \{k_{\theta 1} + B_2^2 k_{y2} + r_{yb}^2 A_5 k_{\theta 2} + r_{yc}^2 B_4^2 k_{x3} + B_6^2 k_{y3} \\
& \qquad + r_{yc}^2 A_{10} k_{\theta 3} + B_8^2 k_{y4} + r_{yc}^2 A_{10} k_{\theta 4}\} q_3^2 \\
& + \{k_{x2} + B_1^2 k_{y2} + A_5 k_{\theta 2}\} q_4^2 \\
& + \{B_3^2 k_{x3} + B_5^2 k_{y3} + A_{10} k_{\theta 3} + k_{x4} + B_7^2 k_{y4} + A_{10} k_{\theta 4}\} q_5^2 \\
& + \{k_{x2} + k_{x3} + k_{x4}\} q_6^2 \\
& + 2\{B_1 k_{y2} + B_5 k_{y3} + B_7 k_{y4}\} q_1 q_2 \\
& + 2\{B_1 B_2 k_{y2} - r_{yb} A_5 k_{\theta 2} - r_{yc} B_4^2 k_{x3} + B_5 B_6 k_{y3} - r_{yc} A_{10} k_{\theta 3} \\
& \qquad + B_7 B_8 k_{y4} - r_{yc} A_{10} k_{\theta 4}\} q_1 q_3 \\
& + 2\{-B_1^2 k_{y2} - A_5 k_{\theta 2}\} q_1 q_4 \\
& + 2\{B_3 B_4 k_{x3} - B_5^2 k_{y3} - A_{10} k_{\theta 3} - B_7^2 k_{y4} - A_{10} k_{\theta 4}\} q_1 q_5 \\
& + 2\{-B_4 k_{x3}\} q_1 q_6 \\
& + 2\{B_2 k_{y2} + B_6 k_{y3} + B_8 k_{y4}\} q_1 q_3 \\
& + 2\{-B_1 k_{y2}\} q_2 q_4 \\
& + 2\{-B_5 k_{y3} - B_7 k_{y4}\} q_2 q_5 \\
& + 2\{-B_1 B_2 k_{y2} + r_{yb} A_5 k_{\theta 2}\} q_3 q_4 \\
& + 2\{-r_{yc} B_3 B_4 k_{x3} - B_5 B_6 k_{y3} + r_{yc} A_{10} k_{\theta 3} - B_7 B_8 k_{y4} \\
& \qquad + r_{yc} A_{10} k_{\theta 4}\} q_3 q_5 \\
& + 2\{r_{yc} B_4 k_{x3}\} q_3 q_6 \\
& + 2\{-k_{x2}\} q_4 q_6 \\
& + 2\{-k_{x4} - B_3 k_{x3}\} q_5 q_6
\end{aligned}
$$

From this, the stiffness matrix elements can be written down as shown in Appendix 7. If hysteretic damping is included, the damping matrix is formed in the same way. If all springs are assumed to have the same loss factor, then the hysteretic matrix is proportional to the stiffness matrix.

For the dissipation function, using the substitutions

$$c_1 = \frac{1}{r_{yg}}, \quad c_2 = 1 + \frac{r_{yb}}{r_{yg}}, \quad c_3 = \frac{1}{r_{yk}}, \quad c_4 = 1 + \frac{r_{yc}}{r_{yk}}$$

we get

$$\begin{aligned} -D = & \left\{ c_1^2 c_b + c_3^2 c_c \right\} \dot{q}_1^2 + \left\{ c_2^2 c_b + c_4^2 c_c \right\} \dot{q}_3^2 \\ & + c_1^2 c_b \dot{q}_4^2 + c_3^2 c_c \dot{q}_5^2 \\ & - 2 \left\{ c_1 c_2 c_b + c_3 c_4 c_c \right\} \dot{q}_1 \dot{q}_3 - 2 c_1^2 c_b \dot{q}_1 \dot{q}_4 \\ & - 2 c_3^2 c_c \dot{q}_1 \dot{q}_5 \\ & + 2 c_1 c_2 c_b \dot{q}_3 \dot{q}_4 + 2 c_3 c_4 c_c \dot{q}_3 \dot{q}_5 \end{aligned}$$

Thus leading to the viscous damping matrix.

APPENDIX 7

EQUATIONS OF MOTION

For computing the response of the lumped parameter models, the equations are required in matrix form. The matrices are:

A - Inertia matrix

E - Stiffness matrix

G - Hysteretic matrix

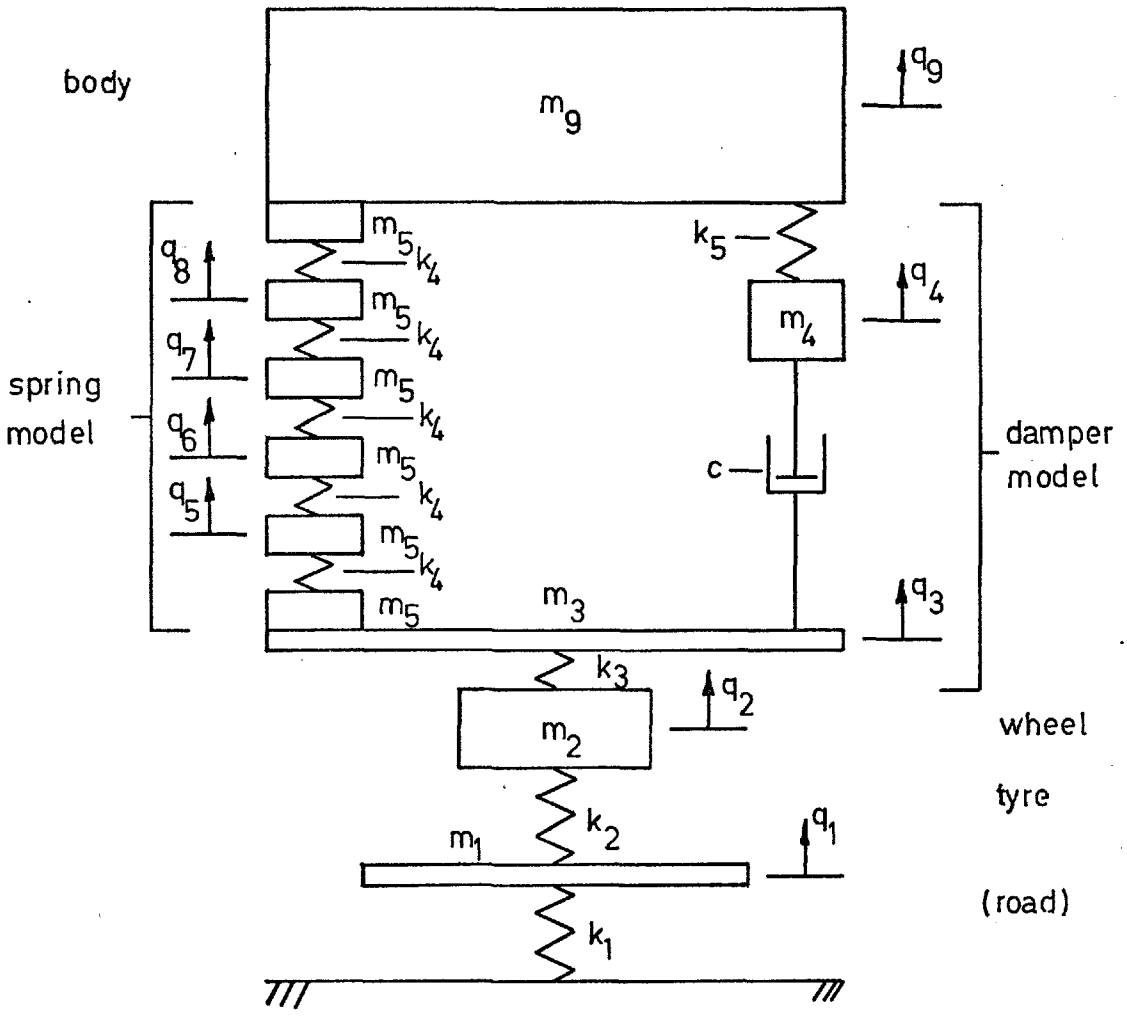
D - Viscous matrix

with the required forcing function provided by the vector F.

This section shows the matrix elements for the models described. For straightforward models without links, the matrix elements can be written down by inspection. Thus only an example is shown below - that for the suspension model including spring surges, §§ 5.4.1 and Figure 5.4.2. A lumped parameter approximation is used for the spring, valid up to the second spring surge. The schematic model is shown in Figure A.7.1, where the springs are permitted to have hysteretic damping.

The matrices for this model are:

$$A = \text{diag}[m_1, m_2, m_3+m_5, m_4, m_5, m_5, m_5, m_9+m_5]$$



m_5 =(total spring mass)/6 ; k_4 =(overall spring stiffness)x5
$=m_s/6$ $=k_s \times 5$

data for Figure 5.4.2 -(transmissibility q_9/q_2 , independent of k_1 , k_2, m_1 & m_2)

m_9 = 500 lb.wt	k_s = 198 lbf/in
m_s = 5.5 lb.wt	k_5 = 4100 lbf/in
m_4 = 0.5 lb.wt	k_3 = 55000 lbf/in
m_3 = 3 lb.wt	c = 18 lbf/in/s

η all springs = 0.01

Figure A.7.1

$$E = \begin{bmatrix} k_1+k_2 & -k_2 & 0 & 0 & 0 & 0 & 0 & 0 & 0 \\ -k_2 & k_2+k_3 & -k_3 & 0 & 0 & 0 & 0 & 0 & 0 \\ 0 & -k_3 & k_4+k_3 & 0 & -k_4 & 0 & 0 & 0 & 0 \\ 0 & 0 & 0 & k_5 & 0 & 0 & 0 & 0 & -k_5 \\ 0 & 0 & -k_4 & 0 & 2k_4 & -k_4 & 0 & 0 & 0 \\ 0 & 0 & 0 & 0 & -k_4 & 2k_4 & -k_4 & 0 & 0 \\ 0 & 0 & 0 & 0 & 0 & -k_4 & 2k_4 & -k_4 & 0 \\ 0 & 0 & 0 & 0 & 0 & 0 & -k_4 & 2k_4 & -k_4 \\ 0 & 0 & 0 & -k_5 & 0 & 0 & 0 & -k_4 & k_4+k_5 \end{bmatrix}$$

G is of the same form as E substituting h for k where $h = \eta k$ where η is the loss factor for the spring.

Finally,

$$D = \begin{bmatrix} 0 & 0 & 0 & 0 & 0 & 0 & 0 & 0 & 0 \\ 0 & 0 & 0 & 0 & 0 & 0 & 0 & 0 & 0 \\ 0 & 0 & C & -C & 0 & 0 & 0 & 0 & 0 \\ 0 & 0 & -C & C & 0 & 0 & 0 & 0 & 0 \\ 0 & 0 & 0 & 0 & 0 & 0 & 0 & 0 & 0 \\ 0 & 0 & 0 & 0 & 0 & 0 & 0 & 0 & 0 \\ 0 & 0 & 0 & 0 & 0 & 0 & 0 & 0 & 0 \\ 0 & 0 & 0 & 0 & 0 & 0 & 0 & 0 & 0 \\ 0 & 0 & 0 & 0 & 0 & 0 & 0 & 0 & 0 \end{bmatrix}$$

For the more complex cases involving links, where the geometry must be considered, the matrix

elements are shown listed, with a schematic diagram of the model. The following pages use part of the computer set routine used in establishing the system matrices to give the equations of motion of each model. The input parameters are read in previously.

A note on reading the computer print-out:

Suffices are not available as such, and appear as full letters or numbers, e.g. A1 is A_1

RXC is r_{xc}

matrix elements are subscripted

e.g. A(I,J) is A_{ij}

and matrix elements not referred to are set to zero.

Also: E(1,1) = KX1 means assign to store E(1,1) value in store KX1 (not 'equals'- can have A = A + A)

* means multiply

** means raise to power

e.g. - C * A4 ** 2 is - CA_4^2 (not-$(CA_4)^2$)

(Precedence rule **; *,/; +,-)

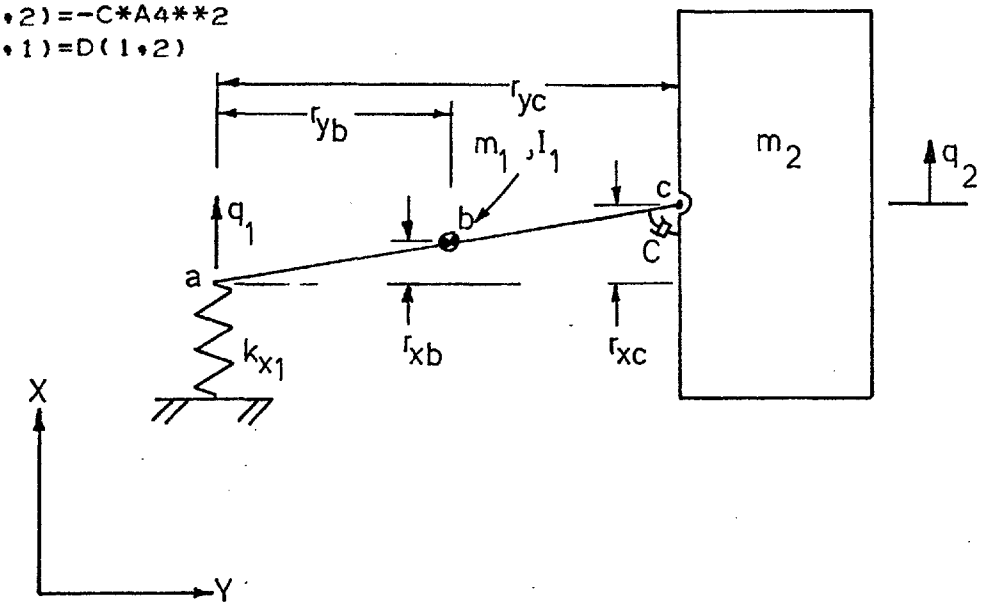
CALL SCAMUL (E, G, M, XXX) means scalar multiply the matrix E by XXX and assign to G, with the matrix order specified by M.

Implicit integer variables, eg. KX1, M2, I4 etc. have all been declared real.

Furthermore, the models all include a spring (or springs) to ground, and sometimes extra mass. The inclusions are for computing purposes, and the effects can be cancelled (see Chapter 3), and can be arranged so as not to affect the transmissibility plots. The spring and mass are also used for rough approximations to the tyre and wheel behaviour.

```
C       THIS PART OF THE SET ROUTINE ESTABLISHES THE INPUT MATRICES FOR
C       THE MODEL SHOWN IN FIGURE 5.3.3, PARA.5.3.1.3 FOR A RIGID,
C       ANGLED LINK WITH A VISCOUSLY DAMPED INBOARD PIVOT.
C       CODE...RLP


        A1=RYB/RYC
        A2=1.-A1
        A3=RXB/RYC-RXC/RYC
        A4=1./RYC
C       SETTING THE INERTIA MATRIX
        A(1,1)=M1*(A2**2+A3**2)+I1*A4**2
        A(2,2)=M1*(A1**2+A3**2)+I1*A4**2+M2
        A(1,2)=M1*(A1*A2-A3**2)-I1*A4**2
        A(2,1)=A(1,2)
C       STIFFNESS MATRIX
        E(1,1)=KX1
C       HYSTERETIC MATRIX
        G(1,1)=HX1
C       VISCOUS MATRIX
        D(1,1)=C*A4**2
        D(2,2)=C*A4**2
        D(1,2)=-C*A4**2
        D(2,1)=D(1,2)
        END
```

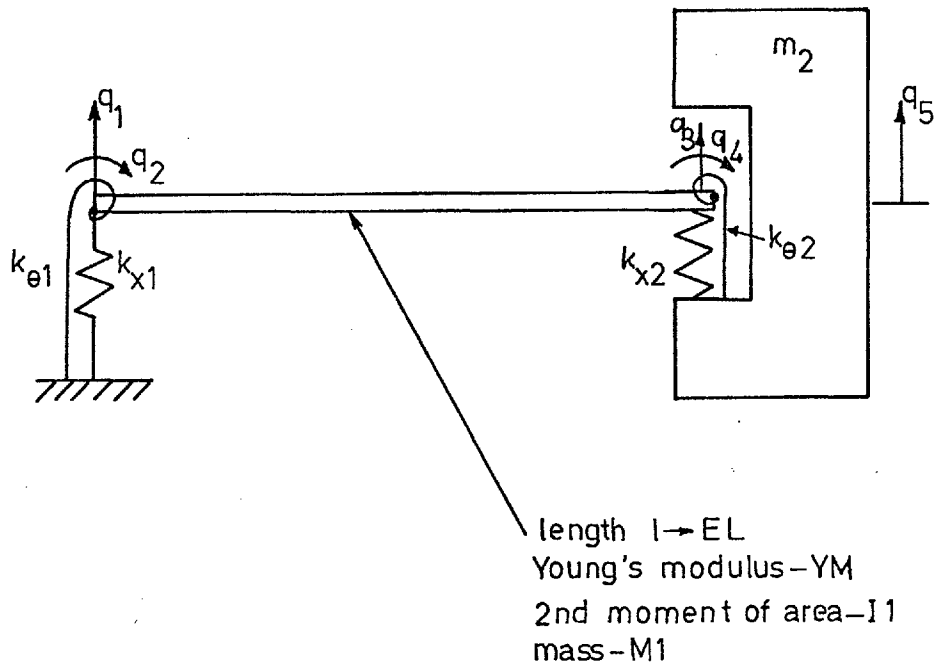


Transmissibility = q_2/q_1 , independent of k_{x1}

b is centre of mass.

```
C       THIS PART OF THE SET ROUTINE ESTABLISHES THE INPUT MATRICES FOR
C       THE MODEL SHOWN IN FIGURE 5.3.3. PARA. 5.3.1.3 FOR A FLEXIBLE
C       LINK (USING AN ASSUMED CUBIC POLYNOMIAL DEFLECTION CURVE).
C       WITH SPRUNG INBOARD PIVOT.
C       CODE...FWB

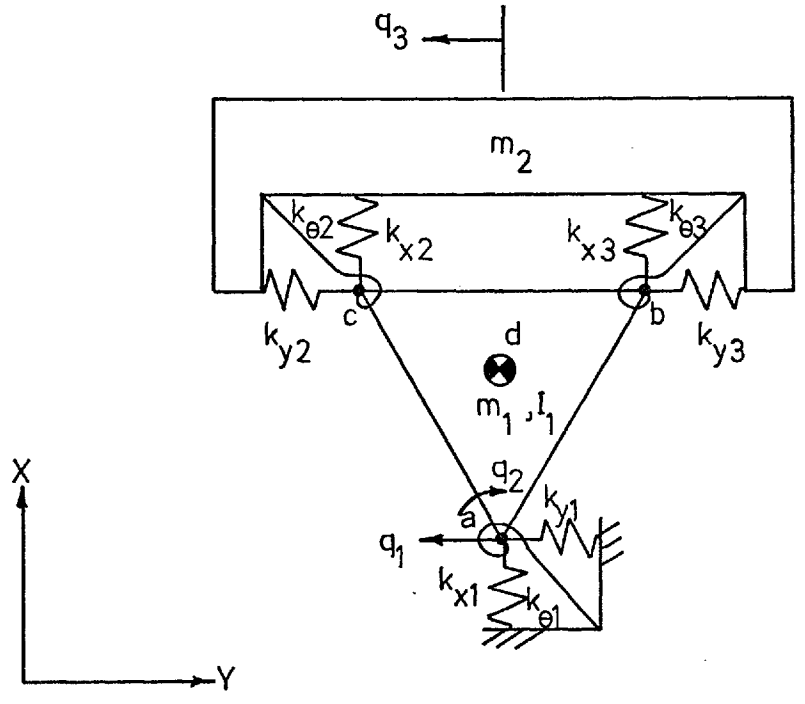

        RO=M1/EL
        CC=YM*I1/EL
        BB=CC/EL
        AA=BB/EL
        DD=RO*EL/420.
        EE=DD*EL
        FF=EE*EL
C       SETTING THE INERTIA MATRIX
        A(1,1)=156.*DD
        A(2,2)=4.*FF
        A(3,3)=156.*DD
        A(4,4)=4.*FF
        A(5,5)=M2
        A(1,2)=22.*EE
        A(1,3)=54.*DD
        A(1,4)=-13.*EE
        A(2,1)=A(1,2)
        A(3,1)=A(1,3)
        A(4,1)=A(1,4)
        A(2,3)=13.*EE
        A(2,4)=-3.*FF
        A(3,2)=A(2,3)
        A(4,2)=A(2,4)
        A(3,4)=-22.*EE
        A(4,3)=A(3,4)
C       STIFFNESS MATRIX
        E(1,1)=12.*AA+KX1
        E(2,2)=4.*CC+KO1
        E(3,3)=12.*AA+KX2
        E(4,4)=4.*CC+KO2
        E(5,5)=KX2
        E(1,2)=6.*BB
        E(1,3)=-12.*AA
        E(1,4)=6.*BB
        E(2,1)=E(1,2)
        E(3,1)=E(1,3)
        E(4,1)=E(1,4)
        E(2,3)=-6.*BB
        E(2,4)=2.*CC
        E(3,2)=E(2,3)
        E(4,2)=E(2,4)
        E(3,4)=-6.*BB
        E(3,5)=-KX2
        E(4,3)=E(3,4)
        E(5,3)=E(3,5)
C       HYSTERETIC MATRIX
        XXX=.01
        CALL SCAMUL (E,G,M,XXX)
C       THIS PRODUCES THE HYSTERETIC MATRIX PROPORTIONAL TO THE
C       STIFFNESS MATRIX, HERE .01X.
        END
```



Transmissibility $= q_5/q_1$, independent of k_{x1}

```
C       THIS PART OF THE SET ROUTINE ESTABLISHES THE INPUT MATRICES FOR
C       THE MODEL SHOWN IN FIGURE 5.3.7, PARA. 5.3.2, FOR THE
C       TRANSMISSION OF VIBRATION IN THE LONGITUDINAL DIRECTION
C       THROUGH THE WISHBONE, WITH A RIGID WISHBONE AND SPRUNG
C       INBOARD PIVOTS
C       CODE...SSH1P

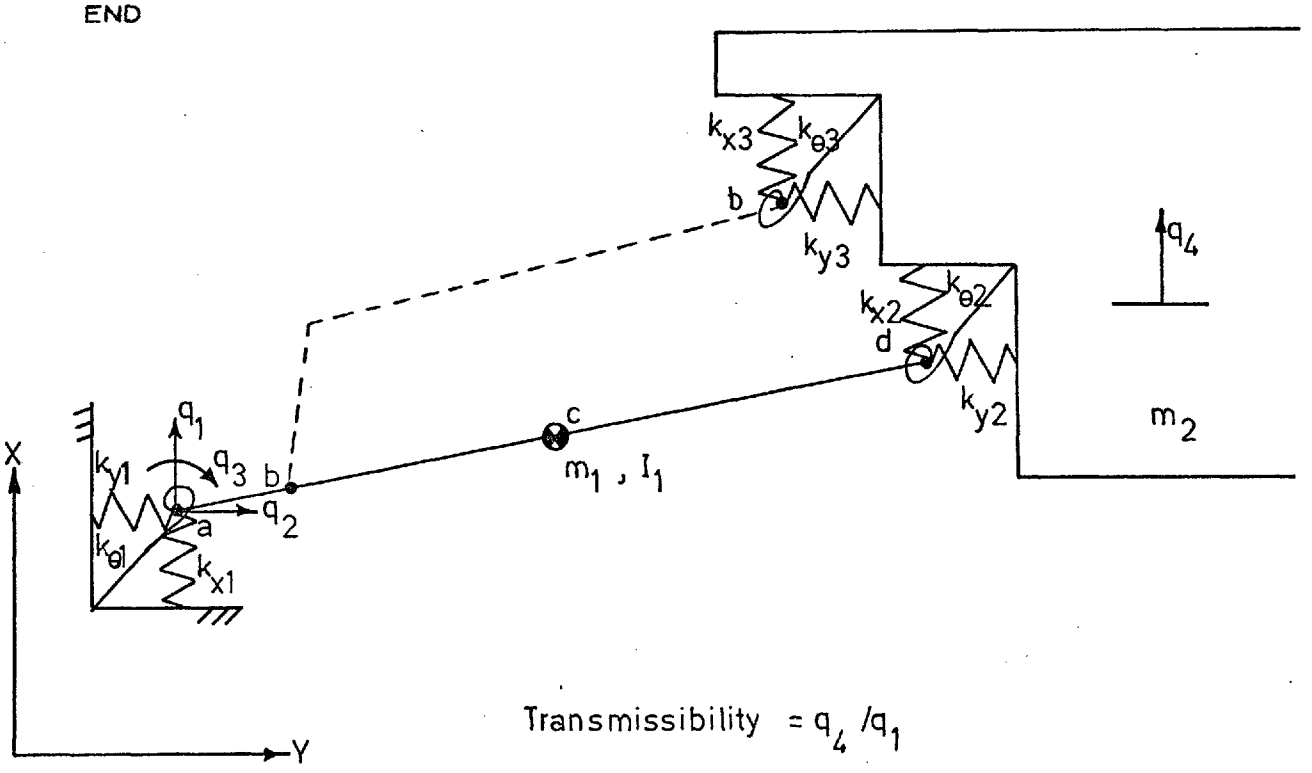

        RD=RXD**2+RYD**2
C       SETTING THE INERTIA MATRIX FOR SSH1P
        A(1,1)=M1
        A(2,2)=M1*RD+I1
        A(3,3)=M2
        A(1,2)=M1*RXD
        A(2,1)=M1*RXD
C        SETTING THE STIFFNESS MATRIX
        E(1,1)=KY1+KY2+KY3
        E(2,2)=KO1+KX2*RYC**2+KY2*RXC**2+KO2+KX3*RYB**2+KY3*RXB**2+KO3
        E(3,3)=KY2+KY3
        E(1,2)=RXC*KY2+RXB*KY3
        E(1,3)=-KY2-KY3
        E(2,1)=E(1,2)
        E(3,1)=E(1,3)
        E(2,3)=-RXC*KY2-RXB*KY3
        E(3,2)=E(2,3)
C       SETTING THE HYSTERETIC MATRIX
        XX=.01
        CALL SCAMUL(E,G,M,XX)
C       THIS PRODUCES THE HYSTERETIC MATRIX PROPORTIONAL TO THE
C       STIFFNESS MATRIX, HERE .01X.
        END
```



Transmissibility = q_3/q_1 , independent of k_{y1}

```
C       THIS PART OF THE SET ROUTINE ESTABLISHES THE INPUT MATRICES FOR
C       THE MODEL SHOWN IN FIGURE 5.4.3, PARA. 5.4.2.1, AND, WITH K3
C       SET TO ZERO, IN FIGURE 5.3.3, PARA. 5.3.1.3. THE MODEL IS
C       FOR ONE RIGID ANGLED WISHBONE, WITH SPRUNG INBOARD BUSH, AND
C       MASSLESS MAIN SPRING.
C       CODE...AWM2V


C       SETTING THE INERTIA MATRIX
        A(1,1)=M1
        A(2,2)=M1
        A(3,3)=M1*(RXC**2+RYC**2)+I1
        A(4,4)=M2
        A(1,3)=-M1*RYC
        A(3,1)=A(1,3)
        A(2,3)=M1*RXC
        A(3,2)=A(2,3)
C       SETTING THE STIFFNESS MATRIX
        E(1,1)=KX1+KX2+KX3
        E(2,2)=KY1+KY2+KY3
        E(3,3)=KO1+KO2+KO3+KX2*RYD**2+KY2*RXD**2+KX3*RYB**2+KY3*RXB**2
        E(4,4)=KX2+KX3
        E(1,3)=-KX2*RYD-KX3*RYB
        E(1,4)=-KX2-KX3
        E(3,1)=E(1,3)
        E(4,1)=E(1,4)
        E(2,3)=KY2*RXD+KY3*RXB
        E(3,2)=E(2,3)
        E(3,4)=RYD*KX2+RYB*KX3
        E(4,3)=E(3,4)
C       SETTING THE HYSTERETIC MATRIX
        XXX=.01
        CALL SCAMUL (E,G,M,XXX)
C       THIS PRODUCES THE HYSTERETIC MATRIX PROPORTIONAL TO THE
C       STIFFNESS MATRIX, HERE .01X.
        END
```

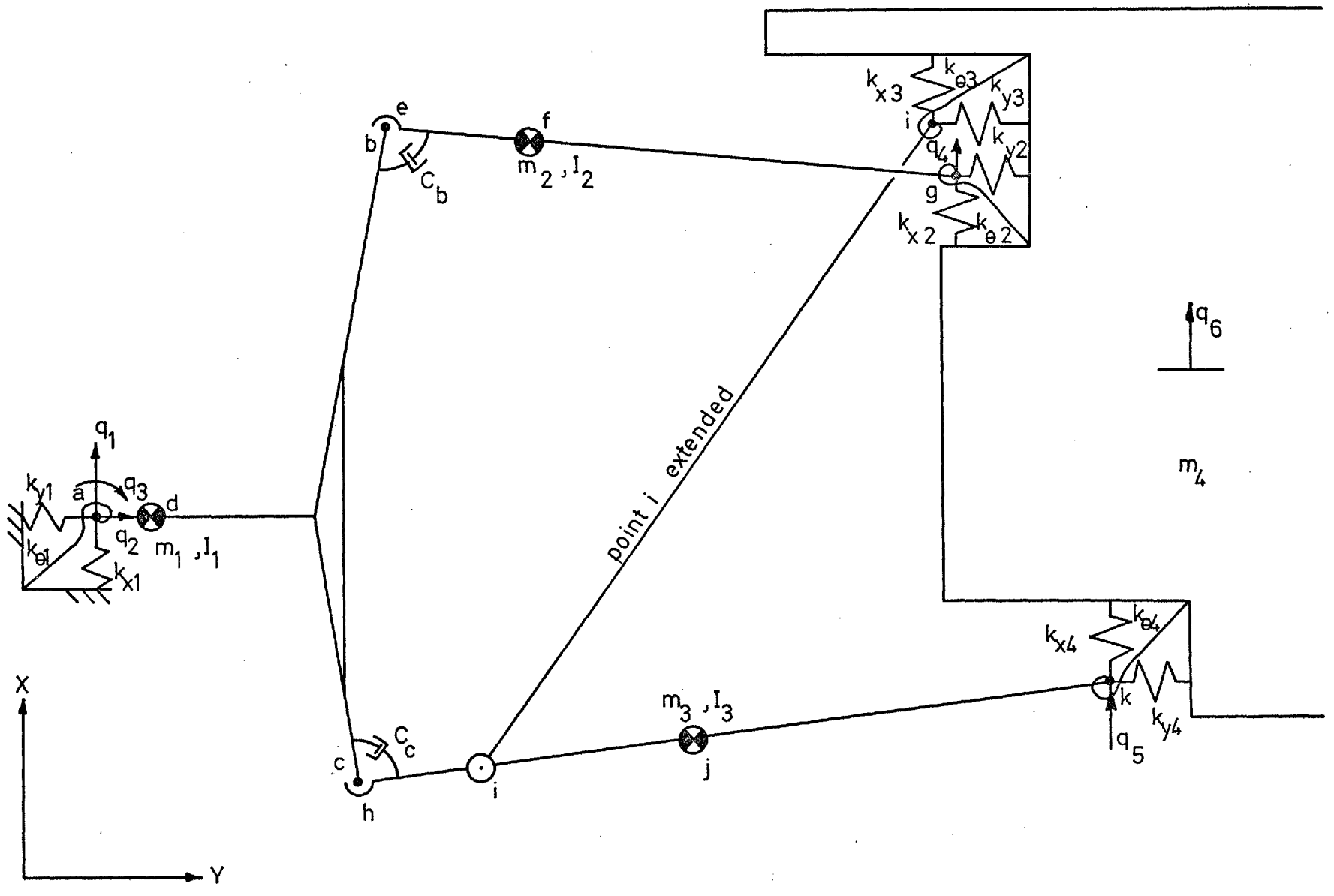


Transmissibility $= q_4 / q_1$

```
C     THIS PART OF THE SET ROUTINE ESTABLISHES THE INPUT MATRICES FOR
C     THE MODEL SHOWN IN FIGURE 5.4.3, PARA. 5.4.2.2. THE MODEL
C     CONSISTS  OF TWO WISHBONES, STUB-AXLE, AND HAS A MASSLESS MAIN
C     SPRING. THE INBOARD PIVOTS ARE SPRUNG, AND THE OUTBOARD PIVOTS
C     ARE ASSUMED TO BE VISCOUSLY DAMPED.
C     CODE...SS2DU


      RD=RXD**2+RYD**2
C     SETTING THE INERTIA MATRIX FOR SS2DU
      A1=RYF/RYG
      A2=1.-A1
      A3=RXF/RYG
      A4=RXB-RYB*RXF/RYG
      A5=1./RYG**2
      A6=RYJ/RYK
      A7=1.-A6
      A8=RXJ/RYK
      A9=RXC-RYC*RXJ/RYK
      A10=1./RYK**2
      A(1,1)=M1+(A2**2+A3**2)*M2+A5*I2+(A7**2+A8**2)*M3+A10*I3
      A(2,2)=M1+M2+M3
      A(3,3)=M1*RD    +I1+((RYB*A2)**2+A4**2)*M2+(RYB**2)*A5*I2
     1                   +((RYC*A7)**2+A9**2)*M3+(RYC**2)*A10*I3
      A(4,4)=(A1**2+A3**2)*M2+A5*I2
      A(5,5)=(A6**2+A8**2)*M3+A10*I3
      A(6,6)=M4
      A(1,2)=A3*M2+A8*M3
      A(1,3)=-RYD*M1+(A3*A4-RYB*A2**2)*M2-RYB*A5*I2
     1                +(A8*A9-RYC*A7**2)*M3-RYC*A10*I3
      A(1,4)=(A1*A2-A3**2)*M2-A5*I2
      A(1,5)=(A6*A7-A8**2)*M3-A10*I3
      A(2,1)=A(1,2)
      A(3,1)=A(1,3)
      A(4,1)=A(1,4)
      A(5,1)=A(1,5)
      A(2,3)=RXD*M1+A4*M2+A9*M3
      A(2,4)=-A3*M2
      A(2,5)=-A8*M3
      A(3,2)=A(2,3)
      A(4,2)=A(2,4)
      A(5,2)=A(2,5)
      A(3,4)=-(RYB*A1*A2+A3*A4)*M2+RYB*A5*I2
      A(3,5)=-(RYC*A6*A7+A8*A9)*M3+RYC*A10*I3
      A(4,3)=A(3,4)
      A(5,3)=A(3,5)
C      SETTING THE STIFFNESS MATRIX
      B1=RXG/RYG
      B2=RXB-RYB*RXG/RYG
      B3=RYI/RYK
      B4=1.-B3
      B5=RXI/RYK
      B6=RXC-RYC*RXI/RYK
      B7=RXK/RYK
      B8=RXC-RYC*RXK/RYK
      E(1,1)=KX1+KY2*B1**2+KO2*A5+KX3*B4**2+KY3*B5**2+A10*KO3+KY4*B7**2
     1+A10*KO4
      E(2,2)=KY1+KY2+KY3+KY4
C     CONTINUED OVER PAGE.........
```

```
      E(3,3)=K01+KY2*B2**2+K02*A5*RYB**2+KX3*(B4*RYC) **2+KY3*B6**2+
     1K03*A10*RYC**2+KY4*B8**2+K04*A10*RYC**2
      E(4,4)=KX2+KY2*B1**2+A5*K02
      E(5,5)=KX3*B3**2+KY3*B5**2+A10*K03+KX4+KY4*B7**2+A10*K04
      E(6,6)=KX2+KX3+KX4
      E(1,2)=B1*KY2+B5*KY3+B7*KY4
      E(1,3)=B1*B2*KY2-RYB*A5*K02-RYC*KX3*B4**2+B5*B6*KY3-RYC*A10*K03
     1+B7*B8*KY4-RYC*A10*K04
      E(1,4)=-KY2*B1**2-A5*K02
      E(1,5)=B3*B4*KX3-KY3*B5**2-A10*K03-KY4*B7**2-A10*K04
      E(1,6)=-B4*KX3
      E(2,1)=E(1,2)
      E(3,1)=E(1,3)
      E(4,1)=E(1,4)
      E(5,1)=E(1,5)
      E(6,1)=E(1,6)
      E(2,3)=B2*KY2+B6*KY3+B8*KY4
      E(2,4)=-B1*KY2
      E(2,5)=-B5*KY3-B7*KY4
      E(3,2)=E(2,3)
      E(4,2)=E(2,4)
      E(5,2)=E(2,5)
      E(3,4)=-B1*B2*KY2+RYB*A5*K02
      E(3,5)=-RYC*B3*B4*KX3-B5*B6*KY3+RYC*A10*K03-B7*B8*KY4+RYC*A10*K04
      E(3,6)=RYC*B4*KX3
      E(4,3)=E(3,4)
      E(5,3)=E(3,5)
      E(6,3)=E(3,6)
      E(4,6)=-KX2
      E(5,6)=-KX4-B3*KX3
      E(6,4)=E(4,6)
      E(6,5)=E(5,6)
C     SETTING THE HYSTERETIC MATRIX
      XX=.01
      CALL SCAMUL(E,G,M,XX)
C     THIS PRODUCES THE HYSTERETIC MATRIX PROPORTIONAL TO THE
C     STIFFNESS MATRIX, HERE .01X.
C     SETTING THE VISCOUS MATRIX
      C1=1./RYG
      C2=1.+RYB/RYG
      C3=1./RYK
      C4=1.+RYC/RYK
      D(1,1)=CB*C1**2+CC*C3**2
      D(3,3)=CB*C2**2+CC*C4**2
      D(4,4)=CB*C1**2
      D(5,5)=CC*C3**2
      D(1,3)=-C1*C2*CB-C3*C4*CC
      D(1,4)=-CB*C1**2
      D(1,5)=-CC*C3**2
      D(3,1)=D(1,3)
      D(4,1)=D(1,4)
      D(5,1)=D(1,5)
      D(3,4)=C1*C2*CB
      D(3,5)=C3*C4*CC
      D(4,3)=D(3,4)
      D(5,3)=D(3,5)
      END
```

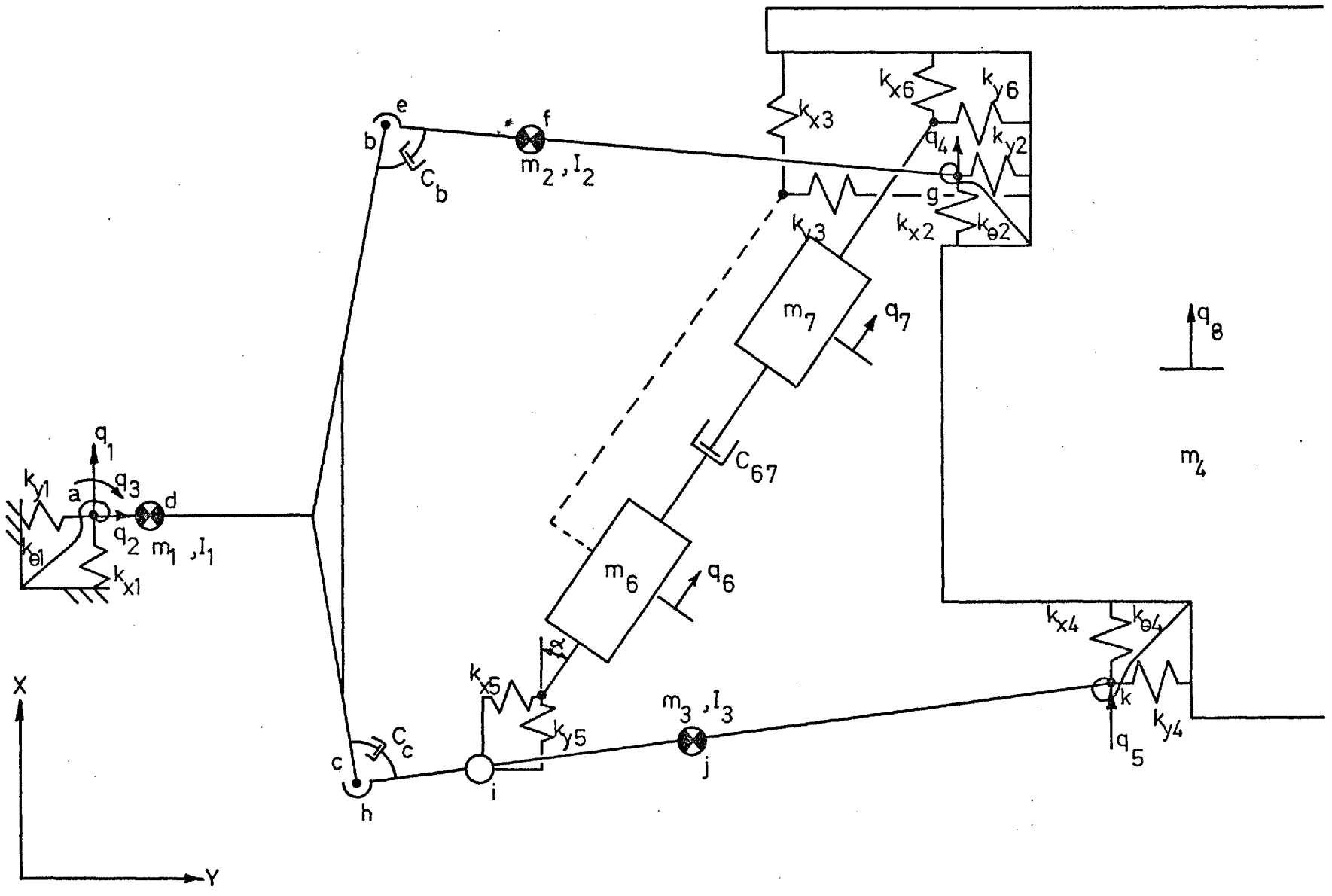

k_{x3}
$k_{\theta 3}$
k_{y3}
i
q_4
k_{y2}
g
k_{x2}
$k_{\theta 2}$
e
f
b
C_b
m_2, I_2
q_6
m_4
q_1
k_{y1}
a
q_3
d
q_2
m_1, I_1
$k_{\theta 1}$
k_{x1}
point i extended
k_{x4}
$k_{\theta 4}$
k
k_{y4}
q_5
m_3, I_3
j
C_c
c
h
i
X
Y

```
C       SPECIFIC MATRIX SETTING BEGINS HERE
C       THIS PART OF THE SET ROUTINE ESTABLISHES THE INPUT MATRICES FOR
C       THE MODEL SHOWN IN FIGURE 5.4.5. PARA. 5.4.2.3.  THE MODEL
C       IS SIMILAR TO THE PREVIOUS MODEL BUT INCLUDES THE DAMPER UNIT.
C       CODE...SS2DD


        P=COS(ALPHA)
        Q=SIN(ALPHA)
        RD=RXD**2+RYD**2
C       SETTING THE INERTIA MATRIX FOR SS2DD
        A1=RYF/RYG
        A2=1.-A1
        A3=RXF/RYG
        A4=RXB-RYB*RXF/RYG
        A5=1./RYG**2
        A6=RYJ/RYK
        A7=1.-A6
        A8=RXJ/RYK
        A9=RXC-RYC*RXJ/RYK
        A10=1./RYK**2
        A(1,1)=M1+(A2**2+A3**2)*M2+A5*I2+(A7**2+A8**2)*M3+A10*I3
        A(2,2)=M1+M2+M3
        A(3,3)=M1*RD    +I1+((RYB*A2)**2+A4**2)*M2+(RYB**2)*A5*I2
     1                     +((RYC*A7)**2+A9**2)*M3+(RYC**2)*A10*I3
        A(4,4)=(A1**2+A3**2)*M2+A5*I2
        A(5,5)=(A6**2+A8**2)*M3+A10*I3
        A(6,6)=M6
        A(7,7)=M7
        A(8,8)=M4
        A(1,2)=A3*M2+A8*M3
        A(1,3)=-RYD*M1+(A3*A4-RYB*A2**2)*M2-RYB*A5*I2
     1                +(A8*A9-RYC*A7**2)*M3-RYC*A10*I3
        A(1,4)=(A1*A2-A3**2)*M2-A5*I2
        A(1,5)=(A6*A7-A8**2)*M3-A10*I3
        A(2,1)=A(1,2)
        A(3,1)=A(1,3)
        A(4,1)=A(1,4)
        A(5,1)=A(1,5)
        A(2,3)=RXD*M1+A4*M2+A9*M3
        A(2,4)=-A3*M2
        A(2,5)=-A8*M3
        A(3,2)=A(2,3)
        A(4,2)=A(2,4)
        A(5,2)=A(2,5)
        A(3,4)=-(RYB*A1*A2+A3*A4)*M2+RYB*A5*I2
        A(3,5)=-(RYC*A6*A7+A8*A9)*M3+RYC*A10*I3
        A(4,3)=A(3,4)
        A(5,3)=A(3,5)
C        SETTING THE STIFFNESS MATRIX
        B1=RXG/RYG
        B2=RXB-RYB*RXG/RYG
        B3=RYI/RYK
        B4=1.-B3
        B5=RXI/RYK
        B6=RXC-RYC*RXI/RYK
        B7=RXK/RYK
        B8=RXC-RYC*RXK/RYK
C       CONTINUED OVER PAGE..........
```

```
      E(1,1)=KX1+KY2*B1**2+KO2*A5+KY4*B7**2+A10*KO4+KX5*B4**2+KY5*B5**2
      E(2,2)=KY1+KY2+KY4+KY5
      E(3,3)=KO1+KY2*B2**2+A5*KO2*RYB**2+KY4*B8**2+A10*KO4*RYC**2+KY5*B6
     1**2+KX5*(RYC*B4)**2
      E(4,4)=KX2+KY2*B1**2+A5*KO2
      E(5,5)=KX4+KY4*B7**2+A10*KO4+KX5*B3**2+KY5*B5**2
      E(6,6)=KX5*P**2+KY5*Q**2+KX3*P**2+KY3*Q**2
      E(7,7)=KX6*P**2
      E(8,8)=KX2+KX4+KX3+KX6
      E(1,2)=B1*KY2+B7*KY4+B5*KY5
      E(1,3)=B1*B2*KY2-RYB*A5*KO2+B7*B8*KY4-RYC*A10*KO4+B5*B6*KY5
     1-RYC*KX5*B4**2
      E(1,4)=-KY2*B1**2-A5*KO2
      E(1,5)=-KY4*B7**2-A10*KO4+B3*B4*KX5-KY5*B5**2
      E(1,6)=-B4*P*KX5-B5*Q*KY5
      E(2,1)=E(1,2)
      E(3,1)=E(1,3)
      E(4,1)=E(1,4)
      E(5,1)=E(1,5)
      E(6,1)=E(1,6)
      E(2,3)=B2*KY2+B8*KY4+B6*KY5
      E(2,4)=-B1*KY2
      E(2,5)=-B7*KY4-B5*KY5
      E(2,6)=-Q*KY5
      E(3,2)=E(2,3)
      E(4,2)=E(2,4)
      E(5,2)=E(2,5)
      E(6,2)=E(2,6)
      E(3,4)=-B1*B2*KY2+RYB*A5*KO2
      E(3,5)=-B7*B8*KY4+RYC*A10*KO4-RYC*B3*B4*KX5-B5*B6*KY5
      E(3,6)=RYC*B4*P*KX5-B6*Q*KY5
      E(4,3)=E(3,4)
      E(5,3)=E(3,5)
      E(6,3)=E(3,6)
      E(4,8)=-KX2
      E(8,4)=E(4,8)
      E(5,6)=-B3*KX5+B5*Q*KY5
      E(5,8)=-KX4
      E(6,5)=E(5,6)
      E(8,5)=E(5,8)
      E(6,8)=-P*KX3
      E(8,6)=E(6,8)
      E(7,8)=-P*KX6
      E(8,7)=E(7,8)
C     SETTING THE HYSTERETIC MATRIX
      XX=.01
      CALL SCAMUL(E,G,M,XX)
C     THIS PRODUCES THE HYSTERETIC MATRIX PROPORTIONAL TO THE
C     STIFFNESS MATRIX, HERE .01X.
C     SETTING THE VISCOUS MATRIX
      C1=1./RYG
      C2=1.+RYB/RYG
      C3=1./RYK
      C4=1.+RYC/RYK
      D(1,1)=CB*C1**2+CC*C3**2
      D(3,3)=CB*C2**2+CC*C4**2
      D(4,4)=CB*C1**2
      D(5,5)=CC*C3**2
C     CONTINUED OVER PAGE.......
```

```
D(6,6)=C67
D(7,7)=C67
D(1,3)=-C1*C2*CB-C3*C4*CC
D(1,4)=-CB*C1**2
D(1,5)=-CC*C3**2
D(3,1)=D(1,3)
D(4,1)=D(1,4)
D(5,1)=D(1,5)
D(3,4)=C1*C2*CB
D(3,5)=C3*C4*CC
D(4,3)=D(3,4)
D(5,3)=D(3,5)
D(6,7)=-C67
D(7,6)=D(6,7)
END
```


e
f
b
C_b
m_2, I_2
k_{x6}
k_{y6}
k_{x3}
q_4
k_{y2}
g
k_{x2}
$k_{\theta 2}$
k_{y3}
m_7
q_7
q_8
m_4
C_{67}
q_1
k_{y1}
a
q_3
d
q_2
m_1, I_1
$k_{\theta 1}$
k_{x1}
m_6
q_6
k_{x4}
$k_{\theta 4}$
α
k_{x5}
m_3, I_3
k
k_{y4}
k_{y5}
C_c
c
i
j
q_5
h
X
Y

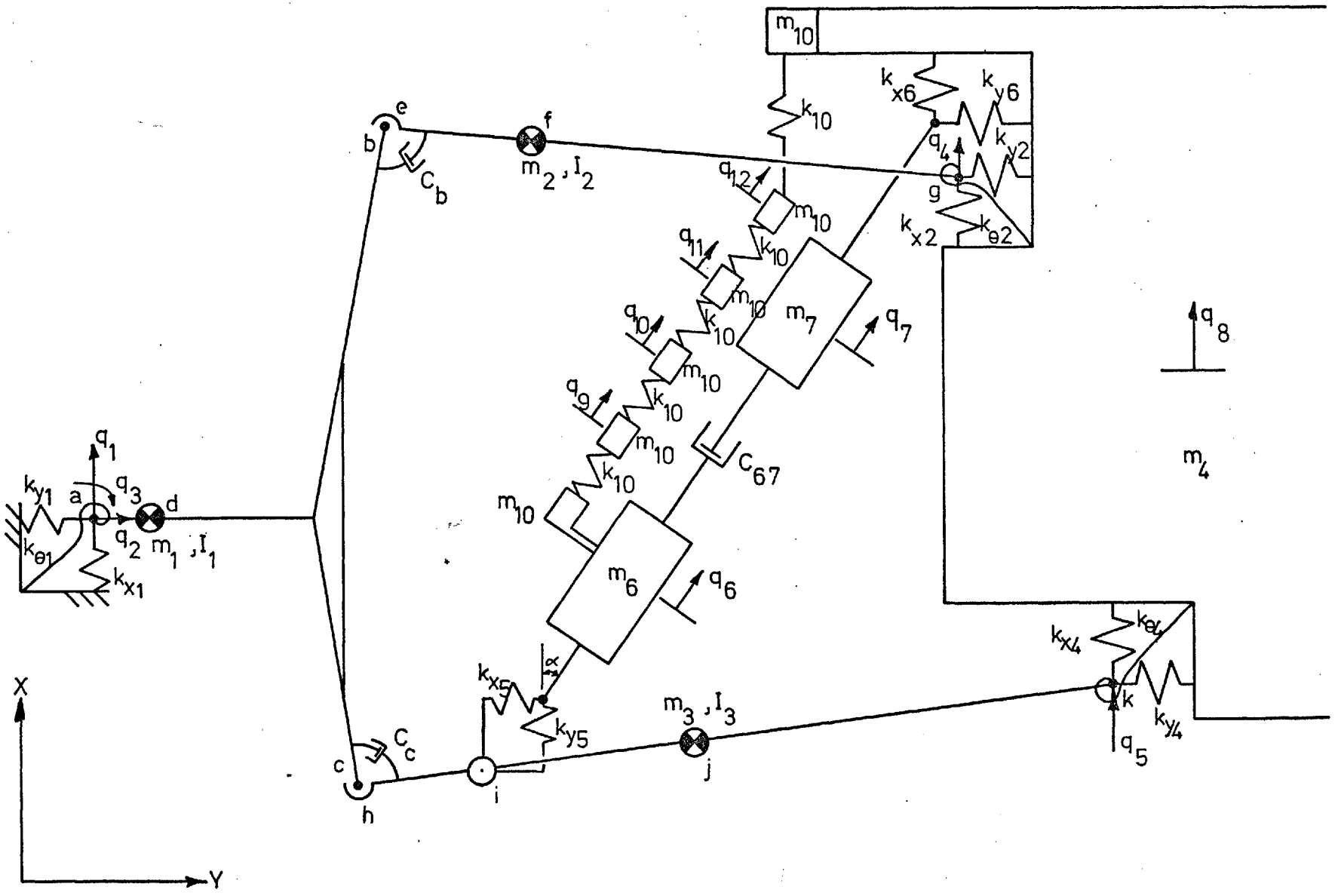
```
C       THIS PART OF THE SET ROUTINE ESTABLISHES THE INPUT MATRICES FOR
C       THE MODEL SHOWN IN FIGURE 5.4.6, PARA. 5.4.2.4.  THE MODEL
C       IS SIMILAR TO THE PREVIOUS MODEL BUT INCLUDES SPRING SURGES.
C       CODE...SS2DDS



        P=COS(ALPHA)
        Q=SIN(ALPHA)
        RD=RXD**2+RYD**2
C       SETTING THE INERTIA MATRIX FOR SS2DDS
        A1=RYF/RYG
        A2=1.-A1
        A3=RXF/RYG
        A4=RXB-RYB*RXF/RYG
        A5=1./RYG**2
        A6=RYJ/RYK
        A7=1.-A6
        A8=RXJ/RYK
        A9=RXC-RYC*RXJ/RYK
        A10=1./RYK**2
        A(1,1)=M1+(A2**2+A3**2)*M2+A5*I2+(A7**2+A8**2)*M3+A10*I3
        A(2,2)=M1+M2+M3
        A(3,3)=M1*RD    +I1+((RYB*A2)**2+A4**2)*M2+(RYB**2)*A5*I2
       1                   +((RYC*A7)**2+A9**2)*M3+(RYC**2)*A10*I3
        A(4,4)=(A1**2+A3**2)*M2+A5*I2
        A(5,5)=(A6**2+A8**2)*M3+A10*I3
        A(6,6)=M6+M10
        A(7,7)=M7
        A(8,8)=M4+M10
        A( 9, 9)=M10
        A(10,10)=M10
        A(11,11)=M10
        A(12,12)=M10
        A(1,2)=A3*M2+A8*M3
        A(1,3)=-RYD*M1+(A3*A4-RYB*A2**2)*M2-RYB*A5*I2
       1                +(A8*A9-RYC*A7**2)*M3-RYC*A10*I3
        A(1,4)=(A1*A2-A3**2)*M2-A5*I2
        A(1,5)=(A6*A7-A8**2)*M3-A10*I3
        A(2,1)=A(1,2)
        A(3,1)=A(1,3)
        A(4,1)=A(1,4)
        A(5,1)=A(1,5)
        A(2,3)=RXD*M1+A4*M2+A9*M3
        A(2,4)=-A3*M2
        A(2,5)=-A8*M3
        A(3,2)=A(2,3)
        A(4,2)=A(2,4)
        A(5,2)=A(2,5)
        A(3,4)=-(RYB*A1*A2+A3*A4)*M2+RYB*A5*I2
        A(3,5)=-(RYC*A6*A7+A8*A9)*M3+RYC*A10*I3
        A(4,3)=A(3,4)
        A(5,3)=A(3,5)
C        SETTING THE STIFFNESS MATRIX
        B1=RXG/RYG
        B2=RXB-RYB*RXG/RYG
        B3=RYI/RYK
        B4=1.-B3
C       CONTINUED OVER PAGE........
```

```
      B5=RXI/RYK
      B6=RXC-RYC*RXI/RYK
      B7=RXK/RYK
      B8=RXC-RYC*RXK/RYK
      E(1,1)=KX1+KY2*B1**2+K02*A5+KY4*B7**2+A10*K04+KX5*B4**2+KY5*B5**2
      E(2,2)=KY1+KY2+KY4+KY5
      E(3,3)=K01+KY2*B2**2+A5*K02*RYB**2+KY4*B8**2+A10*K04*RYC**2+KY5*B6
     1**2+KX5*(RYC*B4)**2
      E(4,4)=KX2+KY2*B1**2+A5*K02
      E(5,5)=KX4+KY4*B7**2+A10*K04+KX5*B3**2+KY5*B5**2
      E(6,6)=KX5*P**2+KY5*Q**2+KX3*P**2+KY3*Q**2+K10
      E(7,7)=KX6*P**2
      E(8,8)=KX2+KX4+KX6+K10/P**2
      E( 9, 9)=2.*K10
      E(10,10)=2.*K10
      E(11,11)=2.*K10
      E(12,12)=2.*K10
      E(1,2)=B1*KY2+B7*KY4+B5*KY5
      E(1,3)=B1*B2*KY2-RYB*A5*K02+B7*B8*KY4-RYC*A10*K04+B5*B6*KY5
     1-RYC*KX5*B4**2
      E(1,4)=-KY2*B1**2-A5*K02
      E(1,5)=-KY4*B7**2-A10*K04+B3*B4*KX5-KY5*B5**2
      E(1,6)=-B4*P*KX5-B5*Q*KY5
      E(2,1)=E(1,2)
      E(3,1)=E(1,3)
      E(4,1)=E(1,4)
      E(5,1)=E(1,5)
      E(6,1)=E(1,6)
      E(2,3)=B2*KY2+B8*KY4+B6*KY5
      E(2,4)=-B1*KY2
      E(2,5)=-B7*KY4-B5*KY5
      E(2,6)=-Q*KY5
      E(3,2)=E(2,3)
      E(4,2)=E(2,4)
      E(5,2)=E(2,5)
      E(6,2)=E(2,6)
      E(3,4)=-B1*B2*KY2+RYB*A5*K02
      E(3,5)=-B7*B8*KY4+RYC*A10*K04-RYC*B3*B4*KX5-B5*B6*KY5
      E(3,6)=RYC*B4*P*KX5-B6*Q*KY5
      E(4,3)=E(3,4)
      E(5,3)=E(3,5)
      E(6,3)=E(3,6)
      E(4,8)=-KX2
      E(8,4)=E(4,8)
      E(5,6)=-B3*KX5+B5*Q*KY5
      E(5,8)=-KX4
      E(6,5)=E(5,6)
      E(8,5)=E(5,8)
      E(6,8)=-P*KX3
      E(8,6)=E(6,8)
      E(7,8)=-P*KX6
      E(8,7)=E(7,8)
      E(6,9)=-K10
      E(8,12)=-K10/P
      E(9,10)=-K10
      E(10,11)=-K10
      E(11,12)=-K10
      E(9,6)=E(6,9)
C     CONTINUED OVER PAGE.....
```

```
      E(12,8)=E(8,12)
      E(10,9)=E(9,10)
      E(11,10)=E(10,11)
      E(12,11)=E(11,12)
CHANGE FOR EXPERIMENTAL RESULTS ONLY-PUTS SPRING FROM END MASS TO GROUND
C     E(8,8)=E(8,8)+303.
C     SETTING THE HYSTERETIC MATRIX
      XX=.001
      CALL SCAMUL(E,G,M,XX)
C     SETTING THE VISCOUS MATRIX
      C1=1./RYG
      C2=1.+RYB/RYG
      C3=1./RYK
      C4=1.+RYC/RYK
      D(1,1)=CB*C1**2+CC*C3**2
      D(3,3)=CB*C2**2+CC*C4**2
      D(4,4)=CB*C1**2
      D(5,5)=CC*C3**2
      D(1,3)=-C1*C2*CB-C3*C4*CC
      D(1,4)=-CB*C1**2
      D(1,5)=-CC*C3**2
      D(3,1)=D(1,3)
      D(4,1)=D(1,4)
      D(5,1)=D(1,5)
      D(3,4)=C1*C2*CB
      D(3,5)=C3*C4*CC
      D(4,3)=D(3,4)
      D(5,3)=D(3,5)
CHANGE TO HYSTERETIC- THIS IS A CHANGE FOR THE OUTBOARD PIVOT FRICTION
      CALL ADD(D,G,G,M)
      CALL SCAMUL(D,D,M,0.)
C     THIS ADDS THE VISCOUS MATRIX TO THE HYSTERETIC MATRIX AND
C     LEAVES THE VISCOUS MATRIX EMPTY
C67 STAYS IN VISCOUS MATRIX FOR DAMPER UNIT
      D(6,6)=C67
      D(7,7)=C67
      D(6,7)=-C67
      D(7,6)=D(6,7)
      END
```


m10
k10
kx6
ky6
ky2
q4
g
kx2
kθ2
e
f
b
Cb
m2 , I2
q12
m10
k10
q11
m10
k10
q10
m10
k10
q9
m10
k10
m10
m7
q7
C67
q8
m4
q1
ky1
a
q3
d
q2
m1 , I1
kθ1
kx1
m6
q6
kx5
kθ5
ky5
m3 , I3
kx4
kθ4
k
ky4
q5
c
Cc
h
i
j
X
Y

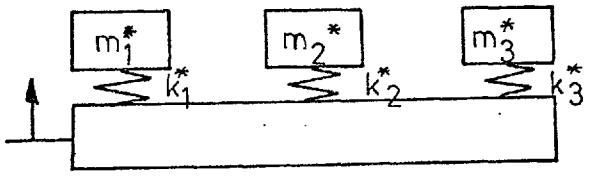
The data for the models shown in Chapters Five and Six are given below in table form.

The units used in the table are as follows:

m	-	lb wt	
I	-	lb wt in^2	
$k_{x,y}$	-	lbf/in	(in phase stiffness)
k_θ	-	lbf in/rad	(in phase stiffness)
$h_{x,y}$	-	lbf/in	(out-of-phase stiffness)
h_θ	-	lbf in/rad	(out-of-phase stiffness)
c	-	lbf/in/S	
$r_{x,y}$	-	in	(system geometry)
α	-	^{o}	(angle)

From the experimental results, a better model for outboard pivot friction was found to be hysteretic damping. Data marked ǂ have thus been modified to this form, as shown in the matrix element listing for SS2 DDS.

For the models with receiver resonances (i.e. Figures 5.4.7, 5.4.8, 6.2.3), resonators are attached as shown below:



For the model shown in Figure 6.2.4, representing the experimental apparatus, a spring value k_3^* (= 303 lbf/in) is attached to ground from the end mass, to represent the combined stiffness of the loading springs.

DATA FOR MODELS SHOWN IN CHAPTERS 5 AND 6

Figure No.	m_1	I_1	m_2	I_2	m_3	I_3	m_4	m_6	m_7	m_{10}	m_1^*	m_2^*	m_3^*
5.3.7	2	24	400										
5.4.3	2	24	500										
5.4.4	10.5	32	2	12	2.9	24	587						
5.4.5	43	129	2	12	2.9	24	587	2.3	0.5				
5.4.6	43	129	2	12	2.9	24	587	2.3	0.5	5.5/6			
5.4.7	43	129	2	12	2.9	24	300				287		
5.4.8	43	129	2	12	2.9	24	100				287	100	100
5.5.1	10	100	2	12	2.9	24	0.1						
5.5.2	10	100	2	12	2.9	24	0.1	2.3	0.5				
6.2.3	5	15	2	23.2	2.915	50	160				23.2		
6.2.4	5	15	2	23.2	2.915	50	160	2.3	0.5	4.46/6			
6.2.6	5	15	2	23.2	2.915	50	500	2.3	0.5	4.46/6			

Contd. over page

Figure No.	k_{x1}	h_{x1}	k_{y1}	h_{y1}	$k_{\theta 1}$	$h_{\theta 1}$	k_{x2}	h_{x2}	k_{y2}	h_{y2}	$k_{\theta 2}$	$h_{\theta 2}$	k_{x3}
5.3.7			20	0.2	10	0.1	1000	10	2000	20	4000	40	1000
5.4.3	400	4	40	0.4	40	0.4	4000	40	4000	40	400	4	200
5.4.4	700	7	70	0.7	10	0.1	1000	10	1000	10	500	5	137
5.4.5	700	7	70	0.7	10	0.1	1000	10	1000	10	500	5	198
5.4.6	700	7	70	0.7	10	0.1	1000	10	1000	10	500	5	
5.4.7	700	7	70	0.7	10	0.1	2000	20	2000	20	1000	10	137
5.4.8	700	7	70	0.7	10	0.1	2000	20	2000	20	1000	10	137
5.5.1							4000	40	4000	40	2000	20	137
5.5.2							1000	10	1000	10	1000	10	198
6.2.3	150	1.5	10	0.1	10	0.1	24000	240	24000	240	60	0.6	
6.2.4	500	0.5	70	0.07	10	0.01	24000	24	24000	24	60	0.6	
6.2.6	500	0.5	70	0.07	10	0.01	24000	24	24000	24	60	0.06	

Contd. over page

Figure No.	h_{x3}	k_{y3}	h_{y3}	$k_{\theta 3}$	$h_{\theta 3}$	k_{x4}	h_{x4}	k_{y4}	h_{y4}	$k_{\theta 4}$	$h_{\theta 4}$	k_{x5}	h_{x5}
5.3.7	10	2000	20	4000	40								
5.4.3	2	20	0.2	20	0.2								
5.4.4	1.37	62	0.62	10	0.1	1000	10	1000	10	500	5		
5.4.5	1.98	10	0.1	0	0	1000	10	1000	10	500	5	1000	10
5.4.6						1000	10	1000	10	500	5	2000	20
5.4.7	1.37	62	0.62	10	0.1	2000	20	2000	20	1000	10		
5.4.8	1.37	62	0.62	10	0.1	2000	20	2000	20	1000	10		
5.5.1	1.37	62	0.62	10	0.1	4000	40	4000	40	2000	20		
5.5.2	1.98	0	0	0	0	1000	10	1000	10	200	5	2000	20
6.2.3						24000	240	24000	240	60	0.6		
6.2.4						24000	24	24000	24	60	0.06	55000	55
6.2.6						24000	24	24000	24	60	0.06	55000	55

Contd. over page

Figure No.	k_{y5}	h_{y5}	k_{x6}	h_{x6}	k_{y6}	h_{y6}	$k_{1\theta}$	$h_{1\theta}$	k_1^*	h_1^*	k_2^*	h_2^*	k_3^*
5.3.7													
5.4.3													
5.4.4													
5.4.5	1000	10	1000	10	1000	10							
5.4.6	2000	20	2000	20	2000	20	198 x 5	1.98 x 5					
5.4.7									7000	70			
5.4.8									7000	70	25000	250	100000
5.5.1													
5.5.2	0	0	2000	20	2000	20							
6.2.3									74.2	0.742			
6.2.4	0	0	8000	8	0	0	198 x 5	0.198 x 5	303	0.303			
6.2.6	0	0	8000	8	0	0	198 x 5	0.198 x 5					

Contd. over page

Figure No.	h_3*	C_b	C_c	C_{67}	r_{xb}	r_{yb}	r_{xc}	r_{yc}	r_{xd}	r_{yd}	r_{xf}	r_{yf}	r_{xg}
5.3.7					10	-8	10	8	6	0			
5.4.3					0.3	2	1	6	2	12			
5.4.4		0.1	0.1		5.4	4.0	-3.65	3.6	0	0.75	-0.2	2.0	-0.72
5.4.5		0.1	0.1	20	5.4	4.0	-3.65	3.6	0	0.75	-0.2	2.0	-0.72
5.4.6		0.1	0.1	10	5.4	4.0	-3.65	3.6	0	0.75	-0.2	2.0	-0.72
5.4.7		0.1	0.1		5.4	4.0	-3.65	3.6	0	0.75	-0.2	2.0	-0.72
5.4.8	1000	0.1	0.1		5.4	4.0	-3.65	3.6	0	0.75	-0.2	2.0	-0.72
5.5.1		1.0	1.0		5.4	4.0	-3.65	3.6	0	0.75	-0.2	2.0	-0.72
5.5.2		0.1	0.1	10	5.4	4.0	-3.65	3.6	0	0.75	-0.2	2.0	-0.72
6.2.3		25200 ‡	63 ‡		5.4	4.0	-3.65	3.6	0	0.75	-0.2	2.0	-0.72
6.2.4		25200 ‡	63 ‡	∞	5.4	4.0	-3.65	3.6	0	0.75	-0.2	2.0	-0.72
6.2.6		25200 ‡	63 ‡	18	5.4	4.0	-3.65	3.6	0	0.75	-0.2	2.0	-0.72

Contd. over page

Figure No.	r_{yg}	r_{xi}	r_{yi}	r_{xj}	r_{yj}	r_{xk}	r_{yk}	α
5.3.7								
5.4.3								
5.4.4	7.8	0.2	1.7	0.6	4.6	1.4	10.3	
5.4.5	7.8	0.2	1.7	0.6	4.6	1.4	10.3	34
5.4.6	7.8	0.2	1.7	0.6	4.6	1.4	10.3	34
5.4.7	7.8	0.2	1.7	0.6	4.6	1.4	10.3	
5.4.8	7.8	0.2	1.7	0.6	4.6	1.4	10.3	
5.5.1	7.8	0.2	1.7	0.6	4.6	1.4	10.3	
5.5.2	7.8	0.2	1.7	0.6	4.6	1.4	10.3	0
6.2.3	7.8	0.2	1.7	0.6	4.6	1.4	10.3	
6.2.4	7.8	0.2	1.7	0.6	4.6	1.4	10.3	34
6.2.6	7.8	0.2	1.7	0.6	4.6	1.4	10.3	34

APPENDIX 8

CONVERSION OF UNITS

Conversion factors for the impedance parameters from British to I.S.O. units are given below

British		I.S.O.
1 in.	=	.0254 m
1 lbf	=	4.448 22 N

Thus, for stiffness (or dynamic stiffness):

1 lbf/in = 175.126 909 549 <u>N/m</u> or kg/s^2

and flexibility (or receptance):

1 in/lbf = $5.710\ 144\ 732 \times 10^{-3}$ <u>m/N</u> or s^2/kg

For impedance:

1 lbf/in/s = 175.1 Ns/m or <u>kg/s</u>

and mobility:

1 in/s/lbf = 5.71×10^{-3} m/Ns (i.e. m/s/N) or <u>s/kg</u>

For (apparent) mass:

1 lbf/in/s^2 = 175.1 Ns^2/m or <u>kg</u>

and inertance

1 in/s^2/lbf = 5.71×10^{-3} m/Ns^2 or <u>1/kg</u>

The preferred I.S.O. forms are shown underlined.

APPENDIX 9

ALTERNATIVE CANCELLATION MODEL

An interesting cancellation model has recently been reported in the literature* which was not considered in Chapter 4. The idea behind the function of the model is to give broad-band cancellation by means of a lever or 'phase-transformer' as shown in Figure A.9.1(a). The fixed point for the fulcrum of the lever is replaced in practice by a mass so that the leverage forces are reacted internally - this is shown in Figure A.9.1(b).

The model analysed here is used to give the transmissibility of this arrangement, and is shown in Figure A.9.1(c). Using the reciprocity theorem, the motion transmissibility q_4/q_1 is seen to be identical to the force transmissibility F_g/F_A (shown dotted) when $q_1 = 0$ (i.e. fixed base).

The system matrices, for the coordinates shown, are:

---

* Fontanet, P. (1971); Study of Engine Hum in an Automobile; Joint Symposium on Vibration and Noise in Motor Vehicles (I.Mech.E. 6-7th July), preprint C110/71.

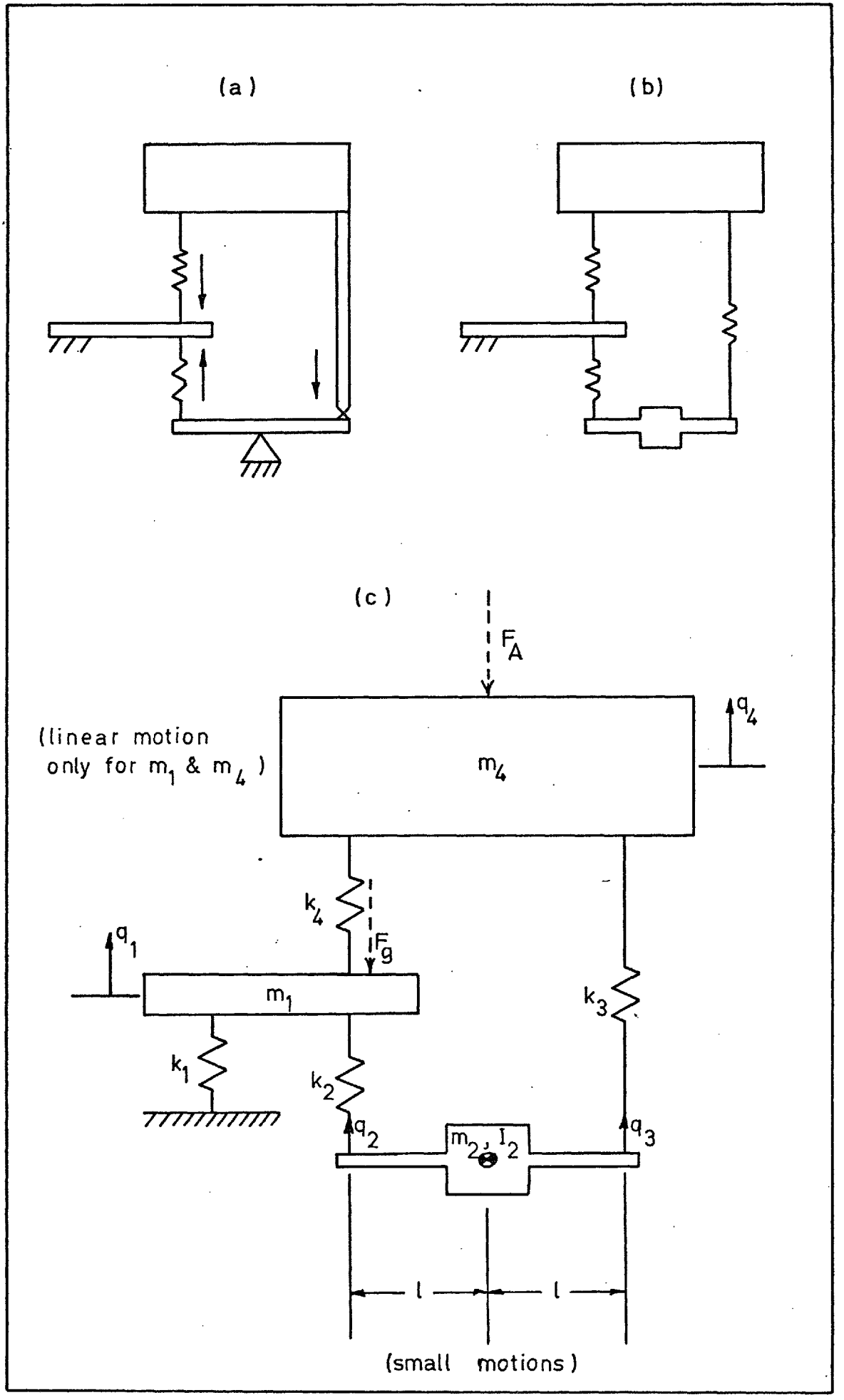

(a)
(b)
(c)
F_A
(linear motion
only for m_1 & m_4)
m_4
q_4
k_4
F_g
q_1
m_1
k_3
k_1
k_2
q_2
m_2, I_2
q_3
l
l
(small motions)

Figure A.9.1

$$[A] = \begin{bmatrix} m_1 & 0 & 0 & 0 \\ 0 & \frac{1}{4}(m_2+I_2/l^2) & \frac{1}{4}(m_2-I_2/l^2) & 0 \\ 0 & \frac{1}{4}(m_2-I_2/l^2) & \frac{1}{4}(m_2+I_2/l^2) & 0 \\ 0 & 0 & 0 & m_4 \end{bmatrix}$$

$$[E] = \begin{bmatrix} k_1+k_2+k_4 & -k_2 & 0 & -k_4 \\ -k_2 & k_2 & 0 & 0 \\ 0 & 0 & k_3 & -k_3 \\ -k_4 & 0 & -k_3 & k_3+k_4 \end{bmatrix}$$

In establishing the system parameters, Figure A.9.1(a) was used as the ideal model. We require:

$$I_2 \longrightarrow 0$$

$$m_2 \longrightarrow \infty$$

and $k_4 = k_2 k_3/(k_2 + k_3)$

to give complete cancellation. But $m_2 = m_4/5$ is a reasonable mass ratio.

On this basis, the parameters for the first calculation are:

m_4	= 500 lb wt	k_4	= 200 lbf/in.
m_2	= 100 lb wt	k_2	= 400 lbf/in.
I_2	= 4 lb wt in^2	k_3	= 400 lbf/in.
l	= 10 in.	η all springs	= .1

The auxiliary mass being less than ideal, but more realistic. The transmissibility for this model is shown as curve 1 on Figure A.9.2. The auxiliary

mass causes a second low-frequency resonance and also a high frequency resonance (rotational resonance of phase transformer), with a final attenuation slope determined by the strongest path - i.e. 12 dB/octave. A fairly broad band low transmissibility region is formed, but not true cancellation. Tuning the response by means of changing k_3 leads to curves 2 (k_3 = 360 lbf/in, i.e. -10%) where two troughs are formed, and 3 (k_3 ∓ 300 lbf/in), i.e. - 25%) where the troughs are spread further apart on the frequency scale. Curve 3 is seen to provide the best initial attenuation slope. The highest mode of the system is seen to be disadvantageous and is controlled by I_2.

Reducing I_2 to 0.04 lb.wt.in.^{2} (an unrealistically low value), shifts the highest mode to a very high frequency. This model, with k_3 ∓ 360 lbf/in is shown as curve 1 on Figure A.9.3. This is compared with an optimised two-stage mount (see Chapter 4) using the same amount of auxiliary mass and for roughly the same fundamental frequency (curve 2). Even for this rather ideal case of the cancellation model, the performance is generally inferior to the two-stage mount. Similar low-frequency resonances are excited, and even in the cancellation region, the two stage mount transmits less. The cancellation model shows one small region only where the transmissibility is less than the two-stage mount.

A full parameter search has not been made, but on the basis of the results shown here it would seem that generally the model is inferior to the two-stage mount.



TCM2R2.3.AND4

Figure A.9.2

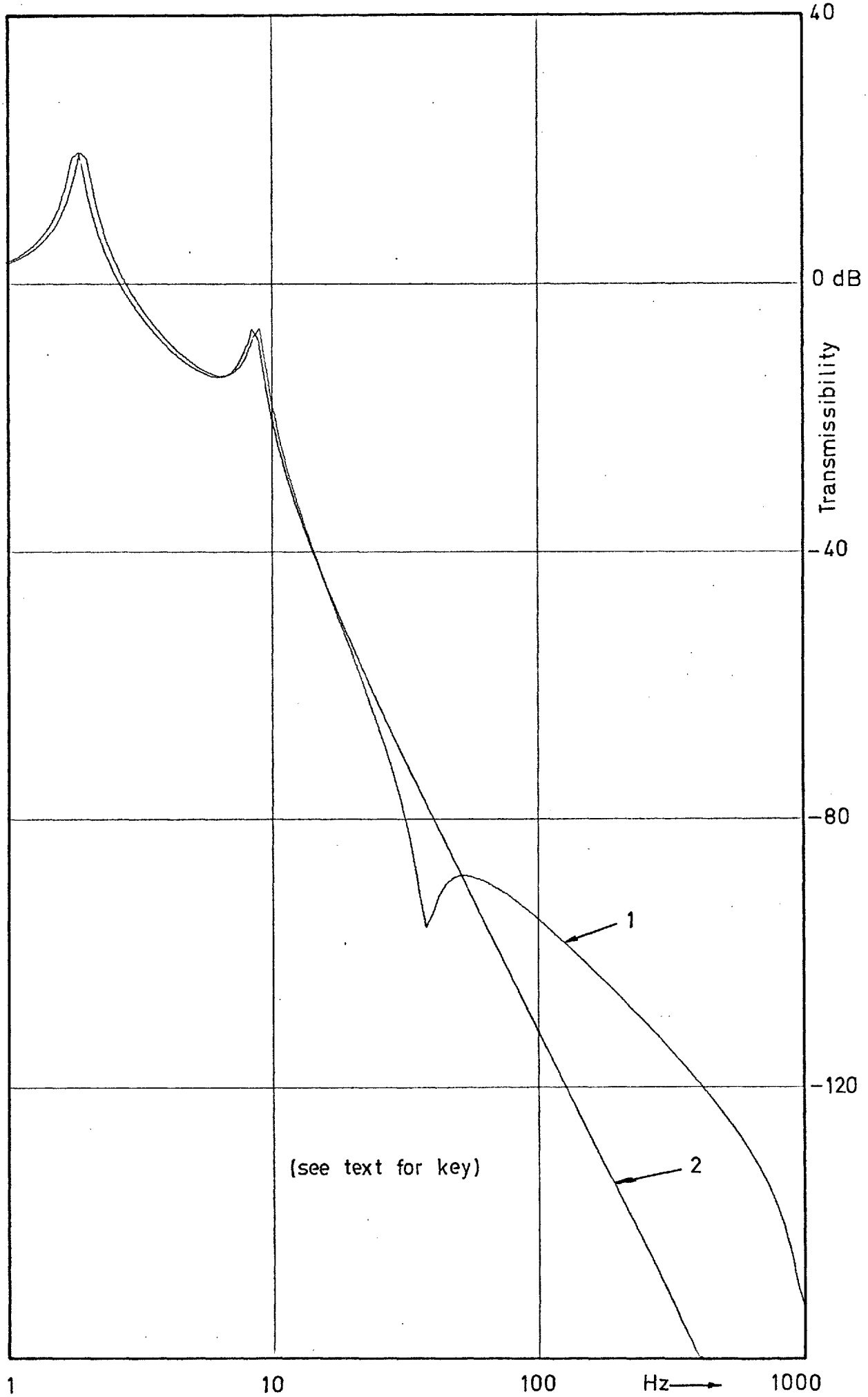


Figure A.9.3

TSM01 AND TCM2R1